Volcanostratigraphy using geophysical methods on La Fossa di Vulcano (S-Italy)

Dissertation zur Erlangung des
naturwissenschaftlichen Doktorgrades
der Bayerischen Julius-Maximilians-Universität Würzburg

vorgelegt von

Iris Gehring

aus
Detmold

Würzburg 2001

Eingereicht am:

1. **Gutachter: Prof. Dr. B. Zimanowski**
2. **Gutachter: Prof. Dr. P. Dellino**

der Dissertation

1. **Prüfer: Prof. Dr. B. Zimanowski**
2. **Prüfer: Prof. Dr. R. Klemd**

der mündlichen Prüfung

Tag der mündlichen Prüfung

Doktorurkunde ausgehändigt am:

Gehring, I. (2001): Volcanostratigraphy using geophysical methods on La Fossa di Vulcano (S-Italy).- Dissertation (Dr. rer. nat.), Universität Würzburg, Germany, 196 pp., 57 figures, 65 tables, 1 CD.

Il ramona soigneusement ses volcans en activité. Il possédait deux volcans en activité. Et c'était bien commode pour faire chauffer le petit déjeuner du matin. Il possédait aussi un volcan éteint. Mais, comme il disait: «On ne sait jamais!» Il ramona donc également le volcan éteint. S'ils sont bien ramonés, les volcans brûlent doucement et régulièrement, sans éruptions. Les éruptions volcaniques sont comme des feux de cheminée. Évidemment sur notre terre nous sommes beaucoup trop petits pour ramoner nos volcans. C'est pourquoi ils nous causent des tas d'ennuis.

(Antoine de Saint~Exupéry: Le Petit Prince)

Abstract

For many active volcanoes all over the world a civil protection program, normally combined with hazard maps, exists. Optimising of hazard maps and the associated hazard assessment implies a detailed knowledge of the volcanostratigraphy, because the deposits provoke information on the potential behaviour during a new activity cycle. Pyroclastic deposits, however, may vary widely in thickness and distribution over very short lateral distances. High resolution characterisation of single strata often cannot be archived, if solely sedimentological and geochemical methods are used. Gamma-ray measurements taken in the field combined with grain-size depended magnetic susceptibility measurements made in the laboratory are used in this work to optimise the resolution of volcanostratigraphic investigations.

The island of Vulcano is part of the Aeolian Archipelago sited of the northern coast of Sicily. La Fossa cone is the active centre of Vulcano, where fumarolic and seismic activity can be observed. The cone was built up during the last 6,000 years, whereby the last eruption period is dated to historic times (1888-1890). For the tuff cone La Fossa the most likely volcanic hazards are the emplacement of pyroclastic deposits as well as gas hazards (especially SO_x and CO_2), due to this the detailed knowledge of the stratigraphy is mandatory. Most of the population resides in Vulcano Porto and the nearby sited peninsula of Vulcanello, which are highly endangered locations for a future eruption scenario.

Measurements, made in standard outcrops, allow a characterisation of the successions Punte Nere, Tufi Varicolori, Palizzi, Commenda, and Cratere Attuale. A discrimination of all successions by solely one of the methods is rarely possible. In some cases, however, the combination of the methods leads to clear results. It can also be noticed that the exposition as well as the sedimentation type (wet-surge or dry-surge deposits) affect the measurements.

In general it can be assumed that the higher the magma is evolved the higher the γ-ray values and the lower the susceptibility values. Measurements from the Wingertsberg (Laacher See deposits, Eifel, W-Germany) show clearly that a higher degree of magma evolution correlates with lower susceptibility and higher gamma-ray values. Variations of the values can be observed not only by the change of the degree of magmatic evolution but also by the inhomogeneous deposition conditions. Particularly the gamma-ray measurements show lower values for the wet-surge deposits than for the dry-surge deposits, even though the erupted material has the same geochemical composition. This can be explained especially by reactions inside of the moist eruption cloud and short-time after deposition, when easily soluble elements like K, U, and Th can be leached by these aggressive fluids. Even extended exposition and high water content can provoke depletion of various elements within the complete or parts of the outcrop, too. If the deposits are affected by a fumarolic activity especially the susceptibility values show significant variations, whereas in general extreme low values are observed.

Contamination of deposits also can occur, if they are overlain by weathered deposits of higher concentration of K, U, and Th. Weathering and mobilisation within the upper deposits can

generate an element enrichment within the lower deposits. In general the element ratios of the barried underlying deposits are less affected than the exposed ones.
After gauging the values of the well defined succession for standard outcrops undefined outcrops were measured. These outcrops are not clearly classified by sedimentological and geochemical methods, thus a correlation with the combined geophysical methods is useful. In general the combination of the methods allows a correlation, although in some cases more than one interpretation is possible. But in connection with time marker horizons as well as sedimentological features an interpretation is feasible. These situations show that a classification solely based on geophysical methods is possible for many cases but, if the volcanic system is more complex, a combination with sedimentological and geochemical methods may be needed.
The investigations on Vulcano, documented in this work, recommend a re-interpretation of the dispersial of some successions of La Fossa cone, especially the presumption that Tufi Varicolori only exist inside of the Caldera of La Fossa. As a consequence the eruption and energy model especially for Tufi Varicolori have to be reviewed.

Zusammenfassung

An den zahlreichen aktiven Vulkanen auf der Erde existiert häufig ein Programm zum Zivilschutz in Kombination mit hazard maps. Die Optimierung von hazard maps und dem damit verbundenen hazard assessement setzt eine detaillierte Kenntnis der Vulkanostratigraphie voraus, da die Ablagerungen Aufschlüsse über ein potentielles Verhalten bei erneuter Aktivität zulassen. Eine detaillierte Stratigraphie pyroklastischen Ablagerungen ist nicht immer eindeutig, da die Verbreitung der Ablagerungen sehr inhomogen sein kann und häufig ein lateraler Fazieswechsel zu beobachten ist. Die Charakterisierung einzelner Horizonte und Einheiten aufgrund von geochemischen und sedimentologischen Untersuchungen ist nicht immer eindeutig. Mit Hilfe von Gamma-ray-Messungen vor Ort und Untersuchungen der korngrößenabhängigen Suszeptibilität wird in dieser Arbeit versucht die Auflösung der Vulkanostratigraphie zu verbessern.
Vulcano gehört zur Inselgruppe der Äolischen Inseln vor der Nordküste von Sizilien. Das derzeit aktive Zentrum, La Fossa cone, zeigt heute vorwiegend fumarolische und seismische Aktivität. Hierbei ist zu beachten, daß die letzte große Eruptionsphase in historischer Zeit stattfand (1888-1890). Aufgrund der Geschichte von La Fossa cone, welche vor rund 6000 Jahren begann, kann man vermuten, daß die aktive Phase noch nicht abgeschlossen ist und weitere Eruptionen folgen können. La Fossa cone ist ein Tuffkegel, dessen größte Gefahr, neben der fumarolischen Aktivität (erhöhte Gehalte an SO_x und CO_2), besonders in der Bildung und Ablagerung von pyroklastischen Strömen liegt, daher ist eine genaue Kenntnis der Stratigraphie unabdingbar. Der Hauptort der Insel, Vulcano Porto, liegt am Fuß von La Fossa cone und ist somit bei einem Ausbruch extrem gefährdet. Hier und auf der

angrenzenden Halbinsel Vulcanello hält sich während der Hauptsaison der Großteil der bis zu 9000 Personen (inklusive Tagestouristen) auf der Insel auf.
Die Kombination der geophysikalischen Methoden hat sich innerhalb der Standardaufschlüsse von Vulcano als geeignete Methode erwiesen, um die bisher definierten Einheiten: Punte Nere, Tufi Varicolori, Palizzi, Commenda und Cratere Attuale voneinander zu unterscheiden. Dabei ist es allerdings wichtig die beiden Methoden zu kombinieren, da nicht alle Einheiten nur anhand von einer Methode zu unterscheiden sind. Auch hat sich gezeigt, daß die jeweilige Exposition wie auch der Ablagerungstyp – wet-surge oder dry-surge Ablagerung – die Werte der Messungen beeinflussen können.
Allgemein gilt, je stärker das Magma differenziert ist umso geringer sind die zu erwartenden Suszeptibilitätswerte und umso höher die zu erwartenden Gamma-ray-Werte. Dies konnte in Vergleichsmessungen am Wingertsberg (Laacher See Ablagerungen, Eifel, W-Deutschland) recht gut beobachtet werden. Solche Ergebnisse sind deutlich bei gleichen Ablagerungsbedingungen zu erkennen, treten jedoch sowohl wet- wie auch dry-surge Ablagerungen auf, so beobachtet man häufig, daß wet-surge Ablagerungen geringere Werte zeigen – besonders für die Gamma-ray-Messungen – als diejenigen von dry-surge Ablagerungen des gleichen Ausgangsmaterial. Dies ist vor allem auf Reaktionen des Materials innerhalb der „feuchten“ Eruptionswolke und des pyroklastischen Stromes (wet-surge Ablagerungen) zurückzuführen, bei denen es zu einer Abreicherung unter anderem von K, U, und Th kommen kann. Auch kurz nach der Ablagerung können bevorzugt Alterationsprozesse auftreten. Eine starke Exposition oder auch eine erhöhte Feuchtigkeit führen häufig zur Abreicherung verschiedener Elemente innerhalb des Aufschlusses. Hiervon sind besonders die Werte von Gamma-ray-Messungen betroffen. An Orten fumarolischer Aktivität ist eine signifikante Änderung der Suszeptibilitätswerte zu beobachten, stark betroffene Bereiche zeigen häufig extrem geringe Suszeptibilitätswerte.
Überlagerung von Einheiten mit hohen Konzentrationen an K, U, und Th kann bei der Verwitterung dieser Lagen eine Kontamination der darunterliegenden Bereiche zur Folge haben. Diese zeigen dann deutlich erhöhte Elementkonzentrationen – im Gegensatz zu den Durchschnittswerten – wobei aber das Verhältnis der Elemente oft nicht signifikant verändert wird.
Nach einer Eichung anhand der Standardprofile wurden Aufschlüsse mit einer nicht immer eindeutigen Zuordnung – durch die „klassischen“ sedimentologischen und geochemischen Methoden – bearbeitet. Hierbei zeigte sich, daß die Kombination der beiden geophysikalischen Methoden durchaus eine Charakterisierung erlaubt. Dabei wurde allerdings auch deutlich, daß eine Korrelation durch die kombinierten geophysikalischen Methoden zwar sinnvoll ist, jedoch stellenweise verschiedene Interpretationen möglich sind, daher ist es sicherlich von Vorteil, wenn zur Charakterisierung auch die „klassischen“ Methoden hinzugezogen werden. Von besonderem Vorteil erwiesen sich bei den Untersuchungen Zeitmarkerhorizonte, durch welche häufig mehrdeutige Interpretationen geklärt werden konnten.

Anhand der Untersuchungen konnten, in dieser Arbeit, nun erstmals die, bisher nur innerhalb der Caldera von La Fossa bekannten, Tufi Varicolori auch außerhalb der Caldera identifiziert werden. Dieser Umstand gibt Anlaß die bisherigen Modelle für den Eruptionsmechanismus und das Energieschema der Tufi Varicolori Eruptionen zu überarbeiten, da für die Überwindung der Calderawand eine deutlich höhere Energie nötig ist als bisher für Tufi Varicolori angenommen wurde.

Acknowledgements

I would like to sincerely thank my supervisors, Prof. Dr. Bernd Zimanowski and Prof. Dr. Pierfrancesco Dellino, who initiated and accompanied this project with continued interest. I wish to thank them for their guidance and assistance throughout the field- and office work, they have always had an open door for problems, questions, and discussions. Prof. Dr. Bernd Zimanowski guided me through the thesis, showed me possibilities to solve the different problems and was like an anchor when I needed a resting point between all these diagrams. Prof. Dr. Pierfrancesco Dellino shared his wide knowledge about the geology of Vulcano with me and showed me not only the outcrops but also all the little things, which had been important to understand Vulcano a little more. Their immense knowledge and enthusiasm were always inspiring and motivating to this thesis.
Many thanks to Prof. Dr. Volker Lorenz for his support and lively interest in the thesis, as well as for fruitful discussions in the field and the office.
I wish to thank Dr. Ralf Büttner for his very helpful co-operation in the field and in the office where he was disclosing the secret of the theory of errors to me. He also gave me many helpful comments and corrections.
I would like to thank Dr. Ulrich Schüssler his patience in teaching me the use of the microprobe.

Concerning headstrong computer and associated programs Christian Lenk and Jan Nestler assisted me in a very helpful way, thanks for that.
Also many thanks to Wolfram Schuhmann for his help with any kind of photographs and slides.
Thank you to Peter Späthe and Rupert Wassermann, who prepared different thin sections. Diverse technical problems in the office were solved by the helpful hand of Anton Uttinger.
I would like to thank Meike Dörnemann and Birgit Mayer for their help in bureaucratic questions and their always constructive assistance.
Many thanks to Laurence Diele who assisted me in the formal regulation of the thesis.
The following people provided helpful comments and corrections on my manuscript: Ralf Büttner, Laurence Diele, Petra Hess, Doris Maicher, Birgit Mayer, Stefan Schröder, Christine Wörrlein, and of course my supervisors Prof. Dr. Pierfrancesco Dellino and Prof. Dr. Bernd Zimanowski.
Lars Tümmler and Harald Kobmann are acknowledged for their team work in summer 2000 during the Eifel-field course, our data let me see clearer some aspects on Vulcano. Lars' refreshing discussions – not only about geology – allowed me another point of view.
I would like to thank my "room mate" Chris for her patience especially during the last time of writing the thesis. Together with Chabba and Chester Chris created an inspiring and relaxing atmosphere.

Cornelia Beck and Petra Meuer are acknowledged for their assistance during different field sessions.

I thank my colleagues Hermann Beyrichen, Steffen Bez, Ralf Büttner, Laurence Diele, Mohammed Hassouneh, Anselm Koopmann, Christian Lenk, Jan Nestler, Hannes Raue, Wolfram Schuhmann, Chris Wörrlein, and Claus Zeller for the good working atmosphere.
I wish to thank Petra Hess for showing me that science is not all as well as for her friendship during all stages of this thesis. She was a real friend.
Thanks to my friends, especially Stefan Behrens, Helge and Nicole Blanke, Jochen Hemmleb, Doris Maicher, Justine Zimmermann, and Bettina and Frank Zuckle, without them it would have been a grey and cold time.
Furthermore, I would like to give special thanks to my mother for her encouragement and understanding on all levels as well as for her generous and widespread support.
Special thanks are owed to Stefan, who not only corrected my work, which often was a good piece of craftsmanship, but who also accompanied me with his patience, love, support, and tolerance during writing this thesis.

The research was financially supported by University of Würzburg (Promotionsstipendium nach dem Gesetz zur Förderung des wissenschaftlichen und künstlerischen Nachwuchses) as well as by the HWP-Program of the University of Würzburg (Hochschul- und Wissenschaftsprogramm “Chancengleichheit für Frauen in Forschung und Lehre”). Logistic support was provided by the Gruppo Nazionale per la Vulcanologia and wondrous sources of the working group.

Table of Contents

1.Introduction

1.1. Overview

Volcanic hazards due to volcanic eruptions can harm population and economy in various ways. Different types of primary and secondary volcanic hazards can be distinguished, for example lava flows, fall out (ash and bombs), gas hazards (BADALAMENTI ET AL., 1998 and WOODS AND PHILLIPS, 1999), collapse of a volcanic dome, pyroclastic surges, giant volcanic landslides, lahars, tsunamis, earthquakes, change of weather, famine and plague. Great historic events of volcanic hazards are the eruption of Mt. Vesuvius documented by Plinius (79 AD), Krakatoa (1883), Santorini (1490 BC), Mont Pelée (1902), Nevado del Ruiz (1985), Tambora (1815), Laki (1783) (LATTER, 1989 and TANGUY ET AL., 1998). Many articles about the victims of volcanic eruptions, hazard assessment, hazard maps (and volcanic hazards) are published (for example ALLEN ET AL., 2000, BADALAMENTI ET AL., 1998, CONIGLIO AND DOBRAN, 1995, DELLINO, 1997, DELLINO AND LA VOLPE, 1997, DELLINO AND LA VOLPE, 1998, DELLINO AND LA VOLPE, 2000, FISHER, 1995, FRAZZETTA AND LA VOLPE, 1991, LATTER, 1989, MASTIN AND WITTER, 2000, NAKADA, 2000, NERI ET AL., 1999, PARESCHI ET AL., 2000, PIERSON, 1998, SAITO ET AL., 2001, SHERIDAN AND MALIN, 1983, TANGUY ET AL., 1998, and THOURET ET AL., 2000). To minimise a few of this consequences a consolidated knowledge about eruption type, deposit dispersal, as well the volcanostratigraphy is necessary, so that dangerous projects (settlement on locations of high potential endangered areas) can be avoided and plans for hazard management made.

What is hazard assessment? How can it be optimised? What does the volcanic history tell the volcanologist about energy and mechanism of an eruption? What can be recognised by the dispersal and sedimentation marks of volcanic deposits? What is the importance of phreatomagmatism and the related deposits? Can volcanic events be calculated by type and energy? Where will the eruption cloud and products go to?

For the island of Vulcano (Aeolian Islands, Southern Tyrrhenian Sea, S-Italy) the most likely volcanic hazards are the emplacement of pyroclastic deposits, gas hazards and fall-out. Because of its velocity, mass and volume, sometimes temperature, toxic composition, and potentially wide dispersal, the emplacement of pyroclastic surge and flow deposits is one of the highest risks for the population living near the volcano and in locations of previous pyroclastic deposition. The main part of the volcanic edifice of La Fossa di Vulcano cone (the centre of recent volcanic activity on Vulcano island) is built up by several pyroclastic deposits and a few lava flows. In principle La Fossa di Vulcano can be called a tuff cone. Maar volcanoes, tuff rings, and tuff cones, are phreatomagmatic subaerial volcanic landforms, usually monogenetic (CAS AND WRIGHT, 1988 and VESPERMANN AND SCHMINCKE, 2000). They are dominated by pyroclastic deposits and may be subdivided as follows: *tuff rings* are positive landforms characterised by a flat morphology, dipping at shallow angles; *tuff cones* feature a steep morphology and steep angles; *maar volcanoes* are negative volcanic

landforms, similar to *tuff rings* but undercutting the prevolcanic surface with deep craters. After FISHER AND SCHMINCKE (1984) wet-surge deposits, which can also be found on La Fossa cone in different pyroclastic successions, are characteristic for tuff rings and tuff cones. These deposits typically originate from violent interaction between magma and subsurface water, which is also assumed for many of the volcanic eruptions of La Fossa di Vulcano.

Investigations and mapping of volcanic areas can be complicated because deposits vary widely in thickness and spatial distribution, sometimes lacking completely due to post-depositional erosion by flowing water, mass wasting and subsequent volcanic events with a high erosional potential. The variation of the different facies types over short distances does not allow the use of only sedimentological or geochemical features for stratigraphical classification and correlation. A detailed knowledge of the volcanostratigraphy is critical for a good hazard assessment. On this basis an attempt can be made to predict which areas are most likely to receive volcanic products, and how it will affect the surrounding areas. Of course, this approach assumes that the volcano behaves in the same manner as before.

The problem of identification and distinction of different ash layers is old, and often geochemical or granulometrical methods are applied (PAWSE ET AL., 1998). Much has been done for accurate identification, for example the use of alpha counting for the determination of U and Th amounts, the analysis of trace elements or the proton-induced X-ray emission for Th geochemical analysis. PAWSE ET AL. (1998) used the hysteresis parameters and electron spin resonance spectroscopy for the identification of different ash layers. A promising tool to solve the problem of volcanostratigraphy is the use of geophysical methods combined with sedimentological and geochemical features. γ-ray-measurements taken in the outcrops layer by layer in combination with grain-size dependent magnetic susceptibility measurements in the laboratory could help to define different successions and probable marker horizons in the stratigraphy. Both methods are more or less easy to carry out, because in general one scientist with a minimum of equipment (except for sus measurements) in the field is sufficient. Samples for the sus measurements can be prepared in a normal sedimentological laboratory. First statements can be made by using solely common computer programs. Both methods are not affected by environmental influences in the same way, so if one method fails, the other may still provide useful information. La Fossa di Vulcano (Isola di Vulcano, S-Italy) is a good study area for this approach, because of its suitable size and the well-preserved and fresh material.

1.2. Geological Setting

1.2.1. Regional Tectonic Setting

The island of Vulcano is part of the Aeolian Archipelago, which is located off the northern coast of Sicily and consists of seven islands and nine seamounts. Three seamounts are found to the NW of Alicudi and the others to the NE of the emergent island arc segment (DE ASTIS ET AL., 2000). West of the island arc another volcanic island, Ustica, rose above sea-level. The Aeolian Archipelago is a typical example for a sub-circular volcanic island arc attributed to a subduction zone sited about 250 km above the Tyrrhenian Benioff zone (BARBERI ET AL., 1973, BARBERI ET AL., 1974, BRUNO ET AL., 2000, DE ASTIS ET AL., 2000, ELLAM ET AL., 1989, FERRARI AND MANETTI, 1993, KELLER, 1974, and PRIVITERA, 1997). Today only Vulcano and Stromboli show "active" volcanism. The Aeolian Arc is one of the two active volcanic island arcs, the Aeolian and the Aegean Arc, of the Mediterranean Sea with calc-alkaline volcanism. It developed at the sutur between the African and European plates (BARBERI ET AL., 1973; BARBERI ET AL., 1974). Geophysical data show an uncommon tectonic situation for both arcs, which can be explained by the complex Mediterranean structure (BARBERI ET AL., 1974). The Aeolian Arc was initiated about 1 Ma ago on the Calabro-Peloritano continental margin in the southern part of the Tyrrhenian Sea, near the SE boundary of the Marsili Basin about 1 Ma ago (DE ASTIS ET AL., 1997b, DE ASTIS ET AL., 2000, FERRARI AND MANETTI, 1993, and VENTURA, 1994). ARGNANI AND SAVELLI (1999) suggest that the Aeolian Islands represent the latest part in the evolution of a steepening slab in the southern Tyrrhenian Basin.

Seismic activity is focussed in the SE part of the Tyrrhenian Basin and at the Calabrian Arc. Intermediate and deep seismic events along a defined zone indicate a narrow Wadati-Benioff zone in NNW-SSE direction with a maximum expected depth of nearly 500 km and an inclination of 50° to 60° (BARBERI ET AL., 1973 and FERRARI AND MANETTI, 1993). Fault plane solutions of intermediate and deep shocks furthermore indicate a relative tension component of 30° ESE (BARBERI ET AL., 1973). The strongest evidence for a subduction of the African plate under Eurasia, especially under the Italian Peninsula, is the seismically defined NW-dipping Benioff zone in a complex state of stress (DE ASTIS ET AL., 1997b). More recent information about the deep structure and the tectonic setting of the Mediterranean Sea is summarized in ARGNANI AND SAVELLI (1999), FACCENNA ET AL. (2001), FERRARI AND MANETTI (1993), GVIRTZMAN AND NUR (2001), and TAMBURELLI ET AL. (2000) (see also figure 1.1). The tectonic movement of the subduction slap in the Central Mediterranean Sea has decreased from 1 - 2 cm/yr to a few mm/yr over the last 20 Ma years (FACCENNA ET AL., 2001). FACCENNA ET AL. (2001) and FERRARI AND MANETTI (1993) give an overview of the development of the Central Mediterranean Sea:

- 80-30 Ma: First signatures of subduction are flysch deposits and high pressure-low temperature metamorphic structures. In the Oligocene (about 32 Ma) first calc-alkaline volcanic activity can be observed in the Sardinia-Provençal region. Extension can be identified at the back of the accreting Apennine edge. 350 km of oceanic lithosphere were subducted in 50 Ma.
- 30-16 Ma: Formation of the first extensional basin, lithospheric rifting and thinning of the Liguro-Provençal Basin. New oceanic crust was formed in the centre of the basin and the Corsica-Sardinia-Calabria block rotated counter-clockwise by 25-30°.
- 16-10 Ma: At the end of the rotation of the Sardinia-Corsica block drifting and spreading of the Liguro-Provençal ended, while subduction of the African plate continued.
- 10-recent: A new phase of extension started, where lithospheric rifting separated the Calabria block and opening of the Southern Tyrrhenian Basin began. During this period local spreading centres with oceanic crust developed (Marcela Basin 2-3 Ma and Vavilov Basin 4-5 Ma).
- recent: Two regions of thinned lithospheric crust, locally with oceanic crust, can be observed. Different geophysical methods describe the often complex structures well (e.g. the slab dips to the NW with 70° to a depth of about 400 km and then bottoms off to depths of about 600 km).

Over the intervening years the subduction slab steepens (FACCENNA ET AL., 2001). This steepening can also be assumed because of the rapid increase in K content of some lavas, restricted for a defined area (BARBERI ET AL., 1974).

The Tyrrhenian Sea belongs to the younger Mediterranean Basins. It is triangular in shape and can be divided into two different parts, shallow in the north and deeper in the south. The basin is bounded by different continental margins of varying nature: the Corsica and Sardinia margin in the west, the Sicilian margin in the south and the Italian peninsular and Calabrian Arc in the east (FERRARI AND MANETTI, 1993). The southern part of the Tyrrhenian Sea is an abyssal plain that can be subdivided into two smaller basins, Vavilov and Marsili, which are characterised by a very thin crust and a similar depth (ARGNANI AND SAVELLI, 1999, and FERRARI AND MANETTI, 1993). The two basins are separated by a fragment of the Campanian Margin as a ridge of thicker crust, and by a volcanic seamount (FERRARI AND MANETTI, 1993). A thin lithosphere of oceanic type is assumed under the central and eastern part of the Tyrrhenian Basin, based on a strong positive Bouguer anomaly, an obvious contrast of the magnetic susceptibility, a relatively high heat flow, and the results of a deep seismic survey (NICOLICH, 1989). These data confirm the presence of a shallow Moho-boundary at about 20 km depth (DE ASTIS ET AL., 2000, FERRARI AND MANETTI, 1993, and PRIVITERA, 1997). Since the late Miocene the Tyrrhenian area evolved from an orogenic belt to a subsiding basin with a depth of 4000 m.

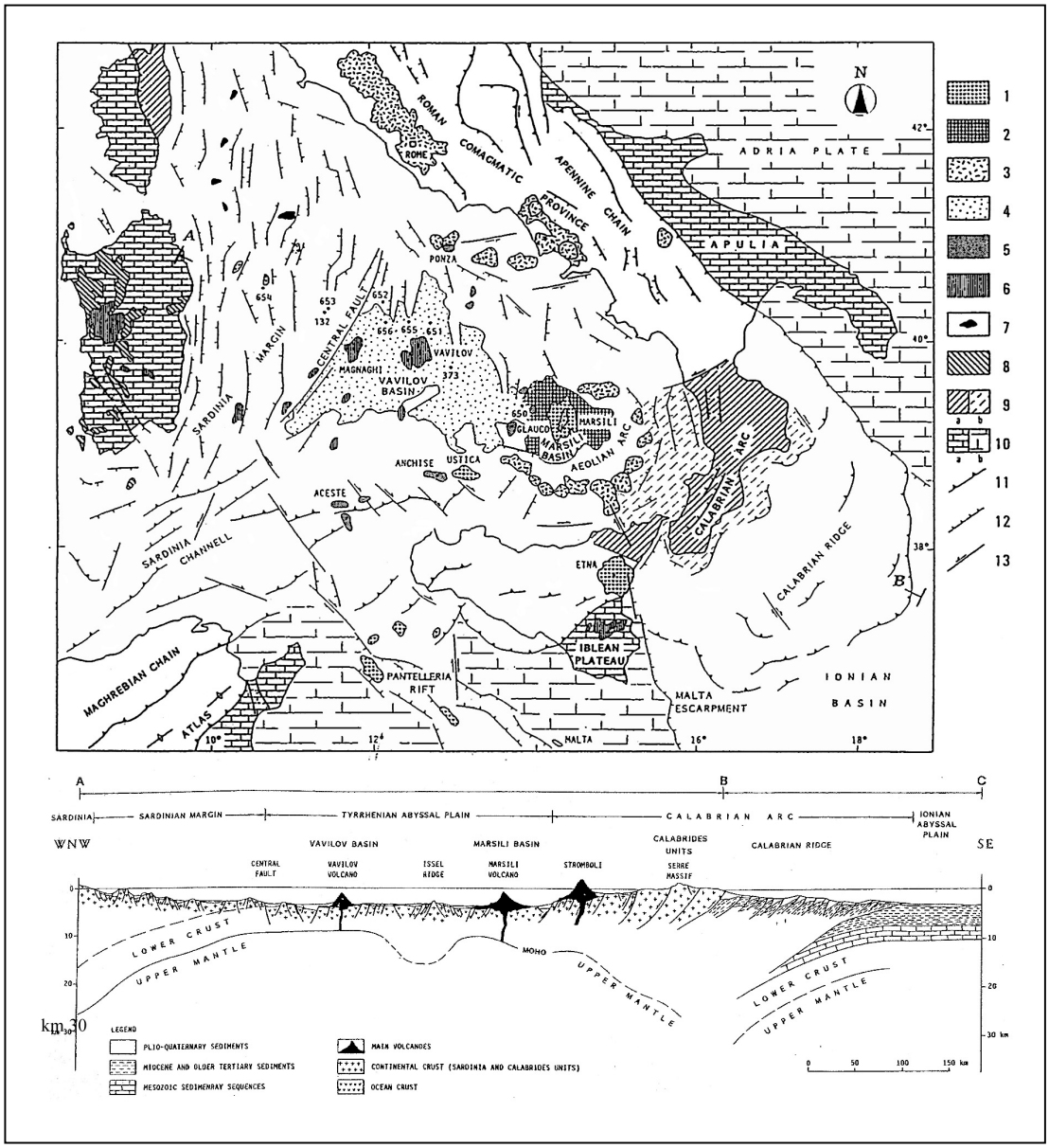

Figure 1.1: Tectonics and volcanism of the Tyrrhenian Sea modified after FERRARI AND MANETTI (1993). **a)** geodynamics and volcanism: 1: extensional-related volcanism in the Pleistocene, 2: Oceanic crust, Pleistocene, 3: subduction-related volcanism, Pleistocene, 4: oceanic crust, Pliocene, 5:subduction related volcanism, Pliocene, 6: extension related volcanism, Pliocene, 7: plutonic bodies, Late Miocene, 8: subduction – related volcanism, Oligocene to Early Miocene, 9: calabrides unit (a = emerged, b = submerged), 10 hinterland and foreland areas (a = emerged, b = submerged), 11: thrust, 12: extensional fault, 13: strike-slip fault. **b)** cross-section through the Tyrrhenian Sea

Two main volcanic types can be identified in the southern Tyrrhenian Sea: a) calc-alkaline volcanism of the Aeolian Islands and andesitic suites with differing potassium amount, related to a Benioff zone, b) volcanism with a basaltic affinity related to extensional tectonics (BARBERI ET AL., 1973) at Etna, Ustica and some seamounts of the abyssal plain, Pantelleria, Linosa and near the eastern side of Sardinia. The Aeolian Islands including the seamounts show a structure similar to the Western Pacific island arcs, whereas the Calabrian Arc can be described as the corresponding outer metamorphic belt (BARBERI ET AL., 1973 and BARBERI ET AL., 1974). In the Tyrrhenian Basin subduction-related volcanism migrated from W to E

between the Oligocene and Pleistocene (FERRARI AND MANETTI, 1993). These authors think that in the Oligocene to Miocene the volcanism was related to the subduction of oceanic crust because of the lack of shoshonite and high-K varieties of magmatic rocks. In the Pliocene different calc-alkaline centres, which form a volcanic arc, for example Glauco and Anchise, can be observed. In view of the geochemistry and the age of the volcanism it can be assumed that this volcanism is related to the opening of the Vavilov Basin and has occurred below sea-level because of the lack of tephra layers in cored Pliocene samples. The Roman Comagmatic Province and the Aeolian Arc show different geochemical and isotopic signatures so it can be supposed that the mantle source has been contaminated by acidic liquids generated by partial melting of the crustal material. The tholeiitic volcanics represent a extension related volcanism.

1.2.2. Volcanism on the Aeolian Islands

Like some circum-Pacific island arcs the Aeolian Islands are in an advanced stage of evolution. In comparison with other fossil island arcs, this stage can be called senile because of the shoshonitic nature of the recent products. The calc-alkaline, high-K-calc-alkaline, shoshonitic and potassic series found on the Aeolian Islands led most authors to suppose a subduction-related origin of the arc (ARGNANI AND SAVELLI, 1999, BARBERI ET AL., 1973, DE ASTIS ET AL., 1997b, DE ASTIS ET AL., 2000, ELLAM ET AL., 1988, FRANCALANCI ET AL., 1993, and VENTURA ET AL., 1999). The calc-alkaline type of volcanism observed at the Aeolian Islands is related to the subduction of oceanic crust under island arcs or continental margins. The high compositional variability of the magma from the Aeolian Arc can be explained as a combined effect of a heterogeneous and metasomatised mantle and a low-pressure magmatic evolution (DE ASTIS ET AL., 2000). Arc tholeiites have only be found on seamounts (DE ASTIS ET AL., 2000). The outcropping products of the islands show ages from more or less 430.000 years until present (VENTURA, 1994). The Aeolian Arc shows the youngest volcanism in the Tyrrhenian Sea Basin, starting in the Pleistocene and continuing until now.

Two main stages of volcanic activity can be discriminated: the first stage, in the Early and Middle Quaternary, formed Panarea, Alicudi, Filicudi and parts of Salina and Lipari; the second stage, in the Upper Pleistocene, completed the island of Salina, most parts of Lipari were build up, and during this time Stromboli and Vulcano rose above sea-level. During historic times eruptions are documented from Lipari, Vulcano and Stromboli (BARBERI ET AL., 1974). A reconstruction of the build up of the Aeolian Islands is made by correlating marine terraces with corresponding levels in continental Italy and radiocarbon dating (KELLER, 1967 and BARBERI ET AL., 1974).

Different authors disagree in their opinion to subdivide the Aeolian Islands into various evolutionary and magmatic stages, some like KELLER (1967) subdivides a K-rich alkaline suite (Vulcano and Stromboli) and a calc-alkaline suite (Salina, Filicudi, Alicudi, Panarea, and Lipari), whereas other authors like BARBERI ET AL. (1973), BARBERI ET AL. (1974), and

KELLER (1974) describe four distinct series, which are originated in one island arc (KELLER, 1980):

calc-alkaline suite:	Salina, Filicudi, Panarea, Alicudi, Lipari, Stromboli
high-K calc-alkaline suite:	Lipari, Stromboli
shoshonitic suite:	Vulcano, Stromboli
leucite-tephritic suite:	

A discrimination based on the composition of volcanic rocks is proposed by e.g. BARBERI ET AL. (1973) and BARBERI ET AL. (1974), who define two volcanic stages of activity. In the first stage a typical calc-alkaline series ranging from high-Al basalts to dacites can be observed. At Lipari high-K andesites emerged at the beginning of the second activity cycle, whereas at Salina a typical calc-alkaline volcanism occurred. For Vulcano, Vulcanello and Stromboli an increase of K-contents can be recognised. In addition, a shoshonitic suite appears on the Aeolian Islands that it ranges from trachy-basalts and shoshonitic basalts to latites and trachytes and in a few cases to rhyolites. The latter are a final member of the magmatic evolution. At Vulcanello a shoshonitic suite with a high-K tendency can also be observed. These volcanics showing geochemical variations from leucite-tephrite to trachyte, formed after caldera collapse. Their isotopic signature in combination with petrological data points to an origin of shallow fragmentation of shoshonitic basalts (BARBERI ET AL., 1974). The western part of the Aeolian Arc with Alicudi, Filicudi and Salina as well as Panarea and the lowest exposed deposits of Lipari and Stromboli have a calc-alkaline composition. Another part with parts of Panarea, Lipari, Stromboli, and Vulcano is dominated by shoshonitic rocks. Only Stromboli and Vulcano also have some leucite-bearing potassic rocks. The most primitive rocks crop out at the western end of the arc: Alicudi (DE ASTIS ET AL., 2000). These basalts to andesites have an age of 90000 to 30000 years. Whereas Stromboli shows the widest range of rock composition, here series from mafic and intermediate calc-alkaline rocks can be observed as well as shoshonitic and leucite-bearing potassic rocks. Also on Vulcano a wide range can be observed, here the composition ranges from high K-calc-alkaline to potassic. The subaerial volcanism on Vulcano migrates from S-SE to N-NW (DE ASTIS ET AL., 2000). BARBERI ET AL. (1974) and DE ROSA AND SHERIDAN (1983) interpreted the rapid change from calc-alkaline to high-K products during the last million years as an indicator for rapid sinking of the subducted slab beneath the islands.

The geochemistry of the Aeolian volcanics can be described as follows: subduction-related calc-alkaline products normally show a high aluminium basalt to rhyodacite sequence, whereas often a dominance of latite and andesite can be observed. Very primitive samples normally are porphyric rocks which show very low silica (48 to 52 wt.%) and an Al_2O_3 content ranging from 16 to 19 wt.%. The common phenocrysts are two types of pyroxene and calcic plagioclase. On Lipari and Vulcano unusual felsic rocks, often rhyolites, can be observed. Vulcanello has occurrences of potassic undersaturated rocks. A plot of water-free

K_2O versus SiO_2 shows the relationship of K_2O content to the depth of the inclined seismic zone below the volcano (BARBERI ET AL., 1973, DICKINSON, 1970, and HATHERTON AND DICKINDON, 1969). These diagrams indicate that Salina should be the nearest island to the trench. For the younger products of Vulcano and Lipari a depth of 250 to 300 km can be assumed, in agreement with the geophysical data (BARBERI ET AL., 1973).
The magmas of the Aeolian Islands originated probably in the Upper Mantle where partial melting of mantle peridotite under hydrous conditions produced an andesitic magma. The descending plate provided the water required for partial melting in the overlying mantle. U and Th amounts and the several isotopic ratios exclude partial melting of oceanic floor basalts as a source of the magmas. More facts about the origin of the magma can be found in ARGNANI AND SAVELLI (1999), BARBERI ET AL. (1973), BARBERI ET AL. (1974), DE ASTIS ET AL. (1997b), PRIVITERA (1997), SANTO (2000), and SBRANA (1997).

Gravimetric surveys on the Aeolian Islands show a Bouguer low for Salina, Vulcano and Lipari, which is very impressive for the active area of Vulcano, Vulcanello and the youngest part of Lipari, where an intensity of about 15 mgal can be observed (BARBERI ET AL., 1973 and BARBERI ET AL., 1974). In combination with seismic data these observations indicate a shallow magma chamber in this area.
Well logging and geophysical surveys indicate continental crust under the central and eastern parts of the arc, whereas oceanic crust of the Tyrrhenian Sea can be observed under the western part of the area. Seismic surveys locate a shallow Moho (less than 20 km) beneath Vulcano (DE ASTIS ET AL., 2000). The tectonic lineaments of the Aeolian Arc are dominated by NW-SE, NE-SW and E-W directions. The NW-SE lineament is the dominant active crustal element with extensional movements, shown by numerous earthquakes in this region. Vulcano, Lipari, and Salina are situated on the same tectonic line. It is also known from NE Sicily where it continues to the Tindari-Letojanni-fault, which is a dextral strike-slip fault (DE ASTIS ET AL., 2000 and PRIVITERA, 1997). It can be assumed that this tectonic element controls magma evolution, even though the other recognised tectonic directions are important for different parts of the evolution of Vulcano. For example, the NE-SW orientation plays an important role for the evolution of the northern part of Vulcano (PRIVITERA, 1997). A dominating NW-SE orientation is interpreted by some authors as a typical pull-apart situation (PRIVITERA, 1997). Geothermal investigations at Vulcano detect a geothermal discontinuity, near La Fossa cone, which can be interpreted as an intrusion of monzonite-diorite at a depth of 1100 to 1360 m below the sea-level (PRIVITERA, 1997). Although much is known about the Aeolian Islands from geophysical and telemetric investigations, the knowledge of the crust and the proportions at greater depth remains very poor (PRIVITERA, 1997).

Lipari is the largest island of the Aeolian Arc. The activity, which build up the island above sea-level, started nearly 223,000 years before present (DELLINO AND LA VOLPE, 1995). Lipari has four distinctive volcanic periods, which can be discriminated by geochemical,

sedimentological and geophysical methods, e.g. gamma-ray surveys (CHIOZZI ET AL., 1998 and DE ROSA AND SHERIDAN, 1983). Two early calc-alkaline to andesitic flows and andesitic composite volcanoes can be distinguished from two later high-K alkalic more rhyolitic flows and related pyroclastic deposits. The latter periods also comprise the so called Liparites (DE ROSA AND SHERIDAN, 1983). The first periods of activity build up the main part of the island and are dominated by effusive and strombolian activity of mafic and intermediate material, these eruptions occurred in the period from 223,000 to 43,000 years before present. The second great period of activity was dominated by rhyolitic material, which often erupted explosive with a high hydromagmatic touch, but also different domes extruded. For the last 10,000 years before present especially the northern part of Lipari shows volcanism and forms some volcanic areas like Canneto Dentro, Gabellotto-Fiume Bianco, Forgia Vecchia and Monte Pilato-Rocche Rosse.

Salina lies in a line with Lipari and Vulcano and can also be called the turning-point in the y-shaped Aeolian Arc. It is composed of five main eruptive centres. Two main volcanic cycles of activity define the volcanic history. The first cycle with Rivi-Capo and Fossa delle Felci (430,000 to 100,000 years before present) is dominated by products with high-alumina basaltic to dacitic composition, and the second (younger) cycle with Fossa delle Felice, Pollara and Porri (100,000 to 13,000 years before present) is characterised by products composed of basaltic andesites and rhyolites (DE ROSA ET AL., 1996).

Stromboli is the northernmost, youngest active volcano of the Aeolian Islands, the characteristic volcanic cone, rise up to nearly 1000 m NN from a depth of about 2000 m below sea-level. Two main eruption cycles can be identified, the oldest is observed at the eastern side of the island, the youngest at the western side, some authors distinguish up to four cycles (NAPPI ET AL., 1999).

1.2.3. Volcanic Evolution of Vulcano Island

Vulcano is the southernmost island of the Aeolian Arc. It has a total surface area of about 22 km^2 and its base lies at a depth of circa 1 km below sea-level (DE ASTIS ET AL., 1997b and GABBIANELLI ET AL., 1991). The base of the volcanic complex has a diameter of about 15 km (GABBIANELLI ET AL., 1991 and VENTURA, 1994). At the surface only volcanic rocks and reworked volcanic material are exposed. The subaerial volcanic activity of Vulcano ranged from 120,000 years before present to the present day. The volcanic and magmatic evolution of Vulcano is coupled with the subduction processes of the Aeolian Arc (SBRANA, 1997). The magmatic evolution of Vulcano is related to the activity of a shear zone, which supports the ascent of material from a high-temperature region and could also be the reason for a higher heat flow through the crust (DE ASTIS ET AL., 1997b). The dominated tectonic orientation on Vulcano is normally NW-SE and NNW-SSE, which is related to the regional tectonic structure of the dextral strike-slip fault Tindari-Letojanni (BARBERI ET AL., 1994, SBRANA, 1997, and VENTURA, 1994). It is parallel to the volcanic axis of Salina-Lipari-Vulcano with

diverse submarine centres. It is a graben-like structure (BARBERI ET AL., 1994, GABBIANELLI ET AL., 1991, and VENTURA, 1994). On the island this tectonic direction is expressed as right-lateral strike-slip faults. Minor directions are N-S and NE-SW. They are related to a local stress field and are expressed as normal faults on the island (VENTURA, 1994). Dislocation of Plio-Pleistocene sediments by these faults is in the order of 6 – 7 km (VENTURA, 1994). A shift of the volcanic activity from SE to NW can be recognised by using different volcanologic and geochronologic methods. The migration of the vents of La Fossa and Vulcanello seems to correspond to the NE-SW trending fractures which are important for the ascent of magma in the inner part of the island. The eruptive centres on the western side are in general related to the N-S trending structures (VENTURA, 1994).

The most important volcanotectonic structures of Vulcano are the Piano Caldera and the La Fossa Caldera. The floor of the Piano Caldera has a mean altitude of 350 m above sea-level and the caldera rims have a maximal altitude of 500 m. In the north-western part of the caldera NE-SW trending sub-vertical scarps can be observed. They dip towards NW and have a maximum height of about 100 m. The maximum thickness of the caldera fill of the Piano Caldera is 200 m. The Fossa Caldera forms the central part of the island. The caldera floor is inclined with the altitude of the base ranging between 7 m (northern part) and 172 m (southern part) above sea-level. The rims at the E- and W- side are orientated N-S, this can be characterised as sub-vertical rectilinging scarps with a maximum height of 40 m (VENTURA, 1994). The La Fossa Caldera and the southern part of Lipari are located in a structural depression or graben, which is defined by N-S and NNW-SSE trending faults (DE ASTIS ET AL., 1997b).

The subsurface stratigraphy and lithology of Vulcano has been investigated by different deep drillings (GIONCADA AND SBRANA, 1991). Perceptions are got by analysing the cuttings because cored wells do not exist, hence textural propositions are rare. Vulcano is a composite volcanic edifice with following evolutionary stages (DE ASTIS ET AL., 1997b, DE ASTIS ET AL., 2000, GIONCADA AND SBRANA, 1991, SBRANA, 1997, and VENTURA, 1994) (see also figure 1.2):

1. The oldest exposed part of Vulcano is named **Vulcano Primordiale** (also called South Vulcano with strato and tuff cones like Monte Aria and Monte Luccia). This part showed activity between 120,000 to 100,000 years before present. Products of this period are exposed at the southern, eastern, and western margins of the island. This period is documented by large stratocones with trachybalsaltic and trachyandesitic lava flows and some intercalations of fall and flow deposits. In general the composition of the material ranges from high–K-calc-alkaline to shoshonitic. In the W of the island the Vulcano Primordiale covers eastward dipping lavas that are assumed to belong to an even older volcanic edifice.
2. The **Piano Caldera** formed between 99,000 to 55,000 years before present by collapse of the Vulcano Primordiale. The caldera, in the S of the island, is a sub-circular depression with a diameter of nearly 2.5 km. Various lava flows and pyroclastic-layers of this period

are preserved. In a the first stage from 99,000 to 78,000 years before present leucitic-tephritic lava was erupted from ring faults. The lava has a maximum thickness of 150 – 170 m. During a second stage intracalderic vents produced trachybasaltic lavas (Timpone del Corvo or Passo del Piano), pyroclastics as well as scoria (e.g. Sommata and Quadrata). Vents north of the caldera produced pyroclastic trachybasalts that were deposited within the caldera.

3. The formation of the Piano Caldera was followed by the collapse of the **Polyphase Caldera of La Fossa** between 50,000 to 24,000 years before present, with associated lava flows and tuffs. Deep drillings give some information about the differential collapse of the caldera (GIONCADA ET AL., 1997).
4. Following, the **Lentia Complex** was built up between 28,000 and 13,000 years before present. Products of this complex, which can be seen in the NW part of the island, e.g. Mt. Lentia. Most of the preserved material of this period is composed of different lava flows and rhyolitic domes. These products emerged along N-S trending fractures and overlie a sequence of effusive and explosive products of latitic composition, the so called Maestro Minico unit. Sometimes also trachytic juvenile clasts can be found in the latter unit. The complex is cut by the western ring faults of the polyphase caldera La Fossa di Vulcano.
5. During the final activity of the Lentia Complex (15,000-8,000 years before present), **intermediate products** like the Tufi di Grotte dei Rossi (TGR) at the Piano Caldera, and the trachytic lava post Lentia were formed. They often show shoshonitic to basaltic and leucit-bearing tephritic composition (KELLER, 1980 and VENTURA, 1994). The TGR unit underwent an inverse evolution, whereby products tend to become more mafic and alkaline in stratigraphic higher eruption cycles. This was interpreted by DE ASTIS ET AL. (1997a) as a mixing process when new magma enters the shallow reservoir, which can also trigger the eruption. The lower TGR unit (TGR inferiore) represents the pyroclastic sequence with the maximal eruption volume formed by a single eruption on Vulcano. Mount Saraceno, who closes this stage of activity, was dominated by strombolian eruption types.
6. The **Cone of La Fossa di Vulcano** was built up during the last 6000 years. It is the central edifice in the northern part of the island, most of which consists of pyroclastic material. In general the pyroclastic deposits and lava flows have an alkali-rich trachytic to rhyolitic composition. Five successions can be distinguished: Punte Nere, Tufi Varicolori, Palizzi, Commenda, and Cratere Attuale, they will be described in chapter 2.
7. The northern part of Vulcano, called **Vulcanello**, was built up in 3 main stages between 183 B.C and 1550 AD. The isthmus of Vulcanello is very young, created during the last eruption and often sized not more than 0.5 to 1 m above the sea-level. At this location the highest intensity of fumarole activity outside of the Gran Cratere can be observed. In contrast to La Fossa cone, Vulcanello is characterised by K-rich, slightly undersaturated, shoshonitic and leucite-bearing scoria and lavas. Sometimes a trachytic composition can be observed as well.

Radiometric data for Vulcano are given by DE ASTIS ET AL. (1997b) and DELITALA ET AL. (1997).

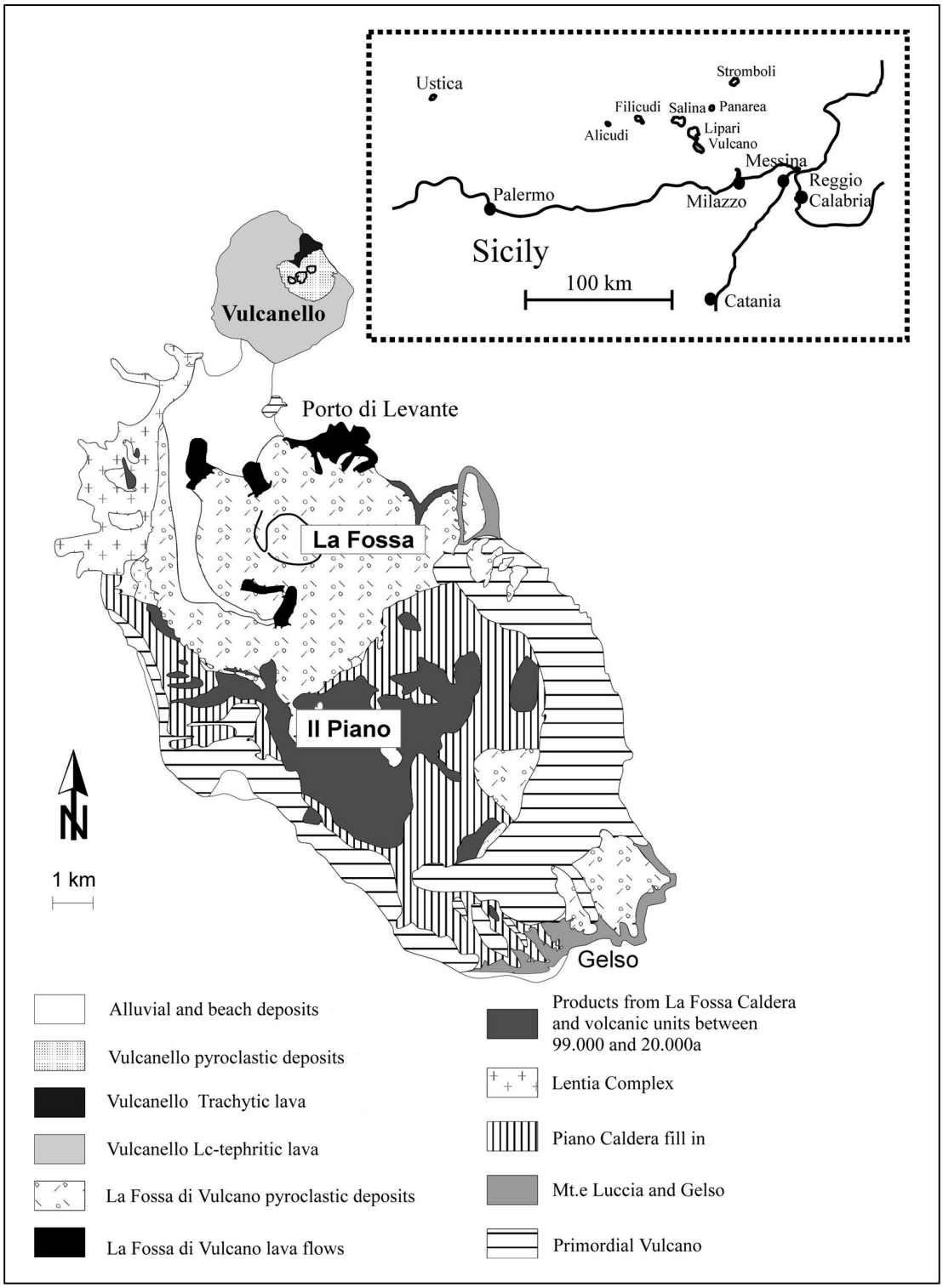

Figure 1.2 Geological map of Vulcano modified after DE ASTIS ET AL. (1997b) and SBRANA (1997)

1.2.4. Petrography and Geochemistry

Volcanic rocks exposed on Vulcano belong to high-K calc-alkaline, shoshonite, leucite tephrite or potassic rocks association (DE ASTIS ET AL., 1997b, DE ASTIS ET AL., 2000, ELLAM ET AL., 1988, and KELLER, 1980). Rocks show different degrees of differentiation from basalt to rhyolite. Mafic rocks are in general porphyric with phenocrysts of plagioclase, Ca-rich clinopyroxene, Fe-Ti-oxides and olivine. The latter can also be found as a relict with resorbed boundaries in rhyolitic suites. Some potassic rocks contain leucite or analcim formed by transformation of leucite (DE ASTIS ET AL., 1997b, DE ASTIS ET AL., 2000, and GIONCADA ET AL., 1997). Phenocryst content in lavas range from 5 to 60% of the total rock volume, whereas the scoria contains a smaller amount of phenocryst (5 to 25%). According to DE FINO ET AL. (1991) the lava flows and bombs of La Fossa di Vulcano, especially these of Palizzi, Commenda and Pietre Cotte, have a SiO_2 content of 58 to 72 wt.%, whereas the glassy matrix of rhyolite contains up to 75 wt.% SiO_2. In addition to their high K_2O content the volcanic rocks normally belong to a shoshonitic suite. In more evolved rock series phenocrysts of K-feldspar and biotite dominate. The groundmass is glassy or microcrystallline. Highly evolved products are limited to the younger deposits of Vulcano, where they form lava flows, pumice layers and some pyroclastic deposits. The texture of these deposits is equally porphyric, but they contain less phenocrysts (1 to 30 %). The mineral assemblage is dominated by plagioclase and salitic to augitic pyroxenes. Accessory minerals are K-feldspars and magnetite, whereas biotite and amphibole are rarely present. Accessory zircon can be found in very felsic rocks of La Fossa cone. Some of the felsic or intermediate rocks contain resorbed phenocrysts as the aforementioned olivine and xenolithes, which belong to less evolved magma sources (DE ASTIS ET AL., 2000).

DE ASTIS ET AL. (2000) distinguish between a young and an old suite of volcanic rocks on Vulcano. The older rocks on Vulcano with an age of 20,000 years and older usually have a high-K calc-alkaline and shoshonitic composition. The younger rocks are in general more enriched in K_2O and incompatible elements than the older products. High-K calc-alkaline, shoshonitic and potassic rocks were produced between 20,000 and 8,000 years before present, have a larger range in the SiO_2 content and a higher amount of incompatible elements. Volcanic products younger than 8,000 years are dominated by shoshonitic and leucite-bearing potassic rocks. Commonly these deposits are of intermediate or silicic composition. Sr isotopic ratios differ from 0.70412 – 0.70520 for the oldest products to 0.70448 – 0.70486 for the intermediate products. Some rhyolites of the youngest products have a Sr isotopic ratio up to 0.70494 – 0.70583 (DE ASTIS ET AL., 1997b). These geochemical data have important implications for the origin of the magma of La Fossa. It is improbable that all series derived from a single homogenous source by different stages of partial melting. DE ASTIS ET AL. (2000) suppose that there is a mixing of a mafic high-K calc-alkaline magma with an evolved rhyolitic melt, which is rich in incompatible elements. A two chamber feeding system for La Fossa di Vulcano was assumed by DE ASTIS ET AL. (1997b), DELLINO (1997), DELLINO AND LA VOLPE (1997), and SBRANA (1997). Some rock suites of La Fossa cone probably originated

by fractional crystallisation, whereas others can be explained as mixing products of intermediate and felsic end-member magmas (DE ASTIS ET AL., 1997b).
Origin and evolution of the magmas erupted at Vulcano is also published by GIONCADA ET AL. (1997), who show a TAS-diagram of samples from Vulcano, where it can be seen that especially the products of La Fossa plot primary in the latitic-trachytic to rhyolitic range. Detailed investigations about the petrology and geochemistry of the deposits of Vulcano are published for example by DE ASTIS ET AL. (1997b) and DE FINO ET AL. (1991).

Vulcano is the type locality for the term “vulcanian” eruption, based on the description of MERCALLI AND SILVESTRI (1890) and SILVESTRI ET AL. (1891) of the great eruption from La Fossa di Vulcano in 1888-1890.
The vulcanian-type eruption is a small to moderate eruption, whereby material is ejected to heights of up to 20 km. A single eruption has the duration of a few seconds to minutes. In general these eruptions with a duration of a few seconds to minutes, are characterised by violent explosions with a ballistic transport of material (e.g. blocks and bombs, bread-crust bombs) and different deposits like pyroclastic avalanches or pyroclastic flows. However, in some cases they can last as a nearly silent, dense cloud of ash for longer time. This eruption style is usually related to the activity of stratovolcanoes with andesitic basalt to dacitic juvenile components. Individual deposits are very thin and often eroded by wind and water on a short time scale. In general eruptions with vulcanian character are typified by higher ejection velocities and greater distances of the ejected material than other eruption types (CAS AND WRIGHT, 1988, FRANCIS, 1993, and MORRISSEY AND MASTIN, 2000). This eruption activity is also documented from a number of historic eruptions like Lascar, Fuego, Irazù, Augustine, Ngauruhoe, Sakurajima, and Galeras (CAS AND WRIGHT, 1988, FRANCIS, 1993, and MORRISSEY AND MASTIN, 2000).

1.3. Name and History

In ancient times Vulcano was called Thermessa (The Hot), with expansion of the cult of the god Hephaestus from Greece it was called Hiera (The Holy) (AMANN, 1999). In the roman mythology Vulcano is the home of the god Vulcan (Greek: Hephaistos), also called Mulciber, where he worked with his three assistants, the Cyclopes. Venus was his wife. He was the god of the blacksmith and a patriot of the cuckolds. In his forge he built the weapons, drinking vessels and golden shoes with magic attributes for other gods. As a son of Jupiter and Juno, Vulcan was crippled at birth, he was thrown from the Pantheon by his mother, who was ashamed by his deformity. The forge of Vulcan has been associated in many places with volcanic activity, including Vulcano and Mt. Etna. Because he is also the god of fire, usually the destructive form like forest fires or volcano eruptions, most of his temples were built outside of town. His attributes in iconography include the axe and tongs. In the classical myth the Aeolian Islands were thought to be the home of Aiolos/Äolus, Lord of the winds.

The first archeologically records on the Aeolian Islands date back to the 5th Millennium BC. The first recorded settlements on Vulcano are known from the 19th century. The populations on the Aeolian Islands fluctuated through time, mainly due to frequent invasions by pirates or conquerors.
The economic factors of Vulcano in former times were agriculture (on the Piano Plateau) and the extraction of sulphur as crystals and alum. The sulphur extraction boomed in roman times and in the 19th century, but was stopped by the last eruption in historical time 1888 – 1890 (Cratere Attuale) at La Fossa di Vulcano. Today the main sources of income are tourism and the business that developed to exploit the medical effects of thermal bathes and mud of Vulcano, which are also a tourist attraction (see figure 1.3).

Likewise the eruptions from Vulcanello were historical documented and holy fairy tales were handed down (AMANN, 1999 and KELLER, 1970). The most important tale was about S. Calogero, who lived as an eremite on Lipari and exorcised devils and demons from Lipari to Vulcano in the 6th century (eruption of the Monte Pilato {Lipari} and eruption of the Commenda succession on Vulcano). An extended list of the historic eruptions and mention of them in the literature can be found in FRAZZETTA ET AL. (1984).

Figure 1.3 Bath in the mud-pool of Vulcano

1.4. Previous Works

Several studies address the complex stratigraphy. Most of the proposed stratigraphic schemes are based on geochemical and sedimentological features (CAPACCIONI AND CONGILIO, 1995, CLOCCHIATTI ET AL., 1994, DE ASTIS ET AL., 1997a, DE ASTIS ET AL., 1997b, DE ASTIS ET AL., 1997c, DE FINO ET AL., 1991, DELITALA ET AL., 1997, DELLINO, 1997, DELLINO ET AL., 1990, DELLINO AND LA VOLPE, 1997, DELLINO AND LA VOLPE, 1998, FRAZZETTA ET AL., 1985, FRAZZETTA AND LA VOLPE, 1991, FRAZZETTA ET AL., 1983, GIONCADA AND SBRANA, 1991, KELLER, 1970, KELLER, 1980, SHERIDAN AND MALIN, 1983, ZANELLA ET AL., 1999, and ZANELLA AND LANZA, 1994). KELLER (1980) published the first comprehensive stratigraphy and a corresponding geological map. Until now geophysical methods have not been applied to the stratigraphy of La Fossa cone on a larger scale. Most of the previous geophysical studies addressed problems related to processes in the magma reservoir, the correlation between groundwater and gas, monitoring the volcano, the magnetic behaviour in past and present (palaeomagnetism), the differentiation of the eruptive phases, structural investigations, tectonic backgrounds, or environmental hazards associated with gas and radioactivity, e.g. ACHILLI ET AL. (1998), BADALAMENTI ET AL. (1991), BARBERI ET AL. (1994), BELLIA ET AL. (1996), BERRINO (1997), BERRINO (2000), BERRINO AND D´ERRICO (1993), BRAI ET AL. (1995), BRANCA ET AL. (1997), BUDETTA ET AL. (1991), BUDETTA AND DEL NEGRO (1995), BUDETTA ET AL. (1993), CAGNOLI AND TARLING (1998), CAPASSO ET AL. (1999), CAPASSO ET AL. (2000), CHEYNET ET AL. (2000), CHIODINI ET AL. (1992), CHIODINI ET AL. (1991), CHIOZZI ET AL. (1999), DEL NEGRO (1997), DEL NEGRO AND FERRUCCI (2000), DELITALA ET AL. (1997), DI MAIO ET AL. (1993), GRAZIANI ET AL. (1997), HARRIS AND MACIEJEWSKI (2000), HAUSER ET AL. (1996), LE CLOAREC ET AL. (1991), LEONARDI ET AL. (1999), MONTALTO (1996), NAPPI ET AL. (1976), NERI ET AL. (1991), NUCCIO (1999), PATELLA ET AL. (1997), RASÀ AND VILLARI (1991), VENTURA (1994), VENTURA ET AL. (1999), ZANELLA ET AL. (1999), and ZANELLA AND LANZA (1994). A classification of the different successions of La Fossa cone using geophysical methods was not done before. This geophysical methods can be a sophisticated tool, but it must be recognised that the La Fossa successions show a similar geochemical evolution and juvenile younger material cannot be discriminated from material of older eruptions.

Reports about hazard potential or hazard assessment on Vulcano island were made by BADALAMENTI ET AL. (1998), BARBERI ET AL. (1991), CHIODINI ET AL. (1991), CONIGLIO AND DOBRAN (1995), DELLINO AND LA VOLPE (1997), DELLINO AND LA VOLPE (1998), FRAZZETTA ET AL. (1984), FRAZZETTA AND LA VOLPE (1991), GRAZIANI ET AL. (1997), NERI ET AL. (1991), and SHERIDAN AND MALIN (1983).

Investigations to distinguish different parts of volcanic island or other stratigraphic problems with gamma-ray measurements were made by BELLIA ET AL. (1996), BRAI ET AL. (1995), CHIOZZI ET AL. (1999), CHIOZZI ET AL. (1998), CIVETTA AND GASPARINI (1973), ETTENSOHN

ET AL. (1979), HECKEMANNS AND KRÄMER (1989), KRASSAY (1999), MYERS AND BRISTOW (1989), PARKINSON (1996), and RUSSELL AND STEINHOFF (1961).

1.5. Objective of this Thesis

Understanding the specific volcano's behaviour in the past is important for modern hazard assessment. The classic approach works with a quantification of different pyroclastic deposits, noticing in particular erupted volumes and spatial distribution. Volcanoes formed by phreatomagmatic eruptions frequently have a very complex stratigraphy, including deposits of maar volcanoes and tuff cones. The edifice of a volcano dominated by phreatomagmatic eruptions can be built up by several hundreds of single eruption deposits, with facies changing over very short lateral distances. In general the classification of the deposits is made by "classic" geochemical and sedimentological investigations, additional geophysics methods shall help for a better classification. In this thesis the combination of geophysical tools with sedimentology and geochemistry is performed. It is searched for a combination of easy handling and fast working methods (γ-ray measurements in the field and grain sized depended magnetic susceptibility measured in the laboratory), which can be combined with sedimentological and geochemical methods to solve stratigraphical problems.

γ-ray-measurements provide information about the magma evolution and in many cases the data allow a distinction between discrete episodes of the eruption history. Combining granulometric analyses with sus measurements provides information on transport and alteration effects as well as about the evolution of the magma. Combined with a "classic" stratigraphic approach these methods have the potential to solve problems during quantitative assessment of complex phreatomagmatic volcanostratigraphy. The young, most probably still active tuff cone of La Fossa di Vulcano (Isola di Vulcano, S-Italy) represents an ideal test ground for these methods, because although much is known about the stratigraphy not all problems are solved and for a correlation of different successions standard outcrops are defined. Results of these standard values are the base of the data set which will be compared with not clear defined outcrops (often also outside of the caldera of La Fossa). Characterising not clearly identified parts is important to optimise the knowledge of deposit dispersion, characterisation of hazard zones (hazard maps) as well as evacuation plans for different eruption types. SHERIDAN AND MALIN (1983) working about hazards of surge eruptions on Vulcano, Lipari and Vesuvius, used a computer model for several surge eruptions. In this case a detailed and complete knowledge of the previous surge eruptions, their emplacement and their energy is very important.

La Fossa di Vulcano is the test area for the new combination of geophysical methods to characterise different pyroclastic deposits by their behaviour in γ-ray- and sus-measurements.

2.La Fossa Stratigraphy

2.1. Introduction

La Fossa cone is the active centre of Vulcano with a height of 391 m and nearly 2 km diameter at its base. Five successions can be distinguished: Punte Nere, Tufi Varicolori, Palizzi, Commenda and Cratere Attuale, that are separated by erosional discontinuities. They are mainly built up by pyroclastic deposits, different lava flows and fall-out deposits.

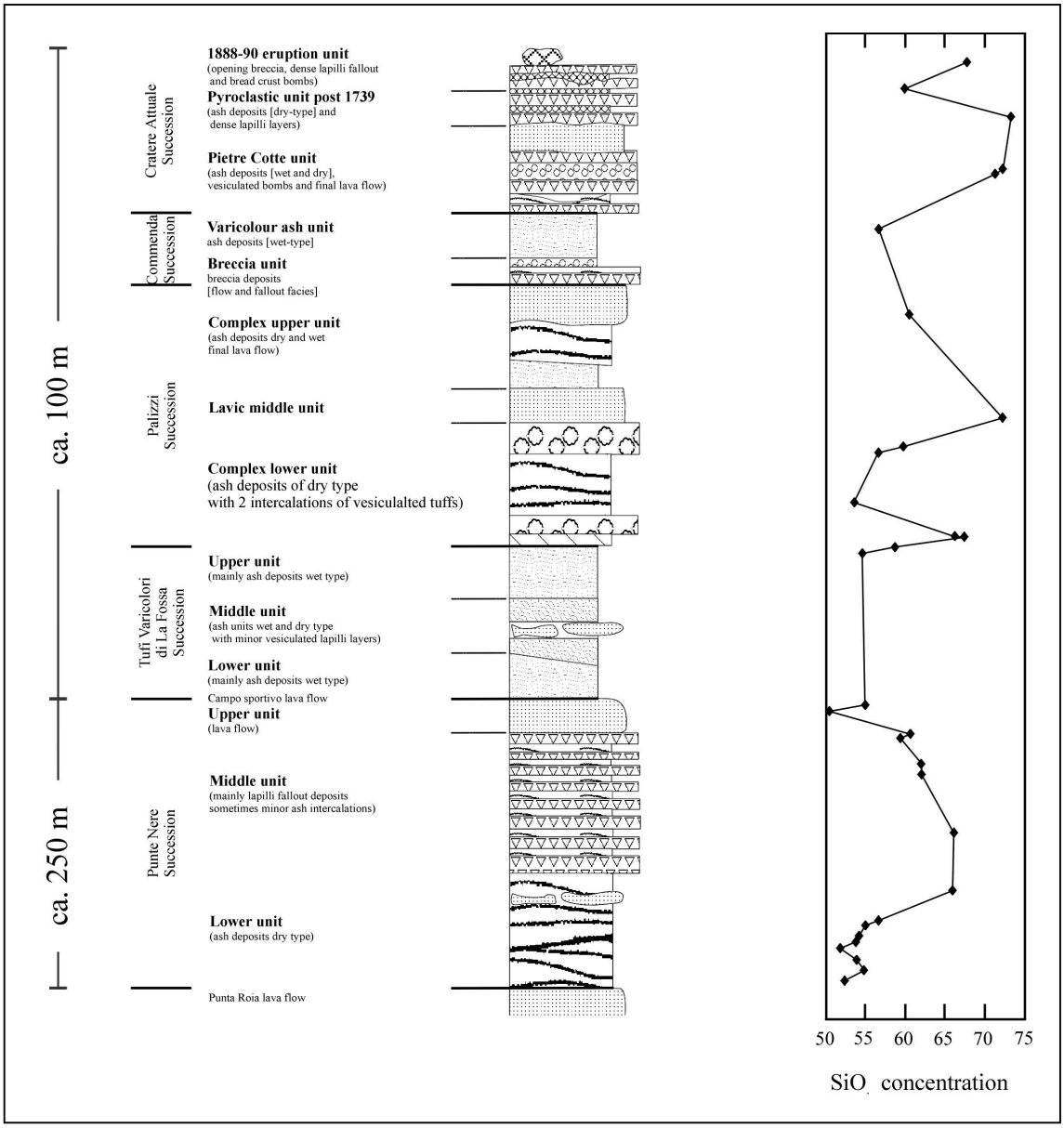

Figure 2.1: Successions of the young La Fossa cone, modern stratigraphy (from Dellino (1997)).

Different lava flows associated with La Fossa cone range in composition between trachyte and rhyolite. Normally they emerge from the crater rim, but only the trachytic lava flows have reached the base of the cone. The rhyolitic lavas like Pietre Cotte and Commenda, as well as

the breadcrust bombs with the same chemical composition (Cratere Attuale), show important internal structures which can be described as relicts of magma mixing (FRAZZETTA ET AL., 1983). The split into five successions is the most modern form of stratigraphy for La Fossa cone (BÜTTNER ET AL., 1999, CAPACCIONI AND CONGILIO, 1995, CONIGLIO AND DOBRAN, 1995, DE ASTIS ET AL., 1997a, DE ASTIS ET AL., 1997b, DE ASTIS ET AL., 1997c, DE FINO ET AL., 1991, DELLINO, 1997, DELLINO, 2000, DELLINO AND LA VOLPE, 1997, DELLINO AND LA VOLPE, 1998, DELLINO AND LA VOLPE, 2000, TONARINI ET AL., 1997, VOLTAGGIO ET AL., 1997, and ZANELLA ET AL., 1999).

Older literature describes different tuff deposits, distinguished by colour, or uses a classification related to the modern stratigraphy but without defining the Tufi Varicolori immediately (e.g. DELLINO ET AL., 1990, FRAZZETTA ET AL., 1985; FRAZZETTA ET AL., 1984, FRAZZETTA AND LA VOLPE, 1991, FRAZZETTA ET AL., 1983, KELLER, 1970, KELLER, 1980, and PICHLER, 1990). The "modern" successions of La Fossa cone can be described as follows (see also figure 2.1).

2.2. Punte Nere

Punte Nere (Black Points) is the oldest succession of La Fossa cone with a thickness of about 250 m. Deposition started before 6,000 years. It makes up the largest part of the La Fossa edifice and can be subdivided into 3 units which can be distinguished by their lithological characteristics and their spatial distinction. Some authors like KELLER (1970) and KELLER (1980) are convinced that Punte Nere starts with a tephritic lava flow, the so-called lava of Pta. Roia in the Vallone della Roia.

The lowermost unit contains mainly latitic to shoshonitic coarse and fine ash deposits of dry-surges. These dry-surges generally have a hydromagmatic origin. Their SiO_2 content ranges between 55.3 to 58.4 wt% (SBRANA, 1997). They have a relatively wide dispersion and can be found inside and outside of the caldera. Deposits from this unit have built up a cone with an angle of 15° and approximately 150 m height. Scoria marker horizons in the upper part have been dated at about 5300 B.C. At the top of this unit sandwave deposits and massive beds may occur. This unit is < 60 m thick (FRAZZETTA AND LA VOLPE, 1991 and FRAZZETTA ET AL., 1983).

The middle unit consists mostly of lapilli fallout deposits which are intercalated by minor ash layers. The geochemical composition of these deposits varies between latite and trachyte with a SiO_2 content of 59 to 66 wt% (SBRANA, 1997). These deposits built up the cone with an angle of 30° and a height of nearly 250 m (DELLINO, 1997 and DELLINO AND LA VOLPE, 1997). The last unit is a lava flow.

Pele´s hair can be found in a couple of surge deposits of Punte Nere. Punte Nere rocks have colours between grey and a dark grey-brown.

2.3. Tufi Varicolori

This succession has been defined only recently, whereas older publications (for example see chapter 2.1) describe only four deposits of La Fossa cone. Sometimes the Tufi Varicolori are mentioned as an undefined unit at the top of Punte Nere containing varicoloured ash layers. The name Tufi Varicolori means varicoloured tuffs, and defined from different colours of the wet-surge deposits which are the dominant deposits of the succession. Tufi Varicolori is a thin succession subdivided into three units separated by erosive surfaces (DELLINO, 1997). All units are composed of ash layers which are discriminated by composition and genesis of the units. They are very similar in texture and composition. They are relatively homogenous and do not show great lithological differences. The first and the last unit show similar composition and behaviour, both are built up by wet-surge deposits and have a latitic to shoshonitic composition. The second unit is dominated by wet-surge deposits intercalated with a few dry-surge deposits, vesiculated lapilli layers, dominant shoshonitic scoria beds, and some bombs. Most of the Tufi Varicolori units are extremely solid and much coarser than the otherwise similar Commenda succession. In general they are much thicker than the Commenda deposits and so far are only known within the former caldera. In the southern part of the cone their thickness can reach up to 20 m. Colours from pale yellow to pale green or soft pink, but also a light greenish grey and some brown layers can be observed. Pele's hair occurs in the second and rarely in the third unit (DELLINO, pers. comm. 2000). A scoria bed in the second unit was dated at 2,390 years B.C..

Some authors attribute the Campo Sportivo lava to the Tufi Varicolori, whereas other place it between Punte Nere and Tufi Varicolori. SBRANA (1997) describes its composition as shoshonitic to latitic with an SiO_2 concentration of 53.4 to 61 wt.%.

2.4. Palizzi

Palizzi is a complex succession with two different pumice layers that are good marker horizons, and a lava flow on top of the last pumice layer. It can be subdivided into three units bounded by erosional surfaces as well as lithological features (DELLINO, 1997). The base of the succession is erosive. The succession starts with a thin stratified unit of latitic dry-surge deposits composed of medium - middle and coarse-grained ashes. Fragments of Pele´s hair and two pumice layers can be found in this unit. Some descriptions of Palizzi notice only one Palizzi pumice marker (CONIGLIO AND DOBRAN, 1995 and FRAZZETTA ET AL., 1984). The first is a rhyolitic lapilli-bomb pumice. The maximum observed thickness of this pumice is about 2.1 m (FRAZZETTA ET AL., 1983). The pumice is graded, grain size ranges from a few centimetres to 15 cm. Some blocks have a diameter up to 30 cm. Lapilli-sized angular obsidian clasts can be observed. Phenocrysts are sanidine, plagioclase, clinopyroxene and some dark mica. This small fall out deposit is covered by a meter-thick surge unit, which is covered by a second layer of fall out products with trachytic composition. The thickness of the deposits varies and reworking – especially of the 1. Palizzi Pumice – is common,

sometimes affecting the entire first part of the unit. This complex unit has a wide distribution from the northern part of Vulcanello to the southern rim of the caldera. Sometimes the deposits can also be found outside of the caldera (Lentia or Piano di Alighieri). The normal thickness of this unit is about 10 m, whereas at the flanks or at the roof of the cone the thickness can be much smaller. Near the vent, this pumice layer is followed by a rhyolitic lava, which is known as the Palizzi-Lava (the so-called lavic middle unit after DELLINO (1997)). The lava is not very thick and can only be seen near the bocca.

The complex last unit consists of different dry-surge deposits which are sporadically intercalated with some wet-surge deposits containing accretionary lapilli. The general grain size varies from fine ash to fine lapilli. A large trachytic lava flow, dated at 1,500 ± 200 years, terminates the succession (DELITALA ET AL., 1997). This lava extends from the vent to the base of the cone. Most of the layers have a more or less dark grey colour which can be similar to the colours of Punte Nere. After GIONCADA ET AL. (1997), the composition of the Palizzi products varies between latite, K-trachyte, and rhyolite. These authors also assume a slightly higher degree of crustal contamination. SBRANA (1997) pointed out that the geochemical composition is very complex; the variability of SiO_2 and Rb is relatively high (SiO_2 ranges between 55 and 73 wt.% whereas the Rb amounts range between 139 and 303 ppm). It is also important to note that in this succession the first significant effusive products of rhoylite – as a lava flow – can be observed.

The sequence has been recently described by DELLINO AND LA VOLPE (2000) (see also figure 2.2), an earlier description of the Palizzi deposits can be found in DE ROSA ET AL. (1992), DELLINO (1997) and DELLINO AND LA VOLPE (1997).

The surges of Palizzi are well sorted, very voluminous and widespread. Nowadays only they can be detected surely outside of the caldera. They are determined by component analysis so far (DELLINO AND LA VOLPE, 2000). Mainly the components of the surges are very fine and coarse components are not found very often.

The dry-surge deposits, especially of the first unit often show high amounts of Pele's hair, which sometimes are nested or enriched at the top of the deposit. DE ROSA ET AL. (1992) and DELLINO AND LA VOLPE (2000) describe especially the dry-surge deposits of Palizzi as follows: In general they are built up by laminated layers. Single layers and laminae are separated by erosional discontinuities. Single surge deposits are often separated by sharp boundaries and can be distinguished by small beds of fine ash found at the top of the surge deposits. After DELLINO AND LA VOLPE (2000) and DELLINO (pers. comm. 1999), this fine ash represents slow settling at the end of the surge-stage. These fine ash beds can be observed very well in outcrop K at the Lentia Complex. They are generally not preserved proximally due to erosion lay the subsequent event. If the layers of fine ash are preserved they show a thickness of < 1 – 2 cm. Internal structures cannot be detected in the field.

Sometimes the surge units following the 1. Palizzi Pumice contain a remarkable amount of Pele's hair. These deposits can be described as dry-surge deposits, because they neither show

accretionary lapilli, nor vesiculated tuffs nor plastic deformation. Two exceptions which can be called wet-surge deposits are located below the 1. Palizzi Pumice and above the 2. Palizzi Pumice.

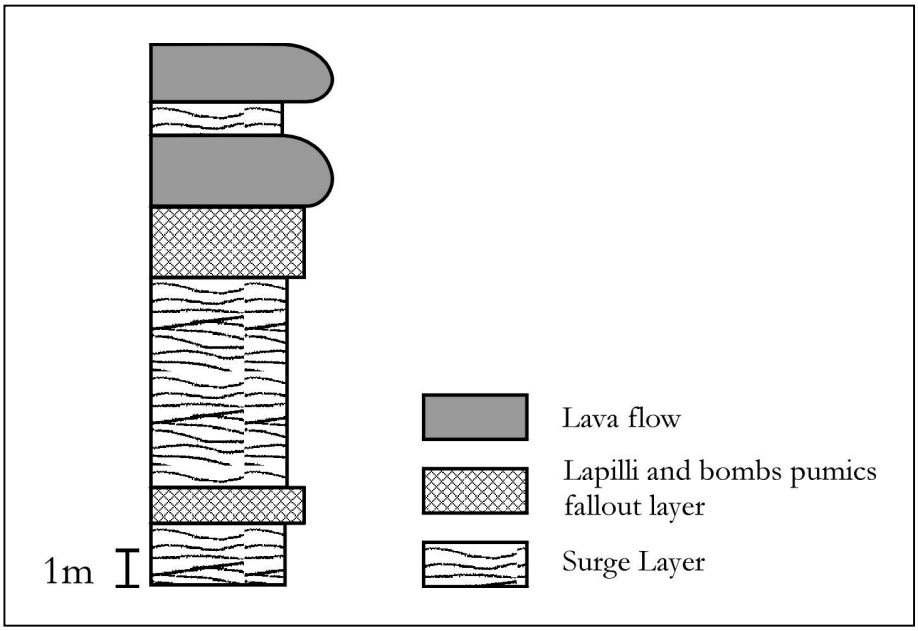

Figure 2.2: Sequence of the Palizzi succession (DELLINO AND LA VOLPE, 2000).

It is important to bear in mind that the surge facies differ from location to location. For example in the Caruggio, the surge deposits show a massive structure with a thickness of 50 cm. The surges could not pass the caldera wall and it seems that the whole surge was completely stopped at the wall, so that the material was deposited at once. The caldera wall was a topographical barrier for coarser material. The topographic obstacle at the Lentia complex has a height of about 70 m, whereas at the Piano Caldera the height is up to 220 m (DELLINO AND LA VOLPE, 2000 and DELLINO, pers. comm. 1999). The latter is an excellent topographic obstacle for coarser material, the higher the barrier and the lower the energy of the surge the finer is the grain size sedimented on the other side of the obstacle. Therefore the deposits at the foot of La Fossa cone are coarser than outside of the caldera rim (DELLINO AND LA VOLPE, 2000). Palizzi probably did not develop a persistent eruption column because of the pulsed phreatomagmatic eruptions, that are significant for the Palizzi surge deposits (DELLINO AND LA VOLPE, 2000). Fine-grained dry-surge deposits of La Fossa cone examined by DE ROSA (1999) are thought to be the result of low-energy eruptions (DE ROSA, 1999 and DE ROSA ET AL., 1992).

2.5. Commenda

The overlying Commenda succession is subdivided into two parts, a breccia and some flow and fall-out deposits at the base followed by a prominent marker, the Upper Pilato Ash, which is not visible in every outcrop and the upper unit composed of different dry-surge deposits. At the base is a breccia unit with flow and fall-out layers. The breccia is a prominent marker horizon that has been interpreted as a phreatic explosive breccia (FRAZZETTA ET AL., 1984 and FRAZZETTA ET AL., 1983). It contains yellow, hydrothermally-alterated clasts in an orange to reddish matrix. This unit is often covered by another important marker, the Upper Pilato Ash, and by a bed of accretionary lapilli ranging from 0.5 to 4 cm in diameter (both markers can be observed in outcrop R, the Pilato Ash also in outcrop N). A prominent 6 cm thick dry-surge deposit with intercalations of Pele's hair occurs sometimes above this marker. The breccia has a rhyolitic to trachytic composition, whereas the trachytic composition based on a mixing between a rhyolitic and a latitic magma (GIONCADA ET AL., 1997). With a lacuna these coarse red and brown layers are followed by multicoloured ashes and lapilli which can be described as wet-surge deposits. Normally the deposits show colours of yellow, orange, pinkish, red, grey, and ochre-green. Often vesiculated tuffs can be observed (DELLINO, 1997). They are dominantly of latitic composition. Their thickness decreases rapidly with distance from the vent. For example at the "recent" La Fossa rim decimetre-scale layers occur, whereas they are a few centimetres thick only a few 100 metres away. The composition is dominated by latitic products and the distribution of the succession is relatively wide around the cone, but spatially more restricted than Palizzi.

The Commenda lava is a glassy lava flow of rhyolitic composition and covers an area of 0.02 km^2 on the southern slope of La Fossa cone. The lava has a constant thickness (DE FINO ET AL., 1991). It is often described as the terminal lava of the Palizzi succession.

SBRANA (1997) noticed a rhyolitic to trachytic composition in the basal deposits, followed by a thin unit of latitic varicoloured ashes. Rhyolitic surge deposits with latitic and trachytic components occur at the top. DE ROSA AND SHERIDAN (1983) suggest that the magmatic history of the Pietre Cotte and Commenda lavas and the products of Monte Guardia (Lipari) can be explained by the rise of a mafic magma which intersects a reservoir of rhyolitic magma. The commonly mafic xenoliths suggest that the magma mixing triggered the eruption.

2.6. Cratere Attuale

Cratere Attuale is the most recent succession and can be subdivided into three main units: 1) Pietre Cotte, 2) Pyroclastics post 1739, 3) Eruption 1888-1890.

The Pietre Cotte unit (cooked stones) starts with wet-surge deposits that cannot be distinguished well from the Upper Commenda. This facies changes upsection to brown-grey wet- and dry-surge deposits that are easily distinguishable from the Upper Commenda. The latter are limited to the near-cone area and have a latitic composition (DELLINO, 1997). Above

it lies a metre thick cycle of fall deposits of rhyolitic bombs and lapilli-pumice. Some vesiculated bombs are observed as well. The microcycle is terminated by a rhyolitic lava-ash-pumice-obsidian-flow. This lava was extruded about 1739. Details about the geochemistry and petrology of this unit are described in DE FINO ET AL. (1991) and GIONCADA ET AL. (1997). Some authors like GIONCADA ET AL. (1997) also define a latitic cycle between Commenda and Pietre Cotte. These authors believe that small amounts of magma were produced between long periods of quiescence from the 6th to the 18th century. The deposits can be observed at the southern edge of the Cratere Attuale. During the same time interval latitic material was erupted at the Forgia Vecchia.

The so-called Pyroclastics post 1739 consist of different ash deposits formed by dry-surges and denser lapilli layers. This unit is dominated by rhyolitic deposits, but also some latitic components can be observed.

The final unit is formed by the products of the eruption 1888-1890. It contains different breccias, dense lapilli fall-out and breadcrust bombs. During this last eruptive episode 5 m of pyroclastic deposits were deposited. Subsequent erosion reduced the thickness to 1 – 2 m. Large breadcrust bombs with diameters up to 1m were ejected over distances up to 1 km from the vent (FRAZZETTA ET AL., 1983). This eruption was documented very well by contemporaneous observers (e.g. SILVESTRI ET AL. (1891)). The scenario can be described as follows:

The eruption started at 2 August 1888 with an initial explosion that emitted no juvenile material. Later eruptions ejected bombs, blocks, and ashes of mostly juvenile material. During the middle part of the activity the breadcrust bombs were produced, which have the similar composition and texture as lavas produced earlier (DE FINO ET AL., 1991). The eruptions were not very continuous, but were interrupted by quiet periods lasting a few minutes and seconds until several days. Only the great explosions ejected bombs and blocks over distances of more than a few 100 m. Intensity of the different eruptions was highly variable. The time between two relatively strong eruptions ejecting bombs and blocks was sometimes long. In the meantime only vapour or small emissions could be recognised. On 22 March 1890 the eruption stopped, but no lava flow has been formed until now (FRAZZETTA ET AL., 1983 and SILVESTRI ET AL., 1891).

The eruption of 1888-1890 is divided into twelve units (CLOCCHIATTI ET AL., 1994). Erosion removed evidence of the last phase of the eruption. These twelve units represent only the high energetic explosions, whereas the other “small” eruptions documented by SILVESTRI ET AL. (1891) did not leave obvious evidence. CLOCCHIATTI ET AL. (1994) grouped these twelve units into three eruptive phases: (1) An opening rhyolitic phase with two phreatomagmatic breccias. (2) A trachytic and latitic phase with pyroclastic surge deposits and fall out deposits. In this second phase the composition evolved from trachytic to latitic. (3) Rhyolitic tephras similar to the products of the initial phase. In the last phase the famous bread crust bombs can be found (CLOCCHIATTI ET AL., 1994). According to GIONCADA ET AL. (1997) the erupted products had

a rhyolitic composition in the beginning and evolved with time to a trachytic and later to a latitic composition.

DE FINO ET AL. (1991) and FRAZZETTA ET AL. (1984) point out that the Pietre Cotte and the following cycles of Cratere Attuale, including the eruption with the breadcrust bombs, emerged from the same vent of La Fossa di Vulcano. DE FINO ET AL. (1991) and FRAZZETTA ET AL. (1983) assumed a four stage model for the evolution of Commenda and Pietre Cotte:

1) mixing of two magmas with different composition (rhyolitic and more primitive),
2) the mixed magma rises to the water table and reacts with the water. In consequence of this reaction eruptions follow and produce surges as well as a tuff cone with a wide crater,
3) after some time the water table can decrease and the eruption style changes to another type of activity (for example vulcanian),
4) the at least in volatile components reduced magma emerged as a lava flow.

2.7. Further information

A more detailed study of the stratigraphy, eruption and sedimentation dynamics, and eruption scenario is given by DELLINO AND LA VOLPE (1997), who also discuss the cycle-hypothesis of FRAZZETTA ET AL. (1983). The geochemistry of La Fossa di Vulcano is described for example by SBRANA (1997). The formation and alternation of the varicoloured wet-surge deposits is recorded by CAPACCIONI AND CONGILIO (1995).

The young La Fossa cone shows an interesting trend of alternating composition of the erupted products. Mafic-intermediate magmas alternate with felsic magmas of a totally different composition over very short time scales. In addition, the volume of the erupted material becomes progressively smaller, the eruptions of Punte Nere produced more than one third of the whole erupted material of La Fossa cone (DE ASTIS ET AL., 1997b). Xenoliths with an intermediate composition and quenched blebs can often be recognised in mafic magmas. It can be assumed that for the evolution of La Fossa cone two magma reservoirs exist (SBRANA, 1997), one shallower at a depth of about 2,000 to 2,500 m and a lower at a depth of about 3,000 to 3,500 m. The observed decrease in volume of the erupted material may indicate that the more evolved shallower reservoir is progressively emptied. The xenoliths which are observed in different states of preservation suggest a significant mass of crystal mush in the lower reservoir. SBRANA (1997) assumed that the shallower reservoir has a pressure of > 300 bar and a temperature of about 1080°C. In this reservoir the latitic-shoshonitic magma differentiates to a K-trachytic magma. The lower reservoir probably has a pressure > 700 bar and a temperature of 1180 – 1080 ± 20°C.

In summary, the following processes may have been responsible for the formation of the La Fossa successions: at the beginning extreme reactions between magma and excess water occurred, leading to wet-surges and phreatic breccias. When the water content decreases dry-surge deposits dominate. The end of the succession is characterised by a low amount of water and lava or pumice were emerged (CONIGLIO AND DOBRAN, 1995 and FRAZZETTA ET AL.,

1984). Erosional gaps between different successions suggest a pause in the eruption. In general such gaps are not observed within a single, genetically related succession.

On La Fossa cone two parasitic cones can be observed at the NW flank of the volcano. They are called Forgia Vecchia (old forge) I and II and their age is not known in detail. FRAZZETTA ET AL. (1983) suppose that Forgia Vecchia I is a large phreatic crater and Forgia Vecchia II is a small phreatic crater of the 1727 eruption, because deposits produced by this crater underlie the Pietre Cotte lava of 1739 (DE ASTIS ET AL., 1997b, DELLINO, 1997, DELLINO AND LA VOLPE, 1997, and FRAZZETTA ET AL., 1983).

A prominent historic marker is the so-called Upper Pilato Ash from Lipari (6^{th} century AD). The deposit is fine grained ash layer with a white to light grey colour. The thickness ranges between 2.5 cm in the northern part of Vulcano and 0.5 to 1.5 cm in the southern part. This layer can be observed at different localities on Vulcano island where it is often intercalated between the Commenda Breccia and Commenda surge-deposits. These marker allows precise dating of the Commenda eruption, because historic observation are not very accurate or scientific (FRAZZETTA ET AL., 1983 and KELLER, 1980). For Vulcano only the last eruption was described in a scientific manner by MERCALLI AND SILVESTRI (1890) and SILVESTRI ET AL. (1891).

The successions of La Fossa can not be distinguished in every outcrop and it is therefore difficult to calculate an exact volume for each eruption phase. This is however necessary for forecasting and hazard assessment. Surges, which represent more than 80 % of the deposits of La Fossa di Vulcano, are the mostly expected eruption type in the future of Vulcano. It is important to understand and distinguish the different successions, because these surges are the most hazardous eruption products for the people on Vulcano (DELLINO AND LA VOLPE, 2000 and FRAZZETTA ET AL., 1983). MONTALTO (1996) expects that the renewed eruptive activity at La Fossa cone will start with an initial phreatic blast, followed by different phreatomagmatic eruptions. In this scenario the village of Vulcano Porto in particular is at risk. SHERIDAN AND MALIN (1983) assumed that only the village of Vulcano Porto is at risk and locations at Vulcanello or at the Piano Plateau are more or less save for the expected eruption. However, some deposits of several younger successions can be found on the Plateau and on Vulcanello as well, and future eruptions may affect the same region again (see also the maps in DELLINO (1997) and DELLINO AND LA VOLPE (1997)).

The fumarolic activity of La Fossa occurs at two different locations: a) at the crater rim, especially at the NE-side of the rim, and b) at the Baia di Levante, especially at the thermal spring with the mud-pool and the shore. The feeding system of both locations is assumed to be different, because changes of composition and temperature are independent at the two locations. At Baia di Levante the source is a shallow aquifer. The fumaroles at the crater rim seem to be originated from a deeper source, probably the magma reservoir. Here, significant changes of temperature and composition can be observed, for example the extreme increase of the temperature since about 1970 which led to increased observations and monitoring on Vulcano. The major chemical compounds of the crater fumaroles are H_2O and CO_2, and sulfur

gases, HCl, HF, B and Br occur in minor amounts (MONTALTO, 1996). Studies of the fumaroles, their geochemistry and changes were made for example by BADALAMENTI ET AL. (1991), BOLOGNESI (2000), BRANCA ET AL. (1997), CAPASSO ET AL. (1999), CAPASSO ET AL. (2000), CHEYNET ET AL. (2000), CHIODINI ET AL. (1992), CHIODINI ET AL. (1991), GRAZIANI ET AL. (1997), HARRIS AND MACIEJEWSKI (2000) LE CLOAREC ET AL. (1991), MONTALTO (1996), NUCCIO (1999), NUCCIO ET AL. (1997), and TEDESCO ET AL. (1995). The fumaroles are also a source of risk for people and pets. For example a gas hazard in 1984 with high CO_2-emissions killed a number of dogs and rabbits (BADALAMENTI ET AL., 1998). As well as BARBERI ET AL. (1991) some other authors suggest a renewal of La Fossa di Vulcano, based on the changes of the fumarolic activity, like geochemistry, temperature, flux, isotopes, that seems to indicate a slow but constant evolution towards a potential new eruption.

3. Methods

The geophysical methods used for a better classification of the different successions are gamma-ray (γ-ray) measurements in the field and measurements of the grain-size depended magnetic susceptibility in the laboratory.

3.1. Gamma-ray

3.1.1. Introduction

γ-ray-measurements are based on the natural radioactivity of rocks. In geology γ-ray-measurements are normally used for sequence-stratigraphy, well logging, and ore prospecting. The natural radioactivity of rocks is also used for the absolute age-determination, for example with Rb-Sr, K-Ar, or U-Th-Pb geochronology. Parts of the internal heat of the earth is induced by radioactive decay, here in general ^{238}U, ^{232}Th, and ^{40}K play an important role (KERTZ, 1992).

Radioactivity is a generic term for events when nuclides change under emission of radiation. The resulting decay is accompanied by the transition from one nuclear energy state to a lower energy state. The exact moment of the decay cannot be predicted because normally it is spontaneous (FAUL, 1954). The radioactive decay can be described by the following equation:

$$N_p = N_i \, e^{-\lambda t}$$

N_i : initial number of atoms at the time zero
N_p : Number of atoms at time t
t : time
λ : decay constant

The decay constant λ is related to the half-life $t_{1/2}$:

$$t_{1/2} = \frac{0.693}{\lambda}$$

Radiation produced by the decay can be of three forms: α-radiation, β-radiation and γ-radiation. An example for the different radioactive decay pathways is given by the radioactive decay of ^{40}K in figure 3.1.

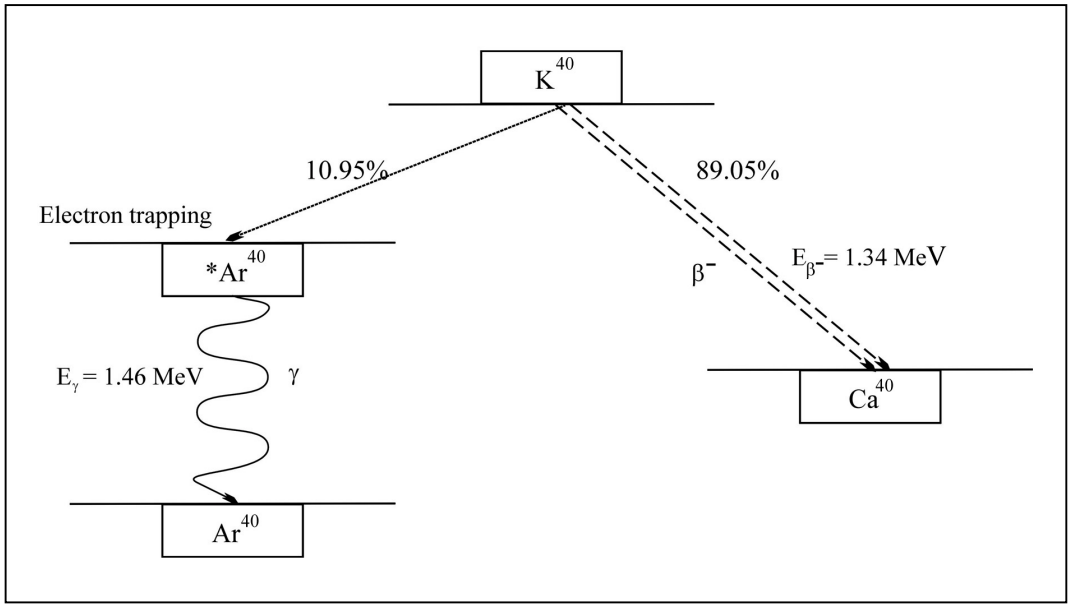

Figure 3.1: Scheme for the radioactive decay of K^{40}, modified after (KERTZ, 1992). $*Ar^{40}$ is the excited state of Ar^{40}, which immediately emits electromagnetic radiation (γ-ray) and decays to the ground state of Ar^{40}. About 10.95% of K^{40} react to Ar^{40} with an energy emission of 1.46 MeV, whereas most of K^{40} degrade to Ca^{40} (β-decay) with an energy emission of 1.34 MeV.

3.1.1.1. Alpha-Radiation

Some radionuclides decay by a spontaneous emission of α-particles. Most of the nuclides producing α-particles have atomic numbers larger than 58, solely a few have lower numbers, like He, Li or Be. α-particles are composed of 2 protons and 2 neutrons, and they are thus equal to a He atom stripped of its electrons. The emission thus reduces the atomic number and the neutron number of the element by 2, hence the mass number is reduced by 4. The isotopic daughter is a different element than the parent element (FAURE**,** 1986). The α-ray particle travels at high velocity on a straight path (FAUL, 1954). (GRASTY, 1979) describes α-particles as doubly positively charged helium nuclei that are absorbed in air within a few centimetres of distance. Thin sheets of paper effectively screen the radiation. The low penetration depth is due to the low energy of the emission, and this characteristic can be used to identify the isotopes. Three decay series can be distinguished: U^{238}, U^{235}, and Th^{232}.

3.1.1.2. Beta-Radiation

The radiation can be split of into different types like electron-emission (β^--decay), positron emission (β^+-decay), and electron catching (e.g. FAUL, 1954 and KUCHLING, 1988). The change of a neutron into a proton associated with the emission of a β-particle (electron) and a neutrino is called β-decay of a nucleus (FAURE, 1986 and SCHÖN, 1983). Because of its negative (electric) charge the β-radiation will be deflected in a magnetic or electric field into the opposite direction as the α-radiation (KOCH, 1984). The energy is variable – from zero to

the maximum set of the energy of the total decay –, and the velocity of β-radiation can be equally variable (HOLLEMANN AND WIBERG, 1985). β-particles have a higher penetration depth than α-rays and can travel up to 1 m (GRASTY, 1979).

3.1.1.3. Gamma-Radiation

γ-radiation is a highly energetic electromagnetic radiation, with wave lengths in the range of 10^{-9} – 10^{-11} cm and frequencies that range between 10^{19}- 10^{21} Hz. Figure 3.2 shows the distribution of γ-ray for 3 naturally occurring radioactive isotopes.

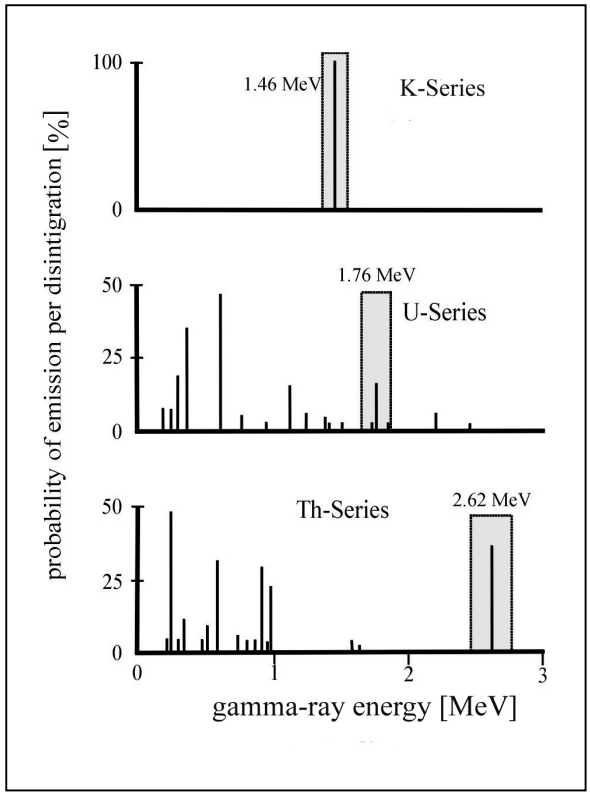

Figure 3.2: The distribution of γ-rays from the 3 naturally occurring radioactive isotopes (modified after LOVBORG AND MOSE (1987) and TITTMAN (1986)). The shadowed areas define the energy windows, which are used for recording counts with the gamma-ray scintillometer in the outcrop.

Gamma-rays can interact with matter in three principal modes: Compton scattering, photoelectric absorption and pair production (e.g. ADAMS AND GASPARINI, 1970, FAUL, 1954, and KOCH, 1984).

Compton scattering: It can be described as an elastic collision between an atomic electron and a γ-quantum. The Compton absorbing and scattering power of a material is more or less proportional to the density of the electrons of the material. If the γ-quantum collides with the electron it changes its direction and transfers parts of its energy to the electron, which is accelerated in a different direction.

Photoelectric absorption: The γ-radiation behaves like a wave and interacts with an atom. The complete energy of the γ-radiation is transferred to a single atomic electron. This electron is ejected from the atom with a discrete kinetic energy that is equal to the energy of the photon minus the binding energy of the electron-atom bond. The free electronic energy levels are filled by the emission of characteristic X-rays.
Pair production: A pair of electrons near the atomic nucleus (positron and negatron) can be produced when the energy of the γ-radiation is twice as high as the remaining mass energy of the electron. The positron lives only very shortly (combines with an atomic electron), produces two quanta of annihilation radiation (FAUL, 1954) and than disappears. This reaction is very rare but very important for the interaction of cosmic rays with the atmosphere and the surface of the Earth. After (GRASTY, 1979) these reactions needs an energy higher than 1.02 MeV.

3.1.2. Method

For this thesis a scintillometer with a NaI(Tl) crystal detector (Exploranium GR-320) is used. It detects the 3 main natural sources ^{40}K, ^{232}Th and ^{238}U, which make up ca. 99 % of the natural γ-ray penetration. The detector probe consists of a 3 x 3 inch NaI(Tl) crystal with associated photomultiplier, high voltage supply and preamplifier. The detector is thermally insulated.
Measurements were taken in the field layer by layer at different distances with an empirical measuring time of 60 sec (see also figure 3.3). Selected outcrops were measured and flat, little weathered outcrop walls were preferred where possible. Because of the relatively dry conditions of the selected outcrops the effects of variation in water content were found to be negligible. Test measurements showed that if the outcrop walls were not inclined more than 60° and the thickness of the single layers exceeded 5 – 7 cm, reproducible measurement could be obtained in the case of La Fossa. Measurements of thinner layers are influenced by γ-radiation from the over- and underlying layers. Measurements with the so called Heger-Scintillometer, which is a γ-ray scintillometer optimised by (KOCH, 1984), show that a mayor fraction of the registered radiation is related to the first third of the ca. 0.4 m penetration depth assumed for the Heger-Scintillometer (HECKEMANNS AND KRÄMER, 1989). For the measurements in this thesis a slightly lower penetration radius of 13 cm is assumed.

In addition to the rocks to be analysed, gamma radiation can be sourced from cosmic rays, the amounts of material in the vicinity, as well as the radioactive impurities of the counter itself. The cosmic rays can be absorbed for example by a lead mantle around the sensor, so that only a small detection fissure is open for the measurements. This small fissure is important for the measurements, because the geometry and layering in the outcrop are important. Figure 3.4 gives a few examples how the layer thickness and the layering can influence the

measurement. The individual layers to be analysed are shown in light grey bars, if the thickness is less than the penetration radius adjacent layers will influence the measurements. This is observable in an extreme manner for vertical bedding. Measurements near the upper edge of a cliff can be influenced by the background radiation, measured from the missing material at the top of a cliff.

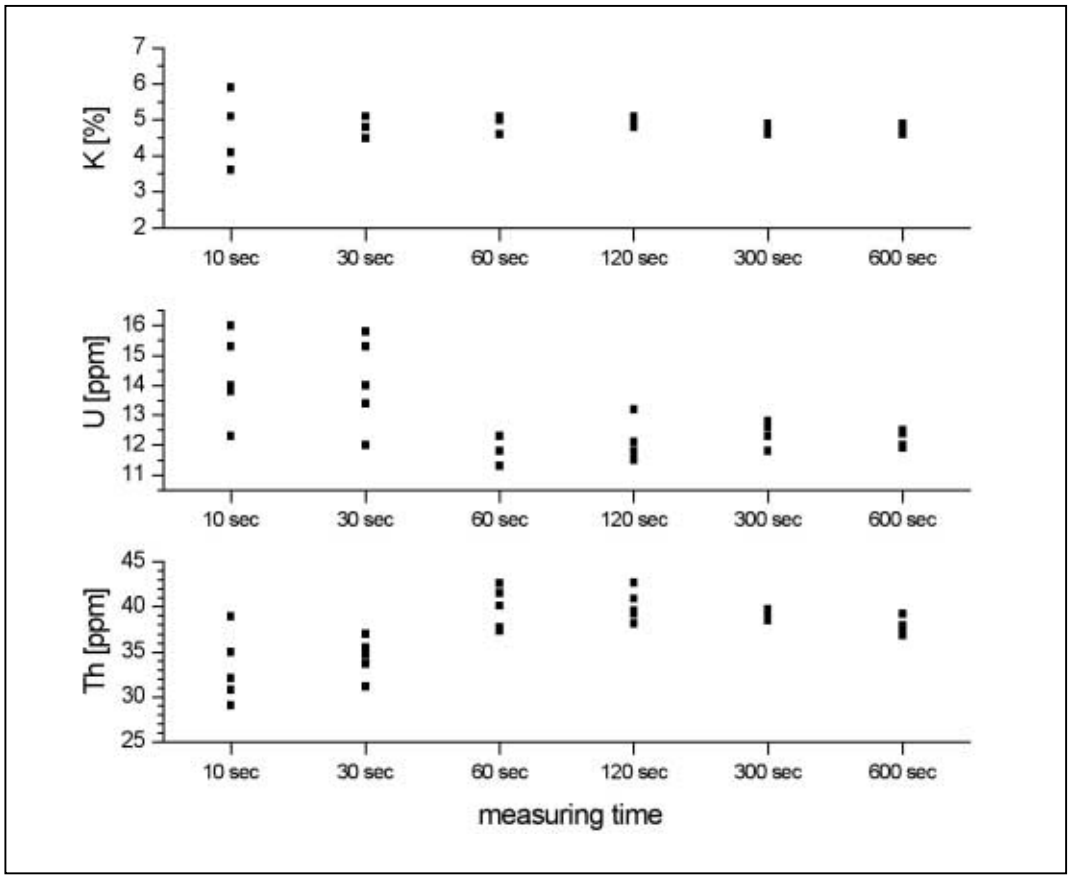

Figure 3.3: Dependence of measured concentration and time for the measurement. A single sample is measured several times and at variable counting times of the spectrometer. Samples measured for 60 sec. combine reasonably short measurement time with acceptable standard deviation and solely a few outliers.

The scintillation counter has the following advantages over the ("old-fashioned") Geiger-Müller counter:

- the efficiency, especially for γ-ray detection, is much higher than with the Geiger-Müller counter.
- the pulse height is more or less proportional to the energy of the ionising particle.
- the effect of cosmic rays in the background is smaller.
- the resolving time is much lower than for the Geiger-Müller counter.

(Bristow, 1979) points out that the Geiger-Müller counter only provides the total count indication, whereas the γ-ray scintillometer can show total counts and the amounts of K, Th, and U. The NaI(Tl) detector is the most common detector for scintillometers used in U exploration. Sometimes other inorganic crystals are also used, especially in borehole logging (e.g. [CsI(Na), CsI(Tl)] and $Bi_4Ge_3O_{12}$) (BRISTOW, 1979).

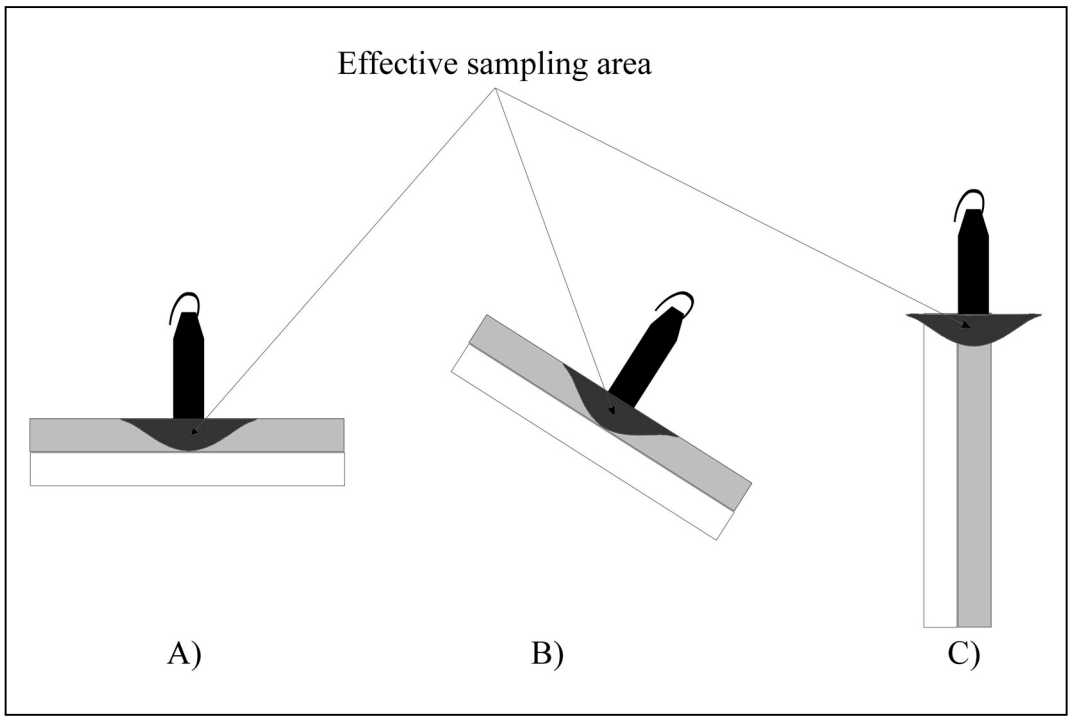

Figure 3.4: Relationship between layering and resolution. Light grey bars represent individual layers to be analysed, dark grey areas indicate area that is effectively sampled. The horizontal bedding (a) and the inclined bedding (b) give the best resolution if the thickness of the layer is higher than the penetration radius, whereas the vertical bedding (c) shows the lowest resolution, depending on the layer thickness (modified after MYERS AND WIGNALL, 1987).

The scintillation counter detects and counts the flashes of light that are produced by the reaction of radioactive radiation with special materials (especially the crystals of the detectors, like NaI(Tl), CsI(Na) and more). These flashes have a characteristic energy that is counted and intensified by a photomultiplier, and then detected by an electronic system. A small computer allows the calculated amounts to be displayed on the scintillometer. For the detection of the photon energies a discrete error has to be considered, because the primary photon energies can decrease due to collisions along the transmission path.

Important minerals for the measurements in our working area are the different K-bearing feldspars and micas (see also table 3.1). Important Th or U bearing minerals are often accessory minerals or heavy minerals, for example rutile, titanite or zircon. The main components of magmatic rocks, feldspars, olivine, pyroxene, quartz and most of the micas, are more or less free of U and Th. U can form different organic complexes and is therefore particularly abundant in organic-rich shales, however the amount of U is low in relation to the dominant clay minerals in shales (TITTMAN, 1986). Especially U can be mobilised in an oxidising environment as the unstable U^{4+} which can form the highly soluble uranyl-ion (UO_2^{2+}) (CHIOZZI ET AL., 2000, DE VOTO, 1978, and MYERS AND WIGNALL, 1987).

Normally the degree of differentiation of the magma is reflected in the γ-radiation emitted by the rock. The more a magma is evolved the higher will be the values. On the Aeolian Islands this has been shown for pyroclastic deposits and lavas (CHIOZZI ET AL., 1998). The correlation between the rock composition and γ-ray radiation on Vulcano Island was seen before by BRAI

ET AL. (1995). To this author's knowledge no correlation has been attempted for pyroclastic deposits based on measurements in the field. It is important to note that pumices show slightly lower values for Th, K, and U than the pyroclastic layers or the lava, and this can be observed especially in more felsic cycles on Lipari (CHIOZZI ET AL., 1998). On Lipari the pyroclastic layers show significant higher values especially for Th and U than samples from the lava flows of the same cycles.

Mineral	*K [%]*	*U [ppm]*	*Th [ppm]*
Major			
Biotite	8.5	1-4	0.5-50
Calcite	0	1.5	0
K-Feldspar	11.8-14	3-7	0.2-5
Hornblende	0	1-30	5-50
Muscovite	7.9	2-8	10-25
Plagioclase	0	0.5-3	0.2-5
Pyroxene	0	2-25	0.01-40
Quartz	0	0.7	2.0
Accessory Minerals			
Allanite	0	30-700	500-2000
Apatite	0	5-150	20-150
Magnetite	0	1-30	0.3-20
Monazite	0	500-3000	25000-200000
Sphene	0	100-700	100-600
Zircon	0	100-6000	50-4000
Clay Minerals			
Illite	6.7	1.5	10-25
Kaolinite	0.3	1.5-9	6-42
Evaporites			
Anhydrite	0	n.d.	n.d.
Halite	0	n.d.	n.d.
Sylvite	52	n.d.	n.d.

Table 3.1: Concentration range of radioactive elements for some minerals (from MYERS AND WIGNALL, 1987, and SERRA, 1984).

γ-ray measurements are also used in sequence stratigraphy, which since now, seems to be the most important tool beside the exploration of ore deposits, examples are given by AIGNER ET AL. (1995), BINOT AND RÖHLING (1988), BRISTOW AND MYERS (1989), ETTENSOHN ET AL. (1979), HECKEMANNS AND KRÄMER (1989), KOCH (1984), KRASSAY (1999), MYERS AND BRISTOW (1989), MYERS AND WIGNALL (1987), and PARKINSON (1996).

In situ measurements in the field were made since the 1970ties by different groups with scientific and industrial background. For these measurements often γ-spectrometers with a NaI(TI) crystal detector were used (e.g. LOVBORG ET AL., 1971). The significance of radioactivity in volcanic products is also assumed by IMBÒ ET AL. (1968), who measures the

radioactivity and the implication for the magmatic evolution in different Italian volcanic areas with variable techniques.

Another problem which has to be discussed is the equilibrium state of the material. When the equilibrium is not reached, either because of loss of daughter products, or because the time since deposition has been too short, then the measurements cannot be assumed to reflect the concentration of the radiogenic elements. In this case it would only be measuring value – not an absolute concentration –, which can be correlated because of the long decay period and the in comparison to the short measuring period of the fieldwork (only differences between two years instead of 10^{6-9} years for the half life time), examples for the equilibrium are given by KILLEEN (1979) and YONEZAWA ET AL. (1996). For the daughter isotopes the half life time is often lower, but after KILLEEN (1979) the equilibrium could be established in approximate five to six half lives (of the daughter isotope). CHIOZZI ET AL. (1998) in his field measurements of the mostly older rocks of Lipari (227,000 to 223,000 years B.C. beginning of activity, 1400 B.C. last eruption (BRUNO ET AL., 2000, DELLINO AND LA VOLPE, 1995, and DELLINO AND LA VOLPE, 1996)), estimates that the equilibrium is reached and the measurements reflect true concentrations of radiogenic elements. The problem of equilibrium is very important in the case where samples are crushed. KILLEEN (1979), RUSSELL AND STEINHOFF (1961), and YONEZAWA ET AL. (1996) show that the mass which could be assumed in the field measurements can reduce the influence of the secular equilibrium. For the measurements on Vulcano Island, especially for the survey at La Fossa cone, the equilibrium can be regarded negligible for the values, because of the consistency of the material. The studied deposits are still relatively soft, whereas during crushing of hard rocks radon can escape and disturb the equilibrium. The influence of radioactive disequilibrium is minimised by large samples sample volumes (KILLEEN AND CARMICHAEL, 1976). Details about counting statistics on γ-ray measurements in the field are given by LOVBORG AND MOSE (1987).

For the early airborne measurements (GRASTY, 1979) estimates a penetration depth of a few ten centimetres when measuring a few hundred meters over the ground. HAUSER ET AL. (1996) make indoor and outdoor measurements of different rocks and soils at Vulcano, he uses thermoluminescent dosimeters to count the radiation of ^{238}U, ^{232}Th and ^{40}K, also Radon measurements are performed, which show a very high seasonal change. The measured radiocativity is relatively high, but does not differ in a significant way from other Southern Italy volcanic areas. Aim of his study was to determine the influence of radioactivity for the inhabitants.

It is important to note that for the γ-ray measurements solely K contains a constant proportion of an observable γ-emitter, whereas ^{232}Th and ^{238}U have to be determined using the amounts of their daughter isotopes ^{208}Tl and ^{214}Bi (MOXHAM ET AL., 1965). It has to be kept in mind that the specific radioactivity of K is much lower than the radioactivity of Th and U, but because of the abundance of K in many rocks the amount is high enough to be detected by the scintillometer (FAUL, 1954).

Background effects can be observed in every outcrop, but they can be reduced by mantling of the detector, so that only the sample area is measured. Initial measurements in the laboratory with a mantling of the detector slot have shown that there is only a small influence for the coating of the sample. Different distance measurements taken at various distances show that for the first centimetre of distance between surface and sensor the values do not change the measurements in a very significant way (see also figure 3.5), but its effect increases with higher distances.

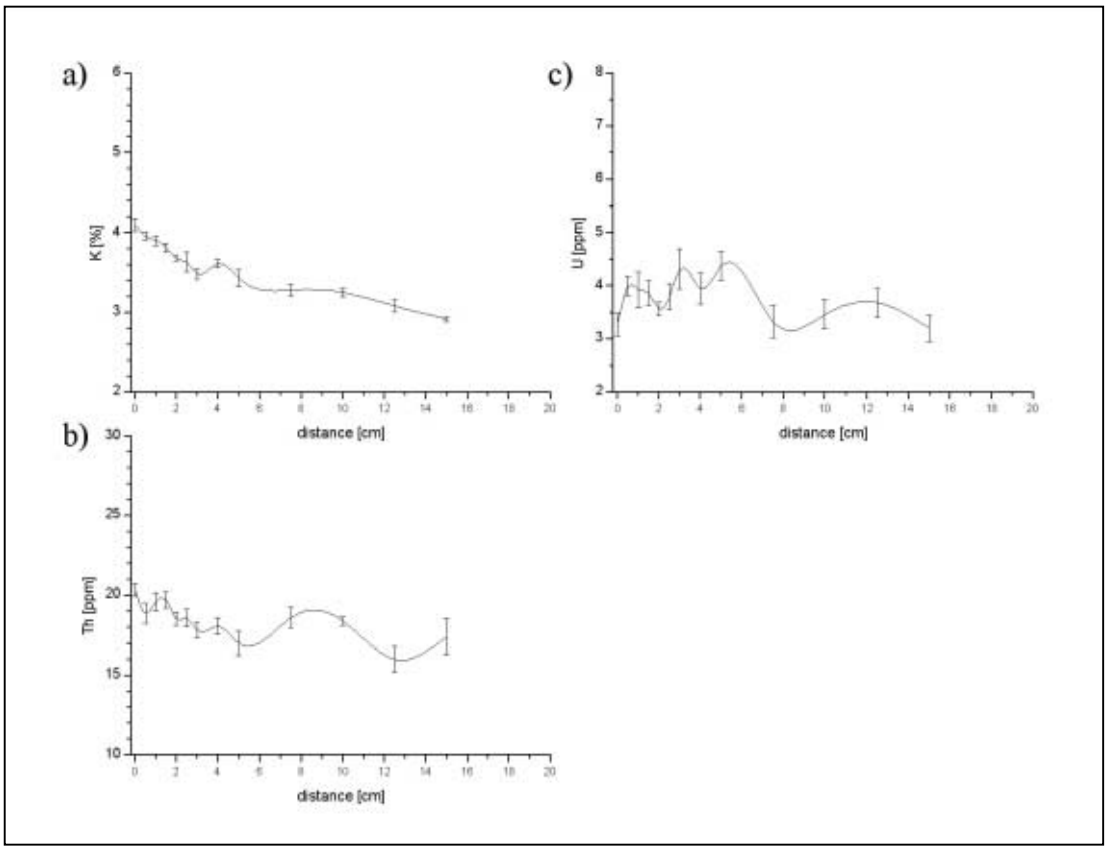

Figure 3.5: Relationship between the measured concentration and the distance from the γ-ray detector to the sample. The first centimetre does not affect the measurement in a very significant way, so the unevenness caused by the preparation mode of the surface does not disturb the measurement in a significant way. a) plot for K with a higher change, b) plot for U shows an extreme change in the first 0.5 cm but the next centimetre does not show significant changes, c) plot for Th shows a similar behaviour as U but with reversed initial conditions.

Measurement errors are caused by the machine and the maximum solution of the spectrometer in correlation to the layer thickness and geometry. They will be described in chapter 4. The influence of high U and Th amounts, which can, if the amount of Th or U concentrations higher than 100 ppm, disturb the measurements of K (LOVBORG AND MOSE, 1987 and LOVBORG ET AL., 1971), but such high concentrations do not occur in the young deposits of La Fossa di Vulcano.

3.2. Magnetic Susceptibility

3.2.1. Introduction

The magnetic susceptibility (sus) is a dimensionless rock parameter that is controlled by its (geochemical/mineralogical) composition. It is possible to discriminate different minerals according to their susceptibility properties. Diverse types of sus can be distinguished:

a) The volume specific sus (K) is often used for measurements of the anisotropy of the sus (AMS). AMS is important for stress and strain analysis, as well as for the correlation of flow directions (ADAMS AND WEAVER, 1958, CAGNOLI AND TARLING, 1998, DELLINO AND LA VOLPE, 1996, FRIEDMAN ET AL., 1976, KOPPELT ET AL., 1998, LE PENNEC ET AL., 1998, ORT ET AL., 1999, PISCITELLO ET AL., 1999, ROCHETTE ET AL., 1992, TAMRAT AND ERNESTO, 1999, TRINDADE ET AL., 1999, WOLFF ET AL., 1989, and ZANELLA ET AL., 1999).

$$M_{ind} = [K] \times H$$

$\mathbf{M_{ind}}$ is the induced magnetisation of the material and **H** is the inducing magnetic field. Both are expressed in amperes per meter, whereas the volumetric susceptibility K is a dimensionless unit.

b) The mass specific magnetic susceptibility (χ) which is defined by

$$\chi = K/\rho$$

with ρ as the density of the specimens (where volume is taken). K is the magnetic volume susceptibility. In this study the mass sus was measured with a mass of generally 7 g for each sample. For a better correlation the data are standardised to 1g and have to be extended by 10^{-6}, they are measured in the cgs-mode.

The sus can be used for AMS as well as for palaeomagnetic observations (KHESIN, 1998, VLAG ET AL., 1999, ZANELLA ET AL., 1999, and ZANELLA AND LANZA, 1994). The sus is also used for environmental investigations, for example (XIE ET AL., 1999), and to study the behaviour of magnetic particles in recent soft sediments (MARCO, 1998). The latter can possibly give some information about the time and mechanism of orientation of magnetic materials.

The orientation of a given magnetic field can be frozen in a rock when it cools below the Curie temperature (T_C) (also important for the AMS). Below the Curie point, the magnetic orientation in a rock cannot change in a wide range, because the dipoles are frozen parallel to the magnetic field lines at the time T_C was reached.

The sus χ and the relative permeability μ (= $1+\chi$) are dimensionless material properties (SCHÖN, 1983). They allow us to distinguish different types of magnetic behaviour for elements and minerals: paramagnetic, diamagnetic, ferromagnetic, ferrimagnetic and

antiferromagnetic. This special behaviour is caused by the arrangement of the crystal grid and the orientation of magnets in the so-called "Weißschen Bezirke". If all atomic magnetic dipoles show a parallel arrangement, for example in Fe, this is called ferromagnetic behaviour. If the magnetic domains can neutralise the magnetic moment, the behaviour is defined as ferrimagnetic. Above T_C the arrangement of domains is impossible and the material will loose its ferro/ferrimagentic properties. The different properties can be described as follows (BERCKHEMER, 1990, CARMICHAEL, 1989, SCHICK AND SCHNEIDER, 1973, and SCHÖN, 1983):

- *paramagnetic*: Material can be magnetised in a magnetic field H in the same direction and the magnetisation will be proportional to the field intensity. The sus of paramagnetic materials is a constant with a positive value which does not depend on the field orientation. Typical values cluster around 10^{-4} to 10^{-6} cgs. In general the magnetic induction of this material is slightly greater than the applied (external) field. The sus of paramagnetic materials depends on the temperature (Curie point and constant).
- *diamagnetism*: If diamagnetic materials are orientated in a magnetic field, they follow the so-called "Lenzsche Regel" and show an inverse orientation, whereas the amount is proportional to the strength of the field. The sus of diamagnetic materials is normally negative and shows values about -10^{-6} cgs. In contrast to paramagnetic materials, the sus of diamagnetic minerals does not depend on the temperature. Normally the induction can be blocked by other para- and ferromagnetic materials.
- *ferromagnetism*: Ferromagnetic materials can show an orientation of their moments parallel to the inducing magnetic field, in particular materials containing Fe, Co and Ni. Ferromagnetic materials contain "Weißschen Bezirke", small areas with equal orientation of the moment (see figure 3.6), which can be aligned in a magnetic field. This alignment is destroyed when the material is heated past T_C, because the temperature-induced particle movement is too high, hence an orientation of the dipoles is impossible. A complete order is only archived at absolute zero temperature, warming up induces disorder and after passing T_C the sus will disappear and the material will behave like a para- or diamagnetic substance, following the "Curie-Weiß"-Law. The sus of ferromagnetic materials is positive and substantially higher than the amounts of para- and diamagnetic materials. Like these, it depends on the field strength and the history of the material.
- *antiferromagnetism*: Antiferromagnetism is a special case of ferromagnetism where groups of ferromagnetic clusters are orientated in a special kind so the resulting magnetisation is zero (see figure 3.6). If the material passes the Néel-temperature – material specific temperature, above which the spin coupling between the paramagnetic centres will break down (HOLLEMANN AND WIBERG, 1985) –, it shows paramagnetic behaviour. The sus can be compared with paramagnetic materials. Prominent antiferromagnetic materials are Cr, Mn, MnO and FeO.

- *ferrimagnetism*: It is a special kind of ferromagnetic orientation, where the orientation of the different groups results in a partial compensation of the magnetic moments and the material shows a spontaneous magnetisation (see figure 3.6). Above T_C paramagnetic behaviour can be observed, below the temperature a remanent magnetisation is noticeable.

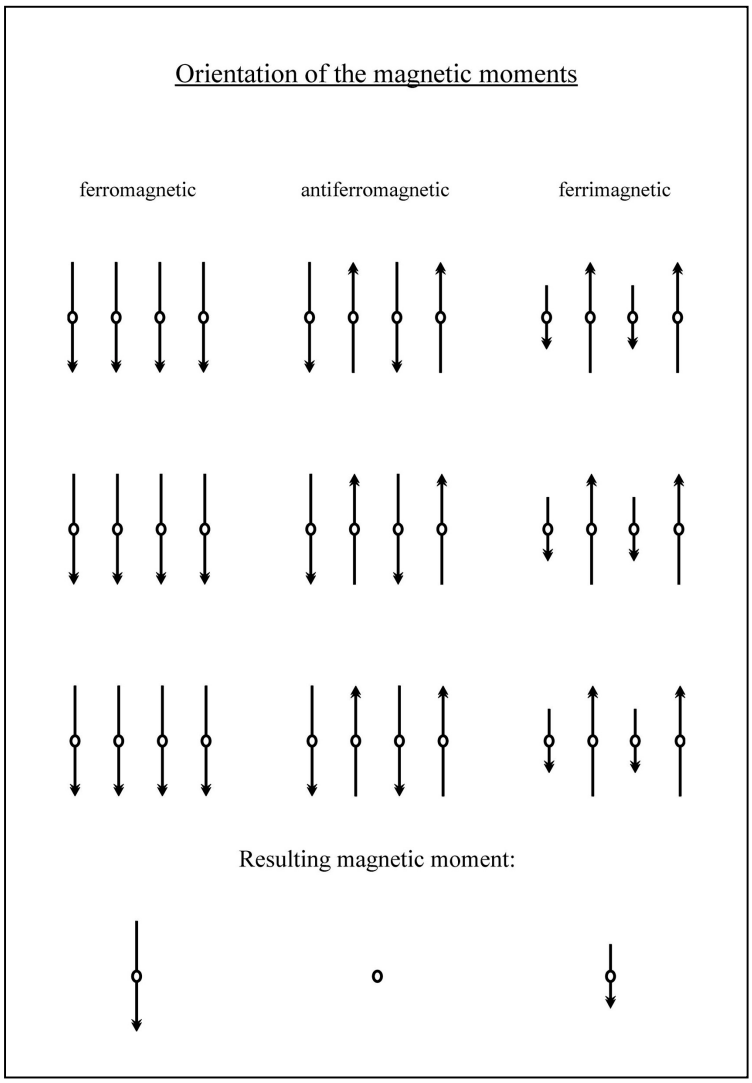

Figure 3.6: Orientation of the magnetic moments for ferro-, antiferro-, and ferrimagnetic materials, after SCHICK AND SCHNEIDER (1973).

Several minerals are susceptible to magnetisation, especially the minerals of the ternary system FeO-TiO_2-Fe_2O_3 show this behaviour (see also figure 3.7). The best known mineral is magnetite (Fe_3O_4), followed by a substituted mineral, where the FeO is partially substituted by TiO. Also strong magnetic properties can be observed for the cubic γ-Fe_2O_3 maghemite, which derives from the oxidation of magnetite. The polymorph equivalent of maghemite, α-Fe_2O_3 hematite, as well as the pyrrhotine FeS, show significant lower values for the magnetic susceptibility. Titanomagnetite can change by hydrothermal and hydritic alteration, involving removal of Fe, into leukoxen, a dark-red to grey-white, fine-grained mineral aggregate of rutile, anatas, titanite, hematite, and other (PICHLER AND SCHMITT-RIEGRAF, 1993).

Ferrimagnetic minerals in rocks generally cause anomalies in the static geomagnetic field. Magnetite and ulvöspinel have the strongest influence, whereas the other members of the series between hematite and ilmenite are less important. For surface anomalies the monoclinic pyrrhotite is significant. Magnetite and titanomagnetite are widespread in different sedimentary, magmatic and metamorphic rock types (RAUEN ET AL., 2000).

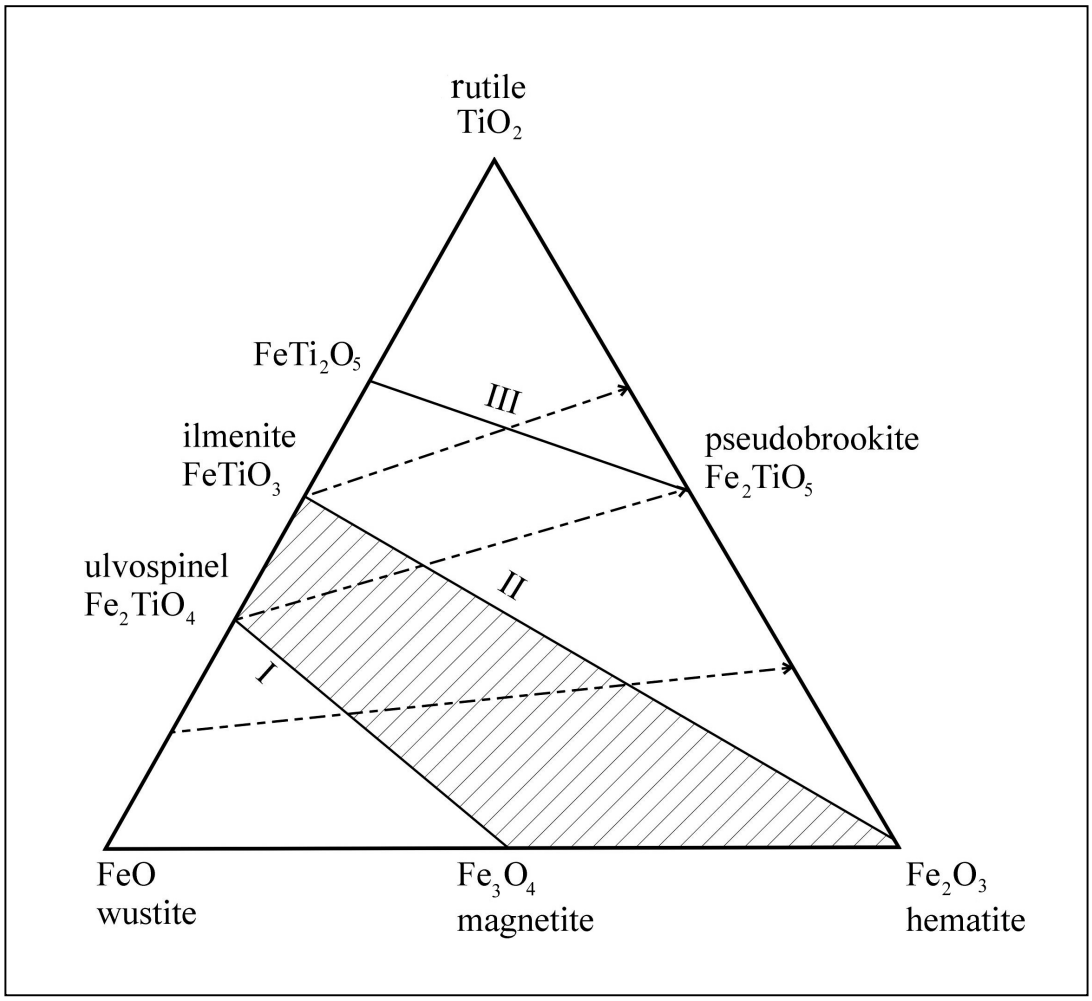

Figure 3.7: Ternary diagram of FeO-TiO_2-Fe_2O_3. Roman numbers mark the lines of solid-solution series, whereas the dotted lines display the directions of oxidation paths (from CARMICHAEL (1989).

LE PENNEC ET AL. (1998) show that the volume dependent sus has lower density and lower amounts when the material is weathered and altered by hydrothermal or meteoric influences. Especially the breakdown of pumice influences the density of the material.

The sus can also be used as a parameter for the magnetite amount in magmatic rocks or ore-deposits, shown by SCHÖN (1983). He explains that there is an empirical relation between sus and the amount of magnetite V_F, with different constants depending on the source:

$$\chi = 0.033 V_F^{1.33}$$

or

$$\chi = 0.0145 V_F^{1.39}$$

3.2.2. Methods

The volume sus (K) is a dimensionless parameter that relates the induced magnetisation of a rock or mineral sample to an applied magnetic field. It is important to note, that rock-forming minerals have a specific magnetic behaviour, which is characteristic for determination and classification. This behaviour depends on the specific property (e.g. diamagnetic like quartz, salts, paramagnetic like dolomite, hornblende and biotite, or ferro-, antiferro- and ferrimagnetic like magnetite, titanomagnetite and ilmenite) (PARASNIS, 1997). In the studied successions of Vulcano the measured sus is entirely controlled by the amount of ferrimagnetic minerals like magnetite (Fe_2O_3), titanomagnetite ($FeO(Fe,Ti)_2O_3$) and ilmenite ($FeTiO_3$).
Susceptibility measurements are performed in the laboratory. Samples are taken in the field and dried at 70-80°C for 12 h, in some cases twice as long. Then the samples are sieved for 15 min at 55 shakes/min. DIN 4188 sieves (Retsch) with a mesh range between 1 and 0.125 mm are used. In order to detect the most sensitive grain size range, initial sus measurements are taken of several grain sizes. For the case of La Fossa surge deposits the grain sizes 0.5 - 0.25 mm and 0.25 - 0.125 mm are found to display the maximum sensitivity. A sample mass of about 7 g is found to be representative. Repeated measurements show reproducibility of the analysis (10 measurements for a sample are representative, see also Appendix VI).
In addition these selected grain sizes have the following advantages:

- There are no scaling problems of sample volume, grain spacing and grain alignment. Alignment of the grains during the measurements is not a geometrical problem. Sample size is relatively small.
- Solely minor depletion or enrichment caused by the surge transport mechanism can be assumed, because of the small and well-defined field area of Vulcano island.

The measurements are made with a magnetic susceptibility meter model Bartington Instruments MS2™ with the sensor type MS2B™. The samples are measured in cgs-mode and this data are standardised to 1 g. For the measurement a frequency of 0.46 kHz and a field strength of 80 A/m RMS is used.
So far, measurements of sus nearly exclusively are performed in the context of paleomagnetic studies. Previous paleomagnetic investigations on different deposits of Vulcano have shown, that susceptibility bearing minerals normally are low-Ti-titanomagnetites, whereas the significant grain size of these titanomagnetites ranges between 25 and 300 µm. These grain sizes are recognised in some older pyroclastic deposits of Vulcano (e.g. Tufi di Grotti Dei Rossi). The magnetites investigated in this thesis are both, single and aggregate crystals (see also figure 3.8). Magnetites are sometimes trapped in other lighter coloured mineral aggregates, so the real grain size is much smaller. These aggregates may be transparent like light glass shards (ZANELLA ET AL., 1999 and ZANELLA AND LANZA, 1994). In other case the magnetites show well developed crystals (or fragments of crystals) with more or less ideal morphology.

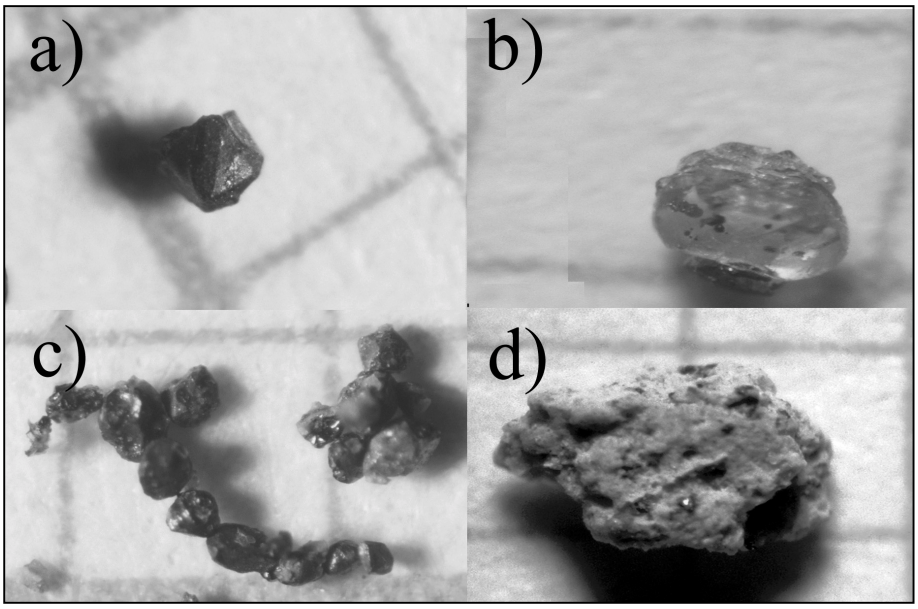

Figure 3.8: Different varieties of magnetite found on Vulcano. a) solitaire mineral with more or less ideal morphology, b) and d) pieces of magnetite embedded in different material, c) chain of solitaire minerals. 1 mm grid.

3.3. Granulometry

The granulometrical data are extracted from the sieved samples prepared for the grain size dependent sus (chapter 3.2). Cumulative grain size curves were generated. The mean (Ms) as well as the median (Md) were calculated on the basis of this data. The Md can be calculated according to the formula of FOLK & WARD in the scale unit Φ (TUCKER, 1985).

$$Md = \Phi_{50}$$

The mean was calculated using the mathematical arithmetic mean, the so-called moments measure, (the Ms is the 1st Moment) (FÜCHTBAUER AND MÜLLER, 1970 and TUCKER, 1985):

$$\bar{x} = \frac{\sum fm\Phi}{100}$$

x = mean (Ms)
f = percentage mass of the gsc
mΦ = mean size of every gsc in the scale unit ϕ

3.4. Microprobe

To characterise the geochemical composition of the sus bearing minerals – described as titanomagnetites to low-Ti-titanomagnetites by ZANELLA ET AL. (2001) and ZANELLA AND LANZA (1994) – magnetites of a few samples from the different successions were analysed by microprobe. Sieved samples were picked, cleaned in an ultrasonic bath with isopropanol, and dried. Thin sections were prepared from the cleaned material and analysed on a CAMECA SX50 microprobe. The following measuring conditions were used: 15 kV, 15 nA, 20 measurements/slide (Matrixcorrection PAP-Correction CAMECA).

The standards for the elements are: MgO for Mg, $MnTiO_3$ for Ti and Mn, Fe_2O_3 for Fe, Al_2O_3 for Al, and Cr_2O_3 for Cr. The measuring times varied between 20 sec/peak for Si, Al, Mg, and Ti, and 30 sec/peak for Mn, Cr, and Fe. Analytical error for the main elements is about < 1% (relative error).

3.5. Example Eifel

3.5.1. Introduction

The methods described before were applied and tested at the Laacher See Tephra, Eifel (Germany). The Laacher See Tephra of the Eifel has been chosen to test the method because of it's well known stratigraphy (for example SCHMINCKE, 1988, SCHMINCKE ET AL., 1973, and WÖRNER AND SCHMINCKE, 1984) and composition. Especially the wide range of composition, not appearing by this clear varieties for La Fossa di Vulcano, is an ideal test ground for both methods. In the course of fieldwork during summer 2000 some samples from the well-known Wingertsberg outcrop were taken. In this location also the difference of sieving and measuring of sus in the field and in the laboratory was tested.

3.5.2. Geological Setting

The Eifel is a quaternary volcanic field in W-Germany (figure 3.9). The area can be subdivided into the West- and East-Eifel volcanic fields. The volcanism is of continental intraplate type and generally monogenetic, with the exception of the Laacher See in the East-Eifel volcanic field.

The West-Eifel volcanic field covers an area of about 600 km^2 and is composed of about 240 volcanoes. The volume of the erupted material in the West-Eifel is much lower than in the East-Eifel. Most of the different volcanoes in the West-Eifel were formed between 0.7 and 0.01 Ma.

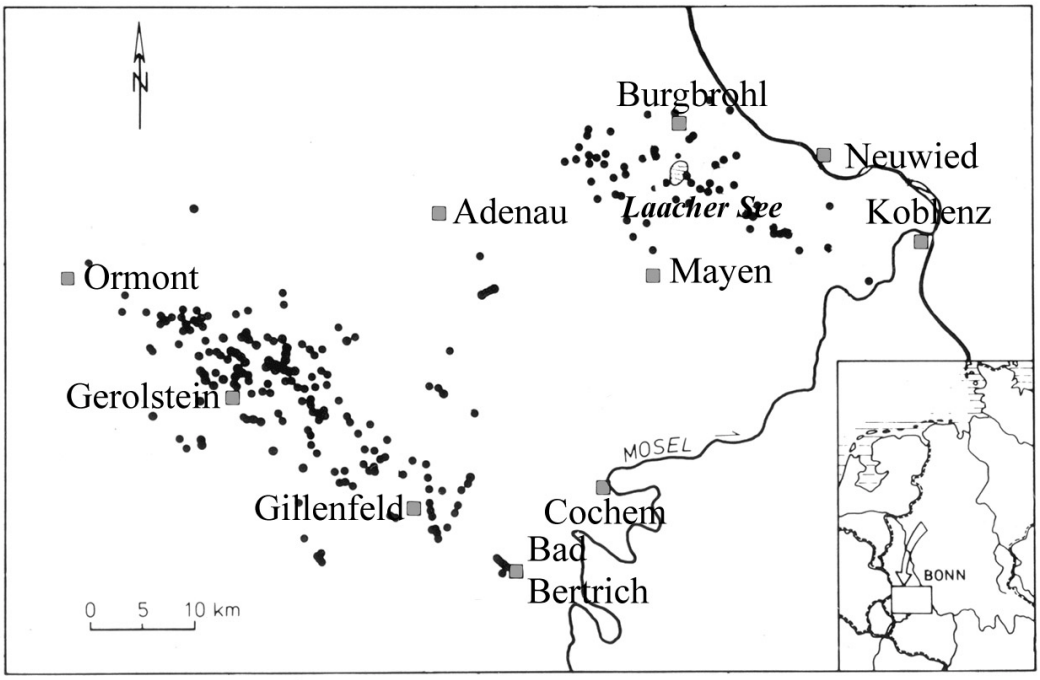

Figure 3.9: Quaternary volcanic fields of the Eifel. Dots are single eruption centre, from SCHMINCKE (1988)

The volcanic field of the East-Eifel consists of about 100 volcanoes on an area of approximately 400 km^2. These volcanoes are normally tuff rings and scoria cones, as well as large phonolithic complexes like the Laacher See, Rieden and Wehr. The activity of the volcanic field can be subdivided into several units, starting about 430,300 years B.C. (SCHMINCKE ET AL., 1990) and ending at 10,000 – 13,000 years B.C. with the great Laacher See eruption. The erupted volume of the Laacher See is assumed to be ca. 5 km^3, which is approximately the mass for the whole erupted volume supposed for the West-Eifel volcanic field. About two thirds of the East-Eifel magma is of mafic composition, in general melilith-nephelinites, nephelinites, leucitites, basanites and tephrites, whereas only one third shows phonolithic composition. This more differentiated material normally occurs in the (so-called) Riedener Caldera and in volcanic complexes like Laacher See, Kempenich and Wehr that are often called caldera-like.
The Wingertsberg (TK 5609 Mayen; R: 2590400; H: 5584800) is a classic outcrop of the Laacher See (proximal Mendinger fan) dominated by surge deposits that are intercalated with some fall- and flow-deposits. At the Wingertsberg the Laacher See Tephra is underlain by loess from the Weichsel cold-period (BÜCHEL ET AL., 2000).

Measuring points belong to the Lower Laacher See Tephra (LLST), the Middle Laacher See Tephra (MLST) and the Upper Laacher See Tephra (ULST) (see Appendix V).
In the MLST several dominant marker beds can be noticed, for example the so-called "Tauchschicht", a light-coloured ignimbrite consisting of different cm-thick layers (BÜCHEL ET AL., 2000). In depressions these thickness can increase to several meters. The sample MLST1 was taken from this layer. The "Tauchschicht" is overlain by the exceptional marker

unit “Autobahn”, which is built up by three layers; two coarse fall-out layers, the so-called “Fahrstreifen” with an intercalated fine ash-layer, the so-called “Mittelstreifen”. Sample MLST2 belongs to the lower “Fahrstreifen” and MLST3 was taken from the Mittelstreifen.

3.5.3. Gamma-ray

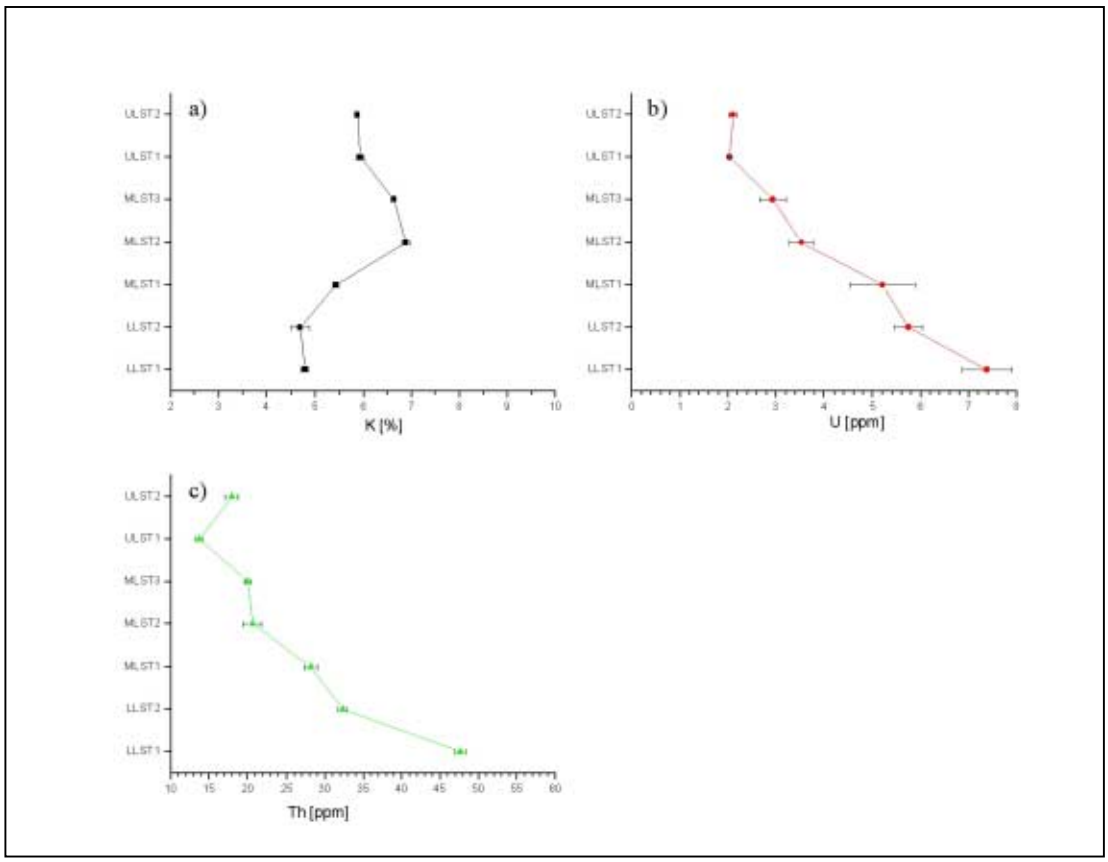

Figure 3.10: Results of the γ-ray measurements for the location Wingertsberg. The evolution of the magma is reflected by the elements. a) plot for K [%], b) plot for U [ppm], c) plot for Th [ppm].

The γ-ray-measurements reflect the magma evolution very well. Especially Th and U show a specific trend, the more evolved the magma is the higher are the values. This behaviour is in contrast to the trend of K that has a positive trend (see also figure 3.10). Th has a wider range than U. The ratio K versus Th shows only a slight increase from the base to the top, whereas the ratio K versus U describes a larger increase. In general plots of the concentration vs. the ratio or the concentration allow a discrimination of the different units, too. Sometimes also a weak linear correlation of the data can be observed in different plots like U vs. Th (see also Appendix V).

3.5.4. Magnetic Susceptibility

The magnetic mass sus is measured in the field during a field course and in the laboratory. Samples for field and laboratory measurements are taken from the same locality. Samples in the field are sieved by hand (DIN 4188 sieves, Retsch, with a mesh range between 1 and 0.125 mm). The varying degree of moisture influenced the quality of sieving in the field. Sample mass for the measurements was about 10 g, but often there was not enough material and the balance used in the field was less precise than the balance used in the laboratory, too. Samples in the laboratory were prepared like the samples from Vulcano, described above (see chapter 3.2).

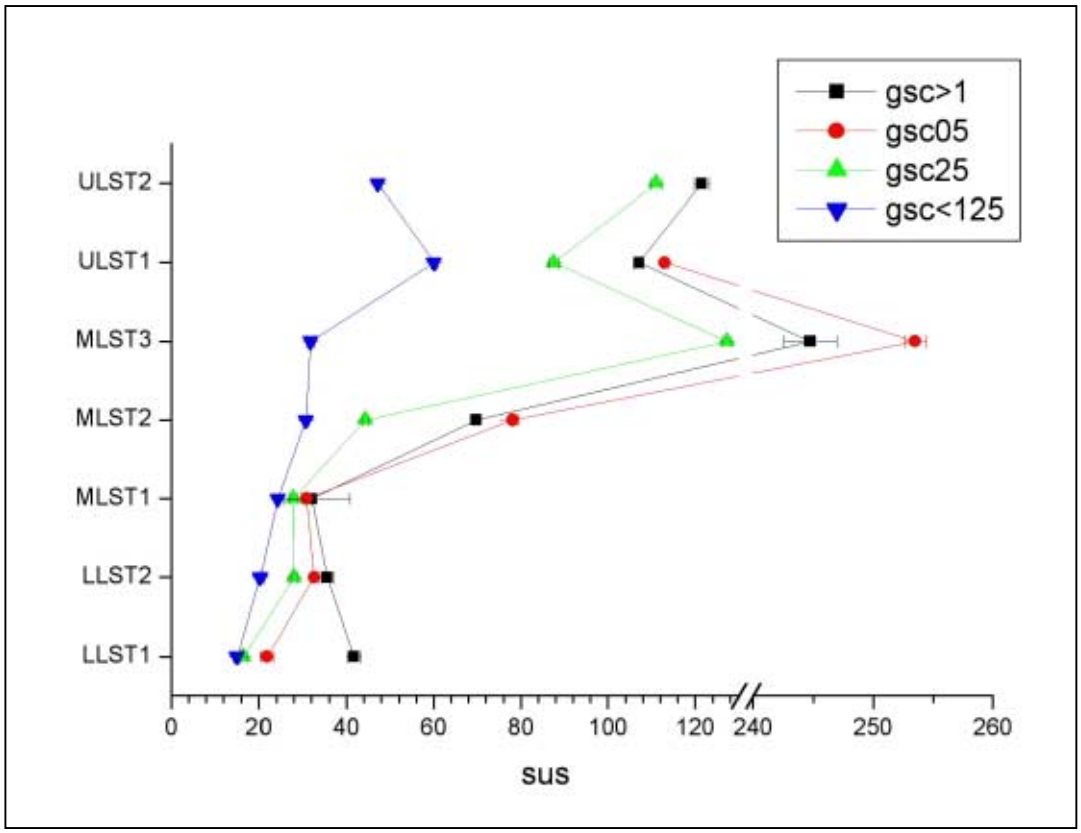

Figure 3.11: Susceptibility samples from the Wingertsberg. This graph solely shows the results of the laboratory measurements.

Figure 3.11 shows the sus of the laboratory measurements for the different gsc. All gsc > 0.125 mm show a more or less similar behaviour. The two gsc 1.0 to 0.5 and 0.5 to 0.25 mm have a significant peak at the sedimentological marker “Autobahn Mittelstreifen” (MLST3). The general trend of all gsc supports the hypothesis that more evolved magma corresponds to a lower sus.

Figure 3.12 gives an example for the difference in absolute values between field and laboratory measurements. It is important to note that laboratory and field measurements do not show the same trend. This may be explained by the different preparation methods; the field measurements are not comparable to the laboratory measurements. For example, a correct sieving was impossible because of sample wetness. The balance used in the field was

not as precise as the model used in the laboratory. These uncertainties are reflected in the wider error bars of the field measurements. Often it was impossible to prepare samples in the field, because they were too wet for exact sieving.

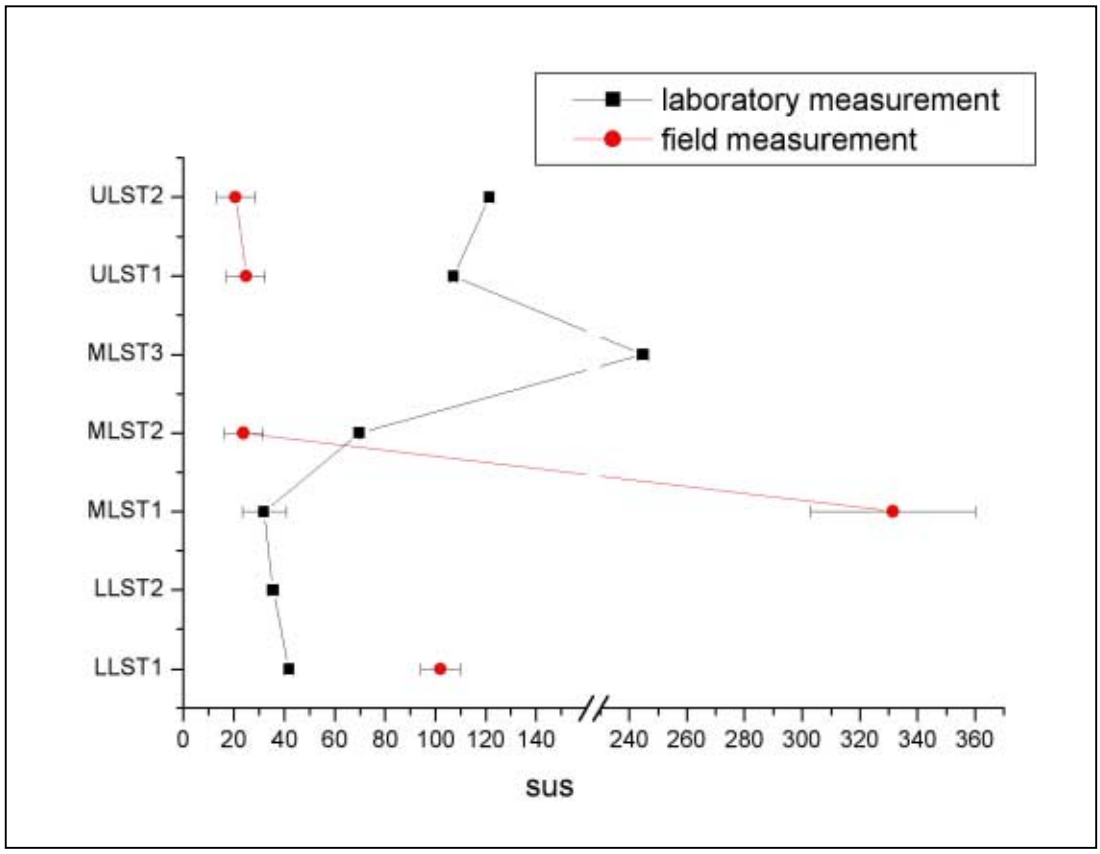

Figure 3.12: Values sus for the gsc for 1.0 to 0.5 mm mesh. Measurements from the field and from the laboratory are plotted.

3.5.4.4. Interpretation

The data from the Wingertsberg clearly show that a higher degree of magma evolution correlates with lower sus and higher γ-ray values. The γ-ray values, especially Th and U, thus reflect removal of material from of a zoned or layered magma reservoir. K on the other hand shows a slight increase at the top where the magma is more basic in composition. The inverse behaviour of K possibly relates to the increase of sanidine to the top of the eruption cycle (SCHMINCKE, 2000).

The increase of titanomagnetite amounts, documented by SCHMINCKE (2000), can be observed in our measurements for the grain size depended magnetic susceptibility. As it can be seen in figure 3.11 the very fine gsc shows a relatively continuous increase of the sus values from the base to the top. A significant peak can only be found in the ULST1, but not in the sedimentological marker horizons MLST2 and MLST3. The gsc coarser than 0.125 mm all show a significant peak at the MLST3 that is also a sedimentological marker horizon. Especially the gsc between 1.0 to 0.5 and 0.5 to 0.25 mm indicate high values of the sus. The

coarser gsc thus mirror the evolution of the magma, and except of the marker MLST3, a well developed trend can be observed (upsection more ti-magnetite = more basic composition). Although all gsc show the same trend, it would be better to choose the same gsc as for the measurements on Vulcano, because, these classes show more or less the same trend for nearly every layer, whereas the coarsest gsc can be affected by geometrical problems during the measurement and the correlation is not as reliable as between the other two gsc.

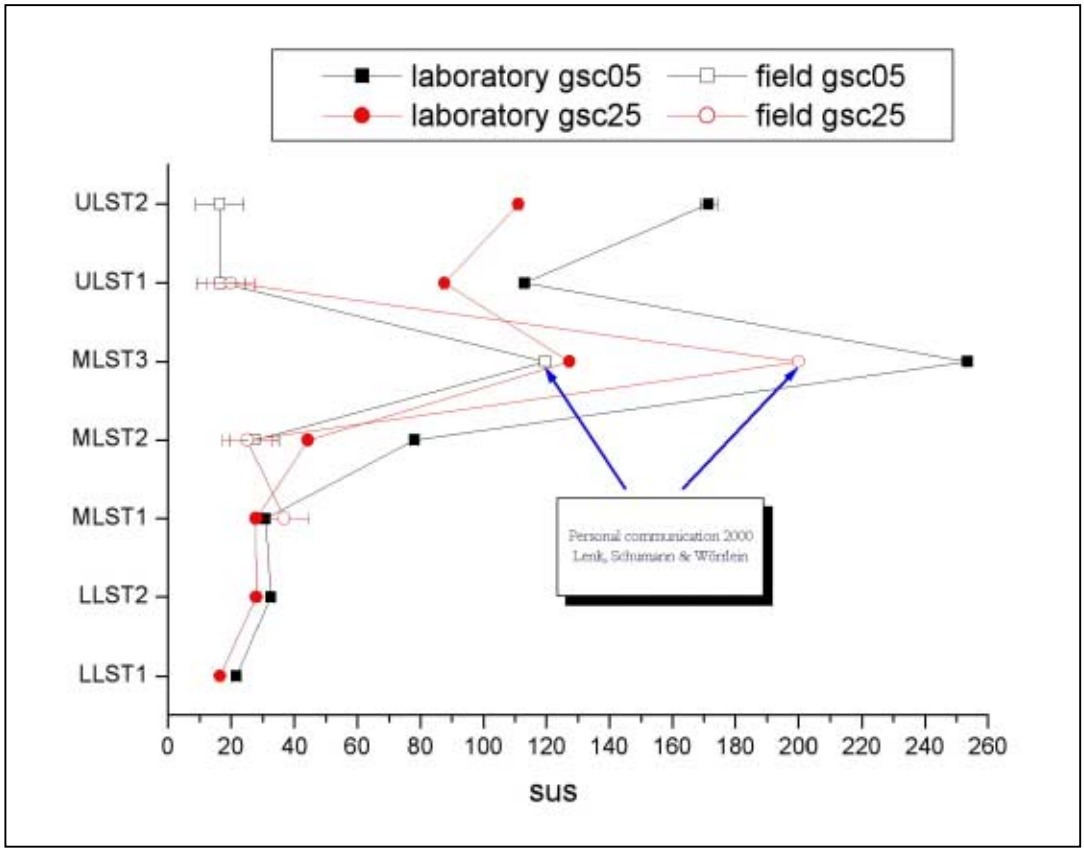

Figure 3.13: Measurements of the sus for the location Wingertsberg, with grain size classes 0.5 to 0.25 and 0.25 to 0.125 mm, shown are both results (field and laboratory), whereas the field values for MLST3 base on data from LENK, SCHUHMANN, AND WÖRRLEIN 2000 (pers. comm.).

The samples measured in the field do not show a clear trend, they only can give an overall value of the sus. Differences between laboratory and field measurements of the sus of the Wingertsberg are shown in figure 3.13, herein solely the gsc used for the characterisation of Vulcano-samples are shown. In general it is noticeable that the prominent marker is visible in the laboratory as well as in the field measurements.

Summarising it can be said that the γ-ray values as well as the sus measurements reflect the magma evolution. The results of sus measurements show that preparation of the samples and measurement in the laboratory is mandatory in respect of the resolution of the method.

4.Data

4.1. Sampling

γ-ray measurements were made in the field, and samples were only taken for sus measurements. In general the sample weight ranged between 600 and 1000 g. This mass is sufficient for the preparation in the laboratory, so that enough material (7 g) for a measurement of one gsc can be obtained.

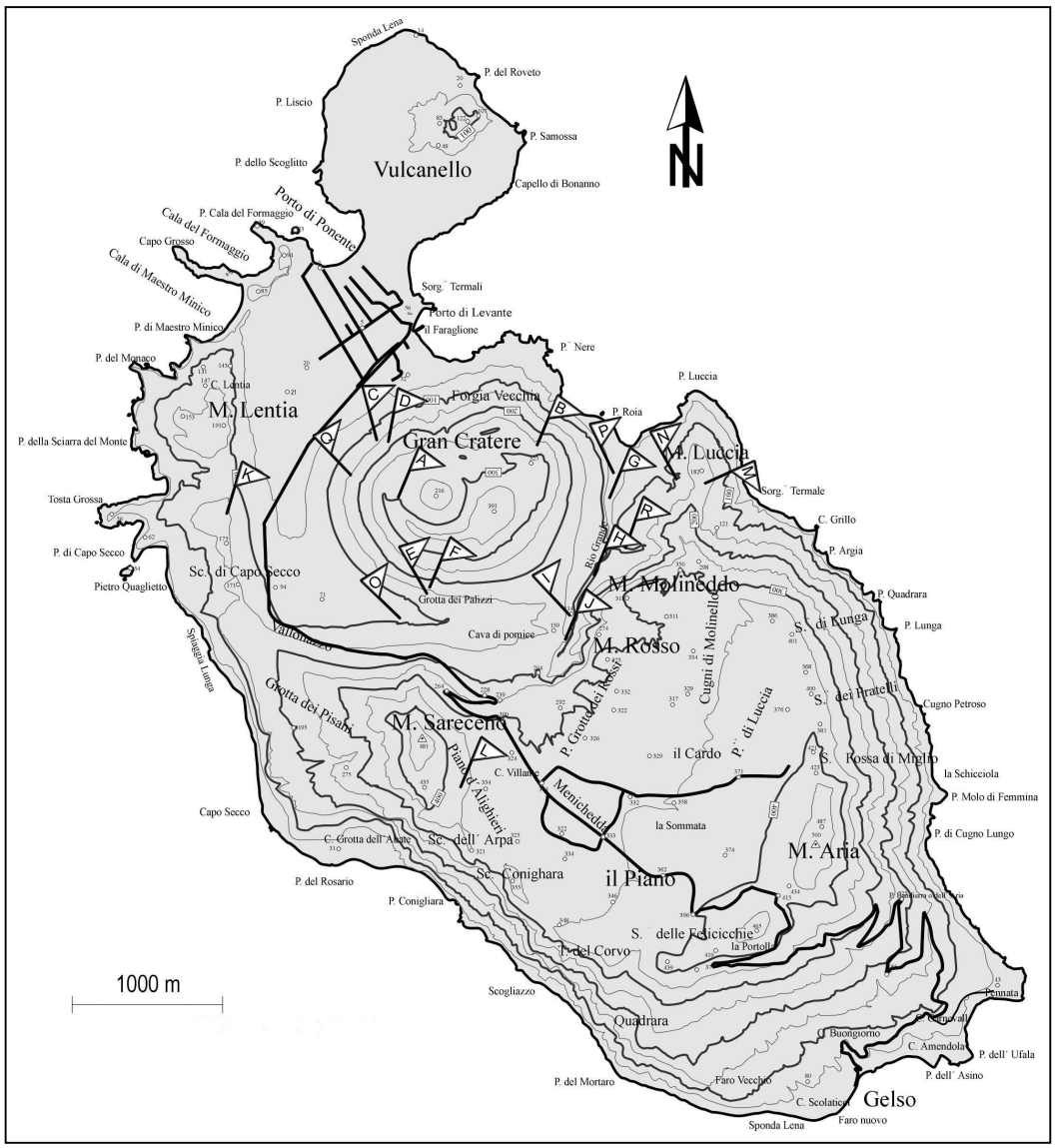

Figure 4.1: Sample locations at Vulcano (digitised and modified map from AGIP, 1981).

Before sampling any surficially altered material was removed. In general the 2 types of surge deposits – dry- and wet-surge deposits – can be distinguished in the field macroscopically: the dry-surge deposits normally consist of grey, loose to semiconsolidated ash layers which can sometimes present intercalations of Pele's hair. The wet-surge deposits generally show a higher degree of consolidation and vary in colour from pale yellow, reddish, pinkish, greenish

and orange to a light grey-green and ochre. Often vesiculated tuffs, accretionary lapilli and plastic deformation can be observed.
The samples were measured (γ-ray measurements) and taken at 17 different outcrops shown in figure 4.1 and prepared for sus measurements as described before (chapter 3.2).

4.2. Gamma-ray

4.2.1. Error

4.2.1.1. General Remarks

The error for the gamma-ray measurements is composed of two main components: the error of the spectrometer measurement and the error related to the thickness and geometry of the layer. The standard error for the measurement is described as:

$$a = \frac{s}{\sqrt{n}}$$

a = standard error for the measurements
s = standard deviation
n = number of measurements

The penetration radius of the gamma ray spectrometer is, in a simplified model for the measurements at La Fossa di Vulcano, assumed to be a semi-sphere with a radius of 13 cm. It is derived from assumptions especially of HECKEMANNS AND KRÄMER (1989), KOCH (1984), and LOVBORG ET AL. (1971) with changes for the fieldwork at La Fossa di Vulcano (see 4.2.1.2).
If the thickness of the layer is lower than the penetration sphere an error caused by the thickness (b) has to be considered. The combination of both errors (thickness error and standard error for the measurement) gives the absolute error for the value, described by the following equation:

$$\sigma = \sqrt{a^2 + b^2}$$

a^2 = standard error for measurement
b^2 = thickness error
σ = standard error, absolute error

The influence of the over- and underlaying deposits is shown below for the location Wingertsberg (Eifel, see chapter 3.5).

4.2.1.2. Thickness Influence

After measurements for the thickness influence at a significant layer at the Wingertsberg (Laacher See, Eifel) (see also figure 4.2) and theoretical calculations of different penetration radii in correlation with layer thickness, a radius of 13 cm for the main penetration area of the gamma-ray was chosen for this study. This value shows a good relation between radius and error, and (KOCH, 1984) demonstrates that this radius contains the area with highest influence on the measurement. For the measurements on Vulcano a simplified model of a sphere is used.

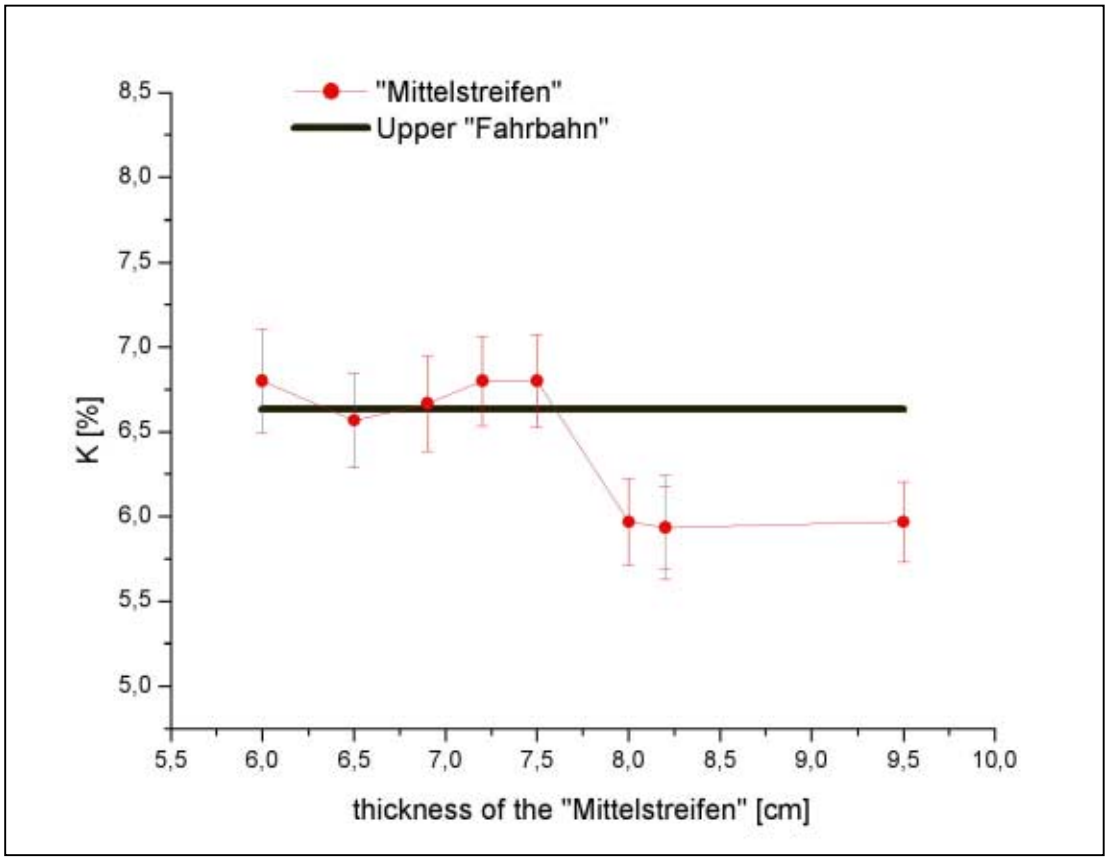

Figure 4.2: γ-ray-measurements of the "Mittelstreifen" (Wingertsberg, Laacher-See, Eifel) in relation to the thickness of the layer. Values of the overlying Upper "Fahrstreifen" are given for comparison. Up to a critical thickness (ca. 7.5cm) the values of the "Mittelstreifen" are affected by the neighbouring "Fahrstreifen".

The intensity of the radiation can change with the distance of the detector. A big gap between detector and sample in the field can generate an error in the measurements, whereas a small gap of a few millimetres (less than 0.5 cm) between detector and sample does not affect the measurement in a significant way (KOCH, 1984). This observation is also valid for samples measured in the laboratory.

4.2.1.3. Influence of Wetness

The influence of wetness on the γ-ray-measurements can be neglected for this study. Measurements made in the laboratory at different degrees of sample wetness showed no significant change of the γ-ray amounts, although higher amounts of water can disturb the measurement itself. As shown in figure 4.3 up to 4% of water in the sample generally do not change the amounts of the measurement in a significant way. The relatively dry environment of Vulcano island, with the exception of heavy rain falls and storms in the winter, allows measurements on more or less dry rocks. Thus the wetness of the deposits can be assumed to be in general less than 4%. MYERS AND WIGNALL (1987) think that variable degrees of moisture can influence the amount of some elements like U in the measurement, thus they prefer sections with constant moisture. According to KOCH (1984), the wetness of the rocks does not disturb the investigation. Nevertheless he worked normally with hard rocks, whereas this study is concerned mainly with semi consolidated rocks.

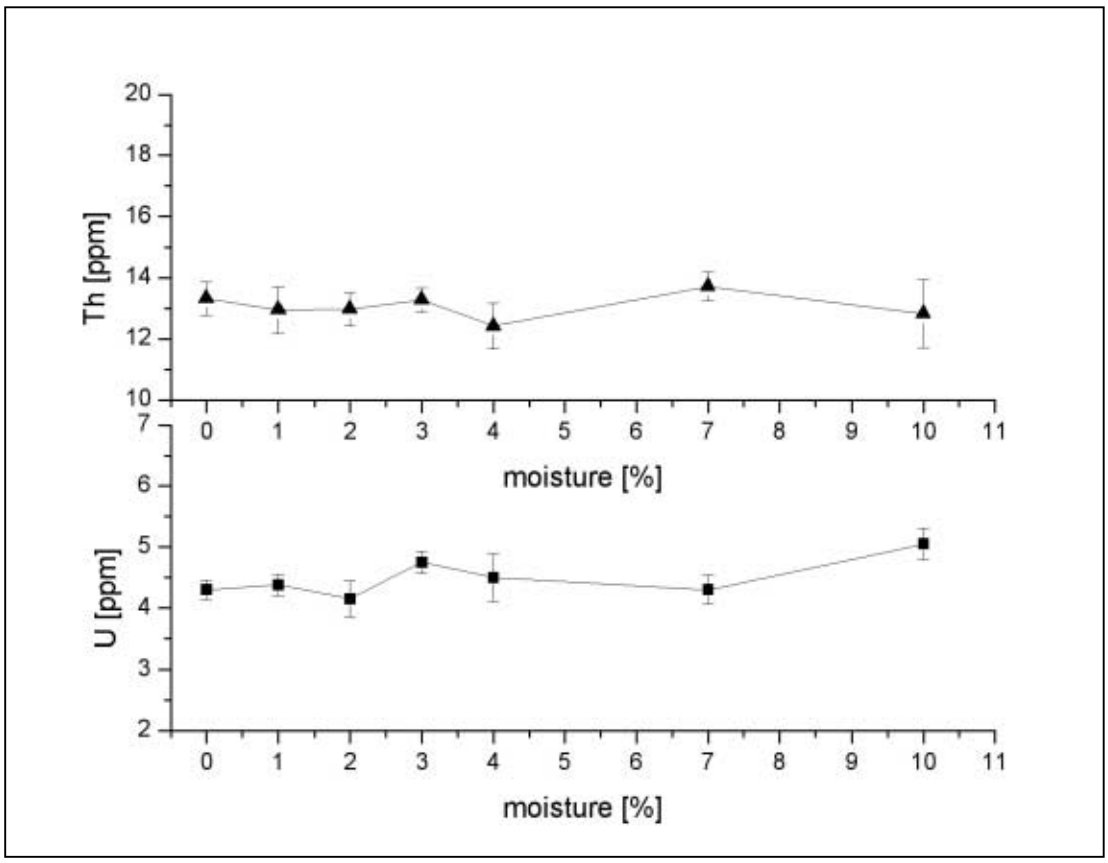

Figure 4.3: Interdependence of wetness γ-ray-measurements. Laboratory measurements of different samples from La Fossa di Vulcano, with increasing wetness.

4.2.2. Data

γ-ray data of the standard outcrop H are shown as an example. This outcrop is attributed to the succession of Punte Nere and located in the Vallone della Roia. The data of the remaining 16 outcrops are shown in Appendices I and II.

sample	K [%]	U [ppm]	Th [ppm]
Ha1	6.03 ± 0.1	14.97 ± 0.1	48.57 + 0.9
Ha2	6.30 ± 0.1	14.33 + 0.2	47.33 + 1.3
Ha3	6.07 ± 0.1	14.20 + 0.0	45.43 + 0.5
Ha4	6.13 ± 0.0	14.37 + 0.7	46.97 + 1.4
Ha5	6.10 ± 0.0	14.87 + 0.2	44.67 + 1.1
Ha6	6.00 ± 0.1	13.67 + 0.3	44.13 + 0.5
Ha7	6.03 ± 0.1	14.40 + 0.1	46.80 + 0.4
Ha8	5.97 ± 0.2	14.20 + 1.1	44.30 + 1.9
Ha9	5.73 ± 0.1	14.20 + 0.6	41.20 + 1.1
Ha10	6.00 ± 0.1	13.07 + 0.5	45.67 + 1.0
Ha11	6.23 ± 0.0	14.00 + 0.7	44.80 + 1.7
Ha12	6.10 ± 0.0	13.73 + 0.3	44.03 + 2.1
Ha13	6.13 ± 0.1	13.70 + 0.2	45.40 + 1.3
Ha14	6.13 ± 0.1	14.90 + 0.4	45.27 + 1.0
Ha15	6.27 ± 0.1	13.73 + 0.7	47.00 + 1.2
Ha16	5.87 ± 0.1	13.93 + 0.6	45.13 + 0.7
Ha17	6.03 ± 0.0	14.13 + 0.4	44.67 + 1.4
Ha18	5.93 ± 0.1	13.77 + 0.7	44.07 + 0.9

Table 4.1: γ-ray values of outcrop H (succession Punte Nere). The error values contain the standard error as well as the thickness influence of the layer.

4.3. Grain size depended magnetic susceptibility

4.3.1. Error

The error for the measurements of the sus can be described as a function of the accurateness of the mass weight and the internal error of the measurement.

The accurateness of the weight depends on where the measurements are performed, because the balance used on Vulcano has a higher error than the balance used in the laboratory where most of the samples were measured. Manual sieving without a machine can also produce higher errors. The weight error is described as:

$$f_M\,\% = \frac{f_W}{m} * 100$$

f_M = weight error

f_W = accurateness of the balance

m = mass of the sample used for the measurement

The second important source of the error is the standard error for the measurement.

$$\sigma = \frac{s}{\sqrt{n}}$$

$$f_{s\tan d}\% = \frac{f_{s\tan d}}{\bar{x}} * 100$$

$\sigma = f_{stand}$ = standard error for the measurement
s = standard deviation
n = number of measurements
$\bar{x}$ = mean value of the measurements

The total error can be described by the following equation:

$$f\% = \sqrt{(f_M\%)^2 + (f_{s\tan d}\%)^2}$$

If the values of the magnetic susceptibility are standardised for 1 g the error can be described by the following equation:

$$f_{norm} = \frac{x_{norm}}{100} * f\%$$

x_{norm} = is the for 1 g standardised mean value of the sample
f_{norm} = absolute error for the standardised mean values

4.3.2. Data

Data for the sus and additional information about location and granulometry of outcrop H, which can attributed to Punte Nere, are shown as an example (see table 4.2). The other outcrops can be found in Appendices I and II.

sample	distance from the vent [m]	Md [ϕ]	Ms [ϕ]	height [m]	sus05	sus25
Ha1	1150	1.42	1.77	0.29	122.52 ± 0.2	127.17 ± 0.3
Ha2	1150	0.28	1.00	0.78	110.69 ± 7.9	113.10 ± 8.1
Ha3	1150	0.98	1.49	0.97	129.04 ± 0.2	137.40 ± 0.2
Ha4	1150	0.92	1.37	1.21	111.15 ± 0.2	131.11 ± 0.3
Ha5	1150	0.63	1.13	1.52	130.10 ± 9.3	121.90 ± 8.7
Ha6	1150	0.92	1.42	1.85	136.04 ± 0.2	142.03 ± 0.2
Ha7	1150	0.97	1.40	2.09	125.39 ± 0.2	113.76 ± 0.1
Ha8	1150	0.62	1.19	2.28	103.11 ± 0.1	98.32 ± 0.2
Ha9	1150	0.66	1.17	2.42	135.24 ± 0.2	132.26 ± 0.2
Ha10	1150	0.66	1.18	2.56	131.99 ± 0.3	145.12 ± 0.2
Ha11	1150	0.72	1.27	2.79	117.35 ± 0.2	94.48 ± 0.2
Ha12	1150	0.74	1.23	3.12	133.53 ± 0.2	142.00 ± 0.2
Ha13	1150	0.90	1.33	3.46	153.50 ± 0.2	135.35 ± 0.3
Ha14	1150	1.14	1.54	3.78	77.93 ± 0.1	86.84 ± 0.1
Ha15	1150	0.78	1.27	4.28	107.48 ± 0.2	98.90 ± 0.1
Ha16	1150	0.76	1.28	4.59	122.51 ± 0.2	170.03 ± 0.3
Ha17	1150	1.07	1.46	4.88	135.82 ± 0.2	142.37 ± 0.2
Ha18	1150	0.75	1.23	5.32	109.66 ± 0.2	107.42 ± 0.2

Table 4.2: sus, common, and granulometric values of outcrop H (succession Punte Nere). The sus is measured in cgs mode, standardised to 1g, and has to be extended to 10^{-6}.

4.4. Microprobe

Samples belong to different successions of La Fossa di Vulcano. Sample characterisation is given in table 4.3.

sample	succession	gsc
Ia9	Punte Nere	gsc25
Ja18	Punte Nere	gsc05
Ob38	Tufi Varicolori	gsc25
Fc10	Palizzi	gsc25
Bd26	Commenda	gsc05
Rs16	dry-surge (possibly Punte Nere or Palizzi)	gsc05

Table 4.3: Samples for the microprobe measurements. Gsc denotes which grain size class the magnetites were taken from.

In each thin section 20 minerals were measured. The mean values of the measurements are shown in table 4.4 as the result of total cations for a unit cell with 32 oxygen and as the result of oxides (below).

a)

Probe	Si^{4+}	Al^{3+}	Mg^{2+}	Ti^{4+}	Mn^{2+}	Cr^{3+}	Fe^{2+}	Fe^{3+}	total cations for a unit cell with 32 oxygen
Ia9	0.028	1.829	1.524	1.736	0.120	0.048	8.077	10.623	23.986
s	0.008	0.123	0.131	0.139	0.030	0.007	0.234	0.320	0.004
Ja18	0.039	1.786	1.536	1.778	0.110	0.045	8.113	10.575	23.981
s	0.039	0.050	0.066	0.059	0.011	0.009	0.119	0.092	0.020
Ob38	0.042	2.049	1.826	1.355	0.078	0.213	7.430	10.987	23.979
sn	0.048	0.069	0.121	0.062	0.011	0.029	0.146	0.152	0.024
Fc10	0.033	1.912	1.592	1.565	0.102	0.044	7.854	10.882	23.984
s	0.008	0.063	0.026	0.070	0.012	0.012	0.074	0.120	0.004
Bd26	0.033	1.446	1.303	1.724	0.119	0.021	8.285	11.053	23.984
s	0.011	0.037	0.029	0.022	0.014	0.010	0.040	0.055	0.006
Rs16	0.032	1.889	1.554	1.557	0.112	0.037	7.875	10.929	23.984
s	0.013	0.079	0.084	0.038	0.025	0.006	0.094	0.074	0.006

b)

Probe	SiO_2	Al_2O_3	MgO	TiO_2	MnO	Cr_2O_3	FeO	Fe_2O_3	total
Ia9	0.10	5.35	3.53	7.96	0.49	0.21	33.30	48.67	99.60
s	0.03	0.37	0.31	0.62	0.12	0.03	0.88	1.55	0.53
Ja18	0.14	5.24	3.56	8.16	0.45	0.19	33.51	48.55	99.79
s	0.14	0.16	0.16	0.26	0.05	0.04	0.44	0.49	0.37
Ob38	0.14	6.01	4.23	6.22	0.32	0.93	30.70	50.45	99.01
sn	0.16	0.22	0.30	0.26	0.05	0.13	0.49	0.92	0.62
Fc10	0.11	5.59	3.68	7.18	0.42	0.19	32.39	49.88	99.45
s	0.03	0.18	0.06	0.33	0.05	0.05	0.37	0.52	0.41
Bd26	0.11	4.18	2.98	7.82	0.48	0.09	33.79	50.09	99.55
s	0.04	0.11	0.07	0.10	0.05	0.04	0.18	0.30	0.29
Rs16	0.11	5.51	3.59	7.12	0.46	0.16	32.40	49.97	99.32
s	0.05	0.24	0.20	0.17	0.10	0.02	0.36	0.42	0.37

Table 4.4: Results for the microprobe measurements. The upper part (a) shows the results for the cations calculated for a unit cell with 32 oxygen and the lower part (b) shows results as oxides. s mean standard deviation.

The cations can occupy different places in the structure, which are characterised by the valence and bonds: for the spinell crystal 2 main types can be distinguished. The spinell-magnetite-chromite group has the common equation AB_2O_4, whereby the elements of group A are located at the tetrahedron location/place of the cell, and the elements of B are located on the octaeder places of the unit cell. Elements can change places within both groups without great difficulties, but a change between the two groups is only possible if the spinell is so-called inverse (for example magnetite). Elements belonging to group A are Mg, Fe^{2+}, and Mn. for B these are Al, Fe^{3+}, and Cr. Figure 4.4 shows the distribution of the elements split up into the two groups for all samples.

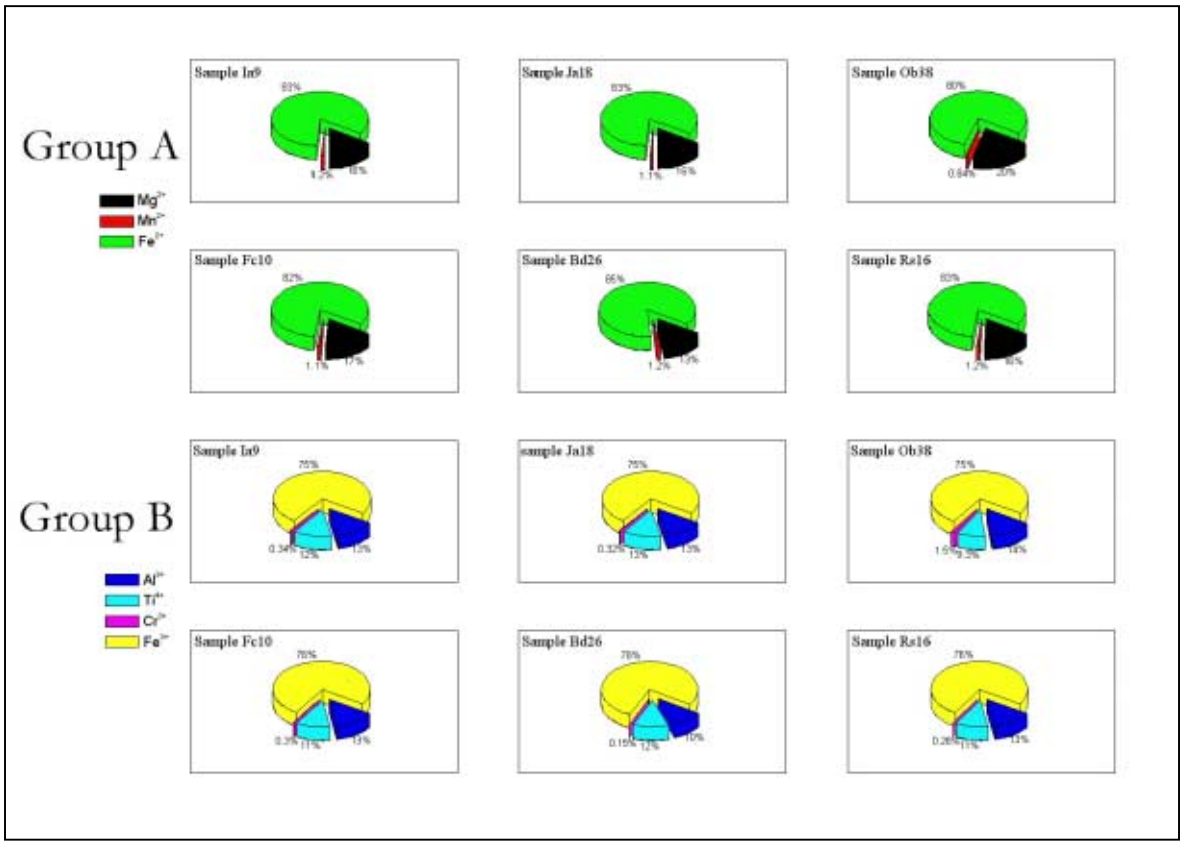

Figure 4.4: Pie charts of the two types of the spinell structure. Microprobe samples show the distribution for the different elements attributed to the same group.

5. Characterisation of Standard Outcrops

5.1. Theoretical Background

5.1.1. Granulometry

The distribution of Ms and Md vs. the distance from the vent can demonstrate elutration, depletion or enrichment of grain size. No significant change of Ms or Md can be observed for the successions of La Fossa (see also figure 5.1 and Appendix VI).

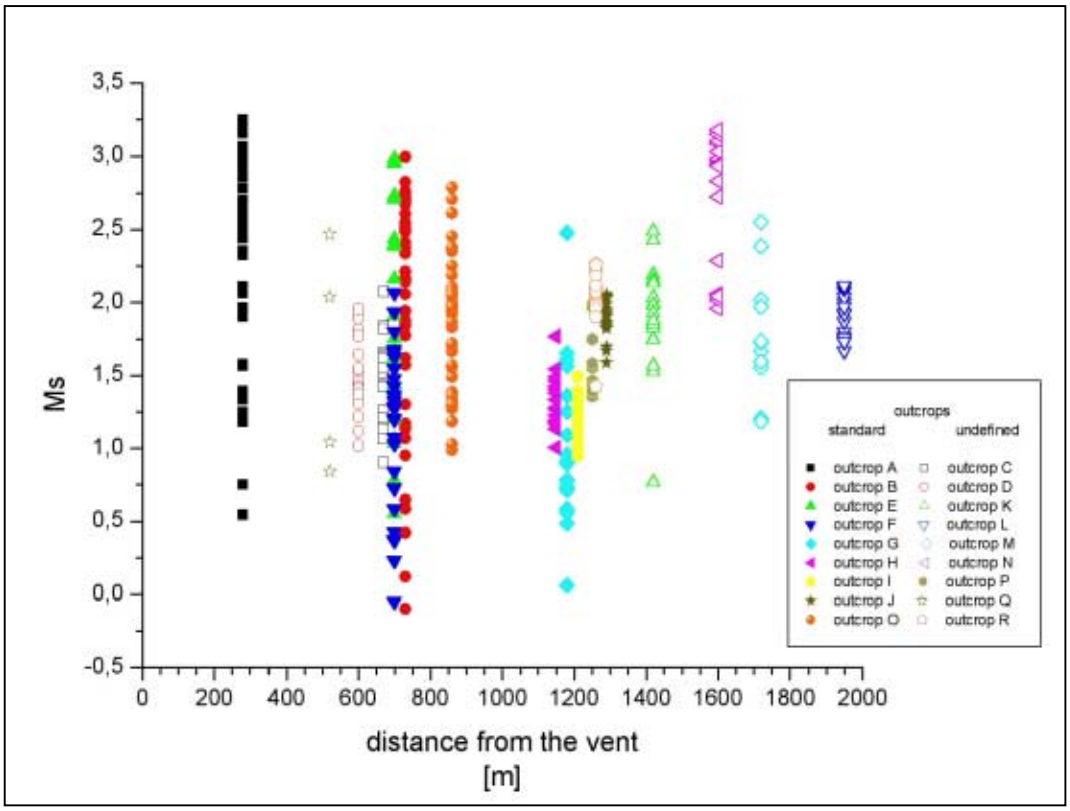

Figure 5.1: Ms vs. distance for the different outcrops at La Fossa cone.

The cumulative grain size curves show the grain-size distribution, without the effect of the non-equidistant mesh-rates. These curves allow to get information about the distribution over the whole grain-size range. Slope and shape of the curves allow interpretation of the depositional system (e.g. FISHER AND SCHMINCKE (1984) and SHERIDAN (1971)).

Histograms or grain distribution curves could be a reference for some successions. Patterns vary for the different successions, in particular in the fine grain size classes where a negative skewness is often observed. The skewness is a symmetry degree of the grain dispersion, when coarser gsc dominate the sample in general the histogram shows a positive (fine skewed) skewness, in contrary if the finer gsc dominate the sample the skewness is so-called negative (coarse-skewed) (TUCKER, 1985).

A scatter diagram where the median grain size is plotted as a function of the standard deviation of the samples allows a classification of the pyroclastic samples (LIRER AND VINCI, 1991, and WALKER, 1971). WOHLETZ (1983) applied this kind of plot to discriminate different sedimentary structures of hydrovolcanic pyroclastics. The samples of La Fossa di Vulcano are generally pyroclastic surge deposits. The scatter plot of gsc vs. standard deviation shows trends particular to each succession. Often a change of the slope can be observed.

5.1.2. Magnetic Susceptibility

The sus reflects the magmatic evolution. A higher degree of magmatic evolution corresponds to lower values of sus. Weathering and leaching do not affect the sus to the same degree as the γ-ray measurements (see chapter 5.1.3). In contrast to the γ-ray measurements no significant difference between dry- and wet-surge deposits can be detected. The successions can often be distinguished by their sus. Sometimes it is possible to observe an internal trend inside a succession. The current accuracy of the method does not allow observations of transport effects.

Important susceptibility-bearing minerals are magnetite, titanomagnetites and their derivates (see also chapter 3.2). The susceptibility-bearing minerals of the La Fossa successions fall into grain size classes of 0.5 to 0.125 mm. Crystals can show ideal morphology as well as subrounded grains sometimes looking like little balls (see also figure 3.8). But also grain fragments embedded in a matrix of crystals (see also figure 3.8) or altered yellow to brownish material (see also figure 3.8) can be observed as well. The latter seem to be small crystals or fragments of crystals. In a single sample solitaire minerals as well as embedded crystals exist, but in the samples the ratio of both components can differ independent of the kind of succession as it is known so far.

The sus is also a powerful tool to define marker horizons. In some successions an important peak, normally positive, can be observed that can be correlated between several outcrops. This marker can occur in both or only in one grain size. It is important to note that because of the sometimes very thin and numerous layers not every potential marker can be found in every potential outcrop with the resolution achieved by this investigation.

Effects of alteration are visible especially near the vent where several fumaroles exist. The layers affected by this alteration are often hardened and bleached. They are equally characterised by highly variable sus values (especially in outcrop A, described in chapter 5.2.4).

A correlation exists between the strength of the oriented sus that is important for the AMS-measurements, and the sedimentation parameters of the deposits (MARCO, 1998 and VEROSUB, 1977). For example, the changes of the detrital remanent magnetisation (DRM) can be used for correlation of the deposits. Aim for the pyroclastic deposits in general the eruption centre is the searched location (LE PENNEC ET AL., 1998, MACDONALD AND PALMER, 1990, ORT ET AL., 1999, and PISCITELLO ET AL., 1999). On Vulcano island in general the location of

the younger deposits of La Fossa is known relatively well and processes like bioturbation are uncommon. The measurements made for this thesis were prepared and carried out in the laboratory, thus the orientation of the sample had no influence.

A sus crossplot for the grain size classes – the coarser is the ordinate and the finer is the abscissa – is another discrimination tool for the different successions. They show the influence of secondary effects like reworking. For example, when weathering and agglomeration preferentially remove the finer material, the residual susceptibility will be higher for the coarse grain size than for the finer grain size. In consequence, the slope will be >1. A higher susceptibility for finer material (slope <1) suggests destruction and weathering of coarser material. A slope = 1 indicates that no secondary processes have altered the original grain size distribution/susceptibility distribution, and will provide information about the magma chamber processes. A flattened slope is an example for reworking or relatively large minerals. The latter indicate either a long residence time inside the magma chamber where they can grow, or the fragmentation energy was very small. Microscopic examination of clast characteristics could help distinguish between the two options. To destroy a mineral very high energy is needed. Another possibility of a potentional coarser grain is that the mineral is embedded into glass or fragments of the melt, which can have high cooling rates, or the fragmentation energy was lower. These assumptions are only realistic if the susceptibility-bearing minerals are most abundant in these two grain size classes. For this thesis an equal dispersion of the susceptibility bearing minerals for the two gsc05 and gsc025 is assumed. These classes show the maximum sus values which are in general similar for one sample.

Weathering conditions can alter magnetite and titanomagnetite into limonite and hematite, but in general these transitions take a long time. Maghemit (γ-Fe_2O_3) can be created by oxidation of magnetite and could retain some magnetic properties.

5.1.3. Gamma-ray

Like the sus, also γ-ray values in a succession depend on the evolution of the magma. The higher the magma is evolved the higher are the γ-ray values (CHIOZZI ET AL., 1999). Transport effects like enrichment or depletion cannot be observed in plots of Ms vs. γ-ray. Changes between wet- or dry-surge conditions can modify the amount of U, Th or K. Weathering is a significant factor. In weathered outcrop faces the amounts e.g. of U and K are significantly lower. Groundwater or hydrothermal water can mobilise U and K as well. NOGAMI AND YOSHIDA (1995) give some experimental examples for leaching through acidic alteration, processes that are also likely on La Fossa di Vulcano. These reactions will be concentrated near the crater rim and in the areas of fumarolic activity.

The scatter plots of the γ-ray values indicate different groups or trends of successions. The difference between dry- and wet-surges can often be observed. A plot of an element against its ratio with another element reflects the degree of dependence of these elements.

An increase of the Th/U ratio suggests that Th is more sensitive than U in the specific process where the measurements are made (IMBÒ ET AL., 1968). These authors show that the values of Th and U in different samples generally behave in the same manner, with only a few exceptions where this covariation is disturbed. An increase of the Th/U ratio can for example indicate a greater degree of weathering or alteration with U being mobilised as an uranyl complex. On some volcanoes in Italy an evolution of the magma is reflected by the evolution of the U- and Th-values (IMBÒ ET AL., 1968). The Th/U ratio probably does not vary significantly during differentiation (IMBÒ ET AL., 1968).

The γ-ray data of IMBÒ ET AL. (1968) for some volcanic rocks on Vulcano where they measure trachybasalts, latites, and rhyolites have the following values for 31 samples:

U 5.0-35.0 ppm

Th 4.0-56.0 ppm

Th/U 1.0-2.0

In the same publication it is pointed out that the volcanics of Southern Italy in comparison with world-wide made investigations have a momentous higher amount of U and Th.

CHIOZZI ET AL. (1999) pointed out that the highest values of U measured on young obsidians of La Fossa cone range between 20 to 25 ppm, and CIVETTA AND GASPARINI (1973) get 57.5 ppm Th, 17.0 ppm U, 4.03 % K and a ratio Th/U of 3.4 for the Pietre Cotte rhyolite. The latter paper contains also data of older units of Vulcano island as well as data from other volcanic areas of Southern Italy like the other Aeolian islands, Ustica, Pantelleria, Linosa, and Mt. Etna. The amounts of U and Th of these areas are in general much smaller than the amounts of Vulcano island. However, especially the younger volcanic islands of the Aeolian Archipelago Stromboli and Vulcano show normally higher amounts of U and Th than the older parts.

5.2. Discussion of Individual Successions

5.2.1. Punte Nere

Standard outcrops: G,H, I, and J

5.2.1.1. Granulometry

The Punte Nere succession is formed by fine and coarse ash layers. In standard outcrops these ash layers have a Ms of about 1.35 ϕ with a standard deviation (s) of 0.5 ϕ. Outcrop G shows the largest variation of the median and the mean size. If the extreme maximum and minimum samples of outcrop G are not considered the Ms and s of Punte Nere is not affected significantly. In this case the standard deviation of outcrop G decreases and the Ms shows lower amounts (see also table 5.1).

sample	outcrop G	outcrop H	outcrop I	outcrop J	Punte Nere
min. value	0.06 (0.48)	1.00	0.95	1.59	0.06 (0.48)
max. value	2.48 (1.65)	1.77	1.49	2.06	2.48 (2.06)
mean	0.97 (0.94)	1.32	1.20	1.90	1.35 (1.36)
standard deviation	0.5 (0.3)	0.2	0.2	0.1	0.5 (0.4)

Table 5.1: Ms of Punte Nere in ϕ. The values in brackets are the corrected data of outcrop G, here the extreme maximum and minimum data are not considered.

The Ms does not change significantly with distance from the vent. All but the above mentioned outcrop G have a relatively small grain size range.

Histograms of the grain sizes in general show a Gaussian normal distribution, especially the data of the outcrops I and J.

The cumulative grain size curves for the data of the 4 outcrops are different (see also Appendix III). The two outcrops I and J, dominated by massive layers, have a more or less sigmoidal curve (the curves of outcrop I are a little bit more pronounced). For outcrop H, dominated by laminated layers, the cumulative grain size curves are flatter, normally without a distinctive sigmoidal curve. Outcrop G can be subdivided into two parts. The first shows laminated and massive dry-surge deposits. This part also has the highest and lowest values of the mean. Both layers are contributed to special deposits with different colour and layer characteristics. The layer with the lowest mean is a very fine and weak yellow to ochre ash-layer with a badly defined top boundary. The layer of the maximum mean has the same colour as the "minimum" layer, but this deposit is more nodular and terminated by a sharp boundary.

Neither in the massive nor in the laminated layer dominated outcrops a significant change in the evolution of Ms with los can be observed. The often relatively closely plotting curves are a reference for rather homogenous energetic condition during the eruptions. If the mean is coarser, as seen especially in outcrop G and parts of H and I, the sigmoidal character of the cumulative grain size curves is reduced. Sometimes there are higher amounts of coarser material as it can be seen for example in the dry-surge deposits of outcrop G. The material in the second part of outcrop G (channel) is coarser – documented by the Ms of 0.81 ϕ (s:0.2) – in comparison with the dry-surge deposits from outcrop G, if the maximum and minimum data of the yellow-ochre layers are corrected a Ms of 1.10 ϕ (s: 0.4) results.

The distribution of the different gsc in the eruption cloud was homogenous and the finer fraction was not depleted. This can be observed especially in cumulative grain size curves of outcrop J showing a relatively well developed sigmoidal shape. Outcrop J also shows a difference between the laminated and the massive layers, here the laminated layers start with a higher value in the cumulative grain size curves, until 2 ϕ they plot a little higher than the massive layers (see also Appendix III). This can be a reference that the massive layers have a higher homogenity of the eruption cloud, whereas the laminated layers possibly have a depletion of fine ash. The Ms of the latter is slightly coarser so that the curve is shifted in comparison with the massive deposits. Type and classification of the cumulative grain size

curves especially of pyroclastic deposits are discussed for example by FISHER AND SCHMINCKE (1984), LIRER AND VINCI (1991), MACDONALD AND PALMER (1990), MOORE (1967), SHERIDAN (1971), WALKER (1984), WATERS AND FISHER (1971), and ZIMANOWSKI (1985).

The Ms and the s (1st and 2nd moment) normally show a linear correlation. Despite some overlap the different outcrops can be differentiated. The data for the linear regression of each outcrop are given in table 5.2. Outcrop I plots a slightly higher, but the kind of line shows the same character as the other outcrops of Punte Nere. The linear regression was done with the method of least squares, where:

$$Y=A+BX$$

A: Intercept value and its standard error.
B: Slope value and its standard error.

sample	A	B	R	SD	N
outcrop G	-0.75 ± 0.5	3.90 ± 0.4	0.94	0.66	16
outcrop H	-0.64 ± 0.3	3.89 ± 0.2	0.97	0.18	18
outcrop I	0.90 ± 1.1	4.37 ± 0.9	0.80	0.61	15
outcrop J	1.62 ± 0.8	2.67 ± 0.4	0.82	0.24	22
Punte Nere	0.26 ± 0.3	3.43 ± 0.2	0.90	0.69	71

Table 5.2: Results for the linear regression of Punte Nere samples in the scatter plot 1st moment vs. 2nd moment. R: correlation coefficient, SD: standard deviation of the linear regression, N: number of data points.

5.2.1.2. Susceptibility

The sus – measured in cgs mode, standardised to 1g, and extended to 10^{-6} – ranges from 44.18 units ± 0.1 to 153.50 units ± 9.3 (mean = 109.28 units, s: 23.0) for the gsc05. In the gsc25 values lie between 48.53 units ± 0.1 and 186.31 units ± 11.2 (mean = 117.18 units, s: 27.4). A change of the sus with distance from the vent cannot be observed. Table 5.3 shows the different values for the Punte Nere standard outcrops and the above mentioned mean sizes for all outcrops.

Generally, no trends in the sus were observed within samples of the same outcrop. However, if only one grain size is considered small trends are visible and some prominent peaks can be detected. The finer gsc in general is the more sensitive.

In contrast, a scatter diagram of the two gsc (sus05 vs. sus25) shows a prominent trend. The linear regression has a slope of 0.75 ± 0.1. The slope changes to 0.74 ± 0.1 if the channel filling from outcrop G is not considered. In general data of the single outcrops show this similar trend.

sample	outcrop G	outcrop G channel	outcrop H	outcrop I	outcrop J	Punte Nere
min. value 0.5-0.25 mm	44.18 ± 0.1	88.46 ± 0.1	77.93 ± 0.1	73.16 ± 0.2	93.55 ± 0.1	44.18 ± 0.1
max. value 0.5-0.25 mm	139.97 ± 0.2	141.55 ± 9.0	153.50 ± 9.3	148.86 ± 8.5	145.23 ± 0.2	153.50 ± 9.3
mean 0.5-0.25 mm	92.90 (s: 22.5)	112.42 (s: 15.3)	121.83 (s: 16.4)	100.65 (s: 19.4)	112.11 (s: 13.7)	109.28 (s: 19.8)
min. value 0.25-0.125 mm	48.53 ±0.1	87.89 ± 0.1	86.84 ± 0.1	75.91 ± 0.3	96.02 ± 0.1	48.53 ±0.1
max. value 0.25-0.125 mm	179.81 ± 0.3	167.03 ± 11.2	170.03 ± 8.7	186.31 ± 9.7	166.58 ± 0.3	186.31 ± 9.7
mean 0.25-0.125 mm	106.84 (s: 33.1)	122.56 (s: 20.6)	124.42 (s: 21.1)	109.15 (s: 27.7)	119.44 (s: 14.4)	117.18 (s: 24.1)

Table 5.3: Mean values of the sus for both gsc of Punte Nere. Outcrop G is split into the part without the channel and the cutting in channel. Samples are measured in cgs-mode and standardised to 1g, they have to be extend by 10^{-6}.

If the sus is plotted vs. the ratio of sus and Ms for most data a linear trend can be observed, its slope is more or less about 1 (see also figure 5.2). Data of outcrop J plots a little higher than the other standard outcrops of Punte Nere. Data of the outcrops H and I in general show similar behaviour for both gsc. As seen before data of outcrop G have been divided into samples of the dry-surges and samples of the channel filling. This channel fill is a secondary deposit that may include reworked epiclastic components. The channel fill samples plot in a different area than the dry-surge deposits of outcrop G and the samples from other outcrops, sometimes data of the dry-surge deposits and of the other outcrops can overlap. Between the two grain size classes no relevant change is visible (figure 5.2 shows the example for one gsc but the other class behaves in the same manner). Only the yellow-ochre nodular layer noticed above shows very high values for the ratio sus/Ms.

No significant trend or distribution can be observed when the sus of one gsc is plotted against the sus ratio of both gsc. Therefore the sus of any one gsc is not affected by the other gsc.

Laminated and massive beds of outcrops G, H, and J do not differ significantly if plotted into scatter diagrams sus05 vs. sus25 (see also Appendix III). Laminated beds of outcrop I show slightly higher values.

The presence of Pele's hair in outcrop I correlates with a lower sus in the coarser gsc, whereas the finer gsc is not affected. This relationship can be explained as follows: Magnetites commonly crystallise from the melt inside the reservoir. Abundance of Pele's hair and enrichment of magnetite in the coarser gsc could be an indicator for a low viscosity of the melt. However, an enrichment of Pele's hair can also indicate high ejection velocities, an intensive fragmentation, and an increment of the specific surface (e.g. ZIMANOWSKI ET AL., 1997 and ZIMANOWSKI ET AL., 1991). The latter implies a higher reaction surface e.g. for leaching that occurs in the eruption cloud. Leaching by aggressive fluids inside the cloud could change the mineral composition and can decrease the measured sus. In principle such early reactions can affect the γ-ray values as well (see also chapter 5.2.1.3). A sus low for

both gsc with Pele's hair is not found. In general the data of the massive layers show the lower values for the sus.

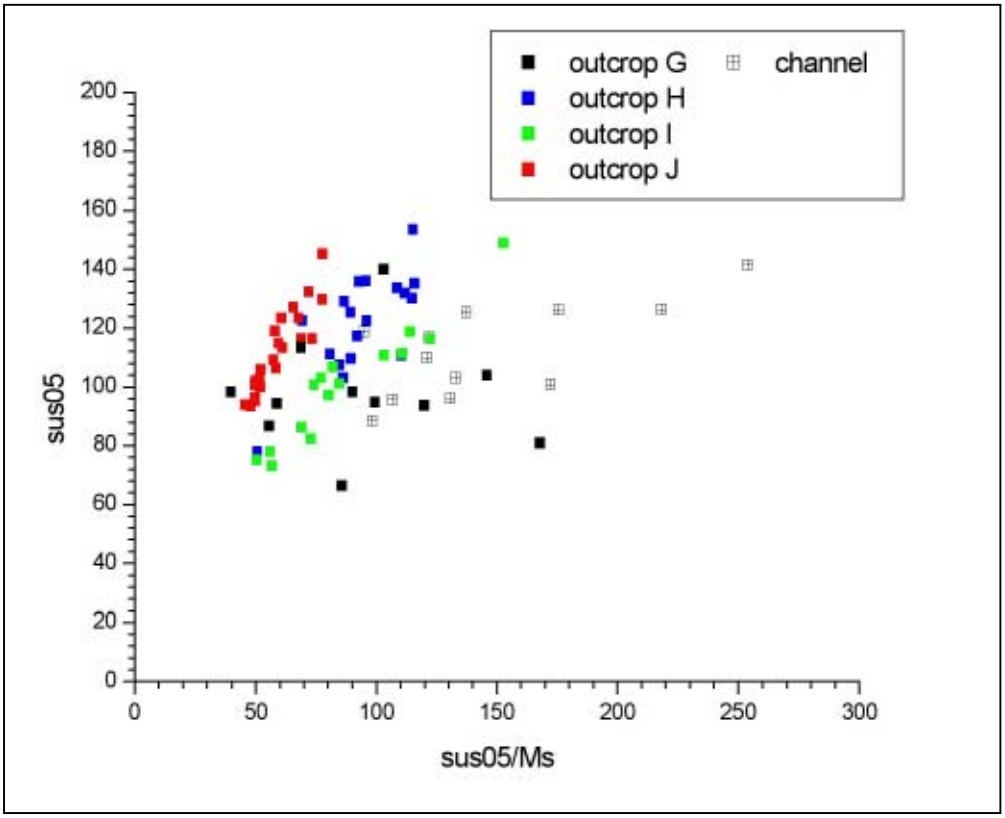

Figure 5.2 Scatter plot of the sus05 vs. the ratio sus05/Ms. Note the distinction between channel deposits and non-channel deposits in outcrop G.

Microprobe samples of Punte Nere magnetites were taken from outcrops I and J. Both samples have a high sus (for further information about the microprobe values see chapters 3 and 4). The Fe^{3+}/Fe^{2+} (1.31) and the Fe^{3+}/Ti^{4+} ratios, as well as the Ti^{4+} concentration are generally much lower than for the other successions (see also table 4.4). The Ti^{4+}/Cr^{3+} and Fe^{3+}/Cr^{3+} ratios are comparable to the data for Palizzi and the dry-surge deposits of outcrop R. The magnetites of Punte Nere are low-chrome titanomagnetites.

5.2.1.3. Gamma-ray

The mean γ-ray values for the standard outcrops are 5.57 % (s: 0.6) for K, 12.76 ppm (s: 1.4) for U, and 40.63 ppm (s: 3.7) for Th. In contrast to the sus values, the data of the channel deposits in outcrop G do not affect the measurements significantly (see also table 5.4). A change of the γ-ray values with distance from the vent cannot be observed.

sample	K [%]	U [ppm]	Th [ppm]
Minimum all samples	4.17 ± 0.3	9.17 ± 0.4	33.90 ± 0.5
Maximum all samples	6.83 ± 0.3	15.97 ± 0.4	49.23 ± 0.7
mean all samples	5.57 (s: 0.6)	12.76 (s: 1.4)	40.63 (s: 3.7)
Minimum without channel	4.17 ± 0.3	10.23 ± 0.9	33.90 ± 0.5
Maximum without channel	6.83 ± 0.3	15.97 ± 0.4	49.23 ± 0.7
mean without channel	5.70 (s: 0.5)	12.91 (s: 1.3)	40.72 (s:3.9)

Table 5.4: Minimum, maximum, and mean values of K [%], U [ppm], and Th [ppm] for Punte Nere standard outcrops.

Individual outcrops are characterised in various ways (see also table 5.5). Where massive deposits dominate in an outcrop, the K, U, and Th amounts are relatively low and comparable between outcrops (e.g. outcrops I and J). Their Th values are remarkable low in comparison to the data of the other outcrops.

sample	K [%]	U [ppm]	Th [ppm]
Minimum outcrop G	4.17 ± 0.3	11.10 ± 0.6	37.37 ± 1.0
Maximum outcrop G	6.20 ± 0.1	14.40 ± 0.2	49.23 ± 0.7
mean outcrop G	5.14 (s: 0.7)	12.95 (s: 1.1)	41.96 (s: 3.1)
Minimum outcrop G channel	4.17 ± 0.1	9.17 ± 0.4	36.27 ± 0.7
Maximum outcrop G channel	5.47 ± 0.1	14.40 ± 0.5	45.13 ± 0.8
mean outcrop G channel	4.80 (s: 0.4)	11.96 (s: 1.6)	40.15 (s: 2.6)
Minimum outcrop H	5.73 ± 0.1	13.07 ± 0.5	41.20 ± 1.1
Maximum outcrop H	6.30 ± 0.1	14.97 ± 0.1	48.57 ± 0.9
mean outcrop H	6.06 (s: 0.1)	14.12 (s: 0.5)	45.30 (s: 1.6)
Minimum outcrop I	5.07 ± 0.1	10.23 ± 0.9	33.90 ± 0.5
Maximum outcrop I	6.83 ± 0.3	15.97 ± 0.4	43.17 ± 0.2
mean outcrop I	5.71 (s: 0.5)	12.50 (s: 1.6)	37.16 (s: 2.7)
Minimum outcrop J	5.20 ± 0.2	10.90 ± 0.3	34.88 ± 0.8
Maximum outcrop J	6.23 ± 0.1	13.96 ± 0.7	42.23 ± 1.0
mean outcrop J	5.71 (s: 0.2)	12.17 (s: 0.8)	38.73 (s: 1.7)

Table 5.5: Maximum, minimum and mean values of K [%], U [ppm], and Th [ppm] for the different standard outcrops of Punte Nere.

Outcrop H, which contains mostly laminated layers, has the highest average values for all measured elements. The data of the channel deposits of outcrop G have relatively low values of K and U which are soluble elements. The channel deposits were formed by wet-surges and can possibly contain reworked material. Therefore, it can be assumed that the channel deposits are weathered because of a higher amount of water, and consequently depleted in the more soluble elements K and U, but not to the same degree compared to the sus data. Layers with Pele's hair usually have slightly higher γ-ray values, but the ratios of U/Th, Th/K, U/K, Th/U, K/U, and K/Th are not significantly changed in layers with Pele's hair.

Scatter plots of Ms vs. element concentration do not show any significant trends. No trends occur within an outcrop, although the data of the dry-surge deposits of outcrop G show a slightly upsection increase in Th, U, and K concentrations. The U/Th ratio does not follow this trend. Table 5.6 shows the range of the values for the different outcrops.

sample	**K** [%]	**U** [ppm]	**Th** [ppm]	**U/Th**
Punte Nere	**4.5-6.25**	**11.0-14.5**	**34-48**	**0.27-0.34**
G	4.5-5.0	11.0-14.5	35-47	0.25-0.34
H	5.75-6.25	13.0-15.0	43-48	0.28-0.34
I	5.0-6.25	11.0-14.5	34-43	0.31-0.36
J	5.25-6.25	11.0-13.5	34-43	0.29-0.34

Table 5.6: Average γ-ray values and the U/Th ratio of the different outcrops.

Data of outcrop H show the smallest range of the values. The relatively high values mirror the high sus values of the gsc05. Large differences between two sampling points can be observed especially in outcrop I and in the lower part of the channel of outcrop G.

Outcrop H is located in a hydraulic active zone and thus is the "wettest" of the Punte Nere standard outcrops. The leachable elements should be depleted, but this was not observed in this study. The vegetation that partly covers the outcrop could have protected it from excessive leaching. In addition, the outcrop is located in a narrow gully where heavy rain falls repeatedly exposed fresh material, thus minimising the time for weathering and leaching. The situation is similar for outcrop G where comparable values of U and K occur at the base of the outcrop. Outcrops I and J are located in a wider valley SW of this outcrops and heavy rainfall does not have the same erosional potential, here more intensive leaching because of the exposed nature of the outcrops is possible.

No significant differences of the data between the laminated and the massive layers of an outcrop can be observed. Only few sections of an outcrop show larger variations of the values that do not significantly affect the general trend.

Plotting element values vs. the ratio of two elements in the case of Th vs. K/Th a strong depletion of K in outcrop G can be observed (see also figure 5.3). This can be explained by the location of the outcrop cut by a channel of wet-surge deposits and the exposure in the

gully, outcrop H which shows some significant peaks for the average values does not react in the same way. It is also interesting to note that the data of outcrop H have slightly elevated Th concentrations relative to the data of outcrops I and J.

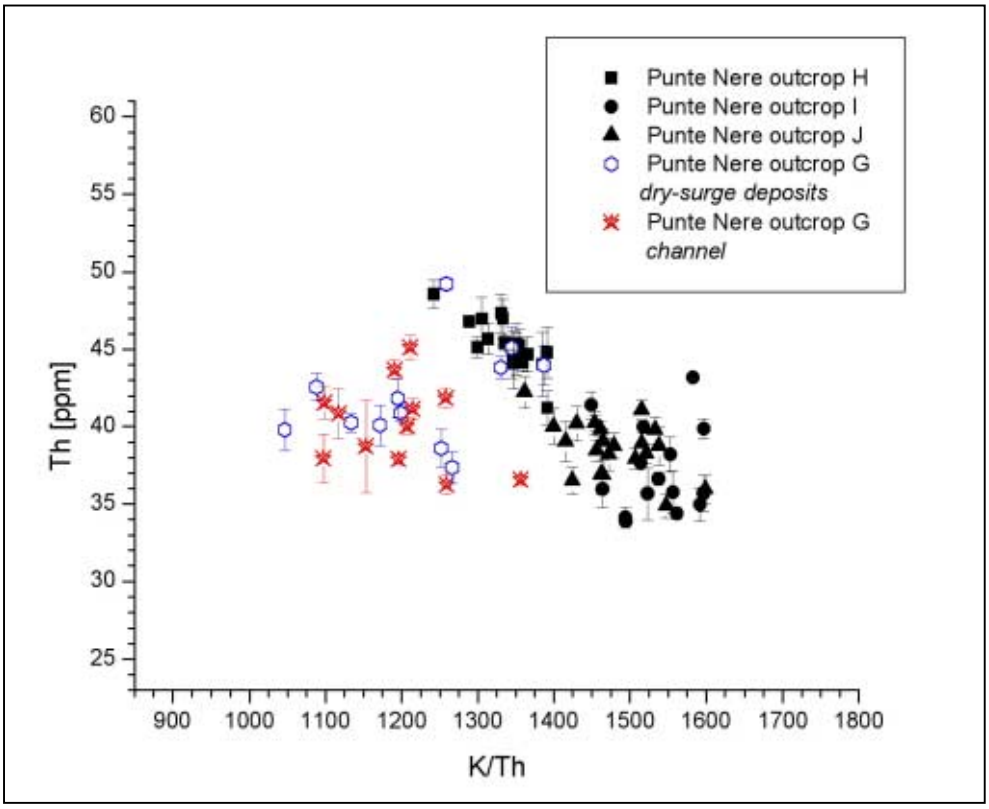

Figure 5.3: Scatter plot of Th vs. K/Th for the succession of Punte Nere. Outcrops are represented by different symbols. Data of outcrop G split into dry-surge deposits and channel deposits and show a significant K-depletion.

Plots of K vs. the Th/K and U/K ratios allow the distinction of Punte Nere from Tufi Varicolori (see also figure 5.4). The other successions cannot be distinguished in the same way, in particular not Palizzi and Cratere Attuale. However, if the data of the K-depleted channel deposits of outcrop G are not considered, the Punte Nere succession is well distinct from the Commenda succession.

Punte Nere can be discriminated from Tufi Varicolori based on the Th concentration vs. the K/Th and U/Th ratios. If again the data of outcrop G are not considered Commenda can also be discriminated. Frequently Palizzi can be discriminated from Punte Nere in a scatter plot of Th vs. U/Th. Uranium is also sensible to define different outcrops. In particular the plot U vs. K/U is also a good tool to distinguish Punte Nere from other successions, as long as the data of outcrop G and the channel are disregarded.

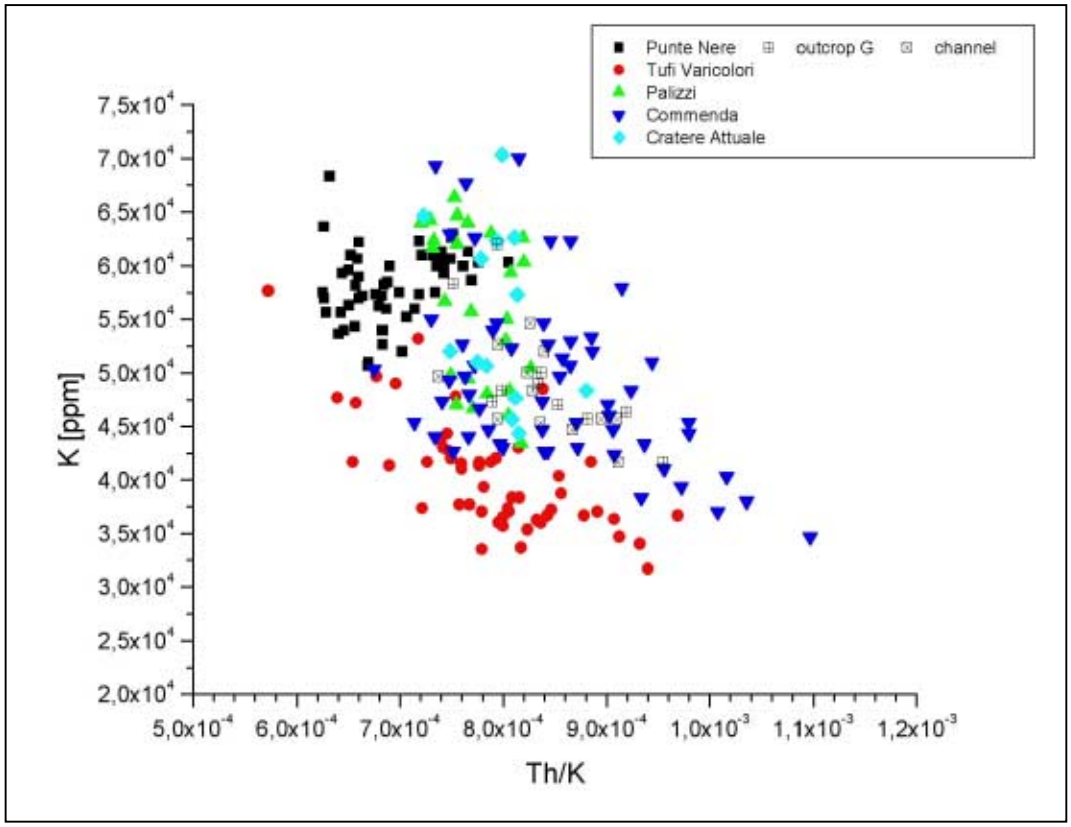

Figure 5.4: Scatter plot of K vs. Th/K for all successions. Punte Nere is split into a group containing outcrops H, I, and J [filled squares], the dry-surge deposits of outcrop G [squares with cross], and outcrop G channel deposits [squares with x]. The main data group of Punte Nere [filled squares] can be distinguished especially from Tufi Varicolori [circles] very well, also Commenda [down triangle] can be discriminated from Punte Nere relatively well.

Plots made for the different elements show that Punte Nere can generally be distinguished from Tufi Varicolori. Its distinction from other successions is only possible when the data of outcrop G are not included in the data set. In the latter case Punte Nere can be distinguished from Palizzi (K vs. U, sometimes Th vs. K), Commenda (Th vs. K, K vs. U), and Cratere Attuale (K vs. U) (for plots see also Appendix III).

The plots discussed above can be quantified by a linear regression that can be used to discriminate Punte Nere from other successions. Data of outcrops with massive layers (I and J) plot in the lower part of the regression line, whereas the dominantly laminated samples of outcrop H plot at the upper end of the regression line (except in the plot U/Th vs. K). Data from outcrop G generally plot outside of the normal trend, because of the K depletion observed in outcrop G. These regression lines could be important for example if in a scatter plot of the ratio no dependence of the elements can be observed - like the plot Th vs. K/Th - a dependence can be assumed, for example the plot of Th vs. U/Th. The construction of linear regression lines shown in table 5.7 is based only on the data of the standard outcrops H, I, and J because of the K depletion and behaviour of outcrop G. The equation is given in chapter 5.2.1.1.

sample	A	B	R	SD	N
K vs. Th/K	34489.08 ± 1574.5	$35.03 * 10^6 \pm 2.2*10^6$	0.53	3.49	55
K vs. U/K	35284.87 ± 1713.3	$106.59*10^6 \pm 7.5*10^6$	0.47	3.63	55
U vs. Th/U	3.94 ± 0.7	3.03 ± 0.21	0.34	5.39	55
U vs. K/U	**35.63 ± 0.6**	**$-0.01 \pm 0.1*10^{-3}$**	**-0.88**	**2.73**	**55**
Th vs. K/Th	**76.03 ± 1.4**	**$-0.02 \pm 0.9*10^{-3}$**	**-0.58**	**5.03**	**55**
Th vs. U/Th	47.23 ± 1.0	-21.83 ± 3.0	-0.16	6.08	55
K vs. U	**32270.43 ± 1100.6**	**2015.11 ± 81.3**	**0.83**	**2.31**	**55**
Th vs. U	**17.26 ± 0.7**	**1.68 ± 0.1**	**0.69**	**4.48**	**55**
Th vs. K	**5.44 ± 1.1**	**$0.6*10^{-3} \pm 18.1*10^{-6}$**	**0.72**	**4.29**	**55**
U/Th vs. K	0.28 ± 0.1	$0.6*10^{-6} \pm 0.9*10^{-6}$	0.09	0.02	55

Table 5.7: Results for the linear fit of Punte Nere for the element scatter plots. Data from outcrop H, I, and J. Plots with trends useful for correlation are highlighted with bold letters..

5.2.2. Tufi Varicolori

Standard outcrops: F and O

5.2.2.1. Granulometry

The succession of Tufi Varicolori is predominantly formed by various wet-surge deposits. Outcrop O belongs to the lower units of Tufi Varicolori (DELLINO, pers. comm. 1999) and outcrop F belongs to a higher stratigraphic section (DELLINO, pers. comm. 1998). The average Ms for the succession is about 1.6 ϕ (s: 0.6). The 2 outcrops show a wide variation of Ms (see also table 5.8). In general the values of outcrop F are smaller than those for outcrop O. Internally, the outcrops show some trends (see also figure 5.5).

sample	outcrop F	outcrop O	Tufi Varicolori
min. value	-0.05	0.99	-0.05
max. value	1.80	2.78	2.78
mean value	0.88	1.86	1.60
standard deviation	0.5	0.5	0.6

Table 5.8: Ms of Tufi Varicolori in ϕ.

Differences between 2 adjacent data points can often be significant, but these differences are smaller for outcrop O than for outcrop F. The Tufi Varicolori section of outcrop F is very exposed, and therefore some of the finer material may be washed out, but also agglomeration processes occur. These newly formed grains are often hard to destroy and result in secondary "coarsening" of the sediment. In outcrop F, the reddish and greenish layers show relatively low Ms values, suggesting an accumulation of agglutinated Fe-grains. The Ms of outcrop O increases up to the middle part of the outcrop. The second part of the outcrop is marked by a prominent crinkly red layer that is bounded by two white bands. The data of prominent layers in outcrop O are often lower compared to the average data, but these layers do not have any obvious components or structures distinguishing them from the other outcrops in the field.

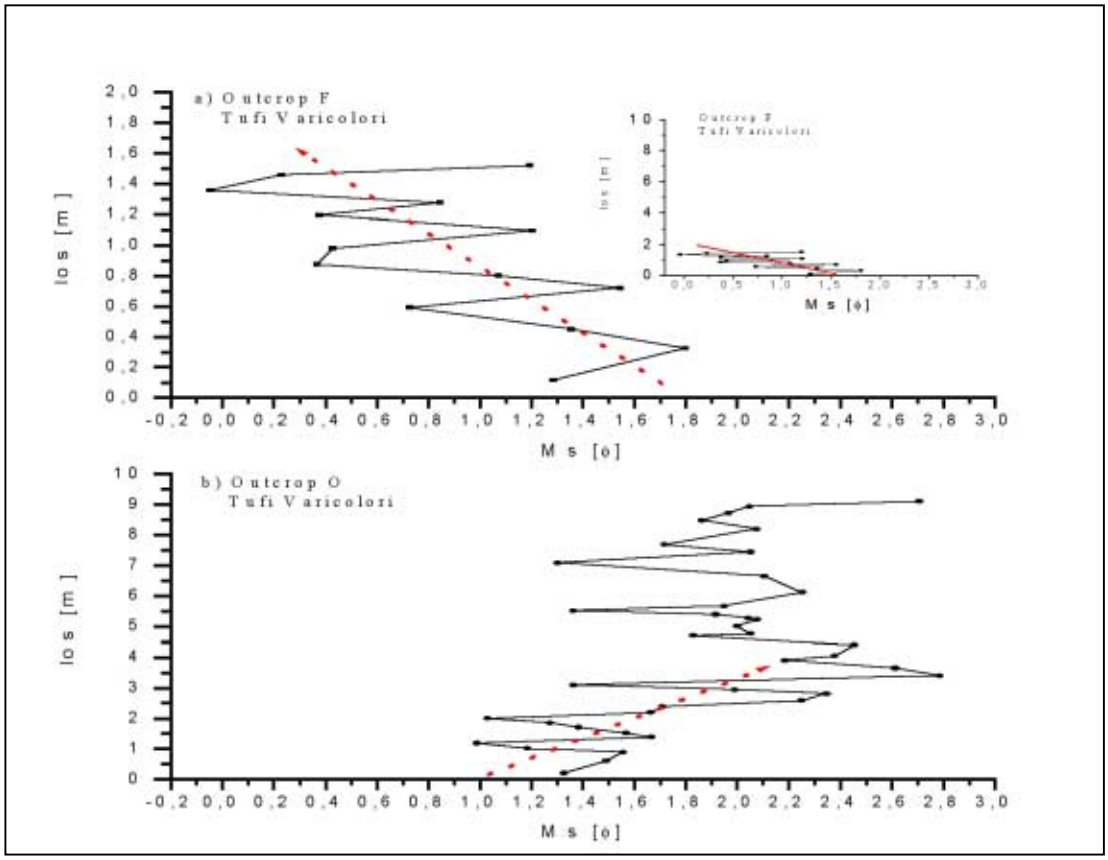

Figure 5.5: Evolution of the Ms for the both standard outcrops of Tufi Varicolori. Data of outcrop F (figure 5.5.a) show a generally positive trend, if high peak differences are not considered. The lower section of outcrop O is characterised by a slightly positive trend of the data (figure 5.5.b), whereas no further trend can be observed in the upper section.

The distance from the vent does not affect the Ms of the samples, thus transport effects influencing the grain size can be excluded. It is important to note that Tufi Varicolori so far are only known inside of the caldera rim. In general they show plastic deformation features. Outcrop O demonstrates the "plastic" character of the surge deposits: the deposits enclose obstacles and the strike and dip can be falsified.

A Gaussian distribution as observed for the Punte Nere deposits is not visible in the histograms for Tufi Varicolori. Especially samples of outcrop O show an increase of the finer grain size classes for the middle and upper sections of this outcrop. A Gaussian distribution is sometimes evident in the lower section of outcrop O. Except of the high accumulation rate in outcrop F the histograms for the grain size plots sometimes show a Gaussian distribution but also an increase to the finer gsc can be remarked.

The cumulative grain size curves of Tufi Varicolori (see also Appendix III) in general do not show a sigmoidal shape as for example many samples of Punte Nere. These curves are often very flat and start with a high fraction of the coarse grain size, but some have a slightly curved shape. These characteristics indicate that the eruption cloud possibly was not as homogeneous as the eruption cloud of Punte Nere. The fine ash is depleted. The Commenda succession

looks similar in the field (colour, wet surge-deposits in general smaller layers than Tufi Varicolori), but has a higher amount of fine ash (see also chapter 5.2.4.1).
Plotting the 1st moment vs. the 2nd moment (Ms vs. s), the correlation is linear with only few outliers. Plots for the data of the single outcrops do not differ from the succession plot. Data for the linear regression are given in table 5.9 (description for the equation see chapter 5.1.1).

sample	A	B	R	SD	N
outcrop F	-0.32 ± 0.7	3.74 ± 0.5	0.95	0.38	8
outcrop O	-0.21 ± 0.2	3.59 ± 0.1	0.99	0.23	39
Tufi Varicolori	-0.16 ± 0.1	3.57 ± 0.1	0.99	0.25	47

Table 5.9: Results for the linear fit of Tufi Varicolori for the scatter plot 1st moment vs. 2nd moment.

In contrast to Punte Nere, the Tufi Varicolori have both a lower correlation coefficient (R) and a smaller SD for the linear fit. The slopes of both successions do not differ in a significant way, although the slope of Tufi Varicolori is slightly higher than the one of Punte Nere and the error for Tufi Varicolori is significant lower than the one for Punte Nere.

5.2.2.2. Susceptibility

The sus is measured in cgs mode, standardised to 1g, and extended to 10^{-6}. The sus05 of the complete succession lies between 42.99 units ± 0.1 and 157.47 units ± 11.2 (mean = 75.20 units, s: 22.3). The sus25 ranges from 38.81 units ± 0.1 to 132.57 units ± 9.5 (mean = 71.67 units, s: 20.7). Minimum and maximum values for the complete succession and for single outcrops are shown in table 5.10. Some prominent peaks in outcrop F possibly indicate marker horizons, but so far they cannot be correlated with peaks in outcrop O. This situation is similar to the problem described in chapter 5.2.1. Table 5.10 also shows that removing the prominent peaks does not affect the overall mean of Tufi Varicolori in a significant way. No change of the sus with distance from the vent can be observed, similar to what has been described for Punte Nere.
In contrast to the granulometric data the sus of both gsc does not show any trend or evolution within the outcrops (see also Appendix III). The different prominent peaks are not distributed in a significant pattern. The average values of the sus of the 2 gsc are different for the single outcrops. They can be classified as follows (cgs-mode, 1g standardised, extension 10^{-6}): the sus05 show average values between 75 and 120 units for outcrop F and between 45 and 70 units for outcrop O, the sus25 range between 70 and 115 units for outcrop F and between 45 and 90 units for outcrop O.

sample	outcrop F	outcrop F without prominent peak	outcrop O	Tufi Varicolori	Tufi Varicolori without the prominent peaks of outcrop F
min. value 0.5-0.25 mm	67.04 ± 4.8	67.04 ± 4.8	42.99 ± 0.1	42.99 ± 0.1	42.99 ± 0.1
max. value 0.5-0.25 mm	157.47 ± 11.2	120.44 ± 0.3	115.89 ± 0.2	157.47 ± 11.2	120.44 ± 0.3
mean 0.5-0.25 mm	99.04 (s: 21.2)	94.54 (s: 14.1)	66.64 (s: 15.4)	75.20 (s: 22.3)	73.61 (s: 19.3)
min. value 0.25-0.125 mm	65.01 ± 0.1	65.01 ± 0.1	38.81 ± 0.1	38.81 ± 0.1	38.81 ± 0.1
max. value 0.25-0.125 mm	132.57 ± 9.5	123.17 ± 0.2	101.32 ± 0.2	132.57 ± 9.5	123.17 ± 0.2
mean 0.25-0.125 mm	91.91 (s: 20.3)	88.78 (s: 17.5)	64.40 (s: 15.3)	71.67 (s: 20.7)	70.50 (s: 19.10)

Table 5.10: Mean values for the sus for both gsc of Tufi Varicolori. In the second data column the data of outcrop F were modified to exclude prominent positive peaks from the average values. Data of the last column show the values for the complete succession with the modified data of outcrop F. Samples are measured in cgs-mode, standardised to 1g, and have to be extended by 10^{-6}.

The sus of the two gsc correlate strongly (see also figure 5.6). The prominent value, marked in the figure, disturbs the linear plot of data of outcrop F, but does not show great effects in the linear plot of the complete succession. The slope of the complete succession is about 0.92 ± 0.01. In general the data of outcrop O are not disturbed, and data of outcrop F often (in many cases they also show a lower error) plot in the same range.

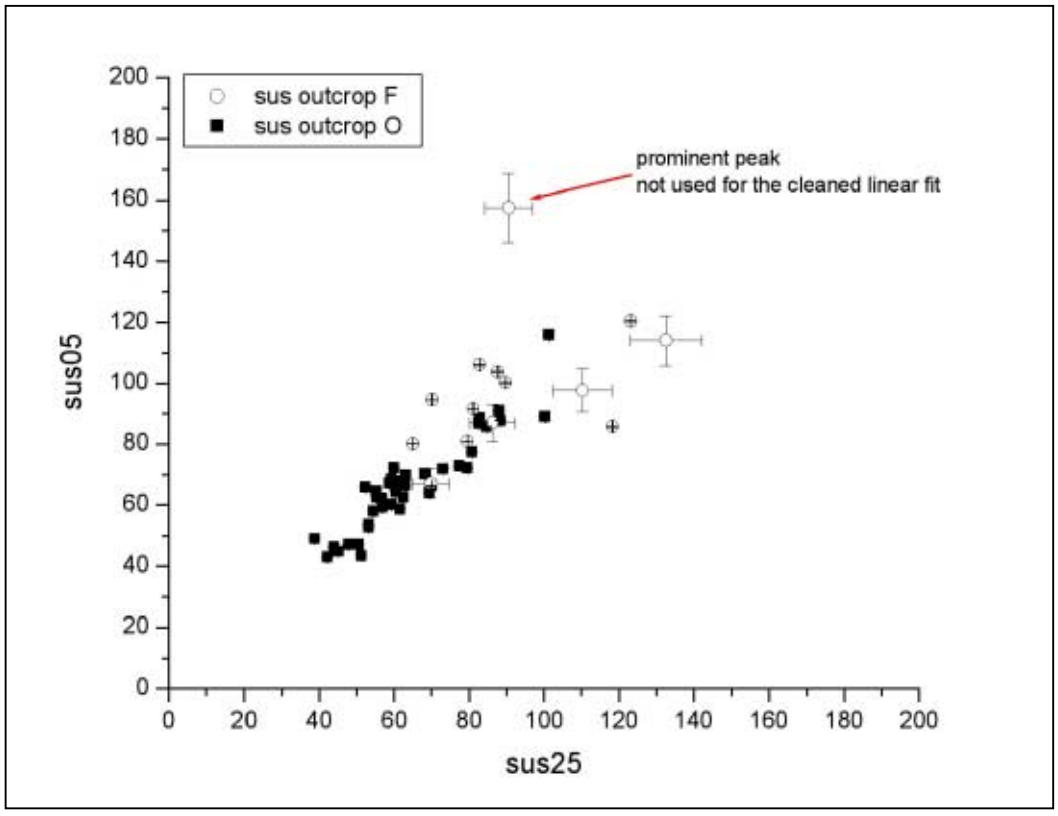

Figure 5.6: Scatter plot of sus05 vs. sus25 of Tufi Varicolori.

Plots of the sus vs. the ratio sus/Ms show an upward trend, in particular for the sus25. However, the relatively high variability, especially for the data of outcrop F, precludes a linear regression of the data and a comparison with other successions (examples can be seen in figure 5.7). For the data points plotting low a slight trend can be observed. This trend cannot be used because of the high variability of the higher plotting data points. Some data points, most of them belonging to the exposed part of outcrop F, may indicate reworking or secondary processes.

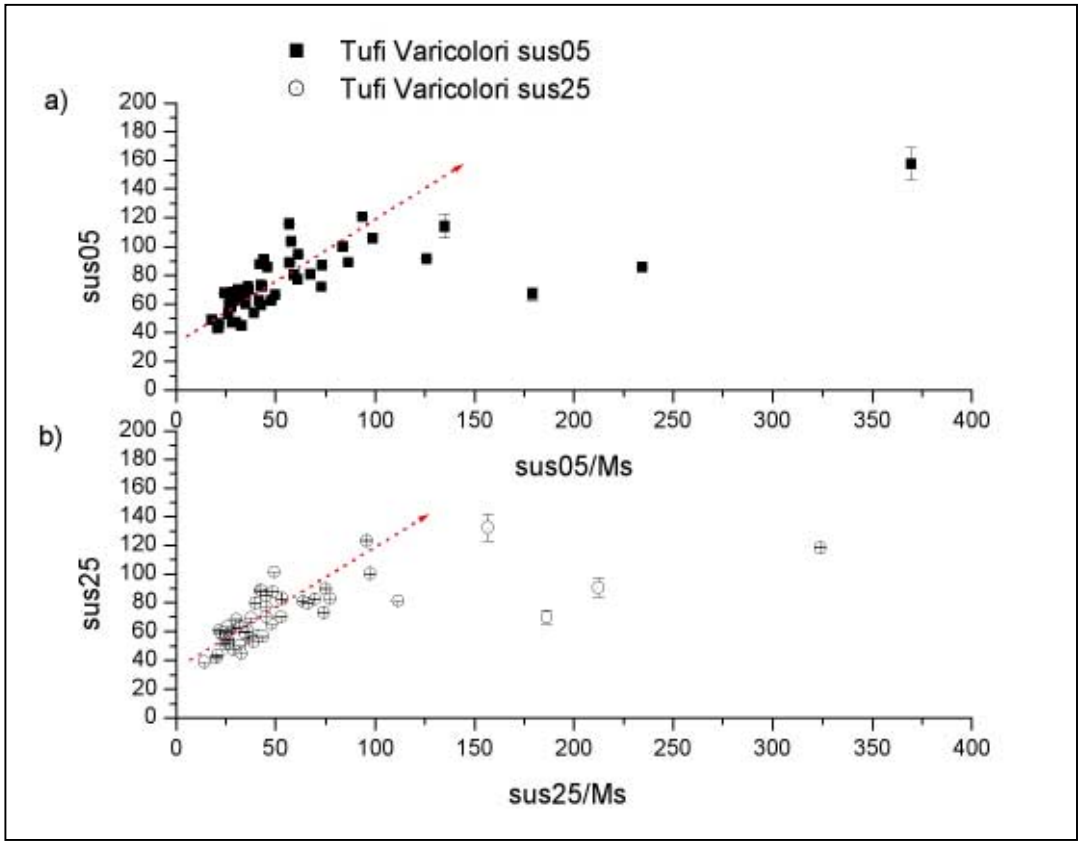

Figure 5.7: Scatter plot of the sus05 (a) and the sus25 (b) vs. the ratio sus/Ms. In general the values show a linear correlation, but the regression error increases with the sus/Ms-ratio.

No trends are visible in a plot of the sus vs. the ratio of both sus for the gsc05 and for the gsc25. This suggests that the sus of one gsc is not affected by the other gsc.

Comparing the data for both gsc in different outcrops it is noticeable that for within outcrop F especially data from layers dominated by red deposits – sometimes characteristic red bands – show higher values for the gsc25 than for the gsc05. In general the finer gsc have slightly lower values than the coarser gsc. The effect described above is not observed in plots of the Ms. The red colour may be related to a higher amount of fine dispersed or agglomerated magnetic minerals, thus increasing the Fe concentration. Weathering of Fe-minerals to limonite or hematite could also cause the red colour. The prominent peak in outcrop F corresponds to a yellow layer that does not show noticeable Ms values. Also this peak can only be observed in the gsc05. In general the values for sus25 are lower than the values for sus05, and this difference is more distinctive for outcrop F. For the data of outcrop O the

difference of the values of adjacent sampling points varies, for the lower part [0-2 m] and the upper part [4-9 m] it is higher than in the middle part [2-4 m] of the outcrop. Prominent positive data peaks – in general for both gsc – are often coupled with layers dominated by grey colours. The uppermost samples of outcrop O with higher sus values come from relatively small layers with more loose material.

One gsc25 sample with relatively high susceptibility from the upper part of outcrop O was selected for microprobe analysis of magnetites of Tufi Varicolori. Magnetites of this sample show a well-developed morphology. They can be found as individual minerals, as well as in accumulations of minerals. The analysis of this sample (see also table 4.4) shows high amounts of Cr^{3+} that distinguish this sample from other samples. The ratio of Fe^{3+}/Fe^{2+} (1.48) is higher than of other comparable samples. In comparison to the other successions the sample of Tufi Varicolori shows relatively high Mg^{2+} and Cr^{3+} amounts, whereas the amounts of Ti^{4+}, Mn^{2+}, and Fe^{2+} in general are lower than for other successions. This can also be observed in the ratios for Fe^{3+}/Cr^{3+} (51.56) and Ti^{4+}/Cr^{3+} (6.36), whereby both show very low amounts in comparison with the other successions. The ratio Fe^{3+}/Ti^{4+} (8.11) is higher than the ratios of other successions. The investigated minerals can be defined as low-Ti-titanomagnetites with a high amount of Cr.

5.2.2.3. Gamma-ray

The standard outcrops of Tufi Varicolori show mean γ-ray values of 4.04 % (s: 0.5) for K, 9.01 ppm (s: 1.3) for U, and 31.57 ppm (s: 2.8) for Th (see also table 5.11). In general the mean values of Tufi Varicolori are lower than the mean values of Punte Nere. Sometimes slight trends can be observed in single outcrops. Changes of the γ-ray values with increasing distance from the vent cannot be observed.

In outcrop F the K values decrease slightly upsection, whereas the values of U increase with a few exceptions. An upsection positive trend is also observed for Th values but the trend is less pronounced. Few outliers occur for Th as well. The ratio of U/Th does not show any kind of trend. The (mostly negative) exceptions within the trends of Th and U in the upper part of the outcrop can be correlated to the red layers that also have unusual positive sus25 values (see also chapter 5.2.2.2). U and K are sensitive recorders for leaching processes. For example, a prominent peak (sample Fb6) in the lower part of outcrop F is characterised by very low U and K values, whereas the Th value compares with values of the surrounding samples. This sample was taken at an exposed part of the outcrop. The soluble elements U and K have apparently been leached, but the less soluble Th was not affected.

sample	K [%]	U [ppm]	Th [ppm]
Minimum outcrop F	3.37 ± 0.1	8.60 ± 0.4	27.27 ± 1.2
Maximum outcrop F	4.77 ± 0.2	11.77 ± 0.4	35.53 ± 1.0
mean outcrop F	3.91 (s: 0.4)	9.92 (s: 0.8)	30.95 (s: 2.2)
Minimum outcrop O	3.17 ± 0.0	6.53 ± 0.3	26.10 ± 1.2
Maximum outcrop O	5.77± 0.8	11.58 ± 0.6	40.68 ± 1.2
mean outcrop O	4.08 (s: 0.5)	8.68 (s: 1.2)	31.79 (s: 2.9)
Minimum Tufi Varicolori	3.17 ± 0.0	6.53 ± 0.3	26.10 ± 1.2
Maximum Tufi Varicolori	5.77 ± 0.8	11.77 ± 0.4	40.68 ± 1.2
mean Tufi Varicolori	4.04 (s: 0.5)	9.01 (s: 1.3)	31.57 (s: 2.8)

Table 5.11: Maximum, minimum and mean values of K [%], U [ppm], and Th [ppm] for the complete succession and single standard outcrops of Tufi Varicolori.

Outcrop O can also be described by different trends (and sections) of the element values and the ratio U/Th (see also Appendix III). All element values show a significant shift in the middle part of the outcrop. Above this point the average values are much smaller. A prominent crinkly layer occurs at the base of this upper part (as aforementioned in chapter 5.2.2.1). The lower part of the outcrop can be described as a long left-handed curve with varying occurrence for the different element values. A few prominent peaks that interrupt the curve correspond to grey layers (not all peaks belong to these layers, but most of them). These layers do not correlate with the evolution of the Ms. No trends of any element can be observed in the upper part of the outcrop. Plotting the data of the ratio U/Th the outcrop is subdivided into 2 parts which are not similar with the parts defined by the element values (the second part of the ratio plot starts 1 m above the crinkling layer, which marks the beginning of the upper section for the elements and the sus). The first part of the ratio plot U/Th does not show a visible trend, in the upper part of outcrop O a slightly decreasing trend can be noticed.

sample	K [%]	U [ppm]	Th [ppm]	U/Th
Tufi Varicolori	**3.25-5.0**	**7-11**	**26-36**	**0.24-0.35**
outcrop F	3.25-4.5	8.5-11	27-33	0.29-0.35
outcrop O	3.25-5.0	7-11	26-38	0.21-0.33
outcrop O lower part defined by elements	4.0-5.0	8.5-11.5	30-38	change not significant
outcrop O upper part defined by elements	3.25-4.0	6.5-11.5	27-33	change not significant

Table 5.12: Average γ-ray values and the U/Th ratio of Tufi Varicolori and the two standard outcrops.

Scatter plots of the Ms vs. K, U, Th, and U/Th do not show any significant trends within the single outcrops or for the complete succession. Often the Ms of outcrop F is (as seen before) lower than the Ms of outcrop O.

When plotting element concentration vs. the ratio of two elements, the following results (for the data of Tufi Varicolori) can be observed (see also table 5.13): Depletion does not occur within the outcrops. Some plots can show trend lines, for example plots of K vs. Th/K or U vs. Th/U, but otherwise data have a diffuse distribution. In the plots K vs. Th/K and U vs. Th/U trends lines can be observed, these lines can be interpreted as the graphic results of the independence of Th vs. the more mobile U and K (see also figure 5.8). A trend line for outcrop F can be observed in a plot of K vs. the ratio U/K and it indicates that K is independent of U. Layer composition or appearance are not obviously reflected in this plot (the distribution of layers with related patterns/profiles). The plot does not show an evolution of values within the outcrop. In the plot U vs. K/U individual outcrops can be discriminated and each shows a good correlation, but the slopes of the regression lines vary significantly. For this plot the data of outcrop F show a distinctive trend line describing the independence of K to U. Plotting Th vs. K/Th, no trends are visible, and especially the data of outcrop O can show a wide dispersion. A linear regression line with a good fit can be calculated for the individual outcrops, but the correlation is not strong when both outcrop data are combined. The plot Th vs. U/Th can be described as a cloud of data points with an indication for the independence of Th and U.

Tufi Varicolori can generally be distinguished well from the other successions, especially from Punte Nere and Palizzi, using the scatter plot K vs. Th/K (see also Appendix III), and in particular from Commenda and Cratere Attuale. Plotting K vs. U/K Tufi Varicolori can be discriminated well from Punte Nere, Palizzi, and Cratere Attuale (see also Appendix III), and the discrimination from Commenda is possible for most of the data. Tufi Varicolori is quite distinct from Palizzi in the plot of U vs. Th/U, whereas the other successions have intermediate values. Most successions can be discriminated from Tufi Varicolori using the plot of U vs. K/U, and again the distinction between Tufi Varicolori and Palizzi is very good (see also Appendix III). The data of Commenda and outcrop G of Punte Nere show larger intersections with the data of Tufi Varicolori than the other successions. Plotting Th vs. K/Th, Tufi Varicolori can be distinguished very well from Punte Nere, the other successions can be distinguished partly. The plot Th vs. U/Th also mirrors a good discrimination from the data of Tufi Varicolori with the data of the other successions (see also Appendix III), here especially the data of Palizzi can be distinguished very well from the data of Tufi Varicolori.

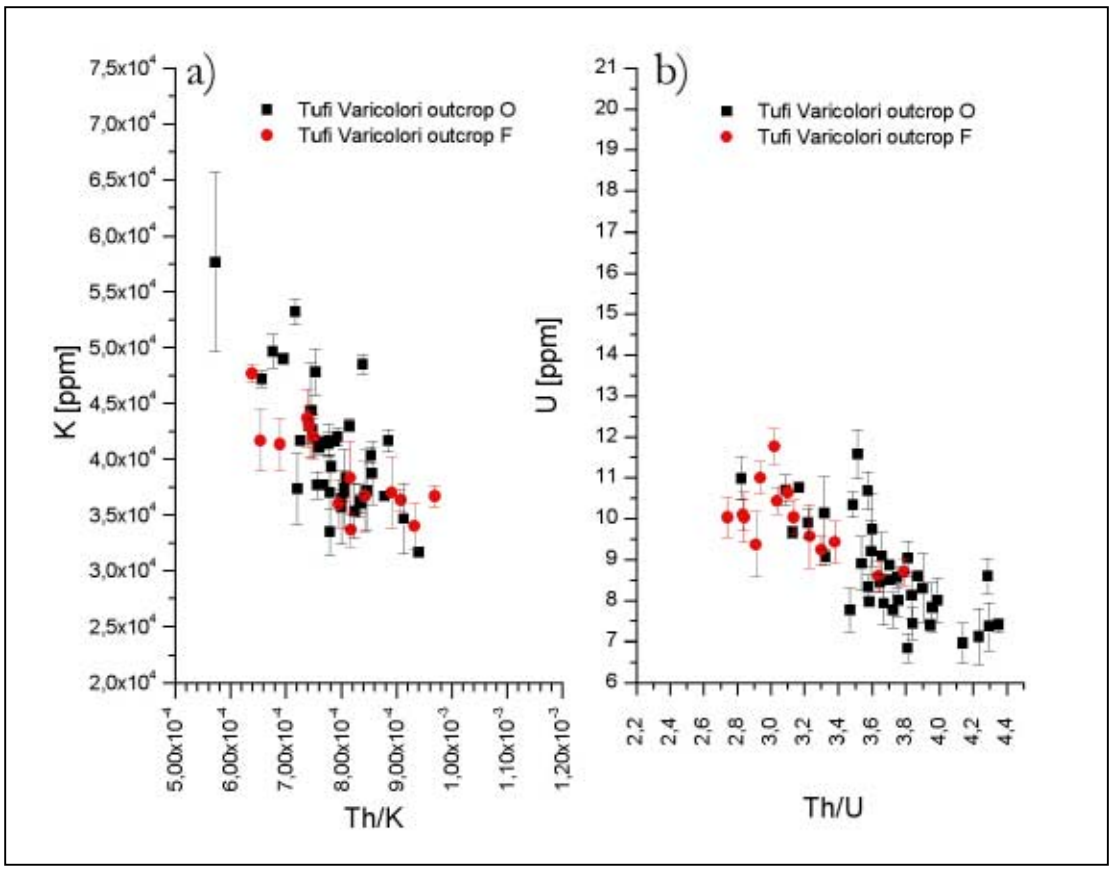

Figure 5.8: Scatter plots of K vs. Th/K (a) and U vs. Th/U (b) for the data of Tufi Varicolori. In both plots the independence of the relationship between Th and K, as well as Th and U can be observed.

Scatter plots of the elements can also give some information to define the successions. The plot K vs. U displays a different slope for Tufi Varicolori than for the Punte Nere succession discussed before (see also Appendix III). Using this plot the data of Tufi Varicolori can be discriminated from the data of Cratere Attuale and Palizzi, whereas the data of Commenda and Punte Nere overlap with the data of Tufi Varicolori, especially with the high-K data points of Tufi Varicolori. The data of the single outcrops of Tufi Varicolori show no significant differences, but they disagree in their linear fit. Plotting Th vs. U a slight slope can be remarked. The data of Tufi Varicolori plot on the same trend as the data of the other successions in the plot Th vs. U (see also Appendix III). This plot discriminates well between the data of Tufi Varicolori and Palizzi. Some overlap exists with the data of the other successions, but in general a distinction is still possible. The linear fit calculated for the Tufi Varicolori succession is relatively flat in comparison with the expected fit fitting on the scatter plot without any mathematical program. Plotting Th vs. K, solely the low-Th data points of Tufi Varicolori can be distinguished from the data of the other successions. Comparing the data of the single outcrops of Tufi Varicolori the linear trends differ in a significant way and the result for the combined data is not usable for the comparison between the different successions. In plots of outcrop O it is important if sample Ob20 - a sample with a very high error - is used or not, because inclusion of this sample reduces the calculated slope. Because of the reproducibility of the data Ob20 failed for the correlation of table 5.13.

The last plot U/Th vs. K does not allow to characterise the data of Tufi Varicolori in comparison with the data of the other successions (see also Appendix III). Solely the data with low K concentrations can be discriminated from the data of the other successions. If outcrop G is not included, the data of Tufi Varicolori can be discriminated well from the data of Punte Nere. The linear fit of this plot is also not sensible for a correlation.

sample	A	B	R	SD	N
K vs. Th/K	**78754.65 ± 1021.2**	**$-48.63*10^6 \pm 1.3*10^6$**	**-0.82**	**3.72**	**53**
K vs. U/K	35074.18 ± 1112.7	$21.68*10^6 \pm 5.1*10^6$	0.09	6.50	53
U vs. Th/U	**21.61 ± 0.2**	**-3.49 ± 0.1**	**-0.91**	**3.62**	**53**
U vs. K/U	21.27 ± 0.4	$-0.002 \pm 78.8*10^{-6}$	-0.51	7.37	53
Th vs. K/Th	32.16 ± 0.9	$-0.001 \pm 0.7*10^{-3}$	-0.06	3.34	53
Th vs. U/Th	36.05 ± 0.6	-18.04 ± 2.2	-0.35	3.14	53
K vs. U	**14265.41 ± 673.2**	**2949.50 ± 76.9**	**0.82**	**3.74**	**52**
Th vs. U	27.78 ± 0.7	0.33 ± 0.1	0.18	3.29	53
Th vs. K	18.69 ± 0.9	$0.30*10^{-3} \pm 0.2*10^{-6}$	0.55	2.78	52
U/Th vs. K	0.22 ± 0.0	$1.69*10^{-6} \pm 0.9*10^{-6}$	0.25	0.03	53

Table 5.13: Results for the linear fit of Tufi Varicolori for the element scatter plots. Data of outcrop F and O. Plots with trends useful for correlation are highlighted with bold letters. The linear fit for Th vs. K does not include the data of sample Ob20 (explanation see text).

5.2.3. Palizzi

Standard outcrops: E and F

5.2.3.1. Granulometry

Different surge deposits of coarse and fine ash form the Palizzi succession. Standard outcrops are dominated by dry-surge deposits. Sometimes these deposits contain Pele's hair or reworked pumice, which in general belongs to the 1st Palizzi pumice that is not everywhere preserved. Stratigraphically outcrop E is located below the 2nd Palizzi pumice, while the 1st Palizzi pumice can be observed as reworked clasts in the lower section of the outcrop. Outcrop F contains the 1st Palizzi pumice that is not reworked significantly in this location. The 2nd Palizzi pumice is not exposed in outcrop F. In standard outcrops the ash layers have an average Ms of about 1.35 ϕ (s: 0.4) (see also table 5.14). Both outcrops do not display the large variations of Ms that can be observed for the data of Tufi Varicolori. The mean Ms values of Palizzi and Punte Nere are similar, whereas the values of Tufi Varicolori are slightly higher (also showing a higher s).

Despite important variation between adjacent data points, both outcrops show an overall upsection increase of Ms that is more pronounced in outcrop E (see also figure 5.9). Layers with Pele's hair often correlate with positive peaks, whereas layers with reworked pumice often show lower values. The relatively higher values in the presence of Pele's hair can be described by the nature of Pele's hair. On the one hand the extremely fine hairs can be

destroyed during short-distance transport, and on the other hand a higher error during the sample preparation can be expected. Pele's hair is not an ideal grain for sieving methods because of its geometry. Thus it is possible that the coarser gsc are thinned and the finer gsc seem to increase because of an higher amount of Pele's hair in the finer gsc. Pumice clasts are generally not very resistant to abrasion by transport, but the Palizzi pumices are still visible macroscopically. Thus, they were not transported over long distances and where present, they shift the Ms to lower values.

sample	outcrop E	outcrop F	Palizzi
min. value	0.55	0.59	0.55
max. value	1.75	2.07	2.07
mean value	1.29	1.39	1.35
standard deviation	0.4	0.4	0.4

Table 5.14: Ms of Palizzi in ϕ.

The extremely coarse peak near the top of outcrop F is caused by the presence of larger dark clasts like small scoria or dark pumice. They shift the Ms to coarser values.
A change of the Ms with distance from the vent cannot be observed.

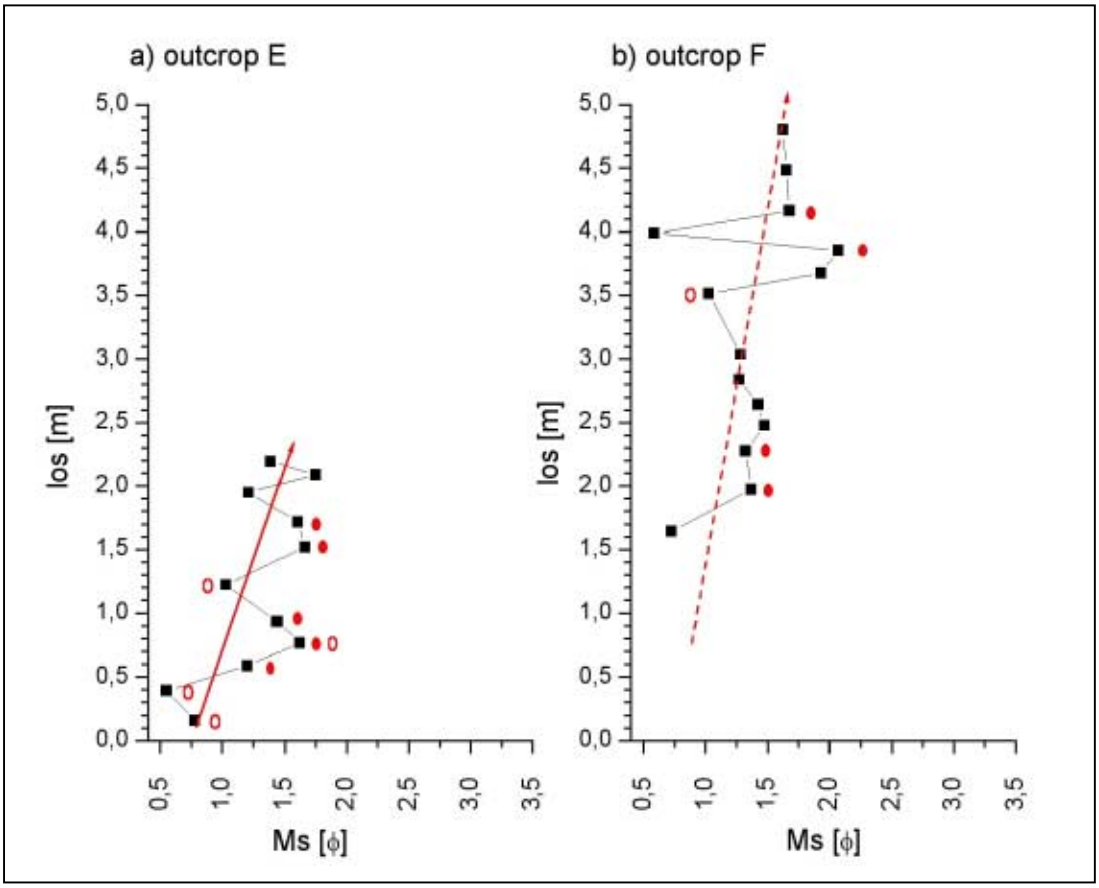

Figure 5.9: Evolution of the Ms for both standard outcrops of Palizzi (a: outcrop E, b: outcrop F). Outcrop E shows a general increase, whereas for outcrop F only a slight trend to higher values can be observed. Filled circles identify layers with Pele's hair and open circles correspond to layers with reworked pumice clasts.

A Gaussian distribution is often present in histogram plots of the gsc. The extremely coarse peaks normally associated with pumice clasts correlate with a slightly positive skewness.
Cumulative grain size curves commonly have slightly sigmoidal shapes (see also Appendix III). Some of these curves are similar to the curves found for the Punte Nere succession. The well-developed curves indicate a homogenous eruption cloud. If pumice is present the curves frequently start with coarser grain sizes and have a more planar shape. Such eruption clouds are less homogeneous than the clouds producing the more sigmoidal shapes. Samples including Pele's hair frequently plot in a smaller range than samples without visible fragments of Pele's hair or pumice. Types with and without Pele's hair show a more or less well developed sigmoidal curve. Samples containing pumice fragments commonly have – especially for the coarser gsc – a wider range and a less sigmoidal shape.
Scatter plots of the 1st vs. the 2nd moment for both outcrops show a gently increasing trend in comparison with Punte Nere and Tufi Varicolori. Results for the linear fit of both outcrops and the complete succession are shown in table 5.15. The slope (2.60 ± 0.4) of the complete successions differs significantly from Punte Nere (3.43 ± 0.2) and Tufi Varicolori (3.57 ± 0.1). The correlation coefficient (R) for Palizzi is smaller than for the other two investigated successions, whereas the SD is much higher (than for the two other successions). These differences allow a good distinction between Palizzi, Tufi Varicolori and Punte Nere.

sample	A	B	R	SD	N
outcrop E	2.91 ± 0.6	2.08 ± 0.4	0.85	0.52	11
outcrop F	1.78 ± 1.0	2.94 ± 0.7	0.78	1.01	14
Palizzi	2.24 ± 0.6	2.60 ± 0.4	0.79	0.82	25

Table 5.15: Results for the linear fit in the scatter plot 1st moment vs. 2nd moment of Palizzi.

5.2.3.2. Susceptibility

Palizzi presents the following mean values for the sus – measured in cgs mode, standardised to 1g, and extended to 10^{-6} – for the two gsc: sus05 ranges from 74.60 ± 5.3 to 166.11 ± 11.9 units (mean = 105.45 units, s: 18.1), sus25 ranges from 74.46 ± 0.1 to 284.29 ± 20.3 units (mean = 117.68 units, s: 43.8). Results for both outcrops and the complete succession can be found in table 5.16. Prominent peaks like the maximum peak for sus25 of outcrop F (284.29 units ± 20.3) are rare. Often they represent marker horizons. These peaks may "disturb" the average data and falsify the mean values of the succession (results are also given in table 5.16). The sus does not change with distance from the vent.
Plotting the sus of both gsc vs. los no trends can be observed (see also Appendix III). The average values of the data for both outcrops plot in general within similar boundaries. In contrary to the successions of Punte Nere the data of Palizzi do not show the same behaviour if coupled with Pele's hair. Although the presence of Pele's hair is often coupled with lower amounts of sus, the data of the samples for Palizzi do not show the same significance –

especially for sus05 – compared to data of the samples of Punte Nere (see also chapter 5.2.1.2). Outcrop E data often shows a similar behaviour as data from Punte Nere but also in this case the variation is much higher. Both samples with dominant peaks within the two outcrops contain pumice clasts. These pumice clasts can include susceptibility bearing minerals. Once abrasion destroys especially the edges of such pumice, the material can enrich the finer gsc with susceptibility bearing minerals and fragments. In the case that susceptibility bearing minerals are not enriched within the pumice, erosion and abrasion of such pumice can thin the resulting sus of the finer gsc. Also the pumice can be destroyed by the sample preparation (especially by sieving), in this case the coarser gsc will be depleted and the finer gsc will be thinned. The behaviour of the pumice of the Palizzi succession can be explained in the first way (enrichment of susceptibility bearing minerals in the finer gsc [finer than the pumice clasts]), because especially the finer gsc shows higher values for the sus (an extreme example is the prominent peak in both outcrops where the values for the gsc25 are definitively higher than the values for the gsc05).

sample	**outcrop E**	**outcrop E** without prominent peak	**outcrop F**	**outcrop F** without prominent peak	**Palizzi**	**Palizzi** without the prominent peaks of outcrops E and F
min. value 0.5-0.25 mm	80.45 ± 0.1	80.45 ± 0.1	74.60 ± 5.3	74.60 ± 5.3	74.60 ± 5.3	74.60 ± 5.3
max. value 0.5-0.25 mm	126.15 ± 0.2	126.15 ± 0.2	166.21 ± 11.9	127.91 ± 0.2	166.21 ± 11.9	127.91 ± 0.2
mean 0.5-0.25 mm	104.07 (s: 15.2)	104.07 (s: 15.2)	106.53 (s: 20.0)	101.94 (s: 11.6)	105.45 (s: 18.1)	102.92 (s: 13.4)
min. value 0.25-0.125 mm	79.90 ± 5.7	79.90 ± 5.7	74.46 ± 0.1	74.46 ± 0.1	74.46 ± 0.1	74.46 ± 0.1
max. value 0.25-0.125 mm	202.01 ± 14.4	148.53 ± 10.6	284.29 ± 20.3	139.38 ± 0.2	284.29 ± 20.3	148.53 ± 10.6
mean 0.25-0.125 mm	115.58 (s: 34.3)	106.94 (s: 21.6)	119.33 (s: 49.9)	106.64 (s: 10.8)	117.68 (s: 43.8)	106.77 (s: 21.2)

Table 5.16: Mean values for the sus for both gsc of Palizzi. In the second and fourth data columns of outcrops E and F the prominent positive peaks are not considered for the average values. Data of the last column show the values for the complete succession with the modified data of outcrops E and F. Samples are measured in cgs-mode, standardised to 1g, and have to be extended by 10^{-6}.

In a scatter plot of sus05 vs. sus25 the data do not allow distinction of the different outcrops. The two prominent peaks do not plot in the data cloud, thus they are not included in the linear fit. The single outcrops differ strongly in their linear fit, and consequently the fits cannot be used for a correlation with other successions.

Plotting the sus vs. the ratio sus/Ms the scatter diagrams for both gsc do not reflect a significant trend, but elongate data clouds can be observed (but also some peaks do not plot in this area). Linear fits for all data or only for corrected data (without the two samples containing prominent peaks described before) cannot be used for a discrimination from other successions. For an acceptable result, too many data points have to be eliminated, and the result for this plot would no longer be representative for the complete succession (see also figure 5.10). The outliers do not show patterns significant for a discrimination.

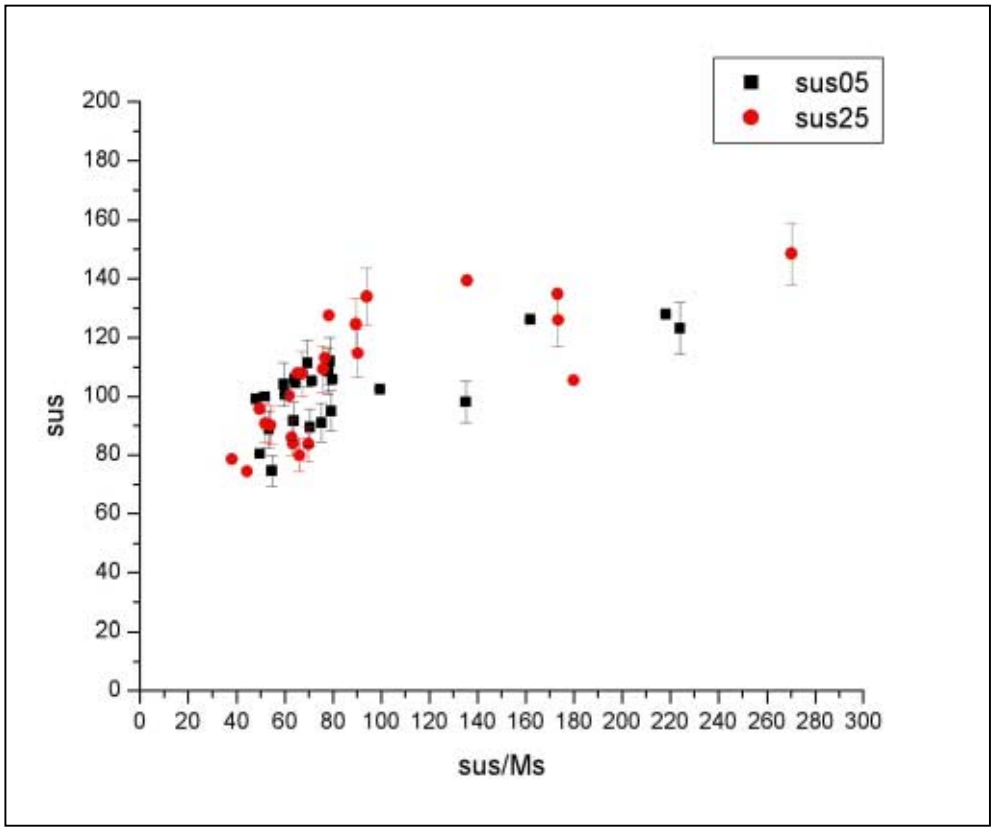

Figure 5.10: Scatter plot for of the sus vs. the ratio sus/Ms for both sus (corrected for the two samples containing the prominent peaks of sus). The data in general plot in an elongated cloud with many outliers. Too many data points have to be eliminated for a representative linear fit of the complete succession.

The microprobe sample of Palizzi magnetites was taken from outcrop F for gsc25 (Ob38 gsc25). In general the data are comparable to the results for the other successions (except Tufi Varicolori) and do not allow discrimination (see also table 4.4). Elemental abundances are particularly similar to the data of Punte Nere, for example Mg^{2+}, Mn^{2+}, and Cr^{3+}. The magnetites of Palizzi are low-chrome titanomagnetites.

5.2.3.3. Gamma-ray

The mean γ-ray values for the standard outcrops of Palizzi are 5.62 % (s: 0.7) for K, 15.52 ppm (s: 2.1) for U, and 43.43 ppm (s: 5.1) for Th (see also table 5.17). A change of the γ-ray values with distance from the vent cannot be observed. The mean values of Palizzi are significant higher than the values of Tufi Varicolori, but only slightly higher than γ-ray values of. Punte Nere (see also table 5.32).

sample	**K** [%]	**U** [ppm]	**Th** [ppm]
Minimum outcrop E	5.93 ± 0.1	14.30 ± 0.2	45.13 ± 0.7
Maximum outcrop E	6.63 ± 0.3	19.53 ± 0.5	49.93 ± 2.6
mean outcrop E	6.28 (s: 0.2)	16.87 (s: 1.6)	47.86 (s: 1.7)
Minimum outcrop F	4.34 ± 0.1	11.98 ± 0.3	35.47 ± 0.4
Maximum outcrop F	6.42 ± 0.3	18.14 ± 0.6	51.28 ± 1.4
mean outcrop F	5.17 (s: 0.6)	14.63 (s: 1.9)	40.48 (s: 4.4)
Minimum Palizzi	4.34 ± 0.1	11.98 ± 0.3	35.47 ± 0.4
Maximum Palizzi	6.63 ± 0.3	19.53 ± 0.5	51.28 ±
mean Palizzi	5.62 (s: 0.7)	15.53 (s: 2.1)	43.43 (s: 5.1)

Table 5.17: Maximum, minimum and mean values of K [%], U [ppm], and Th [ppm] for the complete succession and single standard outcrops of Palizzi.

Within the outcrops E and F sometimes trends can be observed for different elements and in different sections of the outcrops (see also Appendix III). Potassium data of the upper part of outcrop E (until 1.5 m height) increase slightly upsection (see also figure 5.11), and a similar positive trend can be observed for U and Th (the latter starts about 10 cm higher in the section). Potassium and Th also show slightly increasing trends in the lower part of outcrop F up to the 1st Palizzi pumice. No trend can be recognised in outcrop F for U. For both outcrops the ratio U/Th does not show any significant trend, but greater differences can be observed between adjacent sampling points than for the single element plots.

Neither Pele's hair nor the abundance of pumice in the samples affect the values of the different elements as shown by the sus and the values of Punte Nere (see also chapter 5.2.1).

Scatter plots of Ms vs. the elements do not show any trend. Splitting the samples into those with pumice, Pele's hair, and not substituted (with pumice or Pele's hair), samples do not mirror trends. In the case of Palizzi neither the presence of pumice nor of Pele's hair seems to affect the γ-ray values of the samples. However, layers containing pumice often have a smaller range of γ-ray values in contrast to the other groups. Comparable to the observations

made for the granulometry, the samples with Pele's hair have higher mean values (they plot in general in the higher part of the data cloud, not above all data, but not dispersed for the whole cloud).

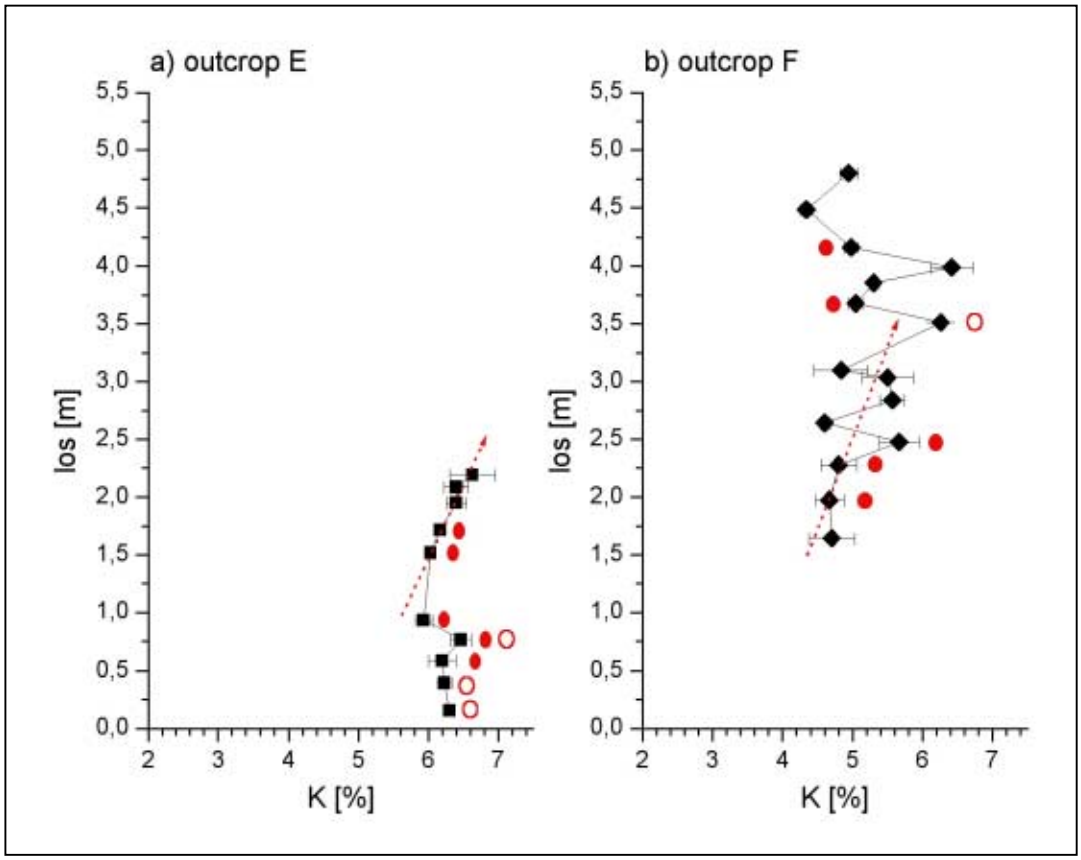

Figure 5.11: Plot of the K values vs. los for both standard outcrops of Palizzi. Filled circles mark samples with Pele's hair and open circles mark samples with pumice. a) outcrop E shows a slightly increasing trend for the upper part; b) in outcrop F a slightly increasing trend in the lower part of the outcrop can be observed.

Similar to the other successions also the outcrops of Palizzi show differences in their average values (see also table 5.18). Here especially the data of outcrop F show a wider range for the single elements. A split within the outcrops as seen for outcrop O of the Tufi Varicolori succession (see also chapter 5.2.2) can not be observed.

sample	**K** [%]	**U** [ppm]	**Th** [ppm]	**U/Th**
Palizzi	**4.5-6.75**	**12-19**	**35-51**	**0.31-0.40**
outcrop E	5.75-6.75	15-19	45-51	0.31-0.40
outcrop F	4.5-6.25	12-18.5	35-51	0.31-0.40

Table 5.18: Average γ-ray values and the U/Th ratio of the different outcrops.

Plots of the element values vs. the ratio of two elements show the following results (see also Appendix III): In all plots the single outcrops can be discriminated by their absolute element values, whereas the ratios commonly do not show differences (for example K vs. Th/K see also figure 5.12.a). Depletion or enrichment of single elements can be observed; for example

the plot U vs. K/U can be interpreted by K depletion in outcrop F, or alternatively by an enrichment of K in outcrop E (see also figure 5.12.b). Outcrop E is located in a small gully and the Palizzi succession is exposed at the base of the outcrop. In this outcrop Palizzi is overlain by Commenda and Cratere Attuale. A K-enrichment may be due to stronger weathering and alternation of the more exposed and possibly more altered successions or especially the overlying 2nd Palizzi pumice containing relatively high γ-ray values (K = 8.40 % ± 0.1, U = 20.53 ppm ± 0.8, and Th = 56.13 ppm ± 0.8). Weathering of this well-exposed layer could have mobilised the elements that subsequently accumulated in the underlying deposits. Outcrop F is a cliff exposed to weathering for example by rainfall. If both processes are considered it is possible that the combination of both outcrops mirror the "real" γ-ray value for the Palizzi succession. The possibility of a magmatic process can be excluded because the sus for both gsc does not reflect a magmatic evolution in a significant way (chapter 5.2.3.2). The sus is also not susceptable to weathering in the same way as the elements of the γ-ray measurement, especially U and K.

Single outcrops show significantly different linear regression fits in a scatter plot of K vs. K/U, therefore the resulting plot for the combined outcrops is not used. When outcrop F is fitted without the layers containing pumice, the results correlate slightly better with the results for outcrop E. The plots of U vs. Th/U and Th vs. U/Th for the single outcrops behave in the same manner. The trends seem to be similar but the fitted results are quite different for the two outcrops. Plotting K vs. Th/K and Th vs. K/Th both outcrops show a similar trend but the variability of the data for outcrop F is higher. The correlation does not improve when the layers with pumice within outcrop F are not considered. The plot of U vs. K/U shows a similar situation as the previous plot, but if the layers with pumice amounts in outcrop F are not considered the trends present a higher similarity.

The plots of the elements vs. the ratios can also be used to distinguish Palizzi from the other successions of La Fossa di Vulcano. A scatter plot of K vs. Th/K allows a discrimination of Palizzi and Tufi Varicolori, but the Palizzi data strongly overlap with data from all other successions. Plots of K vs. U/K and U vs. K/U show a similar situation, but in this case also Punte Nere can be distinguished as well. In comparison with the other successions Palizzi represents extremely high U values in combination with relatively low Th/U ratios. Here the discrimination of Palizzi and Tufi Varicolori is defined very well whereas only parts of Palizzi can be distinguished from Punte Nere, Commenda, and Cratere Attuale. Using the scatter plot of Th vs. U/Th for Palizzi relatively high ratios for U/Th can be observed. This discrimination can be described in the same way as before. The last element-ratio plot Th vs. K/Th allows only the distinction of Palizzi and Tufi Varicolori. In this case Palizzi plots in the middle of a data cloud, whereas the other successions – except of Palizzi – all show different trends.

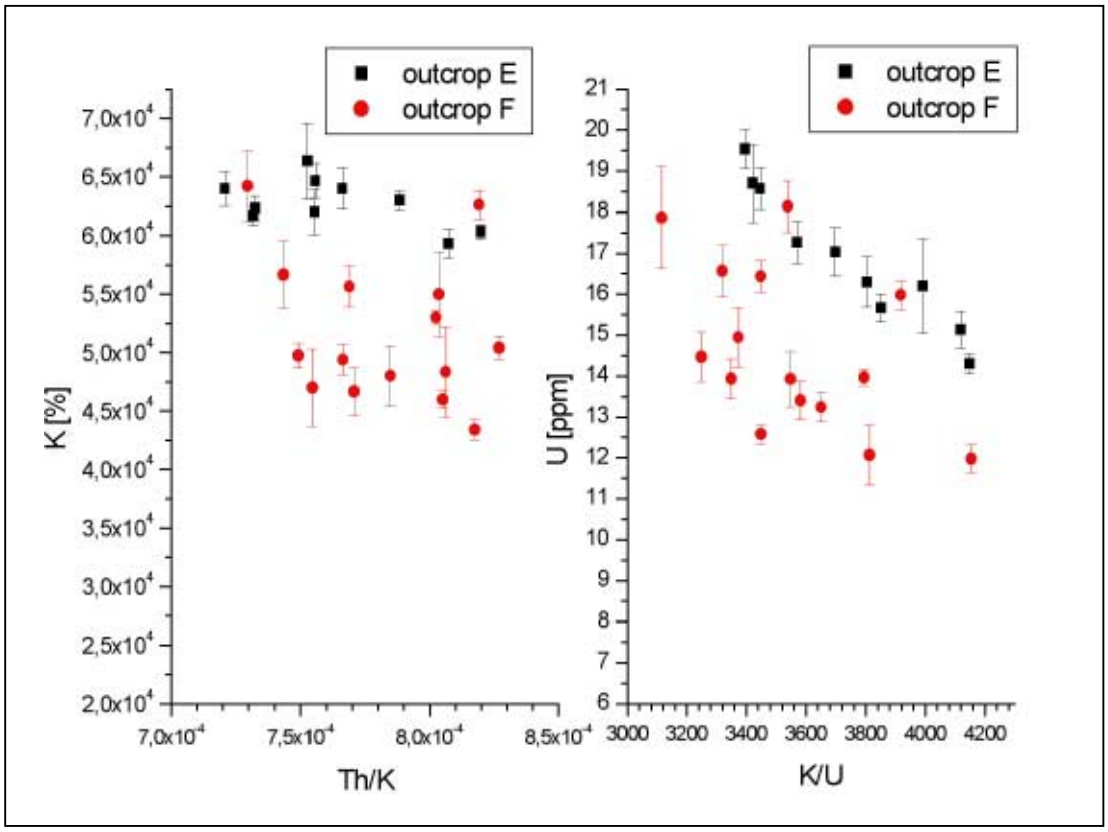

Figure 5.12: Scatter plots for both outcrops of Palizzi a) K vs. Th/K: discrimination of the two outcrops by the values for K but the ratio is similar b) U vs. K/U: depletion of K in outcrop F or enrichment of K in outcrop E (see text).

Scatter plots of single elements can give additional information about the succession when comparing Palizzi with the other successions. In the case of Palizzi also the linear fits in single element plots seem to be more meaningful than fits calculated for the plots of element and ratio. When plotting K vs. U it can be noted that the data of both outcrops of Palizzi plot within different clusters, with only minor overlap that also includes the pumice sample. In general outcrop E has higher element concentrations. The linear fit resulting for the complete successions seems to be usable in the first moment, but if compared with the single outcrops – plotting with highly different linear fits – this result can be described as a real mean value between two points of a scale. Comparing the data of Palizzi with the data of the other successions only Punte Nere – except of outcrop G – and Tufi Varicolori can be distinguished from Palizzi. The data of Palizzi, Commenda, and Cratere Attuale plot in the same range.

A scatter plot of Th vs. U shows again that the single outcrops generally plot in different clusters as observed in the former plot. Like before outcrop E plots slightly higher than outcrop F. Samples of outcrop E containing Pele's hair or pumice often have lower amounts of U than the other samples of outcrop E, whereas the amount of Th is not affected by the presence or absence of these components. This effect cannot be observed in outcrop F where only the sample with pumice shows higher amounts of Th. The Th concentration is comparable to the amounts found in outcrop E samples containing pumice. The results of the

linear fit are significantly different for the two outcrops, and the resulting fit for the complete succession is more similar to the fit of outcrop F. Because of the big differences between the plots for the single outcrops the linear fit of the complete succession seems not to be significant for a correlation with other successions. Comparing Palizzi with the other successions only Tufi Varicolori can be distinguished very well, whereas the other successions overlap.

The following observations can be made in a plot Th vs. K: the data plot on a straight line, but also in this plot the two outcrops can be distinguished as seen before. Splitting up the samples into "normal" samples, samples containing pumice, and samples containing Pele's hair, it can be noted that samples with Pele's hair generally show a smaller K-range. Samples of the outcrops F and E often have the same range of Th values. Samples of outcrop E including Pele's hair also show lower amounts of K than the "normal" samples, but this does not apply to samples of outcrop F that contain Pele's hair. The linear regressions for the single outcrops differ significantly and the result for the complete succession is similar to the result for outcrop F. In the scatter plot Palizzi is quite distinct from Tufi Varicolori and from Punte Nere in particular (without outcrop G). The latter can be discriminated especially from Palizzi samples with lower K and Th values.

Plotting U/Th vs. K the values for the ratio U/Th of both outcrops are similar, but the values of K define the two outcrops as seen before. The samples containing pumice plot in a cluster with similar K-values and a small range of U/Th values. The samples of outcrop E containing Pele's hair can be separated from the "normal" samples of outcrop E, whereas the latter discrimination cannot be used for the samples of outcrop F. The linear regression for outcrop E indicates a good correlation but the plot for outcrop F and the combination for the complete succession are not usable for a sensible correlation. Comparing Palizzi with the other successions especially Tufi Varicolori can be distinguished from Palizzi. Palizzi often plots higher than the other succession but there is also some overlap in the lower part of the Palizzi cluster.

sample	A	B	R	SD	N
K vs. Th/K	119759.14 ± 5423.6	$-81.60*10^{6} \pm 6.9*10^{6}$	-0.39	5.87	25
K vs. U/K	78757.12 ± 3442.6	$-86.48*10^{6} \pm 12.8*10^{6}$	-0.22	6.21	25
U vs. Th/U	22.87 ± 0.9	-2.79 ± 0.3	-0.38	4.44	25
U vs. K/U	20.50 ± 1.1	$-0.002 \pm 0.3*10^{-3}$	0.23	4.67	25
Th vs. K/Th	34.71 ± 3.5	0.002 ± 0.003	0.06	6.58	25
Th vs. U/Th	56.28 ± 1.5	-40.47 ± 4.3	-0.30	6.29	25
K vs. U	**9005.41 ± 1769.1**	**3120.20 ± 117.8**	**0.87**	**3.17**	**25**
Th vs. U	16.55 ± 1.2	1.69 ± 0.1	0.68	4.84	25
Th vs. K	6.20 ± 1.2	$66.01*10^{-3} \pm 22.3*10^{-6}$	0.94	2.31	25
U/Th vs. K	0.35 ± 0.1	$0.04 * 10^{-6} \pm 0.9 * 10^{-6}$	0.01	0.03	25

Table 5.19: Results for the linear fit of Palizzi for the element scatter plots. Data of outcrop E and F. Plots with trends useful for correlation are highlighted with bold letters.

5.2.4. Commenda

Standard outcrops: A, B, and E

5.2.4.1. Granulometry

The investigated part of Commenda is generally formed by wet-surge deposits. In the field these deposits often look similar to the deposits of Tufi Varicolori. However, except of the region near the vent the layers are less thick than the layers of Tufi Varicolori. Fumarolic alteration can be observed in particular near the crater rim (outcrop A).

The standard outcrops of Commenda have an average Ms of about 2.06 ϕ (s: 0.8) (see also table 5.20). Large variations are detectable within the outcrops A and B. Especially outcrop A shows alteration that often derived from fossil fumarolic activity. When samples with possible alteration are excluded, the mean Ms of Commenda increases and is comparable to values of the single outcrops. In comparison with the other successions, Commenda can be distinguished by its higher mean Ms (see also table 5.32). This result also correlates with the fact that Commenda can be discriminated from the otherwise similar succession of Tufi Varicolori by the finer gsc of Commenda (DELLINO, pers. comm. 1997).

sample	outcrop A	outcrop A without visibly altered samples	outcrop B	outcrop B without visibly altered samples	outcrop E	Commenda	Commenda without visibly altered samples
min. value	0.52	1.18	-0.10	0.12	2.16	-0.10	0.12
max. value	3.25	3.25	2.70	2.70	2.98	3.25	3.25
mean	2.22	2.47	2.36	2.36	2.69	2.06	2.47
standard deviation	0.8	0.6	0.3	0.3	0.3	0.8	0.6

Table 5.20: Ms of Commenda in ϕ with original data and data that are corrected because of alteration.

Internally, the outcrops A and B can show slightly positive trends (see also Appendix III). These trends are weak (and not really linear) but visible. In outcrop B especially the upper part shows small variations between adjacent data points, whereas the values in the lower part of the outcrop and in outcrop A present higher variations between adjacent data points. These variations cannot be explained by macroscopically visible features in the outcrop. Some red dominated layers at the base of outcrop B show lower Ms peaks, but to a lesser degree orange or multicoloured layers present a similar pattern. The few samples of outcrop E do not differ significantly.

The Ms values do not change with distance from the vent.

Histograms of the samples generally do not show a Gaussian grain size distribution as seen for most of the other successions. The fine gsc and a negative skewness dominate the Commenda succession. Only for a few sample from outcrop A present a Gaussian distribution might be assumed (see also figure 5.13).

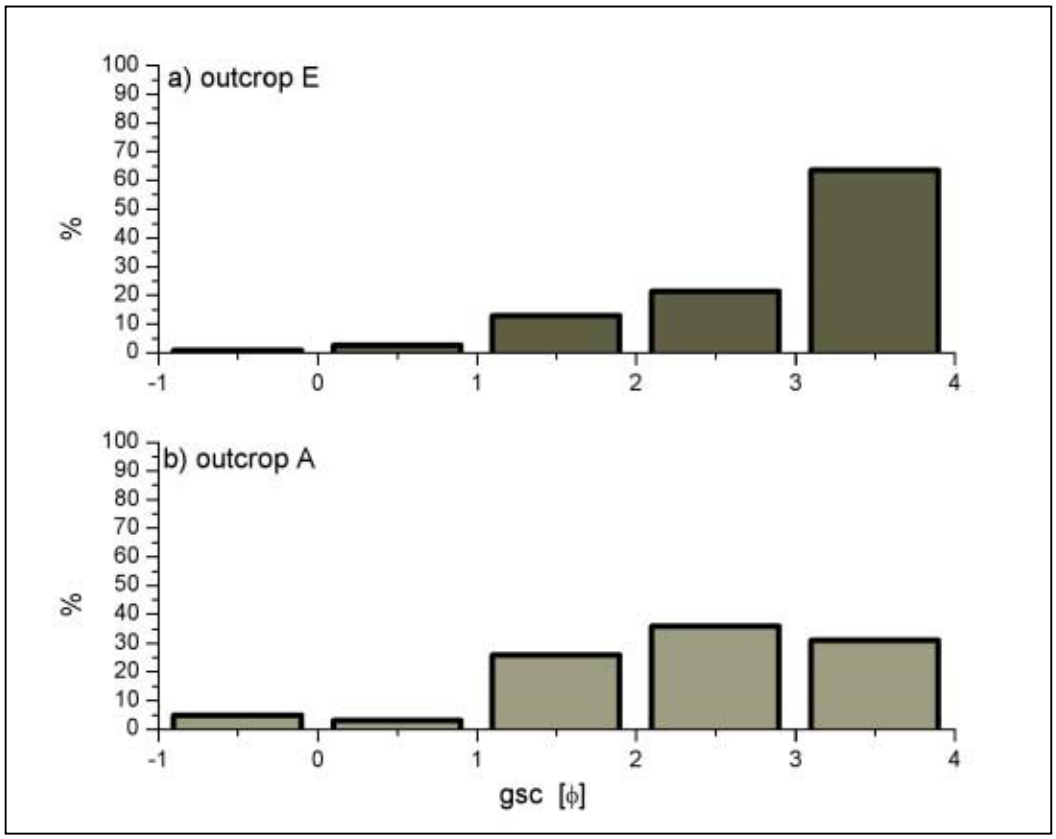

Figure 5.13: Histograms for the gsc of Commenda; a) shows a „normal“ distribution of the Commenda succession of outcrop E; b) shows a slightly Gaussian distribution of outcrop A.

The cumulative grain size curves are normally well developed and do not show a sigmoidal shape. A sigmoidal shape can only be observed when the finer gsc is split up. These shapes indicate a relatively high eruption energy which destroys the magma effectively, or alternatively the eruption cloud was not fully homogenous. Especially the finer material seems to be enriched in the eruption cloud. It has to be noted that in the two outcrops near the crater rim - A and B - the well developed curves decrease if the samples approximate to the base of the outcrops, here the cumulative grain size curves are a straight line. For the former successions this indicates that the eruption cloud is not homogenous; for the succession of Tufi Varicolori it is discussed whether the fine ash is depleted in this samples. In conclusion it can be said that the samples of Commenda in general are more developed and very fine grained, especially in stratigraphically higher positions.

The samples of Commenda show an excellent correlation between the 1st and 2nd moment (see also table 5.21). The plots for the single outcrops do not differ significantly and if the altered samples are cancelled a relatively ideal homogeneity similarity is observed. The resulting slope for the complete succession with the corrected data has a value of 4.92 ± 0.1, which is significantly higher than for the prior successions and in particular Tufi Varicolori can be discriminated very well (see also table 5.32).

sample	A	B	R	SD	N
outcrop A	-2.34 ± 0.5	5.04 ± 0.2	0.97	0.78	37
outcrop B	-1.41 ± 0.4	4.45 ± 0.2	0.98	0.55	23
outcrop E	-5.34 ± 2.2	5.90 ± 0.8	0.95	0.63	7
Commenda	-2.15 ± 0.3	4.88 ± 0.1	0.97	0.73	67
Commenda without the visibly altered samples	-2.26 ± 0.4	4.92 ± 0.1	0.97	0.75	62

Table 5.21: Results for the linear fit of Commenda for the scatter plot 1st moment vs. 2nd moment.

5.2.4.2. Susceptibility

The sus – measured in cgs-mode, standardised to 1g, and extended to 10^{-6} – ranges between 6.06 ± 0.0 and 158.56 ± 0.3 units (mean = 67.22, s: 26.6) for gsc05 and 6.68 ± 0.0 and 183.63 ± 0.3 units (mean = 74.32, s: 30.7) for gsc25 (see also table 5.22).

sample	outcrop A	outcrop A without visibly altered samples	outcrop A without visibly altered samples and extreme peaks	outcrop B	outcrop B without visibly altered samples and extreme peaks	outcrop E
min. value 0.5-0.25 mm	6.06 ± 0.0	14.94 ± 0.0	35.73 ± 0.1	29.29 ± 0.1	29.29 ± 0.1	41.76 ± 0.1
max. value 0.5-0.25 mm	125.88 ± 0.2	125.88 ± 0.2	101.52 ± 0.2	158.56 ± 0.3	109.00 ± 0.2	89.44 ± 0.1
mean 0.5-0.25 mm	65.83 (s:29.1)	68.91 (s: 26.3)	68.93 (s: 20.4)	86.49 (s: 30.5)	76.19 (s: 14.7)	72.30 (s: 14.4)
min. value 0.25-0.125 mm	6.68 ± 0.0	14.59 ± 0.0	26.11 ± 0.0	31.20 ± 0.1	31.20 ± 0.1	58.35 ± 0.1
max. value 0.25-0.125 mm	183.63 ± 0.3	183.63 ± 0.3	124.12 ± 0.2	151.3 ± 0.3	109.69 ± 0.2	98.01 ± 0.2
mean 0.25-0.125 mm	73.8 1 (s: 36.1)	78.25 (35.1)	76.51 (s: 23.5)	92.90 (s:27.0)	84.56 (16.7)	83.85 (s: 11.9)

sample	Commenda	Commenda without visibly altered samples	Commenda without visibly altered samples and extreme peaks
min. value 0.5-0.25 mm	6.06 ± 0.0	14.94 ± 0.0	29.29 ± 0.1
max. value 0.5-0.25 mm	158.56 ± 0.3	158.56 ± 0.3	109.00 ± 0.2
mean 0.5-0.25 mm	67.22 (s: 26.6)	69.07 (s: 24.9)	67.65 (s: 19.3)
min. value 0.25-0.125 mm	6.68 ± 0.0	14.59 ± 0.0	26.11 ± 0.0
max. value 0.25-0.125 mm	183.63 ± 0.3	183.63 ± 0.3	124.12 ± 0.2
mean 0.25-0.125 mm	74.32 (s: 30.7)	76.74 (s: 29.6)	74.66 (s: 21.6)

Table 5.22: Mean values for the sus for both gsc of Commenda. For outcrop A and B data are corrected for alteration occurring especially in the lower part of the outcrops. Also for these outcrops extreme peaks are deleted in a supplementary column. Samples are measured in cgs-mode, standardised to 1g, and have to be extended by 10^{-6}.

Especially the lower part of outcrop A shows relicts of fumarolic alteration, consequently these sampling points are revised to exclude possible influences of the fumaroles and variation in composition. Extreme high peaks, for example Ad19 with sus25 of 183.63 ± 0.3 units, as well as very low peaks like the sample Ad13 – sus05 14.94 ± 0.0 units –, do not belong to the "average peaks". These extreme peaks could be used as marker horizons, but they are not used for the average data values and the calculation of the mean. Outcrop E does not show such significant peaks as outcrops A and B. A significant change of the sus with distance from the vent cannot be observed.

Commenda can be discriminated from Punte Nere and Palizzi by the mean sus values, whereas a discrimination from Tufi Varicolori is not possible using the mean sus values (see also table 5.32). The average values can overlap also for the successions that are otherwise well distinguished (Punte Nere and Palizzi).

In contrast to the granulometry, the plots los vs. sus for both gsc do not show any trend of the sus. Differences between adjacent sampling points are very high, and only a few adjacent sampling points plot in the same range. However, unlike the older successions, Commenda generally has higher sus25 than sus05 values (see also chapters 5.2.1.2, 5.2.2.2, and 5.2.3.2). Such a relationship was only rarely observed within the other successions, especially for some marker horizons or in the presence of Pele's hair. Commenda has a very fine Ms in comparison with the other successions. Both observations indicate a high eruption and fragmentation energy. In outcrop A sus25 is often higher if red colours dominate in the layer, and significant low peaks are often associated with layers dominated by yellow-greenish colours. In outcrop E, where no significant differences of the data points can be observed and the data of sus25 plot generally higher than the data of sus05, red colours dominate the layers. The sus of outcrop B is distinct from the sus of the outcrops A and E; in general the difference between sus05 and sus25 is not as large as for the other outcrops. In particular the multicoloured layers in the middle of the outcrop show lower peaks, whereas a dominance of reddish colours combined with high peaks cannot be observed.

A scatter plot of sus05 vs. sus25 shows a good correlation for Commenda (see also figure 5.14). The single outcrops do not differ significantly and also their individual linear fits are similar. The resulting slope has a value of $0.80 \pm 0.43 * 10^{-3}$. Because of the possible change of composition samples showing signs of alteration are not used to calculate the linear regression (especially samples from outcrop A are concerned).

Plots of sus vs. the ratio sus/Ms show some trends for the succession, but outliers are also common. Thus, a linear fit to distinguish Commenda from the other successions is not sensible. Also the scatter plots of Ms vs. sus do not indicate a useful correlation.

Plotting sus vs. the ratio of the sus for both gsc only data clouds without any trend can be observed. No linear fit useful for a discrimination from other successions can be obtained.

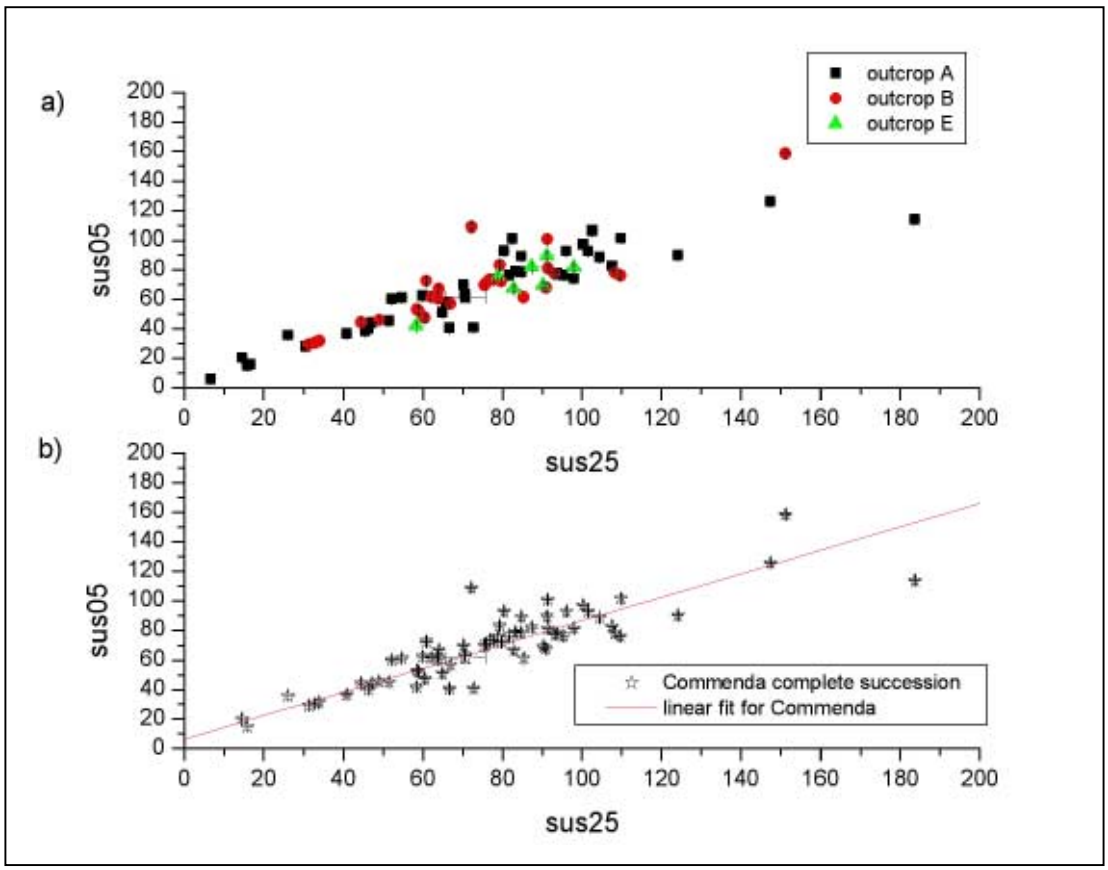

Figure 5.14: Scatter plots of sus05 vs. sus25. a) single outcrops with all data points; b) complete succession and linear fit (without altered samples).

The microprobe sample of Commenda magnetites correlates with the prominent peak of outcrop B Bd26 gsc05. In general the data plot in the same range as the other successions except of Tufi Varicolori (see also table 4.4). The values of Mg^{2+} and Cr^{3+} are relatively low whereas the Ti^{4+} amount is relatively high, close to the amount of Punte Nere. The lower value of Cr^{3+} is also reflected in the ratio of Fe^{3+}/Cr^{3+} and Ti^{4+}/Cr^{3+} that are significantly higher than for every other succession. The magnetites of Commenda – in contrast to the investigated magnetites of the other successions – can be described as very low-Cr titanomagnetites.

5.2.4.3. Gamma-ray

The standard outcrops of Commenda show mean values of 4.93 % (s: 0.8) for K, 13.28 ppm (s: 2.1) for U, and 41.5 ppm for Th (see also table 5.23). These values are obtained from corrected data which do not include samples showing visible alteration. If all samples are considered, however, the mean values do not change as significantly as seen for the Ms. Comparing the mean values of Commenda with the values of the other successions, every element allows distinction of Commenda from Tufi Varicolori. The mean K values of Commenda are slightly lower than those of Punte Nere and Palizzi, but a good discrimination is difficult because the range of Commenda values, as well as the s are higher than for Punte

Nere and Palizzi. Based on the U values, no discrimination from Punte Nere is possible. In addition, U cannot be used to differentiate Commenda from Palizzi because of the higher range of Commenda and the high s for both successions. The amounts of Th do not allow a discrimination between Punte Nere, Palizzi and Commenda because the successions show very similar mean values. Commenda presents the highest maximum values of Th observed so far (see also table 5.32).

sample	**K** [%]	**U** [ppm]	**Th** [ppm]
Minimum outcrop A	3.93 ± 0.1	10.27 ± 0.5	32.07 ± 0.4
Maximum outcrop A	5.50 ± 0.2	14.33 ± 0.9	43.733 ± 1.1
mean outcrop A	4.65 (s: 0.4)	11.93 (s: 1.1)	37.08 (s: 3.1)
Minimum outcrop A without alteration	4.27 ± 0.2	10.27 ± 0.5	32.07 ± 0.4
Maximum outcrop A without alteration	5.50 ± 0.2	14.33 ± 0.9	43.733 ± 1.1
mean outcrop A without alteration	4.69 (s: 0.3)	11.86 (s: 1.2)	36.43 (s: 2.8)
Minimum outcrop B	3.47 ± 0.3	10.97 ± 0.4	35.80 ± 1.7
Maximum outcrop B	5.47 ± 0.1	16.33 ± 0.4	48.17 ± 2.1
mean outcrop B	5.28 (s: 0.2)	14.48 (s: 1.3)	44.70 (s: 1.9)
Minimum outcrop E	5.80 ± 0.3	15.67 ± 0.6	47.17 ± 0.4
Maximum outcrop E	7.00 ± 0.2	19.47 ± 0.4	57.07 ± 0.2
mean outcrop E	6.44 (s: 0.4)	17.14 (s: 1.2)	51.88 (s: 2.9)
Minimum Commenda	3.47 ± 0.3	10.27 ± 0.5	32.07 ± 0.4
Maximum Commenda	7.00 ± 0.2	19.47 ± 0.4	57.07 ± 0.2
mean Commenda	4.87 (s: 0.8)	13.17 (s: 2.0)	41.11 (s: 5.7)
Minimum Commenda without alteration	3.47 ± 0.3	10.27 ± 0.5	32.07 ± 0.4
Maximum Commenda without alteration	7.00 ± 0.2	19.47 ± 0.4	57.07 ± 0.2
mean Commenda without alteration	4.93 (s: 0.8)	13.28 (s: 2.1)	41.3 (s:5.9)

Table 5.23: Maximum, minimum and mean values of K [%], U [ppm], and Th [ppm] for the complete succession and single standard outcrops of Commenda. Data are given with and without samples with visible alteration.

A significant change of the γ-ray values with increasing distance from the vent cannot be observed.

The individual outcrops can differ significantly: while outcrop A does not show significant trends, outcrop B – especially the lower part (0–4 m) – presents increasing values for all elements (see also figure 5.15). Also outcrop E can show a very rough trend for two elements, K slightly increasing and Th slightly decreasing, when differences between the adjacent data points are not considered.

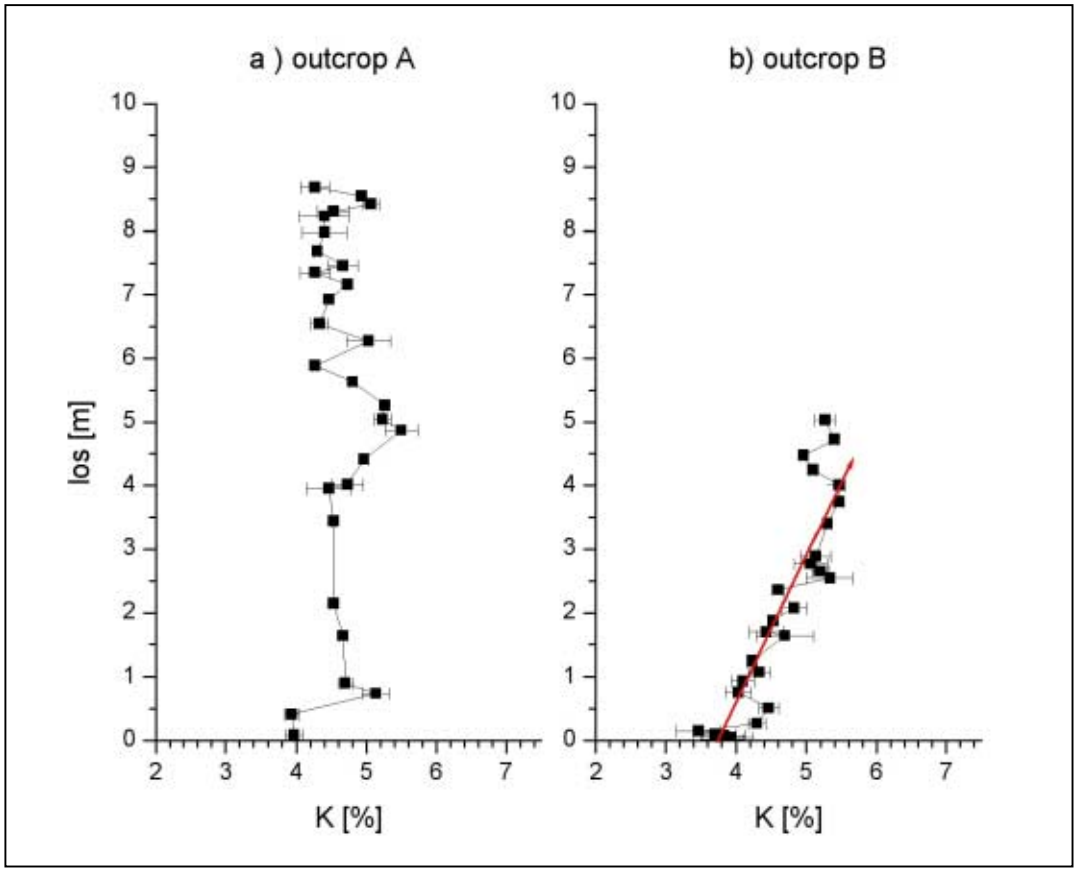

Figure 5.15: los vs. K for outcrop A (a) and outcrop B (b). The first does not show any visible trend, whereas a slightly positive trend can be observed within the latter. It is important to note that the base of the outcrop A (nearly 1m) is built up by layers which in general show visible alteration and have not been used for a correlation.

Individual outcrops not only show individual behaviour but also different ranges of the average data values, as seen in table 5.24. It is remarkable that in particular the data of outcrop E plot slightly higher than the data of the two other outcrops. Outcrops E and B are at similar distances from the vent, thus an influence of vent distance on the values can be excluded. Outcrop A is located near the vent on the crater rim and has average element values close to those of outcrop B. The trend observed in outcrop B could be explained as a magmatic evolution of Commenda, which can admittedly not be recorded by the sus measurements. Outcrop B is the only one with this trend. It does not occur directly near the vent (outcrop A) because of the behaviour of the layer thickness of Commenda that decreases

very rapidly with distance from the vent (see also chapter 2.5). Even though outcrop A at the crater rim has a height of about 10 m (for sampling ground), the stratigraphic section which can be observed is lower than the section which is exposed in outcrop B with about 5 m height for Commenda. In outcrop B, lying a few hundred metres away, layers are one to a few centimetres thick, whereas the layers of outcrop A have a thickness of a few centimetres to decimetres.

The trend which can be observed in outcrop B is particularly well developed for K and Th, whereas the values for U show higher variations and the trend is more blurred. A reason for this variation is possibly the very mobile U which could be leached.

sample	**K** [%]	**U** [ppm]	**Th** [ppm]	**U/Th**
Commenda	**4.00 – 6.50**	**10.5 – 18.5**	**34 – 54**	**0.28 – 0.38**
outcrop A	4.25 – 5.50	10.5 – 14.0	32 – 44	0.29 – 0.36
outcrop B	3.75 – 5.50	11.0 – 16.0	35 – 47	0.28 – 0.36
outcrop E	6.00 – 6.75	15.5 – 19.0	47 – 57	0.30 – 0.37

Table 5.24: Average γ-ray values and the U/Th ratio of the different outcrops.

In plots of the Ms vs. the element concentrations the data of the single outcrops form small overlapping clusters, and no obvious trend can be noted for these plots. Data of outcrop B show a slightly increasing trend in a plot Ms vs. K.

Scatter plots of the element concentration vs. the ratio of elements are useful to give some information about depletion and enrichment of elements in single outcrops. The results for the linear fits of the complete succession, which can possibly be a tool for the discrimination of Commenda from other successions, are given in table 5.25. Plots for data of the single outcrops are given in Appendix III. In these plots it is important to note that the data from outcrop E tend to plot higher for the single element concentrations, while these data normally do not differ significantly in the element ratio. This observation can be explained by enrichment of outcrop E samples in the single elements. This is also indicated in table 5.24 showing that the values for U/Th for all outcrops do not vary as widely as the values for the single element concentrations. Another possibility is the depletion of the elements in outcrops A and B, however it is unlikely that all elements are leached in the same way. K and U are easily leached, whereas Th – in comparison with K and U – is a relatively stable element. For these reasons, an element enrichment in outcrop E is the favoured model possibly originated by the overlying Pietre Cotte pumice (above the successions of Commenda and Cratere Attuale). Interestingly, all successions exposed in outcrop E have γ-ray values that are slightly higher than the corresponding data of other outcrops (see also chapters 5.2.3.3 and 5.3.5.3) (possibly originated by the overlying pumice layers: 2nd Palizzi pumice over Palizzi and Pietre Cotte pumice over Commenda and Cratere Attuale). Outcrop E is located in a closed location where possibly the surrounding is enriched by some unknown activity which also affected the measured not compacted material. No influence on the sus is observed.

The single plots show the following results: plotting K vs. Th/K the individual outcrops can be discriminated relatively well. The outcrops A and B have the same range of K concentration but based the Th/K ratio an enrichment of Th in outcrop B, or alternatively a depletion of Th in outcrop A can be assumed. The plot also indicates that Th is independent of K. The single outcrops show different linear trends so that the slope of the resulting plot of the complete succession is not sensible useful for correlation. The plot K vs. U/K shows similar trends but the differences in the ratio are not as large as in the previous plot. In this diagram a slight dependence of K and U can be assumed but it is not very obvious. Similar to the plot K vs. Th/K the results of the linear regression cannot be used for a correlation. The plot of U vs. Th/U demonstrates very well that the single outcrops only differ in the element concentration whereas the ratio is more or less constant. No evolution can be observed, except in parts of outcrop B. Like before this slope is not useful for a correlation, even though the slopes for the single outcrops and the resulting slope for the complete succession present a higher degree of similarity than the slopes of the other plots. The additional plots U vs. K/U, Th vs. U/Th, and Th vs. K/Th are not significantly different from the former diagrams and also for these plots the results of the linear fits are not useful for a correlation.

Comparing the data of Commenda with the other successions a discrimination from the succession of Tufi Varicolori is generally possible, only sometimes, like in the plot K vs. Th/K, data overlap occurs. Not considering most of the data of outcrop E and the Punte Nere data of outcrop G, the plots K vs. Th/K, U vs. K/U, and Th vs. K/Th allow a discrimination between Commenda and Punte Nere. The successions of Palizzi and Cratere Attuale normally plot in the same range as the data of Commenda. Differences that are observed in a few cases are too small for a sensible discrimination.

Plots of the single elements may also allow a discrimination of the different successions. The scatter plots K vs. U and Th vs. K for the Commenda succession show a positive correlation for the different outcrops, as seen above for the plots element concentration vs. ratio. also in these plots the data of the outcrop E can be distinguished from the other outcrops (this will also be observable for the next plots). As seen before the data of outcrop E follow the same trend as the lower plotting data of outcrops A and B. The resulting trends for Commenda seem to be sensible for a correlation but in comparison with the single outcrops the variability of the slopes is too large to use the resulting slope as a secure correlation tool. In these diagrams Commenda can be distinguished from Punte Nere (without outcrop G) relatively well and also the discrimination between Commenda and Tufi Varicolori is relatively good, except for some small overlap of the higher plotting Tufi Varicolori data with the lower plotting Commenda data. As seen in the plots of element concentration vs. ratio, Commenda, Palizzi, and Crater Attuale cannot be separated using the current scatter plots. The plot of Th vs. U shows a positive correlation, but the results for the linear regression vary too much. Although the resulting plot subjectively allows distinction of the successions by element concentration, the variability of linear regression precludes a good discrimination by the slope of the single plots. In this plot (Th vs. U) only Tufi Varicolori can be well distinguished from

Commenda. The last plot U/Th vs. K shows that the ratio of the elements does not differ for the single outcrops. A useful correlation for the complete succession cannot be found. In the scatter plot with all successions Commenda can be discriminated by parts of the lower plotting Tufi Varicolori, whereas the higher plotting parts overlap. The other successions cannot be distinguished, only Punte Nere is distinguishable if the data of outcrop G and outcrop E are not considered.

sample	A	B	R	SD	N
K vs. Th/K	51261.28 ± 1110.3	$-2.57*10^6 \pm 1.3*10^6$	-0.02	9.57	63
K vs. U/K	40300.88 ± 1082.7	$33.07*10^7 \pm 4.0*10^6$	0.11	9.52	63
U vs. Th/U	17.90 ± 0.4	-1.62 ± 0.1	-0.21	6.77	63
U vs. K/U	20.67 ± 0.4	$-0.002 \pm 0.1*10^{-3}$	-0.37	6.44	63
Th vs. K/Th	52.18 ± 1.3	-0.01277 ± 0.0	-0.48	4.52	63
Th vs. U/Th	33.84 ± 0.6	30.47 ± 1.8	0.15	13.67	63
K vs. U	14434.68 ± 533.9	2643.11 ± 40.2	0.88	4.56	63
Th vs. U	15.96 ± 0.3	1.96 ± 0.0	0.85	7.30	63
Th vs. K	11.76 ± 0.3	$0.61*10^{-3} \pm 6.5*10^{-6}$	0.87	6.91	63
U/Th vs. K	0.30 ± 0.0	$0.43*10^{-6} \pm 0.4*10^{-6}$	0.13	0.03	63

Table 5.25: Results for the linear fit of Commenda for the element scatter plots. Data of outcrops A, B, and E. Useful trends cannot be observed in this succession.

5.2.5. Cratere Attuale

Standard outcrops: B and E

5.2.5.1. Granulometry

The succession of Cratere Attuale is formed by different surge and fall deposits (see also chapter 2.6). The investigated samples normally contain different coarse and fine ash layers. One of the standard outcrops (E) is dominated by dry-surge deposits and covered by the Pietre Cotte pumice, thus these deposits of Cratere Attuale are stratigraphically attributed to the Pietre Cotte unit (the lowermost unit of Cratere Attuale). The other outcrop (B) shows a gradual change from Commenda to Cratere Attuale, and therefore the deposits can be assigned stratigraphically to the Pietre Cotte unit.

The mean Ms of the standard outcrops is about 2.18 ϕ (s: 0.6) (see also table 5.26). The outcrops have different mean values and ranges of Ms. Outcrop E (below the Pietre Cotte pumice) shows a lower mean Ms and a wider range than the samples of outcrop B. Samples of outcrop B can be split into samples clearly attributable to Cratere Attuale, and samples which could be attributed to the top of Commenda. When samples clearly attributable to Cratere Attuale are considered exclusively, only the mean Ms of all outcrops changes its values in a significant way. Admittedly it is reasonable to use all samples for a correlation. Comparing the Ms of Cratere Attuale with the other successions only Commenda has a higher mean Ms than Cratere Attuale, whereas it is significantly lower for the other successions (see also table 5.32).

sample	outcrop B all samples	outcrop B selected samples	outcrop E	Cratere Attuale	Cratere Attuale selected samples
min. value	1.30	1.30	1.06	1.06	1.06
max. value	3.00	2.76	2.43	3.00	2.76
mean	2.37	2.26	1.84	2.18	2.00
standard deviation	0.5	0.7	0.5	0.6	0.6

Table 5.26: Ms of Cratere Attuale in ϕ. Outcrop B can be subdivided into 2 parts. For the upper stratigraphic part the attribution to Cratere Attuale is clear, whereas samples of the lower part could also belong to Commenda. The samples clearly attributable to Cratere Attuale are shown in a separate column (outcrop B selected samples and values for the complete succession only used clearly attributable samples).

A change of the Ms with distance from the vent is not observable. Within the outcrops no obvious trends of the Ms are visible. In outcrop E 3 samples are taken from a single dry-surge deposit (lower, middle, and upper part, with a cumulative thickness of about 40 cm). In this case a trend from coarse to fine can be noted. This reflects the distribution of particles in the eruption cloud and the processes active inside the cloud at different times.

Histograms of the samples show different distributions for the 2 outcrops. Samples of outcrop B present peaks for the extreme coarse as well as for the extreme fine gsc. The extremely coarse parts may be a preparation artifact, because frequently it is not possible to separate grains sticking together. Not considering the coarsest gsc, the plots generally show a negative skewness for Cratere Attuale deposits. Samples of outcrop E often show a less pronounced Gaussian distribution, as well as slightly bimodal distributions. In addition, negative as well as positive skewness can be observed.

Cumulative grains size curves for both outcrops do not show a well developed sigmoidal shape, an observation already made for most of the older successions, except Punte Nere. Some samples of Cratere Attuale have an incipient sigmoidal curve. Samples of outcrop E with a relatively well distribution of gsc show a less developed curve than samples of outcrop B. The observed grain size curves suggest that the eruption cloud was less homogeneous than the clouds for example of Punte Nere where well-developed sigmoidal shapes can be observed.

The scatter plot of the 1st vs. the 2nd moment shows a linear correlation. The resulting fit of the linear regression has a slope of 4.56 ± 0.4 for the complete succession (see also table 5.27). As already seen for the mean Ms, the slope of the complete Cratere Attuale succession allows a distinction from the other successions, only Commenda shows higher values whereas the other successions in general possess lower slope values (see also table 5.32).

sample	A	B	R	SD	N
outcrop B	-1.24 ± 0.7	4.76 ± 0.3	0.99	0.44	9
outcrop E	1.00 ± 0.6	3.10 ± 0.3	0.99	0.35	5
Cratere Attuale	-1.09 ± 0.8	4.56 ± 0.4	0.96	0.8	14

Table 5.27: Results for the linear fit of Cratere Attuale for the scatter plot 1st vs. 2nd moment.

5.2.5.2. Susceptibility

The sus – measured in cgs mode, standardised to 1g, and extended to 10^{-6} – ranges from 45.33 ± 0.2 to 105.15 ± 0.2 units (mean = 77.04 units, s: 18.8) for sus05 and from 48.45 ± 0.1 to 119.1 ± 0.2 units (mean = 91.91 units, s: 19.8) for sus25 (see also table 5.28). Outcrop B can be subdivided into the same 2 groups as has been done for the granulometry. Working solely with samples attributed to Cratere Attuale the mean values are lower than the mean values of all other samples. In comparison, the Palizzi and Punte Nere successions have higher values than Cratere Attuale and can be distinguished relatively well. Tufi Varicolori shows lower mean values for the sus and can thus be distinguished reasonably well from Cratere Attuale. However, there is a strong overlap of minimum and maximum values. Commenda behaves in a special manner (see also chapter 5.2.5.3). Using solely the mean values of the complete successions a discrimination seems to be possible. In this case Cratere Attuale has higher values for both sus. However, in the outcrops it can be noted that for outcrop B sus05 of Cratere Attuale is lower (70.76 units, s: 18.9) than sus05 of the underlying Commenda (76.19 units, s: 14.7); for sus25 the situation is reversed, with 87.74 units (s: 22.8) for Cratere Attuale and 84.56 units (s: 16.7) for Commenda (see also tables 5.22 and 5.28). In outcrop E both sus behave like the samples of the complete successions. This effect of outcrop-dependability of the correlation is even more pronounced for the gamma-ray values (chapter 5.2.5.3) where the possible reasons for this behaviour will be discussed.
A change of the sus with distance from the vent is not observable.

sample	**outcrop B**	**outcrop B** selected samples	**outcrop E**	**Cratere Attuale**	**Cratere Attuale** selected samples
min. value 0.5-0.25 mm	45.33 ± 0.2	66.43 ± 0.1	75.62 ± 0.1	45.33 ± 0.2	66.43 ± 0.1
max. value 0.5-0.25 mm	105.15 ± 0.2	69.00 ± 0.1	104.59 ± 0.2	105.15 ± 0.2	104.59 ± 0.2
mean 0.5-0.25 mm	70.76 (s: 18.9)	67.77 (s: 1.1)	88.3 (s: 11.9)	77.04 (s: 18.8)	80.62 (s: 13.7)
min. value 0.25-0.125 mm	48.45 ± 0.1	78.13 ± 0.1	84.90 ± 0.1	48.45 ± 0.1	78.13 ± 0.1
max. value 0.25-0.125 mm	119.1 ± 0.2	91.09 ± 0.1	111.02 ± 0.2	119.1 ± 0.2	111.02 ± 0.2
mean 0.25-0.125 mm	87.74 (s: 22.8)	85.28 (s: 5.4)	99.11 (s: 8.9)	91.81 (s: 19.8)	93.93 (s: 10.3)

Table 5.28: Mean values for the sus for both gsc of Cratere Attuale. Samples are measured in cgs-mode. standardised to 1g, and have to be extended by 10^{-6}. Columns named selected samples mean that only samples are used which can attributed to Cratere Attuale clearly, the remaining samples also belong to Cratere Attuale but the attribution is only sure for about 90% (columns without explanations).

Similarly, no well developed trends of the sus are observable for the samples of outcrop B (all samples) (see also figure 5.16). It can be noted that in outcrop B, as well as for the data of Commenda, sus25 has higher values than sus05 (in general not observable in Tufi Varicolori). This phenomenon is noticeable for the last samples of outcrop E, too. Outcrop E shows a

slightly positive trend for sus25 and a slightly negative trend for sus05. This does not match with the Ms data, therefore a higher degree of fragmentation that destroyed more larger sus-bearing minerals and aggregates is unlikely. The evolution of the single dry-surge deposit (mentioned in chapter 5.2.5.1) is also remarkable for both sus.

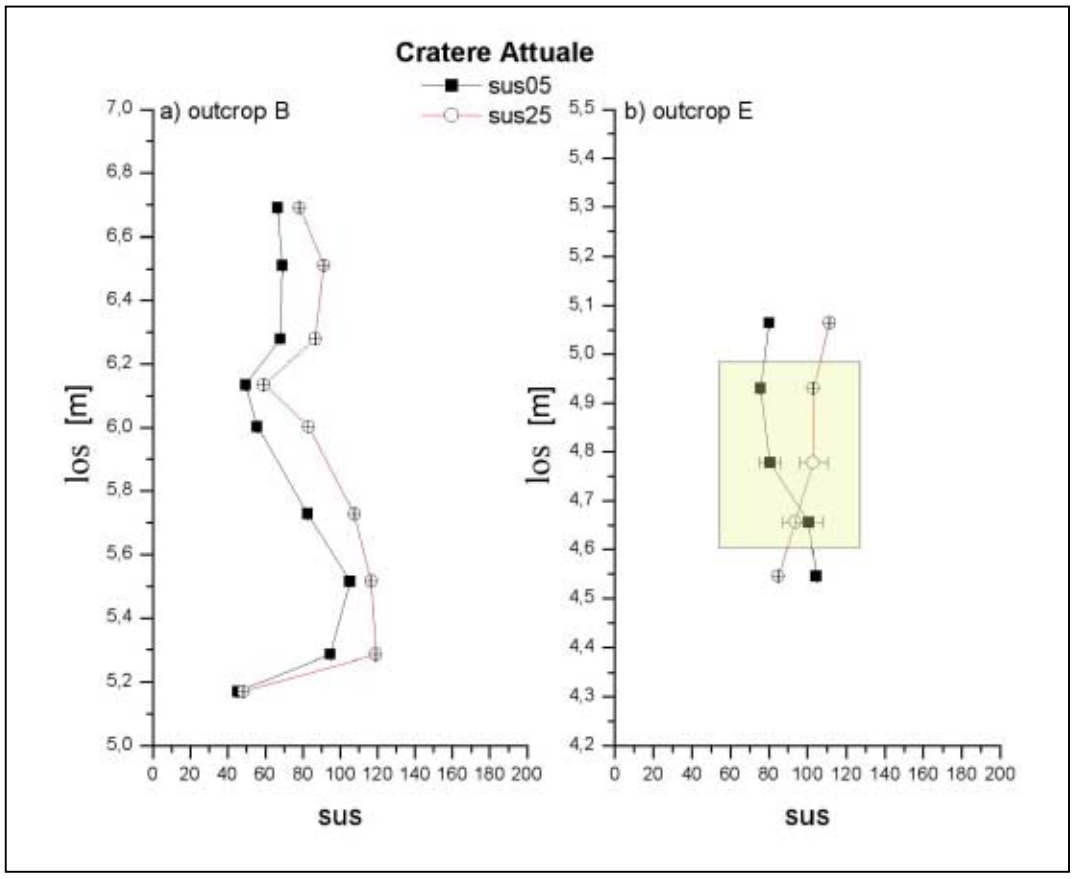

Figure 5.16: Evolution of the los vs. sus of both standard outcrops of Cratere Attuale. a) outcrop B and b) outcrop E. The sus for both gsc are shown, in general sus05 plots lower than sus25, which is contrary to Tufi Varicolori. The highlighted area in outcrop E indicates a single dry-surge deposit where 3 samples were taken.

The plot of sus05 vs. sus25 (see also Appendix III) shows a positive trend. This correlation is mainly made up by the data of outcrop B, whereas data of outcrop E show some outliers. The linear fit of the complete succession is more or less acceptable for a correlation (R: 0.7) and has a slope of 0.63 ± 0.0. In comparison with the significant values of the other successions this is the flattest slope of all investigated successions.

In the scatter plot of sus05 vs. sus05/Ms an elongate cloud of data points can be observed. Although it suggests a slightly positive trend, the linear fit is not useful for a correlation with other successions. The plot for sus25 shows a data cloud, but the data do not show any significant trend and the linear regression is not good. Scatter plots of sus vs. the ratio of both sus also show different clusters without a defined correlation. The results of the linear regressions are not useful for a correlation with other successions.

5.2.5.3. Gamma-ray

The γ-ray values for the standard outcrops of Cratere Attuale are 5.52 % (s: 0.3) for K, 14.27 ppm (s: 2.0) for U, and 43.83 ppm (s: 5.9) for Th (see also table 5.29). Like for the sus measurements all samples were taken into account. Table 5.29 shows the results for the selected samples, too. These results are split into samples which can be attributed clearly to Cratere Attuale and samples attributed to Cratere Attuale with a high probability. In contrast to the sus values, γ-ray exhibits larger differences, following the discussion given above it is better to use the complete sample set. In comparison with values of the other successions all measured elements discriminate Cratere Attuale from Tufi Varicolori. Similarly, the complete succession of Commenda is distinct, but the values for Th tend to be similar. Punte Nere can be distinguished by the U values. The other successions have values that overlap with the values of Cratere Attuale (see also table 5.32).

Comparing solely samples of 2 successions (Cratere Attuale and Commenda) from the same outcrops the following observations can be made (see also tables 5.23 and 5.29): for outcrop B both successions can be distinguished relatively well. Using all samples of Cratere Attuale enhances the discrimination. The discrimination between the 2 successions shows different values if solely a single outcrop a is used or the complete succession (outcrops A, B and E for Commenda and outcrops B and E for Cratere Attuale). For the single outcrop (B) Cratere Attuale normally shows lower values than Commenda, but the situation is reversed when data of the complete succession are used. This can also be observed for outcrop E. It remains open if generally the data of Cratere Attuale plot lower than the data of Commenda. In the case of Commenda possibly the also remaining data of outcrop A (solely Commenda), showing lower values than the other 2 outcrops of Commenda, change the proportion. The little amount of data available for Cratere Attuale is also a problem for a proper interpretation. Outcrop A is a highly exposed outcrop at the crater rim, where fumaroles and gases can occur. Likewise heavy rainfall do not reside in the deposits – located above the ground-water level – and thus an accumulation of elements is not possible. This can influence the element concentration (measured by γ-ray spectroscopy) of this outcrop, too. Element depletion in this outcrop may be due to different effects (especially by weathering). This depletion because of exposition can be adverse when the successions do not differ in a significant way as seen for Commenda and Cratere Attuale. Using data of outcrop A could falsify the mean values of Cratere Attuale and Commenda, and a discrimination as made before for the other successions is not advisable. Thus the data of Cratere Attuale have to be handled with care especially if a distinction from Commenda is required. Commenda and Cratere Attuale are overlain by the Pietre Cotte pumice that shows higher γ-ray values, in particular of U and Th. This pumice can be weathered and the fluids can import certain elements to the underlying deposits. This would also explain the observed higher values for every succession exposed in outcrop E (outcrop B is not overlain by a pumice layer today). Admittedly, the ratio U/Th for the single

outcrops shows the same ranges (see also table 5.30). No significant change with distance from the vent can be observed.

sample	K [%]	U [ppm]	Th [ppm]
Minimum outcrop B	4.43 ± 0.0	11.00 ± 0.5	36.13 ± 1.4
Maximum outcrop B	5.73 ± 0.0	15.43 ± 0.8	46.63 ± 1.3
mean outcrop B	4.96 (s: 0.4)	12.98 (s: 1.3)	39.89 (s: 3.1)
Minimum outcrop B selected samples	4.57 ± 0.1	11.00 ± 0.5	36.93 ± 0.8
Maximum outcrop B selected sample	5.73 ± 0.0	15.43 ± 0.8	46.63 ± 1.3
mean outcrop B selected sample	5.13 (s: 0.5)	13.20 (s: 1.8)	41.03 (s: 4.1)
Minimum outcrop E	6.07 ± 0.2	15.83 ± 0.5	46.77 ± 1.0
Maximum outcrop E	7.03 ± 0.1	16.90 ± 0.3	56.20 ± 4.6
mean outcrop E	6.41 (s: 0.3)	16.35 (s: 0.4)	50.11 (s: 3.4)
Minimum Cratere Attuale	4.43 ± 0.0	11.00 ± 0.5	36.93 ± 0.8
Maximum Cratere Attuale	7.03 ± 0.1	16.90 ± 0.3	56.20 ± 4.6
mean Cratere Attuale	5.52 (s: 0.8)	14.27 (s: 2.0)	43.82 (s: 5.9)
Minimum Cratere Attuale selected sample	4.57 ± 0.1	11.00 ± 0.5	36.93 ± 0.8
Maximum Cratere Attuale selected sample	7.03 ± 0.1	16.90 ± 0.3	56.20 ± 4.6
mean Cratere Attuale selected sample	5.93 (s: 0.7)	15.17 (s: 1.9)	46.70 (s: 5.7)

Table 5.29: Maximum, minimum, and mean values of K [%], U [ppm], and Th [ppm] for the complete succession and single standard outcrops of Cratere Attuale.

Within the outcrops no trends for the single elements can be observed. Scatter plots of Ms vs. the element concentration do not indicate significant new trends or possibilities for a discrimination. As well as before the successions are defined by their element concentration and the relevant scatter plots of concentration vs. ratio or concentration. These plots do not allow a discrimination for the single successions.

Table 5.30 shows the range of the average values for the two outcrops and the complete succession. The range of values is generally different in both outcrops, with only minor overlap, whereas solely the values of the ratio U/Th have a comparable range.

sample	K [%]	U [ppm]	Th [ppm]	U/Th
Cratere Attuale	**4.50 – 6.75**	**11.5 – 17.0**	**37 - 51**	**0.29 – 0.36**
outcrop B	4.50 – 5.50	15.5 – 17.0	36 – 47	0.29 – 0.36
outcrop E	6.00 – 6.75	10.5 – 16.0	46 – 54	0.29 – 0.36

Table 5.30: Average γ-ray values and the U/Th ratio of the different outcrops.

The scatter plots of the element concentration vs. various element ratios (see also Appendix III) reflect the differences between the two outcrops discussed above. However, it is observable that the element ratios are similar and only the concentration of the single elements differ (in a significant way) (also observable for Palizzi [chapter 5.2.3.3]). In general information about depletion and enrichment of elements can be deduced from the few plots. The plot K vs. Th/K shows a well linear correlation for the complete succession but in comparison with the fits of the single outcrops the resulting fit is not sensible for a correlation. In addition, Th seems to be independent of K. A plot of K vs. U/K also exhibits the difference of the 2 outcrops, but outcrop B shows a different behaviour than outcrop E. In the latter, K and U seem to be independent, whereas outcrop B indicates that K seems to be dependent of U (negative trend). The resulting linear fit is not significant for a good correlation with other successions. In general the additional plots U vs. K/U and Th vs. K/Th are not significantly different from the former diagrams and the results of the linear fits are not useful for a correlation, too. The result of the scatter plot U vs. Th/U can be useful for a correlation even though the single outcrops differ slightly. This plot shows only a slight dependence of Th and U. In contrast, the plot Th vs. U/Th does not indicate a correlation if the linear fits are compared. Most of the outcrops do not suggest a well pronounced depletion or enrichment of the different elements, which might be due to the small number of samples.

Using the γ-ray plots to distinguish Cratere Attuale from other successions, by plotting in different clusters and trends, the following observations can be made (see also Appendix III): Tufi Varicolori is distinguishable from Cratere Attuale in every plot, and only very limited overlap occurs. It is also possible to characterise Punte Nere and Cratere Attuale using the plots K vs. Th/K (not considering outcrop G from Punte Nere) and in particular the plots Th vs. K/Th (although a stronger overlap can be noticed), K vs. U/K and U vs. K/U. The plots of Th vs. U/Th and U vs. Th/U display too much overlap of data. The successions of Palizzi and Commenda cannot be distinguished from Cratere Attuale using these plots because their data normally plot in a similar range.

Plots of the single elements can give additional information about the single outcrops as well as about the complete succession when comparing with the other succession (see also Appendix III). Differences between the single outcrops show up clearly in the plots K vs. U,

Th vs. U, and Th vs. K, because their linear fits differ significantly. However, the complete successions mark a positive trend of concentrations, which normally correlates with the linear fit of outcrop B relatively well whereas the fit for outcrop E is not as important as the fit of outcrop B. For the plot U/Th vs. K it can be observed that the element ratio does not differ significantly inside the outcrops, whereas the concentration of the single elements – in this case K – shows wide differences and opposing trends. The resulting fit of the linear regression is not sensible for a correlation.

Tufi Varicolori can be distinguished from Cratere Attuale in every plot of the single element concentration, whereas overlaps in the plot U/Th vs. K are too strong to be sensible for a discrimination of the two successions. Punte Nere is distinguishable from Cratere Attuale using the plots K vs. U and in particular Th vs. K, not considering outcrop G from Punte Nere. As well as for the plots concentration vs. ratio a discrimination of Cratere Attuale from Palizzi and Commenda is not possible because of the high degree of overlap.

sample	A	B	R	SD	N
K vs. Th/K	87811.19 ± 8008.3	$-42.57 * 10^6 \pm 9.9 * 10^6$	-0.13	10.07	13
K vs. U/K	57773.93 ± 5350.6	$-16.32 * 10^6 \pm 20.3 * 10^6$	-0.02	10.15	13
U vs. Th/U	**21.19 ± 1.7**	**-2.62 ± 0.6**	**-0.28**	**4.58**	**13**
U vs. K/U	36.04 ± 2.4	$-0.006 \pm 0.6 * 10^{-3}$	-0.59	3.86	13
Th vs. K/Th	50.00 ± 7.2	-0.005 ± 0.0	-0.04	6.01	13
Th vs. U/Th	46.21 ± 4.4	-7.72 ± 13.3	-0.3	6.02	13
K vs. U	3717.12 ± 1570.0	3531.22 ± 110.5	0.95	3.20	13
Th vs. U	6.94 ± 2.1	2.54 ± 0.1	0.90	2.60	13
Th vs. K	2.94 ± 2.1	$0.74 * 10^{-3} \pm 38.6 * 10^{-6}$	0.95	1.77	13
U/Th vs. K	0.32 ± 0.0	$98.3 * 10^{-9} \pm 84.9 * 10^{-6}$	0.44	0.02	13

Table 5.31: Results for the linear fit of Cratere Attuale for the element scatter plots. Data of outcrops B and E. Plots with trends useful for correlation are highlighted with bold letters.

5.3. Conclusions

The data for the standard outcrops of La Fossa di Vulcano show that in general a characterisation for most of the successions is possible. Table 5.32 shows the characteristics of granulometry, sus, and γ-ray data for the different successions. Furthermore, scatter plots – especially of the γ-ray measurements – often allow a graphic discrimination of the different successions.

Gamma-ray scatter plots of elements vs. the element ratios frequently suggest a linear trend for all successions. These observations allow interpretation of element behaviour. For example, the plot of U vs. the ratio Th/U indicates that the U concentration is in general independent of the Th concentration.

Type	Punte Nere	Tufi Varicolori	Palizzi	Commenda	Cratere Attuale
Grain size					
Ms					
min	0.06	-0.05	0.55	0.12	1.06
max	2.48	2.78	2.07	3.25	3.00
mean	1.35 (s: 0.5)	1.60 (s: 0.6)	1.35 (s: 0.4)	2.47 (s: 0.6)	2.18 (s: 0.6)
1st moment vs. 2nd moment					
slope	3.43 ± 0.2	3.57 ± 0.1	2.60 ± 0.4	4.92 ± 0.1	4.56 ± 0.4
sus					
sus05					
min	44.18 ± 0.1	42.99 ± 0.1	74.60 ± 5.3	14.94 ± 0.0	45.33 ± 0.2
max	153.50 ± 9.3	120.44 ± 0.3	127.91 ± 0.2	158.56 ± 0.3	105.15 ± 0.2
mean	109.28 (s: 19.8)	73.61 (s: 19.3)	102.92 (s: 13.4)	69.07 (s: 24.9)	77.04 (s: 18.8)
sus25					
min	48.53 ±0.1	38.81 ± 0.1	74.46 ± 0.1	14.59 ± 0.0	48.45 ± 0.1
max	186.31 ± 9.7	123.17 ± 0.2	148.53 ± 10.6	183.63 ± 0.3	119.1 ± 0.2
mean	117.18 (s: 24.1)	70.50 (s: 19.1)	106.77 (s: 21.2)	76.74 (s: 29.6)	91.81 (s: 19.8)
sus vs. sus/Ms					
gsc05					
slope	0.58 ± 0.1	not significant	not significant	not significant	not significant
gsc25					
slope	0.58 ± 0.1	not significant	not significant	not significant	not significant
sus05 vs. sus25					
slope	0.74 ± 0.1	0.92 ± 0.0	not significant	$0.80 \pm 0.4 * 10^{-3}$	0.63 ± 0.0
sus05 vs. sus05/sus25					
slope	not significant	not significant	not significant	not significant	not significant
sus05 vs. sus05/sus25					
slope	not significant	not significant	not significant	not significant	not significant
γ-ray					
K [%]					
min	4.17 ± 0.3	3.17 ± 0.0	4.34 ± 0.1	3.47 ± 0.3	4.43 ± 0.0
max	6.83 ± 0.3	5.77 ± 0.8	6.63 ± 0.3	7.00 ± 0.2	7.03 ± 0.1
mean	5.70 (s: 0.5)	4.04 (s: 0.5)	5.62 (s: 0.7)	4.93 (s: 0.8)	5.52 (s: 0.8)
U [ppm]					
min	10.23 ± 0.9	6.53 ± 0.3	11.98 ± 0.3	10.27 ± 0.5	11.00 ± 0.5
max	15.97 ± 0.4	11.77 ± 0.4	19.53 ± 0.5	19.47 ± 0.4	16.90 ± 0.3
mean	12.91 (s: 1.3)	9.01 (s: 1.3)	15.53 (s: 2.1)	13.28 (s: 2.1)	14.27 (s: 2.0)
Th [ppm]					
min	33.90 ± 0.5	26.10 ± 1.2	35.47 ± 0.4	32.07 ± 0.4	36.93 ± 0.8
max	49.23 ± 0.7	40.68 ± 1.2	51.28 ±	57.07 ± 0.2	56.20 ± 4.6
mean	40.72 (s:3.9)	31.57 (s: 2.8)	43.43 (s: 5.1)	41.3 (s:5.9)	43.82 (s: 5.9)
U/Th					
min	0.28	0.22	0.30	0.26	0.29
max	0.39	0.36	0.42	0.39	0.36
mean	0.32 (s: 0.02)	0.29 (s: 0.04)	0.36 (s: 0.03)	0.32 (s: 0.03)	0.33 (s: 0.02)
K vs. Th/K					
slope	not significant	$-48.63*10^{*6} \pm 1.3*10^{6}$	not significant	not significant	not significant

K vs. U/K					
slope	not significant	not significant	not significant	not significant	not significant
U vs. Th/U					
slope	not significant	-3.49 ± 0.1	not significant	not significant	21.19 ± 1.7
U vs. K/U					
slope	$-0.01 \pm 0.1 * 10^{-3}$	not significant	not significant	not significant	not significant
Th vs. K/Th					
slope	$-0.2 \pm 0.9 * 10^{-3}$	not significant	not significant	not significant	not significant
Th vs. U/Th					
slope	not significant	not significant	not significant	not significant	not significant
K vs. U					
slope	2015.11 ± 81.3	2949.50 ± 76.9	3120.20 ± 117.8	not significant	not significant
Th vs. U					
slope	1.68 ± 0.1	not significant	not significant	not significant	not significant
Th vs. K					
slope	$0.6*10^{-3} \pm 18.1*10^{-6}$	not significant	not significant	not significant	not significant
U/Th vs. K					
slope	not significant	not significant	not significant	not significant	not significant
further information					
additional observations	Pele's hair abundant	• Cr^{3+} anomaly in magnetites • sus25 shows lower values than sus05	• Pele's hair abundant	• very fine Ms • very low Mg^{2+} - and Cr^{3+} -amount in magnetites	• samples solely from Pietre Cotte • discrimination from Commenda is not clear for all outcrops; differences between values for single outcrops and the complete succession

Table 5.32: Characteristics and discrimination tools for the different successions of La Fossa di Vulcano. Data based on selected representative samples of different standard outcrops.

It can be noted that the mean values for the sus could be used as a discrimination tool for the different successions. However, figure 5.17 illustrates a significant overlap between the different successions when the complete data range is taken into account. Thus, no single sample of a succession will characterise the succession and allow a discrimination from the others, which will be seen for the identification of unknown units in the next chapter.

The results, summarised in figure 5.17 and table 5.32 demonstrate that no single method is useful to distinguish all successions. Commonly a succession can be discriminated by γ-ray measurements from one or two other successions. The remaining successions do not differ in a significant way, but they may have significantly different sus values. This leads to the conclusion that solely the combination of the two geophysical methods – in addition to

"classic" characterisation methods such as sedimentology and geochemistry – will be successful to discriminate different successions of pyroclastic deposits of La Fossa di Vulcano.

In attempts to correlate to outcrops with strata of unknown stratigraphic affinity, the data often do not indicate clear results (see chapter 6). In that case, and unless tectonics has disturbed the stratigraphic order in a particular outcrop, the best geophysical correlation that leads to a stratigraphically meaningful result will be the most likely.

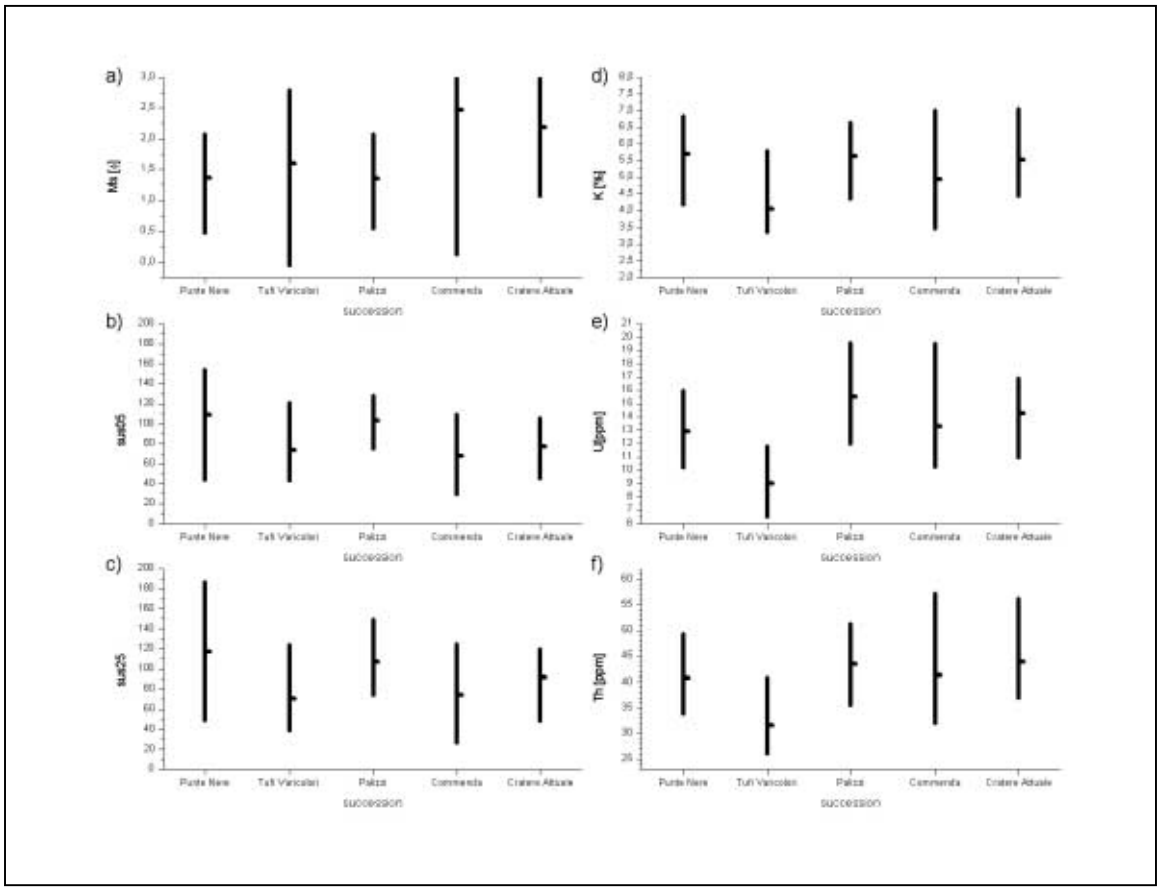

Figure 5.17: Plot of the minimum, maximum, and mean values for the different successions. a) granulometrical data; b) sus for both gsc; c) γ-ray K [%]; d) γ-ray U [ppm]; e) γ-ray Th [ppm]. Punte Nere γ-ray without channel filling, Tufi Varicolori sus without prominent peak.

A further difficulty arises from postdepositional alteration of the successions, due to exposition, weathering etc. In particular the outcrops G of Punte Nere and A of Commenda have to be mentioned. Outcrop G (see also chapter 5.2.1) is located in a small valley and the upper part is built up by a channel containing different wet-surge deposits and reworked material. Especially the γ-ray values show higher differences and a significant depletion of K. Outcrop A (see also chapters 5.2.4 and 5.2.5) is a well-exposed outcrop at the crater rim where fumarolic alteration of the deposits can be observed, especially in the lower part of the selected outcrop. Besides the recent visible fumarolic activity, the vicinity to the crater would allow gases and exhalations to penetrate the outcrop, causing secondary chemical processes

and element depletion. The topographic exposition on top of La Fossa cone leads to increased percolation of rain water and weathering, with depletion or enrichment of elements as a result. All these processes will modify the primary geophysical signal and the data sets will not show the generally determined values (see also chapter 5.2.5.3). This has to be born in mind when comparing different successions in cases where the outcrop location and condition are not similar. However, these processes are not evident for most of the successions because the mean values of Commenda can be discriminated relatively well from most of the other successions, also observable in the different scatter plots (especially γ-ray values). Recognising the potential alteration effects becomes critical when the data of two successions are close, for example Cratere Attuale and Commenda. In this case – in particular for the γ-ray values – the data of outcrop A seem to falsify the mean values of the complete Commenda succession. If the complete successions were compared, the mean values of Cratere Attuale would be higher than the mean values of Commenda. Results of single outcrops where both successions occur show that γ-ray values in particular behave in the opposite way, and Commenda has higher mean values than Cratere Attuale. Thus it can be assumed that a discrimination of Commenda and Cratere Attuale (especially the studied part of Pietre Cotte) is not possible with the methods used in this study.

It is also important to note that single outcrops can differ in their element concentration because of overlying, weathered deposits. Especially the γ-ray values are affected (for example outcrop E, chapters 5.2.3.3, 5.2.4.3, and 5.2.5.3). In contrast, the element ratio is not disturbed in a significant way.

In summary this chapter has shown that the combined geophysical methods allow a characterisation of the different successions of La Fossa di Vulcano, if some exceptions and special situations are taken into account.

6.Characterisation of Undefined Outcrops

6.1. Outcrop C

6.1.1. Introduction

Outcrop C is located on the NW flank of La Fossa cone near the footpath up to the Gran Cratere. It lies in the lower half of the flank in a small erosional gully which changes its appearance with every heavy rainfall (washing out of material and exposition of lower section). The top of the outcrop as well as some parts of the outcrop wall are covered with pioneer vegetation (like small grasses etc.) (see figure 6.1). The height of the outcrop is approximately 2.5 m. The basal part (Cx) is dominated by different multicoloured layers of ash deposits, most of them being similar to wet-surge deposits. One prominent crinkly red layer bounded by two white bands probably correlates to a distinctive layer of Tufi Varicolori found in outcrop O. The upper parts (Cc and Cy) of the outcrop are dominated by different grey loose ash deposits which are reminiscent of Palizzi or parts of Cratere Attuale. It is not possible to exclude that some, possibly the majority of the deposits consists of reworked material. Cc and lower parts of Cy contain Pele's hair. Layers with accretionary lapilli are observable in the upper part of Cy.

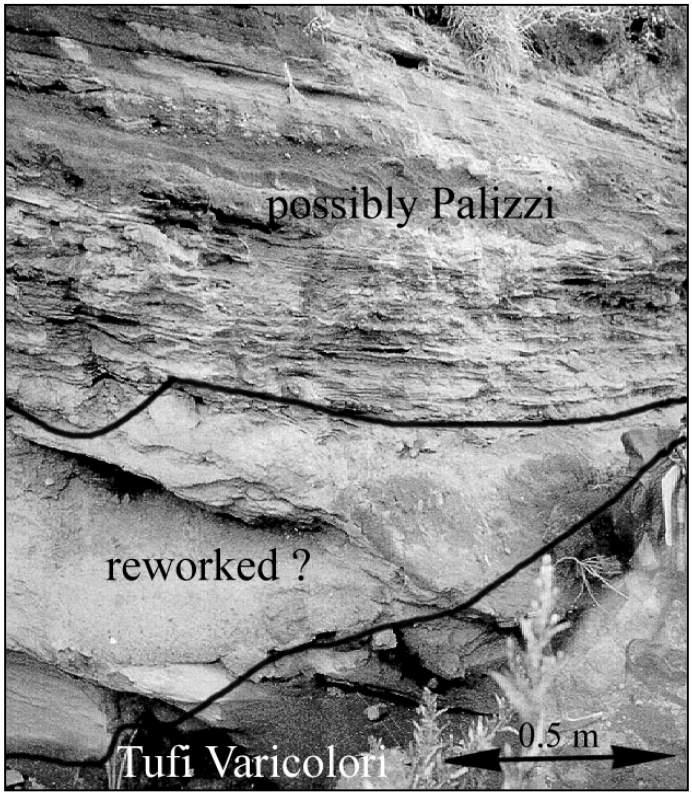

Figure 6.1: Outcrop C, the lower part is possibly build up by Tufi Varicolori followed by a layer of reworked material. The uppermost part may be formed by Palizzi, based on field observations.

Six samples were taken from Cx, 3 from Cc 3 (for γ-ray solely 2), and 9 samples belong to Cy. The uppermost sampling point of Cx may contain reworked material. It has to taken in mind that especially the part belonging to Cc is not significant for a good correlation. Another sample between Cx and Cc includes reworked material and is not used for the correlation.

6.1.2. Granulometry

The three units of outcrop C show the following mean Ms: Cx = 1.68 ϕ (s: 0.3), Cc = 1.27 ϕ (s: 0.3), and Cy = 1.40 ϕ (s: 0.2) (see also table 6.1). In comparison to the standard outcrops the values for Cx are similar to Tufi Varicolori. Cx shows slightly higher mean values than Tufi Varicolori, but the minimum and maximum values are in the same range. The values of Cc and Cy in general are more comparable to the values of Punte Nere and Palizzi. Assuming that the layers are not disturbed tectonically, Cx might belong to Tufi Varicolori rather than beeing part of Punte Nere. Cc and Cy could then be correlated with Palizzi.

sample	**Cx**	**Cc**	**Cy**
min. value	1.19	1.06	0.90
max. value	2.07	1.63	1.62
mean value	1.68	1.27	1.40
standard deviation	0.3	0.3	0.2

Table 6.1: Ms of outcrop C in ϕ.

The histograms of the samples differ and show approximately Gaussian distributions as well as negative or positive skewness. Especially the samples of Cx often show a negative skewness, whereas samples of Cy commonly have a slight Gaussian distribution. The cumulative grain size curves do not represent a well-developed sigmoidal shape, instead they vary between slightly curved and straight (a distribution of the different parts is not significant for the single units). The shape of Cc cumulative grain size curves is less pronounced, which indicates a less homogeneous eruption cloud. Parts of Cy show curves which have shapes similar to curves of Palizzi containing Pele's hair. Indeed, some samples of outcrop C contain Pele's hair.

Using the plot of the 1st vs. the 2nd moment as a discrimination tool (figure 6.2), Cx (4.44 ± 0.4) cannot be correlated with Tufi Varicolori, but Cratere Attuale shows similar values. Cc (3.28 ± 0.4) and Cy (4.03 ± 0.7) cannot be correlated with their slopes, too. Cy does not correlate with any succession and Cc shows values that could be attributed to Punte Nere (solely 3 samples). The plot of the 1st vs. the 2nd moment is shown in figure 6.2, where it can be seen that the samples of Cx behave similar to most plots of Tufi Varicolori whereas most of the samples of Cy plot in a cluster dominated by Palizzi.

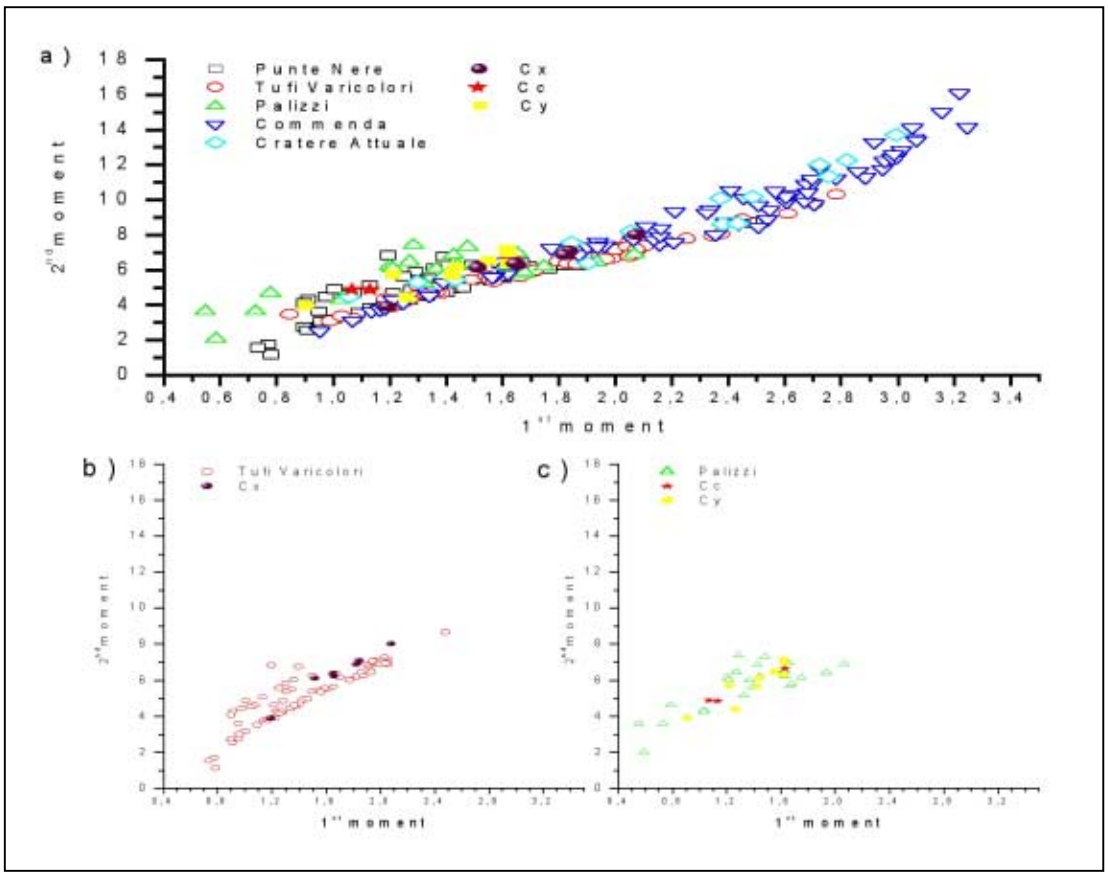

Figure 6.2: 2nd vs. the 1st moment: a) samples of outcrop C (filled objects) in comparison to samples for all successions from standard outcrops (open objects), b) samples of Cx plot in a similar trend as the samples of Tufi Varicolori, c) most samples of Cy plot near clusters of Palizzi.

6.1.3. Susceptibility

The sus – measured in cgs-mode, standardised to 1g, and extended to 10^{-6} – of the 3 units of outcrop C shows the following mean values for sus05: Cx = 71.03 units (s: 14.7), Cc = 89.79 units (s: 14.8), and Cy = 88.07 units (s: 14.1) (see also table 6.2). This increase between Cx and Cc/Cy can also be observed in sus25 (Cx = 59.94 units, s: 6.6, Cc = 83.78, s: 12.3, and Cy = 79.83 units, s: 17.9). In comparison to the standard outcrops, Cx has sus05 values similar to Tufi Varicolori, Commenda or Cratere Attuale, whereas the total range of values (for Cx) shows similarities to the data range of Tufi Varicolori and Cratere Attuale. Using solely the data of outcrop O for Tufi Varicolori the values show an even higher similarity.

For sus05, Cc and Cy plot slightly higher and could be compared with the former successions (Tufi Varicolori and Cratere Attuale) as well as with Palizzi. Cx shows very low sus25 values that could be correlated with Tufi Varicolori, whereas the other successions plot definitively higher than this unit. A correlation with Cratere Attuale, which was possible using sus05, is not indicated. Cc and Cy could belong to Palizzi, Commenda or possibly to Tufi Varicolori, but taken into account the former data, Palizzi seems to be the best choice.

sample	Cx	Cc	Cy
min. value 0.5-0.25 mm	55.06 ± 0.1	73.41 ± 0.1	68.02 ± 0.1
max. value 0.5-0.25 mm	100.1 ± 0.2	109.37 ± 0.2	107.23 ± 0.2
mean 0.5-0.25 mm	71.03 (s: 14.7)	89.79 (s: 14.8)	88.07 (s: 14.1)
min. value 0.25-0.125 mm	49.61 ± 0.1	67.23 ± 01	45.81 ± 0.1
max. value 0.25-0.125 mm	69.22 ± 0.1	96.75 ± 0.1	98.57 ± 0.1
mean 0.25-0.125 mm	59.94 (s: 6.6)	83.78 (s: 12.3)	79.83 (s: 17.9)

Table 6.2: Mean values for the sus for both gsc of outcrop C (C is split into 3 units). Samples are measured in cgs-mode, standardised to 1g, and have to be extended by 10^{-6}.

In general sus05 has higher values than sus25, which can often be observed within the succession of Tufi Varicolori, whereas the other successions in general plot higher in sus25.
The mentioned above, significant red and white layers of Cx (Cx6) and the similar layers of the standard outcrop O (Ob22) do not show obvious similar values, as well the ratios sus05/sus25 are slightly different for Cx 0.98 and for Ob 0.93. In general the ratios of Cx are higher than the ratio of Cx6, within outcrop O the ratio of Ob22 is not as prominent as seen for Cx.
Plotting sus05 vs. sus25 the various data groups plot in diverse clusters, the samples of Cx plot near the cluster of Tufi Varicolori – sometimes also Commenda – but they are normally attributed to Tufi Varicolori. The other 2 groups are more dispersed over the complete plot and do not show a significant clustering in one succession (see also Appendix IV). The slopes of the linear regression do not show a good correlation (Cx: 1.41 ± 0.7; Cc: 0.66 ± 1.0; Cy: 0.68 ± 0.1). Cx plots slightly higher than Tufi Varicolori but in general the slope observable in the graph is more or less similar whereas the slopes of the other units range between Punte Nere and Cratere Attuale.
Plots of the ratio of sus or sus/Ms do not suggest a significant correlation.

6.1.4. Gamma-ray

In comparison to the standard outcrops of La Fossa di Vulcano the γ-ray values of outcrop C show relatively high values for the different units (see also table 6.3). The mean values for K range between 6.75 % (s: 0.2) for Cy and 7.78 % (s: 0.1) for Cc, with intermediate values for Cx (7.74 %, s: 0.2). The mean values of Cc are not really meaningful because γ-ray measurements were taken only at two sampling points. The mean values for U are 12.79 ppm (s: 0.3) for Cx, 13.01 ppm (s: 0.5) for Cc, and 11.10 ppm (s: 0.6) for Cy. The Th values decrease from Cx (58.93 ppm, s: 1.6) through Cc (56.32 ppm, s: 0.6) to Cy (47.21 ppm, s: 3.7) in a similar fashion to the K values. In comparison to the data of the standard outcrops

the values of K and Th for all units are significant higher than the respective average mean values. For Cy, having slightly lower values, possibly a correlation with Palizzi or Cratere Attuale can be assumed. Using the U values for a discrimination, the data of outcrop C plot inside the normal ranges. Using solely the amounts of U Cx can be correlated with Punte Nere and possibly Commenda, but the range of maximum and minimum is more in the range of Punte Nere than of Commenda. Unit Cc falls between Punte Nere and Commenda, and the very small data set further precludes a clear correlation. Cy shows very low U values which are similar to the higher U concentrations of Tufi Varicolori.

sample	**K** [%]	**U** [ppm]	**Th** [ppm]
Minimum Cx	7.46 ± 0.1	12.18 ± 0.5	56.56 ± 1.2
Maximum Cx	8.03 ± 0.4	13.18 ± 0.6	61.12 ± 0.6
mean Cx	7.74 (s: 0.2)	12.79 (s: 0.3)	58.93 (s: 1.6)
Minimum Cc	7.72 ± 0.1	12.52 ± 0.3	55.68 ± 0.9
Maximum Cc	7.84 ± 0.2	13.50 ± 0.4	56.96 ± 1.2
mean Cc	7.78 (s: 0.1)	13.01 (s: 0.5)	56.32 (s: 0.6)
Minimum Cy	6.38 ± 0.2	10.35 ± 0.5	44.40 ± 1.5
Maximum Cy	7.85 ± 0.3	12.25 ± 0.9	56.95 ± 1.5
mean Cy	6.75 (s: 0.2)	11.10 (s: 0.6)	47.21 (s: 1.1)
Minimum Cy not considering Cy1	6.38 ± 0.2	10.35 ± 0.5	44.40 ± 1.5
Maximum Cy not considering Cy1	6.84 ± 0.3	12.25 ± 0.9	47.80 ± 1.0
mean Cy not considering Cy1	6.61 (s: 0.1)	11.11 (s: 0.7)	46.00 (s: 1.3)

Table 6.3: Maximum, minimum and mean values of K [%], U [ppm], and Th [ppm] for outcrop C. Unit Cc contains solely 2 samples, and these values are not really meaningful. In the last lines sample Cy1 showing an outlier for the values of Th and K for the unit Cy is not considered.

In general the plots of los vs. concentration (see also Appendix IV) do not show significant trends for single units. Using scatter plots of concentration vs. ratio and concentration (see also Appendix IV) and the slope of the single plots – as the linear fits, including the slope of the trend, of the standard successions are significant – for a discrimination of Cx, Cc, and Cy. The plot K vs. Th/K shows that although the ratios of the units in outcrop C are comparable to standard outcrops, the relatively high K amounts preclude a good correlation with any of the

successions. Only Cy shows some overlap with Punte Nere, some parts of Palizzi, as well as with Commenda. The plot indicates a depletion of K for Cy in comparison to Cx and Cc. As a result of the linear fits solely the slope of Tufi Varicolori is significant but it is not comparable to the slopes calculated for the units. The plot K vs. U/K does not allow any correlation for outcrop C. In the plot U vs. Th/U the samples of outcrop C are distinct from the "normal" plot of the successions. In general the values are higher but the trends (described by the linear regression and the resulting slope, significant for the successions of Tufi Varicolori and Cratere Attuale) of the single units indicate some references for a calculation: Cx –2.54 ± 2.2, Cc –4.32 (solely 2 samples), and Cy –0.82 ± 0.4. The slope for Cx shows the same direction as the slope for Tufi Varicolori although the calculated slope values are not similar (Tufi Varicolori: -0.49 ± 0.1). Using the plot U vs. K/U the linear fits do not correlate with the only significant fit of Punte Nere (this fit shows a high negative slope), instead the fits of outcrop C show slightly negative slopes. The trends look like the graphic visible trends of Tufi Varicolori, but the values are definitively higher. A correlation is not possible because of affiliation to a special cluster or because of the slope. The plots Th vs. K/Th and Th vs. U/Th do not provide new information for a correlation.

Because of the relatively high element concentration in the samples of outcrop C the scatter plots for the element concentration (of all successions) cannot be used for a correlation. In addition, the slopes do not indicate any significant correlation. An exception is the plot of Th vs. K where all successions and the samples of outcrop C approximately fall on a line. In this plot unit Cy overlaps with parts of the Palizzi cluster.

The high values of K, U, and Th in outcrop C suggest a general enrichment. Concentrations decrease in the upper part of the outcrop, containing unit Cy, which is possibly due to reworking and secondary element depletion. The vegetation may play a role as well in retarding rain water. The lower part of the outcrop, especially unit Cx, is formed by deposits which can also behave like an impermeable layer, possibly resulting in accumulation of elements along this layer. Its function as an aquitard is also observable after heavy rains, because the water remains for a relatively long time period in the gully. Depletion caused by fumarolic activity was not observed in this outcrop. The distribution of the concentration depletion and enrichment for K, U, and Th can be seen as a small problem, because Th as well as K are enriched in the base of the outcrop whereas the U concentration seems to be more widely dispersed. The nature of the problem can be described by the distribution of depletion and enrichment: normally it can be assumed that the soluble elements as K and U will give likewise trends whereas the relatively unsoluble Th not. The eye catching factor in this outcrop is that especially at the base of the outcrop the element concentrations are relatively high, the sus values, however, do not show this effect. This part of the outcrop is a very close part of the gully; possibly the background radiation affects the measurements more than in a "normal" situation (the situation of the closed gully – not as extreme as here – can also be found for the lower parts of outcrop E (Palizzi and parts of Commenda [chapter 5.2.3.3 and

5.2.4.3]). It is significant that the concentration decreases when the walls of the gully widened. For this situation it can be assumed that U is affected by depletion and enrichment in a more significant way than K and Th.
A clear classification based solely on γ-ray mean values is not possible for outcrop C.

6.1.5. Interpretation

Based on the results shown above, only parts of outcrop C can be correlated with the known successions of La Fossa cone. Cx is possibly correlated to Tufi Varicolori, as indicated by the Ms, the results for the sus values, as well as the plot sus05 vs. sus25. This interpretation is supported by field evidence, especially the prominent crinkly red layer bounded by two white bands, that occurs also in one of the standard outcrops for Tufi Varicolori (outcrop O). Gamma-ray, on the other hand, does not allow an unequivocal correlation.
Unit Cc could be correlated with Palizzi, but the Ms data would also allow an attribution to Punte Nere. This is however not very likely unless the stratigraphic superposition is disturbed. The sus data indicate an attribution to either Palizzi or Commenda, but the field appearance does not favour a correlation with Commenda. The upper part of Commenda is usually formed by multicoloured wet-surge deposits, only on the base a few look-like dry-surge deposits are noticeable. Likewise the occurrence of Pele's hair can be used as an indicator that the unit rather belongs to Palizzi, where Pele's hair is also visible, than to the upper part of Commenda.
For unit Cy the same arguments as for unit Cc can be used. In addition, some cumulative grain size curves look similar to cumulative grain size curves of Palizzi samples containing Pele's hair. The samples of Cy sometimes contain fragments of Pele's hair, but Pele's hair is more common in Cc. In general the data show similar behaviour as most of the samples of Cc. Possibly also some of these samples contain reworked material (in particular at the top of the outcrop).

6.2. Outcrop D

6.2.1. Introduction

Outcrop D is located a few tens of metres below outcrop C in the same gully, and is approximately 3 m high. Deposits at the base are dominantly multicoloured wet-surge deposits, whereas the upper part of the outcrop is formed mainly by dry-surge deposits. The top layer shows beginning soil formation. Based on the different types of the deposits, the outcrop can be split into Dy1 (lower part, multicoloured wet surges, 12 sampling points) and Dy2 (upper part, grey dominated, transition between wet- and dry-surge deposits, 7 sampling points). Parts of Dy2 contain Pele's hair. Reworked material occurs in upper part of the outcrop.

6.2.2. Granulometry

The mean Ms of the two units of outcrop D are 1.56 ϕ (s: 0.2) for Dy1 and 1.46 ϕ (s: 0.3) for Dy2. In comparison to mean Ms of the standard outcrops Dy1 shows results close to Tufi Varicolori, although the range between minimum and maximum is higher for Tufi Varicolori than for Dy1. The values of Dy2 are between those for Tufi Varicolori and Punte Nere/Palizzi. The granulometry suggests that Dy1 can be attributed to the succession of Tufi Varicolori. Consequently, Dy2 can only belong to Palizzi or possibly to Tufi Varicolori.

sample	**Dy1**	**Dy2**
min. value	1.11	1.02
max. value	1.89	1.95
mean value	1.56	1.46
standard deviation	0.2	0.3

Table 6.4: Ms of outcrop D in ϕ.

The Ms remains relatively constant throughout los. Histograms show Gaussian distribution as well as negative and positive skewness. The distribution is not clearly defined for other samples. This lack of a unequivocal grain size distribution in outcrop D precludes a correlation based on grain size alone. With few exceptions, the cumulative grain size curves do not show any well developed sigmoidal shape, instead curves have slightly curved shapes. The highly variable grain size distribution suggests a heterogeneous eruption cloud. Alternatively, some curves could be shifted to a higher gsc not investigated by this measurements.

Plotting all successions as well as the samples of outcrop D in a scatter plot 2^{nd} vs. 1^{st} moment the data of outcrop D normally plot within the lower part of the average trend. The samples of Dy1 generally follow the trend of Tufi Varicolori whereas the data of Dy2 plot higher. The latter have a wider range and they do not show the same clear trend. The slopes resulting from the linear regression show values which are near to Commenda (Dy1 4.81 ± 0.3) and Cratere Attuale (Dy2 4.52 ± 0.4). Tufi Varicolori has lower slope values.

6.2.3. Susceptibility

The sus is measured in cgs-mode, standardised to 1g, and extended to 10^{-6}. Dy1 has a mean value of 60.46 units (s: 24.2) for sus05, the value for Dy2 lies by 61.90 units (s: 31.4). sus25 ranges from 60.91 units (s: 16.1) for Dy2 to 63.54 units (s: 15.7) for Dy1. Minimum and maximum values are shown in table 6.5.

Based on the mean values neither Dy1 nor Dy2 can be correlated with Punte Nere or Palizzi that both have higher values. Instead, Tufi Varicolori and Commenda seem to be the best choice for both units. Cratere Attuale would be possible based on sus05, but the difference for sus25 is too high. Similar to the granulometry results the mean sus values do not differ significantly throughout the outcrop, but sus25 tends to be slightly smaller than sus05.

sample	Dy1	Dy2
min. value 0.5-0.25 mm	26.97 ± 0.1	27.81 ± 0.1
max. value 0.5-0.25 mm	113.01 ± 0.2	142.15 ± 0.2
mean 0.5-0.25 mm	60.46 (s: 24.2)	61.90 (s: 31.4)
min. value 0.25-0.125 mm	34.62 ± 0.1	31.49 ± 0.1
max. value 0.25-0.125 mm	85.81 ± 0.1	82.32 ± 0.1
mean 0.25-0.125 mm	63.54 (s: 15.7)	60.91 (s: 16.1)

Table 6.5: Mean values for the sus from both gsc of outcrop D. Samples are measured in cgs-mode, standardised to 1g, and have to be extended by 10^{-6}.

The data do not show a significant change within los, in general sus05 and sus25 are located in the same range whereby normally this situation is also visible within outcrop C and for the succession of Tufi Varicolori, whereas for the other successions sus25 is generally greater than sus05. Plots of sus vs. the ratio sus/sus or sus/Ms do not show significant new correlation patterns.

Most of the data plot in the lower left part of the plot sus05 vs. sus25. Dy1 plots in the same area as most of the Commenda or Palizzi data, whereas the data of Dy2 normally follow the trend of Tufi Varicolori. The results for the linear fits show that the slope of Dy1 (0.75 ± 0.0) is more similar to the slope of Punte Nere than for Tufi Varicolori. The results could possibly also be correlated to Commenda. For Dy2 (0.96 ± 0.0) the slope can be best correlated with the values of Tufi Varicolori.

6.2.4. Gamma-ray

The γ-ray data, especially the values of Th and K, show relatively high values, similar to outcrop C, here a correlation because of the concentration is difficult. Dy1 shows the following mean values: K = 7.29 % (s: 0.2), U = 12.82 ppm (s: 0.9), and Th = 59.30 ppm (s: 1.7). The values for Dy2 are 7.12 % (s: 0.2) for K, 12.53 ppm (s: 0.7) for U, and 56.38 ppm (s: 2.1) for Th (see also table 6.6). The comparison to the average mean values of the standard outcrops does not allow a correlation based on K and Th. The data of outcrop D have higher values than the data of the standard outcrops. The U values of both units are similar to the mean values of Punte Nere, whereas the values of Tufi Varicolori are lower. It seems that U is depleted in comparison to the other element concentrations, possibly because of the outcrop location.

sample	**K** [%]	**U** [ppm]	**Th** [ppm]
Minimum Dy1	6.92 ± 0.2	10.33 ± 0.2	56.28 ± 1.8
Maximum Dy1	7.53 ± 0.4	13.60 ± 0.7	61.52 ± 1.3
mean Dy1	7.29 (s: 0.2)	12.82 (s: 0.9)	59.30 (s: 1.7)
Minimum Dy2	6.83 ± 0.2	11.43 ± 0.4	52.73 ± 0.9
Maximum Dy2	7.55 ± 0.3	13.63 ± 0.8	60.00 ± 1.2
mean Dy2	7.12 (s: 0.2)	12.53 (s: 0.7)	56.38 (s: 2.1)

Table 6.6: Maximum, minimum and mean values of K [%], U [ppm], and Th [ppm] for outcrop D.

The plots of los vs. element concentration (see also Appendix IV) do not show significant trends, solely the last 2-3 samples at the top mirror a decrease for all element values. This can be observed in particular for U, which can be explained by soil formation and influence of vegetation at the top of the outcrop.

The plots of element concentration vs. ratio do not allow a graphical discrimination of the units. In general the plots for outcrop D follow the “normal” trends of the successions but a clear classification is not possible (see also figure 6.3). A correlation between outcrop D and the standard outcrop by the calculated slope is not useful. In the plot U vs. Th/U the slope of Dy2 (-3.16 ± 0.8) shows values similar to Tufi Varicolori (-3.49 ± 0.1), whereas the value of Dy1 (-2.04 ± 0.2) is lower.

Also scatter plots of the element concentrations do not show a graphical correlation pattern for the data of outcrop D plotting in general higher than the data of the standard outcrops (except of the U-values). In the plot Th vs. K the 2 units of outcrop D follow the average observable trend at the higher end of the trend line.

For this outcrop the situation is not as close as for outcrop C at it’s base. In outcrop D a change of the values especially of Th and K, as a consequence of topography, is not observable. It seems that K and Th are enriched whereas the highly mobile U is depleted. However, K generally tends to be very mobile as well and an enrichment of K in combination with a depletion of U is not usual. ADAMS ET AL. (1959) describe that an average U content in intrusive rocks can be explained as the hydrothermal escapement of U from a slow crystallising magma. This would be a good description for the two outcrops but in other outcrops these observation is not possible and the exploration of a newly succession with long residual times in the reservoir is implausible. It is more likely that recent fumarolic activity above the outcrop leached the U. The alteration by magmatic gases, fossil fumarolic and hydrothermal activity, as well as weathering are additional leaching processes.

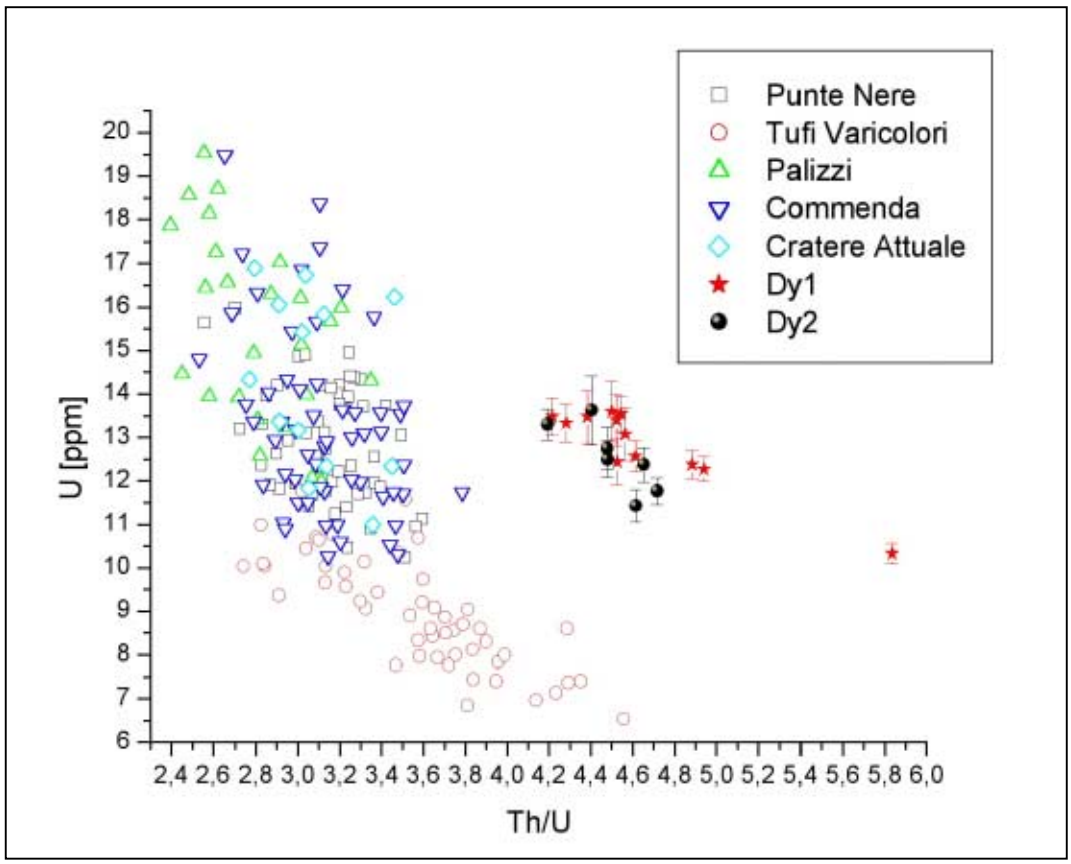

Figure 6.3: Scatter plot of U vs. Th/U to identify the samples of outcrop D in comparison to the other successions. Open objects mark data points from standard outcrops whereas filled objects mark the unknown units of outcrop D. Because of the high K values the data plot outside of the data cloud of the successions, but similar trends can be assumed.

6.2.5. Interpretation

As for outcrop C the significant results for a correlation are provided by granulometry and the sus measurements. The γ-ray measurements have relatively high values which in general do not show similarities with the standard outcrops of La Fossa di Vulcano. As discussed above, the low U concentrations may reflect secondary processes rather than a primary signal. Only the slope of the plot U vs. Th/U suggests an affiliation to Tufi Varicolori. Using the element concentration solely U could be combined with the Punte Nere succession.

The appearance in the field suggests that Dy1 may correlate with parts of Tufi Varicolori, as well as reworked sections whereas Dy2 seems to correlate with parts of Palizzi or Cratere Attuale. Reworking may have occurred as well. The granulometric data indicate that Dy1 belongs to Tufi Varicolori whereas Dy2 can be attributed to Punte Nere, Tufi Varicolori or Palizzi, whereby Punte Nere can be excluded because this would require tectonic superposition of units not normally superposed. The shape of the cumulative grain size curves sometimes indicate a correlation with Tufi Varicolori. Results for the plot of the 2nd vs. the 1st moment differ in the graphic statement – both units plot near the Tufi Varicolori cluster, especially Dy2 – and the calculated slope of the plot, here both units are more attributed to Commenda and Cratere Attuale. Using the data of the sus measurements generally the 2 units

can be attributed to Tufi Varicolori or Commenda. Cratere Attuale, which shows similarities for sus05, has higher differences for sus25. Normally sus25 shows lower values than sus05, which is mostly observable within the succession of Tufi Varicolori. The plot sus05 vs. sus25 confuse the observations made before because Dy1 plots in the range of Commenda and Palizzi, and also the slope value is better correlated with Commenda than with Tufi Varicolori. The data of Dy2 normally follow the cluster of Tufi Varicolori and the slope correlated by the linear fit shows the best correlation with Tufi Varicolori. If these results are taken into account the "normal" stratigraphic concept is not usable anymore, a slide or inversal bedding has to be assumed. Near the outcrop no references for a tectonic event can be observed.

In summary, Dy1 most likely belongs to Tufi Varicolori, but a high degree of reworking has to be assumed. Dy2 can be attributed to Tufi Varicolori, but some data may also suggest a correlation with Palizzi. Reworking is likely as well. A good distinction between the two parts of the outcrop by geophysical methods is not possible.

6.3. Outcrop K

6.3.1. Introduction

The outcrop is located on the westernmost part of the island, the so-called Lentia Complex. Whereas the first 2 outcrops (C and D) are located at the flank of the volcano, inside of the La Fossa Caldera, the position of outcrop K lies outside of the La Fossa Caldera. There the caldera walls do not reach their maximum height as observable near the Piano Caldera on the southern and southeastern boundary of the Fossa Caldera (near outcrops M, N, and R). The outcrop is distributed over a larger area of the Lentia Complex. In the field 3 units can be distinguished form their appearance, starting with a few wet-surge deposits (Kw, 5 samples) at the base, demonstrating plastic behaviour, e.g. mantling a lava-block of the Lentia Complex (see also figure 6.4.a). A few metres beside different dry-surge deposits (Kc, 6 samples, see also figure 6.4.b) can be found. These distal deposits show well developed grading, which demonstrates the energy evolution and distribution with time in the eruption cloud (pers. comm. DELLINO, 1999). This unit starts with thinly laminated, coarse – sometimes only few grains thick – deposits passing into more massive deposits of finer gsc. Often the upper massive part is erosionally cut by the next set of deposits. These deposits are discordantly cut by surge deposits which show massive as well as laminated structures (Ke, 9 samples). Deposits of Ke are often solidified, in contrast to most of the deposits of the standard outcrops, which are generally less solidified than most of the deposits of Ke.

VALENTINE ET AL. (1998) do not agree with the common explanation of this outcrop, they describe the deposits appearing here as the so-called Cuesta succession. In their opinion the Cuesta succession was formed before the main formation of the La Fossa Caldera.

Figure 6.4 Different parts of outcrop K. a) wet-surge deposits of the 1st unit (Kw) showing plastic behaviour by mantling lava-block of the Lentia complex, b) deposits of the 2nd unit (Kc) a few metres away of the Kw deposits, cut discordantly by deposits of the 3rd unit (Ke) (arrow) c) deposits of the 3rd unit (Ke) on the top of the cliff, d) middle and upper part of outcrop K, at the bottom deposits of Kc can be seen which are overlaid by deposits of Ke; the top is covered by fruze and grass.

6.3.2. Granulometry

The mean Ms of the 3 units from outcrop K shows slightly different values (Kw = 1.65 ϕ, s: 0.6; Kc = 2.03 ϕ, s: 0.3; Ke = 1.85 ϕ, s: 0.2). The minimum and maximum data have a wide variation, this can be observed especially for the units Kw and Ke, which show similar mean Ms. In this case Kw has a wider range of data.

Comparing these data with the average mean Ms of the standard outcrops a sensible correlation is not possible in any case. Taking into account slightly differences, Kw and Ke could be correlated with the lower plotting Tufi Varicolori or the higher plotting Cratere Attuale, whereas the data of Kc are only correlated with Cratere Attuale. If the deposits are layered in a normal tectonic superposition a correlation of Kw with Cratere Attuale is not probable. Considering that this outcrop is not located inside of the caldera it is possible that the Ms could have been resulting in a higher Ms. The reason for the different composition is originated in the transport-energy overtaking the barrier (about 100 m for this location), possibly coarser particles cannot overtake the barrier and the eruption-cloud is thinned.

sample	Kw	Kw without extreme peaks	Kc	Kc without extreme peaks	Ke
min. value	0.77	1.88	1.53	1.85	1.57
max. value	2.43	2.43	2.48	2.16	2.13
mean value	1.85	2.12	2.03	2.05	1.85
standard deviation	0.6	0.2	0.3	0.1	0.2

Table 6.7: Ms of outcrop K in ϕ. The modified columns show data without the extreme peaks of the units (1st sample of Kw and 1st and 3rd sample of Kc).

The evolution of the Ms shows that the different units, especially Kw and Kc represent wide variations (see also figure 6.5). Not taken into account these extreme sampling points the mean Ms of Kc does not change in a significant way whereas the mean Ms of Kw now is much finer, and shows values in the range of Cratere Attuale.

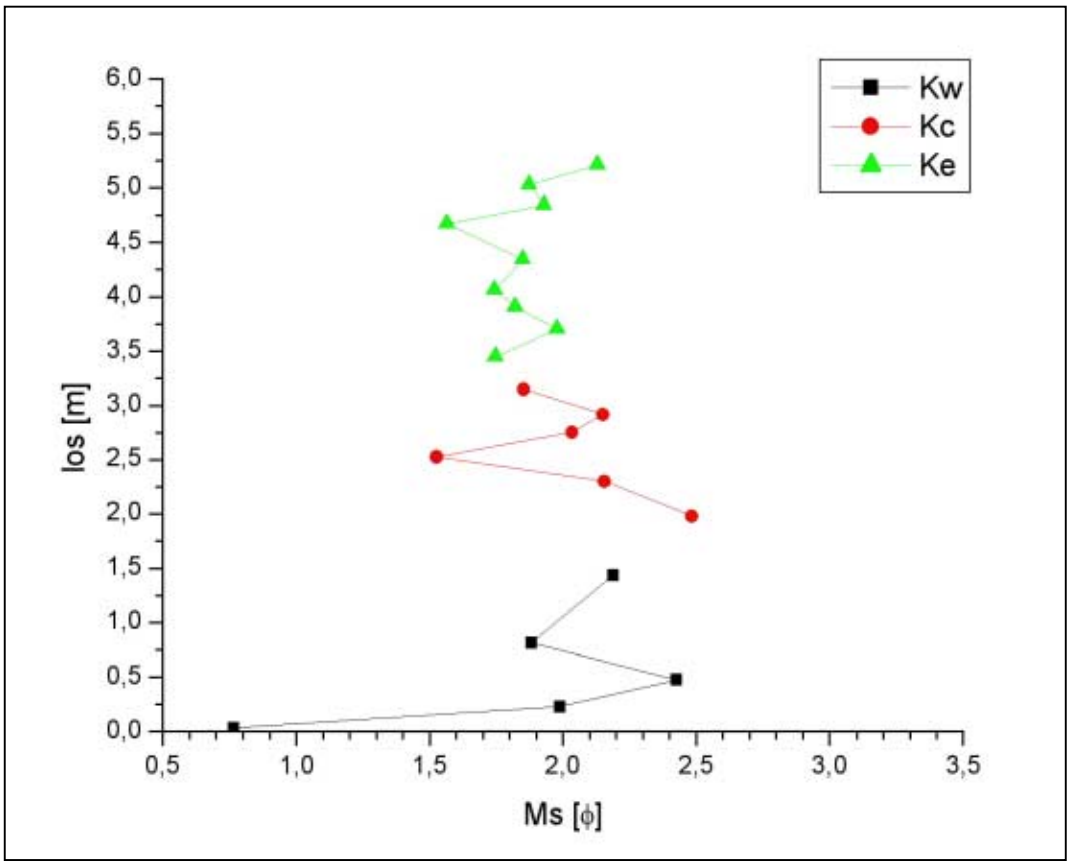

Figure 6.5: Ms of outcrop K in ϕ as a plot vs. los. It has to be remarked, that especially the 1st sample of Kw (dark squares) represents an extreme coarse peak, also the 1st and the 3rd sample of Kc (circles) show values that do not plot in the average range of Kc.

The histograms of the gsc generally show a negative skewness – except for the 1st sample – whereas the diagrams of Kc vary in different ways. Samples of Ke can define an approximately Gaussian distribution as well as a slight negative skewness for most of it's samples. The slight negative skewness, observable of Kw, is also known from standard outcrops of Tufi Varicolori as well as from some outcrops of Commenda. Kc shows graphs

which sometimes can be compared with a few graphs of Palizzi. The cumulative grain size curves have similar starting points with solely a few outliers (for example Kw1). In general the curves of Kw show a slight shape but no a well defined sigmoidal shape, which can also be observed for Kc, whereas the curves steepen faster than the curves of Kw. Ke shows well defined curves with a slight sigmoidal touch. The latter can be observed for some samples of Punte Nere. Tufi Varicolori has some curves that look likewise as some curves for Kw and Kc, especially the curves of the upper part of outcrop O, but also a few samples of Kc can be correlated with curves for Palizzi (sometimes also some samples of Ke). A few parts of Commenda are solely comparable with some curves of Kw. These results smear definitive statements, if it is assumed that all samples belong to the successions of La Fossa di Vulcano and the deposits show a primary layering, because if samples of Kw can belong to Punte Nere, Tufi Varicolori or Commenda, the latter can be excluded because the other units are not comparable with the same or a higher succession. Kc may belong to both expected successions whereas the affiliation of Ke to the succession of Punte Nere is not very probable; an affiliation with Palizzi could be assumed, but the appearance does not show the usual type of Palizzi (possibly as wet surge-deposits, which can also be found in the locations outside of the caldera).

Plotting the 2^{nd} vs. the 1^{st} moment the different samples generally follow the average trend of all successions. Kw follows the trend of Tufi Varicolori and often plots near the samples of Tufi Varicolori, but also the samples of Punte Nere are involved. Kc also shows a trend near Tufi Varicolori, but a special trend cannot be assumed, the samples of Palizzi sometimes plot higher, but also here an overlap can be observed. Ke plots within all samples without a distinctive trend. Using the slope for a correlation for all units the slope ranges about 3.03 and 3.04. This can be correlated with Punte Nere or Palizzi, the data for the complete outcrop plot between this two with an equal distance.

6.3.3. Susceptibility

The sus – measured in cgs-mode, standardised to 1g, and extended to 10^{-6} – of the 3 units of outcrop K shows for Kw mean values of 63.57 units (s: 8.0) for sus05 and 69.86 units (s: 15.8) for sus25. Kc shows likewise values, here 63.90 units (s: 2.4) for sus05 and 73.53 units (s: 6.5) for sus25 can be observed. The values of Ke plot noticeable higher (sus05 = 74.56 units, s: 4.5; sus25 = 93.12 units, s: 13.0). Kc has the lowest range between minimum and maximum whereas the other units show higher variations especially for sus25 (see also table 6.8).

Comparing the results for outcrop K with the mean values of the standard outcrops, Kw can be characterised by Tufi Varicolori or Commenda, whereas Commenda seems to be the better choice due to the ratio between the sus. Values for Punte Nere and Palizzi are much higher as showing a good correlation with Kw, but the values – except for the ratio between the values of sus05 and sus25 – of outcrop O for Tufi Varicolori show related amounts. The other

possibility, Commenda, shows also related values, here especially the corrected outcrop A gives a good correlation. Values for Kc show more or less related combinations, solely sus25 has a higher mean value. Ke demonstrates higher sus mean values with a wider range between the two sus. For this unit Cratere Attuale is a relatively good correlation, especially the amounts of the sus differ not in a significant way (for all this reflections the range of maximum and minimum has been taken into account less or not at all). It has to be noted, that comparing both parts Kc has a very low s in contrast to the other units and also to the standard outcrops.

sample	Kw	Kc	Ke
min. value 0.5-0.25 mm	50.91 ± 0.1	60.22 ± 0.1	67.96 ± 0.1
max. value 0.5-0.25 mm	72.36 ± 0.1	67.63 ± 0.2	82.08 ± 0.1
mean 0.5-0.25 mm	63.57 (s: 8.0)	63.90 (s: 2.4)	74.56 (s: 4.5)
min. value 0.25-0.125 mm	47.69 ± 0.1	65.18 ± 0.1	78.24 ± 0.1
max. value 0.25-0.125 mm	94.66 ± 0.2	82.80 ± 0.1	122.65 ± 0.2
mean 0.25-0.125 mm	69.86 (s:15.8)	73.52 (s: 6.5)	93.12 (s: 13.0)

Table 6.8: Mean values of the sus for both gsc of outcrop K.

In contrast to the outcrops mentioned above in outcrop K sus25 plots higher than sus05, which is observable for most of the successions of La Fossa (except of Tufi Varicolori). Especially sus25 represents higher variations (normally Kw and Ke), but the slightly observable trend is mirrored for this sus better.

Plots of the sus vs. the ratio sus/Ms and sus/sus do not show significant new trends or correlation tools. Using the plot sus05 vs. sus25 Kw plots in the range of Tufi Varicolori overlapping with Commenda. Kc plots in the same part but here the abundance of Commenda dominates. Ke plots in the range of Commenda and Cratere Attuale. Using the slope as a discrimination tool solely Kw shows $R < 0.9$, with it's 0.52 ± 0.0 it plots in the nearer range of Cratere Attuale, the other successions show too high values for a good correlation. The slope values 0.31 ± 0.0 for Kc and 0.26 ± 0.0 for Ke are too low in comparison to the "useful" slopes of the different successions

6.3.4. Gamma-ray

The γ-ray values for outcrop K show different amounts for the single units, especially Ke has low values, which could be explained by exposure and following leaching. This can also be observed in the plot of the elements vs. los (see also figure 6.6). Kw has a mean value for K of 4.31 % (s: 0.1), for U of 11.80 ppm (s: 1.1), and 38.28 ppm Th (s: 1.0), the values for Kc are more or less likewise (K = 4.51 %, s: 0.5; U = 10.72 ppm, s: 1.2; Th = 34.60 ppm, s: 1.9). Ke

shows noticeable lower values for all elements (K = 3.56 %, s:0.4; U = 8.67 ppm, s: 1.1; Th = 29.33. s: 2.5), which, as mentioned above, may be explained by leaching due to the exposed nature of the sampling points (see also table 6.9 and figure 6.4).

sample	**K** [%]	**U** [ppm]	**Th** [ppm]
Minimum Kw	4.13 ± 0.1	13.40 ± 0.4	36.67 ± 0.6
Maximum Kw	4.43 ± 0.1	10.27 ± 0.6	39.67 ± 0.6
mean Kw	4.31 (s: 0.1)	11.80 (s: 1.1)	38.28 (s: 1.0)
Minimum Kc	3.70 ± 0.1	8.90 ± 0.5	31.90 ± 0.5
Maximum Kc	5.23 ± 0.1	12.65 ± 0.4	37.60 ± 0.5
mean Kc	4.51 (s: 0.5)	10.72 (s: 1.2)	34.60 (s: 1.9)
Minimum Ke	2.90 ± 0.1	6.40 ± 0.5	25.90 ± 0.9
Maximum Ke	4.40 ± 0.1	10.27 ± 0.4	35.03 ± 1.0
mean Ke	3.56 (s: 0.4)	8.67 (s: 1.1)	29.33 (s: 2.5)

Table 6.9: Maximum, minimum and mean values of K [%], U [ppm], and Th [ppm] for outcrop K.

Considering the data of Punte Nere, in this case especially the data of outcrop G (especially the channel-data), generally the data of Kw show similar behaviour. This can often be observed in the plots of the concentration vs. the ratio, too (see Appendix IV). Most of the samples measured normally for Punte Nere belong to dry-surge deposits or deposits with less wet-surge portion. The deposits of Kw are definitively wet-surge deposits, their lower γ-ray values may be originated by leaching within the eruption cloud. The mean values of outcrop K in comparison to the standard outcrops show the following results: Considering the values of Th and U Kw can be compared to Punte Nere, although the data of Kw are slightly lower. Considering the data of outcrop G and the channel, the data of Kw show likewise values and it seems to be that the data can be compared to this outcrop. Kw is also comparable to Tufi Varicolori using the slightly higher K and U values. The data of Kw are a little higher but show the best correlation with Tufi Varicolori. For the other successions solely Commenda shows low correlation possibilities but the data in general have too wide ranges. For Kc a correlation with Tufi Varicolori is possible for most of the elements, but often solely the values of Tufi Varicolori plot lower than the samples. Also a correlation with Punte Nere, using the data of U and Th, is possible. The data of these successions are higher than the measured data. A comparison to Commenda is practical using K, whereas Commenda holds higher values than Kw, but in general the correlation is not useful. Ke, the unit with the lower

amounts, shows only similarities to Tufi Varicolori, whereas the values of the standard Tufi Varicolori show higher ranges.

In plots of los vs. element concentration (see also figure 6.6) especially unit Ke demonstrates a significant decrease of concentration with increasing los, which may be explained by leaching and weathering. This can also be seen by the consistence of the samples, especially the samples of the upper part are noticeable solidified. Kw shows solely some differences for the trend of U whereby the first and the last sample have higher values than the average samples; the other elements do not show significant peaks. Kc has lower values – except for K – than Kw but the range of the values is much wider than for Kw. For the last sample, located beneath (ca. 1m) the former samples (here also the discordant contact between Kc and Ke can be observed), the values for all elements rise. As mentioned above Ke shows a noticeable decrease for all elements, which have values lower than the mean values of Tufi Varicolori. This can be explained by leaching.

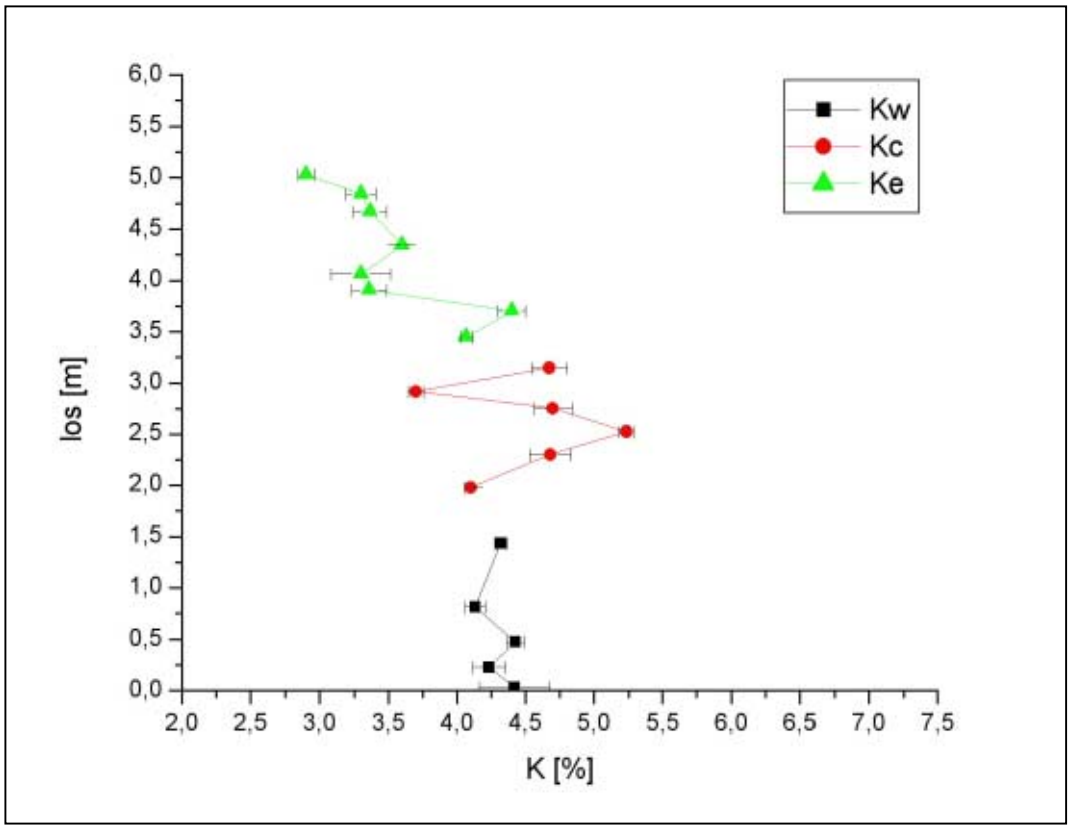

Figure 6.6: Element concentration vs. height of the outcrop, example for the good leachable K. It has to be noted that especially the values of the higher exposed Ke indicate hints for leaching.

The plots of element concentration vs. the ratio show various results. Kw can be compared to Punte Nere, especially the deposits of outcrop G, where consensus can be observed in every plot. Kw is present in the cluster of Commenda as well as in the cluster of Punte Nere, intersections with other successions, for example Palizzi, are rare. The unit of Kc normally plots between many successions so a characterisation is not easy or possible. Sometimes

larger intersections with margins of the data for Punte Nere as well as the data of outcrop G are observable (for example K vs. U/K and Th vs. U/Th), but also overlaps with Commenda in U vs. Th/U and Th vs. U/Th are remarkable. Ke plots dominantly in the cluster of Tufi Varicolori, whereas it normally shows lower values than Tufi Varicolori. It has to take into account that the values of Ke are probably leached because of the exposure, thus their γ-ray values are not very meaningful. The slopes which can be used for a characterisation show solely similarities for Kw and Kc with Tufi Varicolori in the plot U vs. U/Th (Kw = -3.82 ± 0.8, Kc = -3.66 ± 0.7, and Tufi Varicolori = -3.49 ± 0.1).

Scatter plots of the element concentrations have comparable distributions as the data in the plots before. In general Ke plots in cluster than Tufi Varicolori, Kw plots in the Commenda cluster as well as inside cluster of the data of outcrop G. Whereas unit Kc normally plots in the area of all successions with intersections everywhere, sometimes (for example K vs. U) also an affiliation with the data of outcrop G is noticeable. A correlation of slope values with defined succession is not possible.

6.3.5. Interpretation

Outcrop K is the first outcrop out of the caldera so the facies could have changed during overriding the barrier. Because of the exposition of the upper part especially the γ-ray values for unit Ke have to be interpreted carefully.

The data of unit Kw indicate different classification possibilities for the standard outcrops. Based on the granulometric data Kw can be classified as Tufi Varicolori as well as for the higher plotting Cratere Attuale. The plots indicate a characterisation possibility of Punte Nere, Tufi Varicolori or Commenda. For the scatter plot of the 2^{nd} vs. the 1^{st} moment Kw plots in the ranges of Punte Nere and Tufi Varicolori, whereas the slope can be correlated with Tufi Varicolori or Palizzi. These successions show the lowermost slope values, which are still higher than the measured for this outcrop. The sus indicates an affiliation to Tufi Varicolori or Commenda, whereas in this case Commenda has a better correlation of the ratio, too. A small reference that the comparison to Tufi Varicolori is not as good as it would be can be seen for sus25 which is slightly higher than sus05 in this outcrop. This is observable in most of the standard outcrops except for Tufi Varicolori. In plots of sus05 vs. sus25 a correlation with Tufi Varicolori as well as with Commenda is possible. The γ-ray values differ in a significant way if they are compared to the results of sus. Taking into account that in the samples of outcrop G, belonging to Punte Nere, the values for Kw show an affinity with the succession of Commenda as well as with Punte Nere (especially the data of outcrop G overlap). Using solely the mean values Kw is comparable with Punte Nere, Tufi Varicolori, and Commenda; using especially the plots Commenda as well as Punte Nere dominate. In this case it has to take into account that from Punte Nere in general most of the data belong to samples of dry-surge deposits, thus the in this outcrop exposed wet-surge deposits may show slightly different values because of the conditions inside of the cloud (more leached material, lower

values because of early reactions before deposition). Kw is not defined clearly, 3 solutions are given, whereas the characterisation of b or c seems to be most sensible:

a) Punte Nere, whereby especially the data of outcrop G are considered (more wet-surge deposits than the generally measured dry-surge dominated standard outcrops), is one possibility, but for this definition the sus values do not correlate. The γ-ray values overlap with Commenda, so a certain characterisation is not possible.
b) Tufi Varicolori are defined by different granulometric and sus measurements, whereas the data for the γ-ray measurements plot in different ranges. The appearance in the field is more or less similar, but since now Tufi Varicolori has not been described outside of the caldera (because of it's energy level and behaviour).
c) Commenda looks like most of these deposits, but the mean values of Ms differ significantly, whereas likewise some shapes of the different grain size curves are comparable with Commenda. For the sus investigations a characterisation by Commenda dominates and the plots of the γ-ray values show similar results, although the mean values do not present a perfect correlation for every time.

Kc also shows different possibilities for a correlation. The granulometric data allow a comparison to Cratere Attuale by the values, with Punte Nere, Tufi Varicolori, and Palizzi by the different graphs and histograms, and with Punte Nere as well as with Palizzi using the slope of the plot 2^{nd} vs. 1^{st} moment. The sus values indicate an affiliation to Tufi Varicolori or Commenda by the mean values, whereas Commenda can also be defined by the plot sus05 vs. sus25. The γ-ray values allow solely a characterisation using the mean values, because Kc plots in different clusters or overlapping parts of various successions thus a characterisation by the plot is not sensible. The mean values allow a correlation with Punte Nere, Tufi Varicolori, and Commenda. In general whether Tufi Varicolori nor Commenda build up dry-surge deposits in the same volume as observed in Kc (as known now), so a correlation which is likely for the results shown above is not reasonable. If it is assumed that also a part of this unit is weathered, the results of the γ-ray measurements may plot also in the range of Palizzi which would be a well choice for the outer appearance of the outcrop. An affiliation to Punte Nere is unlikely taken into account the possible stratigraphic location of the underlying Kw. It may also be assumed that this succession belongs to Cratere Attuale, for example the values of Pietre Cotte (but solely the values of the granulometry show similarities). Possibly it can be defined as a part of the Pyroclastics post 1739 with a latitic to rhyolitic composition.

Ke can only be characterised by it's appearance, granulometric and sus data, because especially the top of the unit shows very low values for the γ-ray measurements thus it can be assumed that this part of the outcrop is weathered and the data of the measurements are not sensible for a correlation, which can also be observed in the scatter plots where the data of Ke plot lower than the data of Tufi Varicolori (samples with the lowest known γ-ray values for the younger successions of La Fossa di Vulcano). The mean Ms of Ke is comparable with values of Tufi Varicolori and Cratere Attuale, whereas it's graphs as well as the slope of the

plot of the 2nd vs. the 1st moment correlate more with Punte Nere and Palizzi. The data for the sus show a correlation with Cratere Attuale and sometimes also with Commenda. In the context of the characterisation of the other units solely a correlation with the Cratere Attuale succession seems to be useful, whereby these units can be correlated with Pietre Cotte or the Pyroclastics post 1739, which depends on the classification of Kc.
Concluding the following feasibilities can be assumed:

- Kw belongs to Punte Nere or Tufi Varicolori (first time that Tufi Varicolori is described outside of the caldera), Kc to Palizzi or Cratere Attuale, and Ke to Cratere Attuale.
- Kw is defined as Commenda, Kc is correlated with Cratere Attuale, and Ke belongs to a higher stratigraphic unit of Cratere Attuale (possibly Pyroclastics post 1739).
- The definition of VALENTINE ET AL. (1998) is correct and the units belong to pre-La Fossa cone successions.

6.4. Outcrop L

6.4.1. Introduction

Outcrop L is located on the Piano Caldera near the Monte Saraceno on the so-called Piano d' Alighieri. 3 units can be characterised in this outcrop (see also figure 6.7) which lies at the top of a gully. Normally the same deposits as in outcrop K should occur [DELLINO, pers. comm., 1999], solely because of the location the deposits in the middle part (Palizzi as the field description of DELLINO [pers. comm., 1999]) are not prepared in the same way as before (former described Kc) because at the top of the gully the thickness decreases. For the present knowledge this is the furthermost distal outcrop in which Palizzi as a solid type can be observed.
The lower part of outcrop L is built up by various wet-surge deposits, which often incude vesiculated tuffs. The layers are dominated by reddish to brownish colours with grey, white and ochre intercalations. These deposits are consolidated in unit Lw (8 samples for sus and 7 for γ-ray measurements). The unit is covered by different wet- as well as dry-surge deposits dominated by grey to brown/ochre layers and sometimes intercalated by red bands. This unit Lc (3 samples for sus and 2 samples for γ-ray) has a thickness less than 1 metre. The last unit Le (4 samples) contains various wet-surge deposits, which are highly exposed thus weathering or leaching can be assumed. This is demonstrated very well by the γ-ray measurements. These measurements are not sensible for a correlation because they show lower values than the lowest known values of Vulcano (La Sommata → basic lava). The caldera wall, which was surmounted by the cloud, is higher for outcrop L than the caldera wall of the last outcrop (K, approximately 100 m caldera wall height), so a depletion of coarse material can be assumed.

Figure 6.7: Outcrop L with the different units. The upper unit Le is not shown completely. Most of the samples of this unit are taken above the visible part from the background of the outcrop.

6.4.2. Granulometry

The mean Ms for the units of outcrop L differ slightly compared to the values of outcrop K and do not show extreme peaks which may falsify the results. The mean Ms decreases with increasing unit: Lw has the highest values with 1.93 ϕ (s: 0.1) followed by Lc with 1.88 ϕ (s: 0.2), and Le 1.84 ϕ (s: 0.1). Samples belonging to Le on the higher part of the outcrop are solidified and it may be difficult to destroy their agglomerates, thus the mean value can be slightly falsified. Comparing the mean values of outcrop L with standard outcrops of La Fossa di Vulcano the data of the younger successions of Vulcano (Commenda and Cratere Attuale) show higher values, whereas the older successions (Punte Nere, Tufi Varicolori, and Palizzi) represent lower values. The data of outcrop L plot between the 2 types with slight tendencies to Cratere Attuale or Tufi Varicolori, not considering possible enrichment or depletion because of overriding the caldera wall. The coarser material may be depleted by the override of the wall and the resulting mean values seem to be higher as the they are in comparison to the standard outcrops.

sample	**Lw**	**Lc**	**Le**
min. value	1.73	1.67	1.73
max. value	2.09	2.11	1.97
mean value	1.93	1.88	1.84
standard deviation	0.1	0.2	0.1

Table 6.10: Ms of outcrop L in ϕ.

In plots of los vs. Ms no significant trends can be observed. Histograms of all units often show a slight negative skewness. The curves of Lw and in particular Le normally have similar shapes, whereas the curves of Lc differ in their expressions, especially the laminated part (Lc2) shows a well developed sigmoidal shape and owns the highest Ms of unit Lc. Sometimes the cumulated grain size curves of Lc look similar as some Palizzi curves. This indicates a homogenous cloud which overrides the wall without wide depletion. Possibly in this case the energy budget of the eruption cloud was so high, that it could surmount the obstacle without the depletion seen otherwise. It is possible that because of the high Ms the energy budget was low and the cloud was thinned by coarser particles. This can effect a depletion of particles of the sus (gsc05 and gs505), which would result in lower sus values.
Plotting the data in the scatter plot of the 2^{nd} vs. 1^{st} moment in general they follow the line of the standard successions. Lw falls on the line of Tufi Varicolori overlapped by the other successions. Lc plots near Palizzi and parts of Commenda whereas the values of Le do not point out a specific trend, this can also be caused by their exposed and possibly varied situation. The slopes of the linear fit (Lw = 3.07 ± 0.1, Lc = 6.27 ± 1.0, and Le = 3.70 ± 0.3) do not allow a correct correlation. Lw lies between Punte Nere and Palizzi, whereas Le shows higher similarities to the data of Tufi Varicolori, especially the latter is not very meaningful and weathering processes have to take into account.

6.4.3. Susceptibility

The values for the sus – measured in cgs-mode, standardised to 1g, and extended to 10^{-6} – for the units of outcrop L show slightly increasing mean values from the lower to the upper units. Herein for Lw the values range between 53.77 units (s: 3.4) for sus05 and the more or less similar sus25 with 53.92 units (s: 4.3). The following unit plots slightly higher in both sus whereas the difference between sus05 and sus25 is also higher (this may be originated by the low number of sampling points [3]), here values of 60.51 units (s: 1.7) for sus05 and 65.97 units (s: 6.4) for sus25 are observable. The last unit (Le) is widely exposed and alteration may be mirrored in the last sample with very low amounts, except for this sampling point, the remaining sampling points (3 samples) show a higher increase as the complete unit, the modified values range between 72.69 units (s: 5.8) for sus05 and 86.65 units (s:5.3) for sus25. Likewise in this unit the gap between the single sus increases.
Comparing the samples of outcrop L with the data of the standard outcrops it can be noticed that Lw plots lower than all known mean values. Possibly a correlation with low plotting Tufi Varicolori or Commenda may be feasible, because in addition both successions have relatively low differences between the two measured sus classes. In this case also the fact whether sus05 plots higher than sus25 or not is not clear because the values do not show wide differences for both sus. Lc has a correlation less similar to Lw, which possesses only slightly higher values. For this unit a correlation with Palizzi is not obvious – the field theory said that Lc belongs to the wet-surge dominated type of Palizzi, which was not measured for the

standard outcrops – but the raw data are lower than the data of standard outcrops. If a depletion of coarser elements is assumed in this context also some of the susceptibility bearing minerals are depleted, the lower sus values may be explained partly. Le shows a relatively good correlation with Commenda (taken into account all samples) as well as a correlation with Cratere Attuale, taken into account solely the samples plotting in the average range.

sample	**Lw**	**Lc**	**Le**	**Le** without the last sampling point
min. value 0.5-0.25 mm	49.87 ± 0.1	58.18 ± 0.1	47.07 ± 0.1	64.84 ± 0.1
max. value 0.5-0.25 mm	61.28 ± 0.1	62.13 ± 0.1	78.70 ± 0.1	78.70 ± 0.1
mean 0.5-0.25 mm	53.77 (s: 3.4)	60.51 (s: 1.7)	66.29 (s: 12.2)	72.69 (5.8)
min. value 0.25-0.125 mm	48.64 ± 0.1	57.26 ± 0.1	46.01 ± 0.1	69.38 ± 0.1
max. value 0.25-0.125 mm	61.72 ± 0.1	72.22 ± 0.1	106.65 ± 0.2	106.65 ± 0.2
mean 0.25-0.125 mm	53.92 (s: 4.3)	65.97 (s: 6.4)	76.49 (s: 22.0)	86.65 (5.3)

Table 6.11: Mean values for the sus for both gsc of outcrop L. Samples are measured in cgs-mode, standardised to 1g, and have to be extended by 10^{-6}. Lc contains solely 3 samples and the last sample of Le is significant low, according to the values of the γ-ray measurements this sampling point may be described as strongly weathered and leached.

Plotting the mean values vs. los solely Lw does not show a trend-line. The values of Lc increase with los whereas Le decreases. For every unit the values of sus25 demonstrate wider variations than sus05. Furthermore most of sus25 plot higher than sus05, except for the lower part of Lw pointing out an inverted appearance.

Plots of sus05 vs. sus25 demonstrate that the values of outcrop L in general plot in the "normal trend" without many outliers. Correlating the data graphically within the plots Lw can be defined as a part of Tufi Varicolori or Commenda. Lc shows similarities to Commenda and parts of Tufi Varicolori (using solely the raw data). For the highest values of Lc, supposing a potential depletion, a correlation with the lower plotting part of Palizzi may be possible (although it is not clear how intense the depletion affects the resulting lower sus values). Le can be observed in many clusters, but Commenda and Cratere Attuale dominate for most of the samples and seem to have the highest influence. A characterisation of the different units based on the slopes of the linear fits cannot be made, solely Le with a slope of 0.51 ± 0.0 can be compared with Cratere Attuale in particular (Lw: 0.42 ± 0.0, Lc: 0.27 ± 0.0). Comparing outcrops L and K – pursuant to the field theory that both outcrops own the same successions – the samples of Kw have a higher range than the samples of Lw. The samples of Ke have a lower range but show a higher affinity to Cratere Attuale, and the values of Kc and Le plot more or less similar. Now taking into account, that also Kc maybe depleted

by the overriding of the barrier, also the values of Kc could plot higher and be defined as samples of Palizzi (here dominantly dry-surge deposits).

6.4.4. Gamma-ray

The γ-ray data of the different units show high differences. Unit Lc is not very representative, because here solely 2 samples occur showing high differences especially in U and Th. The samples of Le are not sensible for a correlation because they are too low and due to their exposition it can be assumed that they are falsified as a result of leaching. In general a decreasing trend of the mean values for the different units can be observed. This can be explained by the exposition, as well as by the type of deposit (wet-surge or dry-surge deposits) and possibly also by their composition.

sample	**K** [%]	**U** [ppm]	**Th** [ppm]
Minimum Lw	4.60 ± 0.1	9.50 ± 0.9	33.10 ± 0.5
Maximum Lw	4.90 ± 0.2	10.53 ± 0.3	35.93 ± 1.3
mean Lw	4.72 (s: 0.1)	10.09 (s: 0.4)	34.46 (s: 0.9)
Minimum Lc	4.37 ± 0.1	7.70 ± 0.6	30.40 ± 0.6
Maximum Lc	4.63 ± 0.2	10.33 ± 0.4	36.57 ± 1.1
mean Lc	4.50 (s: 0.1)	9.02 (s: 1.3)	33.48 (s: 3.1)
Minimum Lc	2.57 ± 0.0	5.73 ± 0.2	20.73 ± 0.7
Maximum Le	2.73 ± 0.0	6.53 ± 0.2	23.40 ± 0.6
mean Le	2.65 (s: 0.1)	6.21 (s: 0.3)	22.04 (s: 1.0)

Table 6.12: Maximum, minimum and mean values of K [%], U [ppm], and Th [ppm] for outcrop L. Lc contains solely 2 sampling points.

The mean values (see also table 6.12) of K range between 2.65 % (s: 0.1) for Le, 4.50 % (s: 0.1) for Lc and 4.72% (s: 0.1) for Lw. The values of U show amounts of 6.21 ppm (s: 0.3) for Le, about 9.02 ppm (s: 1.3) for Lc, and for Lw 10.09 ppm (s: 0.4). Th shows great differences between the single units, the highest values can be observed for Lw with about 34.46 ppm (s: 0.9) followed by Lc with 33.48 ppm (s: 3.1), whereas the lowest values are represented by Le with 22.04 ppm (s: 1.0). Because of the above mentioned exposed location of Le and the small sample amount of Lc solely Lw is useful to be compared with the other successions by it's mean values. These data show a correlation for Commenda by K, taken into account also depletion because of weathering in the eruption cloud in comparison to the data of dry-surge dominated deposits (known from standard outcrops like Palizzi and Punte

Nere) the data may be higher but because of the uncertainty of the degree of depletion a sensible correlation is not possible. The not modified values of Th and U in general show the best correlation with Tufi Varicolori, which plots slightly lower. The ratio U/Th of Lw 0.29 (s: 0.01) correlates well with the ratio of Tufi Varicolori (0.29, s: 0.04). In the context of possible leaching because of deposition and transportation type possibly Punte Nere is a probable correlation.

The plots of los vs. the element values represent the great differences of the units. Lw does not show a visible trend or high variations, whereas the two samples of Lc differ in a significant way (especially for Th and U). The noticeable difference between this 2 units to the depleted unit Le is mirrored in this plots very well (see also figure 6.8).

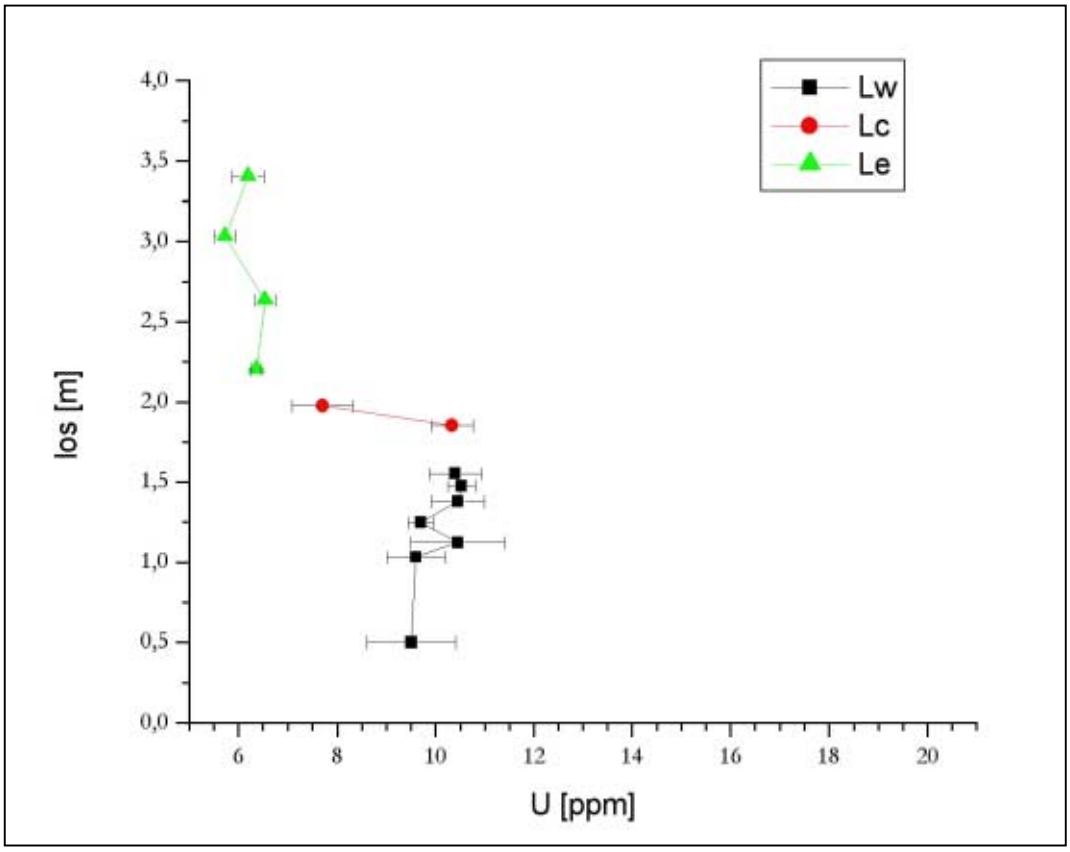

Figure 6.8: Plot of U vs. los. Remark the well defined zone of depletion in the uppermost part, caused by leaching.

Plotting the data of this outcrop within scatter plots concentration vs. ratio with the standard outcrops (see also Appendix IV) the following results can be summarised: in all cases Le shows a significant depletion and cannot be characterised by plotting in a special cluster. Lw in general shows references to Tufi Varicolori (normally to the higher plotting data of Tufi Varicolori) as well as to the lower plotting parts of Commenda, in contrast to the data of Kw the data of outcrop G and the channel (Punte Nere) do not show the same significance for the characterisation. Partly intersections with Punte Nere and Cratere Attuale can be observed. For Lc, with it's solely 2 sampling points, normally a correlation with Tufi Varicolori is the

best choice, sometimes also intersections with Palizzi or Commenda can be observed. Even if lower values because of depletion inside of the eruption cloud can be assumed anyhow a correlation with Palizzi is rare. Correlation of the slopes with significant slopes of standard outcrops are possible in particular, for example Lw can be correlated with Tufi Varicolori by the plot U vs. Th/U (Tufi Varicolori: -3.49 ± 0.1, Lw: -3.26 ± 1.4).

The scatter plots for the concentration (see also Appendix IV) show a correlation of Lw with Tufi Varicolori (upper plotting part) and often also probable correlation with Commenda (normally lower plotting part of Commenda). The 2 samples of Lc often plot in the cluster of Tufi Varicolori, but also Commenda and in particular Palizzi overlap. The correlation of the slopes for the single element concentrations allows solely a weak correlation of Lw with Punte Nere using the plot Th vs. K (Punte Nere: $-0.6*10^{-3} \pm 18.2*10^{-6}$, Lw $-0.5*10^{-3} \pm 0.3*10^{-3}$).

6.4.5. Interpretation

Also as for the outcrops before these data cannot be used for an identification by all methods. The special location and exposition of some units have to take into account when characterising the samples. Even the fact that samples, which are known solely as dry-surge deposits from the standard outcrops could be observed as wet-surge deposits in this location plays an important role.

Lw, which is built up by different wet-surge deposits, in general shows a dominance of indications for Tufi Varicolori, also Commenda often gives a good correlation with this unit. Solely a few links in the granulometry allow also a slight correlation with Palizzi or Punte Nere. The override of the barrier can change the Ms and on this basis these data are not as significant as inside of the caldera of La Fossa. Bearing in mind a change of the Ms also a change of the concentration of the sus-bearing minerals can be assumed, possibly they are depleted because many of them are hold back on the barrier. Due to that also the sus values can be depleted or enriched. Since now Tufi Varicolori is only known inside of the caldera and the normally plastical behaviour and less energy do not allow a settlement over the barrier, but the raw data show a good correlation to Tufi Varicolori. Commenda has been observed outside of the caldera and because of the intersections especially within the γ-ray plots a clear classification for this unit is not possible. Punte Nere in general shows too high values, so a depletion in the deposits can be the only reason for the great differences between the raw data and the values of Punte Nere.

Lc shows only a few data which are useful for a correlation. The γ-ray data have to be handled with care because here solely 2 sampling points occur. The unit shows references for many successions, in the outcrop it looks like some wet-surge deposits of Commenda or Tufi Varicolori, whereas the granulometric data also allow a correlation with Palizzi (cumulative grain size curves and 1^{st} vs. 2^{nd} moment) sometimes also Commenda seems to correlate, the raw data for sus show characterisations for Commenda as well as for Tufi Varicolori. Taking

into account a possible change of the composition (possibly depletion of sus-bearing minerals) a slight increase can shift the data of unit Lc into the lower part of the Palizzi-cluster. The γ-ray data in general show plots between different successions or inside of Tufi Varicolori, because of the small sample mass a correlation is not sensible. The best correlation for this unit seems to be Palizzi or Commenda, but the definition as Palizzi is solely feasible if Lw is attributed to Tufi Varicolori and an inversion of the deposits is not assumed.
Le can solely identified by the granulometric and sus data. As a result an attribution to Cratere Attuale may occur, although the granulometric data represent a few references to Tufi Varicolori, whereby the correlation is not very useful. Some data of the sus data set also allow a correlation with Commenda. The references for Cratere Attuale prevail and also inside of the outcrop stratigraphy this result is consequential.
Summarising the analysis for the complete outcrop the following results are possible, whereby the 1st or 2nd possibility is most likely:

- Lw belongs to Tufi Varicolori, Lc to Palizzi, and Le to Cratere Attuale
- Lw belongs to Tufi Varicolori, Lc to Commenda, and Le to Cratere Attuale
- Lw and Lc belong to Commenda and Le to Cratere Attuale

6.5. Outcrop M

6.5.1. Introduction

Outcrop M (see also figure 6.9) is located on the NE side of the Piano Caldera, the so-called area of Mt. Luccia, an exposed formation located on a cliff above the Vallone della Roia and the Caruggi. This location is situated at a high part of the caldera wall with more than 300 m of maximum height. As a result of the barrier in this outcrops solely parts of the eruption cloud are documented. Parts or even complete eruption clouds are deposited at the base of the wall, if the energy was too low to override the wall. Massive dominated deposits of the Vallone can show a laminated counterpart above the caldera wall (the finer part which has surmounted the barrier).
The outcrop has a height of about 4.5 m and is highly exposed, especially at the top; this way so that – as well as for the outcrops K and L – a depletion because of leaching in the upper sections can be assumed. At the base of the deposits TGR (Tufi dei Grotti Rossi) can be observed, which are not considered in the geophysical measurements. The remaining outcrop is built up by various wet- and dry-surge deposits, whereas the dry-surge deposits dominate at the base (near the TGR), upwardly a change to a higher amount of wet-surge deposits can be observed. Inside of the dry-surge deposits sometimes Pele's hair occurs. Clearly defined boundaries inside of the outcrop are not easy to find and thus 4 different units are characterised, dominated by the type of deposits. Above the deposits of TGR the investigated outcrop starts with a sequence of dry-surge deposits (Ms, 3 sampling points) followed by a unit of dry- and wet-surge deposits (Msw, 3 sampling points). These deposits result in unit

Mw (2 sampling points) dominated by wet-surge deposits. The top of the outcrop is built up by wet-surge deposits (Mwe, 3 sampling points), which are solidified on a highly exposed position.

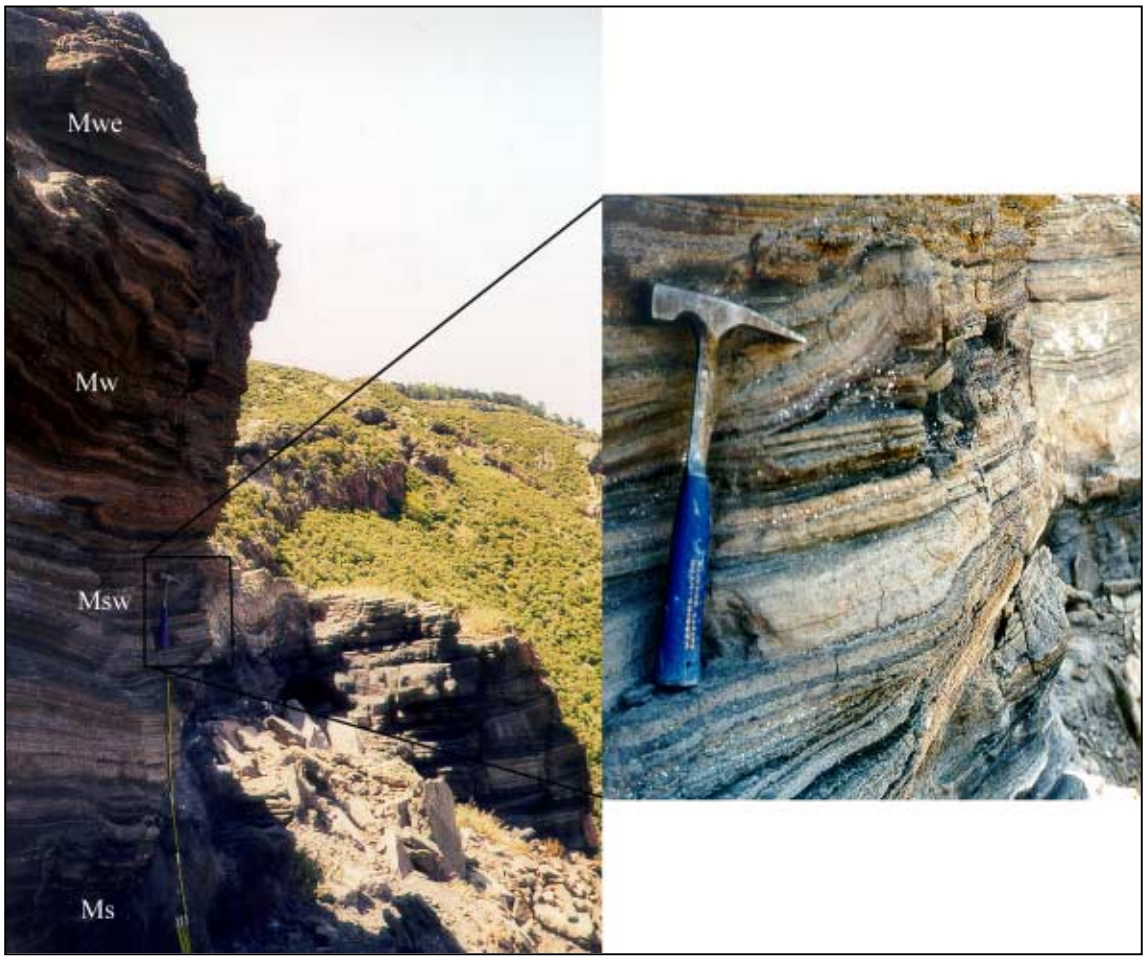

Figure 6.9: Outcrop M on the cliff of Mt. Luccia. a) complete outcrop, b) transition between dry- and wet-surge deposits (between unit Ms and Msw).

6.5.2. Granulometry

The granulometric data for the different units show high differences, especially the not solidified wet-surge deposits have relatively low values, whereas the solidified types show similar ranges as the dry-surges. The mean values of the Ms (see also table 6.13) range between 1.20 ϕ (s: 0.0) for Mw, 1.71 ϕ (s: 0.2) for Mwe, 1.80 ϕ (s: 0.2) for Ms, and 2.22 ϕ (s: 0.4) for Msw. The strongly solidified samples of Mwe and slightly solidified samples of Mw may be falsified due to the preparation mode or agglomeration processes.

Comparing these data with standard outcrops of La Fossa di Vulcano unit, Msw shows the best correlation with Cratere Attuale, possibly also Commenda can taken into account for the characterisation, whereby the value of Commenda shows a higher difference. The 2 samples of Mwe and Ms with likewise amounts can be best characterised by Tufi Varicolori, whereas for the slightly higher amount of unit Ms also a correlation with Cratere Attuale may be

possible. The latter is not very common. The lowest value (Mw, with solely 2 samples) shows the best correlation with Punte Nere and Palizzi. Most of these deposits do not allow a sensible correlation solely because of their mean Ms.

sample	Ms	Msw	Mw	Mwe
min. value	1.66	1.74	1.19	1.56
max. value	2.02	2.55	1.21	1.97
mean value	1.80	2.22	1.20	1.71
standard deviation	0.2	0.4	0.0	0.2

Table 6.13: Ms of outcrop M in ϕ.

The Ms do not show significant trends, normally a wide range can be observed. The histograms of unit Ms represent a relatively well Gaussian distribution that continues in the basal unit Msw. The remaining histograms of the upper Msw have a negative skewness. Nevertheless, the transition between Ms and Msw is smooth. The following 2 samples of Mw do not represent a significant distribution, whereas the upper unit (Mwe) demonstrates a slightly negative skewness. Caused by the distribution Ms and the basal Msw can be compared with parts of Punte Nere or Palizzi. A slightly negative skewness is observable in many successions. The cumulative grain size curves for the different units sometimes vary noticeable in their shape. The lower units Ms and Msw have a well defined shape, whereby especially Ms and Msw1 represent relatively well formed sigmoidal shapes, most notably comparable with curves of Punte Nere, partly also some samples of Palizzi are comparable with these shapes. These shapes indicate a homogenous distribution in the eruption cloud, which overrides the barrier. This allows the assumption that the transport as well as the eruption energy of the early events was relatively high and a significant part of the cloud can override the obstacle. On the other hand, it could be assumed that the barrier height was not as high as observed today, thus the energy to override the obstacle had to be lower.

The samples of Mw have a straight form without any type of curve, this behaviour is also observable in some samples of outcrop G of Punte Nere, a few samples of Tufi Varicolori, and basal samples for 2 standard outcrops (A and B, especially at the base) of Commenda. The upper unit (Mwe) whether shows a well defined shape like Ms nor a straight line like Mw, it plots between with a light curved shape and a very low sigmoidal touch. This type is observable for example in Cratere Attuale as well as in the solidified part of outcrop L (Le).

When plotting the samples in the diagram 2^{nd} vs. 1^{st} moment they do not show significant outliers and follow the average direction of the plot. Samples of Ms and Msw plot in the middle to upper part, whereas Mw plots much lower. The covering Mwe represents it's data in the lower part of the plot, but in general higher than Mw. Comparing the slopes (linear regression) as a discrimination tool, Ms (3.50 ± 1.2) can be compared with the lower plotting Punte Nere (3.43 ± 0.2) or the higher plotting Tufi Varicolori (3.57 ± 0.1); the transition unit Msw (3.56 ± 0.3) has a high affinity to Tufi Varicolori. Caused by the small numbers of samples the plot of Mw is not sensible for a correlation, whereas the covering Mwe (3.76 ± 0.4) shows a similarity to the lower plotting Tufi Varicolori.

6.5.3. Susceptibility

The mean values for the sus – measured in cgs-mode, standardised to 1g, and extended to 10^{-6} – of outcrop M differ slightly solely in the miscellaneous units (see also table 6.14). In comparison to the standard outcrops, most of the data show low values. Sus05 for Ms has values about 67.27 units (s: 2.7) whereas sus25 possess slightly higher values of 72.93 units (s: 4.0). In general, Msw shows lower values (sus05 = 52.87 units, s: 6.1, sus25 = 56.64 units, s: 6.2), whereby Mw with it's 2 samples plots in the same range (sus05 = 52.75 units, s: 2.0; sus25 = 58.33 units, s: 4.0). Likewise the last unit (Mwe) shows similar values, whereas in this case the difference between both sus (sus05 = 57.46 units. s: 7.6, and sus25 = 59.43 units, s: 8.2) is not very high, but the standard deviation is higher than for most of the other units.
Using the standard outcrops for a characterisation nearly all samples of outcrop M show similar correlation because of their relatively close fitting values. The best correlation can be made with Tufi Varicolori and in particular also with Commenda, whereby the lowest unit near TGR (Ms) fits the best correlation. The other units solely show the various similarities with these successions but a satisfactory correlation cannot be made. For Ms the best characterisation can be made with Commenda, where both sus demonstrate only small variations to the values of Commenda. In every unit (of the outcrop) it is possible that the amounts of susceptibility bearing minerals are depleted because solely a part of the eruption cloud overrides the barrier.

sample	**Ms**	**Msw**	**Mw**	**Mwe**
min. value 0.5-0.25 mm	63.96 ± 0.1	46.31 ± 0.1	50.76 ± 0.1	48.94 ± 0.1
max. value 0.5-0.25 mm	70.45 ± 0.1	60.91 ± 0.1	54.74 ± 0.1	67.39 ± 0.1
mean 0.5-0.25 mm	67.27 (s: 2.7)	52.87 (s: 6.1)	52.75 (s: 2.0)	57.46 (s: 7.6)
min. value 0.25-0.125 mm	68.39 ± 0.1	49.84 ± 0.1	54.29 ± 0.1	52.91 ± 0.1
max. value 0.25-0.125 mm	78.21 ± 0.1	64.92 ± 0.1	62.36 ± 0.1	71.03 ± 0.1
mean 0.25-0.125 mm	72.93 (s: 4.0)	56.64 (s: 6.2)	58.33 (s: 4.0)	59.43 (s: 8.2)

Table 6.14: Mean values for the sus for both gsc of outcrop M. Samples are measured in cgs-mode, standardised to 1g, and have to be extended by 10^{-6}. Mw contains solely 2 samples.

In the plots of los vs. sus significant trends cannot be observed, only Mwe shows a slight decrease and sus25 of Ms an increase. For all units sus25 generally plots higher than sus05, which is noticeable for all other succession (except of Tufi Varicolori).
Plots of the ratio of sus or sus/Ms do not denote significant correlation. Plots of sus05 vs. sus25 give the following information: Data of Ms can be found in clusters of Tufi Varicolori as well as Commenda, partly an intersection with Cratere Attuale is observable but in general all samples of outcrop M show higher sus05 values than samples of Cratere Attuale with a similar sus25 amount. The data of Mws plot in a lower part than the samples of Ms but also

an intersection with Tufi Varicolori as well as with Commenda is noticeable. The wet-surge deposits Mw and Mwe have the same preferences as the units before, as sensible discrimination is not possible. In comparison to the standard outcrops of La Fossa the slopes (as a result of the linear fits) for the single units do not allow any correlation of Ms (0.32 ± 0.0). Msw (0.97 ± 0.0) mirrors similarities with Tufi Varicolori, whereas Mw is not comparable because of the small number of samples. The result for Mwe (0.89 ± 0.0) ranges between the values of Tufi Varicolori and Commenda, whereby the amounts of Tufi Varicolori are closer to the amounts of Mwe as the values of Commenda.

6.5.4. Gamma-ray

The γ-ray data of outcrop M can split of into 2 groups: samples of the basal units Ms and Msw with higher plotting element values and the group of lower plotting samples containing the pure wet-surge deposits (Mw and Mwe) (see also table 6.15). For Ms the following mean values can be noticed: K = 4.80 % (s: 0.4), U = 9.01 ppm (s: 1.3), and Th 32.35 ppm (s: 0.9). The values for Msw are often similar (K = 4.62 %, s: 0.4; U = 9.87 ppm, s: 0.9; Th = 32.74 ppm, s: 1.1). Mw shows related values for it's 2 samples except of Th (K = 2.02 %, s: 0.0; U = 7.25 ppm, s: 0.1; Th = 22.45 ppm, s: 2.3). For example the covering and higher weathered Mwe has likewise values with a K amount of 2.25 % (s: 0.1), U ranges at 6.64 ppm (s: 0.7), and Th has a mean value of 22.20 ppm (s: 0.3). The comparison of these data with standard outcrops of La Fossa allows the following characterisations: Using K Ms shows the best correlation with Commenda, also the very high plotting Tufi Varicolori may be possible. For the U values Tufi Varicolori seems to be the best choice and even the Th values indicate an attribution to Tufi Varicolori. For Msw the correlation shows strong similarities, whereby the values for K have a higher affinity to Tufi Varicolori than to Commenda. The upper units Mw and Mwe do not show sensible correlations, both plot lower than the known values of La Fossa standard outcrops. For Mwe a depletion because of weathering is supposed. The similar γ-ray data for Mw also indicate a depletion due to weathering, although the appearance in the field does not point this out as seen for Mwe.

Using the plots of los vs. element concentration (see also figure 6.10) the similar units of Ms and Msw show opposite trends, whereby Ms increases and Msw decreases. Taken into account that the values of the γ-ray measurements can reflect the composition of the erupted material and an evolution of the magma chamber, it can be assumed that the erupted magma of Ms seems to be less evolved with increasing eruption. The values for Msw show a newly increase of the values which indicates a higher evolved magma-type. Considering that the degree of wet-surge deposits rise with higher position and that the γ-ray values of wet-surge deposits normally plot lower than the γ-ray values of dry-surge deposits of the same magmatic composition, the trend in Msw mirrors a rapid increase of highly evolved material (base to top of unit Msw). This behaviour is also noticeable in the U/Th ratio. The behaviour of Msw may

indicate that the reservoir geometry can be more complex – different possibilities of emptying the reservoir, whereby parts of a former hydraulic or hydrostatic disabled part of the reservoir gets more influence with ongoing eruption and higher amounts of this magma-type participate on the eruption – as assumed by KOKELAAR (1998) –, or the dynamics of the eruptions are more complex as assumed in the recent case. For the uppermost units Mw and Mwe, no significant trends can be observed.

sample	**K** [%]	**U** [ppm]	**Th** [ppm]
Minimum Ms	4.28 ± 0.1	8.18 ± 0.4	30.10 ± 0.7
Maximum Ms	5.23 ± 0.1	11.45 ± 0.5	33.10 ± 0.8
mean Ms	4.80 (s: 0.4)	9.01 (s: 1.3)	32.35 (s: 0.9)
Minimum Msw	4.20 ± 0.0	9.00 ± 0.6	31.68 ± 0.9
Maximum Msw	5.23 ± 0.2	11.10 ± 0.4	32.23 ± 0.1
mean Msw	4.62 (s: 0.4)	9.87 (s: 0.9)	32.74 (s: 1.1)
Minimum Mw	2.00 ± 0.0	7.03 ± 0.3	20.20 ± 0.5
Maximum Mw	2.03 ± 0.1	7.27 ± 0.5	24.70 ± 0.4
mean Mw	2.02 (s: 0.0)	7.25 (s: 0.1)	22.45 (s: 2.3)
Minimum Mwe	2.18 ± 0.1	5.87 ± 0.3	21.80 ± 1.3
Maximum Mwe	2.38 ± 0.1	7.65 ± 0.4	22.50 ± 1.2
mean Mwe	2.25 (s: 0.1)	6.64 (s: 0.7)	22.20 (s: 0.3)

Table 6.15: Maximum, minimum and mean values of K [%], U [ppm], and Th [ppm] for outcrop M. Mw contains solely 2 samples.

Using the plots of element concentration vs. the ratio of the concentrations (see also Appendix IV) to characterise the different units, a graphical characterisation of Mw and Mwe is not sensible because both units plot out of range, although their ratio often shows values near the data of the standard outcrops. Ms and Msw in general plot in the same range and overlap with the cluster of Tufi Varicolori in every plot. Sometimes also intersections with small parts of the Punte Nere cluster (Th vs. U/Th, K vs. Th/K, K vs. U/K, and U vs. K/U) and the Commenda cluster (Th vs. U/Th, Th vs. K/Th, K vs. Th/K, and U vs. Th/U) can be observed. A correlation using the slopes is not possible for Mw and also the other units have solely a few data points so the correlation is not as sensitive as for units with a larger data set. A possible correlation with Punte Nere can be found for Ms in the plot U vs. K/U.

The plots of concentration vs. concentration for K, U, and Th do also allow some correlation, as well as in the scatter plots before the data of Mw and Mwe plot out of range in the lower part of the graphs. In all plots Ms and Msw plot dominantly in the cluster of Tufi Varicolori, but for this plots more intersections with Punte Nere (K vs. U, possibly Th vs. K) and Commenda (Th vs. U, possibly Th vs. K) can be recognised. Even so a correlation by the slopes cannot be observed.

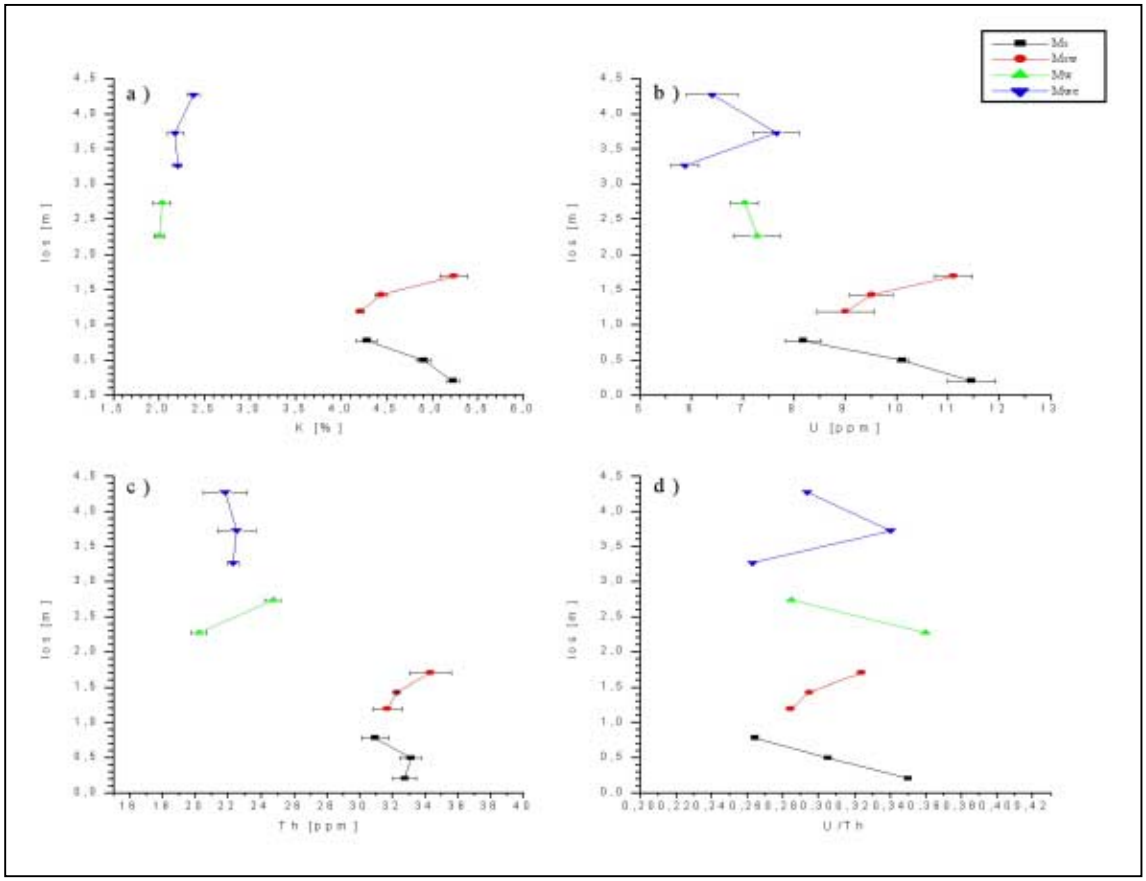

Figure 6.10: Plots of the element concentrations and the ratio U/Th vs. los. a) los vs. K, b) los vs. U, c) los vs. Th, and d) los vs. U/Th. For all plots except of d) a clear differentiation between the basal, dry-surge dominated and the upper wet-surge dominated deposits can be made. Here the high probability of weathering and leaching for the upper parts has to taken in mind. The lower units – with similar mean values – show opposite trends (vs. los), which can also be observed in d).

6.5.5. Interpretation

Summarising the results of each method the outcrop can be classified using the following way. The units Ms and Msw in general show likewise results and maybe merged for the interpretation. For these units any method indicates data implicating secondary influences, which can influence the results. This can be observed for Mw and Mwe, where the γ-ray values indicate leaching, whereby the solidified consistence and the exposure of Mwe is also a reference for the changed situation.

The granulometry data allow a characterisation of Ms as Punte Nere, Tufi Varicolori or Palizzi, whereas the sus values indicate a classification as Tufi Varicolori or Commenda, whereby the constellation of sus05 and sus25 is not characteristic for Tufi Varicolori. Taken into account solely the γ-ray data the best correlation seems to be Tufi Varicolori, admittedly also Punte Nere and Commenda show slight correlation with the plots, but the dominating part is Tufi Varicolori. All these consolidate a classification of Tufi Varicolori, but the deposits of Tufi Varicolori as known so far do not possess many dry-surge deposits, the few are normally intercalated in wet-surge deposits known so far. Similar arguments can be used to refute a correlation with Commenda, which is the other succession with a possible correlation for Ms. A correlation with Palizzi is – except of the appearance – only based on the plots of cumulative grain size curves and histograms and thus not powerful. Characterising Ms as Punte Nere solely the appearance, the partial correlation of the γ-ray and some granulometric data allow a weak correlation. The intersections of the γ-ray plots used for a characterisation are small. Taken into account that the eruption cloud overrides the high barrier (highest part of the recent barrier) it is possible that the composition of the cloud has changed and possibly larger fragments, which can also contain sus-bearing minerals or important minerals for the γ-ray measurements, do not cross the barrier and can be observed as massive beds in the Vallone. This stays in contrast to the well defined sigmoidal shape of the grain size curves, which indicate a higher homogeneity of the eruption cloud. According to the data the unit can be characterised as Tufi Varicolori.

The correlation for Msw is likewise, also for this unit the preferred correlation is Tufi Varicolori, if only used the data without the appearance of the deposits in the field. Especially the basal part of this unit is comparable with Ms (unit).

For Mw and Mwe the γ-ray-data are out of range, solely the granulometrical and sus-values can taken into account. The mean values of sus represent the best correlation with Tufi Varicolori, but also a correlation with Commenda is possible, using the plot sus05 vs. sus25. The granulometric data of Mw show the best correlation with Punte Nere and Palizzi, whereas it's cumulative grain size curves show good correlation with outcrop G of Punte Nere, parts of Tufi Varicolori and the basal samples of Commenda (especially outcrops A and B). A clear classification without γ-ray data is not sensible and because of that Mw can belong to Tufi Varicolori as well as to Commenda. Mwe shows good correlation of the sus values (mean, slope, scatter plot) with Tufi Varicolori. A characterisation as Commenda is also possible using the slope (linear fit sus05 vs. sus25) in a wider range as well as the graphic result of the plot sus05 vs. sus25. The latter shows also small intersections with the lower plotting Cratere Attuale, whereby it has to bear in mind that this data solely belong to Pietre Cotte not to all units of Cratere Attuale. Using the granulometric data to describe Mwe it has to taken into account that the material is secondary solidified most likely by weathering processes. The mean values and partly also the slope (2^{nd} vs. 1^{st} moment) describe a good correlation with Tufi Varicolori. The cumulative grain size curves are very similar to the curves of the

likewise weathered and indurated unit Le of outcrop L, that is correlated with Cratere Attuale. Comparing the sus values of Mwe with the values of Le, a similarity to the upper samples of Le with the samples of Mwe can be noticed. Mwe can be described as Tufi Varicolori, Commenda or Cratere Attuale. If Mw is defined as Commenda a characterisation for Mwe as Tufi Varicolori is not meaningful.
Concluding the following characterisation possibilities can be expected, whereas the 2nd possibility with Mwe belonging to Cratere Attuale seems to be the best correlation:

- Ms and Msw belong to Tufi Varicolori, Mw to Tufi Varicolori, and Mwe to Tufi Varicolori, Commenda, or Cratere Attuale.
- Ms and Msw belong to Tufi Varicolori, Mw to Commenda, and Mwe to Commenda or Cratere Attuale, whereby Cratere Attuale seems to be the better choice.

6.6. Outcrop N

6.6.1. Introduction

The Caruggi is a flat upland area (inside of the Fossa Caldera above the Vallone della Roia) about 100 to 150 m above the ground of the Fossa Caldera, bounded by the high caldera wall of the Fossa Caldera in transition to the Piano Caldera. Outcrop N is located on the northern part of this area below the Mt. Luccia and has a height of about 3 m. In this outcrop a prominent marker horizon – the Upper Pilato Ash, originated in Lipari – is observable in 2 layers (see also figure 6.11). The base of the outcrop is dominated by various greyish dry-surge deposits, often including Pele's hair, which change to wet-surge deposits. These deposits are merged in unit Nc and contain 5 sampling points. Because of the defined overlaying deposits this unit can be classified as pre-Commenda (Punte Nere, Tufi Varicolori, or Palizzi). Nc is covered by the conspicuous Commenda fall-out deposits – containing flamboyantly yellow to orange coloured, highly altered, up to hand sized clasts – which, in this outcrop, are followed by another prominent marker horizon (Upper Pilato Ash). The latter is coated by multicoloured wet-surge deposits. On the base these deposits are dominated by ochre-grey-reddish layers, whereby the ochre colour fades out to the top. The unit is bounded by a remarkable pinkish layer. Up to this layer the unit is defined as Nd and contains 7 sampling points; above the pinkish layer a slight change of the appearance in the field is observable and orange to greyish colours dominate the deposits (unit Nw, containing 4 sampling points). The deposits of the units Nd and Nw have to be attributed to Commenda or Cratere Attuale, caused by the stratigraphic situation observed the outcrop (marker horizons). Figure 6.11 shows the basal to middle part of outcrop N, also containing the Commenda fall-out deposits and the Upper Pilato Ash.

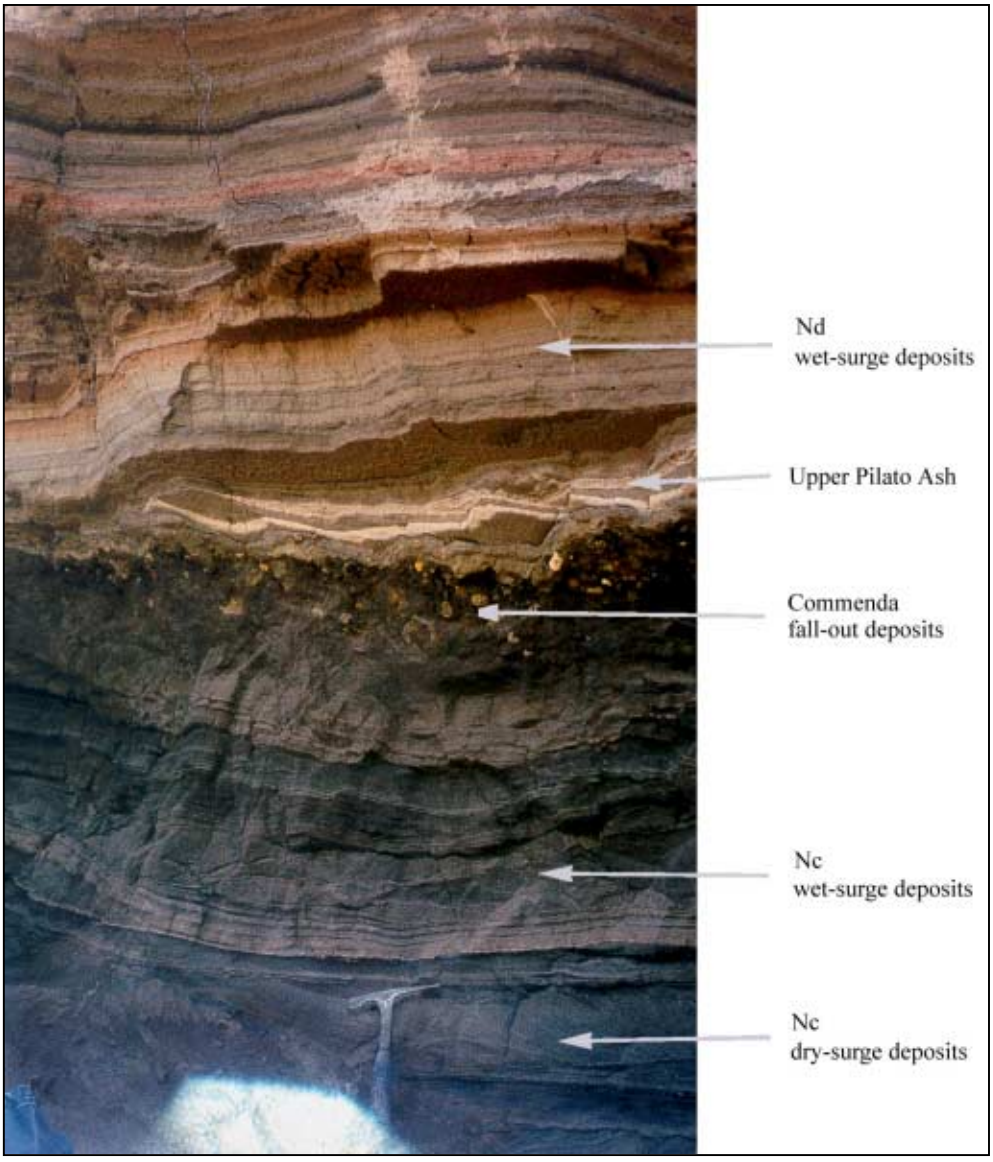

Figure 6.11: Lower part of outcrop N, the base is dominated by unit Nc, build up by grey dry- and wet-surge deposits, and covered by the Commenda fall-out deposits followed by 2 layers of the Upper Pilato Ash. These prominent marker horizon is followed by unit Nd, dominated by wet-surge deposits.

6.6.2. Granulometry

The granulometric data of outcrop N posses different mean values of the Ms, whereby the difference between Nd and Nw is not significant (see also table 6.16). The mean Ms value (2.07 ϕ, s: 0.1) for Nc is significant lower than the nearby plotting values of Nd (3.02 ϕ, s: 0.1) and Nw (2.94 ϕ, s: 0.2). In comparison to the standard outcrops of La Fossa Nc correlates with Cratere Attuale (the range of Nc is very small) and even a correlation with Tufi Varicolori could be possible; considering the marker horizons (Upper Pilato Ash) the correlation with Cratere Attuale is unrealistic. For Nd and Nw a correlation with Commenda seems to be the best choice, whereby the mean values of both units are higher than the average mean values of Commenda. But solely Commenda has likewise maximum Ms values as those observable for the average Ms values of Nd and Nw. The relatively high Ms values

could be explained by the override of the barrier by the eruption cloud, whereby the cloud could be thinned by a hydraulic jump.

sample	Nc	Nd	Nw
min. value	1.96	2.83	2.72
max. value	2.29	3.15	3.18
mean value	2.07	3.02	2.94
standard deviation	0.1	0.1	0.2

Table 6.16: Ms of outcrop N in ϕ.

The plot of los vs. Ms demonstrates the differences in Ms size between Nc on the one hand and Nd and Nw on the other hand. Trends inside of the units are not observable. Nd and Nw plot in the same range of the Ms but the difference between adjacent data points for Nd is lower than for Nw, which cannot be explained solely by a higher data density.

The histograms for the different units show mostly a pronounced negative skewness especially for the wet-surge deposits of Nd and Nw. In general the samples of Nd show a slightly higher rate of gsc < 0.125 mm than most of the samples of Nw. The samples of Nc can be split into the part containing wet-surge deposits, showing an approximately Gaussian distribution, and the part dominated by dry-surge deposits, also showing a slight negative skewness not pronounced as well as for the wet-surge deposits of Nd and Nw. A slight negative skewness is observable in Tufi Varicolori, whereas many samples of Punte Nere have a well pronounced Gaussian distribution, also a few Palizzi samples can show Gaussian distribution, often combined with the presence of Pele's hair or pumice clasts. For Commenda a distinct negative skewness is visible, which is sometimes also observable for Cratere Attuale, admittedly here Gaussian distribution is remarkable, too.

Comparing the cumulative grain size curves for Nd and Nw no significant differences can be seen; a slightly shape with a steep increase of the finer gsc is observable. The curves of Nc often represent a sigmoidal shape – the wet-surge deposits are less pronounced as the dry-surge deposits –, which is often observable in Punte Nere and parts of Palizzi. Curves with similar shape as the curves of Nd and Nw are normally observable inside of the Commenda successions as well as in parts of Cratere Attuale.

In the plot of the 2^{nd} vs. the 1^{st} moment the data of Nc plot in the middle of the average trend-line, whereby they do not fall on a line. In general they cluster in the zone where most of the successions can be observed. The values of Nd and Nw overlap and plot in a line slightly below the upper part of the trend line dominated by Commenda, a discrimination between the two units is not possible. A correlation by the slope is not possible for any unit.

6.6.3. Susceptibility

The mean values of the sus – measured in cgs-mode, standardised to 1g, and extended to 10^{-6} – show a split for the units in outcrop N, which is also observable for the granulometrical values discussed above. Nc is distinguishable from Nd and Nw, which plot in a similar range (see also table 6.17). The mean value for sus05 of Nc is about 96.34 units (s: 13.3) and for sus25 about 88.76 units (s: 14.2). Nd and Nw have mean values of Nd = 59.30 units (s: 7.8) and Nw = 61.60 units (s: 15.1) for sus05 and Nd = 64.31 units (s: 8.7) and Nw = 59.85 units (s: 15.7) for sus25. It has to be noticed that s for Nc and Nw is higher than for Nd, in spite of the latter contains more samples for a better correlation. Although the values of Nd and Nw are likewise, they differ in the range of their mean values, whereas Nd has a higher mean for sus25 and Nw for sus05. Even in Nc sus05 shows higher amounts than sus25. In the standard outcrops this is only (well pronounced) observable in the succession of Tufi Varicolori.
Using the mean values of the sus to characterise the units, the following results can be seen: Nc does not show a good correlation with any succession except of sus25 for Cratere Attuale, this correlation is not possible due to the defined marker horizons. sus05 maybe correlates with sus05 of Punte Nere or Palizzi. Nd and Nw show the best correlation with Commenda whereby these data also do not represent an ideal correlation, but both units ranges inside of the boundaries defined by Commenda.

sample	**Nc**	**Nd**	**Nw**
min. value 0.5-0.25 mm	82.86 ± 0.2	47.01 ± 0.1	39.93 ± 0.1
max. value 0.5-0.25 mm	116.13 ± 0.2	71.97 ± 0.2	81.46 ± 0.6
mean 0.5-0.25 mm	96.34 (s: 13.3)	59.30 (s: 7.8)	61.60 (s: 15.1)
min. value 0.25-0.125 mm	70.07 ± 0.2	49.04 ± 0.1	34.24 ± 0.1
max. value 0.25-0.125 mm	111.80 ± 0.2	75.05 ± 0.1	74.67 ± 0.1
mean 0.25-0.125 mm	88.76 (s: 14.2)	64.31 (s: 8.7)	59.85 (s: 15.7)

Table 6.17: Mean values for the sus for both gsc of outcrop N. Samples are measured in cgs-mode, standardised to 1g, and have to be extended by 10^{-6}.

Looking on the plots of los vs. sus a significant trend is not observable, only the wet-surge deposits of Nc show a higher value than the average data. Not taken into account this 2 samples the sus of Nc would be solely slightly higher than the sus of Nd and Nw.
Plots of the ratio of sus or sus/Ms do not point out a significant correlation. The plot of sus05 vs. sus25 (see also figure 6.12) gives a better classification of the 3 single units as assumed by the mean values. It is obvious that Nd and most parts of Nw plot in the same cluster as Commenda, although a few intersections, especially with Tufi Varicolori, can be observed, a correlation with Commenda seems to be possible (also because of the time marker). Nc plots

in a cluster where many successions can occur, but in general the data of Punte Nere as well as of Palizzi dominate, whereby many samples plot in the lower part of the cluster of Punte Nere. A correlation of the units with successions by the slope for this plot does not show very probable results: Nc (0.88 ± 0.0) has it's best correlation with Tufi Varicolori, which will be possible because of time horizon but do not have more correlation for Nc so far. Also a weak correlation with Commenda can be assumed, which is implausible because of the time marker horizon. Nd (0.75 ± 0.0) and Nw (0.69 ± 0.0) show a relatively good correlation with Punte Nere, which is not realistic because of the time marker horizon.

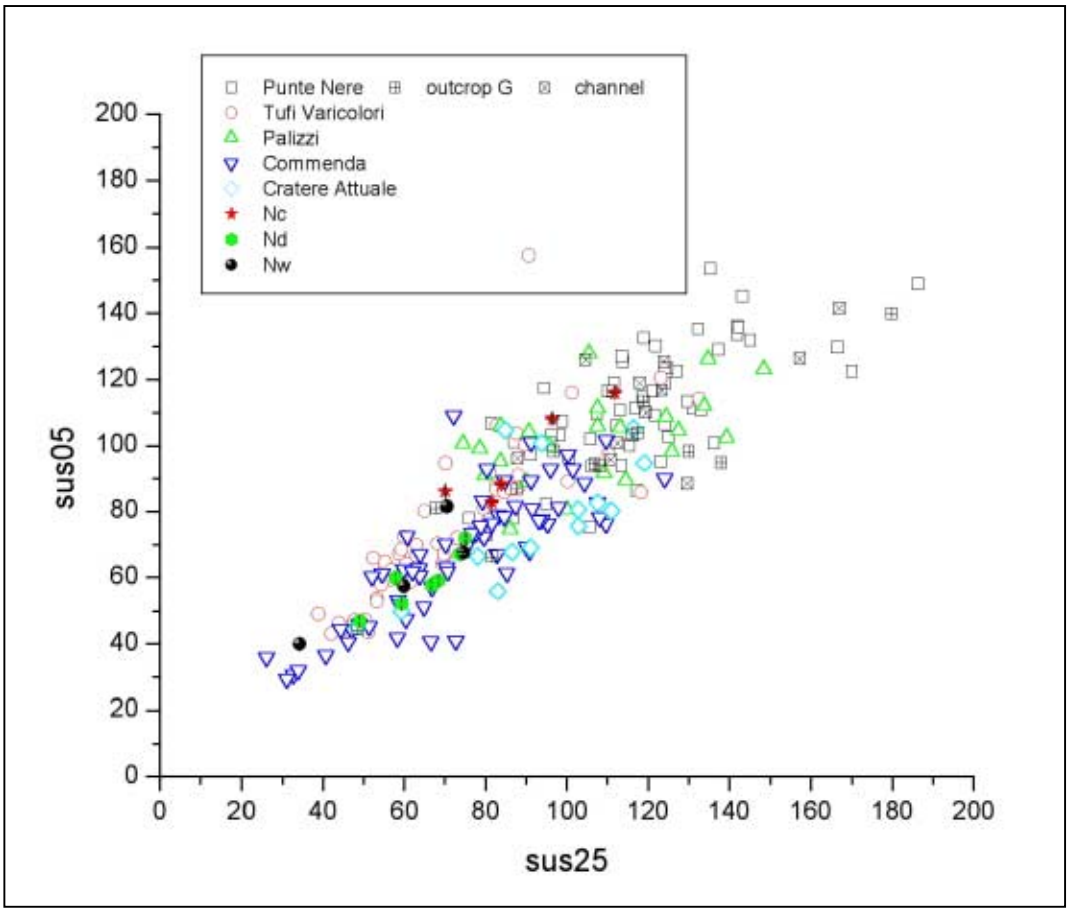

Figure 6.12: sus05 vs. sus25 for the samples of outcrop N (filled marks) in comparison to standard outcrops of La Fossa di Vulcano.

6.6.4. Gamma-ray

The mean sizes of the γ-ray values for outcrop N are shown in table 6.18. For Nc the following mean values can be observed: K = 6.17 % (s: 0.3), U = 14.02 ppm (s: 0.7), and Th = 43.44 ppm (s:1.2). These values are the lowest plotting mean values in this outcrop, but also the values with a very low s. The data of Nd and Nw do not correlate in the same way as observed above for the granulometry and the sus. This can be seen especially for U, where the values for Nd with 16.88 ppm (s: 2.2) are noticeable higher than the values for Nw (15.53 ppm, s: 0.3). In general all mean values of Nw (K = 6.36 %, s: 0.3 and Th = 49.17 ppm, s:

2.0) are lower than the mean values of Nd (K = 6.46 %, s: 0.7 and Th 51.93 ppm, s: 6.7). The ratios of all units are more or less equal.

A comparison to standard outcrops of La Fossa with Nc by single elements gives up to 3 different results: K is partly comparable with Punte Nere or Palizzi, whereas the best correlation for U can be observed with Cratere Attuale. The less soluble Th shows a very good correlation with Palizzi. U and K differ in a wider range and the correlation is more vague. Nd is characterised especially by some of it's maximum γ-ray values as Palizzi, as well the choice of Palizzi is not very sensible because of the time marker (Upper Pilato Ash). The situation of Nw is more or less similar for K. Because of the lower mean value of U for this element concentration a good correlation with Palizzi is observable, whereas the correlation based on Th is not as specific as U seems to be. With the high plotting Th also a correlation with Cratere Attuale is possible. As well as for Nd the classification of Nw as Palizzi is impossible because of the time marker.

sample	**K** [%]	**U** [ppm]	**Th** [ppm]
Minimum Nc	5.60 ± 0.1	13.15 ± 0.5	41.40 ± 1.5
Maximum Nc	6.43 ± 0.2	14.93 ± 0.6	44.60 ± 0.6
mean Nc	6.17 (s: 0.3)	14.02 (s: 0.7)	43.44 (s: 1.2)
Minimum Nd	5.133 ± 0.2	13.13 ± 0.3	40.97 ± 0.9
Maximum Nd	7.33 ± 0.3	20.43 ± 1.0	62.70 ± 1.2
mean Nd	6.46 (s: 0.7)	16.88 (s:2.2)	51.93 (s: 6.7)
Minimum Nw	6.00 ± 0.1	15.27 ± 0.8	46.58 ± 0.7
Maximum Nw	6.80 ± 0.2	15.97 ± 0.6	52.10 ± 1.1
mean Nw	6.36 (s: 0.3)	15.53 (s: 0.3)	49.17 (s: 2.0)

Table 6.18: Maximum, minimum and mean values of K [%], U [ppm], and Th [ppm] for outcrop N.

The plot of los vs. concentration does not show significant trends for Nc and Nw but inside of Nd a splitting of the unit can be observed. The change occurs between Nd4 and Nd5, whereby for Th Nd4 can belong to the lower as well as to the higher plotting part (see also figure 6.13). The values for the ratio U/Th do not demonstrate this split. The change of values correlates with a change of colours in the deposits: the lower sampling points are dominated by ochre to reddish-violet slightly grey substituted colours, the upper part is dominated by reddish-greyish layers terminated by the pinkish layer. Dividing Nd into 2 new subgroups – Nd_{base} and Nd_{upper} – the γ-ray mean values will change significantly. The subgroup Nd_{base}, containing the sampling points Nd1 to Nd4, represents a mean K value of 6.98 % (s: 0.2), for U 18.55 ppm

(s: 1.1), and for Th 56.63 ppm (s: 4.1). These values do not show a significant correlation with any succession based solely on the mean values. The remaining subgroup Nd_{upper}, containing the sampling points Nd5 to Nd6, have lower mean values like 5.77 % (s: 0.5) for K, 14.65 ppm (s: 1.2) for U, and 45.73 ppm (s: 4.0) for Th. These values can be correlated with Punte Nere, Palizzi or Cratere Attuale by K, with Cratere Attuale by U, and with Palizzi or Cratere Attuale by Th. An absolute match is not observable, but in the case of Nd_{upper} a correlation with Cratere Attuale seems to be useful, because whether Punte Nere nor Palizzi are available for a correlation due to the time marker. This split up could be originated because of the composition mirrored by the change of colour dominance.

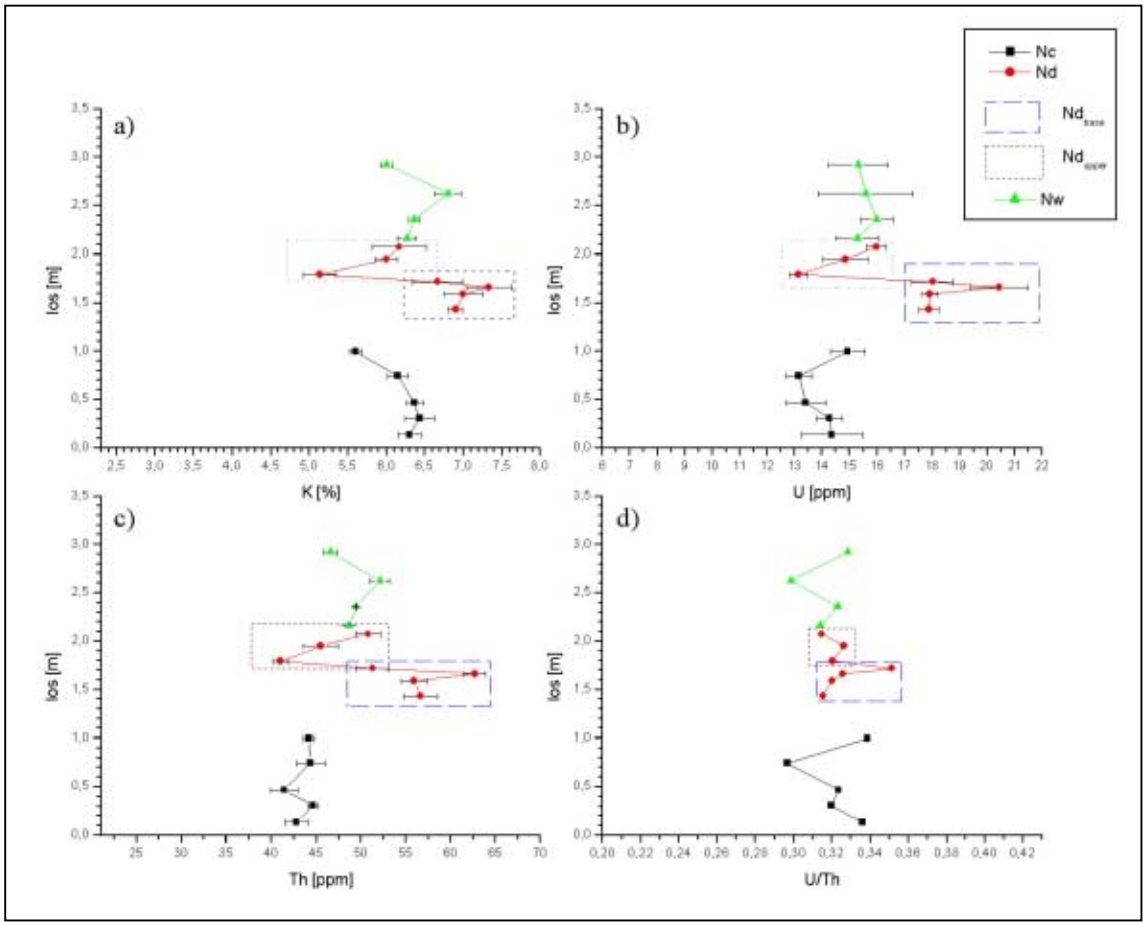

Figure 6.13: Development of the γ-ray data for outcrop N with los. Note the transition in Nd (2 subgroups Nd_{base} and Nd_{upper} plotting in different ranges, not observable for the sus or Ms development).

Plotting concentration vs. the ratio of element concentration for outcrop N (see also Appendix IV) the data of the Nc can be classified as Palizzi as well as Punte Nere, whereby the concentration often indicates an affiliation to Palizzi whereas the ratio allows an attribution to Punte Nere. Summarising all plots, the affiliation of Nc with Punte Nere is better for most of the plots. Nd often plots in the concentration range of Commenda as well as in the same range as Cratere Attuale, whereby the clustering in the ratio is dominated by marginal spheres of Commenda, likewise Palizzi can be identified in the clusters of Nd. But the latter (Palizzi) can

be excluded because of the time marker. In contrast to Nc the cluster of this unit in general do not plot in a defined area of only 1 or 2 successions, here often the clusters of many successions overlap. Normally the situation for Nw is comparable. A good discrimination between Commenda and Cratere Attuale cannot be made for this plots as seen before (chapters 5.2.4 and 5.2.5). For unit Nd more similarities with Commenda can be noticed but also a correlation with Cratere Attuale is possible. The values of Nw often show similar behaviour and thus a likewise characterisation as Nd with a slightly higher affinity to Cratere Attuale can be assumed. Using also the results of the linear fits for this plots Nd has a similar slope as Punte Nere in the plot U vs. K/U. Due to the time marker this correlation is not possible.

Using the single element concentrations illustrated in scatter plots for 2 elements, in general unit Nc can be defined as Punte Nere, although single plots show a few intersections with other successions. In the plot Th vs. K Nc is located in a window of "free space" between Punte Nere and Palizzi, a few overlaps with outcrop G and the channel (Punte Nere) are observable. Nd shows the same problems as seen for the former plots. A clear classification is not possible, whereby a characterisation as Palizzi can be excluded because of the position above the Upper Pilato Ash. The situation for Nw is more or less equal, whereby here Cratere Attuale shows a higher influence. A correlation based on the slopes can be made for Nd (3152.46 ± 713.8) in the plot K vs. U, this unit correlates with Palizzi, which is not possible in the known stratigraphic context (the Upper Pilato Ash is observable below). For the plot Th vs. U Nw (1.71 ± 0.6) can be compared with Punte Nere, this situation is not possible in the known stratigraphic context.

6.6.5. Interpretation

For this outcrop the difference between appearance and correlation based on the data set is lower than for many outcrops described before. Furthermore the presence of prominent marker horizons – the Commenda Breccia and the Upper Pilato Ash (see also chapter 2.5) – restricts the possible correlation for units deposited above or below the marker. Nc is located below the marker horizon, thus only a correlation with Punte Nere, Tufi Varicolori or Palizzi is sensible. According to the data Punte Nere is the best characterisation to choose for this unit, because here the most junctures are observable. The likewise very good correlating succession of Palizzi is placed back especially because of the better correlation of the γ-ray plots for Punte Nere (even the shape of the cumulative grain size curves gives some references for Punte Nere). In this situation the appearance in the field – structure, existence of Pele's hair, colour, consistence – is no discrimination tool between the 2 successions.

Nd and Nw, wet-surge deposits located above the marker, are allowed to be correlated solely with Commenda or Cratere Attuale. As seen before (chapters 5.2.4 to 5.2.5) the discrimination of these 2 successions is not very sensible for most situations. Correlation with Punte Nere or Palizzi by γ-ray results or Punte Nere and Tufi Varicolori by sus are not

realistic. According to the majority of intersections and correlation by single plots and mean values, the best characterisation for Nd can be made by Commenda. Few links for Cratere Attuale, as seen especially in the split-of into Nd_{base} and Nd_{upper}, do not agree with the context. A correlation of Nw, often similar to Nd, is based on an equal data set as for Nd. But for this unit also a correlation with Cratere Attuale can be assumed, verified especially by the plots of the γ-ray values (scatter plots of concentration vs. ratio or concentration). Considering the dominance of the other references a correlation with Commenda and a high affinity to Cratere Attuale is the best choice.

6.7. Outcrop P

6.7.1. Introduction

Many undefined outcrops located outside of the caldera of La Fossa, outcrop P is situated in the Vallone della Roia. It is located above a steep step near the end of the valley (seaward direction). The standard outcrops in the Vallone are located more southward. The measured and sampled part of the steep-sited outcrop has a height of about 5 m and has at the base of the outcrop an altered lava-flow (see also figure 6.14). The outcrop is built up by massive and laminated deposits of ochre to greyish-reddish colours. In general these deposits are more solidified than most of the deposits sampled and measured in other outcrops. Inside of the outcrop a tectonic lineament is observed (marked with an arrow in figure 6.14). This dip-slip fault seems to be postsedimentary, because upward or downward drags of the layers are not observable. The deposits of the outcrop are not split up into different units (10 sampling points [Pa]).

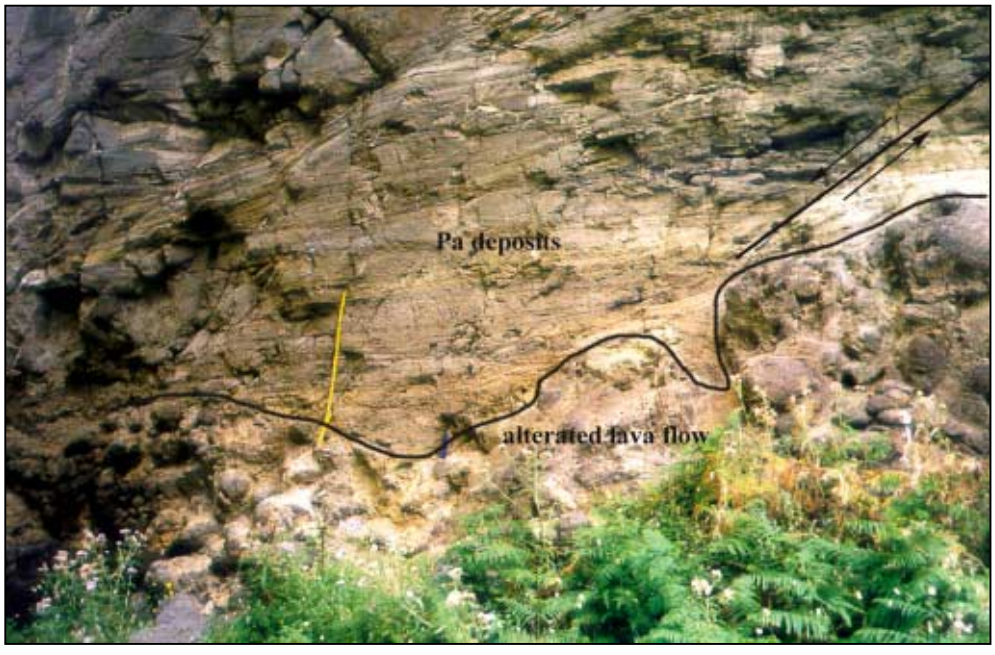

Figure 6.14: Outcrop P located in the Vallone della Roia. The outcrop has an altered lava-flow at it's base (boundaries are marked). On the right side a tectonic lineament (dip-slip fault) can be noticed (arrow).

6.7.2. Granulometry

The mean Ms of the Pa is about 1.64 ϕ (s: 0.2). In comparison to standard outcrops it can be classified as Tufi Varicolori, whereby colour and solidification partly agree with this correlation. Minimum, maximum and mean values for Pa can be seen in table 6.19.

sample	**Pa**
min. value	1.36
max. value	1.99
mean value	1.64
standard deviation	0.2

Table 6.19: Ms of outcrop P in ϕ.

The plot of Ms vs. los shows a slight negative trend, observable especially in samples from the upper part of the outcrop. The histograms generally show a Gaussian distribution whereby a touch of skewness (positive as well as negative) can be observed sometimes. This distribution is often noticeable for the succession of Punte Nere and for a few times also in Palizzi. The cumulative grain size curves can be subdivided into 2 parts, the 1st, basal, part shows more curves with a slightly sigmoidal shape. The curves flatten towards the top where less curved fits dominate (2nd part). Good developed shapes are often observable in Punte Nere and parts of Palizzi, whereas the slightly curved fits normally can be found in the samples of outcrop G (Punte Nere).
Using the results of the 2nd vs. the 1st moment as a discrimination tool, the graphic result do not allow a clear correlation, because Pa plots without a distinctive cluster on the same trend-line as a great part of the standard outcrops. The slope, resulting on the linear fits for the different successions, allows a correlation of Pa (3.34 ± 0.4) with Punte Nere (3.43 ± 0.2). Tufi Varicolori shows the next best slope with 3.58 ± 0.1, but the correlation of Punte Nere with Pa more appropriate.

6.7.3. Susceptibility

The mean values of the sus – measured in cgs-mode, standardised to 1g, and extended to 10^{-6} – are shown in table 6.20. Comparing the mean value of sus05 (113.50 units, s: 11.1) with standard outcrops, Pa has a high affinity to Punte Nere. For sus25 (115.09 units, s: 15.9) a characterisation as Punte Nere (117.18 units. s: 24.1) is again the best correlation. Taking into account, that also Palizzi or Cratere Attuale have comparable values, the range of variation between these successions and outcrop P however, is relatively wide.
Plotting los vs. sus, especially near the base, adjacent sampling points show high variations of their values. In general the values of sus25 are slightly higher than those of sus05. With increasing los the situation changes. The variation inside of the basal part is sometimes correlated with a change between massive and more laminated deposits. In the case of outcrop P samples of the more massive deposits plot slightly higher than the samples of the more

laminated deposits. A similar situation is also observable for Punte Nere, but in this case the more laminated deposits show higher values. The upper part of Pa shows a slight negative trend of the values, whereby now sus05 plots higher than sus25 (a situation normally observed for Tufi Varicolori).

sample	Pa
min. value 0.5-0.25 mm	97.44 ± 0.1
max. value 0.5-0.25 mm	136.61 ± 0.2
mean 0.5-0.25 mm	113.50 (s: 11.1)
min. value 0.25-0.125 mm	101.17 ± 0.1
max. value 0.25-0.125 mm	144.58 ± 0.2
mean 0.25-0.125 mm	115.09 (s: 15.9)

Table 6.20: Mean values for the sus for both gsc of outcrop P. Samples are measured in cgs-mode, standardised to 1g, and have to be extended by 10^{-6}.

From the plot of sus vs. sus/Ms no significant new information is gained. Using the scatter plot sus vs. sus/sus, for example sus05 vs. sus05/sus25, Pa plots in the wider range of Punte Nere, with a small overlap over the other successions (especially Palizzi). A positive trend for Pa can be observed in the plot sus05 vs. sus25 using all standard outcrops, herein Pa overlaps with the lower part of the Punte Nere and the higher parts of the Palizzi cluster, as well as with single values of Tufi Varicolori. Even in this plot a characterisation as Punte Nere has the highest probability. Using the slope of the resulting linear fit for this plot Pa does not show any good correlation.

6.7.4. Gamma-ray

In contrast to the sus mean values the mean values of the γ-ray measurements for Pa (see also table. 6.21) do not correlate with standard outcrops as well as the sus values. The mean value of K, of about 4.50 % (s: 0.3), is located between the mean values of Tufi Varicolori and Commenda. U with a mean value of 11.72 ppm (s: 1.0) shows solely a weak correlation with Punte Nere. Th, showing a mean value of about 39.39 ppm (s: 2.6), is also characterised by the slightly higher plotting Punte Nere, but the range between Pa and the values of the other successions is too wide for a sensible characterisation. Having a look at the mean values of outcrop G and the channel (see also table 5.5), which both belong to Punte Nere, most of the mean values for Pa can be correlated excellently with the data of the channel, which contains dominantly wet-surge deposits and partly reworked material. The wet-surge deposits generally have lower amounts for the γ-ray values caused by early alteration processes in the cloud and during deposition.

sample	K [%]	U [ppm]	Th [ppm]
Minimum	4.10 ± 0.1	10.33 ± 0.4	35.83 ± 1.1
Maximum	5.00 ± 0.1	13.10 ± 0.6	43.58 ± 1.1
mean	4.50 (s: 0.3)	11.72 (s: 1.0)	39.39 (s: 2.6)

Table 6.21: Maximum, minimum and mean values of K [%], U [ppm], and Th [ppm] for outcrop P.

In the plots of los vs. concentration generally a wide positive trend can be observed. With this method the difference between laminated and massive deposits is not as well pronounced as seen for the sus-measurements. Further, the behaviour is inverse, which means that the more massive dominated deposits show lower values than most of the laminated deposits. As a result the external form for the curve is very weak, except of the plot of K.

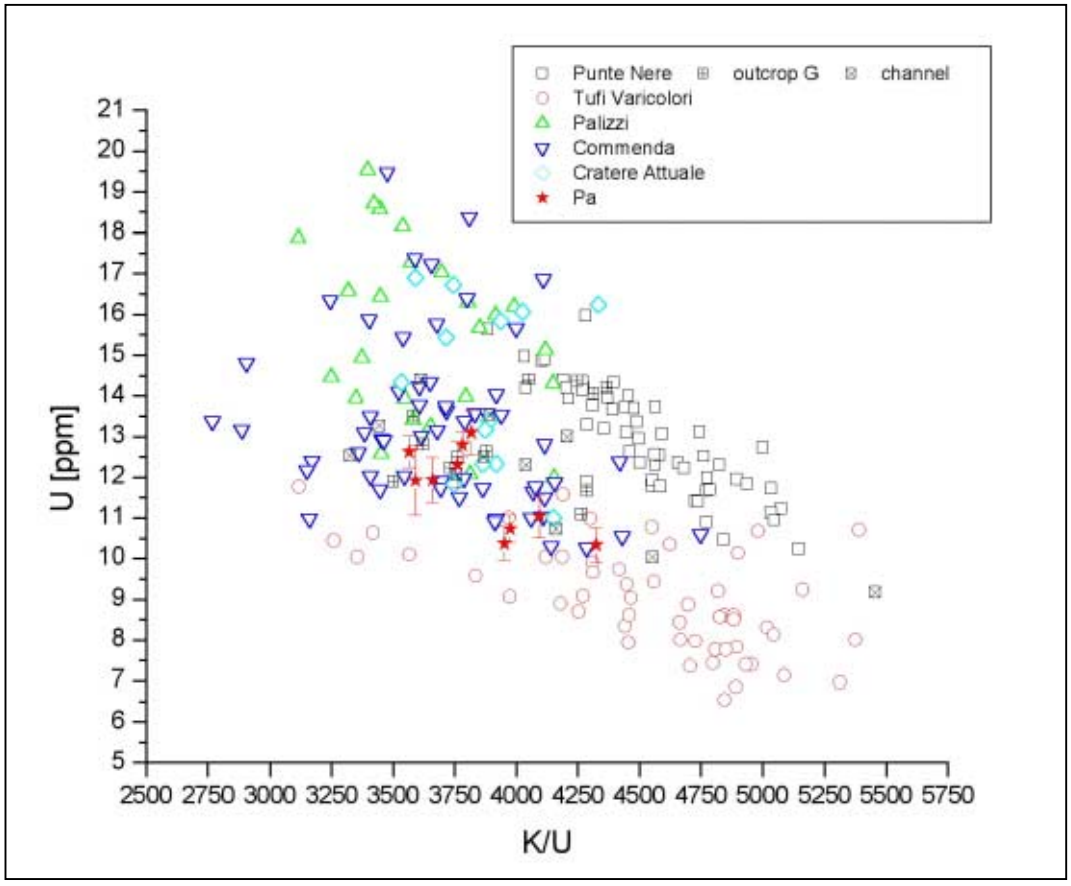

Figure 6.15: Scatter plot of U vs. K/U for all standard outcrops (open objects) and Pa (filled star). Pa plots in the same range as Commenda and the deposits of outcrop G and the channel, belonging to Punte Nere.

Using the plots of the concentration vs. the ratio (see also Appendix IV) as a discrimination tool, Pa plots in a cloud containing mainly 2 successions. The 1st definition may be Commenda and the 2nd Punte Nere, whereby for the latter especially the values of outcrop G and the channel show a distinct correlation. Not taken into account the samples of outcrop G and the channel – both belong to Punte Nere – Pa can be correlated with Commenda, because for this the overlap with clusters of Commenda dominate the other correlation. For most of

the samples a correlation with the channel and outcrop G is also a good choice (see for example also figure 6.15). Slopes for the plots U vs. K/U and Th vs. K/Th may allow a weak correlation with Punte Nere (Pa: U vs. K/U $0.01 \pm 0.6*10^{-3}$, and Th vs. K/Th -0.03 ± 0.0), whereby R as the correlation coefficient points out that the correlation is not perfect (low coefficient).
Plots of concentration vs. concentration of K, U, and Th (see also Appendix IV) do not show a probable correlation, because the values of nearly all standard outcrops plot in the same range as the values of Pa.

6.7.5. Interpretation

Outcrop P, located in the same valley as the standard outcrops of Punte Nere and thus inside of the caldera of La Fossa, shows a good correlation with Punte Nere. Especially the granulometric values have a noticeable consistence with Pa and Punte Nere, although the mean values of Ms tend to correlate with Tufi Varicolori. The sus-measurements show that the characterisation as Punte Nere is the best solution for Pa, although not all points agree perfectly. The γ-ray values for example show a wider variation. The mean values do not correlate with the standard outcrops as ideal as the values of the other methods. The best correlation can be observed with the data of the channel of outcrop G (Punte Nere). In the scatter plots of the concentration the affinity to deposits of outcrop G and the channel can also be observed, the “normal” parts of Punte Nere do not overlap in every plot. In this plots also a correlation with Commenda could be imagined, but due to the results of the other methods this is rejected.
Summarising Pa can be described as a part of the Punte Nere successions, whereby a high affinity to the slightly more altered wet-surge deposits of the channel of outcrop G is recognised.

6.8. Outcrop Q

6.8.1. Introduction

Beside the footpath up to the Gran Cratere outcrop Q is located half-way up the flank in a gully. The outcrop is highly erosive and changes its appearance after every heavy rainfall and after every tourist season. With a height of about 1.6 to 2.0 m the outcrop is relatively small. Different types of reworked material are observable and 4 measurements, covering most of the different appearances, are made solely to demonstrate the material’s variability. Besides variable, often blocky, flows and matrix supported deposits also pockets containing Pele’s hair can be observed (see also figure 6.16).

Figure 6.16: Pocket in the reworked material outcrop Q containing Pele's hair.

6.8.2. Granulometry

The minimum, maximum and mean values for outcrop Q are given in table 6.22. The mean value is comparable with Tufi Varicolori, but also a correlation with Punte Nere and Palizzi seems to be slightly possible.

sample	**Qr**
min. value	0.84
max. value	2.47
mean value	1.60
standard deviation	0.7

Table 6.22: Ms of outcrop Q in ϕ.

The plot of los vs. Ms shows strong differences between the various layers without a visible trend. The histograms do not show an uniform behaviour, positive as well as negative skweness is observable. The cumulative grain size curves change in various ways. This is also noticeable in the plot of the 2^{nd} vs. the 1^{st} moment, although the values of Qr plot in the same range as the values of the standard outcrops, a clear definition cannot be seen.

6.8.3. Susceptibility

The sus values of Qr – measured in cgs-mode, standardised to 1g, and extended to 10^{-6} –, shown in table 6.23, range between the values of the lower plotting successions like Tufi Varicolori, Commenda, and Cratere Attuale.

sample	Qr
min. value 0.5-0.25 mm	46.72 ±0.1
max. value 0.5-0.25 mm	111.00 ± 0.2
mean 0.5-0.25 mm	74.63 (s: 23.3)
min. value 0.25-0.125 mm	56.20 ± 0.1
max. value 0.25-0.125 mm	97.17 ± 0.1
mean 0.25-0.125 mm	72.03 (s: 15.3)

Table 6.23: Mean values for the sus for both gsc of outcrop Q. Samples are measured in cgs-mode, standardised to 1g, and have to be extended by 10^{-6}.

The plot los vs. sus do not show significant trends and both sus do not show a high difference, often sus25 plots slightly lower than sus05. In plots sus vs. sus, sus/sus, and sus/Ms the data scatters widely and no matching trend is recognised.

6.8.4. Gamma-ray

The mean γ-ray values of Qr (see also table 6.24) show high concentrations especially for K (6.98 %, s: 0.6) and Th (56.08 ppm, s: 7.6), which are not comparable with average mean values of the standard outcrops. U with a mean value of 11.55 ppm (s: 1.0) is situated between the values of Tufi Varicolori and Punte Nere. A good correlation is not possible.

sample	K [%]	U [ppm]	Th [ppm]
Minimum	5.97 ± 0.1	10.05 ± 0.6	46.17 ± 1.0
Maximum	7.62 ± 0.1	12.46 ± 0.6	67.17 ± 1.64
mean	6.98 (s: 0.6)	11.55 (s: 1.0)	56.08 (s: 7.6)

Table 6.24: Maximum, minimum and mean values of K [%], U [ppm], and Th [ppm] for outcrop Q.

Looking at the plots of los vs. element concentration in general a slight positive trend of the high values can be observed. The different scatter plots of concentration vs. ratio and concentration do not show any correlation possibility because the data of Qr in general plot out of range.

6.8.5. Interpretation

Outcrop Q contains solely deposits of reworked material, which are not comparable with parts of the standard outcrops. At times a slight correlation tentatively appears possible, but for the complete outcrop a good and logical characterisation is impossible.

6.9. Outcrop R

6.9.1. Introduction

Outcrop R is located in a lateral valley of the Vallone della Roia on the rise up to Caruggi outcrop N. This outcrop, forming a wall 6.5 to 7 m high, consists of nearly 5.5 m of different grey, mostly dry-surge deposits of fine and coarse ash, and solely in a few cases also indicators for a higher moisture content in the depositional environment, like vesiculated tuffs, can be observed. Laminated as well as massive layers, both with variable proportions of Pele's hair, exist. Reworked pumice can be seen in the upper section of unit Rs, above the reworked pumice also references for a wet milieu can be observed. After a few centimetres layers of this more wet character gradually change into layers with more dry-surge characteristics. These layers are covered by the Commenda Breccia and the Upper Pilato Ash (marker horizons). They are topped by a horizon of fine, light grey, which is variable in thickness (Rd1) and a horizon with inverse graded accretionary lapilli (Rd2). Above these deposits different wet-surge deposits of grey to ochre colour at the base to red dominated deposits towards the top occur. For the measurements the outcrop is split up into 2 units: unit Rs, containing the grey dry-surge deposits (16 sampling points) and unit Rd above the Upper Pilato Ash, containing 4 sampling points. Because of the marker horizons in this outcrop as well as in outcrop N a few characterisation possibilities for the units Rd and Rs can be excluded. Rs can solely be defined as Punte Nere, Tufi Varicolori or Palizzi, whereas Rd can only be characterised as Commenda or Cratere Attuale, assuming that the normal bedding is not disturbed.

6.9.2. Granulometry

For outcrop R the mean values show no wide differences between the 2 units (see also table 6.25), Rs has a value of about 2.06 ϕ (s: 0.1) and Rd of about 2.00 ϕ (s: 0.3). The values of Rs do not show wide variations whereas for Rd a negative outlier (Rd2) can be observed, not taken into account this outlier the mean value of Rd ranges about 2.19 ϕ (s: 0.1). The outlier is mainly built up by the accretionary lapilli.

Comparing the mean Ms values of Rs and Rd with standard outcrops of La Fossa, both units are best comparable with Cratere Attuale. The other successions, except of Commenda, show significantly lower values of their mean Ms.

sample	Rs	Rd	**Rd** without the outlier (Rd2)
min. value	1.90	1.42	2.12
max. value	2.27	2.25	2.25
mean value	2.06	2.00	2.19
standard deviation	0.1	0.3	0.1

Table 6.25: Ms of outcrop R in ϕ. Value of Rd are given for the complete unit and without a prominent lower peak (Rd2).

The plot of los vs. Ms does not show a significant trend. An interference by different depositional types like laminated or massive layers, content of Pele's hair or pumice is not observable in the values of Rs. For Rd the content of accretionary lapilli in sample Rd2 shows a significant impact.

Histograms of Rs in general represent a negative skewness with a maximum peak for gsc25, the finer gsc is in general lower than gsc05 and can be compared with the values of the coarser gsc. This behaviour is comparable with parts of the successions of Punte Nere – especially outcrop J, which is dominated by massive layers – and some sampling points of Palizzi. The upper wet-surge deposits of Rd have a negative skewness, and also indicate a negative skewness, which is not as symmetric as observable for Rs. The cumulative grain size curves normally show a well developed shape, which can often be described as a sigmoidal shape. These shapes, generally are characteristic for the successions of Punte Nere and Palizzi. They indicate a relative homogenous distribution inside of the cloud, possibly before a hydraulic step, as it can be seen outside of the caldera.

In the plot of the 2^{nd} vs. the 1^{st} moment the values of the samples plot inside the average trend-line for the standard outcrops. Rs plots near Rd, and both overlap with Commenda as well as with Tufi Varicolori. Rs, plotting slightly lower than most of the data of Rd, plots in the top part of the Punte Nere cluster and sometimes overlaps partly with Palizzi. Rd shows solely 1 outlier, plotting inside of Palizzi and Punte Nere in the lower part of the plot. This data point (Rd2) is characterised by a high amount of accretionary lapilli. No correlation of the slopes of Rs and Rd with slopes of the standard outcrops appear possible.

6.9.3. Susceptibility

In outcrop R the mean values of sus – measured in cgs-mode, standardised to 1g, and extended to 10^{-6} – differ noticeably for the 2 units (see also table 6.26). Rs shows mean values for sus05 of about 102.49 units (s: 23.8) and of about 96.99 units (s: 15.4) for sus25. Not considering the prominent peak (Rs13) in the upper part of Rs, the values range between 97.80 units (s: 16.0) for sus05 and 95.23 units (s: 14.3) for sus25. In contrast the values of Rd are definitively lower with amounts of 61.18 units (s: 11.2) for sus05 and 67.12 units (s: 11.8) for sus25. The last sample of Rd exhibits values lower than the average values. Excluding

these low values, the mean values for Rd range between 66.99 units (s: 5.6) for sus05 and 73.60 units (s: 4.3) for sus25.
Using the mean values as a characterisation tool, Rs shows the best correlation with Palizzi but partly also with Punte Nere. The values of Rd can be defined as Commenda relatively well, though a less accurate correlation with Tufi Varicolori is partly possible.

sample	**Rs**	**Rs** without prominent peak	**Rd**	**Rd** without prominent peak
min. value 0.5-0.25 mm	62.46 ± 0.1	62.46 ± 0.1	43.76 ± 0.1	61.15 ± 0.1
max. value 0.5-0.25 mm	172.80 ± 0.2	127.93 ± 0.2	74.59 ± 0.1	74.59 ± 0.1
mean 0.5-0.25 mm	102.49 (s: 23.8)	97.80 (s: 16.0)	61.18 (s: 11.2)	66.99 (s: 5.6)
min. value 0.25-0.125 mm	70.42 ± 0.1	70.42 ± 0.1	47.71 ± 0.1	70.43 ± 0.1
max. value 0.25-0.125 mm	123.42 ± 0.2	119.79 ± 0.2	79.71 ± 0.1	79.71 ± 0.1
mean 0.25-0.125 mm	96.99 (s: 15.4)	95.23 (s: 14.3)	67.12 (s: 11.8)	73.60 (s: 4.3)

Table 6.26: Mean values for the sus of both gsc of outcrop R. Both units are shown by the data for the whole unit and by a corrected version, where an outlier is not taken into account. Samples are measured in cgs-mode, standardised to 1g, and have to be extended by 10^{-6}.

In the plot of los vs. sus (see also figure 6.17) a negative trend of Rd is observable for both sus, sus05 in general plots lower than sus25. The prominent marker of the granulometry (Rd2) does not show any irregularities to become a prominent outlier for this method, neither. For Rs no obvious trend is noticeable, though in the upper part of this unit adjacent sampling points often have higher differences in their values than the sampling points of the basal part. A dependence based on sedimentary and depositional features, or the occurrence of accessory components is not observable.
The scatter plot of sus05 vs. sus25 indicates a correlation between Rd and Commenda, whereby also a less accurate correlation with Tufi Varicolori (not possible because of the marker) and Cratere Attuale may be possible. Most samples of Rs plot in the range of Punte Nere and Palizzi, a useful correlation for these samples is not possible (both successions Punte Nere and Palizzi show the same correlation degree). Comparing the slopes solely Rd 0.91 ± 0.0 can be correlated with Tufi Varicolori (0.92 ± 0.0), which, however, is not possible because of the time marker horizon.
Microprobe analyses of magnetites of Rs (Rs16; sus05; see also chapter 4.4) show similar values as those for Palizzi. Furthermore, the ratios of Fe^{3+}/Fe^{2+}, Fe^{3+}/Ti^{4+}, and less well also Ti^{4+}/Cr^{3+} show a likewise agreement. The analysed grains can be classified as low-chrome titanomagnetites.

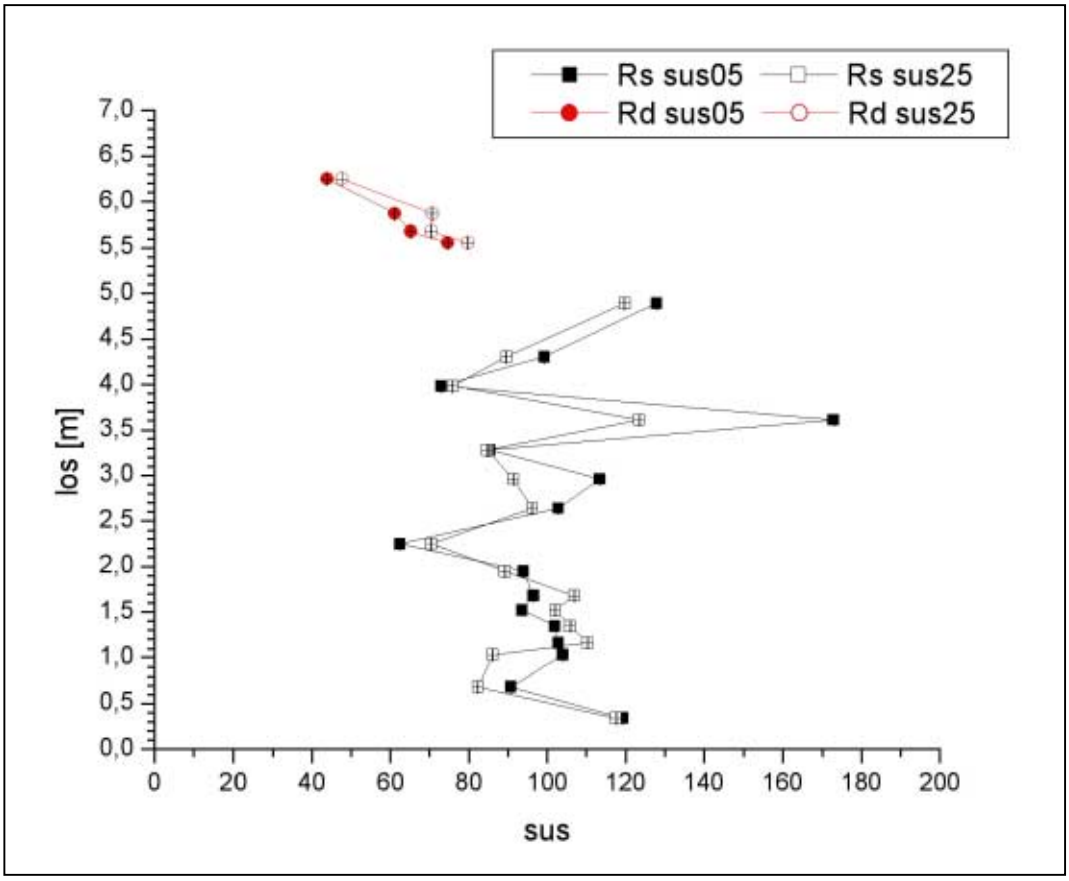

Figure 6.17: Plot of los vs. sus show solely negative trends for Rd, whereas within Rs no obvious trend is observable.

6.9.4. Gamma-ray

The mean values of the γ-ray measurements are in general relatively high (see also table 6.27) and do not show a good correlation with the standard outcrops. The K values range between 7.15 % (s: 0.5) for Rs and 7.80 % (s: 0.5) for Rd. For U variations between 12.42 ppm (s: 1.1) for Rs and 13.59 ppm (s: 0.9) for Rd occur. Also Th has differences between 49.53 ppm (s: 3.0) for Rs and 60.10 ppm (s: 3.4) for Rd. Comparing these values with standard outcrops of La Fossa di Vulcano, for K and Th a useful correlation is not possible. Only the values of U may correlate Rs with Punte Nere and Rd with Commenda as well as with Cratere Attuale because the values of Rd plot more or less between both successions.

As well as seen for the sus measurements the plots of los vs. concentration do not have an obvious trend for Rs, whereas Rd shows a positive trend for most of the single elements. The upper part of Rs has high variations between adjacent sampling points, which are not explained by the type of deposits or by the components.

sample	K [%]	U [ppm]	Th [ppm]
Minimum Rs	6.43 ± 0.1	10.63 ± 0.4	44.83 ± 0.4
Maximum Rs	8.18 ± 0.1	14.38 ± 0.5	55.40 ± 0.7
mean Rs	7.15 (s: 0.5)	12.42 (s: 1.1)	49,53 (s: 3.0)
Minimum Rd	7.17 ± 0.1	12.13 ± 0.4	56.07 ± 0.6
Maximum Rd	8.33 ± 0.1	14.53 ± 0.5	64.40 ± 2.0
mean Rd	7.80 (s: 0.5)	13.59 (s: 0.9)	60.10 (s: 3.4)

Table 6.27: Maximum, minimum and mean values of K [%], U [ppm], and Th [ppm] for R.

The plots of element concentration vs. ratio as well as the plots of element concentration vs. element concentration do not allow a simple correlation because in general the values of outcrop R plot out of range (for example see also figure 6.18).

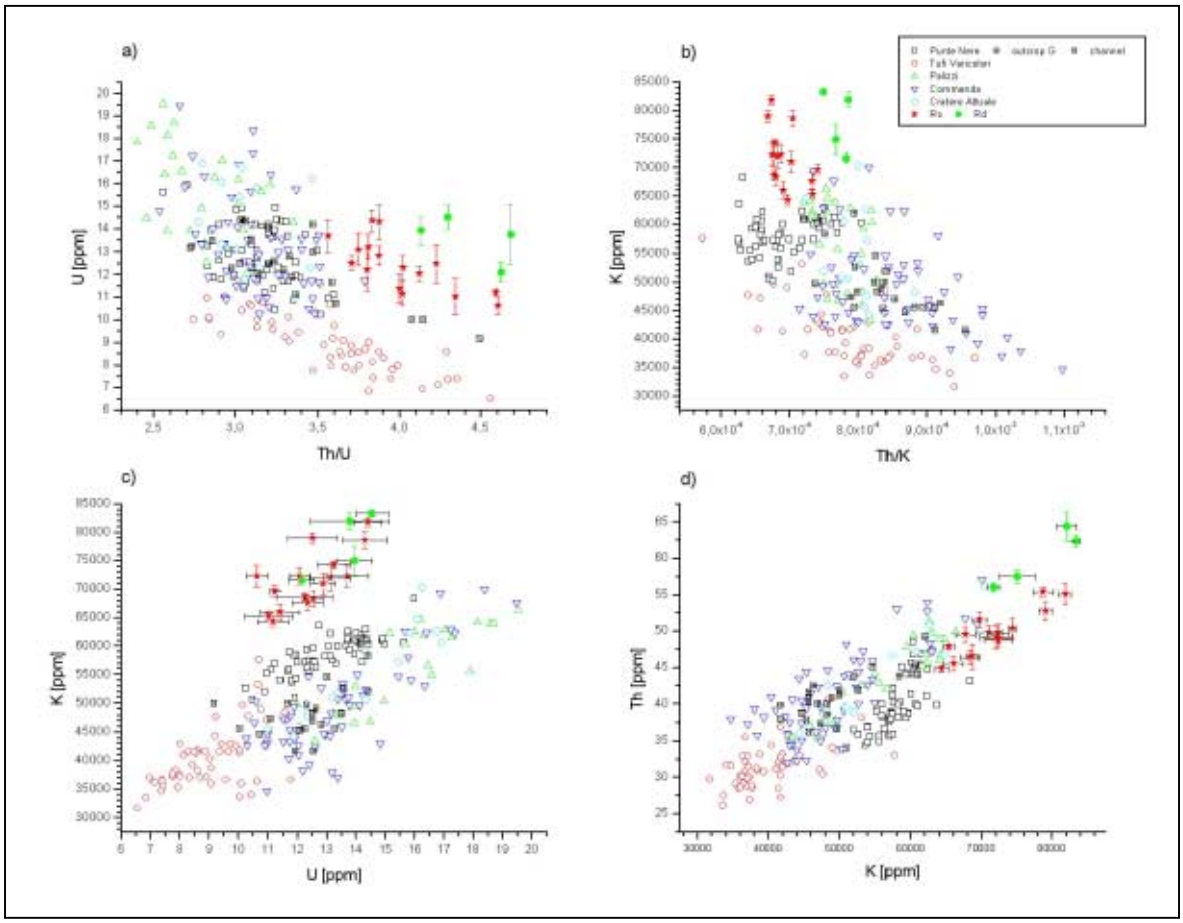

Figure 6.18: Scatter plots of U vs. Th/U (a), K vs. Th/K (b), K vs. U (c), and Th vs. K (d). All sketches show very well that all values of outcrop R plot out of the average range.

Assuming that elements are enriched above or in an impermeable or less permeable layer or a trap, and also assuming that the enrichment is homogenous, the plotted values possibly can be shifted linearly into the average plot. In that case Rd may plot in the clusters of Commenda and Cratere Attuale, whereas Rs could plot near Punte Nere or also near Palizzi. As observed in several outcrops before, U does not plot in the assumed range. It may be possible that whereas Th and K are enriched U may be depleted. The resulting question is: why is the soluble U depleted whereas the also very soluble K is enriched? A satisfying answer is not possible within the limits of this thesis.
A comparison of the slopes is useful if a homogenous enrichment of all elements is assumed, in that case the amounts of the slope will not change significantly and the slope can be used as a correlation tool. In outcrop R no correlation is possible.

6.9.5. Interpretation

The characterisation of outcrop R is not possible with any method, and the γ-ray values do not allow an average characterisation. As mentioned above it could be possible to shift the values into the average plot assuming that the enrichment is homogenous, in that case Rs may correlate with Punte Nere or Palizzi and Rd with Commenda or Cratere Attuale.
The granulometric data indicate a classification of Rs to Punte Nere as well as to Palizzi, whereas Rd could be correlated with Commenda, but the references are weak. The sus investigation gives additional references for a classification. Rs is comparable with Punte Nere and Palizzi as before, but the results for the microprobe analyses indicate a higher affinity to Palizzi. This is supported by the of reworked pumice in the upper part of the unit. Rd is best characterised as Commenda, also indicated by the presence of the Commenda Breccia and the Upper Pilato Ash below; a wide erosional gap inside of the sequence is not observable.
As a resume it can be said that Rs is defined as Palizzi whereas Rd can be characterised as Commenda.

6.10. Conclusions

The combination of sus- and γ-ray-measurements in general allows an identification for most of the unknown outcrops. The results are shown in table 6.28. It has to be noticed that the utility of the methods is limited by a variety of factors. For example, dependent on whether the entire eruption cloud or solely a few components of the eruption cloud can surmount obstacles, the granulometric composition may be changed. This will also affect the sus-measurements, because susceptibility-bearing minerals can be depleted or enriched within the overriding cloud. Alteration and weathering affect both sus and γ-ray data. Fumarolic activity will influence the sus more than the γ-ray data. The γ-ray data, on the other hand, reflect especially the effects of weathering and leaching. For example, the highly exposed part of

outcrop L (Le) shows a significant decrease of the γ-ray values (see also figure 6.8), whereas the sus values are solely affected in the last sample showing decreasing values. Not only good visible weathering of highly exposed and often solidified deposits can be detected by the γ-ray data, weathering may also cause depletion or enrichment of elements in outcrops less exposed to weathering (for example Mw or Rd). Differences between wet- and dry-surge deposits have to be taken into account when using the γ-ray values: wet-surge deposits are more likely to be altered in the eruption cloud or during deposition, which will affect especially the γ-ray values.

As seen in table 6.28 a clear identification of all successions is not always possible, but for all outcrops the correlation options are limited to a few successions. A correlation solely based on 1 method is relatively weak, but in combination with granulometric data, marker horizons and sedimentological characteristics (for example reworked pumices, scoria layers, or occurrence of Pele's hair), a correlation is normally possible.

For some outcrops the surficial appearance and affinity to a succession are not confirmed by the geophysical data. In outcrop M the basal dry-surge units show a high similarity to Palizzi or Punte Nere. The geophysical data, however, suggest a correlation of the units Ms and Msw with Tufi Varicolori. Interestingly, Tufi Varicolori has not yet been described from outside of the La Fossa Caldera and generally has a significant different appearance since now. The outcrop is located at the highest point of the caldera wall, thus the energy to surmount this obstacle has to be very high. If the correlation with Tufi Varicolori is correct, this implies that the energy and possibly also the eruption scheme for Tufi Varicolori has to be revised, and this will affect potential hazard plans, too.

Some correlations are also weak because of the low number of sampling points, illustrating that a characterisation based on 1 or 2 samples is not very useful. Trends within the units can be better identified with more sampling points, which are in general better for a better stratigraphical correlation, showing clusters in sometimes overlapping parts of different successions.

Although the deposits of outcrop K look like deposits of La Fossa cone – especially the dry-surge deposits of Kc seem to correlate with Palizzi based on sedimentological investigations in the outcrop and the appearance in the field – they may not correlate with the standard outcrops of La Fossa cone. The geophysical data do not allow a clear correlation (to any of the known successions), and it is possible that these deposits are pre-la Fossa in age. The deposits of La Fossa may have been deposited at this location but are not preserved due to erosion.

unit	*probable succession*	*probability*	*remarks*
outcrop C			
Cx	Tufi Varicolori	o	• γ-ray values cannot be used because of the outcrop's nature • occurrence of a prominent marker which can also be observed within a standard outcrop of Tufi Varicolori (crinkly red layer that is bounded by two white bands; Ob22 and Cy6) • last sample is possibly reworked
Cc	Palizzi	- (-)	• occurrence of Pele's hair • dry-surge deposits
Cy	Palizzi and reworked parts	- (-)	
outcrop D			
Dy1	possibly Tufi Varicolori and reworked parts	-	
Dy2	reworked, possibly upper Tufi Varicolori or Palizzi	- (-)	• occurrence of Pele's hair in a few layers • soil formation at the top of the unit
outcrop K			
Kw	pre-La Fossa or Punte Nere or Tufi Varicolori or Commenda	-	
Kc	pre-La Fossa or Palizzi or Cratere Attuale	-	• appearance of Palizzi dry-surge deposits
Ke	pre-La Fossa or Cratere Attuale	-	• slightly leached, most of the γ-ray values are not sensible
outcrop L			
Lw	Tufi Varicolori or Commenda	o to +	• wet surge that surmounted the barrier, possibly depletion or enrichment • data in general indicate Tufi Varicolori or Commenda, because both parts can overlap in the scatter plots as well as using the range of the values
Lc	Commenda, possibly Palizzi	-	• solely a few samples which are not meaningful for every method.

unit	*probable succession*	*probability*	*remarks*
Le	Cratere Attuale	o	• highly exposed part of the outcrop and strongly leached samples • γ-ray data are not sensible because of leaching
outcrop M			
Ms	Tufi Varicolori	+	• often behave in the same way and can be merged • do not show the "classic" appearance of Tufi Varicolori known until now
Msw	Tufi Varicolori	+	
Mw	Tufi Varicolori or Commenda	o	• depletion of γ-ray values
Mwe	Tufi Varicolori, Commenda or Cratere Attuale	o	• depletion of γ-ray values • the deposits are solidified, possibly by weathering
outcrop N			
Nc	Punte Nere	++	• most of the values also allow a correlation with Palizzi but the γ-ray plots are more characteristic for Punte Nere
Nd	Commenda	++	• γ-ray plots also suggest a slight affinity to Cratere Attuale
Nw	Cratere Attuale	+	• some values often behaves like Commenda
outcrop P			
Pa	Punte Nere	++	• very similar to outcrop G and the channel with slightly altered material
outcrop Q			
Qr	reworked	o	• occurrence of Pele's hair in a pocket • fast changes of outcrop appearance
outcrop R			
Rs	Palizzi	+	• good correlation using sus data • no sensible γ-ray • occurrence of Pele's hair • occurrence of reworked pumice
Rd	Commenda	+	• γ-ray cannot be used

Table 6.28: Characterisation of the not clearly defined outcrops with geophysical tools. These results are the best characterisations which could be made. Probability: ++ very well, + well, o possibly, - vague, -- only few indications.

7.Discussion

Summarising the results for the standard outcrops and the correlation with the undefined outcrops it can be said that:

The case study of La Fossa di Vulcano shows that the combination of γ-ray and sus measurements to characterise different successions of the pyroclastic deposits is a powerful tool in volcanostratigraphy. The standard outcrops, located inside of the Caldera of La Fossa have a clearly defined stratigraphy, which can be used for calibration, and which can then allow a characterisation of undefined outcrops. Mean values and scatter plots, sometimes combined with slopes for the single successions within the scatter plots, normally allow a classification of the different successions. As shown for the standard outcrops in chapter 5, no single method can characterise all successions, but a combination of different geophysical methods with sedimentological markers allows a good correlation and discrimination of the individual successions.

Undefined outcrops of the younger deposits of La Fossa cone in general can be characterised by the geophysical methods. However, the correlation has not always a single solution (for example some units in the outcrops K, L or N; see also chapter 6). This is often originated by the change of the behaviour of some deposits beyond the caldera wall (DELLINO AND LA VOLPE, 2000), caused by modified energy conditions. Thus, the appearance and composition of the deposits would have been changed. Surface exposition of deposits can cause leaching processes, which specially affect the γ-ray measurements, thence a few units cannot be defined clearly in every case solely by the use of geophysical methods because some successions do not differ in sus and γ-ray values. In this situation often diverse solutions can be found, which have to be discussed in the geological and logical context. Enrichment and depletion – especially on location outside of the Piano Caldera – can also cause a larger error of the geophysical methods. When the degree of the exchange is not known exactly a characterisation of single units can be complicated.

In general it can be assumed that increased magma evolution goes along with higher γ-ray values and lower sus-values (CHIOZZI ET AL., 1999). These parameters may thus reflect evolutionary processes in the reservoir, pulses of fresh material which could trigger the eruption, but also the internal stratigraphy of a magma reservoir.

The test measurements in the Eifel, an area with well defined stratigraphy and significant changes in the chemical composition, have shown that the differentiation of the magma and a compositionally change is mirrored by the sus and γ-ray values very well. On Vulcano island the situation is more complex and the magma reservoir was certainly not homogenously erupted in a single great eruption cycle. Often a refilling or a new pulse, introducing more primitive material, can be assumed. Some authors like DE ASTIS ET AL. (1997), DE FINO ET AL. (1991), DELLINO (1997), DELLINO AND LA VOLPE (1997), and SBRANA (1997) have

supposed two reservoirs. The complexity of the magma feeding and reservoir system is reflected by the values for the different successions. Usually the single successions can be identified by varying sus and γ-ray values, but in a few cases the values look similar for different successions, and consequently a similar composition must be assumed. These circumstances can confuse the discrimination of the single successions and it is not possible to correlate solely on the basis of the γ-ray and sus values the stratigraphic height and affiliation to a distinct succession. It is however feasible to identify different distinctive characteristics (see also chapter 5, especially table 5.32) for the various successions. Although it is normally possible to characterise individual samples with geophysical methods, sometimes also the combination with sedimentological or geochemical features and with distinct marker horizons allows a more precise correlation. The Upper Pilato Ash is a prominent marker horizon, mentioned before, and it allows – as seen for example in the outcrops N and R – a limitation of correlation possibilities because of the chronology: Punte Nere, Tufi Varicolori, Palizzi, Commenda Breccia, Upper Pilato Ash, Commenda, Cratere Attuale.

Alteration of the sus values derives mostly from fumarolic activity. This is especially the case for the investigated younger deposits of La Fossa di Vulcano, whereas older deposits may also show signs of alteration by oxidation or mineral transformation. In contrast, the γ-ray values are more affected by the historical and present environment. Sedimentation and transport processes also have a big influence. If an eruption cloud contains a higher amount of water (leading to wet-surge deposits), the material can be leached or altered easily within the cloud and after deposition, especially by aggressive fluids (for example CAPACCIONI AND CONGILIO (1995) and CAPACCIONI ET AL. (1991)). When comparing dry-surge- and wet-surge deposits from the same magma reservoir with The same initial composition, the dry-surge deposits often show higher values than the wet-surge deposits. Sometimes even dry-surge deposits of less evolved magma can show higher values than wet-surge deposits of a more evolved magma. The γ-ray values also mirror effects of secondary processes like enrichment or depletion of the elements, especially the soluble elements K and U. Depletion can be observed especially in highly exposed outcrops, where leaching and cementation of the deposits as well as the formation of surficial crusts can be observed. Weathering, hydrothermal activity, reworking, or groundwater may also cause depletion or enrichment of elements in outcrops less exposed to weathering. Deposits with high element concentrations, undergoing alteration, can contaminate underlying deposits, and element enrichment can occur (for example Palizzi, Commenda, and Cratere Attuale in outcrop E [chapter 5]).

A general problem of the volcanostratigraphy of pyroclastic deposits is that an ideal radial dispersion around the cone is rare. Consequently, potential markers may not be found on all sides of the cone. Obviously, some layers may be subject to subsequent erosion. Thus, a

correlation layer by layer – also taken into account the huge number of pyroclastic deposits – may not be very useful in every case.
For Vulcano island a correlation layer by layer could be interesting and useful for an excellent knowledge of the volcanic behaviour and history, but because of the changing direction of the eruption clouds (mentioned above) and the low thickness of many layers, sampling of every layer in every outcrop is not possible. The layer thickness also limits the use of the γ-ray measurements. As mentioned in the chapters 3 and 4, the penetration depth of γ-ray measurements is restricted. When layers are much smaller than the penetration radius the over- and underlying deposits will influence the measurement, and this effect increases with decreasing thickness. As a consequence, not every single bed will yield a precise measurement of its (γ-ray) composition. Susceptibilty measurements are also influenced (contamination during the sampling by over- and underlying deposits as well as a small sample volume for very thin beds) by this effect, although to a lesser degree.

The equipment for the measurements is easy to handle and the measurements are not very time-consuming. For the γ-ray-measurements in the field one person is sufficient for easily accessible outcrops. The battery power for the spectrometer lasts for a minimum of 1 to 2 days. Measuring times depend on the concentration in the deposits; in the case of La Fossa 60 seconds are adequate for repeatable measurements. Depending on the material consistency the preparation of a measuring surface takes a few minutes. Thus the average time for a single measurement ranges from about 10 to 20 minutes. A team of two persons can measure and sample one outcrop in one day and is also necessary if the outcrop is not easy to reach.
The preparation of the samples for the sus measurements in the laboratory lasts 1 to 2 days, whereas the measurement takes a few minutes. The sample can be prepared easily if it consists of soft rocks or relatively loose ash, otherwise a preparation method destroying the agglomeration but not the grains has to be used, which can be relatively time intensive. Alteration, except of fumarolic activity, does not influence the sus measurements in the same way as the γ-ray measurements, at least for the standard outcrops of La Fossa di Vulcano. Prominent peaks could be used as marker horizons in the different successions. It is important to exclude these extreme markers from the average values of the defined successions, which can be falsified in that way. Consequently a small number of samples – for example one or two sampling points – may be not very representative for a correlation.

The results may require a re-interpretation of the distribution of the La Fossa successions. Until now Tufi Varicolori were not reported outside of the Fossa Caldera. The results of the geophysical measurements allow a characterisation of some deposits outside of the Fossa Caldera, as Tufi Varicolori. These observations contradict the assumption of a very plastic behaviour of Tufi Varicolori base surges that prevents them to override higher obstacles because of their low energy of the eruption cloud. Hazard plans for an eruption of the type of

Tufi Varicolori have to reflect the potentially wider spreading and higher energy level. Such an eruption would also endanger locations on the Piano Caldera, previously thought to be more or less save for eruptions of the Tufi Varicolori-type. Most of this area is also assumed to be safe for the eruptions of Commenda–type (producing wet-surges), for example DELLINO AND LA VOLPE (1997). Also some assumptions about other locations have to be changed. For example the deposits located at the Lentia complex (outcrop K) may not have been originated from the younger La Fossa cone. Deposits of La Fossa cone may be deposited also on this location but they are most probably not preserved.

In the future more outcrops have to be investigated and studied by geophysical, geochemical and sedimentological methods to get more information about the dispersion of the different successions and internal variation. Also investigation of the susceptibility-bearing minerals using microprobe can be interesting, because their composition may vary between successions. This will be especially useful for outcrops where the characterisation by the combined geophysical methods gives two or more solutions.
Further investigations may involve taking more samples of standard outcrops and define marker horizons to enhance the correlation between different standard outcrops. In addition, the behaviour of the deposits in and outside of the caldera would be interesting to investigate. What happens with the susceptibility-bearing minerals when the eruption cloud surmounts the caldera wall? At what amount of energy loss will an effect be visible? Is it possible to find layers attributed to the same eruption cloud in- and outside of the caldera? How is the γ-ray value affected by the overriding cloud?

As a summary it can be said that the combination of grain size depended sus and γ-ray measurements, together with sedimentological and geochemical investigations allow a better stratigraphic correlation of pyroclastic deposits. These methods are ideal for younger and softer deposits, but also older, consolidated deposits can be investigated when applying longer measurement times, especially for the γ-ray measurements. The magma evolution is reflected relatively well in the measurements, and new pulses or replenishing of the reservoir can be detected easily. More investigations about depletion and enrichment of highly soluble elements due to weathering and alteration as well as processes in wet eruption clouds have to be carried out. A correlation based solely on the geophysical methods is in some cases possible, but in general the combination of all methods is the best choice. The geophysical methods can give first clues and indications about the possible stratigraphic height of the sample can be made, if the stratigraphy is not too complex. Full understanding of the stratigraphic successions and their characteristic parameters, based on standard outcrops, is essential. When the geochemical composition does not vary as on Vulcano island, but evolved along simple pathways (like for example the Wingerstberg location of the Laacher See, Eifel), geophysical measurements alone allow a classification of the stratigraphic height of the deposits.

8.References

- ACHILLI, V. ET AL., 1998. Digital photogrammetric survey on the island of Vulcano. Acta Vulcanol., 10(1): 1-5.
- ADAMS, J. A. S. AND GASPARINI, P., 1970. Gamma-ray spectrometry of rocks. Methods in geochemistry and geophysics, 10. Elsevier, Amsterdam, 295 pp.
- ADAMS, J. A. S., OSMOND, J. K. AND ROGERS, J. J. W., 1959. The geochemistry of uranium and thorium. Physics and Chemistry of the Earth, 3: 299-348.
- ADAMS, J. A. S. AND WEAVER, C. E., 1958. Thorium-to-uranium ratios as indicators of sedimentary processes: example of concept of geochemical facies. AAPG Bulletin, 42(2): 387-430.
- AGIP, 1981: Isola di Vulcano (map), scale 1:10000.
- AIGNER, T., SCHAUER, M., JUNGHANS, W., JUNGHANS, D. AND REINHARD, L., 1995. Outcrop gamma-ray logging and its applications: Examples from the German Triassic. Sedim. Geol., 100: 47-61.
- ALLEN, A. G., BAXTER, P. J. AND OTTLEY, C. J., 2000. Gas and particle emissions from Soufrière Hills Volcano, Montserrat, West Indies: characterization and health hazard assessment. Bull. Volcanol., 62(1): 8-19.
- AMANN, P., 1999. Liparische Inseln. Iwanowski's Reisebuchverlag, Dormagen, 300 pp.
- ARGNANI, A. AND SAVELLI, C., 1999. Cenozoic volcanism and tectonics in the Southern Tyrrhenian Sea: space-time distribution and geodynamic significance. Journal of Geodynamics, 27(4-5): 409-432.
- BADALAMENTI, B. ET AL., 1991. Special Field Workshop at Vulcano (Aeolian Islands) during summer 1988: Geochemical results. Acta Vulcanol., 1: 223-228.
- BADALAMENTI, B., DILIBERTO, I. S., GURRIERI, S. AND VALENZA, M., 1998. Gas Hazard at Vulcano Porto (Eolian Island, Italy), Cities on Volcanoes. Osservatorio Vesuviano & Gruppo Nazionale per La Vulcanologia, Rome & Naples, pp. 158.
- BARBERI, F. ET AL., 1994. The deep structure of the Aeolian Arc (Filicudi-Panarea-Vulcano sector) In light of gravity magnetic and volcanological data. J. Volcanol. Geotherm. Res., 61(3/4): 189-206.
- BARBERI, F., GASPARINI, P., INNOCENTI, F. AND VILLARI, L., 1973. Volcanism of the Southern Tyrrhenian Sea and its geodynamical implications. J. Geophys. Res., 78(23): 5221-5232.
- BARBERI, F., INNOCENTI, F., FERRARA, G., KELLER, J. AND VILLARI, L., 1974. Evolution of Eolian arc volcanism (Southern Tyrrhenian Sea). Earth Planet. Sci. Letters, 21: 269-276.
- BARBERI, F., NERI, G., VALENZA, M. AND VILLARI, L., 1991. 1987-1990 unrest at Vulcano. Acta Vulcanol., 1: 95-106.
- BELLIA, S., BRAI, M., HAUSER, S., PUCCIO, P. AND RIZZO, S., 1996. Environmental radioactivity and volcanological features of three islands of the Mediterranean Sea (Pantelleria, Ustica and Vulcano). Chemistry-and-Ecology, 12(4): 297-302.
- BERCKHEMER, H., 1990. Grundlagen der Geophysik. Wissenschaftliche Buchgesellschaft, Darmstadt, 201 pp.

- BERRINO, G., 1997. Prospezioni gravimetriche a mare perla definizione del quadro geologico-strutturale di Vulcano e delle Isole Eolie. In: L. LA VOLPE, P. DELLINO, M. NUCCIO, E. PRIVITERA AND A. SBRANA (Editors), Progetto Vulcano Risultati delle attivita di ricerca 1993-1995. C.N.R. Gruppo Nazionale Per La Vulcanologia Italy, Pisa, pp. 284.
- BERRINO, G., 2000. Combined gravimetry in the observation of volcanic processes in Southern Italy. Journal of Geodynamics, 30(3): 371-388.
- BERRINO, G. AND D´ERRICO, V., 1993. Vulcano: Gravity and gradiometric observations. Acta Vulcanol., 3: 295-298.
- BINOT, F. AND RÖHLING, H.-G., 1988. Lithostratigraphie und natürliche Gammastrahlung des Mittleren Buntsandsteins von Helgoland.- Ein Vergleich mit der Nordseebohrung J/18-1. Z. dt. geol. Ges., 139: 33-49.
- BOLOGNESI, L., 2000. Earthquake-induced variations in the composition of the water in the geothermal reservoir at Vulcano Island, Italy. J. Volcanol. Geotherm. Res., 99(1-4): 139-150.
- BRAI, M. ET AL., 1995. Natural γ-radiation of rocks and soils from Vulcano. Nucl. Geophys., 9(2): 121-127.
- BRANCA, M., TUCCIMEI, P. AND VOLTAGGIO, M., 1997. Disequilibri della serie dell Uranio nei sublimati dell isola di Vulcano. In: L. LA VOLPE, P. DELLINO, M. NUCCIO, E. PRIVITERA AND A. SBRANA (Editors), Progetto Vulcano Risultati delle attivita di ricerca 1993-1995. C.N.R. Gruppo Nazionale Per La Vulcanologia Italy, Pisa, pp. 67-69.
- BRISTOW, C. S. AND MYERS, K. J., 1989. Detailed sedimentology and gamma-ray log characteristics of a Namurian deltaic succession I: Sedimentology and facies analysis. In: M. K. G. WHATELEY AND K. T. PICKERING (Editors), Deltas Sites and traps for fossil fuels. Geological Society Special Publication. The Geological Society, Oxford, pp. 75-80.
- BRISTOW, Q., 1979. Gamma-ray spectrometric methods in uranium exploration - airborne instrumentation. In: P. J. HOOD (Editor), Geophysics and Geochemistry in the Search for Metallic Ores. Economic Geology Report. Geological Survey of Canada, Ottawa, pp. 135-146.
- BRUNO, P. P. G., PAOLETTI, V., GRIMALDI, M. AND RAPOLLA, A., 2000. Geophysical exploration for geothermal low enthalpy resources in Lipari Island, Italy. J. Volcanol. Geotherm. Res., 98(1-4): 173.
- BÜCHEL, G., NEGENDANK, J. F. W., WUTTKE, M. AND VIERECK, L., 2000. Quarternary and Tertiary Eifel maars, Enspel (Westerwald) and Laacher See: Volcanology, sedimentology and hydrogeology. In: F. O. NEUFFER AND H. LUTZ (Editors), International Maar Conference. Mainzer Naturwissenschaftliches Archiv. Mainzer Naturwissenschaftliches Archiv, Daun, pp. 112-123.
- BUDETTA, G., CALTABIANO, T., DEL NEGRO, C. AND FERRUCCI, F., 1991. A permanent array for magnetic observation at Vulcano. Acta Vulcanol., 1: 275-277.
- BUDETTA, G. AND DEL NEGRO, C., 1995. Piezomagnetic field variation expected at Vulcano. Acta Vulcanol., 7(1): 93-94.
- BUDETTA, G., DEL NEGRO, C. AND FERRUCCI, F., 1993. Vulcano: Continuous magnetic measurements. Acta Vulcanol., 3: 293-295.

- BÜTTNER, R., DELLINO, P. AND ZIMANOWSKI, B., 1999. Identifying magma-water interaction from the surface features of ash particles. Nature, 401 (14 October 1999): 688-690.
- CAGNOLI, B. AND TARLING, D. H., 1998. A consolidation technique enabling the study of the anisotropy of magnetic susceptibility of friable pyroclastic rocks from Los Humeros Volcanic Center (Mexico). Acta Vulcanol., 10(1): 13-17.
- CAPACCIONI, B. AND CONGILIO, S., 1995. Varicolored and vesiculated tuffs from La Fossa volcano, Vulcano Island (Aeolian Archipelago, Italy): evidence of syndepositional alteration processes. Bull. Volcanol., 57(1): 61-70.
- CAPACCIONI, B., CONIGLIO, S. AND FRATINI, F., 1991. Clay minerals on recent products of hydromagmatic activity: considerations on their genesis. Acta Vulcanol., 1: 69-78.
- CAPASSO, G., FAVARA, R., FRANCOFORTE, S. AND INGUAGGIATO, S., 1999. Chemical and isotopic variations in fumarolic discharge and thermal waters at Vulcano Island (Aeolian Islands, Italy) during 1996: evidence of resumed volcanic activity. J. Volcanol. Geothem. Res., 88(3): 167-175.
- CAPASSO, G., FAVARA, R. AND INGUAGGIATO, S., 2000. Interaction between fumarolic gases and thermal groundwaters at Vulcano Island (Italy): evidences from chemical composition of dissolved gases in waters. J. Volcanol. Geotherm. Res., 102(3-4): 309-318.
- CARMICHAEL, R. S. (Editor), 1989. Practical handbook of physical properties of rocks and minerals. CRC Press, Boston, 741 pp.
- CAS, R. A. F. AND WRIGHT, J. V., 1988. Volcanic successions - modern and ancient. Chapman & Hall, London, 528 pp.
- CHEYNET, B. ET AL., 2000. Trace elements from fumaroles at Vulcano Island (Italy): rates of transport and a thermochemical model. J. Volcanol. Geotherm. Res., 95(1-4): 273-283.
- CHIODINI, G. ET AL., 1992. Geochemical and seismological investigations at Vulcano (Aeolian Islands) during 1978-1989. J. Geophys. Res., 97(B7): 11025-11032.
- CHIODINI, G., CIONI, R., RACO, B. AND TADDEUCCI, G., 1991. Gas geobarometry applied to evalute phreatic explosion hazard at Vulcano Island (Sicily, Italy). Acta Vulcanol., 1: 193-197.
- CHIOZZI, P., DE FELICE, P., FAZIO, A., PASQUALE, V. AND VERDOYA, M., 2000. Laboratory application of NaI(Tl) gamma-ray spectrometry to studies of natural radioactivity in geophysics. Applied Radiation and isotopes, 53(1-2): 215-220.
- CHIOZZI, P., DE FELICE, P., PASQUALE, V., RUSSO, D. AND VERDOYA, M., 1999. Field gamma-ray spectrometry on the Vulcano island (Aeolian Arc, Italy). Applied radiation and isotopes, 51(2): 247-253.
- CHIOZZI, P., PASQUALE, V. AND VERDOYA, M., 1998. Ground radiometric survey of U, Th, and K on the Lipari Island, Italy. Journal of Applied Geophysics, 38(3): 209-217.
- CIVETTA, L. AND GASPARINI, P., 1973. U and Th distributions in recent volcanics from Southern Italy: magmatological and geophysical implications. Riv. Ital. Geofis., 22(3/4): 127-139.
- CLOCCHIATTI, R. ET AL., 1994. Assessment of a shallow magmatic system: the 1888-90 eruption, Vulcano Island, Italy. Bull. Volcanol., 56: 466 - 486.
- CONIGLIO, S. AND DOBRAN, F., 1995. Simulations of magma ascent and pyroclast dispersal at Vulcano (Aeolian Islands, Italy). J. Volcanol. Geotherm. Res., 65(3-4): 297-317.

- DE ASTIS, G., DELLINO, P., DE ROSA, R. AND LA VOLPE, L., 1997a. Eruptive and emplacement mechanisms of fine-grained pyroclastic deposits widespread on Vulcano Island. Bull. Volcanol., 59(2): 87-102.
- DE ASTIS, G., LA VOLPE, L., PECCERILLO, A. AND CIVETTA, L., 1997b. Volcanological and petrological evolution of Vulcano island (Aeolian Arc, southern Tyrrhenian Sea). J. Geophys. Res., 102: 8021-8050.
- DE ASTIS, G., PECCERILLO, A., KEMPTON, P. D., LA VOLPE, L. AND WU, T. W., 2000. Transition from calc-alkaline to potassium-rich magmatism in subduction environments: geochemical and Sr, Nd, Pb isotopic constraints from the island of Vulcano (Aeolian arc). Contrib. Mineral. Petrol., 139(6): 684-703.
- DE ASTIS, G., DELLINO, P., DE ROSA, R. AND LA VOLPE, L., 1997c. Transition between laminated and massive surge deposits at La Fossa di Vulcano (Italy), IAVCEI, General Assembly, Puerto Vallarta, Mexico, pp. 9.
- DE FINO, M., LA VOLPE, L. AND PICCARRETA, G., 1991. Role of magma mixing during recent activity of La Fossa di Vulcano (Aeolian Islands, Italy). J. Volcanol. Geotherm. Res., 48: 385-398.
- DE ROSA, R., 1999. Compositional modes in the ash fraction of some modern pyroclastic deposits: their determination and significance. Bull. Volcanol., 61(3): 162-173.
- DE ROSA, R., FRAZZETTA, G. AND LA VOLPE, L., 1992. An approach for investigating the depositional mechanism of fine-grained surge deposits. The example of the dry surge deposits at "La Fossa di Vulcano". J. Volcanol. Geotherm. Res., 51: 305-321.
- DE ROSA, R., MAZZUOLI, R. AND VENTURA, G., 1996. Relationships between deformation and mixing processes in lava flows: a case study from Salina (Aeolian Islands, Tyrrhenian Sea). Bull. Volcanol., 58: 286-297.
- DE ROSA, R. AND SHERIDAN, M. F., 1983. Evidence for magma mixing in the surge deposits of the Monte Guardia sequence, Lipari. J. Volcanol. Geotherm. Res., 17: 313-328.
- DE VOTO, R. H., 1978. Uranium geology and eploration. Lecture notes and references. Colorado School of Mines, Golden, Colorado, 396 pp.
- DEL NEGRO, C., 1997. Il rilievo magnetico ad alta risoluzione dell'isola di Vulcano. In: L. LA VOLPE, P. DELLINO, M. NUCCIO, E. PRIVITERA AND A. SBRANA (Editors), Progetto Vulcano Risultati delle attivita di ricerca 1993-1995. C.N.R. Gruppo Nazionale Per La Vulcanologia Italy, Pisa, pp. 252-254.
- DEL NEGRO, C. AND FERRUCCI, F., 2000. Volcanomagnetic effects at Vulcano Island (Aeolian archipelago, Italy). Geophys. J. Int., 140(1): 83-94.
- DELITALA, C., DI LISA, G. A., TADDEUCCI, A., TUCCIMEI, P. AND VOLTAGGIO, M., 1997. Studio geochronologico e isotopico dei prodotti eruttivi dell'isola di Vulcano, basato sui metodi del disequilibrio radioattivo della serie dell'uranio. In: L. LA VOLPE, P. DELLINO, M. NUCCIO, E. PRIVITERA AND A. SBRANA (Editors), Progetto Vulcano Risultati delle attivita di ricerca 1993-1995. C.N.R. Gruppo Nazionale Per La Vulcanologia Italy, Pisa, pp. 207-213.
- DELLINO, P., 1997. Scenario eruttivo ed eruzione massima attesa a La Fossa. In: L. LA VOLPE, P. DELLINO, M. NUCCIO, E. PRIVITERA AND A. SBRANA (Editors), Progetto Vulcano Risultati

delle attivita di ricerca 1993-1995. C.N.R. Gruppo Nazionale Per La Vulcanologia Italy, Pisa, pp. 37-48.

- DELLINO, P., 2000. Phreatomagmatic deposits: fragmentation, transportation and deposition mechanisms. In: A.-W. Stiftung (Editor), Inernational Maar Conference. Terra Nostra. Alfred-Wegener Stiftung, Daun, pp. 99-105.
- DELLINO, P., FRAZZETTA, G. AND LA VOLPE, L., 1990. Wet surge deposits at La Fossa di Vulcano: depositional and eruptive mechanisms. J. Volcanol. Geotherm. Res., 43: 215-233.
- DELLINO, P. AND LA VOLPE, L., 1995. Fragmentation versus transportation mechanisms in the pyroclastic sequence of Monte Pilato-Rocche Rosse (Lipari, Italy). J. Volcanol. Geotherm. Res., 64: 211-231.
- DELLINO, P. AND LA VOLPE, L., 1996. Image processing analysis in reconstructing fragmentation and transportation mechanism of pyroclastic deposits. The case of Monte Pilato-Rocche Rosse eruptions, Lipari (Aeolian islands, Italy). J. Volcanol. Geotherm. Res., 71: 13-29.
- DELLINO, P. AND LA VOLPE, L., 1997. Stratigrafia, dinamiche eruttive e deposizionali, scenario errutivo e valutazioni di pericolosita a La Fossa di Vulcano. In: L. LA VOLPE, P. DELLINO, M. NUCCIO, E. PRIVITERA AND A. SBRANA (Editors), Progetto Vulcano Risultati delle attivita di ricerca 1993-1995. C.N.R. Gruppo Nazionale Per La Vulcanologia Italy, Pisa, pp. 214-237.
- DELLINO, P. AND LA VOLPE, L., 1998. Hazard related to pyroclastic surges at La Fossa di Vulcano (Aeolian Islands, Italy) as deduced by field evidence and sedimentological constraints, Cities on Volcanoes. Osservatotio Vesuviano & Gruppo Nazionale per La Vulcanologia, Rome and Naples, pp. 158.
- DELLINO, P. AND LA VOLPE, L., 2000. Structures and grain size distribution in surge deposits as a tool for modelling the dynamics of dilute pyroclastic density currents at la Fossa di Vulcano (Aeolian Islands, Italy). J. Volcanol. Geotherm. Res., 96(1-2): 57-78.
- DI MAIO, R., PATELLA, D. AND TREMACERE, A., 1993. Vulcano: Self-potential mapping and profiling. Acta Vulcanol., 3: 298-300.
- DICKINSON, W. R., 1970. Relation of andesites, granites, and derivative sandstones to arc-trench tectonics. Rev. Geophys. Space Phys., 8: 813-859.
- ELLAM, R. M., HAWKESWORTH, C. J., MENZIES, M. A. AND ROGERS, N. W., 1989. The volcanism of southern Italy: role of the subduction and the relationships between potassic and sodic alkaline magmatism. J. Geophys. Res., 94(B4): 4589-4601.
- ELLAM, R. M. ET AL., 1988. The transition from calc-alkaline to potassic, orogenic magmatism in the Aeolian Islands, Southern Italy. Bull. Volcanol., 50: 386-398.
- ETTENSOHN, F. R., PROVO-FULTON, L. AND KEPFERLE, R. C., 1979. Use of scintillometer and gamma-ray logs for correlation and stratigraphy in homogenous black shales: Summary. GSA Bull., 90: 421-423.
- FACCENNA, C., FUNICIELLO, F., GIARDINI , D. AND LUCENTE, P., 2001. Episodic back-arc extension during restricted mantle convection in the Central Mediterranean. Earth Planet. Sci. Letters, 187(1-2): 105-116.
- FAUL, H. (Editor), 1954. Nuclear geology. John Wiley and Sons, New York.
- FAURE, G., 1986. Principles of Isotope Geology. Wiley & Sons, New York, 589 pp.

- FERRARI, L. AND MANETTI, P., 1993. Geodynamic framework of the Tyrrhenian volcanism: a review. Acta Vulcanol., 3: 1-9.
- FISHER, R. V., 1995. Decoupling of pyroclastic currents: hazards assessments. J. Volcanol. Geotherm Res., 66(1-4): 257-263.
- FISHER, R. V. AND SCHMINCKE, H.-U., 1984. Pyroclastic rocks. Springer-Verlag, Berlin, Heidelberg, New York, Tokyo, 472 pp.
- FRANCALANCI, L., TAYLOR, S. R., MCCULLOCH, M. T. AND WOODHEAD, J. D., 1993. Geochemical and isotopic variations in the calc-alkaline rocks of the Aeolian arc, southern Tyrrhenian sea, Italy. Contrib. Mineral. Petrol., 113: 300-313.
- FRANCIS, P., 1993. Volcanoes: a planetary perspective. Claredon Press, 443 pp.
- FRAZZETTA, G., GILLOT, P. Y. AND LA VOLPE, L., 1985. The island of Vulcano. In: IAVCEI (Editor), IAVCEI 1985 Scientific Assembly Potassic volcanism- Mt. Etna Volcano Excursions Guidebook. IAVCEI, Gardini-Naxos (Italy), pp. 125-140.
- FRAZZETTA, G., GILLOT, P. Y., LA VOLPE, L. AND SHERIDAN, M. F., 1984. Volcanic hazard at La Fossa of Vulcano: data from the last 6000 years. Bull. Volcanol., 47(1): 105-124.
- FRAZZETTA, G. AND LA VOLPE, L., 1991. Volcanic history and maximum expected eruption at "La Fossa di Vulcano" (Aeolian Island, Italy). Acta Vulcanol., 1: 107-114.
- FRAZZETTA, G., LA VOLPE, L. AND SHERIDAN, M. F., 1983. Evolution of the Fossa Cone, Vulcano. J. Volcanol. Geotherm. Res., 17: 329-360.
- FRIEDMAN, J. F., HEIKEN, G., RANDERSON, D. AND MCKAY, D. S., 1976. Observations of eruption clouds from Sakura-Zima volcano, Kyushu, Japan from Skylab 4. J. Volcanol. Geotherm. Res., 1: 305-329.
- FÜCHTBAUER, H. AND MÜLLER, G., 1970. Sedimente und Sedimentgesteine. Sediment-Petrologie, 2. E. Schweizerbartsche Verlagsbuchhandlung, Stuttgart, 726 pp.
- GABBIANELLI, G., ROMAGNOLI, C., ROSSI, P. L., CALANCHI, N. AND LUCCHINI, F., 1991. Submarine morphology and tectonics of Vulcano (Aeolian Islands, Southeastern Tyrrhenian Sea). Acta Vulcanol., 1: 135-141.
- GIONCADA, A. AND SBRANA, A., 1991. "La Fossa caldera", Vulcano: inferences from deep drillings. Acta Vulcanol., 1: 115-126.
- GIONCADA, A. ET AL., 1997. Il sistema di alimentazione di La Fossa. In: L. LA VOLPE, P. DELLINO, M. NUCCIO, E. PRIVITERA AND A. SBRANA (Editors), Progetto Vulcano Risultati delle attivita di ricerca 1993-1995. C.N.R. Gruppo Nazionale Per La Vulcanologia Italy, Pisa, pp. 178-198.
- GRASTY, R. L., 1979. Gamma-ray spectrometric methods in uranium exploration - theory and operational procedures. In: P. J. HOOD (Editor), Geophysics and Geochemistry in the Search for Metallic Ores. Economic Geology Report. Geological Survey of Canada, Ottawa, pp. 147-161.
- GRAZIANI, G., MARTILLI, A., PARESCHI, M. T. AND VALENZA, M., 1997. Atmospheric dispersion of natural gases at Vulcano Island. J. Volcanol. Geotherm. Res., 75(3-4): 283-308.
- GVIRTZMAN, Z. AND NUR, A., 2001. Residual topography, lithospheric structure and sunken slabs in the central Mediterranean. Earth Planet. Sci. Letters, 187(1-2): 117-130.

- HARRIS, A. J. L. AND MACIEJEWSKI, A. J. H., 2000. Thermal surveys of the Vulcano Fossa fumarole field 1994-1999: evidence for fumarole migration and sealing. J. Volcanol. Geotherm. Res., 102(1-2): 119-147.
- HATHERTON, T. AND DICKINDON, W. R., 1969. The relationship between andesitic volcanism and seismicity in Indonesia, the lesser Antilles, and other island arcs. J. Geophys. Res., 74: 5301-5310.
- HAUSER, S., BRAI, M. AND BELLIA, S., 1996. Indoor and outdoor mesasurements of natural radioactivity al Vulcano (Aeolian Islands). Acta Vulcanol., 8(2): 161-165.
- HECKEMANNS, W. AND KRÄMER, F., 1989. Radiometrie und Sedimentationscharakteristik der Trifels-Schichten (sT) im Raum Wilgartswiesen (Pfälzer-Wald). Oberrhein. geol. Abh., 35: 245-257.
- HOLLEMANN, A. F. AND WIBERG, E., 1985. Lehrbuch der Anorganischen Chemie. Walter de Gruyter, Berlin-New York, 1451 pp.
- IMBÒ, G., GASPARINI, P., LUONGO, G. AND RAPOLLA, A., 1968. Contribution to the volcanological researches by determination of radioactivity of eruptive products. Bull. Volcanol., 32(2): 317-342.
- KELLER, J., 1967. Alter und Abfolge der vulkanischen Ereignisse auf den Aeolischen Inseln/ Siziliens. Berichte der Naturforschenden Gesellschaft zu Freiburg im Breisgau, 57(1): 33-67.
- KELLER, J., 1970. Die historischen Eruptionen von Vulcano und Lipari. Z. dt. geol. Ges., 121: 179-185.
- KELLER, J., 1974. Petrology of some volcanic rock series of the aeolian Arc, Southern tyrrhenian sea: calcalkaline and shoshonitic associations. Contrib. Mineral. Petrol., 45: 29-47.
- KELLER, J., 1980. The island of Vulcano. Rend. Soc. It. Miner. Petrol., 36(1): 369-414.
- KERTZ, W., 1992. Einführung in die Geophysik. B.I. -Hochschultaschenbuch. Bibliographisches Institut, Mannheim, Mannheim, 440 pp.
- KHESIN, B. E., 1998. Effective magnetization of the Precambrian in Sinai and southern Israel: Implication of new methods for ΔT field analysis. Isr. J. Earth Sci., 47(1): 47-60.
- KILLEEN, P. G., 1979. Gamma-ray spectrometric methods in uranium exploration - applications and interpretation. In: P. J. HOOD (Editor), Geophysics and Geochemistry in the Search for Metallic Ores. Economic Geology Report. Geological Survey of Canada, Ottawa, pp. 163-229.
- KILLEEN, P. G. AND CARMICHAEL, C. M., 1976. Radioactive disequilibrium determinations, Part 1: Determination of radioactive disequilibrium in uranium ores by alpha-spectrometry. Geol. Surv. Can., Pap., 75(38): 1-18.
- KOCH, G., 1984. Entwicklung und Anwendung einer radiometrischen Meßmethode (Heger-Sonde) zur Kennzeichnung klastischer Gesteinsfolgen in Aufschlüssen. Dissertation Thesis, Universität Karlsruhe, Karlsruhe, 304 pp.
- KOKELAAR, P., 1998. Volcanic processes and deposits (course notes), Würzburg/Liverpool, pp. 87.
- KOPPELT, U., ABRAHAMSEN, N. AND VOSS, O., 1998. Magnetic modelling of strongly magnetized bodies. Phys. Chem. Earth, 23(9-10): 1009-1014.

- KRASSAY, A. A., 1999. Outcrop and drill core gamma-ray logging integrated with sequence stratigraphy: examples from Proterozoic sedimentary successions of Northern Australia. AGSO Journal of Australian Geology and Geophysics, 17(4): 285-299.
- KUCHLING, H., 1988. Taschenbuch der Physik. Verlag Harri Deutsch, Thun und Frankfurt/Main, 672 pp.
- LATTER, J. H., 1989. Volcanic hazards, assessment and monitoring. Springer, Berlin, 625 pp.
- LE CLOAREC, M. F., CORAZZA, E., PENNISI, M. AND LAMBERT, G., 1991. Radioactivity of fumarolic gases at Vulcano (Italy). Acta Vulcanol., 1: 211-214.
- LE PENNEC, J.-L., CHEN, Y., DIOT, H., FROGER, J.-L. AND GOURGAUD, A., 1998. Interpretation of anisotropy of magnetic susceptibility fabric of ignimbrites in terms of kinematic and sedimentological mechanisms: An Anatolian case-study. Earth Plan. Sci. Letters, 157(1-2): 105-127.
- LEONARDI, S. ET AL., 1999. Cross-correlation between volcanic tremor and SO_2 flux at Mt. Etna volcano, 1987-1995. Acta Vulcanol., 11(2): 255-258.
- LIRER, L. AND VINCI, A., 1991. Grain-size distributions of pyroclastic deposits. Sedimentology, 38: 1075-1083.
- LOVBORG, L. AND MOSE, E., 1987. Counting statistics in radioelement assaying with a portable spectrometer. Geophysics, 52(4): 555-563.
- LOVBORG, L., WOLLENBERG, H., SORENSEN, P. AND HANSEN, J., 1971. Field determination of uranium and thorium by gamma-ray spectrometry, exemplified by measurements in the Ilimaussaq alkaline intrusion, South Greenland. Econ. Geol., 66: 368-384.
- MACDONALD, W. D. AND PALMER, H. C., 1990. Flow directions in ash-flow tuffs: a comparison of geological and magnetic susceptibility measurements, Tshirege member (upper Bandalier Tuff), Valles caldera, New Mexico, USA. Bull. Volcanol., 53: 45-59.
- MARCO, S., 1998. Magnetization of recent mud. GSI Current Research, 11: 123-126.
- MASTIN, L. G. AND WITTER, J. B., 2000. The hazards of eruptions through lakes and seawater. J. Volcanol. Geotherm. Res., 97(1-4): 195-214.
- MERCALLI, G. AND SILVESTRI, O., 1890. Le eruzioni dell'isola di Vulcano incominciate il 3 agosto 1888 e terminate il 22 marzo 1890, relazione scientifica. Annali dell'Ufficio Centrale Metereologico e Geodinamico Italiano, 10: 1-23.
- MONTALTO, A., 1996. Signs of potential renewal of eruptive activity at La Fossa (Vulcano, Aeolian Islands). Bull. Volcanol., 57(7): 483 - 492.
- MOORE, J. G., 1967. Base surge in recent volcanic eruptions. Bull. Volcanol., 30: 337-363.
- MORRISSEY, M. M. AND MASTIN, L. G., 2000. Vulcanian eruptions. In: H. SIGURDSSON (Editor), Encyclopedia of volcanoes. Academic Press, San Diego, pp. 463-475.
- MOXHAM, R. M., FOOTE, R. S. AND BUNKER, C. M., 1965. Gamma-ray spectrometer studies of hydrothermally alterated rocks. Econom. Geol., 60(4): 653-670.
- MYERS, K. J. AND BRISTOW, C. S., 1989. Detailed sedimentology and gamma-ray log characteristics of a Numurian deltaic succession II: Gamma-ray logging. In: M. K. G. WHATELEY AND K. T. PICKERING (Editors), Deltas: Sites and traps for fossil fuels. Geological Society Special Publication. The Geological Society, Oxford, pp. 81-88.

- MYERS, K. J. AND WIGNALL, P. B., 1987. Understanding Jurassic organic-rich mudrocks- New concepts using gamma-ray spectrometry and palaeoecology: Examples from the Kimmeridge Clay of Dorset and the Jet Rock of Yorkshire. In: J. K. LEGGETT AND G. G. ZUFFA (Editors), Marine clastic sedimentology. Graham and Trotman, pp. 172-189.
- NAKADA, S., 2000. Hazards from pyroclastic flows and surges. In: H. SIGURDSSON (Editor), Encyclopedia of volcanoes. Academic Press, San Diego, pp. 945-955.
- NAPPI, G., BONASIA, V., FERRI, M., MONTAGNA, S. AND PINGUE, F., 1976. Primi resultati sulla sorveglianza del complesso vulcanico Lipari-Vulcano. Boll. Soc. Geol. It., 95(5): 967-980.
- NAPPI, G., CAPACCIONI, B., BIAGIOTTI, F. AND VASELLI, O., 1999. Upper pyroclastic sequence of the Scari formation: a paroxistic eruption from Stromboli volcano (Aeolian Islands, Italy). Acta Vulcanol., 11(2): 259-264.
- NERI, A., MACEDONIO, G. AND GIDASPOV, D., 1999. Phreatic Explosion Hazard Assessment by Numerical Simulation. Physics and Chemistry of the Earth, Part A: Solid Earth and Geodesy, 24(11-12): 989-995.
- NERI, G., MONTALTO, A., PATANE, D. AND PRIVITERA, E., 1991. Earthquake space-time-magnitudo patterns at Aeolian Islands (Southern Italy) and implications for the volcanics surveillance of Vulcano. Acta Vulcanol., 1: 163-169.
- NICOLICH, R., 1989. Crustal structures from seismic studies in the frame of the EGT (Southern segment) and CROP Projects. Atti Conegni Acc. Naz. Lincei, 80: 157-176.
- NOGAMI, K. AND YOSHIDA, M., 1995. Leaching rates of rock-forming components through acidic alteration. J. Volcanol. Geotherm. Res., 65(1-2): 41-49.
- NUCCIO, P. M., 1999. Geochemical modeling of mixing between magmatic and hydrothermal gases: the case of Vulcano Island, Italy. Earth Plan. Sci. Letters, 167(3-4): 321-334.
- NUCCIO, P. M., PAONITA, A. AND SORTINO, F., 1997. Processi di miscelazione tra gas magmatici ed idrotermali. In: L. LA VOLPE, P. DELLINO, M. NUCCIO, E. PRIVITERA AND A. SBRANA (Editors), Progetto Vulcano Risultati delle attivita di ricerca 1993-1995. C.N.R. Gruppo Nazionale Per La Vulcanologia Italy, Pisa, pp. 133-140.
- ORT, M. H., ROSI, M. AND ANDERSON, C. D., 1999. Correlation of deposits and vent locations of the proximal Campanian Ignimbrite deposits, Campi Flegrei, Italy, based on natural remanent magnetization and anisotropy of magnetic susceptibility characteristics. J. Volcanol. Geotherm. Res., 91(2-4): 167-178.
- PARASNIS, D. S., 1997. Principles of Applied geophysics. Chapman & Hall, London, 434 pp.
- PARESCHI, M. T. ET AL., 2000. May 5, 1998, debris flows in circum-Vesuvian areas (southern Italy): Insights for hazard assessment. Geology, 28(7): 639-643.
- PARKINSON, D. N., 1996. Gamma-ray spectrometry as a tool for stratigraphical interpretation: examples from the western European Lower Jurassic. In: S. P. HESSELBO AND D. N. PARKINSON (Editors), Sequence stratigraphy in British Geology. Geological Society, pp. 231-255.
- PATELLA, D., DI MAIO, R., DE MARTINO, P. AND VIETRI, P., 1997. Rilievi areali di potenziale spontaneo e tomografie di geoelettrica dipolare all'isola di Vulcano. In: L. LA VOLPE, P. DELLINO, M. NUCCIO, E. PRIVITERA AND A. SBRANA (Editors), Progetto Vulcano Risultati

delle attivita di ricerca 1993-1995. C.N.R. Gruppo Nazionale Per La Vulcanologia Italy, Pisa, pp. 255-257.

- PAWSE, A., BESKE-DIEHL, S. AND MARSHALL, S. A., 1998. Use of magnetic hysteresis properties and electron spin resonance spectroscopy for the identification of volcanic ash a preliminary study. Geophys. J. Int., 132(3): 712-720.
- PICHLER, H., 1990. Italienische Vulkangebiete III: Lipari, Vulcano, Stromboli und Tyrrhenisches Meer. Sammlung geologischer Führer, 69. Gebrüder Bornträger, Berlin, 272 pp.
- PICHLER, H. AND SCHMITT-RIEGRAF, C., 1993. Gesteinsbildene Minerale im Dünnschliff. Ferdinand Enke Verlag, Stuttgart, 233 pp.
- PIERSON, T. C., 1998. An empirical method for estimating travel times for wet volcanic mass flows. Bull. Volcanol., 60: 98-109.
- PISCITELLO, M., NARDI, G. AND OLIVETTA, L., 1999. Anisotropy of magnetic susceptibility study on the Orvieto-Bagnoregio ignimbrite (Vulsini district, Central Italy). Acta Vulcanol., 11(2): 293-296.
- PRIVITERA, E., 1997. Stato delle conoscenze sulla struttura di Vulcano. In: L. LA VOLPE, P. DELLINO, M. NUCCIO, E. PRIVITERA AND A. SBRANA (Editors), Progetto Vulcano Risultati delle attivita di ricerca 1993-1995. C.N.R. Gruppo Nazionale Per La Vulcanologia Italy, Pisa, pp. 49-63.
- RASÀ, R. AND VILLARI, L., 1991. Geomorphological and morpho-structural investigations on the Fossa cone (Vulcano, Aeolian islands): a first outline. Acta Vulcanol., 1: 127-133.
- RAUEN, A., SOFFEL, H. C. AND WINTER, H., 2000. Statistical analysis and origin of the magnetic susceptibility of drill cuttings from the 9.1-km-deep KTB drill hole. Geophys. J. Int., 142(1): 83-94.
- ROCHETTE, P., JACKSON, M. AND AUBOURG, C., 1992. Rock magnetism and the interpretation of anisotropy of magnetic susceptibility. Rev. Geophys., 30(3): 209-226.
- RUSSELL, W. L. AND STEINHOFF, R. O., 1961. Radioactivity of volcanic sediments in Brazos County, Texas. Geophysics, 26(5): 618-625.
- SAITO, T., EGUCHI, T., TAKAYAMA, K. AND TANIGUCHI, H., 2001. Hazard predictions for volcanic explosions. J. Volcanol. Geotherm. Res., 106(1-2): 39-51.
- SANTO, A. P., 2000. Volcanological and geochemical evolution of Filicudi (Aeolian Islands, south Tyrrhenian Sea, Italy). J. Volcanol. Geotherm. Res., 95(1-2): 79-101.
- SBRANA, A., 1997. Il sistema magmatico di La Fossa. In: L. LA VOLPE, P. DELLINO, M. NUCCIO, E. PRIVITERA AND A. SBRANA (Editors), Progetto Vulcano Risultati delle attivita di ricerca 1993-1995. C.N.R. Gruppo Nazionale Per La Vulcanologia Italy, Pisa, pp. 22-36.
- SCHICK, R. AND SCHNEIDER, G., 1973. Physik des Erdkörpers. Enke Verlag, Stuttgart, 267 pp.
- SCHMINCKE, H.-U., 1988. Vulkane im Laacher See-Gebiet. Doris Bode Verlag GmbH, Haltern, 119 pp.
- SCHMINCKE, H.-U., 2000. Vulkanismus. Wissenschaftliche Buchgesellschaft, Darmstadt, 264 pp.
- SCHMINCKE, H.-U., BOGAARD, P. V. D. AND FREUNDT, A., 1990. Quaternary Eifel Volcanism. In: IAVCEI (Editor), IAVCEI International Volcanological Congress Mainz (FRG). IAVCEI, Mainz, pp. 188.

- SCHMINCKE, H.-U., FISHER, R. V. AND WATERS, A. C., 1973. Antidune and chute and pool structures in the base surge deposits of the Laacher See area, Germany. Sedimentology, 20(4): 553-574.
- SCHÖN, J., 1983. Petrophysik: physikalische Eigenschaften von Gesteinen und Mineralen. Enke Verlag, Stuttgart, 405 pp.
- SERRA, O., 1984. fundamentals of well-log interpretation. Developments in Petroleum Science, 15a. Elsevier, Amsterdam, 423 pp.
- SHERIDAN, M. F., 1971. Particle-Size charakteristics of pyroclastic tuffs. J. Geophys. Res., 76(23): 5627-5634.
- SHERIDAN, M. F. AND MALIN, M. C., 1983. Application of computer-assisted to volcanic hazard evaluation of surge eruptions: Vulcano, Lipari, and Vesuvius. J. Volcanol. Geotherm. Res., 17: 187-202.
- SILVESTRI, O., MERCALLI, G., GRABLOWITZ, G. AND CLERICI, V., 1891. Le eruzioni dell´isola di Vulcano incominiciate il 3 agosto 1988 e terminate il 22 Marzo 1890. Ann. Uff. Centr. Meteor. Geod., 10: 212.
- TAMBURELLI, C., BABBUCCI, D. AND MANTOVANI, E., 2000. Geodynamic implications of subduction related magmatism: insights from the Tyrrhenian-Apennines region. J. Volcanol. Geotherm. Res., 104(1-4): 33-43.
- TAMRAT, E. AND ERNESTO, M., 1999. Magnetic fabric and rock-magnetic character of the Mesozoic flood basalts of the Paraná Basin, Brazil. Journal of Geodynamics, 28(4-5): 419-437.
- TANGUY, J.-C., RIBIÈRE, C., SCARTH, A. AND TETJEP, W. S., 1998. Victims from volcanic eruptions: a revised database. Bull. Volcanol., 60: 137-144.
- TEDESCO, D., GERARDA MIELE, G., SANO, Y. AND TOUTAIN, J. P., 1995. Helium isotopic ratio in Vulcano island fumaroles: temporal variations in shallow level mixing and deep magmatic supply. J. Volcanol. Geotherm. Res., 64(1-2): 117-128.
- THOURET, J.-C., LAVIGNE, F., KELFOUN, K. AND BRONTO, S., 2000. Toward a revised hazard assessment at Merapi volcano, Central Java. J. Volcanol. Geotherm. Res., 100(1-4): 479-502.
- TITTMAN, J., 1986. Geophysical well logging. Methods of experimental Physics, 24. Academic Press, Orlando, 175 pp.
- TONARINI, S., PENNISI, M., FERRARA, G. AND LEEMAN, W. P., 1997. Delta^{11}B nelle lave di Vulcano: implicazioni sulla petrogenesi dei magmi. In: L. LA VOLPE, P. DELLINO, M. NUCCIO, E. PRIVITERA AND A. SBRANA (Editors), Progetto Vulcano Risultati delle attivita di ricerca 1993-1995. C.N.R. Gruppo Nazionale Per La Vulcanologia Italy, Pisa, pp. 199-203.
- TRINDADE, R. I. F., RAPOSO, M. I. B., ERNESTO, M. AND SIQUEIRA, R., 1999. Magnetic susceptibility and partial anhysteretic remanence anisotropies in the magnetite-bearing granite pluton of Tourao, NE Brazil. Tectonophysics, 314(4): 443-468.
- TUCKER, M. E., 1985. Einführung in die Sedimentpetrologie. Enke, Stuttgart, 265 pp.

- VALENTINE, G. A., PALLADINO, D. M., AGOSTA, E., TADDEUCCI, J. AND TRIGILA, R., 1998. Volcaniclastic aggregation in a semiarid environment, northwestern Vulcano Island, Italy. GSA Bull., 110(5): 630-643.
- VENTURA, G., 1994. Tectonics, structural evolution and caldera formation in Vulcano Island (Aeolian Archipelago, southern Tyrrhenian Sea). J. Volcanol. Geotherm. Res., 60(3-4): 207-224.
- VENTURA, G., VILARDO, G., MILANO, G. AND PINO, N. A., 1999. Relationships among crustal structure, volcanism and strike--slip tectonics in the Lipari-Vulcano Volcanic Complex (Aeolian Islands, Southern Tyrrhenian Sea, Italy). Physics of the Earth and Planetary Interiors, 116(1-4): 31-52.
- VEROSUB, K. L., 1977. Depositional and postdepositional processes in the magnetization of sediments. Rev. Geophys. Space Phys., 15(2): 129-143.
- VESPERMANN, D. AND SCHMINCKE, H.-U., 2000. Scoria cones and tuff rings. In: H. SIGURDSSON (Editor), Encyclopedia of volcanoes. Academic Press, San Diego, pp. 683-694.
- VLAG, P., ALVA-VALDIVIA, L., DE BOER, C. B., GONZALEZ, S. AND URRUTIA-FUCUGAUCHI, J., 1999. A rock- and paleomagnetic study of a Holocene lava flow in Central Mexico. Physics of the Earth and Planetary Interiors, 118(3-4): 259-272.
- VOLTAGGIO, M. ET AL., 1997. Calcite in fractures in a volcanic environment (Vulcano Island, Italy): contribution of geochronological and isotopic studies to volcanotectonics. J. Volcanol. Geotherm. Res., 75(3-4): 271-282.
- WALKER, G. P. L., 1971. Grain-size charakteristics of pyroclastic deposits. J. Geol., 79: 696-714.
- WALKER, G. P. L., 1984. Characteristics of dune-bedded pyroclastic surge bedsets. J. Volcanol. Geotherm. Res., 20: 281-296.
- WATERS, A. G. AND FISHER, R. F., 1971. Bas surges and their deposits: Capelinhos and Taal volcanoes. J. Geophys. Res., 76(23): 5596-5614.
- WOHLETZ, K. H., 1983. Mechanisms of hydrovolcanic pyroclast formation: Grain-size, scanning electron microscopy, and experimental studies. J. Volcanol. Geotherm. Res., 17: 31-64.
- WOLFF, J. A., ELLWOOD, B. B. AND SACHS, S. D., 1989. Anisotropy of magnetic susceptibility in welded tuffs: application to a welded-tuff dyke in the Tertiary Trans-Pecos Texas volcanic province, USA. Bull. Volcanol., 51(4): 299-310.
- WOODS, A. A. AND PHILLIPS, J. C., 1999. Turbulent bubble plumes and CO2-driven lake eruptions. J. Volcanol. Geotherm. Res., 92(3-4): 159-170.
- WÖRNER, G. AND SCHMINCKE, H.-U., 1984. Mineralogical and chemical zonation of the Laacher See Tephra (East Eifel Germany). J. Petrol., 25(4): 836-851.
- XIE, S., DEARING, J. A. AND BLOEMENDAL, J., 1999. A partial susceptibility approach to analysing the magnetic properties of environmental materials: a case study. Geophys. J. Intern., 138(3): 851-856.
- YONEZAWA, C., TANAKA, T. AND KAMIOKA, H., 1996. Water-rock reactions during gamma-ray irradiation. Applied Geochemistry, 11(3): 461-469.
- ZANELLA, E., DE ASTIS, G., DELLINO, P., LANZA, R. AND LA VOLPE, L., 1999. Magnetic fabric and remanent magnetization of pyroclastic surge deposits from Vulcano (Aeolian Islands, Italy). J. Volcanol. Geotherm. Res., 93(3-4): 217-236.

- ZANELLA, E., DE ASTIS, G. AND LANZA, R., 2001. Palaeomagnetism of welded, pyroclastic-fall scoriae at Vulcano, Aeolian Archipelago. J. Volcanol. Geotherm. Res., 107(1-3): 71-86.
- ZANELLA, E. AND LANZA, R., 1994. Remanent and induced magnetisation in the volcanites of Lipari and Vulcano (Aeolian Islands). Ann. Geofis., 37(5): 1149-1156.
- ZIMANOWSKI, B., 1985. Fragmentationsprozesse beim explosiven Vulkanismus. PhD Thesis Thesis, Johannes Gutenberg - Universität Mainz, Mainz, 251 pp.
- ZIMANOWSKI, B., BÜTTNER, R., LORENZ, V. AND HÄFELE, H.-G., 1997. Fragmentation of basaltic melt in the course of explosive volcanism. J. Geophys. Res., 102(B1): 803-814.
- ZIMANOWSKI, B., FRÖHLICH, G. AND LORENZ, V., 1991. Quantitative experiments on phreatomagmatic explosions. J. Volcanol. Geotherm. Res., 48: 341-358.

Notation

Anisotropy of magnetic susceptibility	AMS
Curie temperature	T_C
decay constant	λ
density	ρ
gamma-ray	γ-ray
grain sized class 0.25 to 0.125	gsc25
grain sized class 0.5 to 0.25	gsc05
half-life	$t_{1/2}$
induced magnetisation	M_{ind}
inducing magnetic field	H
initial number at the time zero	N_i
local outcrop stratigraphic height	los
Magnetic susceptibility	sus
Magnetic susceptibility for the grain sized classes < 0.125 mm	sus125
Magnetic susceptibility for the grain sized classes 0.25 to 0.125 mm	sus25
Magnetic susceptibility for the grain sized classes 0.5 to 0.25 mm	sus05
Magnetic susceptibility for the grain sized classes 1.0 to 0.5 mm	sus1
mass specific magnetic susceptibility	χ
mean grain size	Ms
Median	Md
Number of particles at time t	N_p
relative permeability	μ
remanent magnetisation	M_{rem}
specific magnetisation	M
standard deviation	s
time	t
volumetric susceptibility	K

Lebenslauf

Name:	Iris Gehring
Geburtsdatum:	03.10.1967
Geburtsort:	Detmold
Wohnort:	Würzburg
Familienstand:	ledig

Ausbildung	1974 - 1978	Weerthschule (Grundschule) (Detmold)
	1978 - 1987	Leopoldinum II (Gymnasium) (Detmold)
	1987	Abitur
	1987 – 1988	Praktikum an der Bundesforschungsanstalt für Getreide und Kartoffelverarbeitung, Institut für Bäckereitechnologie-Bereich Mikrobiologie (Detmold)
	1988 – 1992	Bayerische Julius-Maximilians-Universität Würzburg (Grundstudium Chemie)
	Oktober 1992	Bayerische Julius-Maximilians-Universität Würzburg Beginn des Studiums im Fach Geologie/Paläontologie
	10.11.1994	Vordiplom im Fach Geologie/Paläontologie
	22.06.1998	Diplom im Fach Geologie/Paläontologie
	seit 1.8.1998	Dissertation im Fach Geologie: Volcanostratigraphy using geophysical methods on La Fossa di Vulcano (S-Italy) (Bayerische Julius-Maximilians-Universität Würzburg)

Würzburg, den 03.12.2001

Erklärung
Hiermit erkläre ich, dass ich die vorliegende Dissertation in allen Teilen selbstständig angefertigt und keine anderen als die genannten Quellen und Hilfsmittel verwendet habe.

Würzburg, den 03.12.2001

Iris Gehring

Table of Contents Appendix

I. Appendix I: Data for Standard Outcrops

I.A. Punte Nere

I.A.1. Susceptibility Data and Additional Information

I.A.1.a. Outcrop G

sample	distance from the vent [m]	Md [ϕ]	Ms [ϕ]	los [m]	sus05 [*10^{-6}] e	sus25 [*10^{-6}] e
Ga1	1180	1.18	1.56	0.14	86.75 ± 0.2	87.63 ± 0.1
Ga2	1180	1.28	1.65	0.50	113.40 ± 0.2	118.91 ± 0.2
Ga3	1180	-0.35	0.71	0.75	103.87 ± 0.2	117.56 ± 0.2
Ga4	1180	1.18	1.61	1.13	94.36 ± 0.2	106.90 ± 0.2
Ga5	1180	-1.13	0.48	1.57	80.92 ± 0.1	67.82 ± 0.1
Ga6	1180	-0.09	0.77	1.81	66.34 ± 0.1	81.65 ± 0.1
Ga7	1180	-4.05	0.06	1.96	44.18 ± 0.1	48.53 ± 0.1
Ga8	1180	2.21	2.48	2.04	98.22 ± 0.1	96.84 ± 0.1
Ga9	1180	-0.25	0.78	2.23	93.73 ± 0.1	108.25 ± 0.2
Ga10	1180	0.81	1.36	2.50	139.97 ± 0.2	179.81 ± 0.3
Ga11	1180	0.20	0.95	2.64	94.81 ± 0.2	138.10 + 0.2
Ga12	1180	0.51	1.09	2.73	98.21 ± 0.2	130.08 ± 0.2
outcrop G channel deposits						
Ga13	1180	-1.30	0.77	2.97	103.06 ± 0.2	116.19 ± 0.2
Ga14	1180	0.87	1.25	3.48	118.88 ± 0.2	117.88 ± 0.2
Ga15	1180	-0.50	0.56	3.75	141.55 ± 0.2	167.03 ± 0.2
Ga16	1180	0.13	0.90	4.09	95.69 ± 0.1	110.84 ± 0.2
Ga17	1180	0.16	0.91	4.35	109.99 ± 0.2	119.45 ± 0.2
Ga18	1180	-0.44	0.72	4.70	126.09 ± 0.2	104.63 ± 0.2
Ga19	1180	-0.69	0.59	5.04	100.77 ± 0.1	112.49 ± 0.2
Ga20	1180	0.55	0.91	5.34	125.38 ± 0.2	123.92 ± 0.2
Ga21	1180	-0.12	0.74	5.64	96.13 ± 0.2	87.89 ± 0.1
Ga22	1180	0.42	0.90	5.83	88.46 ± 6.3	129.69 ± 9.3
Ga23	1180	-0.50	0.58	6.06	126.37 ± 9.0	157.39 ± 11.2
Ga24	1180	0.29	0.96	6.23	116.69 ± 0.2	123.35 ± 0.2

e: standardised to 1g, measured in cgs-mode

I.A.1.b. Outcrop H

sample	distance from the vent [m]	Md [ϕ]	Ms [ϕ]	los [m]	sus05 [*10^{-6}] e	sus25 [*10^{-6}] e
Ha1	1150	1.42	1.77	0.29	122.52 ± 0.2	127.17 ± 0.3
Ha2	1150	0.28	1.00	0.78	110.69 ± 7.9	113.10 ± 8.1
Ha3	1150	0.98	1.49	0.97	129.04 ± 0.2	137.40 ± 0.2
Ha4	1150	0.92	1.37	1.21	111.15 ± 0.2	131.11 ± 0.3
Ha5	1150	0.63	1.13	1.52	130.10 ± 9.3	121.90 ± 8.7
Ha6	1150	0.92	1.42	1.85	136.04 ± 0.2	142.03 ± 0.2
Ha7	1150	0.97	1.40	2.09	125.39 ± 0.2	113.76 ± 0.1
Ha8	1150	0.62	1.19	2.28	103.11 ± 0.1	98.32 ± 0.2
Ha9	1150	0.66	1.17	2.42	135.24 ± 0.2	132.26 ± 0.2
Ha10	1150	0.66	1.18	2.56	131.99 ± 0.3	145.12 ± 0.2
Ha11	1150	0.72	1.27	2.79	117.35 ± 0.2	94.48 ± 0.2
Ha12	1150	0.74	1.23	3.12	133.53 ± 0.2	142.00 ± 0.2
Ha13	1150	0.90	1.33	3.46	153.50 ± 0.2	135.35 ± 0.3
Ha14	1150	1.14	1.54	3.78	77.93 ± 0.1	86.84 ± 0.1
Ha15	1150	0.78	1.27	4.28	107.48 ± 0.2	98.90 ± 0.1
Ha16	1150	0.76	1.28	4.59	122.51 ± 0.2	170.03 ± 0.3
Ha17	1150	1.07	1.46	4.88	135.82 ± 0.2	142.37 ± 0.2
Ha18	1150	0.75	1.23	5.32	109.66 ± 0.2	107.42 ± 0.2

e: standardised to 1g, measured in cgs-mode

I.A.1.c. Outcrop I

sample	distance from the vent [m]	Md [ϕ]	Ms [ϕ]	los [m]	sus05 [*10^{-6}] e	sus25 [*10^{-6}] e
Ia1	1210	0.86	1.29	1.03	73.16 ± 5.2	80.31 ± 5.7
Ia2	1210	0.93	1.36	1.26	100.64 ± 7.2	136.23 ± 9.7
Ia3	1210	1.01	1.49	1.56	75.16 ± 5.4	105.73 ± 7.6
Ia4	1210	0.31	0.95	1.77	116.29 ± 8.3	110.21 ± 7.9
Ia5	1210	0.82	1.34	2.07	103.00 ± 7.4	96.27 ± 6.9
Ia6	1210	0.74	1.13	2.32	82.31 ± 5.9	95.07 ± 6.8
Ia7	1210	0.77	1.20	2.56	101.16 ± 7.2	87.07 ± 6.2
Ia8	1210	0.88	1.30	2.91	106.81 ± 7.6	81.44 ± 5.8
Ia9	1210	0.62	0.98	3.28	148.86 ± 0.2	186.31 ± 0.3
Ia10	1210	0.88	1.25	3.60	86.30 ± 6.2	117.26 ± 8.4
Ia11	1210	0.70	1.07	3.93	110.64 ± 7.9	133.09 ± 9.5
Ia12	1210	0.76	1.21	4.23	97.23 ± 6.9	91.20 ± 6.5
Ia13	1210	0.57	1.04	4.49	118.89 ± 8.5	124.33 ± 8.9
Ia14	1210	0.66	1.00	4.78	111.30 ± 8.0	116.80 ± 8.3
Ia15	1210	0.96	1.39	5.12	77.94 ± 5.6	75.91 ± 5.4

e: standardised to 1g, measured in cgs-mode

I.A.1.d. Outcrop J

sample	distance from the vent [m]	Md [ϕ]	Ms [ϕ]	los [m]	sus05 [*10^{-6}] e	sus25 [*10^{-6}] e
Ja1	1290	1.58	2.03	0.12	100.68 ± 0.1	96.02 ± 0.2
Ja2	1290	1.36	1.82	0.24	106.28 ± 0.2	124.22 ± 0.2
Ja3	1290	1.58	2.04	0.44	101.98 ± 0.2	105.85 ± 0.2
Ja4	1290	1.59	2.05	0.67	119.04 ± 0.2	111.65 ± 0.2
Ja5	1290	1.50	1.96	0.98	93.55 ± 0.2	106.19 + 0.2
Ja6	1290	1.29	1.70	1.13	116.47 ± 0.2	111.16 ± 0.1
Ja7	1290	1.37	1.84	1.24	132.40 ± 0.2	119.03 ± 0.2
Ja8	1290	1.40	1.93	1.42	114.83 ± 0.2	118.63 ± 0.2
Ja9	1290	1.19	1.59	1.57	116.38 ± 0.2	121.20 ± 0.2
Ja10	1290	1.49	1.99	1.68	102.61 ± 0.2	124.97 ± 0.2
Ja11	1290	1.34	1.82	1.79	123.41 ± 0.2	124.86 ± 0.2
Ja12	1290	1.43	1.91	1.94	95.26 ± 0.2	123.17 ± 0.2
Ja13	1290	1.31	1.85	2.25	113.24 ± 0.2	129.73 ± 0.2
Ja14	1290	1.42	1.93	2.46	99.99 ± 0.1	115.46 ± 0.2
Ja15	1290	1.56	2.06	2.67	93.88 ± 0.2	113.47 ± 0.2
Ja16	1290	1.33	1.87	2.89	145.23 ± 0.2	143.24 ± 0.2
Ja17	1290	1.58	2.04	3.04	105.95 ± 0.2	112.34 ± 0.2
Ja18	1290	1.12	1.67	3.23	129.65 ± 0.2	166.58 ± 0.3
Ja19	1290	1.37	1.90	3.38	109.16 ± 0.2	121.63 + 0.3
Ja20	1290	1.44	1.93	3.53	96.20 ± 0.2	100.60 ± 0.2
Ja21	1290	1.53	2.03	3.74	123.34 ± 0.2	124.09 + 0.2
Ja22	1290	1.42	1.94	4.15	126.97 ± 0.2	113.54 ± 0.2

e: standardised to 1g, measured in cgs-mode

I.A.2. Gamma-ray Data

I.A.2.a. Outcrop G

sample	K [%]	U [ppm]	Th [ppm]
Ga1	6.20 ± 0.0	14.20 ± 0.4	49.23 ± 0.4
Ga2	6.10 ± 0.0	14.37 ± 0.5	43.97 ± 1.3
Ga3	5.83 ±0.1	14.40 ± 0.2	43.83 ± 0.7
Ga3scoria	6.23 ±0.4	13.10 ± 0.9	49.17 ± 2.9
Ga4	6.07 ±0.1	14.07 ± 0.6	45.10 ± 1.4
Ga5	5.00 ±0.1	11.67 + 0.7	41.83 ± 1.3
Ga6	4.63 ±0.1	12.80 ± 1.2	42.57 ± 0.9
Ga7	4.70 ± 0.3	12.50 ± 0.3	40.10 ± 1.3
Ga8	4.90 ± 0.2	12.63 ± 0.5	40.87 + 0.6
Ga9	4.57 ±0.1	12.23 ± 0.3	40.27 ± 0.6
Ga10	4.83 ± 0.1	13.50 ± 0.6	38.60 ± 1.2
Ga11	4.73 ± 0.3	11.10 ± 0.6	37.37 ± 1.0
Ga12	4.17 ± 0.3	11.90 ± 0.3	39.80 ± 1.3
outcrop G channel deposits			
Ga13	4.83 ± 0.1	12.50 ± 0.2	40.03 ± 0.6
Ga14	5.00 ± 0.1	9.17 ± 0.4	41.17 ± 0.6
Ga15	4.47 ± 0.1	10.73 ± 1.1	38.73 ± 3.0
Ga16	4.57 ± 0.1	10.03 ± 0.2	41.57 ± 1.1
Ga17	4.57 ± 0.0	10.03 ± 0.7	40.87 ± 1.6
Ga18	4.97 ± 0.1	12.30 ± 0.2	36.60 ± 0.3
Ga19	4.17 ± 0.1	12.53 ± 0.1	37.97 ± 1.6
Ga20	4.57 ± 0.1	13.27 + 0.7	36.27 ± 0.7
Ga21	4.53 ± 0.1	12.07 ± 0.4	37.90 ± 0.3
Ga22	5.47 ± 0.1	13.00 ± 0.6	45.13 ± 0.8
Ga23	5.27 ± 0.0	13.53 ± 0.2	41.87 ± 0.6
Ga24	5.20 ± 0.0	14.40 ± 0.5	43.67 ± 0.6

I.A.2.b. Outcrop H

sample	K [%]	U [ppm]	Th [ppm]
Ha1	6.03 ± 0.1	14.97 ± 0.1	48.57 + 0.9
Ha2	6.30 ± 0.1	14.33 + 0.2	47.33 + 1.3
Ha3	6.07 ± 0.1	14.20 + 0.0	45.43 + 0.5
Ha4	6.13 ± 0.0	14.37 + 0.7	46.97 + 1.4
Ha5	6.10 ± 0.0	14.87 + 0.2	44.67 + 1.1
Ha6	6.00 ± 0.1	13.67 + 0.3	44.13 + 0.5
Ha7	6.03 ± 0.1	14.40 + 0.1	46.80 + 0.4
Ha8	5.97 ± 0.2	14.20 + 1.1	44.30 + 1.9
Ha9	5.73 ± 0.1	14.20 + 0.6	41.20 + 1.1
Ha10	6.00 ± 0.1	13.07 + 0.5	45.67 + 1.0
Ha11	6.23 ± 0.0	14.00 + 0.7	44.80 + 1.7
Ha12	6.10 ± 0.0	13.73 + 0.3	44.03 + 2.1
Ha13	6.13 ± 0.1	13.70 + 0.2	45.40 + 1.3
Ha14	6.13 ± 0.1	14.90 + 0.4	45.27 + 1.0
Ha15	6.27 ± 0.1	13.73 + 0.7	47.00 + 1.2
Ha16	5.87 ± 0.1	13.93 + 0.6	45.13 + 0.7
Ha17	6.03 ± 0.0	14.13 + 0.4	44.67 + 1.4
Ha18	5.93 ± 0.1	13.77 + 0.7	44.07 + 0.9

I.A.2.c. Outcrop I

sample	K [%]	U [ppm]	Th [ppm]
Ibase (lava)	4.13 ± 0.1	6.67 ± 0.4	24.53 ± 0.9
Ia1	5.57 ± 0.2	11.67 ± 0.8	35.77 ± 1.3
Ia2	5.57 ± 0.1	12.37 ± 0.4	34.97 ± 1.1
Ia3	5.93 ± 0.2	12.30 ± 0.3	38.20 ± 1.1
Ia4	5.70 ± 0.1	13.30 ± 1.0	37.63 ± 0.2
Ia5	6.07 ± 0.1	15.63 ± 0.4	39.97 ± 0.4
Ia6	6.83 ± 0.3	15.97 ± 0.4	43.17 ± 0.2
Ia7	5.27 ± 0.1	10.23 ± 0.9	35.97 ± 1.2
Ia8	5.63 ± 0.1	12.63 ± 0.2	36.63 ± 0.4
Ia9	5.37 ± 0.1	11.80 ± 0.5	34.37 ± 0.4
Ia10	6.00 ± 0.2	13.37 ± 0.6	41.40 ± 0.9
Ia11	5.43 ± 0.1	11.93 ± 0.1	35.67 ± 1.7
Ia12	5.70 ± 0.1	11.23 ± 1.0	35.70 ± 1.2
Ia13	5.10 ± 0.1	11.90 ± 0.2	34.13 ± 0.6
Ia14	5.07 ± 0.1	10.47 ± 0.2	33.90 ± 0.5
Ia15	6.37 ± 0.1	12.73 ± 0.4	39.87 ± 0.7

I.A.2.d. Outcrop J

sample	K [%]	U [ppm]	Th [ppm]
Ja1	5.85 ± 0.1	11.95 ± 0.5	40.23 ± 0.8
Ja2	5.63 ± 0.3	12.33 ± 0.4	38.20 ± 1.0
Ja3	5.85 ± 0.2	11.85 ± 0.8	40.23 ± 0.5
Ja4	5.40 ± 0.1	11.43 ± 0.2	34.88 ± 0.8
Ja5	5.40 ± 0.1	11.78 ± 0.5	36.93 ± 1.3
Ja6	5.75 ± 0.3	12.55 ± 0.6	42.23 ± 1.0
Ja7	5.72 ± 0.1	11.98 ± 0.5	37.94 ± 0.7
Ja8	5.60 ± 0.2	11.13 ± 0.7	40.00 ± 1.2
Ja9	5.53 ± 0.3	10.95 ± 0.6	39.03 ± 1.3
Ja10	5.75 ± 0.1	12.35 ± 0.8	40.20 ± 1.1
Ja11	5.40 ± 0.4	11.40 ± 0.7	36.86 ± 1.0
Ja12	5.75 ± 0.1	13.20 ± 0.5	35.95 ± 0.9
Ja13	5.96 ± 0.1	12.52 ± 0.5	38.74 ± 1.3
Ja14	5.72 ± 0.4	12.22 ± 0.7	39.04 ± 0.9
Ja15	6.23 ± 0.1	13.13 ± 0.7	41.08 ± 0.6
Ja16	5.90 ± 0.4	11.72 ± 0.9	38.92 ± 1.1
Ja17	5.83 ± 0.1	13.10 ± 0.5	39.85 ± 0.5
Ja18	5.20 ± 0.2	10.90 ± 0.3	36.50 ± 0.9
Ja19	5.82 ± 0.1	12.94 ± 0.3	38.24 ± 0.6
Ja20	5.60 ± 0.2	11.70 ± 0.7	38.45 ± 0.7
Ja21	5.73 ± 0.1	12.57 ± 0.2	38.77 ± 0.8
Ja22	6.10 ± 0.1	13.96 ± 0.7	39.78 ± 0.9

I.B. Tufi Varicolori

I.B.1. Susceptibility Data and Additional Information

I.B.1.a. Outcrop F

sample	**distance from the vent** [m]	**Md** [ϕ]	**Ms** [ϕ]	**los** [m]	**sus05** [*10^{-6}] e	**sus25** [*10^{-6}] e
Fb1	700	0.84	1.29	0.12	120.44 ± 0.3	123.17 ± 0.2
Fb2	700	1.38	1.80	0.32	103.72 ± 0.2	87.59 ± 0.2
Fb3	700	0.76	1.36	0.45	80.12 ± 0.1	65.01 ± 0.1
Fb4	700	-1.18	0.73	0.59	91.65 ± 0.2	81.10 ± 0.1
Fb5	700	1.36	1.54	0.72	94.60 ± 0.2	70.12 ± 0.1
Fb6	700	0.45	1.07	0.80	106.02 ± 0.1	82.83 ± 0.1
Fb7	700	-2.73	0.37	0.88	85.71 ± 0.2	118.30 ± 0.2
Fb8	700	-0.89	0.43	0.98	157.47 ± 11.2	90.56 ± 6.5
Fb9	700	0.64	1.20	1.10	80.98 ± 0.1	79.53 ± 0.1
Fb10	700	-3.09	0.37	1.19	67.04 ± 4.8	69.76 ± 5.0
Fb11	700	0.43	0.85	1.28	114.04 ± 8.1	132.57 ± 9.5
Fb12	700	-5.04	-0.05	1.36	87.00 ± 6.2	86.21 ± 6.2
Fb14	700	-2.05	0.23	1.46	97.63 ± 7.0	110.27 ± 7.9
Fb15	700	0.76	1.19	1.52	100.11 ± 0.2	89.70 ± 0.1

e: standardised to 1g, measured in cgs-mode

I.B.1.b. Outcrop O

sample	distance from the vent [m]	Md [ϕ]	Ms [ϕ]	los [m]	sus05 [*10^{-6}] e	sus25 [*10^{-6}] e
Ob1	860	0.80	1.33	0.20	66.28 ± 0.1	70.01 ± 0.1
Ob2	860	1.08	1.49	0.59	62.55 ± 0.1	55.33 ± 0.1
Ob3	860	1.04	1.56	0.89	88.66 ± 0.2	82.75 ± 0.1
Ob4	860	0.60	1.19	1.01	86.81 ± 0.1	82.58 ± 0.1
Ob5	860	0.23	0.99	1.18	71.97 ± 0.1	73.02 ± 0.1
Ob6	860	1.31	1.67	1.38	47.16 ± 0.1	47.86 ± 0.1
Ob7	860	1.18	1.57	1.51	47.13 ± 0.1	50.51 ± 0.1
Ob8	860	0.79	1.38	1.70	59.34 ± 0.1	56.88 ± 0.1
Ob9	860	0.61	1.27	1.85	77.48 ± 0.1	80.84 ± 0.1
Ob10	860	0.26	1.03	1.99	89.06 ± 0.1	100.21 ± 0.1
Ob11	860	1.16	1.66	2.19	72.29 ± 0.1	59.97 ± 0.1
Ob12	860	1.30	1.71	2.38	73.01 ± 0.1	77.39 ± 0.1
Ob13	860	1.99	2.25	2.58	70.24 ± 0.1	68.24 ± 0.1
Ob14	860	2.00	2.35	2.80	64.39 ± 0.1	60.49 ± 0.1
Ob15	860	1.49	1.99	2.94	72.26 ± 0.1	79.55 ± 0.1
Ob16	860	0.83	1.37	3.09	53.73 ± 0.1	53.23 ± 0.1
Ob17	860	2.55	2.78	3.40	67.83 ± 0.1	60.67 ± 0.1
Ob18	860	2.33	2.61	3.64	67.28 ± 0.2	58.82 ± 0.1
Ob19	860	1.97	2.19	3.90	58.72 ± 0.1	61.53 ± 0.1
Ob20	860	2.06	2.38	4.04	68.54 ± 0.2	59.22 ± 0.1
Ob21	860	2.30	2.45	4.39	66.60 ± 0.1	63.02 ± 0.1
Ob22	860	1.39	1.83	4.69	64.19 ± 0.1	69.41 ± 0.1
Ob23	860	1.97	2.05	4.76	42.99 ± 0.1	42.13 ± 0.1
Ob24	860	1.78	2.00	5.01	52.77 ± 0.1	53.23 ± 0.1
Ob25	860	1.73	2.08	5.22	87.72 ± 0.1	88.37 ± 0.1
Ob26	860	1.84	2.04	5.27	43.55 ± 0.1	51.22 ± 0.1
Ob27	860	1.66	1.92	5.39	69.91 ± 0.1	63.06 ± 0.1
Ob28	860	0.56	1.36	5.51	44.83 ± 0.1	45.10 ± 0.1
Ob29	860	1.71	1.95	5.66	62.60 ± 0.1	62.36 ± 0.1
Ob30	860	2.01	2.25	6.12	64.71 ± 0.1	55.22 ± 0.1
Ob31	860	1.92	2.11	6.64	46.19 ± 0.1	43.95 ± 0.1
Ob32	860	0.91	1.30	7.08	62.30 ± 0.1	56.71 ± 0.1
Ob33	860	1.58	2.05	7.43	91.03 ± 0.1	88.04 ± 0.1
Ob34	860	1.38	1.72	7.68	60.22 ± 0.1	59.24 ± 0.1
Ob35	860	1.82	2.08	8.19	58.03 ± 0.1	54.34 ± 0.1
Ob36	860	1.55	1.86	8.47	85.70 ± 0.2	84.71 ± 0.1
Ob37	860	1.64	1.97	8.71	65.96 ± 0.1	52.32 ± 0.1
Ob38	860	1.55	2.05	8.94	115.89 ± 0.2	101.32 ± 0.2
Ob39	860	2.24	2.71	9.10	48.98 ± 0.1	38.81 ± 0.1

e: standardised to 1g, measured in cgs-mode

I.B.2. Gamma-ray Data

I.B.2.a. Outcrop F

sample	K [%]	U [ppm]	Th [ppm]
Fb1	4.8 ± 0.1	9.23 ± 0.3	30.47 ± 0.8
Fb2	4.3 ± 0.1	9.43 ± 0.5	31.90 ± 1.2
Fb3	4.2 ± 0.3	9.37 ± 0.8	27.27 ± 1.2
Fb4	4.1 ± 0.2	10.03 ± 0.6	28.50 ± 0.3
Fb6	3.83 ± 0.3	8.60 ± 0.4	31.27 ± 1.2
Fb7	4.20 ± 0.2	10.03 ± 0.4	31.47 ± 1.0
Fb8	3.60 ± 0.2	10.10 ± 0.4	28.63 ± 1.0
Fb9	3.37 ± .2	10.03 ± 0.5	27.50 ± 0.3
Fb10	3.67 ± 0.3	9.57 ± 0.8	30.90 ± 1.3
Fb11	3.40 ± 0.2	10.43 ± 0.3	31.70 ± 0.8
Fb12	3.70 ± 0.3	8.70 ± 0.3	32.97 ± 0.7
Fb13	3.63 ± 0.1	10.63 ± 0.2	32.97 ± 0.8
Fb14	3.67 ± 0.1	11.77 ± 0.4	35.53 ± 1.1
Fb15	4.37 ± 0.3	11.00 ± 0.4	32.30 ±0.6

I.B.2.b. Outcrop O

sample	K [%]	U [ppm]	Th [ppm]
Ob1	4.85 ± 0.1	11.58 ± 0.6	40.68 ± 1.2
Ob2	4.17 ± 0.1	8.60 ± 0.4	36.87 ± 1.6
Ob3	4.30 ± 0.1	9.73 ± 0.9	35.03 ± 1.5
Ob4	4.43 ± 0.4	9.20 ± 0.7	33.07 ± 0.9
Ob5	4.20 ± 0.1	8.60 ± 0.1	33.30 ± 0.9
Ob6	4.27 ± 0.1	9.90 ± 0.4	31.90 ± 0.4
Ob7	3.67 ± 0.0	7.40 ± 0.2	32.20 ± 0.8
Ob8	4.17 ± 0.1	8.30 ± 0.9	32.37 ± 1.1
Ob9	3.88 ± 0.3	9.08 ± 0.6	33.18 ± 1.7
Ob10	4.13 ± 0.1	8.57 ± 0.2	32.10 ± 0.9
Ob11	3.93 ± 0.1	8.43 ± 0.2	30.73 ± 1.0
Ob12	4.03 ± 0.1	9.03 ± 0.4	34.43 ± 1.2
Ob13	4.17 ± 0.0	9.67 ± 0.2	30.27 ± 0.6
Ob14	4.15 ± 0.1	8.50 ± 0.1	31.50 ± 0.4
Ob15	4.78 ± 0.2	10.34 ± 0.3	36.04 ± 1.0
Ob16	4.17 ± 0.0	8.87 ± 0.1	32.83 ± 0.5
Ob17	4.72 ± 0.1	10.98 ± 0.5	31.02 ± 1.0
Ob18	4.90 ± 0.0	10.77 ± 0.0	34.10 ± 1.1
Ob19	4.97 ± 0.1	10.13 ± 0.9	33.63 ± 0.9
Ob20	5.77 ± 0.8	10.70 ± 0.4	33.03 ± 0.6
Ob21	5.32 ± 0.1	10.68 ± 0.5	38.18 ± 1.1
Ob22	3.73 ± 0.3	7.77 ± 0.5	26.93 ± 1.1
Ob23	3.53 ± 0.2	7.93 ± 0.5	29.10 ± 1.4
Ob24	3.77 ± 0.1	7.97 ± 0.1	28.53 ± 1.4
Ob25	3.57 ± 0.3	7.43 ± 0.4	28.53 ± 0.9
Ob26	3.73 ± 0.4	8.00 ± 0.4	30.03 ± 1.1
Ob27	3.83 ± 0.1	7.83 ± 0.6	31.00 ± 0.7
Ob28	3.72 ± 0.4	8.90 ± 0.7	31.48 ± 1.5
Ob29	3.60 ± 0.1	9.06 ± 0.2	30.12 ± 1.4
Ob30	4.30 ± 0.2	8.00 ± 0.5	31.90 ± 0.3
Ob31	4.10 ± 0.1	8.13 ± 0.6	31.15 ± 0.8
Ob32	3.63 ± 0.1	7.13 ± 0.7	30.18 ± 1.2
Ob33	3.70 ± 0.3	6.97 ± 0.5	28.83 ± 0.6
Ob34	3.65 ± 0.1	7.40 ± 0.1	29.20 ± 0.8
Ob35	3.70 ± 0.1	8.33 ± 0.3	29.80 ± 1.1
Ob36	3.47 ± 0.3	7.37 ± 0.6	31.63 ± 1.0
Ob37	3.17 ± 0.0	6.53 ± 0.3	29.77 ± 0.5
Ob38	3.35 ± 0.2	6.85 ± 0.3	26.10 ± 1.2
Ob39	3.77 ± 0.0	7.77 ± 0.4	28.90 ± 0.4

I.C. Palizzi

I.C.1. Susceptibility Data and Additional Information

I.C.1.a. Outcrop E

sample	distance from the vent [m]	Md [ϕ]	Ms [ϕ]	los [m]	sus05 [*10^{-6}] e	sus25 [*10^{-6}] e
Ec1	700	0.10	0.78	0.16	126.15 ± 0.2	134.83 ± 0.2
Ec2	700	0.01	0.55	0.39	123.14 ± 8.8	148.53 ± 10.6
Ec3	700	0.76	1.20	0.59	95.06 ± 6.8	83.67 ± 6.0
Ec4	700	1.07	1.62	0.77	80.45 ± 0.1	100.23 ± 0.2
Ec5	700	0.94	1.44	0.93	91.66 ± 6.5	109.23 ± 7.8
Ec6	700	0.50	1.03	1.22	124.61 ± 8.9	202.01 ± 14.4
Ec7	700	1.17	1.66	1.52	88.77 ± 6.3	90.16 ± 6.4
Ec8	700	1.10	1.60	1.72	111.24 ± 7.9	107.71 ± 7.7
Ec9	700	0.84	1.21	1.95	91.10 ± 6.5	79.90 ± 5.7
Ec10	700	1.24	1.75	2.09	104.07 ± 7.4	90.67 ± 6.5
Ec11	700	0.88	1.39	2.19	108.56 ± 7.8	124.46 ± 8.9

e: standardised to 1g, measured in cgs-mode

I.C.1.b. Outcrop F

sample	distance from the vent [m]	Md [ϕ]	Ms [ϕ]	los [m]	sus05 [*10^{-6}] e	sus25 [*10^{-6}] e
Fc1	700	0.18	0.73	1.64	98.10 ± 7.0	125.93 ± 9.0
Fc2	700	0.95	1.37	1.97	74.60 ± 5.3	86.06 ± 6.1
Fc3	700	0.82	1.32	2.28	105.71 ± 0.1	83.84 ± 0.2
Fc4	700	0.99	1.48	2.48	105.25 ± 0.1	113.09 ± 0.2
Fc5	700	1.05	1.42	2.64	111.91 ± 8.0	133.89 ± 9.6
Fc6	700	0.79	1.27	2.84	89.39 ± 6.4	114.60 ± 8.2
Fc7	700	0.88	1.28	3.04	166.21 ± 11.9	284.29 ± 20.3
Fc9	700	0.56	1.03	3.51	102.36 ± 0.2	139.38 ± 0.2
Fc10	700	1.47	1.93	3.68	99.89 ± 0.2	95.74 ± 0.1
Fc11	700	1.69	2.07	3.86	99.11 ± 0.2	78.61 ± 0.1
Fc12	700	-0.12	0.59	3.99	127.91 ± 0.2	105.49 ± 0.2
Fc13	700	1.20	1.68	4.16	100.62 ± 0.1	74.46 ± 0.1
Fc14	700	1.17	1.65	4.48	105.86 ± 0.2	107.72 ± 0.2
Fc15	700	1.31	1.63	4.80	104.53 ± 0.1	127.54 ± 0.3

e: standardised to 1g, measured in cgs-mode

I.C.2. Gamma-ray Data

I.C.2.a. Outcrop E

sample	K [%]	U [ppm]	Th [ppm]
Ec1	6.30 ± 0.1	17.03 ± 0.6	49.67 ± 0.8
Ec2	6.23 ± 0.1	15.13 ± 0.5	45.67 ± 0.8
Ec3	6.20 ± 0.2	16.30 ± 0.6	46.83 ± 0.9
Ec4	6.47 ± 0.1	16.20 ± 1.1	48.87 ± 1.6
Ec5	5.93 ± 0.1	14.30 ± 0.2	47.90 ± 0.9
Ec7	6.03 ± 0.1	15.67 ± 0.3	49.47 ± 1.5
Ec8	6.17 ± 0.1	17.27 ± 0.5	45.13 ± 0.7
Ec9	6.40 ± 0.1	18.57 ± 0.5	46.13 ± 0.8
Ec10	6.40 ± 0.2	18.70 ± 0.9	49.03 ± 1.1
Ec11	6.63 ± 0.3	19.53 ± 0.5	49.93 ± 2.7
Ec 2nd pumice	8.40 ± 0.0	20.53 ± 0.8	56.13 ± 0.8

I.C.2.b. Outcrop F

sample	K [%]	U [ppm]	Th [ppm]
Fc1	4.70 ± 0.3	14.47 ± 0.6	35.47 ± 0.4
Fc2	4.67 ± 0.2	13.93 ± 0.5	35.97 ± 1.0
Fc3	4.80 ± 0.3	13.40 ± 0.5	37.67 ± 1.3
Fc4	5.67 ± 0.3	16.43 ± 0.4	42.13 ± 0.8
Fc5	4.60 ± 0.1	12.07 ± 0.7	37.03 ± 0.6
Fc6	5.57 ± 0.2	17.87 ± 1.2	42.80 ± 1.0
Fc7	5.50 ± 0.4	16.57 ± 0.6	44.20 ± 0.8
Fc8	4.83 ± 0.4	13.23 ± 0.4	38.97 ± 2.1
Fc 1st pumice1	4.10 ± 0.1	12.03 ± 0.3	33.40 ± 0.9
Fc 1st pumice2	4.58 ± 0.1	14.28 ± 0.3	39.33 ± 0.5
Fc9	6.26 ± 0.1	15.98 ± 0.3	51.28 ± 1.4
Fc10	5.04 ± 0.1	14.94 ± 0.7	41.68 ± 0.8
Fc11	5.30 ± 0.1	13.97 ± 0.2	42.53 ± 0.3
Fc12	6.42 ± 0.3	18.14 ± 0.6	46.84 ± 0.6
Fc13	4.98 ± 0.1	11.98 ± 0.3	37.28 ± 0.8
Fc14	4.34 ± 0.1	12.58 ± 0.2	35.48 ± 0.8
Fc15	4.94 ± 0.1	13.92 ± 0.7	37.86 ± 0.5

I.D. Commenda

I.D.1. Susceptibility Data and Additional Information

I.D.1.a. Outcrop A

sample	distance from the vent [m]	Md [ϕ]	Ms [ϕ]	los [m]	sus05 [*10^{-6}] e	sus25 [*10^{-6}] e
Ad1	280	1.08	1.57	0.08	106.53 ± 0.2	102.64 ± 0.1
Ad2	280	1.38	1.56	0.41	73.99 ± 0.1	98.00 ± 0.1
Ad3	280	-4.34	0.75	0.74	38.38 ± 0.1	45.48 ± 0.1
Ad4	280	1.08	1.39	0.90	57.91 ± 0.1	65.93 ± 0.1
Ad5	280	-1.74	0.54	1.18	15.97 ± 0.0	16.78 ± 0.0
Ad6	280	0.79	1.25	1.64	27.99 ± 0.1	30.48 ± 0.1
Ad7	280	-2.00	0.54	1.92	6.06 ± 0.0	6.68 ± 0.0
Ad8	280	1.94	1.96	2.14	101.26 ± 0.2	82.48 ± 0.1
Ad9	280	1.56	1.57	2.48	70.07 ± 0.1	70.22 ± 0.1
Ad10	280	2.90	3.16	2.80	78.90 ± 0.5	83.28 ± 0.1
Ad11	280	0.77	1.34	3.03	78.53 ± 0.1	84.72 ± 0.1
Ad12	280	2.82	3.06	3.44	36.57 ± 0.4	40.77 ± 0.1
Ad13	280	0.93	1.34	3.86	14.94 ± 0.0	15.89 ± 0.0
Ad14	280	0.45	1.18	3.95	45.30 ± 0.1	51.40 ± 0.1
Ad15	280	2.59	2.68	4.02	97.22 ± 0.2	100.37 ± 0.1
Ad16	280	1.97	2.36	4.41	92.80 ± 0.2	101.57 ± 0.1
Ad17	280	1.99	1.90	4.76	62.53 ± 0.1	59.94 ± 0.1
Ad18	280	2.21	2.44	4.87	92.86 ± 0.2	96.14 ± 0.2
Ad19	280	2.08	2.51	5.04	113.79 ± 0.2	183.63 ± 0.3
Ad20	280	2.67	2.89	5.26	101.53 ± 0.2	109.84 ± 0.2
Ad21	280	1.60	1.94	5.43	125.88 ± 0.2	147.47 ± 0.2
Ad22	280	0.24	1.21	5.64	44.34 ± 0.1	47.09 ± 0.1
Ad23	280	2.05	2.06	5.89	20.42 ± 0.1	14.59 ± 0.0
Ad24	280	2.47	2.33	6.10	63.26 ± 0.1	70.51 ± 0.1
Ad25	280	2.68	2.78	6.28	76.29 ± 0.1	95.45 ± 0.2
Ad26	280	2.82	2.92	6.55	77.64 ± 0.2	93.87 ± 0.1
Ad27	280	2.59	2.62	6.78	76.49± 0.1	81.69 ± 0.1
Ad28	280	2.58	2.61	6.93	89.38 ± 0.2	84.79 ± 0.1
Ad29	280	2.67	2.70	7.16	88.65 ± 0.1	104.48 ± 0.1
Ad30	280	2.87	3.05	7.35	40.80 ± 0.2	72.73 ± 0.1
Ad31	280	2.62	2.57	7.46	82.74 ± 0.2	107.64 ± 0.2
Ad32	280	2.76	3.00	7.69	90.08 ± 0.2	124.12 ± 0.2
Ad33	280	2.94	3.22	7.91	40.68 ± 1.0	66.62 ± 0.1
Ad34	280	2.28	2.11	7.98	40.40 ± 0.1	46.24 ± 0.1
Ad35	280	2.71	2.86	8.09	92.90 ± 0.2	80.39 ± 0.1
Ad36	280	2.82	3.07	8.23	51.19 ± 0.2	64.88 ± 0.1
Ad37	280	2.79	3.01	8.30	61.30 ± 0.2	54.64 ± 0.1
Ad38	280	2.85	3.25	8.42	60.23 ± 0.3	52.13 ± 0.1
Ad39	280	2.57	2.46	8.55	61.80 ± 4.4	70.76 ± 5.1
Ad40	280	2.77	2.99	8.68	35.73 ± 0.1	26.11 ± 0.0

e: standardised to 1g, measured in cgs-mode

I.D.1.b. Outcrop B

sample	distance from the vent [m]	Md [ϕ]	Ms [ϕ]	los [m]	sus05 [*10^{-6}] e	sus25 [*10^{-6}] e
Bd1	730	-7.77	-0.10	0.01	53.04 ± 0.2	58.48 ± 0.3
Bd2	730	-2.24	0.42	0.05	72.33 ± 0.1	79.75 ± 0.1
Bd3	730	-0.99	0.65	0.07	57.11 ± 0.1	66.90 ± 0.1
Bd4	730	-0.65	0.59	0.10	71.24 ± 0.2	75.95 ± 0.1
Bd5	730	-2.52	0.12	0.15	47.39 ± 0.2	60.49 ± 0.2
Bd6	730	-0.22	0.95	0.27	80.93 ± 0.1	91.52 ± 0.1
Bd7	730	1.30	1.62	0.51	67.08 ± 0.1	63.98 ± 0.1
Bd8	730	0.29	1.14	0.76	67.90 ± 0.1	90.97 ± 0.2
Bd9	730	-0.80	0.58	0.93	45.82 ± 0.1	48.95 ± 0.1
Bd10	730	1.97	2.14	1.08	62.69 ± 0.1	63.70 ± 0.1
Bd11	730	2.03	1.94	1.25	60.59 ± 0.1	63.91 ± 0.1
Bd12	730	2.49	2.61	1.53	83.10 ± 0.1	79.31 ± 0.1
Bd13	730	2.20	2.54	1.64	72.59 ± 0.1	60.80 ± 0.1
Bd14	730	2.45	2.67	1.70	100.87 ± 0.2	91.34± 0.2
Bd15	730	0.14	1.07	1.88	30.56 ± 0.1	32.77 ± 0.0
Bd16	730	2.09	2.16	2.08	69.66 ± 0.1	75.52 ± 0.1
Bd17	730	0.41	1.17	2.36	29.29 ± 0.1	31.20 ± 0.1
Bd18	730	1.88	1.77	2.55	51.98 ± 0.2	58.96 ± 0.1
Bd19	730	1.92	2.21	2.65	77.38 ± 0.1	93.13 ± 0.1
Bd20	730	2.09	2.55	2.77	44.29 ± 0.1	44.43 ± 0.1
Bd21	730	1.28	1.57	2.89	31.91 ± 0.1	33.94 ± 0.1
Bd22	730	1.85	1.87	3.13	73.52 ± 0.1	77.68 ± 0.1
Bd23	730	2.22	2.16	3.40	73.37 ± 0.1	76.79 ± 0.1
Bd24	730	2.53	2.21	3.75	61.34 ± 0.1	85.30 ± 0.2
Bd25	730	2.53	2.51	4.01	109.00 ± 0.2	72.17 ± 0.1
Bd26	730	2.65	2.70	4.24	158.56 ± 0.3	151.27 ± 0.3
Bd27	730	2.65	2.68	4.48	61.78 ± 0.1	62.06 ± 0.1
Bd28	730	2.65	2.41	4.73	76.15 ± 0.2	109.69 ± 0.2
Bd29	730	2.52	2.34	5.03	78.20 ± 0.2	108.23 ± 0.2

e: standardised to 1g, measured in cgs-mode

I.D.1.c. Outcrop E

sample	distance from the vent [m]	Md [ϕ]	Ms [ϕ]	los [m]	sus05 [*10^{-6}] e	sus25 [*10^{-6}] e
Ed2	700	1.45	2.16	3.06	41.77 ± 0.1	58.35 ± 0.1
Ed3	700	2.47	2.70	3.42	67.07 ± 0.1	82.83 ± 0.1
Ed4	700	2.71	2.95	3.52	89.44± 0.1	91.23 ± 0.2
Ed5	700	2.75	2.95	3.72	81.30 ± 0.1	98.01 ± 0.2
Ed7	700	2.72	2.73	4.02	81.81 ± 0.2	87.41 ± 0.2
Ed8	700	2.76	2.98	4.26	69.24 ± 0.1	90.23 ± 0.1
Ed1	700	2.26	2.39	4.45	75.47 ± 0.1	78.87 ± 0.1

e: standardised to 1g, measured in cgs-mode

I.D.2. Gamma-ray Data

I.D.2.a. Outcrop A

sample	K [%]	U [ppm]	Th [ppm]
Ad1	3.97 ± 0.1	11.63 ± 0.4	35.13 ± 0.2
Ad2	3.93 ± 0.1	12.00 ± 0.1	36.40 ± 1.4
Ad3	5.13 ± 0.2	12.97 ± 0.1	43.73 ± 1.1
Ad4	4.70 ± 0.1	12.33 ± 0.5	42.07 ± 0.4
Ad6	4.67 ± 0.1	12.57 ± 0.4	41.53 ± 1.1
Ad8	4.53 ± 0.1	11.60 ± 0.6	38.03 ± 1.0
Ad12	4.53 ± 0.0	11.97 ± 0.3	39.50 ± 0.7
Ad14	4.47 ± 0.3	12.93 ± 0.5	37.43 ± 0.6
Ad15	4.73 ± 0.2	11.63 + 0.2	39.67 ± 1.0
Ad16	4.97 ± 0.1	13.77 + 1.0	37.90 ± 1.1
Ad18	5.50 ± 0.2	14.03 ± 0.7	40.17 ± 1.0
Ad19	5.23 ± 0.1	14.33 ± 0.9	42.30 ± 1.2
Ad20	5.27 ± 0.0	12.80 ± 0.5	40.07 ± 1.5
Ad22	4.80 ± 0.1	11.77 ± 0.1	36.83 ± 0.3
Ad23	4.27 ± 0.0	12.03 ± 0.2	35.97 ± 1.3
Ad25	5.03 ± 0.3	10.60 ± 0.4	33.97 ± 0.5
Ad26	4.33 ± 0.1	11.50 ± 0.9	34.53 ± 0.6
Ad28	4.47 ± 0.0	11.00 ± 0.2	35.10 ± 1.8
Ad29	4.73 ± 0.0	11.50 ± 0.1	35.07 ± 0.4
Ad30	4.27 ± 0.2	10.30 ± 0.3	35.83 ± 1.1
Ad31	4.67 ± 0.2	10.53 ± 0.4	36.27 ± 2.2
Ad32	4.30 ± 0.0	10.97 ± 0.1	34.40 ± 1.3
Ad34	4.40 ± 0.3	11.90 ± 0.5	33.73 ± 0.6
Ad36	4.40 ± 0.4	10.27 ± 0.5	32.30 ± 0.5
Ad37	4.53 ± 0.2	11.03 ± 0.4	32.37 ± 0.7
Ad38	5.07 ± 0.1	13.37 ± 0.1	39.13 ± 0.8
Ad39	4.93± 0.0	11.87 ± 0.4	36.90 ± 0.8
Ad40	4.27 ± 0.2	10.90 ± 0.8	32.07 ± 0.4

I.D.2.b. Outcrop B

sample	K [%]	U [ppm]	Th [ppm]
Bd1	3.80 ± 0.3	13.17 ± 0.6	39.37 ± 1.2
Bd2	3.93 ± 0.3	12.40 ± 0.4	38.27 ± 1.1
Bd3	3.83 ± 0.3	12.17 ± 0.5	35.80 ± 1.7
Bd4	3.70 ± 0.3	13.37 ± 0.9	37.30 ± 2.1
Bd5	3.47 ± 0.3	10.97 ± 0.4	38.03 ± 0.9
Bd6	4.30 ± 0.1	14.80 ± 0.4	37.50 ± 1.1
Bd7	4.47 ± 0.1	12.90 ± 0.7	40.50 ± 1.6
Bd8	4.03 ± 0.2	11.70 ± 0.7	41.00 ± 1.2
Bd9	4.10 ± 0.2	12.03 ± 0.4	39.20 ± 0.8
Bd10	4.33 ± 0.2	11.73 ± 1.0	40.60 ± 1.9
Bd11	4.23 ± 0.1	12.60 ± 0.6	38.43 ± 1.1
Bd13	4.70 ± 0.4	13.00 + 0.9	42.37 ± 1.5
Bd14	4.43 ± 0.3	13.10 ± 0.7	43.47 ± 1.5
Bd15	4.53 ± 0.1	11.73 ± 0.3	44.43 ± 0.2
Bd16	4.83 ± 0.2	13.13 ± 0.1	44.67 ± 0.2
Bd17	4.60 ± 0.1	13.50 ± 0.4	41.53 ± 1.6
Bd18	5.33 ± 0.3	13.53 ± 0.4	47.23 ± 1.4
Bd19	5.20 ± 0.1	13.57 ± 0.2	46.10 ± 1.0
Bd20	5.07 ± 0.2	13.63 ± 0.6	43.83 ± 1.6
Bd21	5.13 ± 0.2	14.23 ± 0.6	44.03 ± 1.7
Bd23	5.30 ± 0.0	16.33 ± 0.4	45.87 ± 0.6
Bd24	5.47 ± 0.1	12.37 ± 0.2	43.40 ± 0.4
Bd25	5.47 ± 0.1	15.43 ± 0.8	45.90 ± 0.6
Bd26	5.10 ± 0.0	13.73 ± 0.6	48.17 ± 2.1
Bd27	4.97 ± 0.0	14.10 ± 0.5	42.47 ± 0.9
Bd28	5.40± 0.0	15.87 ± 0.2	42.67 ± 0.3
Bd29	5.27 ± 0.1	13.57 ± 1.5	44.43 ± 1.3

I.D.2.c. Outcrop E

sample	K [%]	U [ppm]	Th [ppm]
Ed1	6.93 ±0.4	16.87 ±0.5	50.93 ±1.1
Ed2	6.23 ±0.0	17.37 ±0.7	53.97 ±1.5
Ed3	5.80 ±0.3	15.77 ±1.2	53.07 ±0.7
Ed4	6.23 ±0.1	16.40 ±0.1	52.73 ±0.5
Ed5	6.77 ±0.3	19.47 ±0.4	51.70 ±0.2
Ed6	7.00 ±0.2	18.37 ±0.5	57.07 ±0.2
Ed7	6.27 ±0.2	15.67 ±0.6	48.43 ±0.9
Ed8	6.30 ±0.1	17.23 ±0.7	47.17 ±0.4

I.E. Cratere Attuale

I.E.1. Susceptibility Data and Additional Information

I.E.1.a. Outcrop B

sample	distance from the vent [m]	Md [ϕ]	Ms [ϕ]	los [m]	sus05 [*10^{-6}] e	sus25 [*10^{-6}] e
Bd/e1	730	2.04	1.85	5.17	45.33 ± 0.2	48.45 ± 0.1
Bd/e2	730	2.16	2.05	5.29	94.69 ± 0.1	119.10 ± 0.2
Bd/e3	730	2.59	2.49	5.52	105.15 ± 0.2	116.48 ± 0.2
Bd/e4	730	2.76	2.82	5.73	82.61 ± 0.2	107.63 ± 0.2
Bd/e5	730	2.84	2.99	6.00	55.91 ± 0.2	82.98 ± 0.1
Bd/e6	730	2.59	2.37	6.13	49.83 ± 0.2	59.24 ± 0.1
Be1	730	2.68	2.76	6.28	67.88 ± 0.1	86.61 ± 0.1
Be2	730	2.75	2.73	6.51	69.00 ± 0.1	91.09 ± 0.1
Be3	730	0.25	1.30	6.69	66.43 ± 0.1	78.13 ± 0.1

e: standardised to 1g, measured in cgs-mode

I.E.1.b. Outcrop E

sample	distance from the vent [m]	Md [ϕ]	Ms [ϕ]	los [m]	sus05 [*10^{-6}] e	sus25 [*10^{-6}] e
Ee1	700	2.20	2.38	4.55	104.59 ± 0.2	84.90 ± 0.1
Ee2	700	0.46	1.06	4.66	100.71 ± 7.2	93.81 ± 6.7
Ee3	700	0.92	1.43	4.78	80.60 ± 5.8	102.91 ± 7.4
Ee4	700	2.21	2.43	4.93	75.62 ± 0.1	102.92 ± 0.2
Ee5	700	1.38	1.90	5.06	80.11 ± 0.1	111.02 ± 0.2

e: standardised to 1g, measured in cgs-mode

I.E.2. Gamma-ray Data

I.E.2.a. Outcrop B

sample	K [%]	U [ppm]	Th [ppm]
Bd/e1	5.07 ± 0.3	14.33 ± 0.4	39.70 ± 0.7
Bd/e2	4.43 ± 0.0	11.83 ± 0.7	36.13 ± 1.4
Bd/e3	4.83 ± 0.2	12.33 ± 0.5	42.57 ± 1.9
Bd/e4	5.20 ± 0.1	13.37 ± 0.1	38.93 ± 0.8
Bd/e6	4.77 ± 0.1	12.33 ± 0.8	38.70 ± 1.1
Be1	5.73 ± 0.0	15.43 + 0.8	46.63 ± 1.3
Be2	5.10 ± 0.1	13.17 ± 0.3	39.53 ± 1.7
Be3	4.57 ± 0.1	11.00 ± 0.5	36.93 ± 0.8

I.E.2.b. Outcrop E

sample	K [%]	U [ppm]	Th [ppm]
Ee1	7.03 ± 0.1	16.23 ± 0.9	56.20 ± 4.6
Ee2	6.07 ± 0.2	16.90 ± 0.3	47.23 ± 1.1
Ee3	6.23 ± 0.1	15.83 ± 0.5	49.50 ± 0.6
Ee4	6.47 ± 0.3	16.07 ± 1.0	46.77 ± 1.0
Ee5	6.27 ± 0.2	16.73 ± 0.6	50.83 ± 0.8
Ee pumice	6.13 ± 0.1	17.50 ± 0.4	61.03 ± 0.8

II. Appendix II: Data for Undefined Outcrops

II.A. Outcrop C

II.A.1. Susceptibility Data and Additional Information

sample	**distance from the vent** [m]	**Md** [ϕ]	**Ms** [ϕ]	**los** [m]	**sus05** [*10^{-6}] e	**sus25** [*10^{-6}] e
Cx1	670	1.80	2.08	0.07	58.65 ± 0.1	49.61 ± 0.1
Cx2	670	1.66	1.84	0.21	67.96 ± 0.1	58.53 ± 0.1
Cx3	670	1.49	1.82	0.32	100.10 ± 0.2	69.22 ± 0.1
Cx4	670	1.33	1.66	0.44	75.76 ± 0.1	58.98 ± 0.1
Cx5	670	1.35	1.51	0.51	68.67 ± 0.1	67.10 ± 0.1
Cx6	670	0.47	1.19	0.55	55.06 ± 0.1	56.22 ± 0.1
Cx7	670	1.43	1.64	0.71	53.55 ± 0.1	36.60 ± 0.1
Cc1	670	0.58	1.13	1.04	109.37 ± 0.2	87.34 ± 0.1
Cc2	670	1.21	1.63	1.25	73.41 ± 0.1	67.23 ± 0.1
Cc3	670	0.58	1.07	1.31	86.59 ± 0.1	96.75 ± 0.1
Cy1	670	0.93	1.44	1.38	92.38 ± 0.1	98.57 ± 0.1
Cy2	670	0.68	1.26	1.46	81.46 ± 0.1	59.67 ± 0.1
Cy3	670	0.32	0.90	1.51	101.43 ± 0.2	93.18 ± 0.2
Cy4	670	0.98	1.42	1.59	96.82 ± 0.1	95.03 ± 0.2
Cy5	670	1.48	1.62	1.69	68.02 ± 0.1	45.81 ± 0.1
Cy6	670	1.12	1.62	1.77	101.22 ± 0.1	90.27 ± 0.1
Cy7	670	0.67	1.21	1.86	107.23 ± 0.2	95.50 ± 0.1
Cy8	670	1.04	1.55	1.98	75.65 ± 0.1	73.58 + 0.1
Cy9	670	1.10	1.62	2.16	68.45 ± 0.1	66.86 ± 0.1

e: standardised to 1g, measured in cgs-mode

II.A.2. Gamma-ray Data

sample	K [%]	U [ppm]	Th [ppm]
Cx1	7.76 ± 0.2	12.94 ± 0.6	61.12 ± 0.6
Cx2	7.46 ± 0.1	12.18 ± 0.5	57.74 ± 1.2
Cx3	7.90 ± 0.2	13.10 ± 0.2	59.66 ± 0.9
Cx4	7.74 ± 0.3	12.66 ± 0.6	56.56 ± 1.2
Cx5	7.55 ± 0.3	13.18 ± 0.5	60.33 ± 1.8
Cx6	8.03 ± 0.4	12.67 ± 0.5	58.17 ± 1.2
Cx7	7.68 ± 0.1	14.16 ± 0.4	58.04 ± 0.9
Cc1	7.73 ± 0.1	12.53 ± 0.3	55.68 ± 0.9
Cc3	7.84 ± 0.2	13.50 ± 0.4	56.96 ± 1.2
Cy1	7.85 ± 0.3	11.00 ± 0.5	56.95 ± 1.5
Cy2	6.83 ± 0.3	11.48 ± 0.6	45.98 ± 1.2
Cy3	6.60 ± 0.3	10.50 ± 0.4	47.72 ± 0.8
Cy4	6.62 ± 0.2	11.12 ± 0.2	44.70 ± 0.9
Cy5	6.84 ± 0.3	10.82 ± 0.5	45.86 ± 0.9
Cy6	6.60 ± 0.3	10.35 ± 0.5	47.80 ± 1.0
Cy7	6.58 ± 0.3	10.44 ± 0.4	44.42 ± 1.1
Cy8	6.38 ± 0.2	12.25 ± 0.9	44.40 ± 1.5
Cy9	6.48 ± 0.1	11.95 ± 0.4	47.10 ± 1.1

II.B. Outcrop D

II.B.1. Susceptibility Data and Additional Information

sample	distance from the vent [m]	Md [ϕ]	Ms [ϕ]	los [m]	sus05 [*10^{-6}] e	sus25 [*10^{-6}] e
Dy1	600	0.97	1.45	0.08	102.18 ± 0.2	142.15 ± 0.2
Dy2	600	0.69	1.21	0.21	75.45 ± 0.1	81.14 ± 0.1
Dy3	600	1.70	1.89	0.38	57.91 ± 0.1	51.61 ± 0.1
Dy4	600	1.42	1.89	0.51	113.01 ± 0.2	103.42 ± 0.2
Dy5	600	0.85	1.42	0.62	57.16 ± 0.1	68.59 ± 0.1
Dy6	600	0.33	1.12	0.75	57.84 ± 0.1	57.42 ± 0.1
Dy7	600	1.62	1.78	0.90	42.92 ± 0.1	40.95 ± 0.1
Dy8	600	1.21	1.46	1.19	48.58 ± 0.1	43.39 ± 0.1
Dy9	600	1.31	1.53	1.36	26.97 ± 0.1	27.81 ± 0.1
Dy10	600	1.71	1.81	1.42	36.07 ± 0.1	37.41 ± 0.1
Dy11	600	1.40	1.55	1.50	52.58 ± 0.1	44.06 ± 0.1
Dy12	600	1.47	1.64	1.71	54.87 ± 0.1	44.85 ± 0.1
Dy13	600	1.03	1.42	1.88	67.94 ± 0.1	70.26 ± 0.1
Dy14	600	1.55	1.95	2.00	59.52 ± 0.1	56.79 ± 0.1
Dy15	600	0.85	1.31	2.07	34.62 ± 0.1	31.49 ± 0.1
Dy16	600	0.34	1.02	2.17	69.53 ± 0.1	69.29 ± 0.1
Dy17	600	1.04	1.41	2.21	76.53 ± 0.1	70.39 ± 0.1
Dy18	600	1.31	1.77	2.35	85.81 ± 0.1	82.32 ± 0.1
Dy19	600	0.97	1.37	2.69	50.81 ± 0.1	45.86 ± 0.1

e: standardised to 1g, measured in cgs-mode

II.B.2. Gamma-ray Data

sample	K [%]	U [ppm]	Th [ppm]
Dy1	7.38 ± 0.1	13.54 ± 0.4	61.52 ± 1.3
Dy2	7.37 ± 0.2	13.40 ± 0.6	60.60 ± 0.9
Dy3	7.35 ± 0.1	12.28 ± 0.3	60.65 ± 1.2
Dy4	7.02 ± 0.2	13.48 ± 0.4	56.84 ± 1.1
Dy5	7.00 ± 0.1	13.33 ± 0.4	57.10 ± 0.9
Dy6	6.92 ± 0.2	12.44 ± 0.5	56.28 ± 1.8
Dy7	7.30 ± 0.1	13.48 ± 0.6	59.05 ± 0.6
Dy8	7.27 ± 0.1	10.33 ± 0.2	60.30 ± 1.4
Dy9	7.30 ± 0.3	12.57 ± 0.3	57.97 ± 0.8
Dy10	7.53 ± 0.4	13.60 ± 0.7	61.20 ± 1.1
Dy11	7.48 ± 0.2	13.08 ± 0.6	59.65 ± 1.1
Dy12	7.53 ± 0.2	12.38 ± 0.3	60.43 ± 0.6
Dy13	7.55 ± 0.3	13.63 ± 0.8	60.00 ± 1.2
Dy14	7.23 ± 0.1	12.38 ± 0.4	57.58 ± 2.4
Dy15	7.03 ± 0.1	12.50 ± 0.4	56.00 ± 1.0
Dy16	6.93 ± 0.3	13.30 ± 0.4	55.78 ± 1.5
Dy17	7.08 ± 0.3	12.75 ± 0.5	57.10 ± 2.1
Dy18	6.83 ± 0.2	11.43 ± 0.4	52.73 ± 0.9
Dy19	7.23 ± 0.1	11.77 ± 0.3	55.50 ± 0.2

II.C. Outcrop K

II.C.1. Susceptibility Data and Additional Information

sample	distance from the vent [m]	Md [ϕ]	Ms [ϕ]	los [m]	sus05 [*10^{-6}] e	sus25 [*10^{-6}] e
Kw1	1420	0.06	0.77	0.04	72.36 ± 0.1	94.66 ± 0.2
Kw2	1420	1.63	1.99	0.23	70.40 ± 0.1	73.31 ± 0.1
Kw3	1420	2.12	2.43	0.47	50.91 ± 0.1	47.69 ± 0.1
Kw4	1420	1.53	1.88	0.81	65.96 ± 0.1	74.49 ± 0.1
Kw5	1420	1.98	2.19	1.43	58.21 ± 0.1	59.15 + 0.1
Kc1	1420	2.10	2.48	1.98	60.22 ± 0.1	65.18 ± 0.1
Kc2	1420	1.75	2.16	2.30	64.59 ± 0.1	81.80 ± 0.1
Kc3	1420	1.02	1.53	2.52	62.01 ± 0.1	68.79 ± 0.1
Kc4	1420	1.69	2.03	2.75	67.63 ± 0.1	81.43 ± 0.1
Kc5	1420	1.73	2.15	2.92	63.53 ± 0.1	68.66 ± 0.1
Kc6	1420	1.30	1.85	3.15	65.39 ± 0.1	75.27 ± 0.1
Ke1	1420	1.30	1.75	3.45	67.96 ± 0.1	82.27 ± 0.1
Ke2	1420	1.59	1.98	3.70	72.05 ± 0.1	92.46 ± 0.1
Ke3	1420	1.36	1.82	3.91	71.80 ± 0.1	78.24 ± 0.1
Ke4	1420	1.42	1.74	4.06	70.78 ± 0.1	97.00 ± 0.1
Ke5	1420	1.54	1.85	4.35	71.79 ± 0.1	89.41 ± 0.1
Ke6	1420	1.06	1.57	4.67	79.01 ± 0.1	95.74 ± 0.2
Ke7	1420	1.60	1.93	4.84	79.39 ± 0.1	101.44 ± 0.1
Ke8	1420	1.60	1.87	5.03	82.08 ± 0.1	122.65 ± 0.2
Ke9	1420	1.72	2.13	5.21	76.17 ± 0.1	78.90 ± 0.1

e: standardised to 1g, measured in cgs-mode

II.C.2. Gamma-ray Data

sample	K [%]	U [ppm]	Th [ppm]
Kw1	4.42 ± 0.3	13.40 ± 0.4	38.40 ± 1.6
Kw2	4.23 ± 0.1	11.37 ± 0.8	39.67 ± 0.6
Kw3	4.43 ± 0.1	11.35 ± 0.5	38.93 ± 1.3
Kw4	4.13 ± 0.1	10.27 ± 0.6	36.67 ± 0.6
Kw5	4.32 ± 0.0	12.60 ± 0.5	37.72 ± 1.3
Kc1	4.10 ± 0.0	10.10 ± 0.6	32.90 ± 1.4
Kc2	4.68 ± 0.2	10.56 ± 0.4	36.38 ± 0.9
Kc3	5.23 ± 0.1	11.47 ± 0.3	37.60 ± 0.5
Kc4	4.70 ± 0.1	10.63 ± 1.1	34.17 ± 0.4
Kc5	3.70 ± 0.1	8.90 ± 0.5	31.90 ± 0.5
Kc6	4.68 ± 0.1	12.65 ± 0.4	34.65 ± 0.7
Ke1	4.07 ± 0.0	10.00 ± 0.4	35.03 ± 1.0
Ke2	4.40 ± 0.1	10.27 ± 0.4	30.67 ± 0.3
Ke3	3.36 ± 0.1	7.80 ± 0.3	28.92 ± 1.1
Ke4	3.30 ± 0.2	8.37 ± 0.2	30.10 ± 0.6
Ke5	3.60 ± 0.1	8.73 ± 0.3	29.38 ± 0.7
Ke6	3.37 ± 0.1	8.90 ± 0.7	25.90 ± 0.9
Ke7	3.30 ± 0.1	8.27 ± 0.6	26.67 ± 0.7
Ke8	2.90 ± 0.1	6.40 ± 0.5	27.36 ± 1.0
Ke9	3.73 0.1	9.27 ± 0.5	29.97 ± 0.2

II.D. Outcrop L

II.D.1. Susceptibility Data and Additional Information

sample	distance from the vent [m]	Md [ϕ]	Ms [ϕ]	los [m]	sus05 [*10^{-6}] e	sus25 [*10^{-6}] e
Lw1	1950	1.87	2.07	0.50	54.70 ± 0.1	48.64 ± 0.1
Lw2	1950	1.67	1.80	1.03	55.76 ± 0.1	51.11 ± 0.1
Lw3	1950	1.63	1.73	1.12	51.42 ± 0.1	49.88 ± 0.1
Lw4	1950	1.55	1.76	1.25	49.87 ± 0.1	52.32 ± 0.1
Lw5	1950	1.85	2.00	1.38	54.04 ± 0.1	59.51 ± 0.2
Lw6	1950	1.84	2.03	1.48	50.90 ± 0.1	54.39 ± 0.1
Lw7	1950	1.87	2.09	1.55	61.28 ± 0.1	61.72 ± 0.1
Lw8	1950	1.77	1.92	1.64	52.20 ± 0.1	53.80 ± 0.1
Lc1	1950	1.49	1.67	1.75	58.18 ± 0.1	57.26 ± 0.1
Lc2	1950	1.72	2.11	1.85	61.21 ± 0.1	68.44 ± 0.1
Lc3	1950	1.56	1.87	1.98	62.13 ± 0.1	72.22 ± 0.1
Le1	1950	1.59	1.75	2.20	78.70 ± 0.1	83.92 ± 0.1
Le2	1950	1.59	1.92	2.64	74.53 ± 0.1	106.6 ± 0.2
Le3	1950	1.54	1.73	3.03	64.84 ± 0.1	69.39 ± 0.1
Le4	1950	-0.02	1.97	3.40	47.07 ± 0.1	46.01 ± 0.1

e: standardised to 1g, measured in cgs-mode

II.D.2. Gamma-ray Data

sample	K [%]	U [ppm]	Th [ppm]
Lw1	4.78 ± 0.1	9.50 ± 0.9	34.60 ± 1.4
Lw2	4.90 ± 0.3	9.60 ± 0.6	33.10 ± 0.5
Lw3	4.73 ± 0.2	10.45 ± 0.9	34.80 ± 1.7
Lw4	4.60 ± 0.1	9.70 ± 0.3	33.68 ± 1.2
Lw5	4.65 ± 0.2	10.45 ± 0.5	34.95 ± 0.9
Lw6	4.68 ± 0.3	10.53 ± 0.3	34.18 ± 0.6
Lw7	4.70 ± 0.3	10.40 ± 0.5	35.93 ± 1.3
Lc2	4.37 ± 0.1	10.33 ± 0.4	30.40 ± 0.6
Lc3	4.63 ± 0.2	7.70 ± 0.6	36.57 ± 1.1
Le1	2.60 ± 0.0	6.37 ± 0.1	21.43 ± 0.3
Le2	2.73 ± 0.0	6.53 ± 0.2	23.40 ± 0.6
Le3	2.70 ± 0.1	5.73 ± 0.2	22.60 ± 0.3
Le4	2.57 ± 0.0	6.20 ± 0.3	20.73 ± 0.7

II.E. Outcrop M

II.E.1. Susceptibility Data and Additional Information

sample	distance from the vent [m]	Md [ϕ]	Ms [ϕ]	los [m]	sus05 [*10^{-6}] e	sus25 [*10^{-6}] e
Ms1	1720	1.47	2.02	0.21	63.96 ± 0.1	68.39 ± 0.1
Ms2	1720	1.18	1.66	0.50	70.45 ± 0.1	72.20 ± 0.1
Ms3	1720	1.20	1.72	0.78	67.41 ± 0.1	78.21 ± 0.1
Msw1	1720	1.29	1.74	1.43	60.91 ± 0.1	64.92 ± 0.1
Msw2	1720	2.18	2.38	1.70	46.31 ± 0.1	49.84 ± 0.1
Msw3	1720	2.23	2.55	1.70	51.39 ± 0.1	55.16 ± 0.1
Mw1	1720	0.54	1.21	2.28	50.75 ± 0.1	54.29 ± 0.1
Mw2	1720	0.49	1.19	2.74	54.74 ± 0.1	62.36 ± 0.1
Mwe1	1720	1.27	1.56	3.27	67.39 ± 0.1	71.03 ± 0.1
Mwe2	1720	1.42	1.59	3.73	56.04 ± 0.1	54.34 ± 0.1
Mwe3	1720	0.71	1.97	4.28	48.94 ± 0.1	52.91 ± 0.1

e: standardised to 1g, measured in cgs-mode

II.E.2. Gamma-ray Data

sample	K [%]	U [ppm]	Th [ppm]
Ms1	5.23 ± 0.1	11.45 ± 0.5	32.73 ± 0.8
Ms2	4.90 ± 0.1	10.10 ± 0.1	33.10 ± 0.7
Ms3	4.28 ± 0.1	8.18 ± 0.4	30.93 ± 0.8
Msw1	4.20 ± 0.0	9.00 ± 0.6	31.68 ± 0.9
Msw2	4.43 ± 0.1	9.50 ± 0.4	32.23 ± 0.1
Msw3	5.23 ± 0.2	11.10 ± 0.4	34.30 ± 1.3
Mw1	2.00 ± 0.0	7.27 ± 0.5	20.20 ± 0.5
Mw2	2.03 ± 0.1	7.03 ± 0.3	24.70 ± 0.4
Mwe1	2.20 ± 0.0	5.87 ± 0.3	22.30 ± 0.4
Mwe2	2.18 ± 0.1	7.65 ± 0.4	22.50 ± 1.2
Mwe3	2.38 ± 0.1	6.40 ± 0.5	21.80 ± 1.3

II.F. Outcrop N

II.F.1. Susceptibility Data and Additional Information

sample	distance from the vent [m]	Md [ϕ]	Ms [ϕ]	los [m]	sus05 [*10^{-6}] e	sus25 [*10^{-6}] e
Nc1	1600	1.65	2.06	0.14	88.33 ± 0.2	83.82 ± 0.1
Nc2	1600	1.53	1.96	0.31	86.20 ± 0.2	70.07 ± 0.2
Nc3	1600	1.57	2.01	0.47	82.86 ± 0.2	81.58 ± 0.1
Nc4	1600	1.86	2.29	0.75	116.13± 0.2	111.80 ± 0.2
Nc5	1600	1.53	2.04	1.00	108.18 ± 0.2	96.42 ± 0.1
Nd1	1600	2.59	2.83	1.43	67.15 ± 0.1	73.75 ± 0.1
Nd2	1600	2.76	3.08	1.59	59.13 ± 0.1	68.39 ± 0.1
Nd3	1600	2.76	3.10	1.66	47.01 ± 0.1	49.04 ± 0.1
Nd4	1600	2.64	2.97	1.72	52.10 ± 0.1	59.31 ± 0.1
Nd5	1600	2.76	3.15	1.79	59.91 ± 0.1	57.87 ± 0.1
Nd6	1600	2.62	2.98	1.95	71.97 ± 0.2	75.05 ± 0.1
Nd7	1600	2.64	3.03	2.07	57.84 ± 0.1	66.75 ± 0.2
Nw1	1600	2.52	2.94	2.16	81.46 ± 0.6	70.55 ± 0.1
Nw2	1600	2.82	3.18	2.36	57.40 ± 0.1	59.95 ± 0.1
Nw3	1600	2.30	2.72	2.63	67.61 ± 0.1	74.67 ± 0.1
Nw4	1600	2.46	2.93	2.92	39.93 ± 0.1	34.24 ± 0.1

e: standardised to 1g, measured in cgs-mode

II.F.2. Gamma-ray Data

sample	K [%]	U [ppm]	Th [ppm]
Nc1	6.30 ± 0.1	14.35 ± 1.1	42.75 ± 1.3
Nc2	6.43 ± 0.2	14.27 ± 0.5	44.60 ± 0.6
Nc3	6.37 ± 0.1	13.40 ± 0.7	41.40 ± 1.5
Nc4	6.15 ± 0.1	13.15 ± 0.5	44.33 ± 1.6
Nc5	5.60 ± 0.1	14.93 ± 0.6	44.13 ± 0.6
Nd1	6.90 ± 0.1	17.87 ± 0.3	56.63 ± 1.9
Nd2	7.00 ± 0.3	17.90 ± 0.3	55.90 ± 1.4
Nd3	7.33 ± 0.3	20.43 ± 1.0	62.70 ± 1.2
Nd4	6.67 ± 0.3	18.00 ± 0.8	51.27 ± 1.8
Nd5	5.13 ± 0.2	13.13 ± 0.3	40.97 ± 0.9
Nd6	6.00 ± 0.1	14.85 ± 0.8	45.48 ± 2.0
Nd7	6.17 ± 0.3	15.97 ± 0.4	50.73 ± 1.4
Nw1	6.27 ± 0.1	15.27 ± 0.8	48.60 ± 0.5
Nw2	6.37 ± 0.1	15.97 ± 0.6	49.40 ± 0.0
Nw3	6.80 ± 0.2	15.57 ± 1.7	52.10 ± 1.1
Nw4	6.00 ± 0.1	15.30 ± 1.1	46.58 ± 0.7

II.G. Outcrop P

II.G.1. Susceptibility Data and Additional Information

sample	distance from the vent [m]	Md [ϕ]	Ms [ϕ]	los [m]	sus05 [*10^{-6}] e	sus25 [*10^{-6}] e
Pa1	1250	1.02	1.46	0.79	105.91 ± 0.2	110.07 ± 0.1
Pa2	1250	1.16	1.97	1.63	97.44 ± 0.1	104.57 ± 0.2
Pa3	1250	1.52	1.99	1.87	112.98 ± 0.2	134.99 ± 0.2
Pa4	1250	0.84	1.97	2.00	99.90 ± 0.1	107.25 ± 0.2
Pa5	1250	1.10	1.55	2.19	120.43 ± 0.2	136.70 ± 0.2
Pa6	1250	1.35	1.75	2.36	107.70 ± 0.2	101.27 ± 0.1
Pa7	1250	1.12	1.58	2.65	136.62 ± 0.2	144.58 ± 0.2
Pa8	1250	0.81	1.42	3.78	122.82 ± 0.2	107.32 ± 0.2
Pa9	1250	0.78	1.36	4.19	118.47 ± 0.2	102.98 ± 0.2
Pa10	1250	0.74	1.39	4.63	112.68 ± 0.2	101.17 ± 0.1

e: standardised to 1g, measured in cgs-mode

II.G.2. Gamma-ray Data

sample	K [%]	U [ppm]	Th [ppm]
Pa1	4.27± 0.1	10.73 ± 0.3	37.77 ± 0.6
Pa2	4.47 ± 0.2	10.33 ± 0.4	37.27 ± 0.4
Pa3	4.10 ± 0.1	10.38 ± 0.4	35.83 ± 1.1
Pa4	4.52 ± 0.2	11.04 ± 0.5	38.14 ± 1.6
Pa5	4.28 ± 0.1	11.92 ± 0.8	36.36 ± 1.5
Pa6	4.37 ± 0.1	11.93 ± 0.5	42.53 ± 0.9
Pa7	4.50 ± 0.0	12.63 ± 0.4	41.10 ± 1.2
Pa8	4.63 ± 0.1	12.30 ± 0.6	39.20 ± 1.3
Pa9	4.84 ± 0.1	12.80 ± 0.3	42.16 ± 1.4
Pa10	5.00 ± 0.1	13.10 + 0.6	43.58 ± 1.1

II.H. Outcrop Q

II.H.1. Susceptibility Data and Additional Information

sample	distance from the vent [m]	Md [ϕ]	Ms [ϕ]	los [m]	sus05 [*10^{-6}] e	sus25 [*10^{-6}] e
Qr1	520	1.62	2.04	0.44	74.70 ± 0.1	69.74 ± 0.1
Qr2	520	1.93	2.47	0.88	66.10 ± 0.1	64.99 ± 0.1
Qr3	520	0.29	0.84	1.29	111.00 ± 0.2	97.17 ± 0.1
Qr4	520	0.09	1.04	1.53	46.72 ± 0.1	56.20 ± 0.1

e: standardised to 1g, measured in cgs-mode

II.H.2. Gamma-ray Data

sample	K [%]	U [ppm]	Th [ppm]
Qr1	5.98 ± 0.1	10.05 ± 0.6	46.18 ± 1.0
Qr2	6.96 ± 0.1	11.38 ± 0.5	53.30 ± 1.6
Qr3	7.37 ± 0.1	12.30 ± 0.2	57.70 ± 1.1
Qr4	7.62 ± 0.1	12.46 ± 0.6	67.16 ± 1.6

II.I. Outcrop R

II.I.1. Susceptibility Data and Additional Information

sample	**distance from the vent** [m]	**Md** [ϕ]	**Ms** [ϕ]	**los** [m]	**sus05** [*10^{-6}] e	**sus25** [*10^{-6}] e
Rs1	1260	1.54	2.01	0.34	119.25 ± 0.2	117.63 ± 0.2
Rs2	1260	1.80	2.22	0.69	90.70 ± 0.1	82.30 ± 0.1
Rs3	1260	1.57	1.99	1.03	103.94 ± 0.2	86.03 ± 0.1
Rs4	1260	1.68	2.09	1.16	102.83 ± 0.1	110.25 ± 0.2
Rs5	1260	1.77	2.22	1.35	101.99± 0.2	105.82 ± 0.2
Rs6	1260	1.64	2.08	1.52	93.59 ± 0.1	102.12 ± 0.1
Rs7	1260	1.59	2.02	1.68	96.50 ± 0.1	106.93 ± 0.2
Rs8	1260	1.84	2.27	1.95	93.88 ± 0.1	89.22 ± 0.1
Rs9	1260	1.59	2.01	2.25	62.46 ± 0.1	70.42 ± 0.1
Rs10	1260	1.53	1.98	2.64	102.79 ± 0.2	96.26 ± 0.2
Rs11	1260	1.62	1.95	2.96	113.44 ± 0.2	91.35 ± 0.1
Rs12	1260	1.62	2.10	3.28	85.38 ± 0.1	84.80 ± 0.1
Rs13	1260	1.62	2.06	3.61	172.80 ± 0.2	123.42 ± 0.2
Rs14	1260	1.55	1.96	3.98	73.00 ± 0.1	75.92 ± 0.1
Rs15	1260	1.51	1.90	4.30	99.30 ± 0.2	89.62 ± 0.1
Rs16	1260	1.64	2.07	4.89	127.92 ± 0.2	119.79 ± 0.2
Rd1	1260	1.87	2.12	5.56	74.59 ± 0.1	79.71 ± 0.1
Rd2	1260	1.19	1.42	5.68	65.22 ± 0.1	70.43 ± 0.1
Rd3	1260	1.77	2.19	5.87	61.15 ± 0.1	70.66 ± 0.1
Rd4	1260	1.96	2.25	6.25	43.76 ± 0.1	47.71 ± 0.1

e: standardised to 1g, measured in cgs-mode

II.I.2. Gamma-ray Data

sample	K [%]	U [ppm]	Th [ppm]
Rs1	7.23 ± 0.2	13.70 ± 0.7	48.80 ± 0.4
Rs2	7.10 ± 0.2	12.87 ± 0.4	49.83 ± 1.0
Rs3	7.43 ± 0.1	13.23 ± 0.5	50.40 ± 1.5
Rs4	7.20 ± 0.2	13.13 ± 0.7	49.18 ± 1.6
Rs5	6.60 ± 0.1	11.40 ± 0.7	45.57 ± 1.0
Rs6	6.77 ± 0.1	12.33 ± 0.5	49.57 ± 1.0
Rs7	6.53 ± 0.1	11.03 ± 0.8	47.90 ± 0.3
Rs8	6.97 ± 0.1	11.23 ± 0.1	51.57 ± 1.0
Rs9	8.18 ± 0.1	14.38 ± 0.5	55.08 ± 1.4
Rs10	7.23 ± 0.2	10.63 ± 0.4	48.93 ± 1.1
Rs11	6.83 ± 0.1	12.53 ± 0.3	46.43 ± 0.9
Rs12	7.23 ± 0.2	12.07 ± 0.3	49.70 ± 1.3
Rs13	6.43 ± 0.1	11.17 ± 0.5	44.83 ± 0.4
Rs14	7.90 ± 0.1	12.50 ± 0.9	52.80 ± 1.3
Rs15	7.87 ± 0.1	14.30 ± 0.8	55.40 ± 0.7
Rs16	6.87± 0.1	12.23 ± 0.9	46.50 ± 1.7
Rd1	7.17 ± 0.1	12.13 ± 0.4	56.07 ± 0.6
Rd2	7.50 ± 0.3	13.93 ± 0.6	57.53 ± 1.0
Rd3	8.20 ± 0.1	13.77 ± 1.3	64.40 ± 2.0
Rd4	8.33 ± 0.1	14.53 ± 0.5	62.40 ± 0.9

III. Appendix III: Plots for Standard Outcrops

III.A. Punte Nere

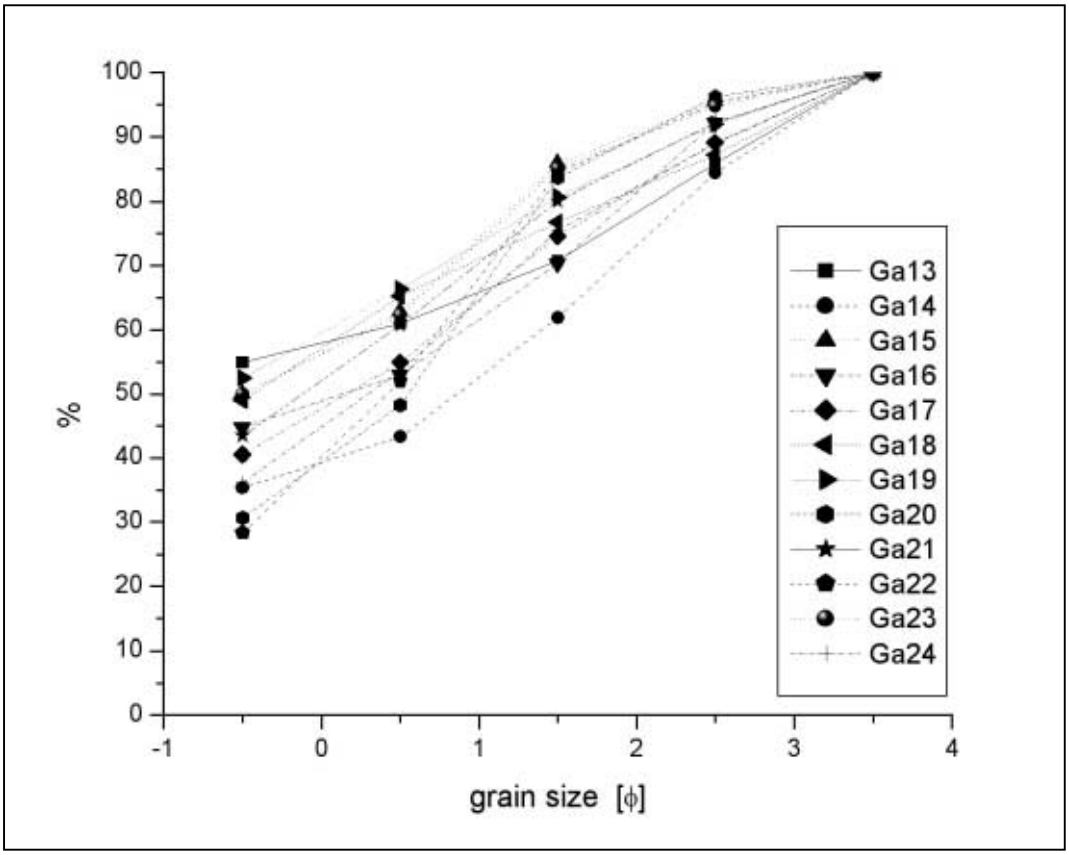

Figure III.1: Cumulative grain size curve for the deposits of the channel (upper part of outcrop G).

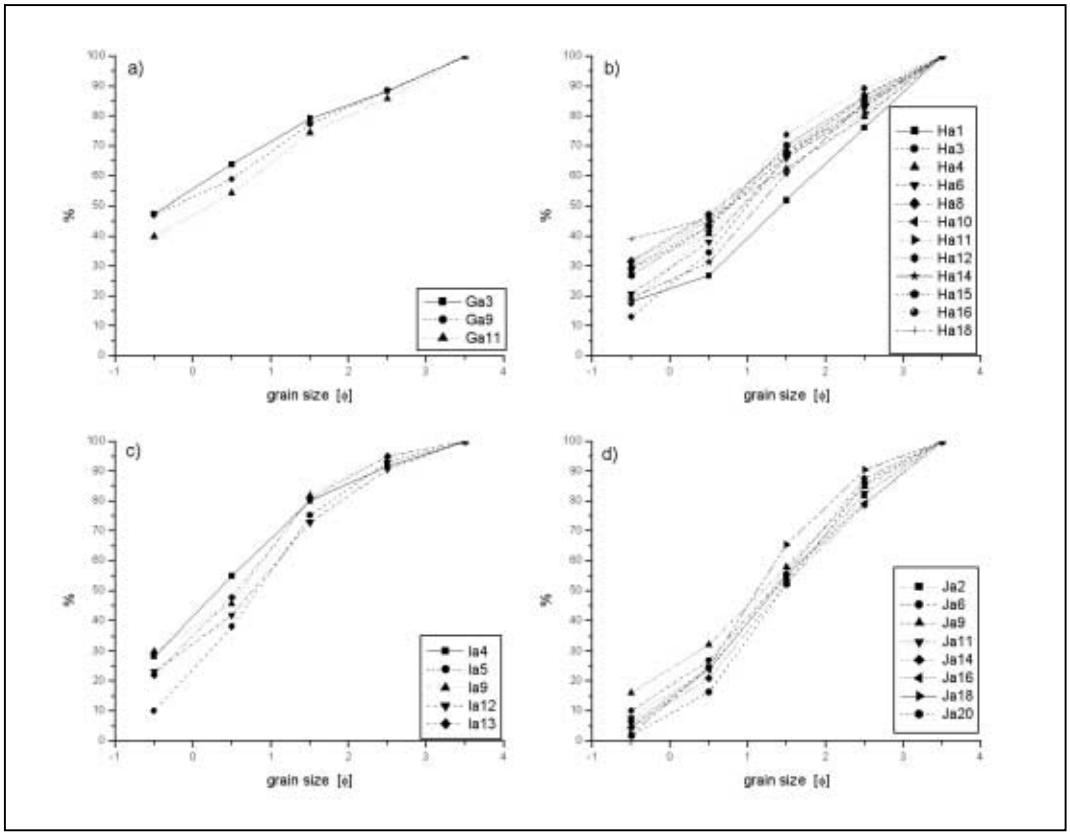

Figure III.2: Cumulative grain size curve for laminated deposits of Punte Nere. a) outcrop G, b) outcrop H, c) outcrop I, and d) outcrop J.

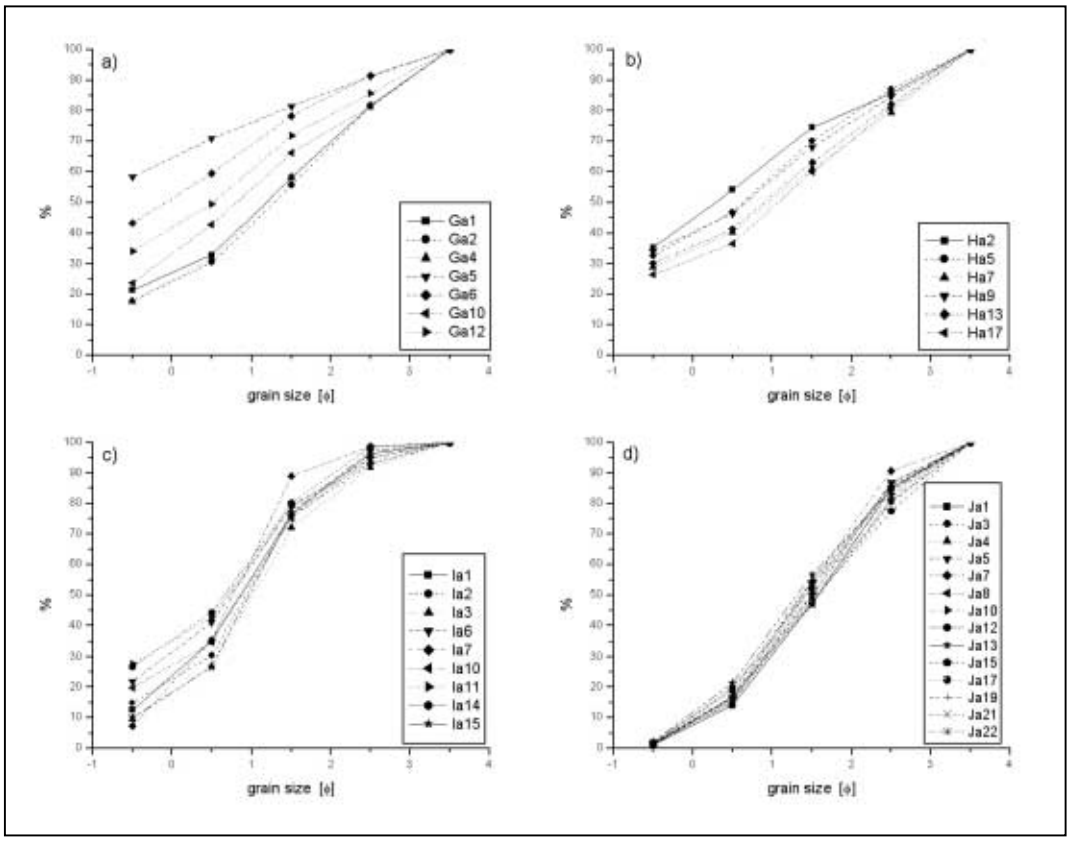

Figure III.3: Cumulative grain size curve for massive deposits of Punte Nere. a) outcrop G, b) outcrop H, c) outcrop I, and d) outcrop J.

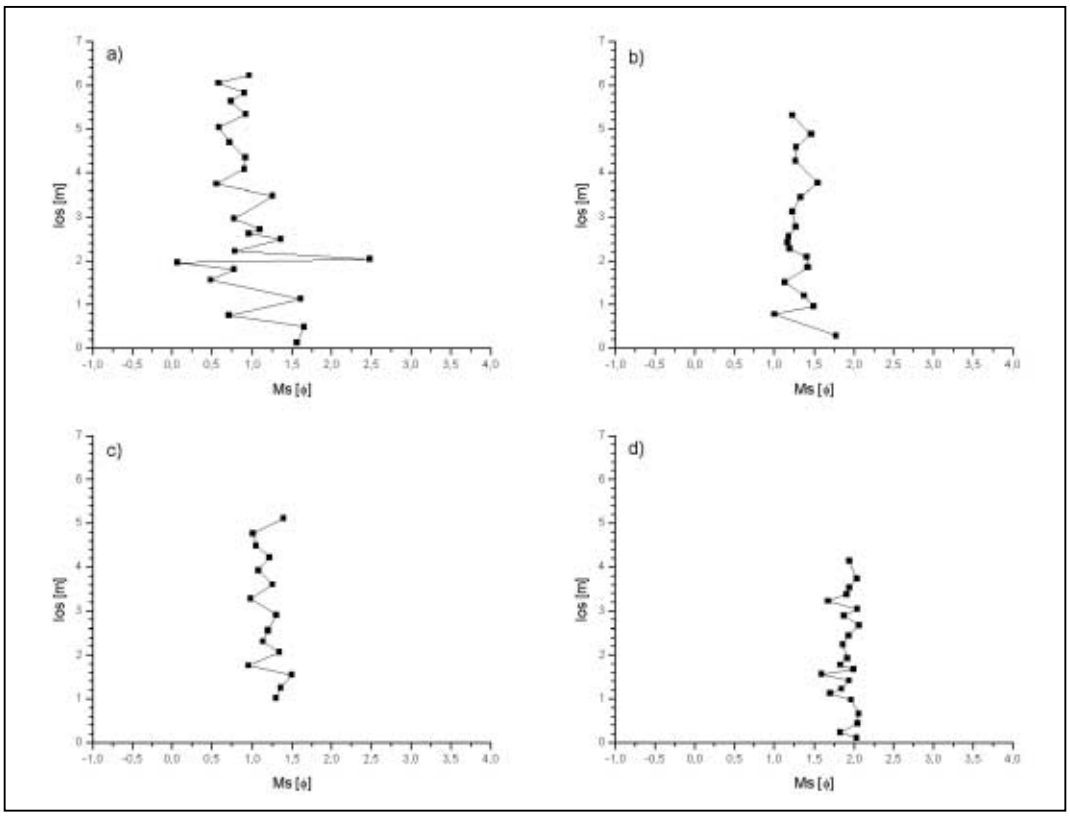

Figure III.4: los vs. Ms [ϕ] for Punte Nere; a) outcrop G, b) outcrop H, c) outcrop I, and d) outcrop J.

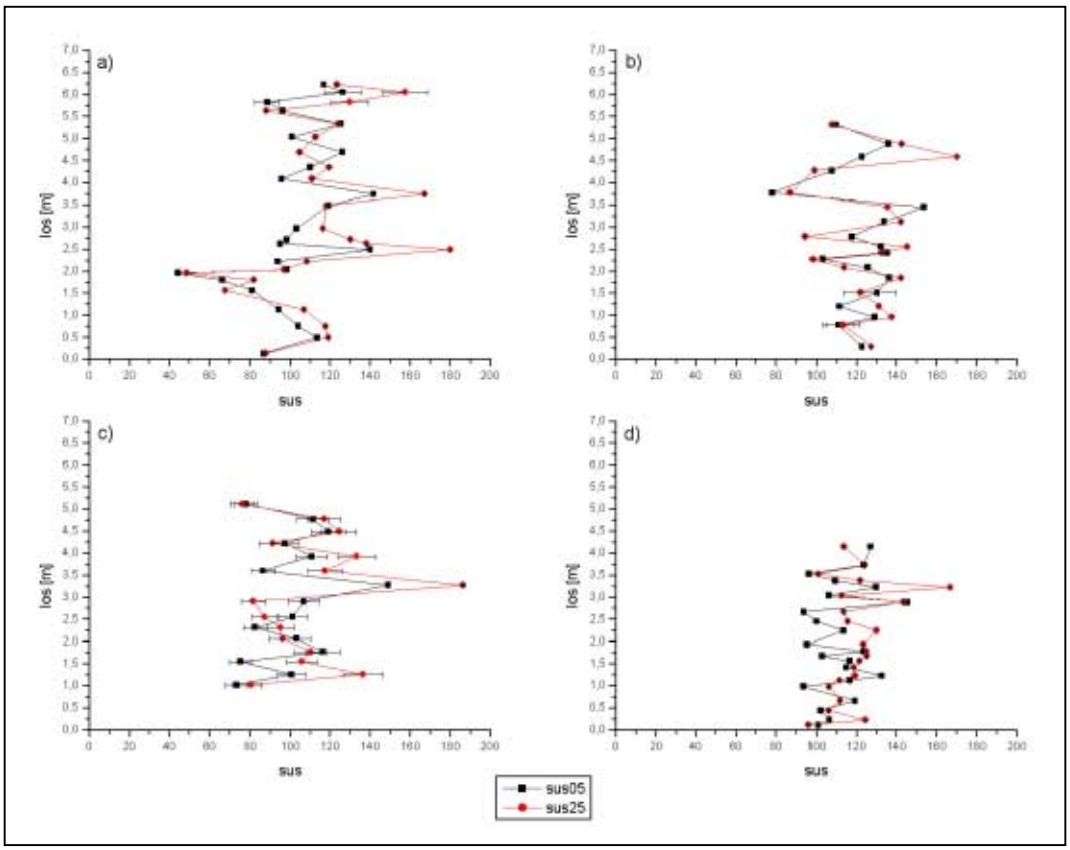

Figure III.5: los vs. sus05 and sus25 (measured in cgs-mode, standardised to 1g, extension 10-6) for Punte Nere; a) outcrop G, b) outcrop H, c) outcrop I, and d) outcrop J.

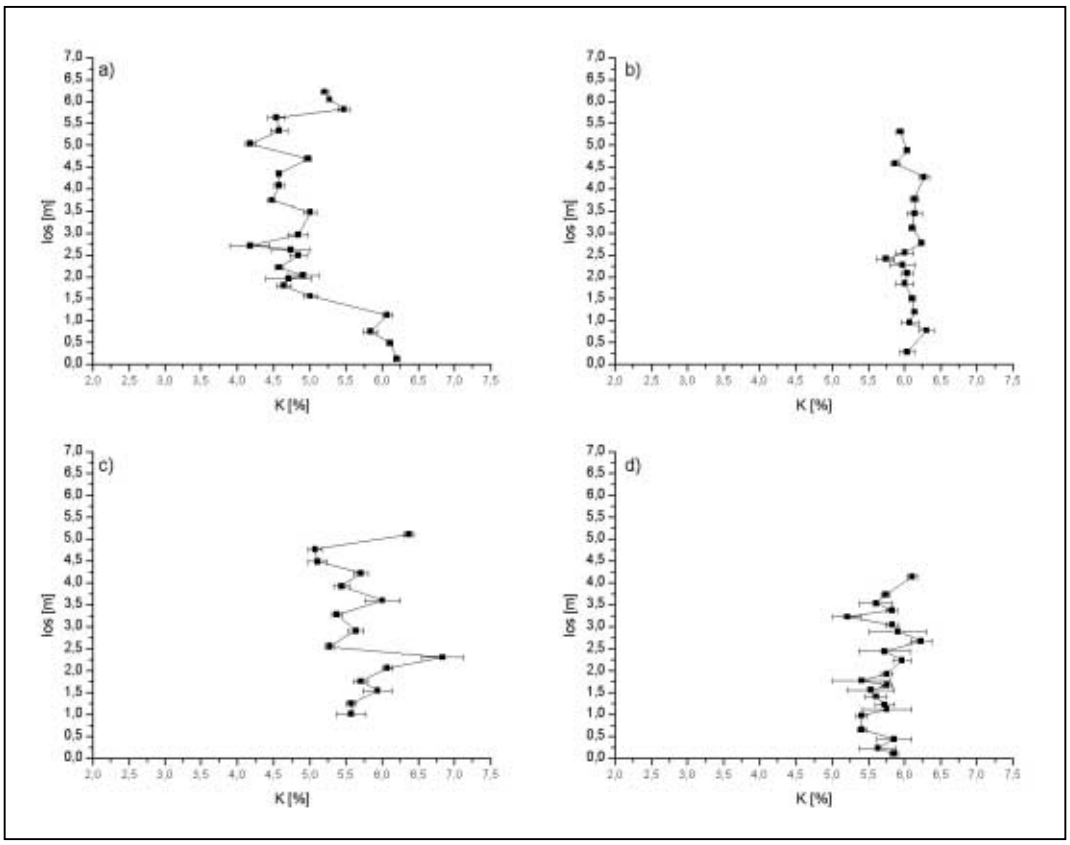

Figure III.6: los. vs. K [%] for Punte Nere; a) outcrop G, b) outcrop H, c) outcrop I, and d) outcrop J.

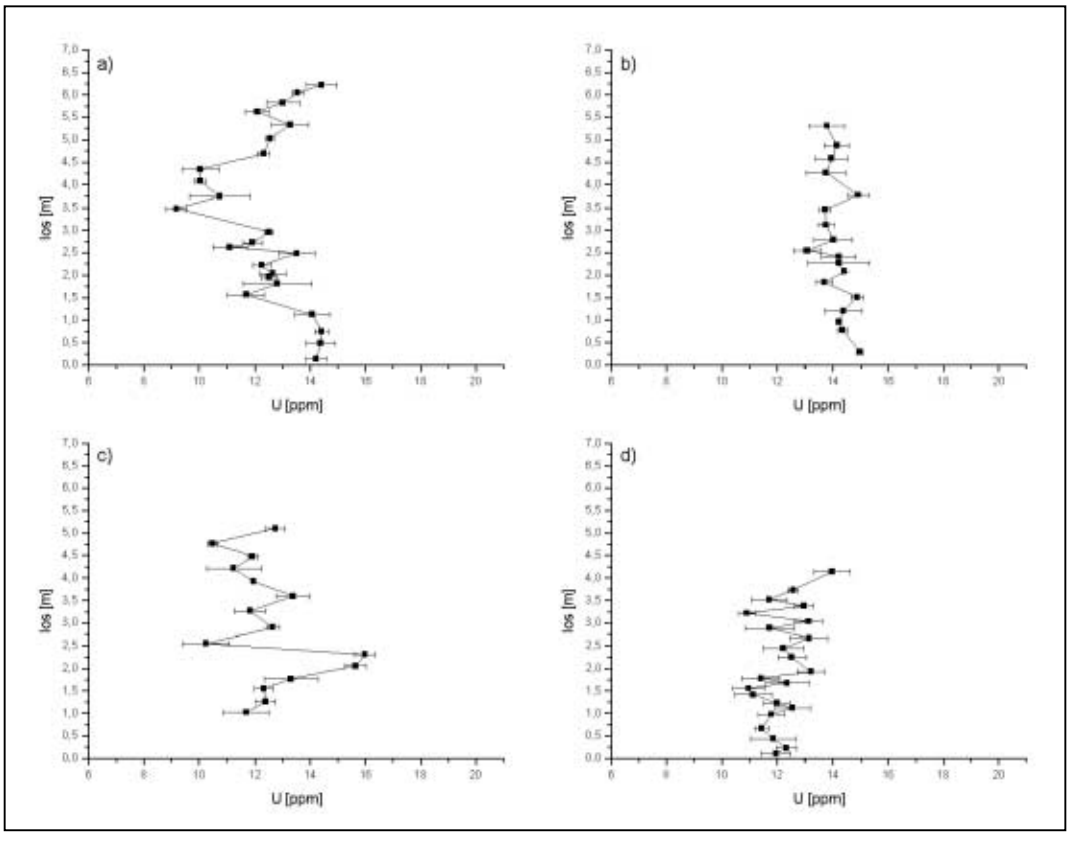

Figure III.7: los vs. U [ppm] for Punte Nere; a) outcrop G, b) outcrop H, c) outcrop I, and d) outcrop J.

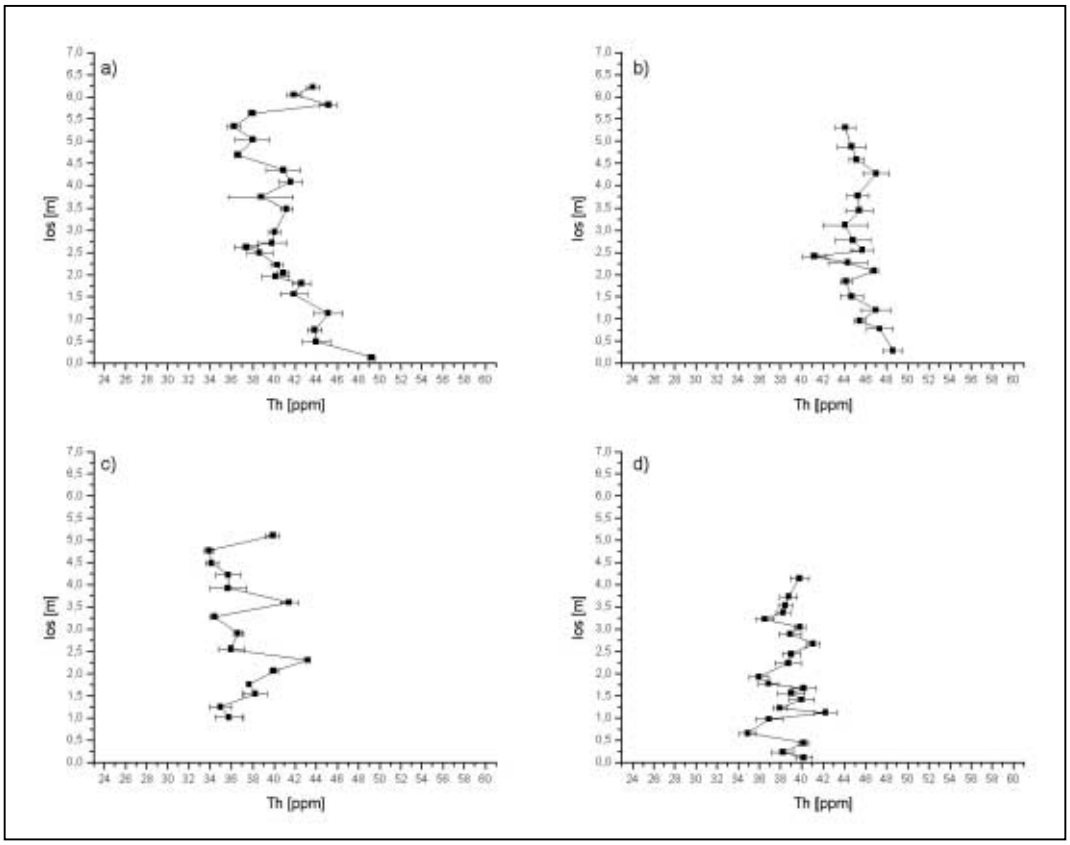

Figure III.8: los vs. Th [ppm] for Punte Nere; a) outcrop G, b) outcrop H, c) outcrop I, and d) outcrop J.

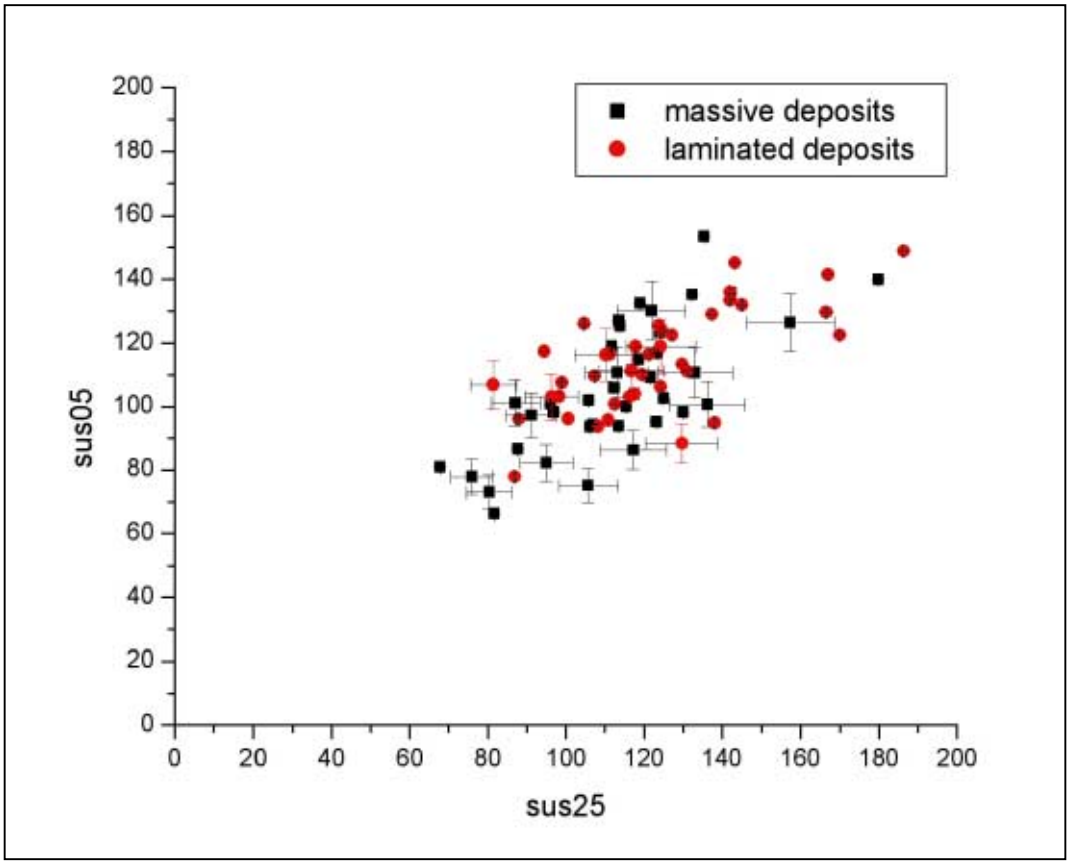

Figure III.9: sus05 vs. sus25 (measured in cgs-mode, standardised to 1g, extension 10-6) for Punte Nere, split up into laminated and massive deposits.

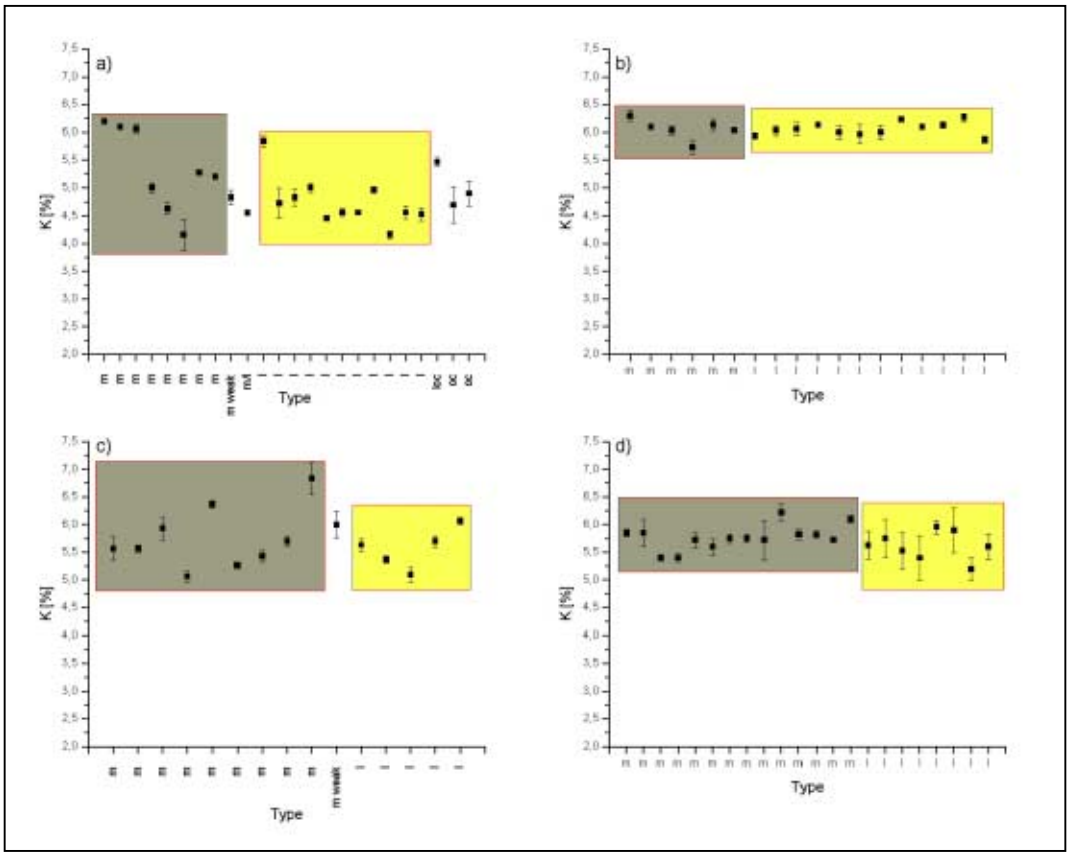

Figure III.10: Plot of K [%] for Punte Nere showing the influence of laminated (l), massive (m), and ochre (oc) deposits; a) outcrop G, b) outcrop H, c) outcrop I, and d) outcrop J.

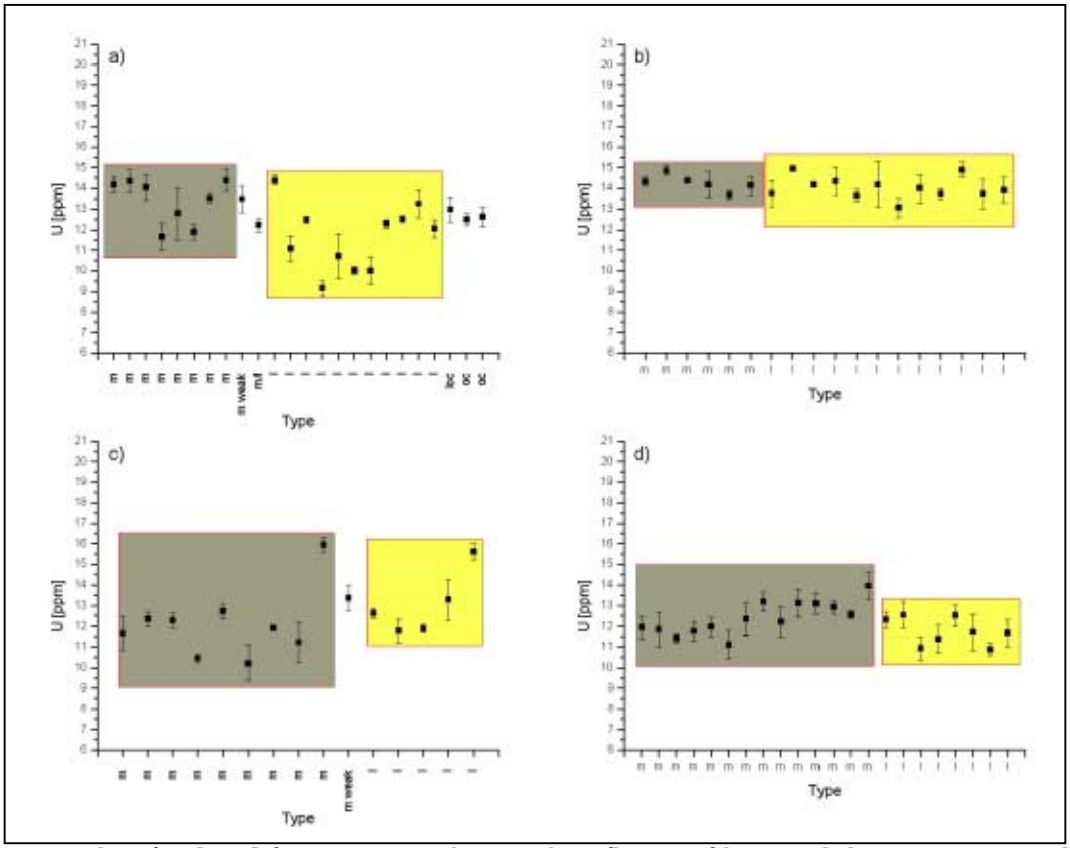

Figure III.11: Plot of U [ppm] for Punte Nere showing the influence of laminated (l), massive (m), and ochre (oc) deposits; a) outcrop G, b) outcrop H, c) outcrop I, and d) outcrop J.

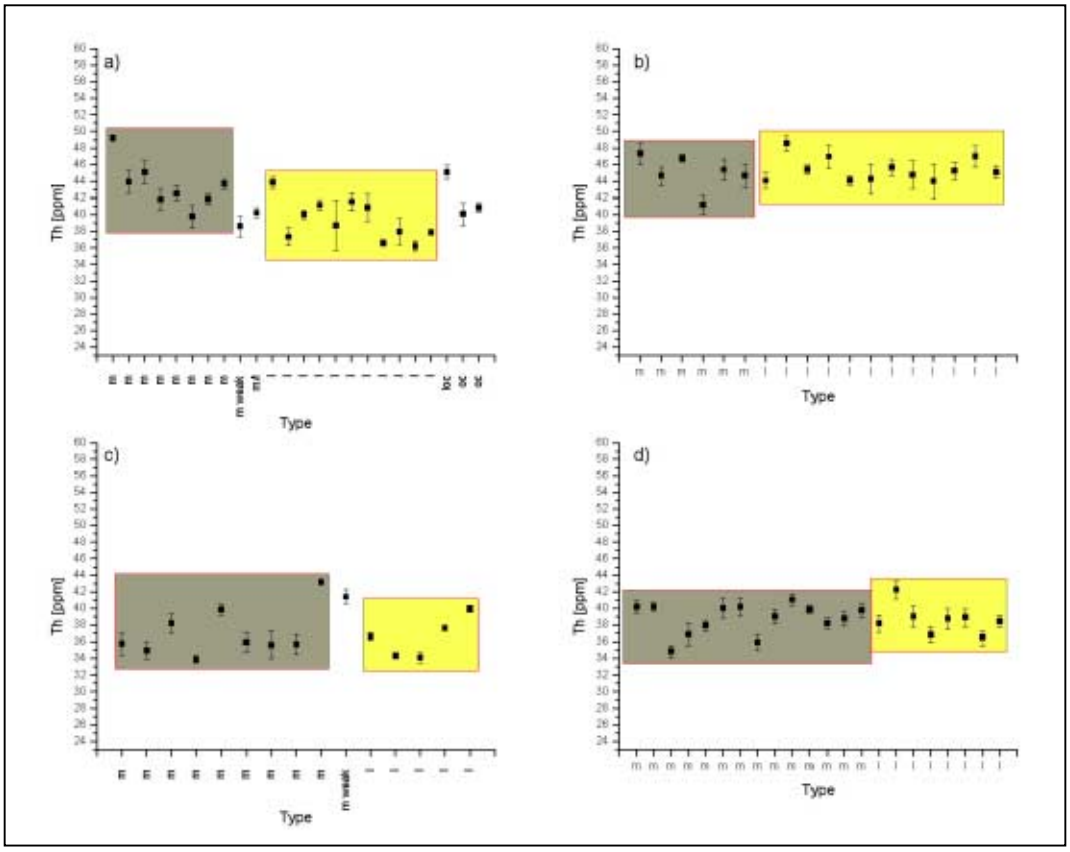

Figure III.12: Plot of Th [ppm] for Punte Nere showing the influence of laminated (l), massive (m), and ochre (oc) deposits; a) outcrop G, b) outcrop H, c) outcrop I, and d) outcrop J.

III.B. Tufi Varicolori

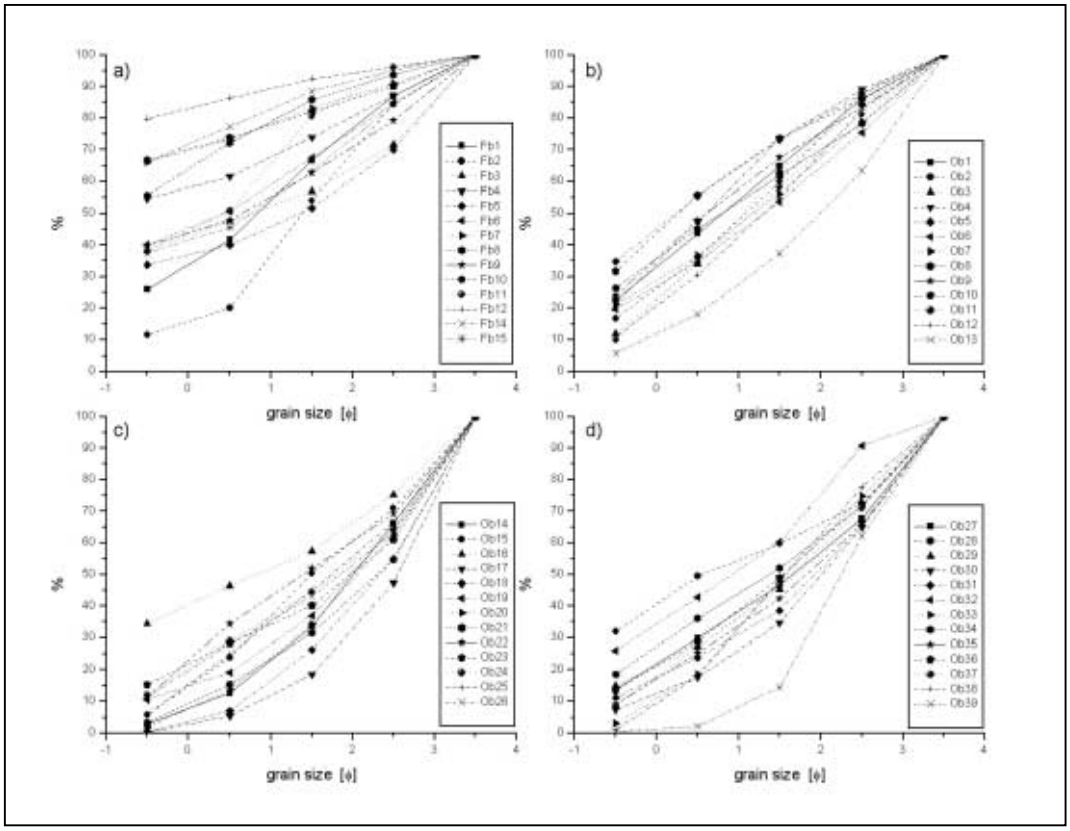

Figure III.13: Cumulative grain size curves for Tufi Varicolori. a) outcrop F, b) to d) outcrop O.

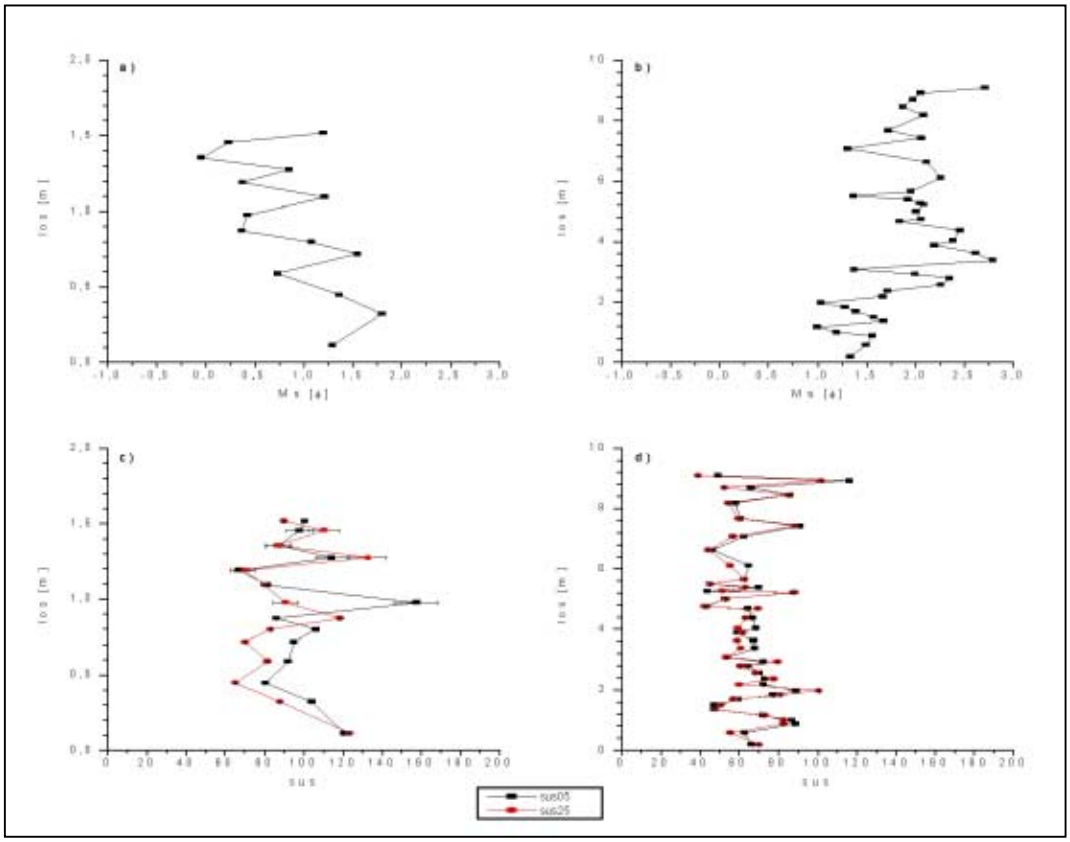

Figure III.14: los vs. Ms [ϕ] and sus for Tufi Varicolori. a) los vs. Ms for outcrop F; b) los vs. Ms for outcrop O; c) los vs. sus05 and sus25 for outcrop F; d) los vs. sus05 and sus25 for outcrop O.

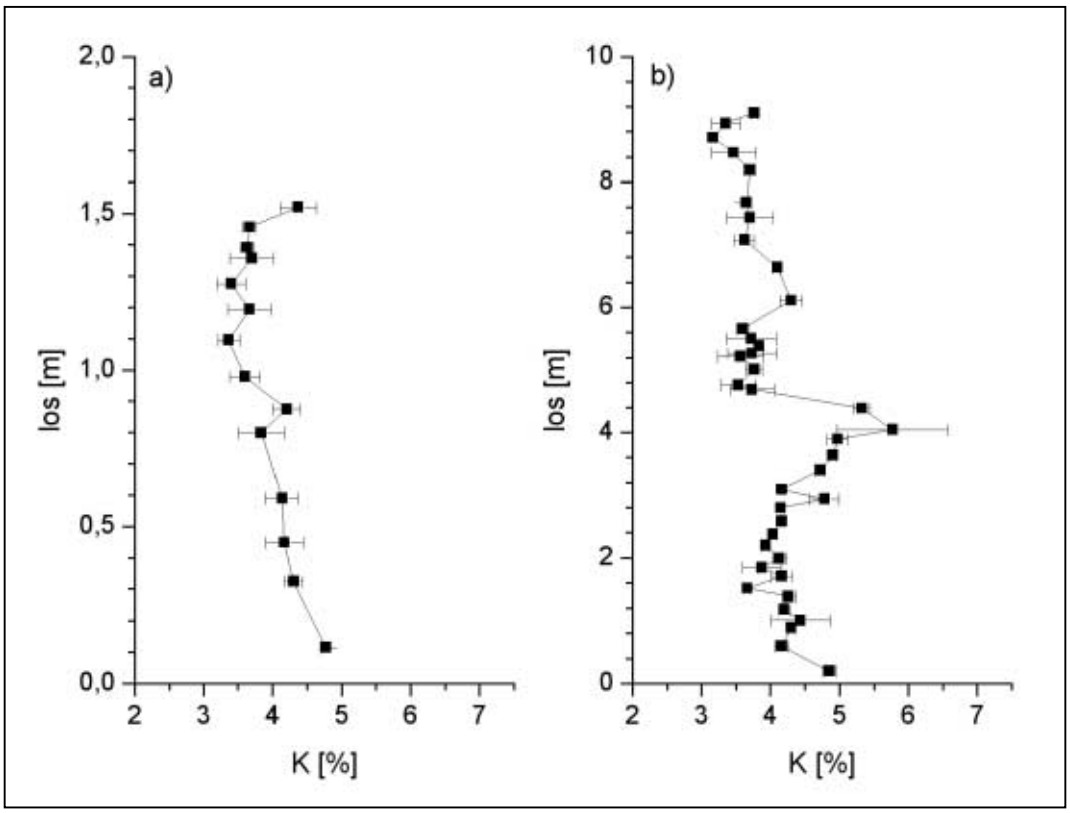

Figure III.15: los vs. K [%] for Tufi Varicolori; a) outcrop F; b) outcrop O.

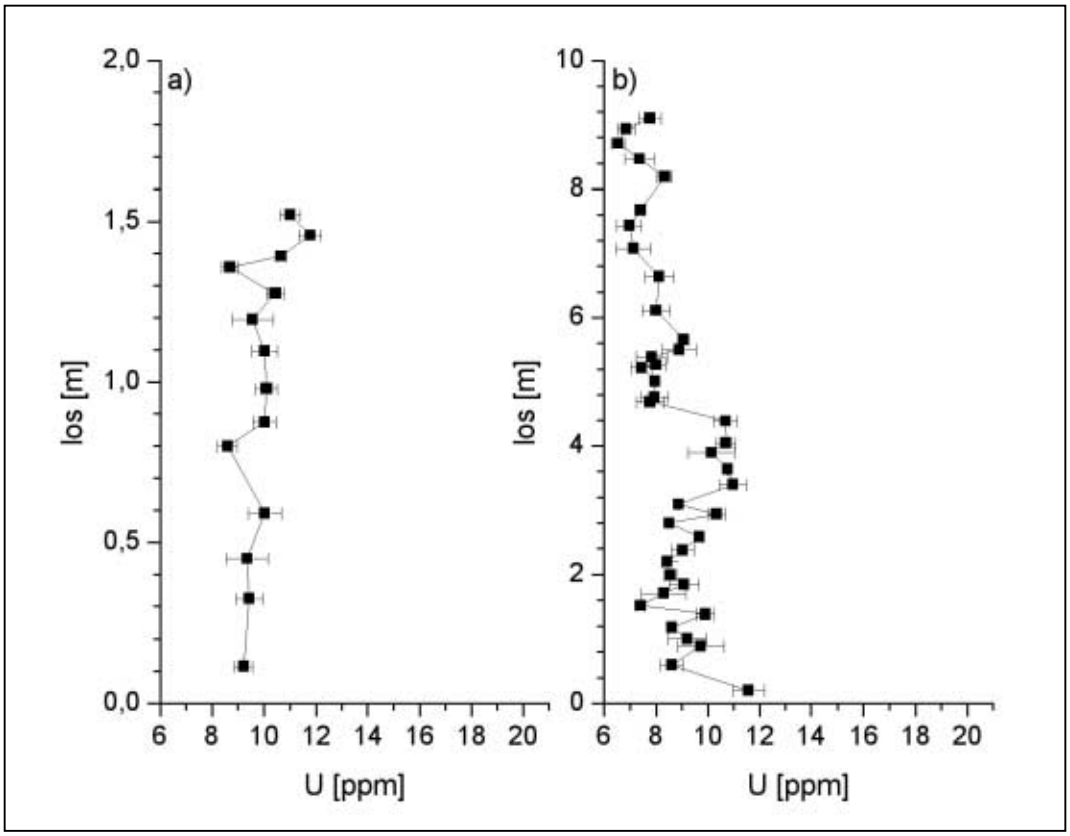

Figure III.16: los vs. U [ppm] for Tufi Varicolori; a) outcrop F; b) outcrop O.

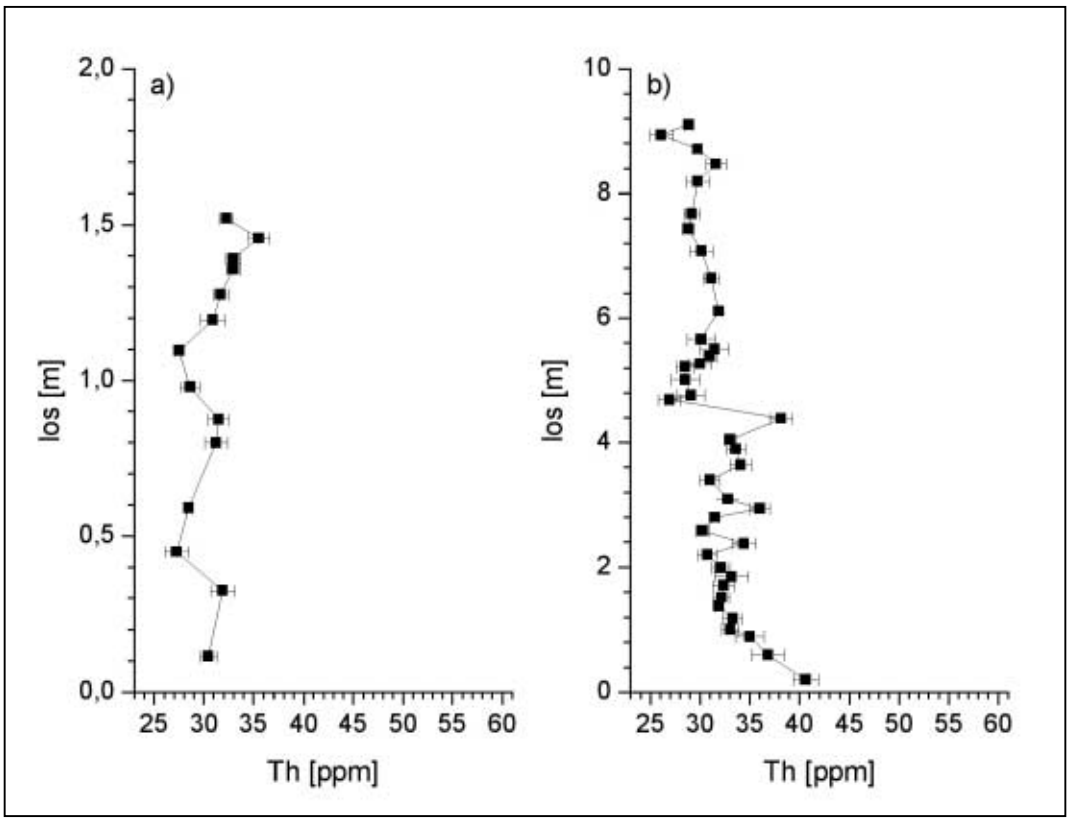

Figure III.17: los vs. Th [ppm] for Tufi Varicolori. a) outcrop F; b) outcrop O.

III.C. Palizzi

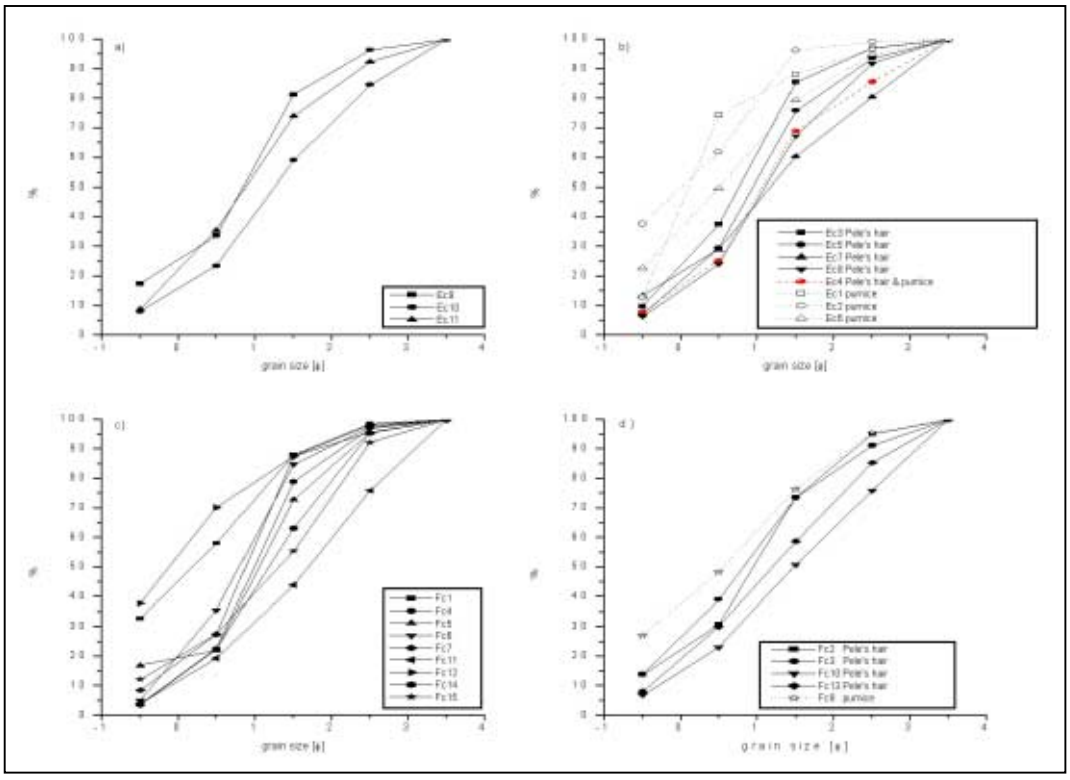

Figure III.18: Cumulative grain size curves for Palizzi. a) outcrop E without any marks, b) outcrop E containing Pele's hair or pumice, c) outcrop F without any marks, d) outcrop F containing Pele's hair or pumice.

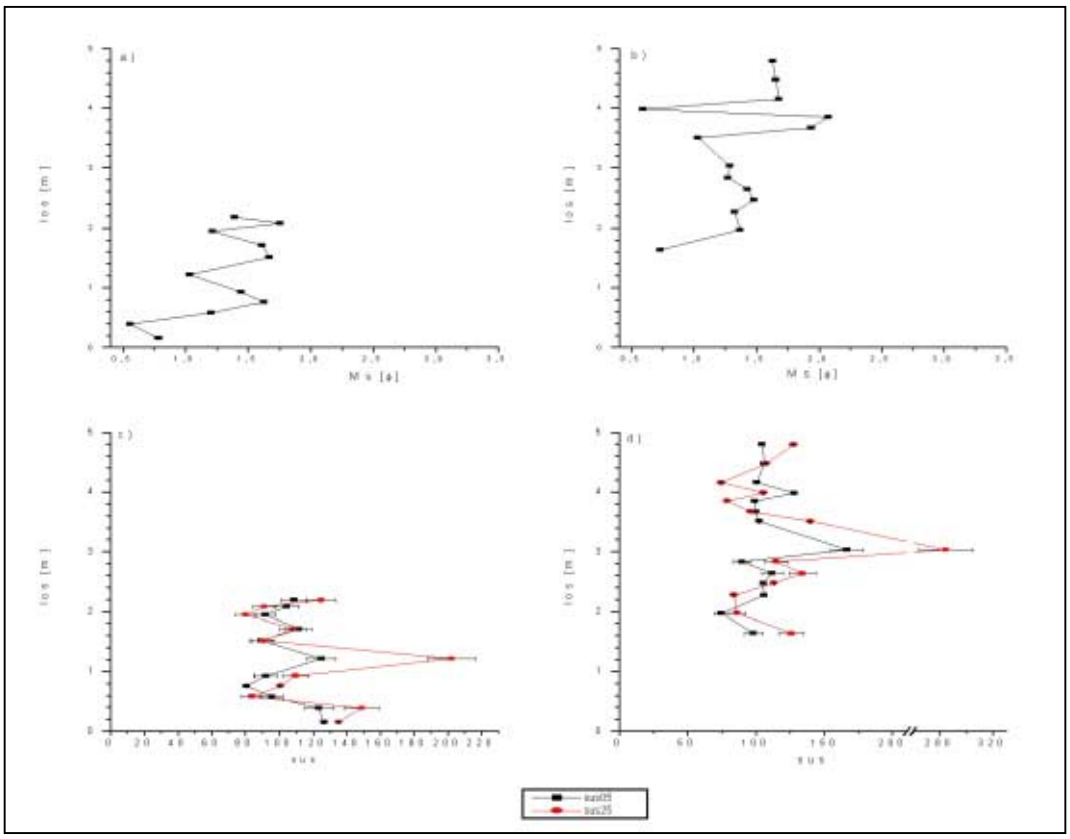

Figure III.19: los vs. Ms [ϕ] and sus for Palizzi. a) los vs. Ms for outcrop E; b) los vs. Ms for outcrop F; c) los vs. sus05 and sus25 for outcrop E; d) los vs. sus05 and sus25 for outcrop F.

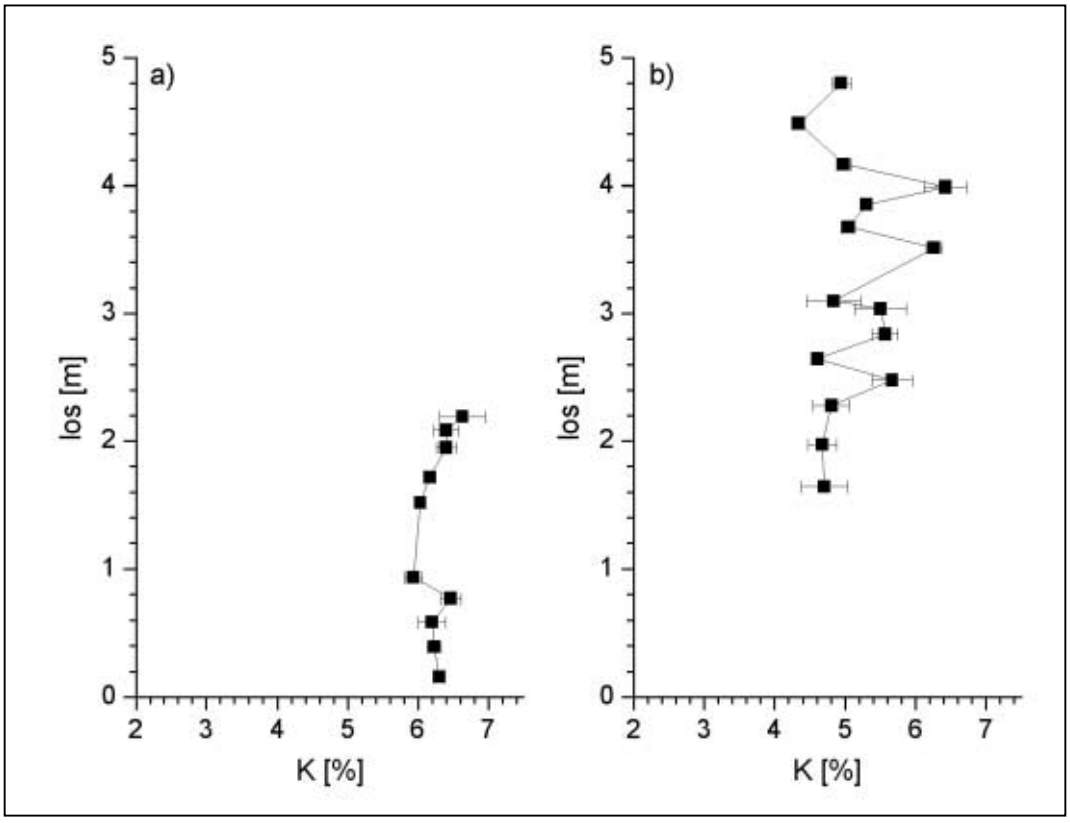

Figure III.20: los vs. K [%] for Palizzi; a) outcrop E; b) outcrop F.

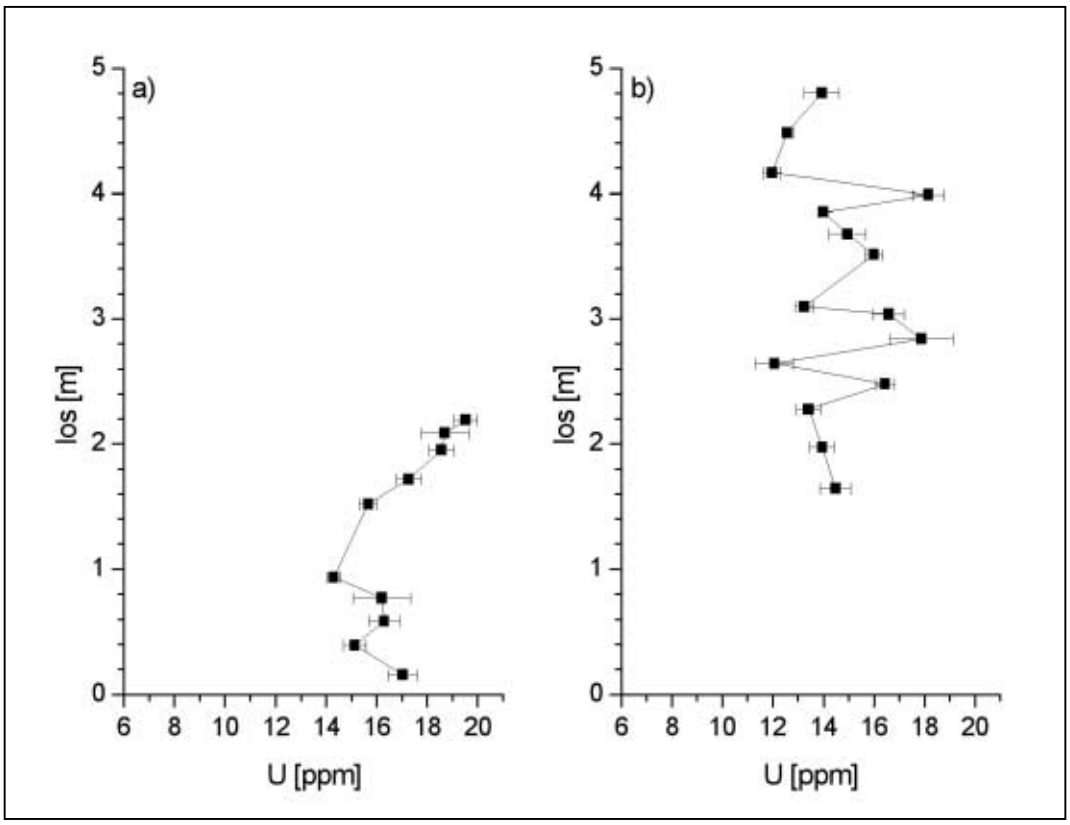

Figure III.21: los vs. U [ppm] for Palizzi; a) outcrop E; b) outcrop F.

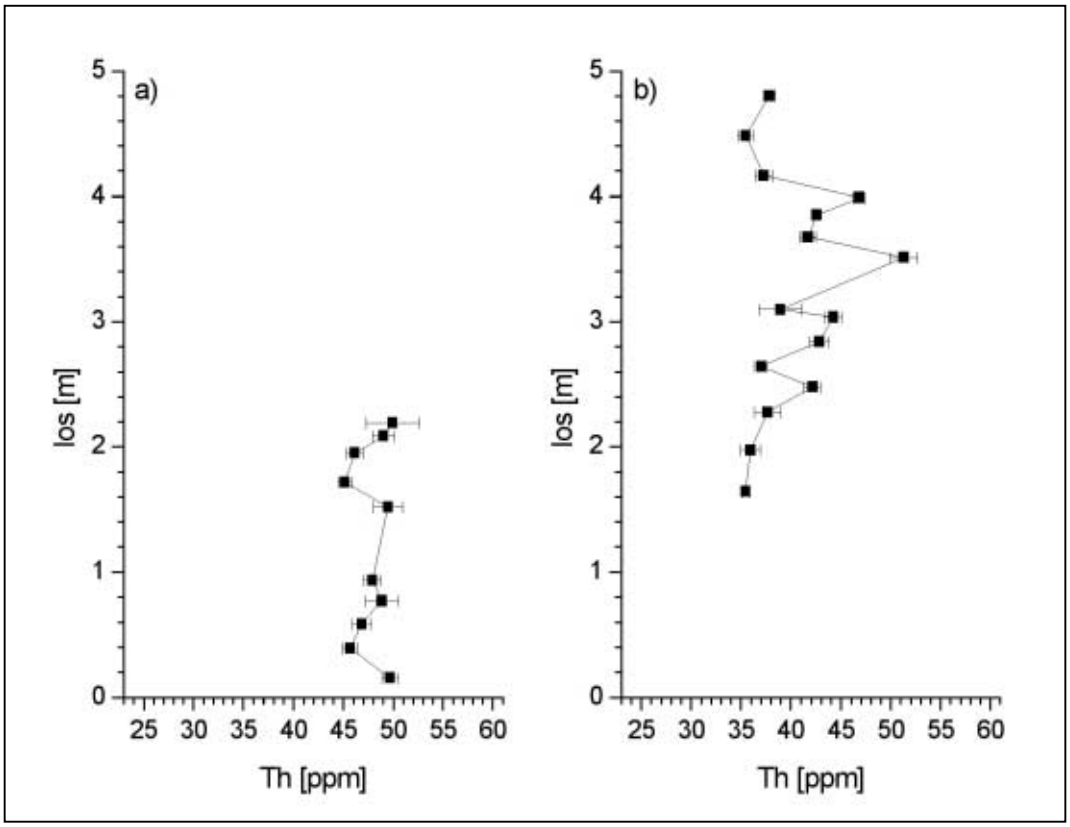

Figure III.22: los vs. Th [ppm] for Palizzi. a) outcrop E; b) outcrop F.

III.D. Commenda

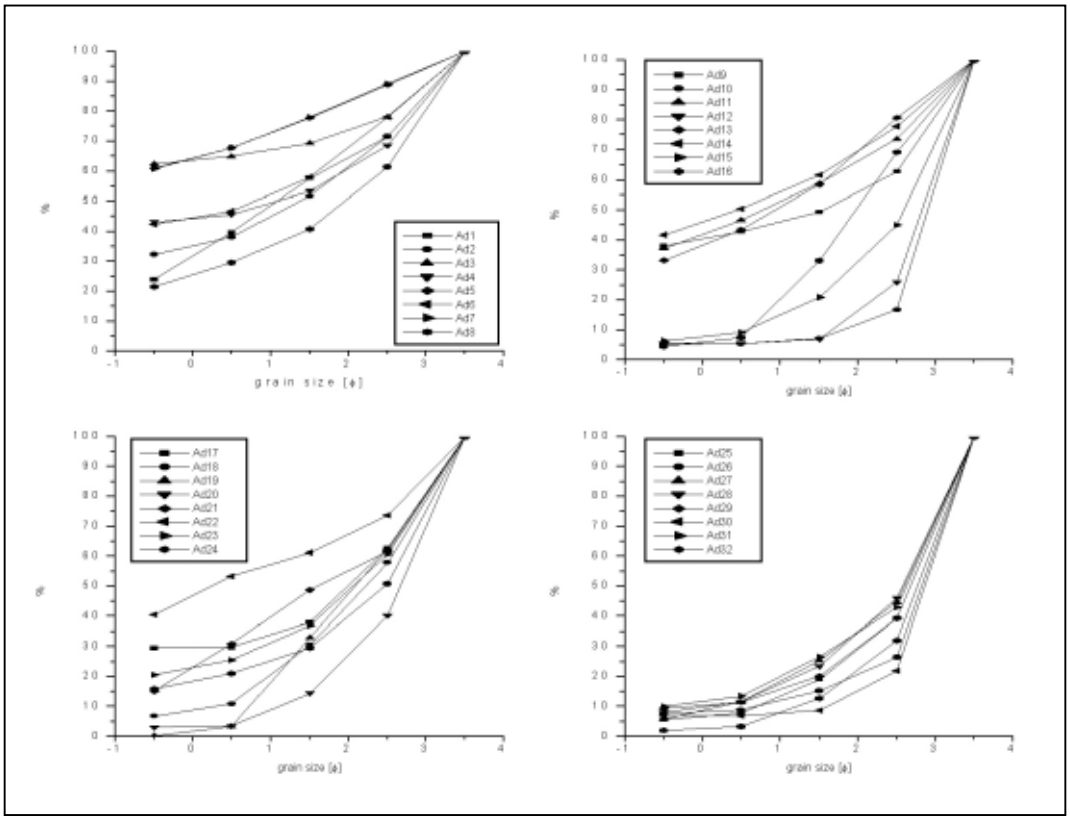

Figure III.23: Cumulative grain size curves for parts of outcrop A (Commenda).

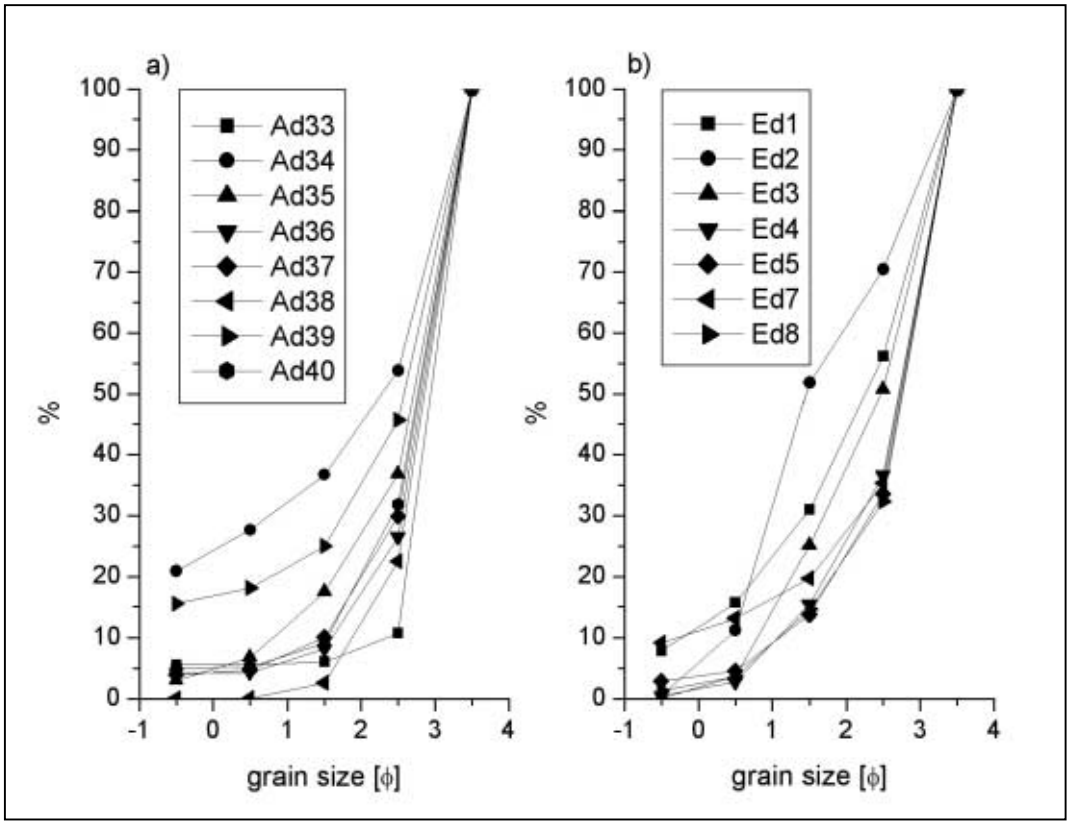

Figure III.24: Cumulative grain size curves for Commenda. a) parts of outcrop A, b) outcrop E.

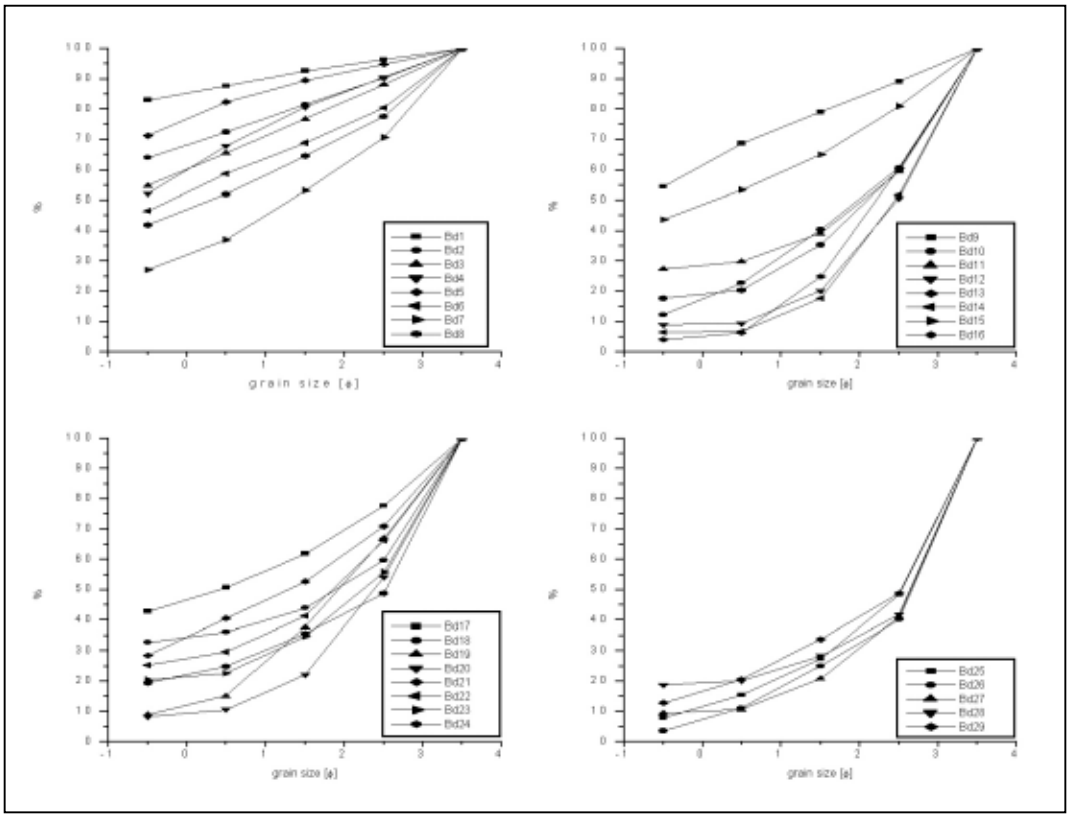

Figure III.25: Cumulative grain size curves of outcrop B (Commenda).

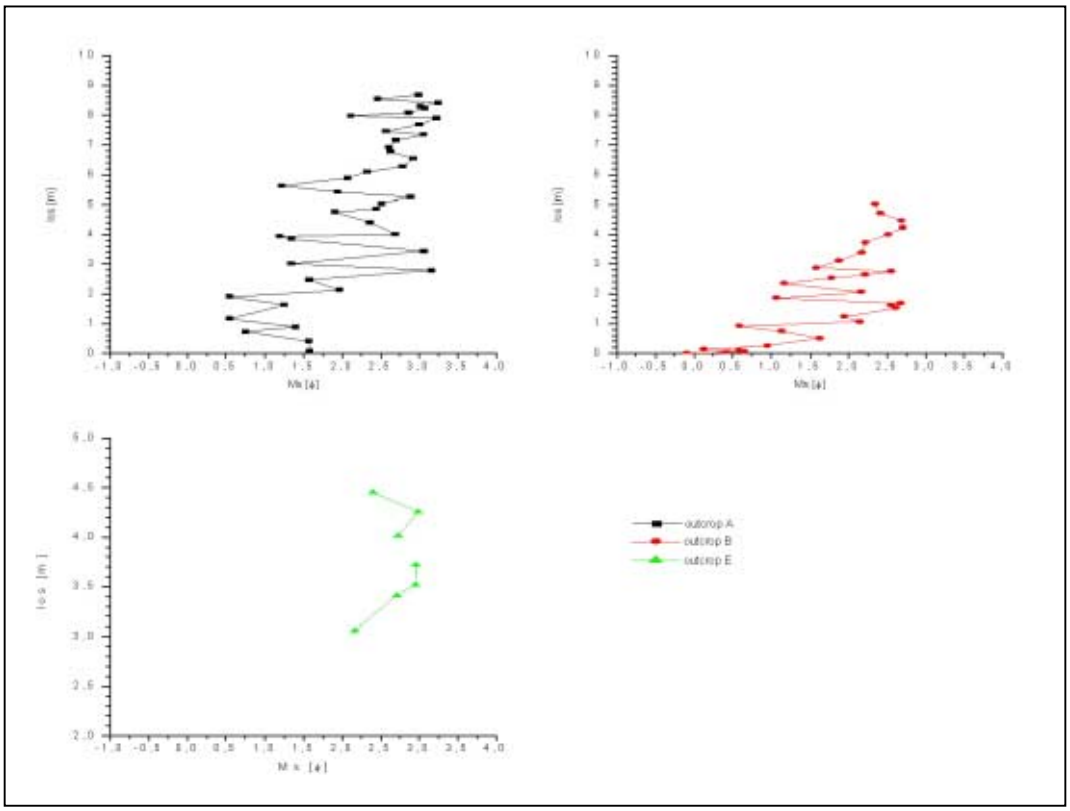

Figure III.26: los vs. Ms [ϕ] for Commenda.

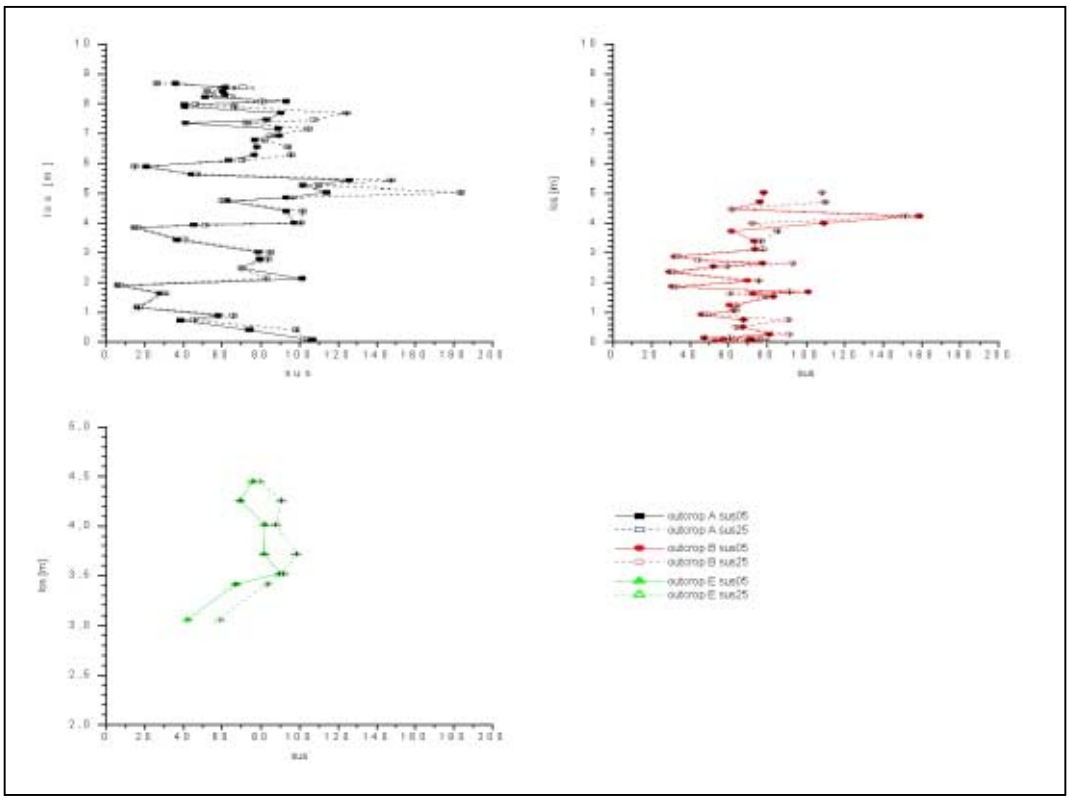

Figure III.27: los vs. sus for Commenda.

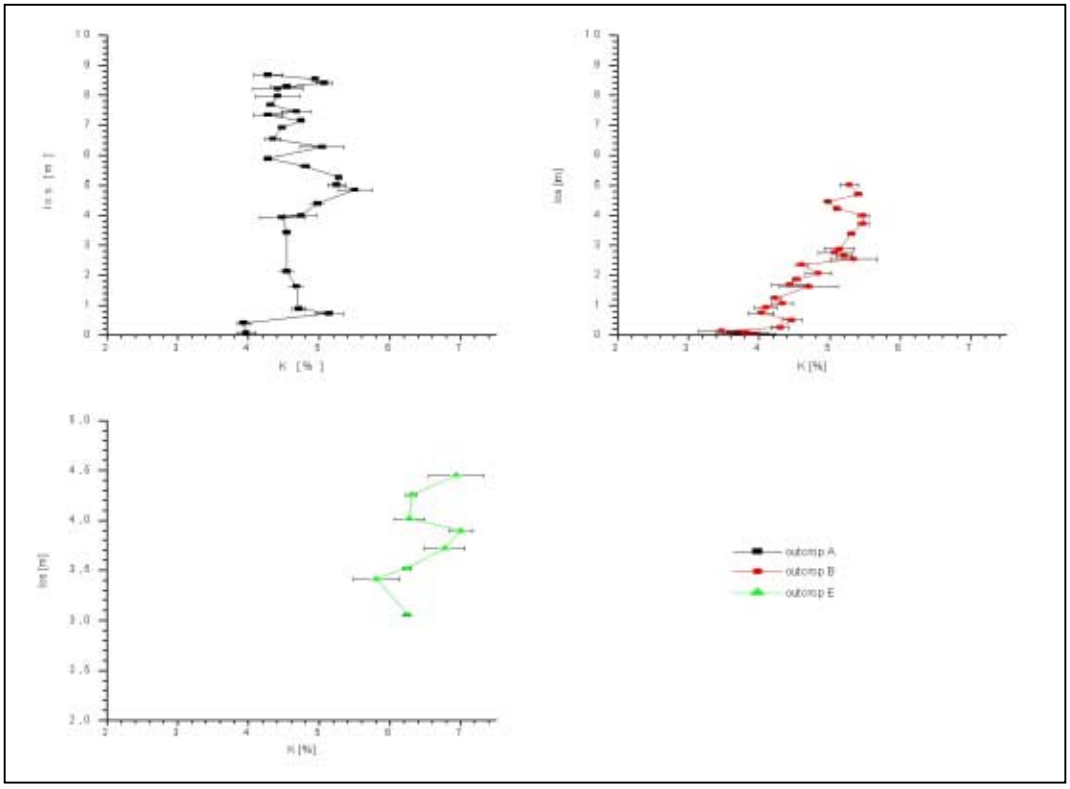

Figure III.28: los vs. K [%] for Commenda.

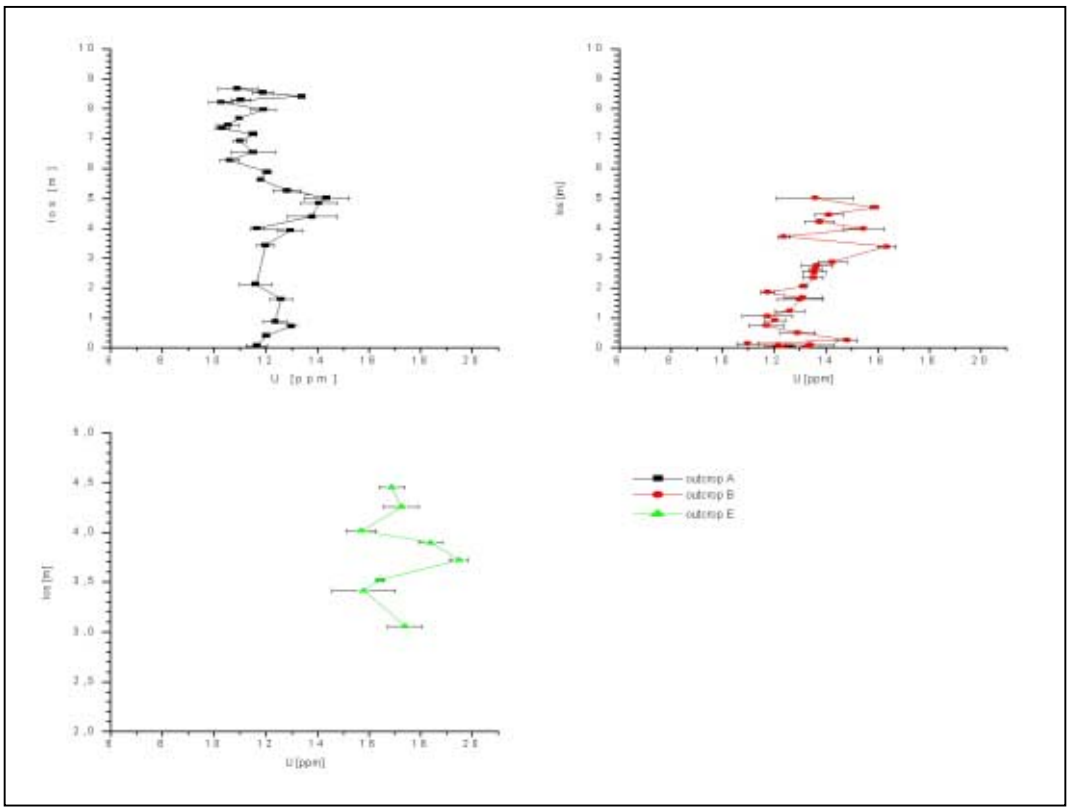

Figure III.29: los vs. U [ppm] for Commenda.

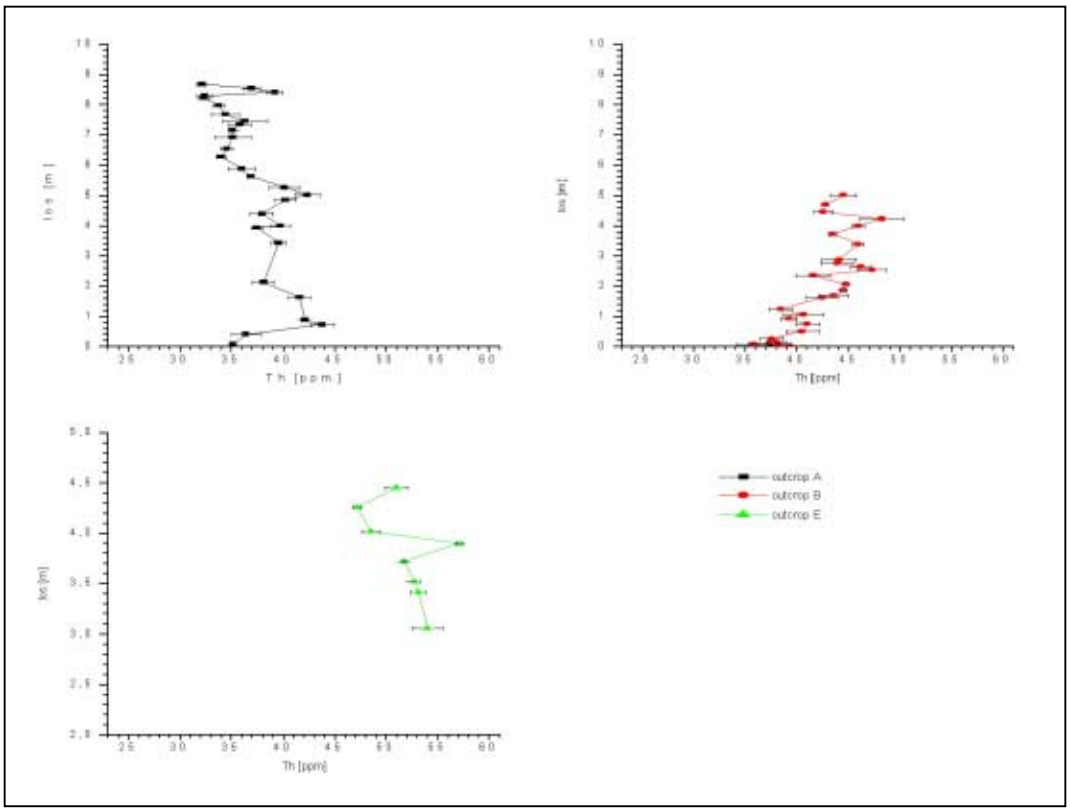

Figure III.30: los vs. Th [ppm] for Commenda.

III.E. Cratere Attuale

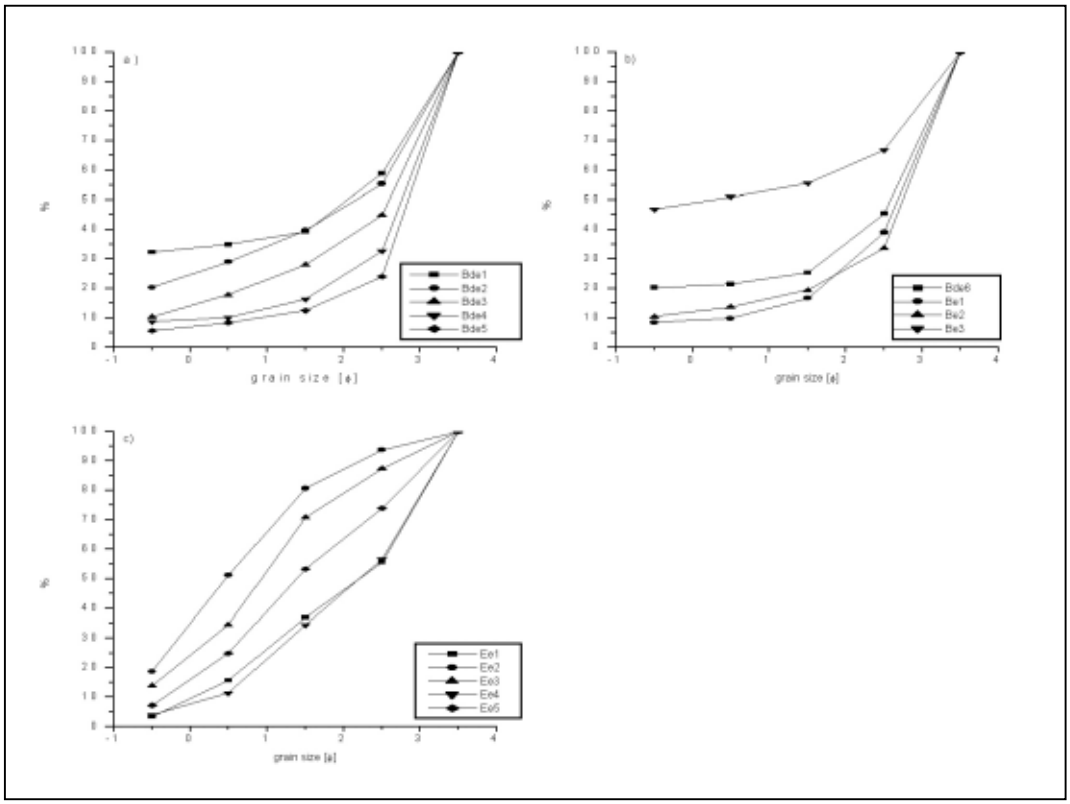

Figure III.31: Cumulative grain size curves for Crater Attuale. a) outcrop B, b) outcrop B, c) outcrop E.

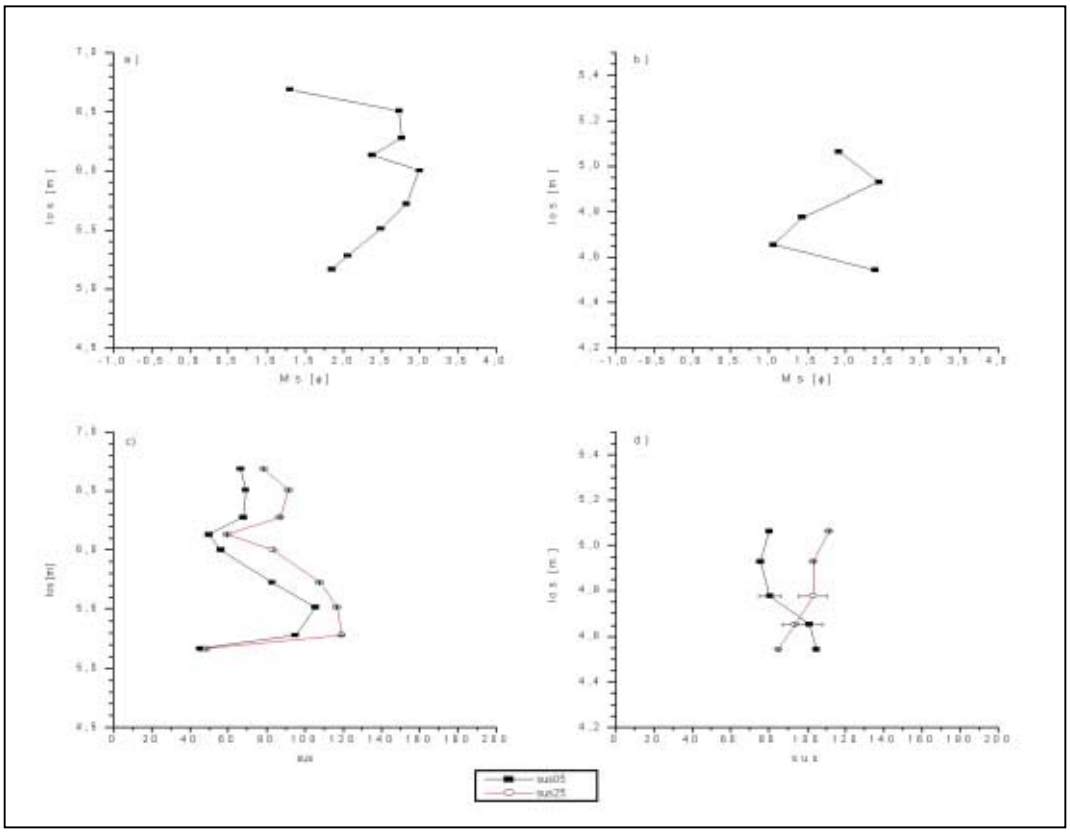

Figure III.32: los vs. Ms [ϕ] and sus for Cratere Attuale. a) los vs. Ms for outcrop B; b) los vs. Ms for outcrop E; c) los vs. sus05 and sus25 for outcrop B; d) los vs. sus05 and sus25 for outcrop E.

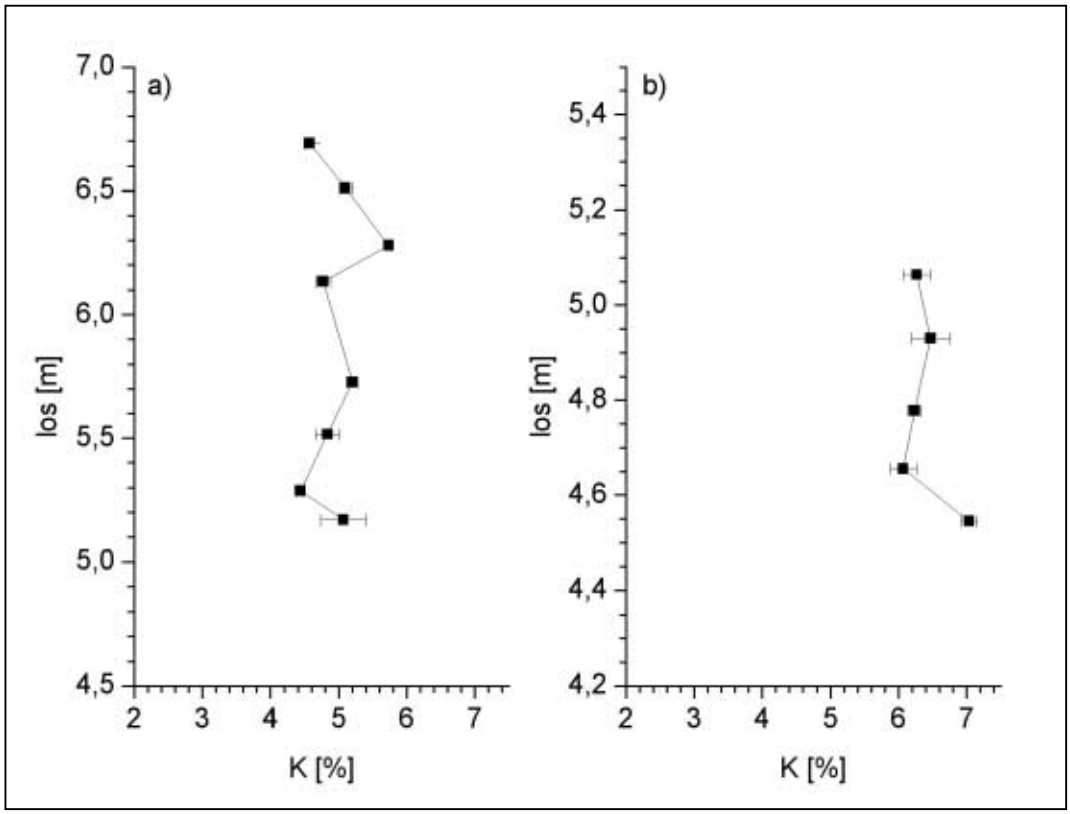

Figure III.33: los vs. K [%] for Cratere Attuale; a) outcrop B; b) outcrop E.

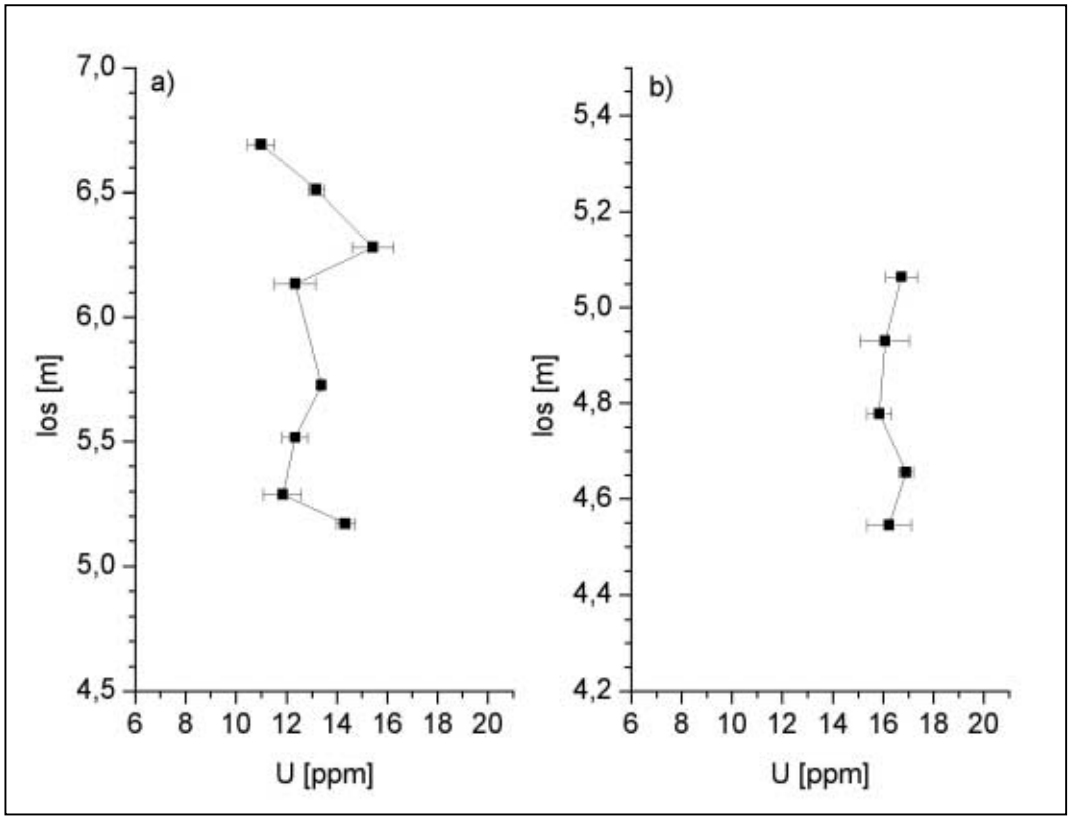

Figure III.34: los vs. U [ppm] for Cratere Attuale; a) outcrop B; b) outcrop E.

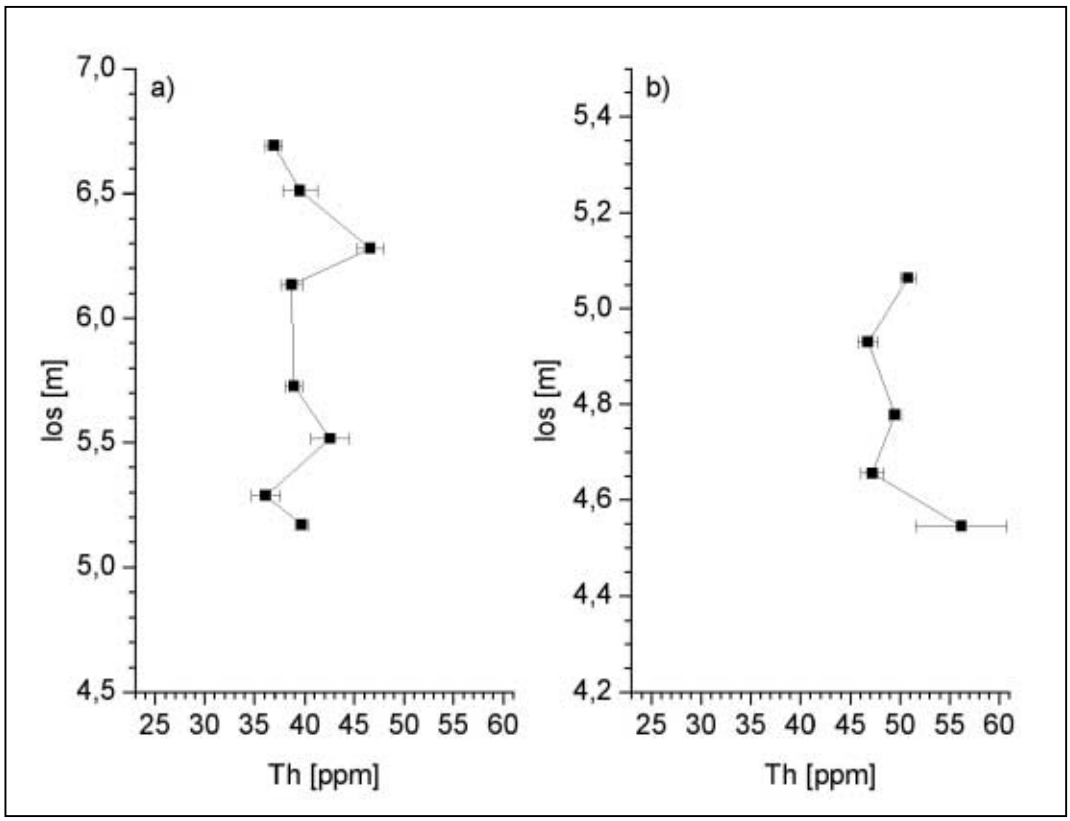

Figure III.35: los vs. Th [ppm] for Cratere Attuale. a) outcrop B; b) outcrop E.

III.F. Granulometric Plots for all Successions

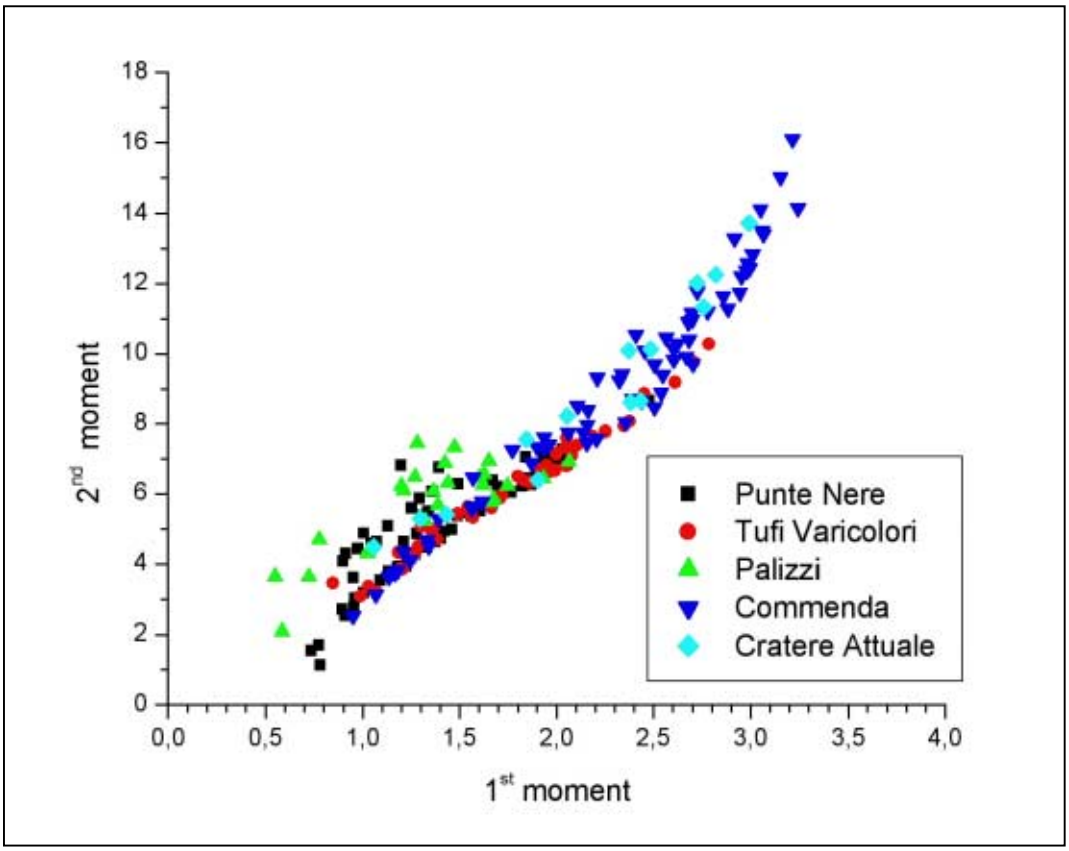

Figure III.36: 1st vs. 2nd moment for all successions.

III.G. Susceptibility Plots for all Successions

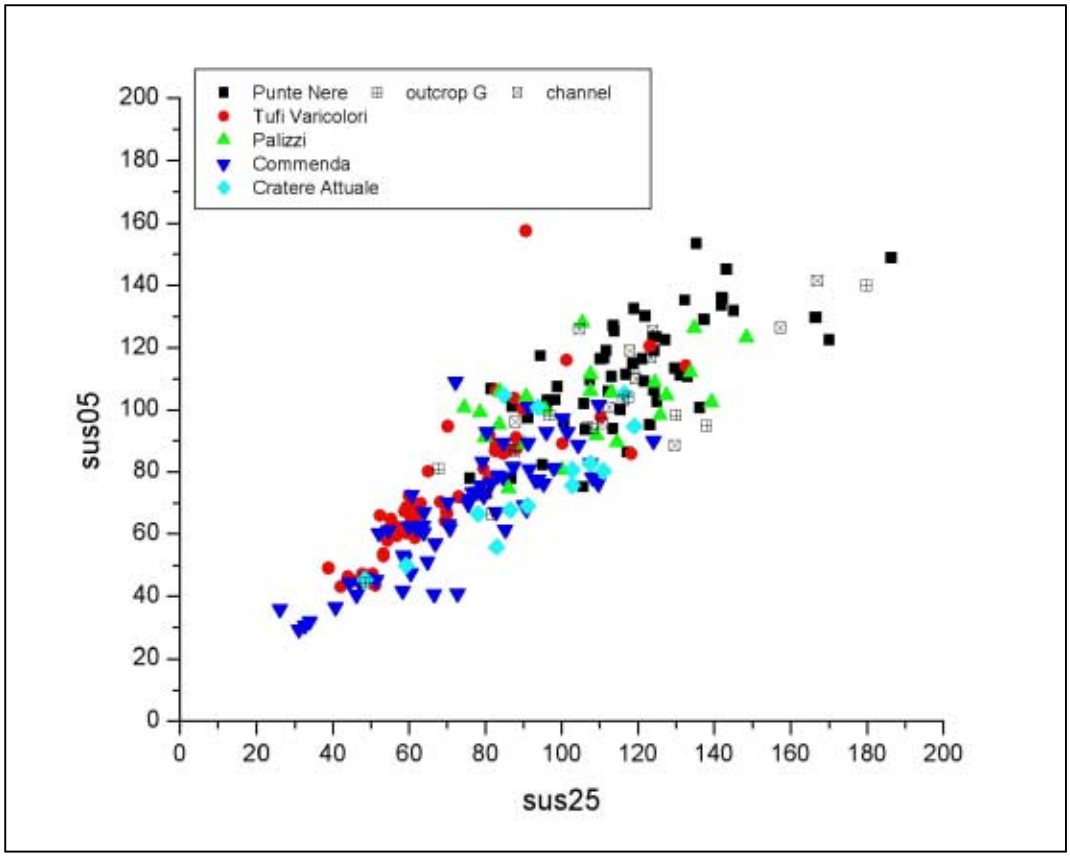

Figure III.37: Scatter plot sus05 vs. sus25 for all successions.

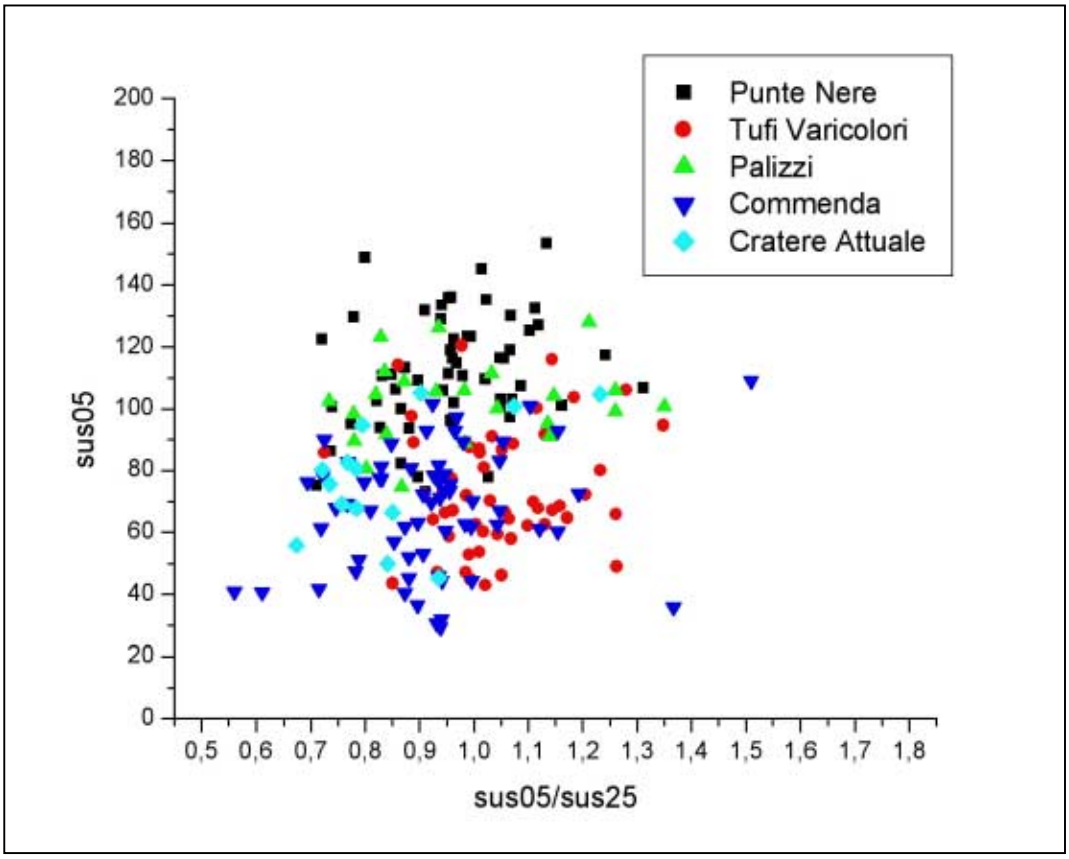

Figure III.38: Scatter plot sus05 vs. sus05/sus25 for all successions.

III.H. Gamma-ray Plots for all Successions

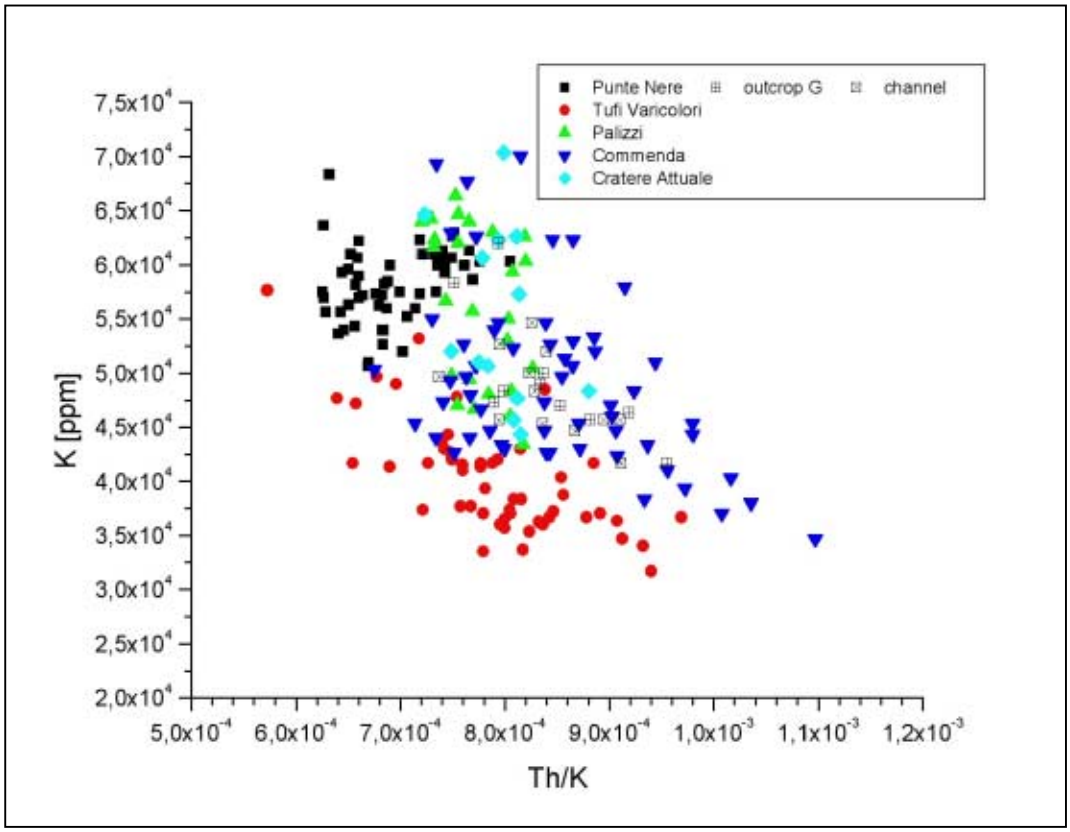

Figure III.39: Scatter plot K vs. Th/K for all successions.

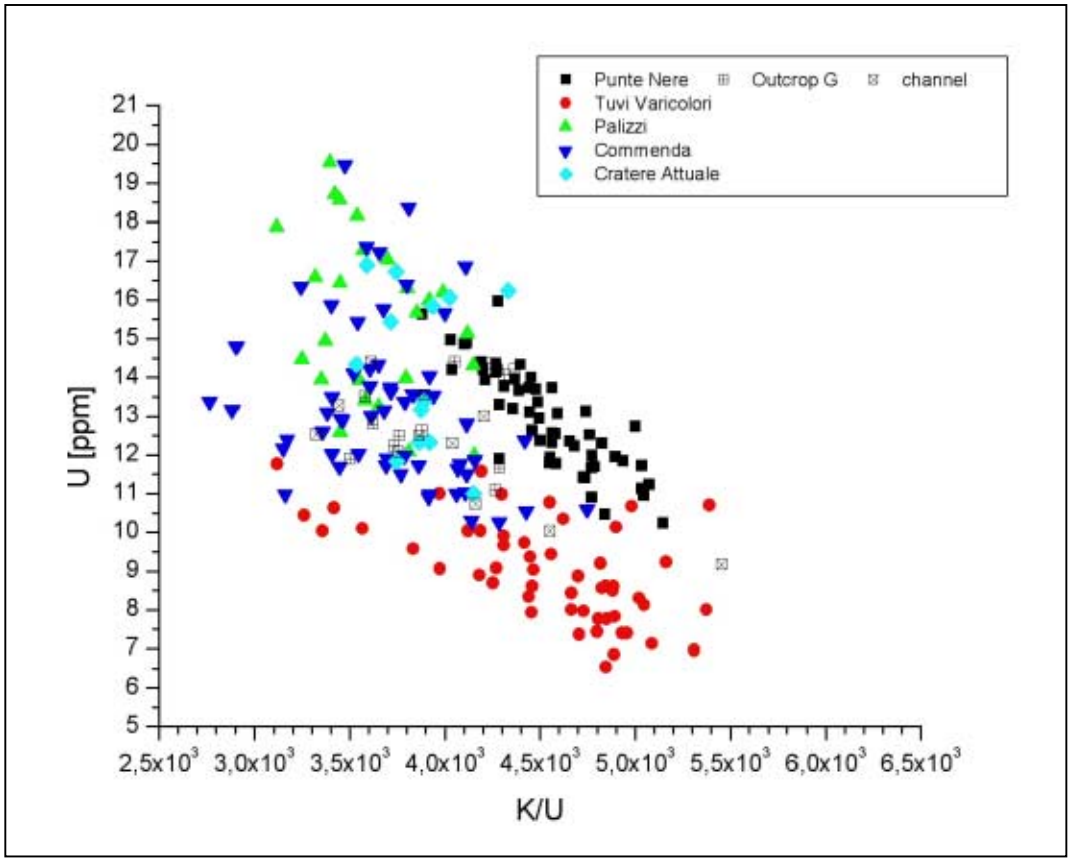

Figure III.40: Scatter plot K vs. U/K for all successions.

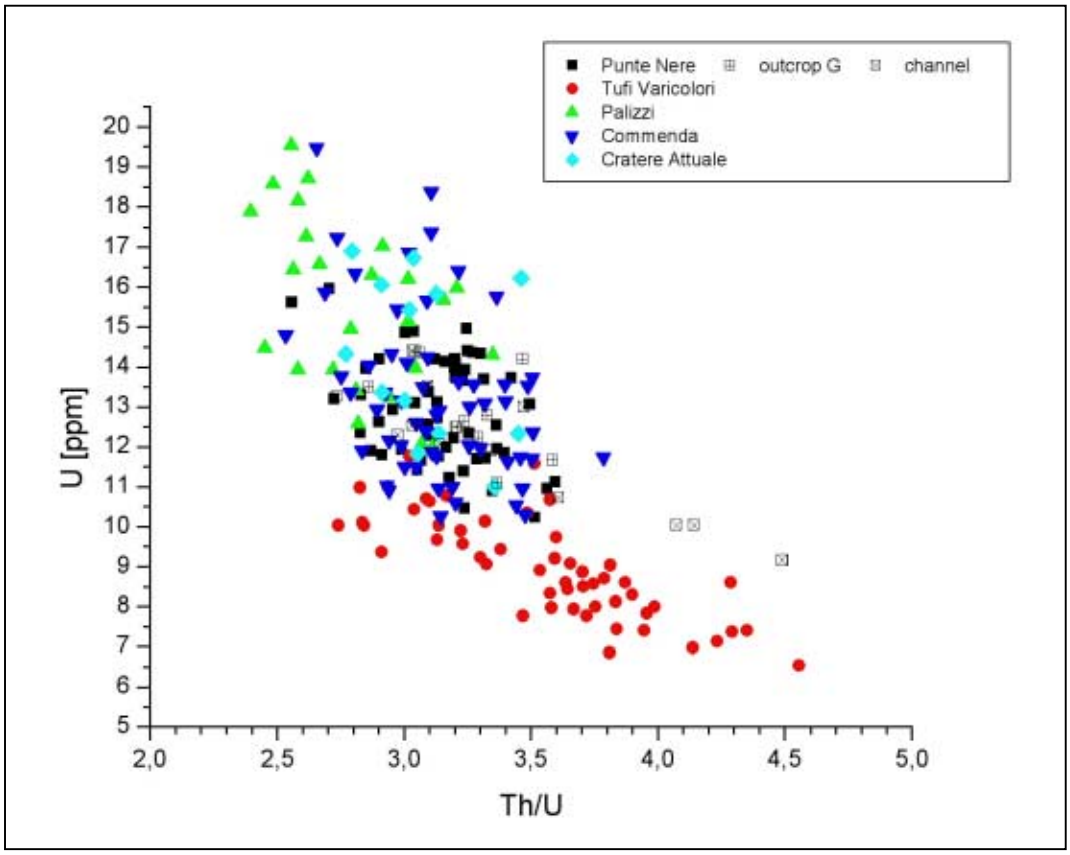

Figure III.41: Scatter plot U vs. Th/U for all successions.

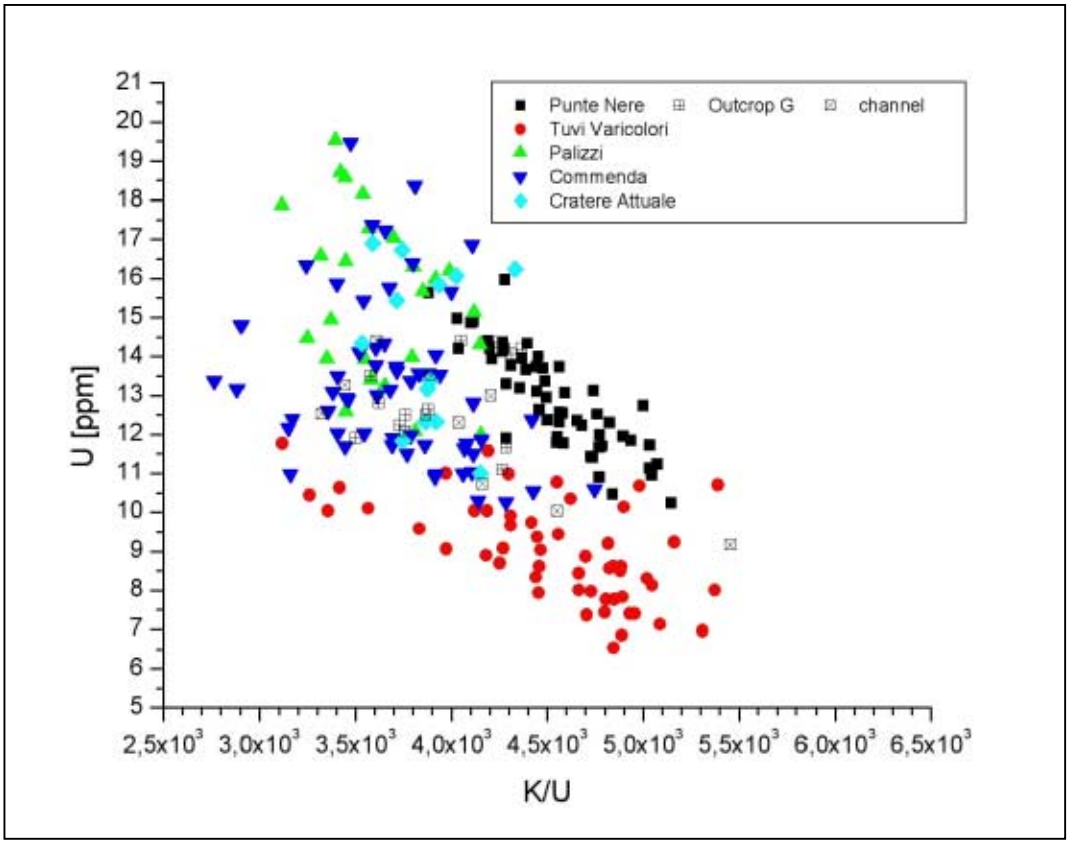

Figure III.42: Scatter plot U vs. K/U for all successions.

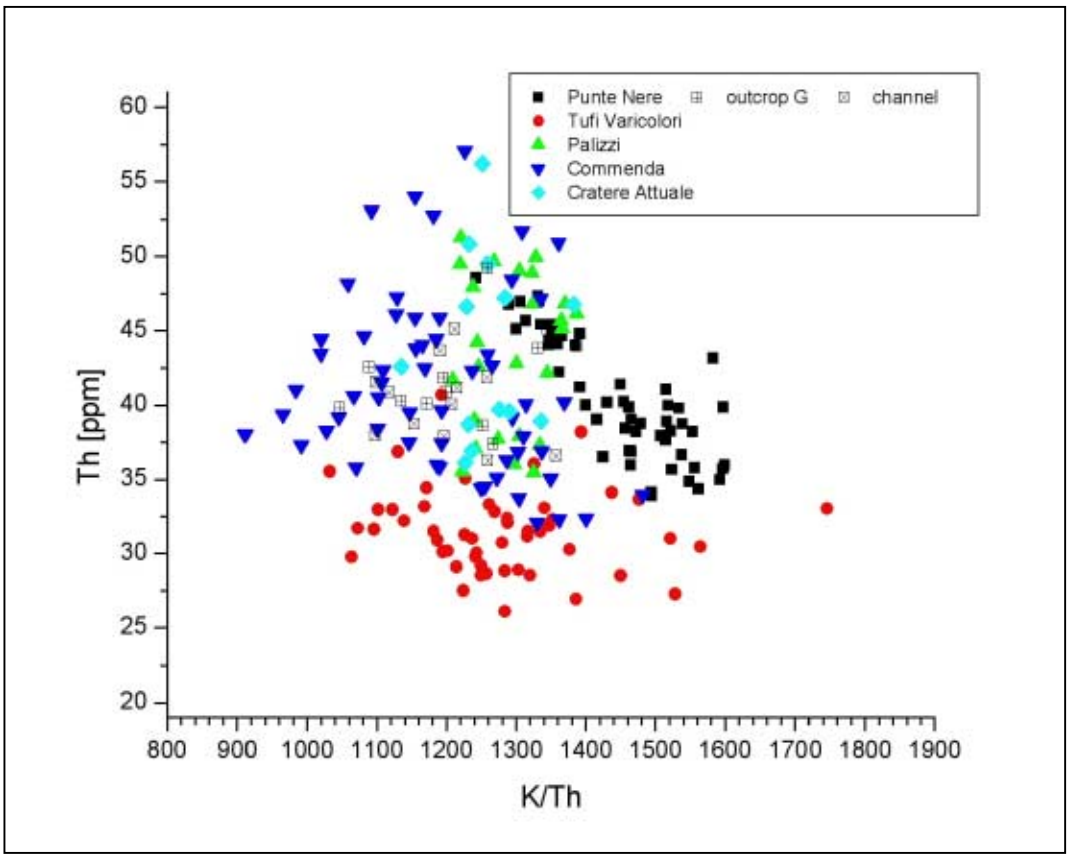

Figure III.43: Scatter plot Th vs. K/Th for all successions.

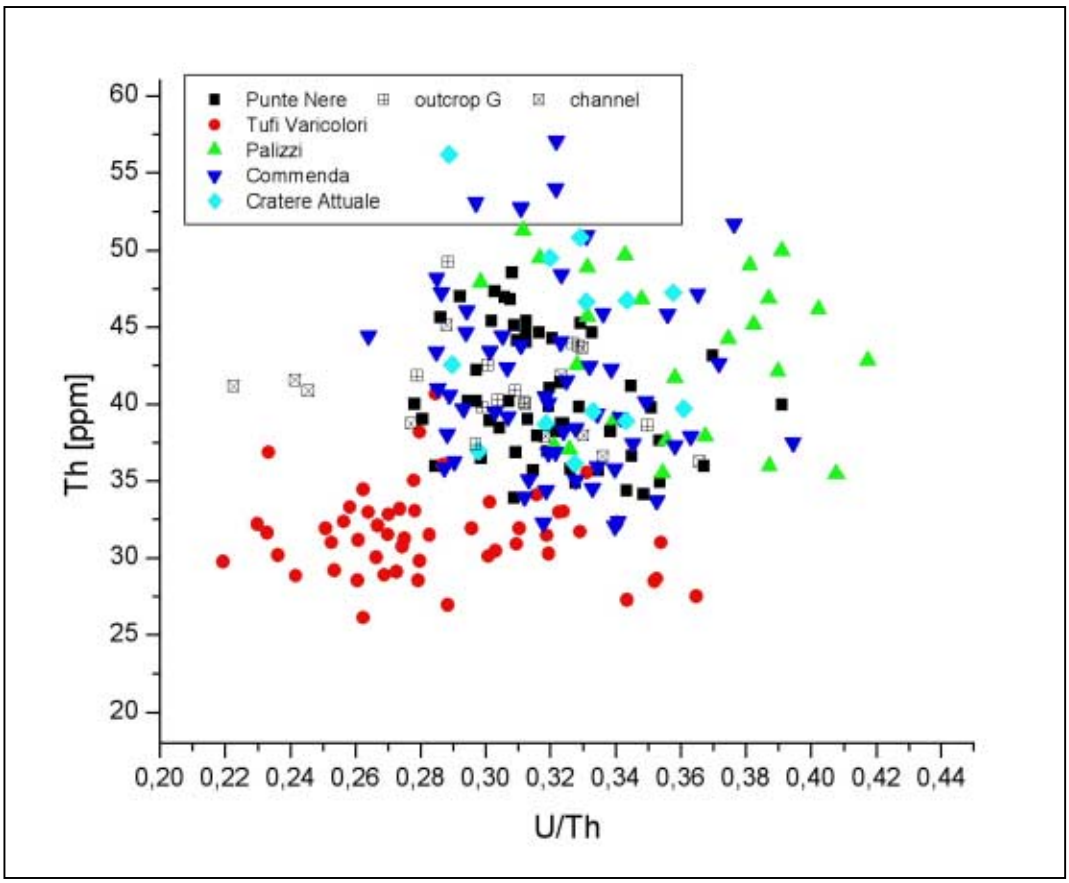

Figure III.44:Scatter plot Th vs. U/Th for all successions.

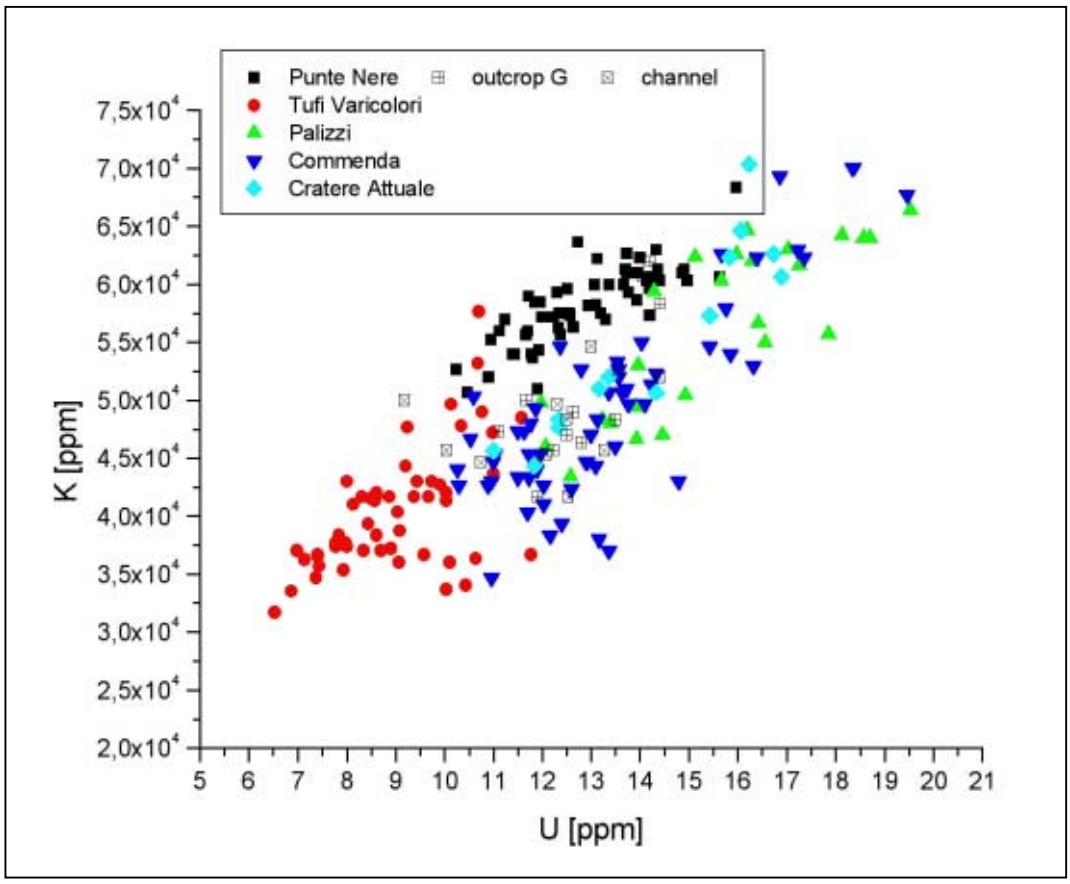

Figure III.45: Scatter plot K vs. U for all successions.

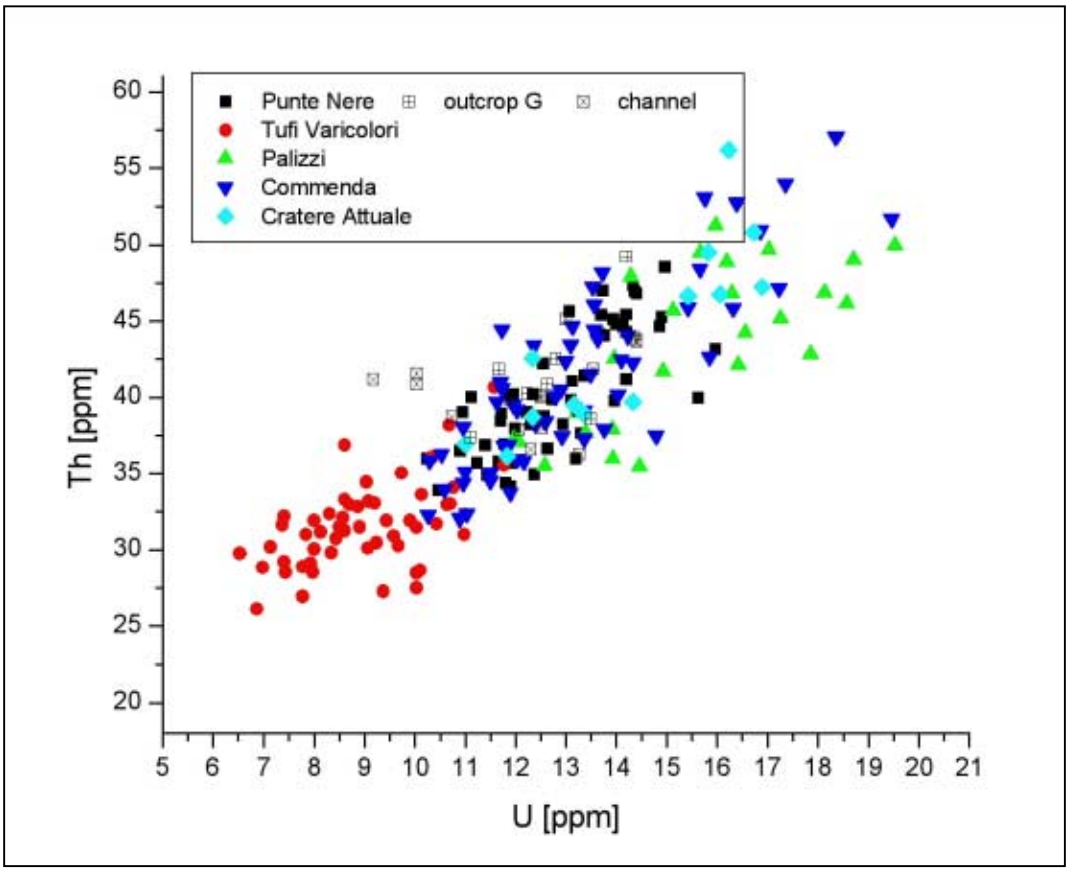

Figure III.46: Scatter plot Th vs. U for all successions.

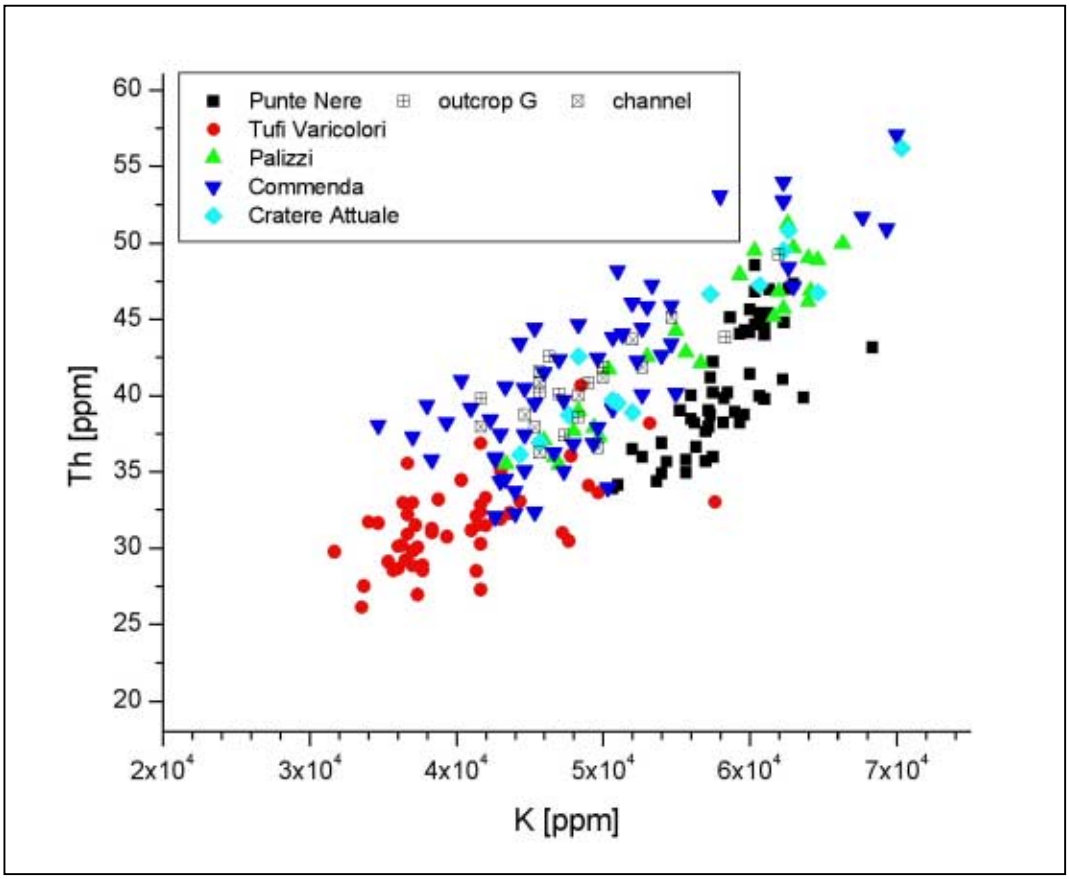

Figure III.47: Scatter plot Th vs. K for all successions.

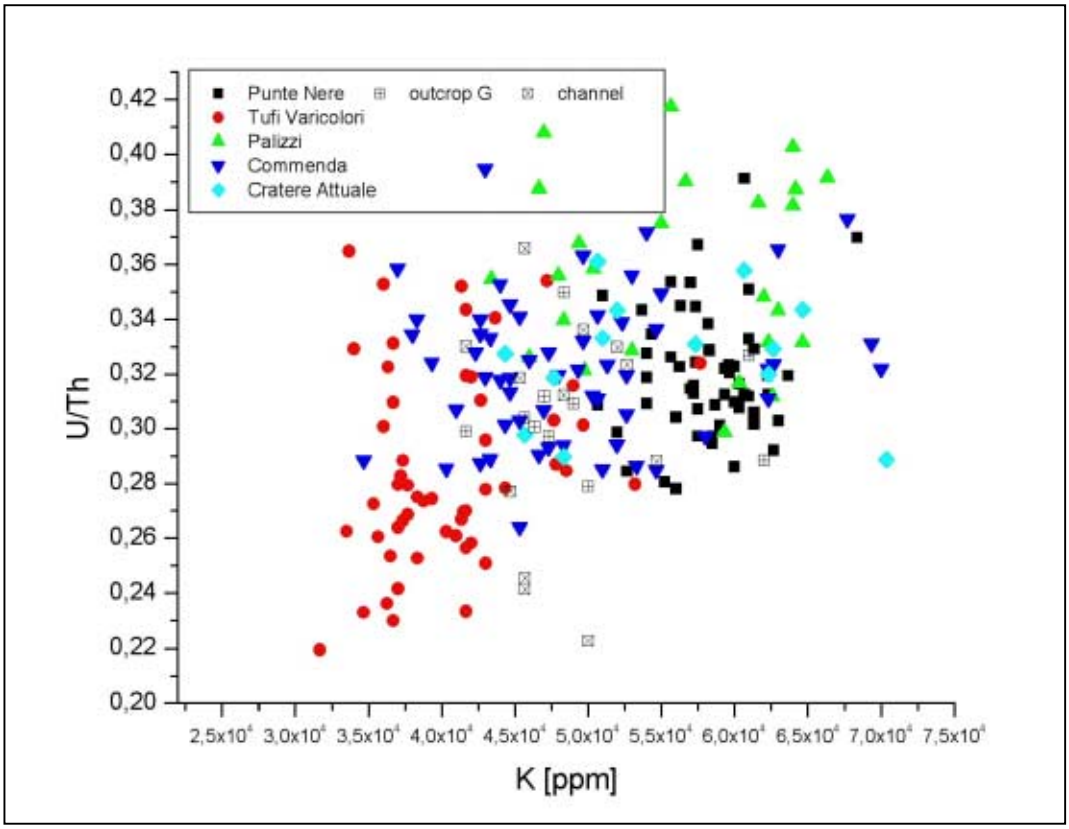

Figure III.48: Scatter plot U/Th vs. K for all successions.

IV. Appendix IVa: Plots for Undefined Outcrops

IV.A. Outcrop C

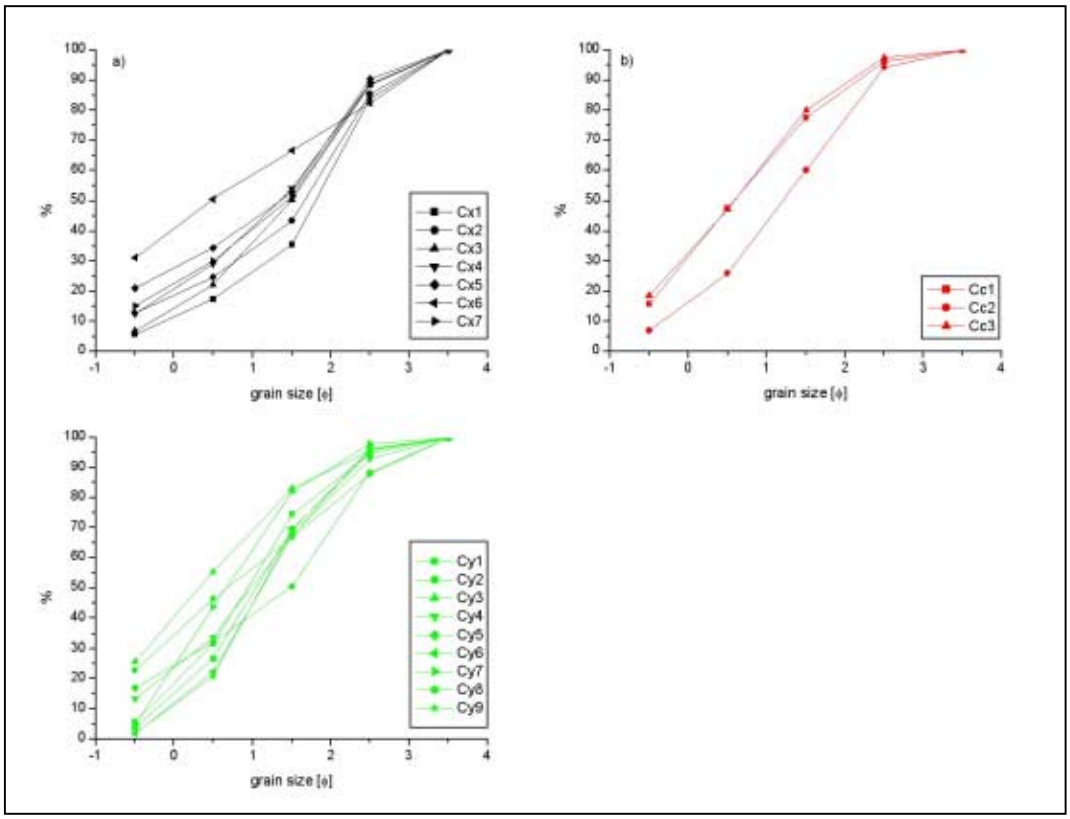

Figure IV.A.1: Cumulative grain size curve for outcrop C. a) unit Cx, b) unit Cc, and c) unit Cy.

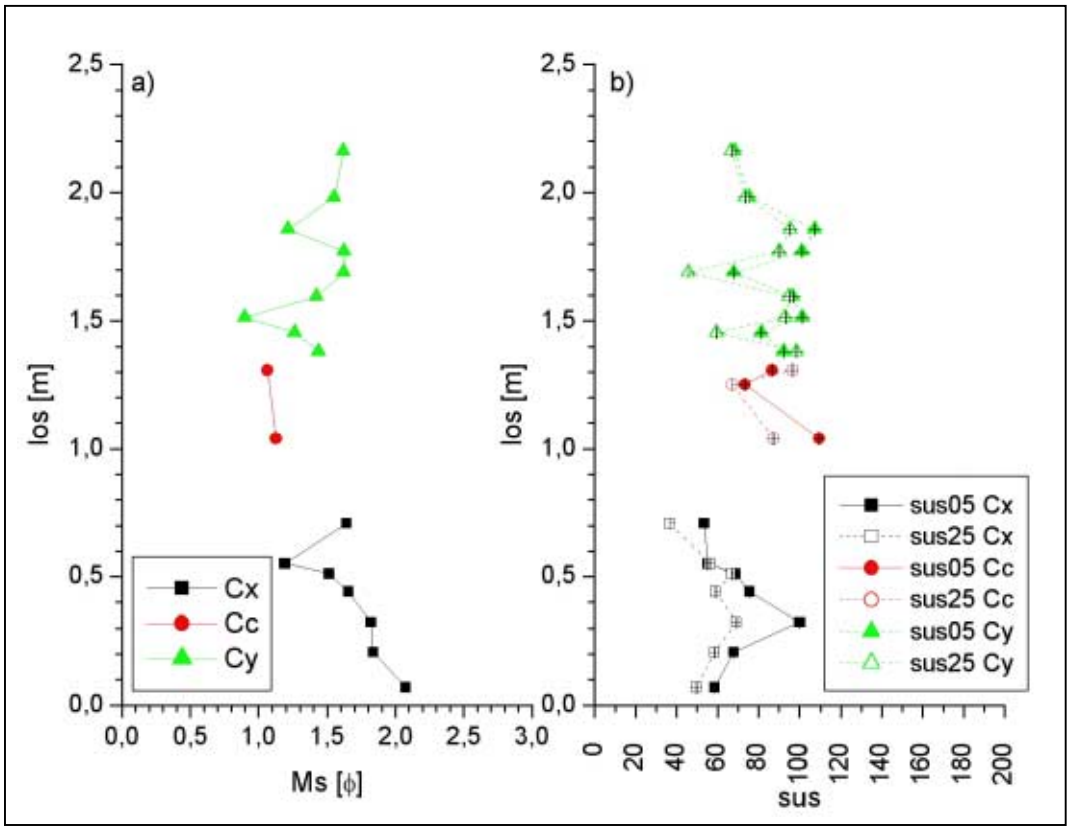

Figure IV.A.2: los vs. Ms [ϕ] and sus for outcrop C. a) los vs. Ms; b) los vs. sus05 and sus25.

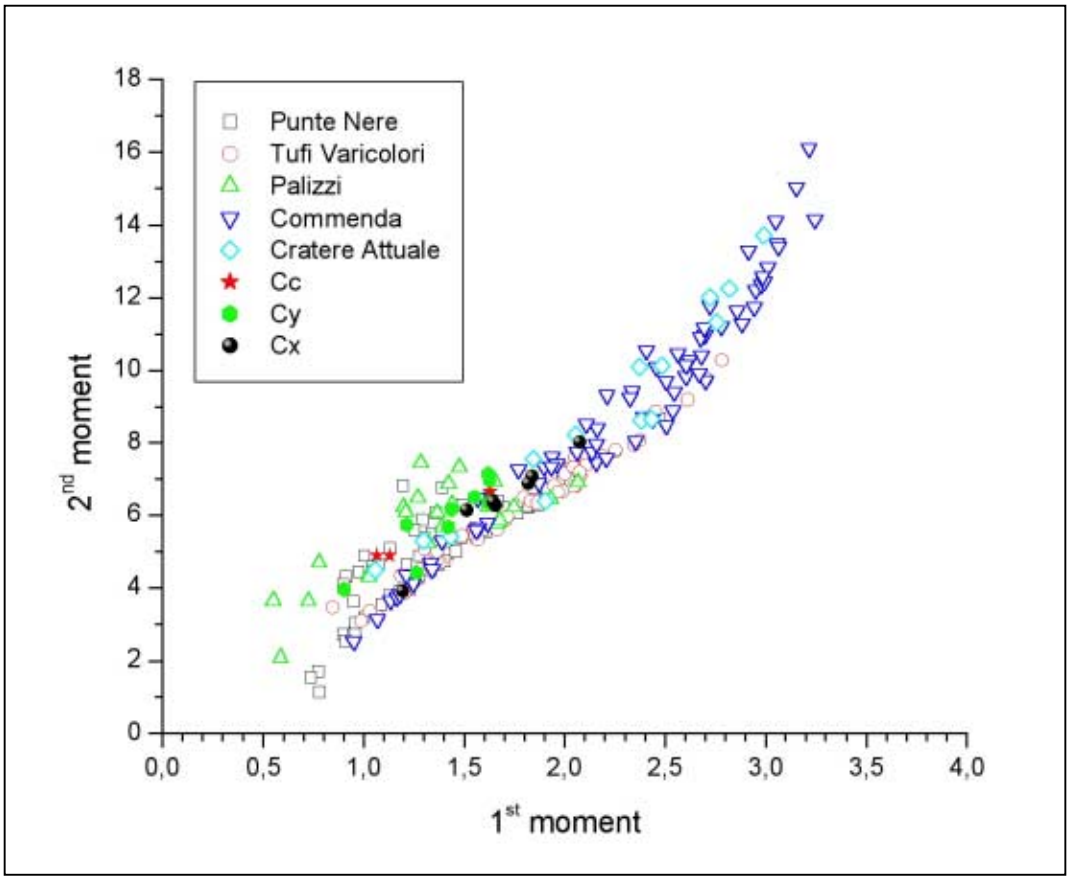

Figure IV.A.3: 1st vs. 2nd moment for outcrop C in comparison with the standard outcrops.

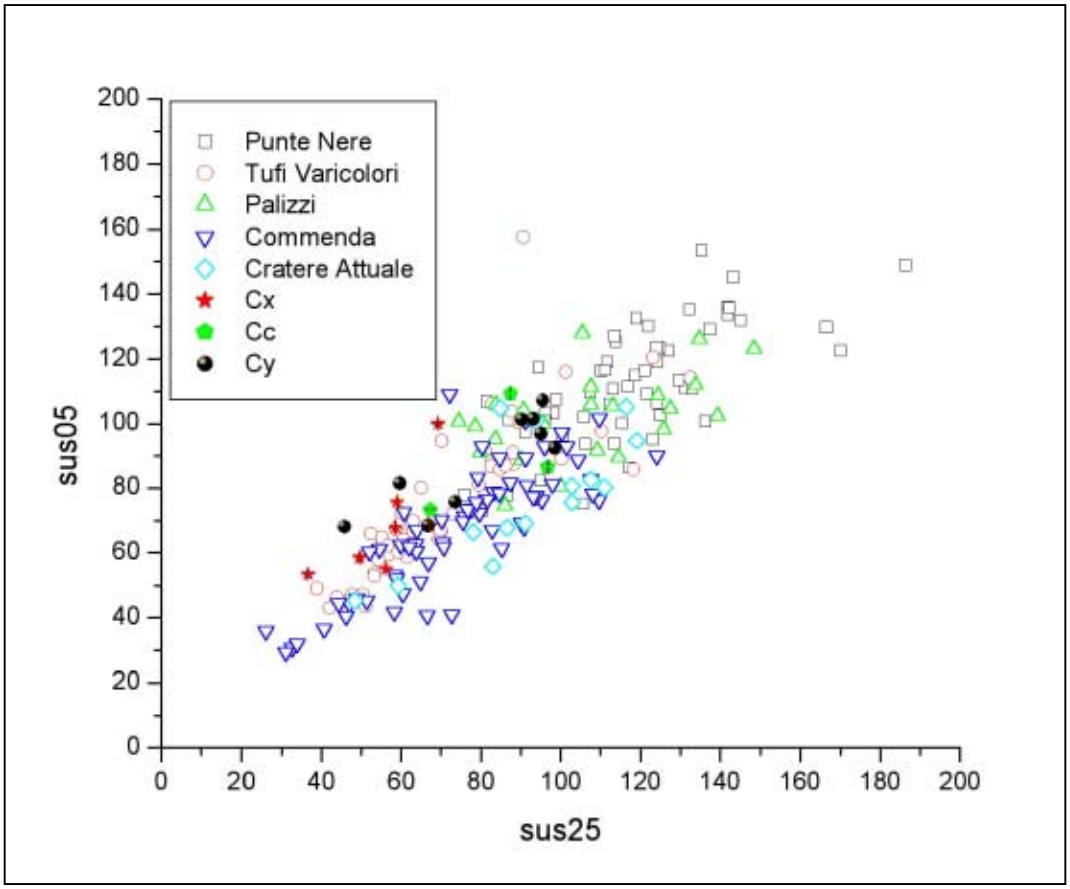

Figure IV.A.4: Scatter plot sus05 vs. sus25 for outcrop C in comparison with the standard outcrops.

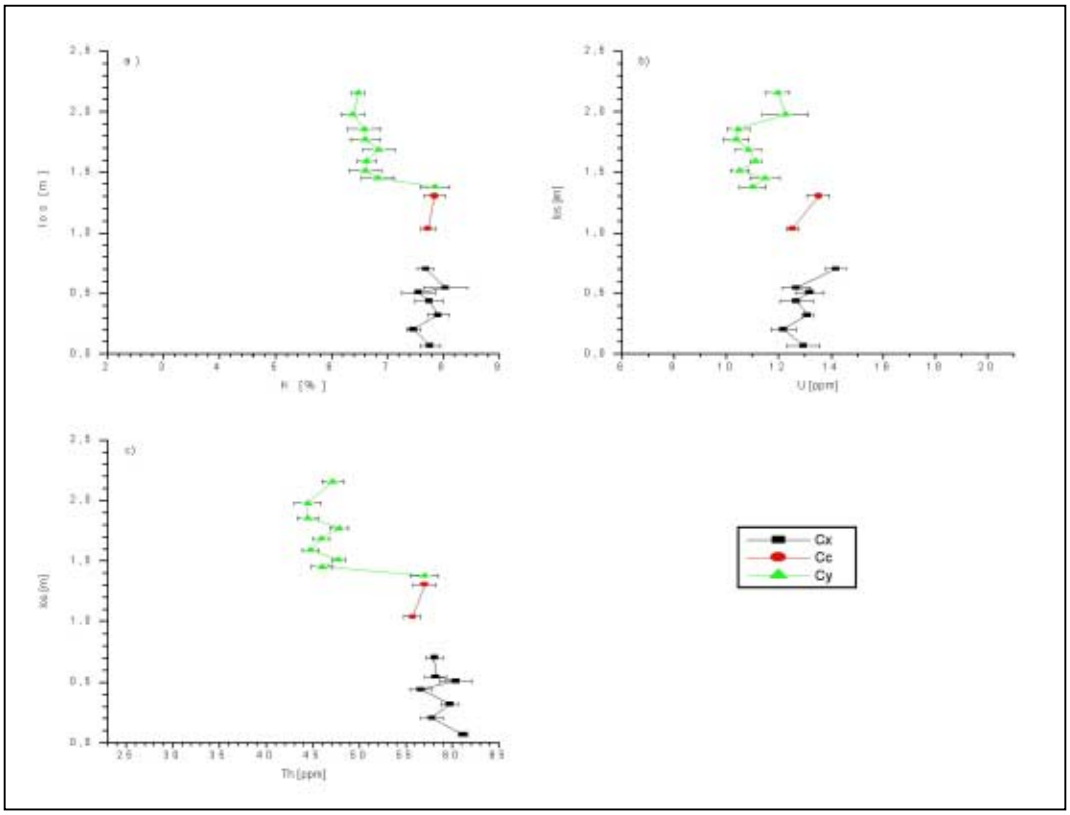

Figure IV.A.5: los. vs. γ-ray values for outcrop C. a) K [%], b) U [ppm], c) Th [ppm].

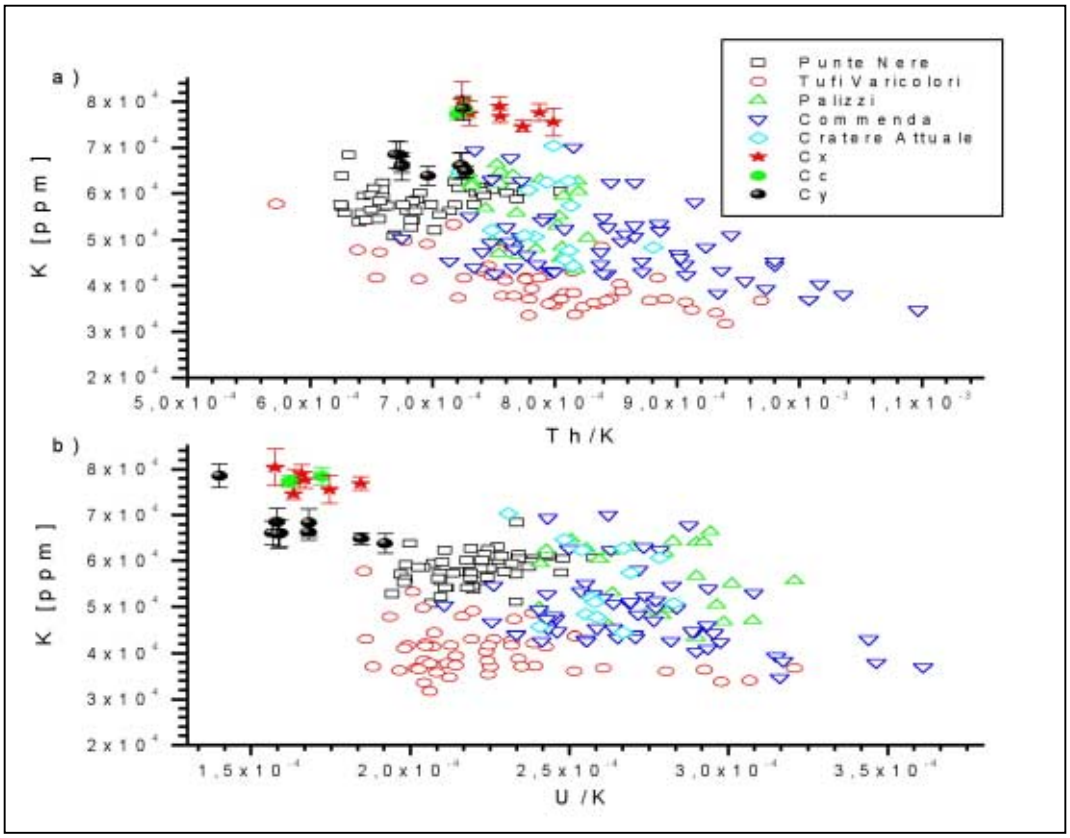

Figure IV.A.6: Scatter plots K vs. Th/K and K vs. U/K for outcrop C in comparison with the standard outcrops. a) K vs. Th/K, b) K vs. U/K.

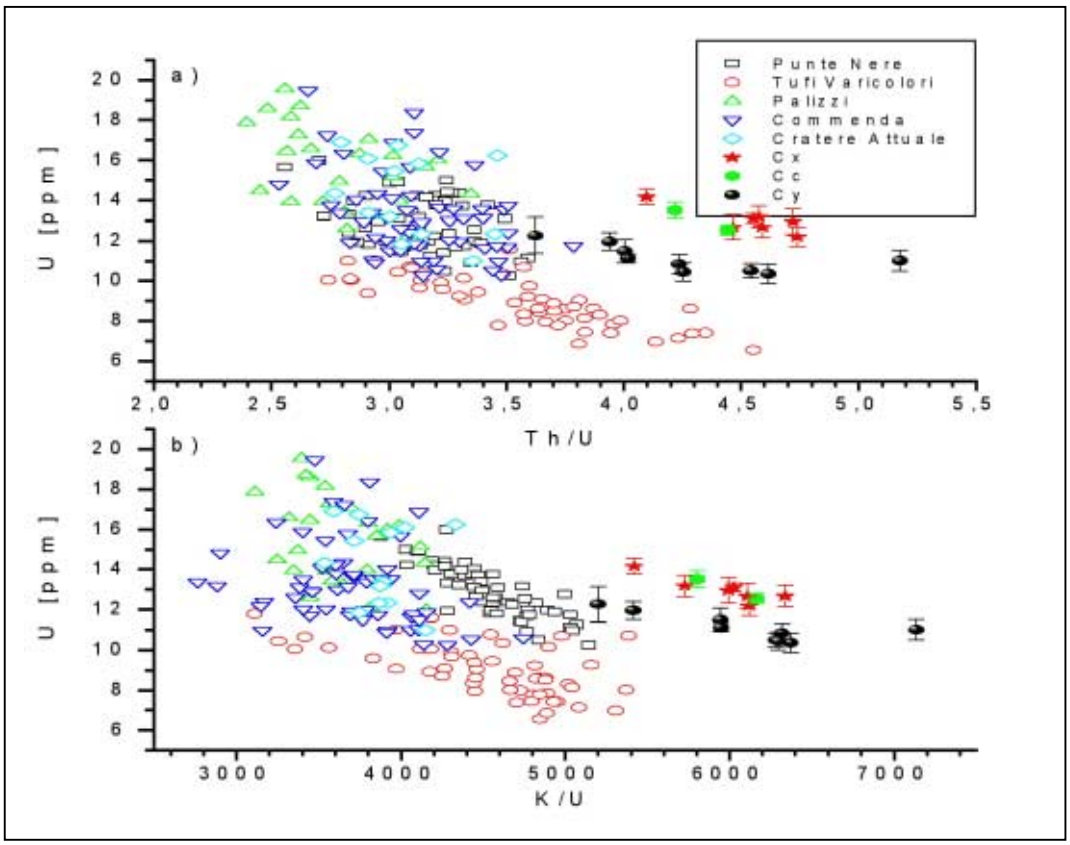

Figure IV.A.7: Scatter plots U vs. Th/U and U vs. K/U for outcrop C in comparison with the standard outcrops. a) U vs. Th/U, b) U vs. K/U.

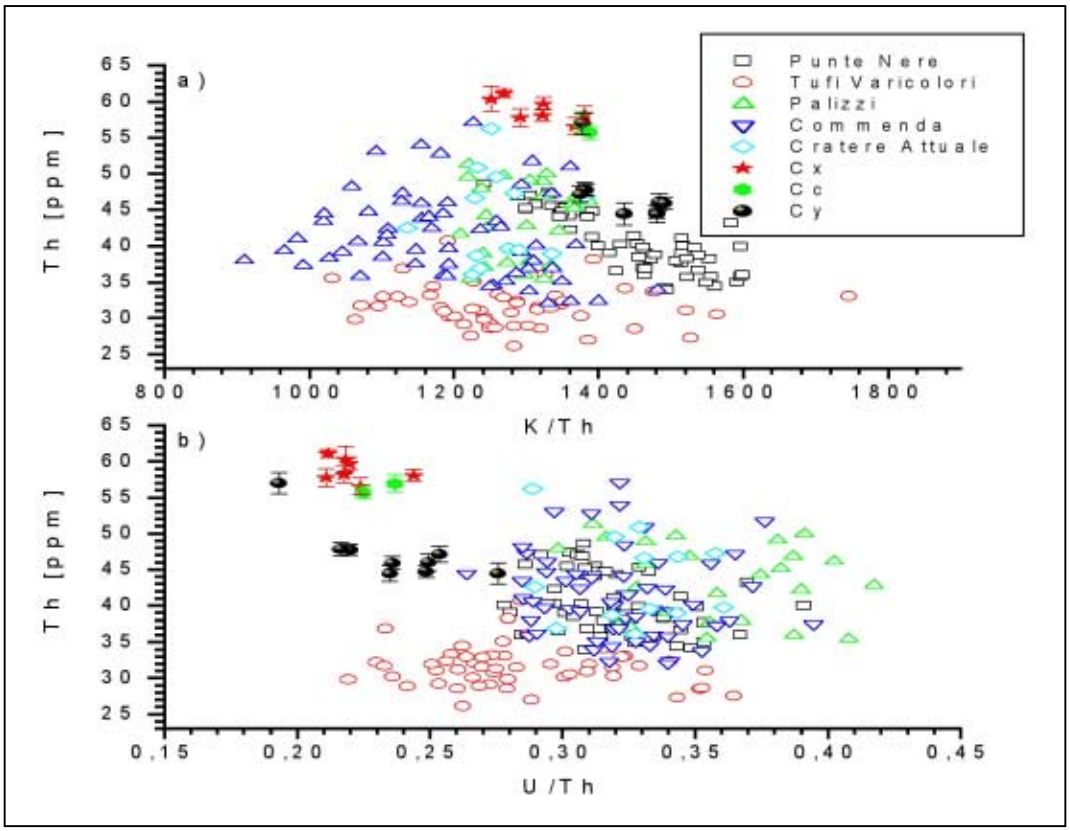

Figure IV.A.8: Scatter plots Th vs. K/Th and Th vs. U/Th for outcrop C in comparison with the standard outcrops. a) Th vs. K/Th, b) Th vs. U/Th.

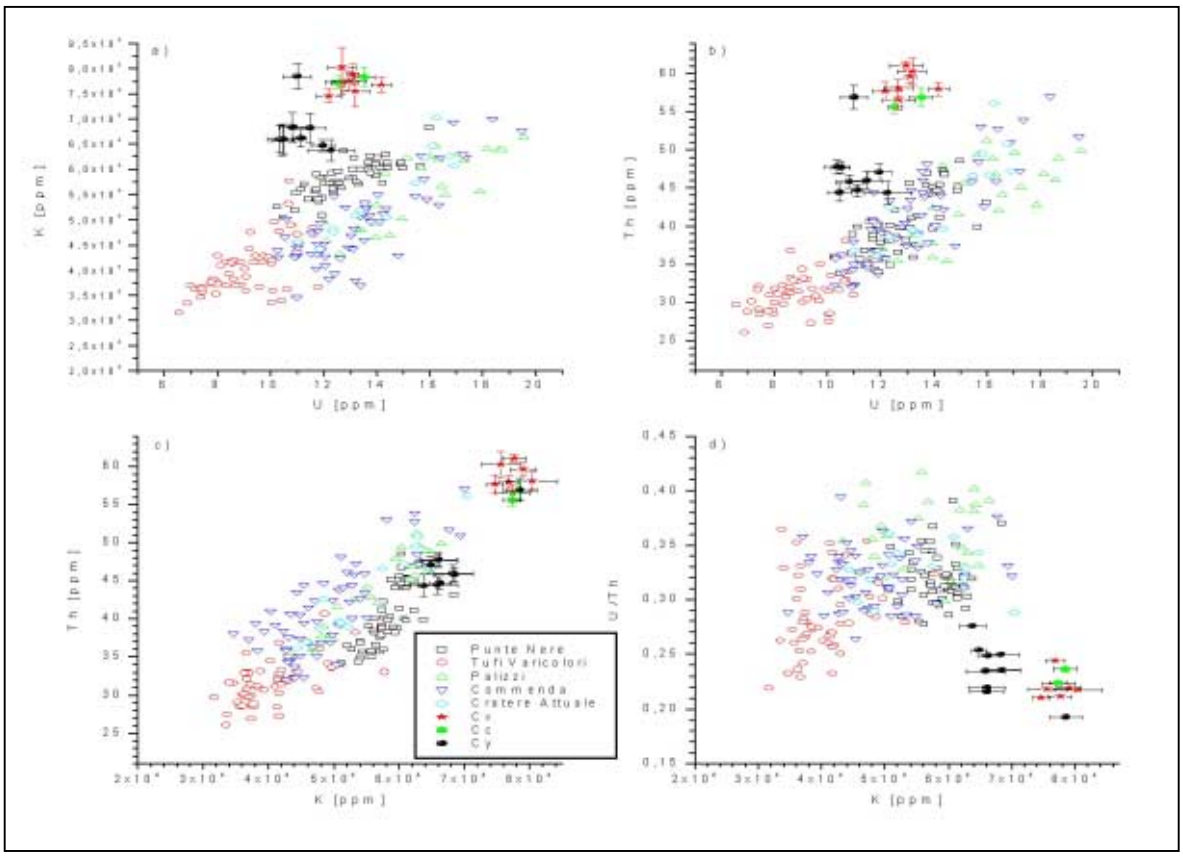

Figure IV.A.9: Scatter plots K vs. U, Th vs. U, Th vs. K, and U/Th vs. K for outcrop C in comparison with the standard outcrops. a) K vs. U, b) Th vs. U), c) Th vs. K, d) U/Th vs. K.

IV. Appendix IVb: Plots for Undefined Outcrops

IV.B. Outcrop D

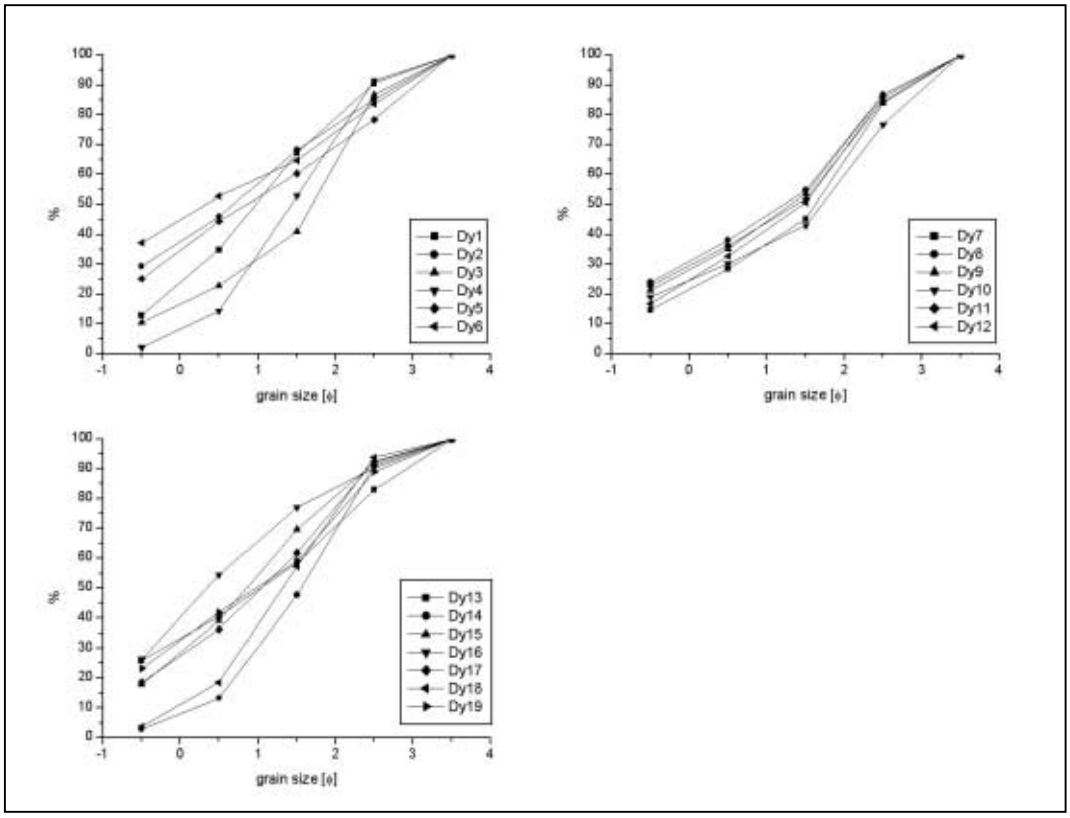

Figure IV.B.1: Cumulative grain size curve for outcrop D.

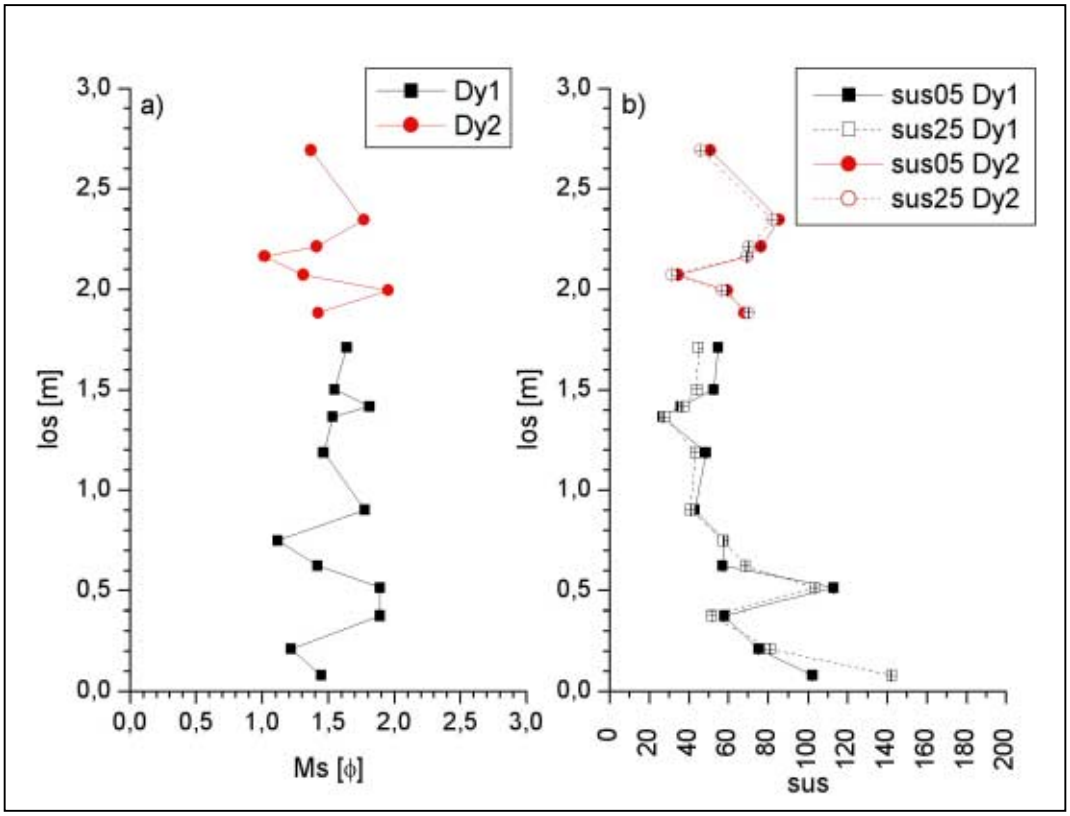

Figure IV.B.2: los vs. Ms [ϕ] and sus for outcrop D. a) los vs. Ms; b) los vs. sus05 and sus25.

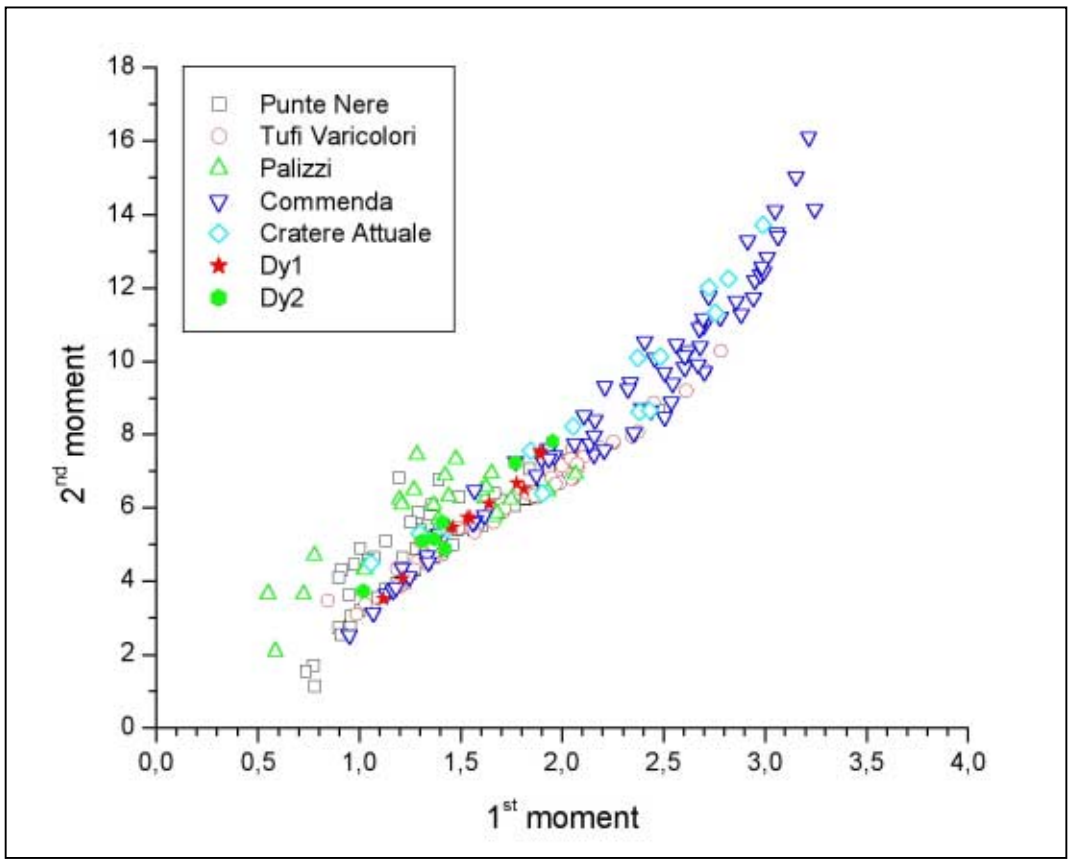

Figure IV.B.3: 1st vs. 2nd moment for outcrop D in comparison with the standard outcrops.

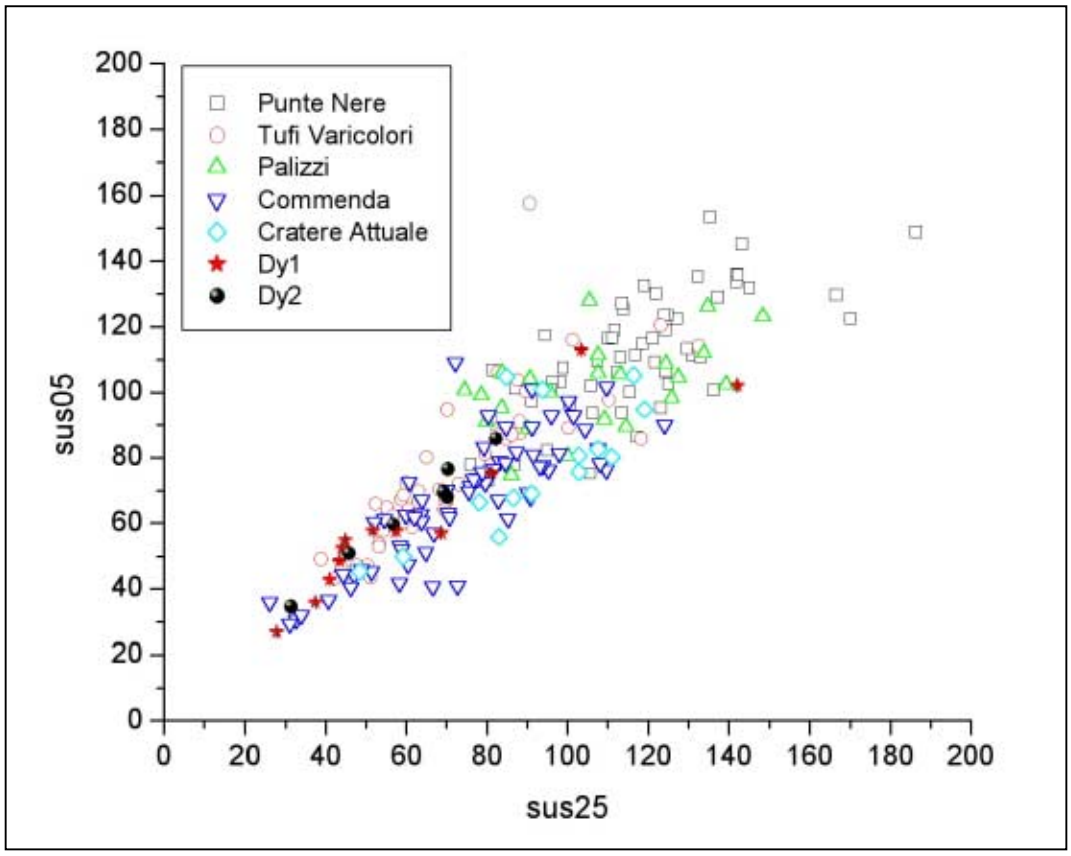

Figure IV.B.4: Scatter plot sus05 vs. sus25 for outcrop D in comparison with the standard outcrops.

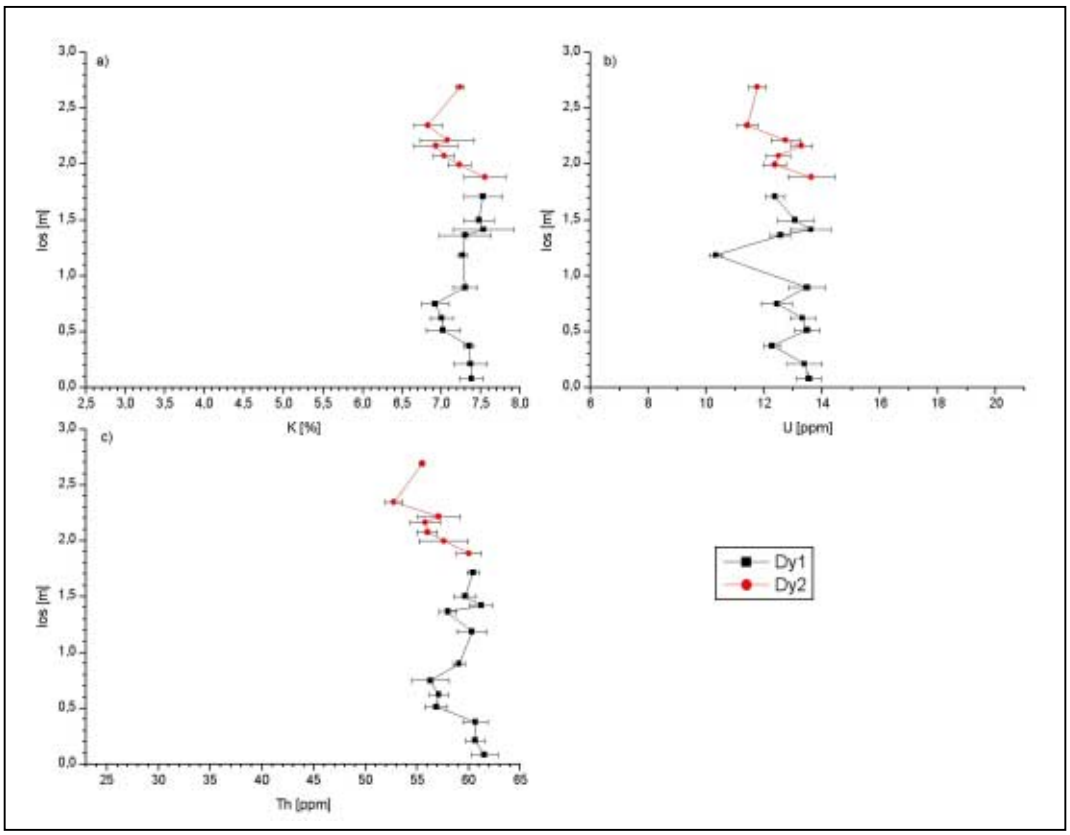

Figure IV.B.5: los. vs. γ-ray values for outcrop D. a) K [%], b) U [ppm], c) Th [ppm].

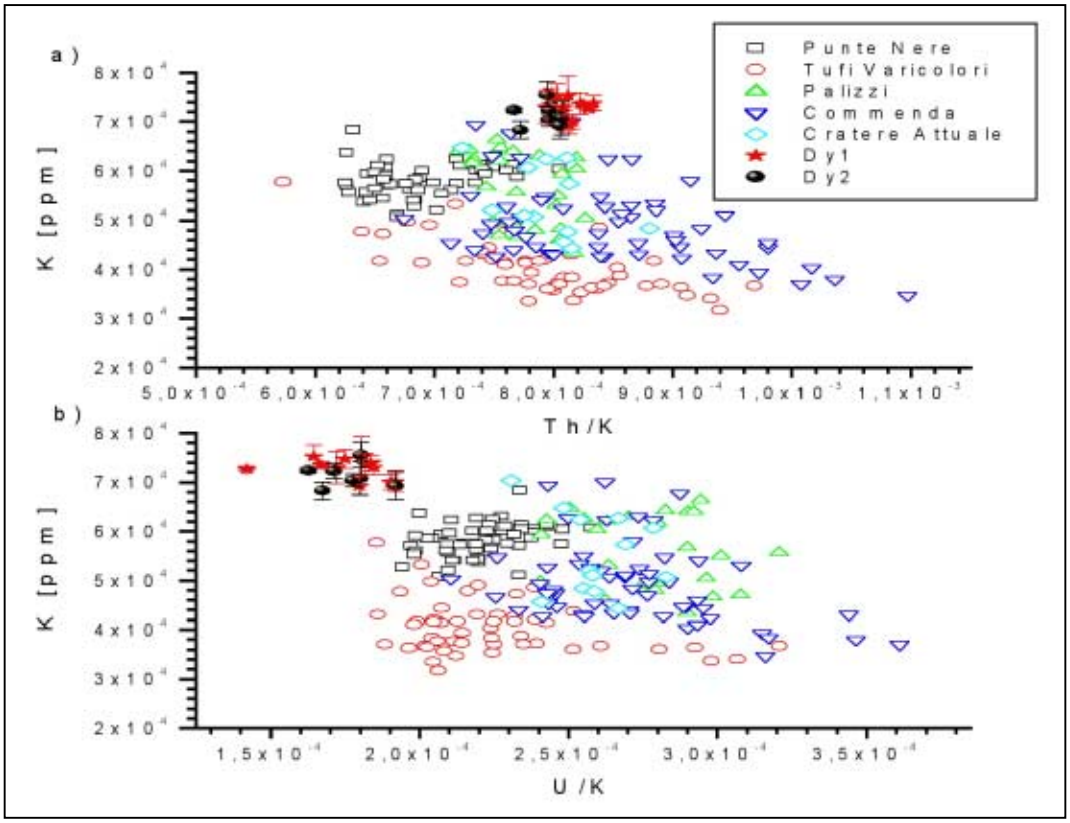

Figure IV.B.6: Scatter plots K vs. Th/K and K vs. U/K for outcrop D in comparison with the standard outcrops. a) K vs. Th/K, b) K vs. U/K.

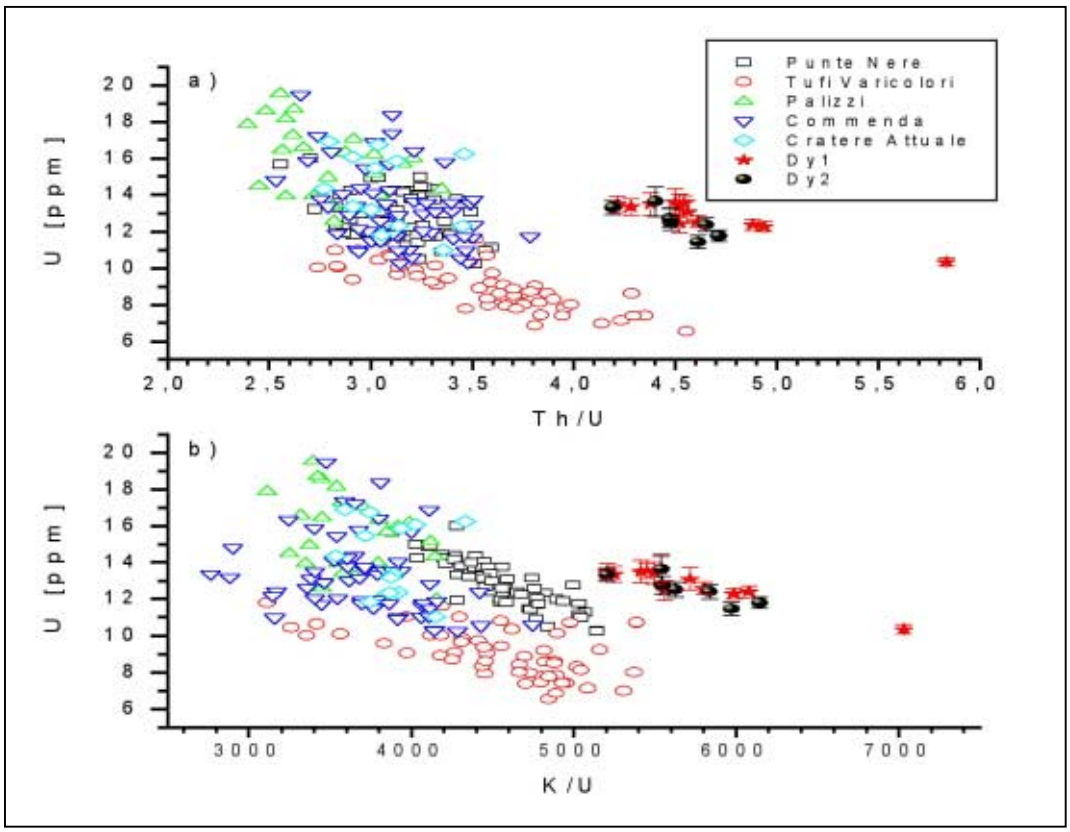

Figure IV.B.7: Scatter plots U vs. Th/U and U vs. K/U for outcrop D in comparison with the standard outcrops. a) U vs. Th/U, b) U vs. K/U.

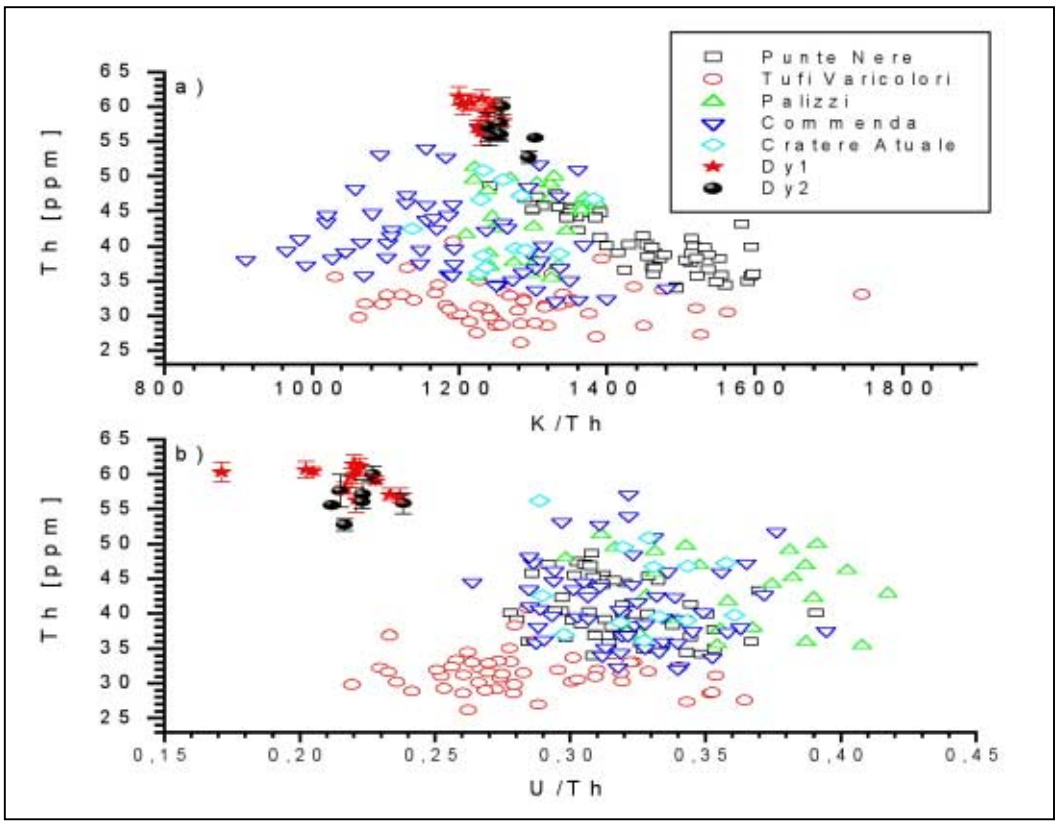

Figure IV.B.8: Scatter plots Th vs. K/Th and Th vs. U/Th for outcrop D in comparison with the standard outcrops. a) Th vs. K/Th, b) Th vs. U/Th.

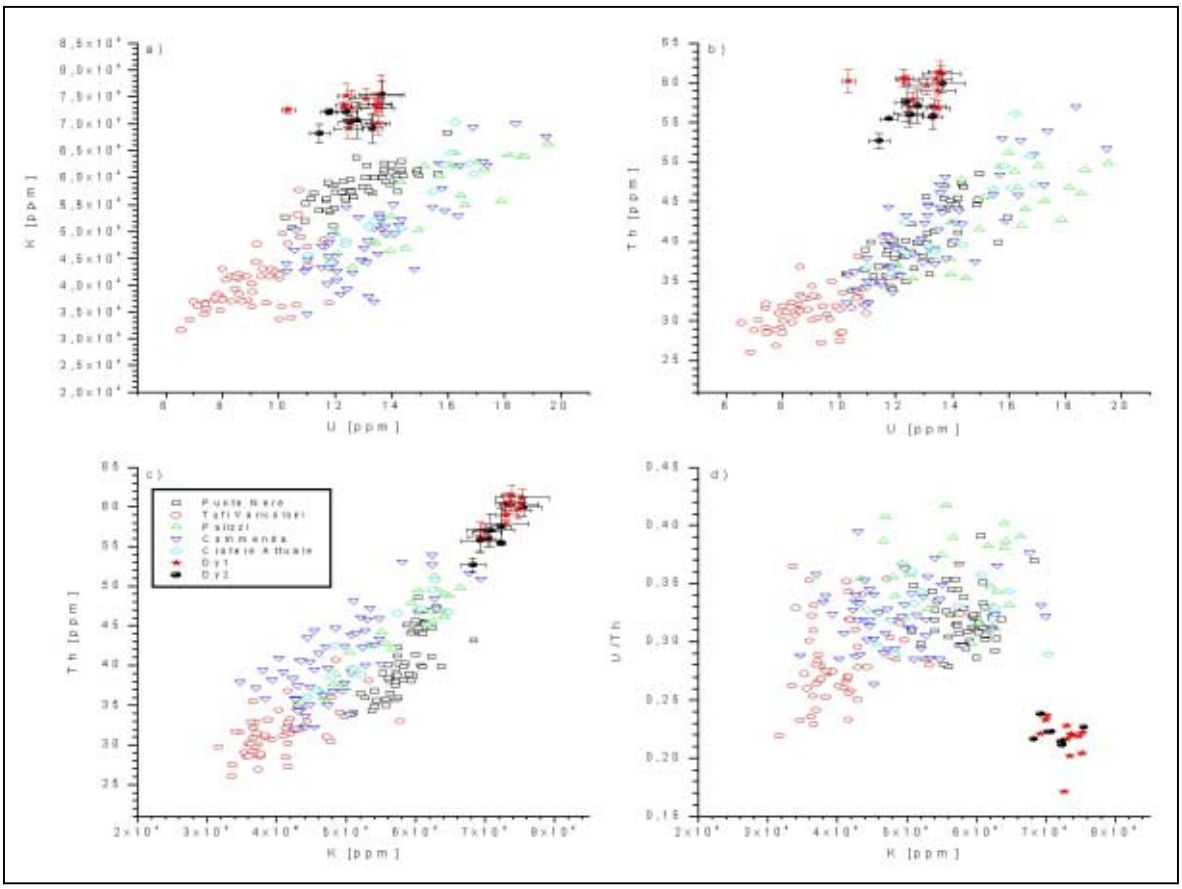

Figure IV.B.9: Scatter plots K vs. U, Th vs. U, Th vs. K, and U/Th vs. K for outcrop D in comparison with the standard outcrops. a) K vs. U, b) Th vs. U), c) Th vs. K, d) U/Th vs. K.

IV. Appendix IVc: Plots for Undefined Outcrops

IV.C. Outcrop K

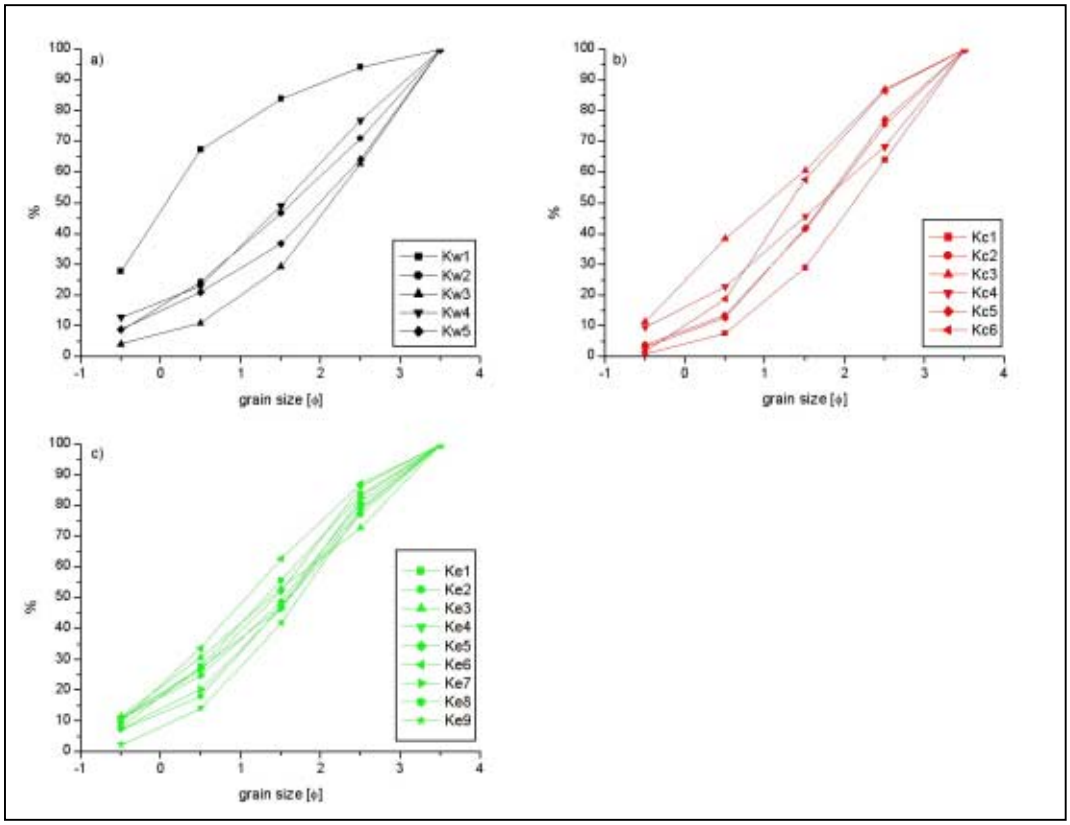

Figure IV.C.1: Cumulative grain size curve for outcrop K. a) unit Kw, b) unit Kc, and c) unit Ke.

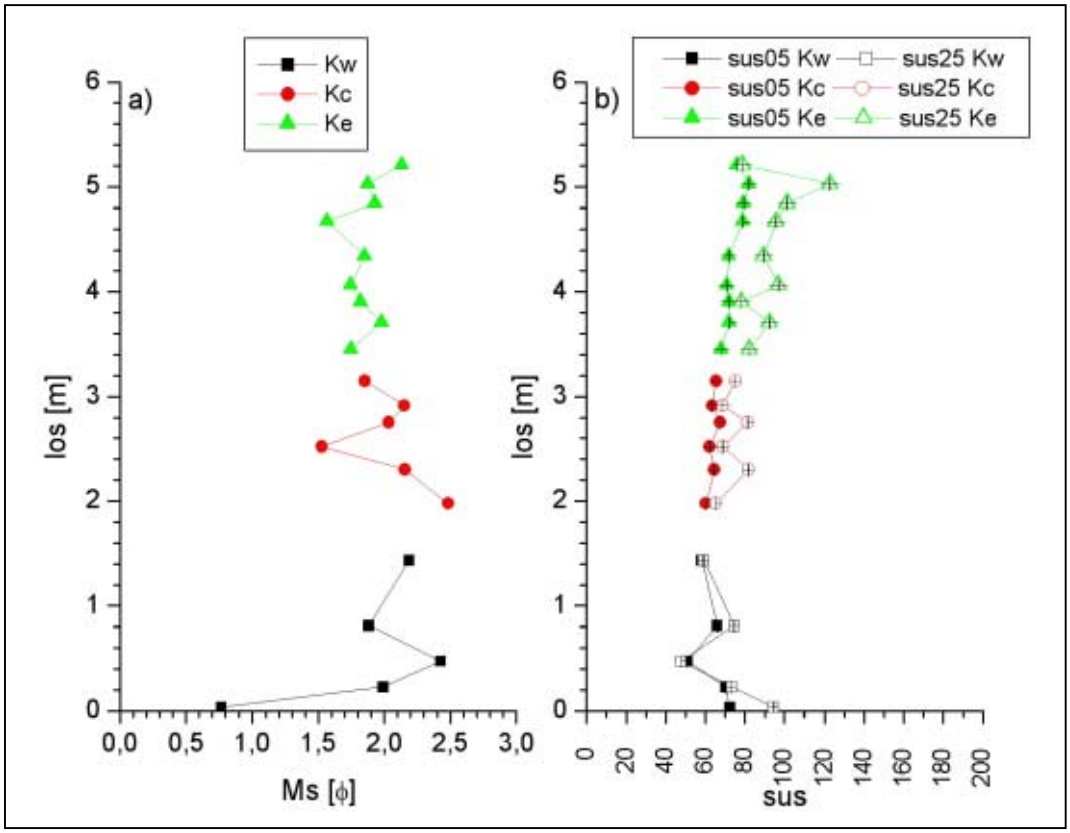

Figure IV.C.2: los vs. Ms [ϕ] and sus for outcrop K. a) los vs. Ms; b) los vs. sus05 and sus25.

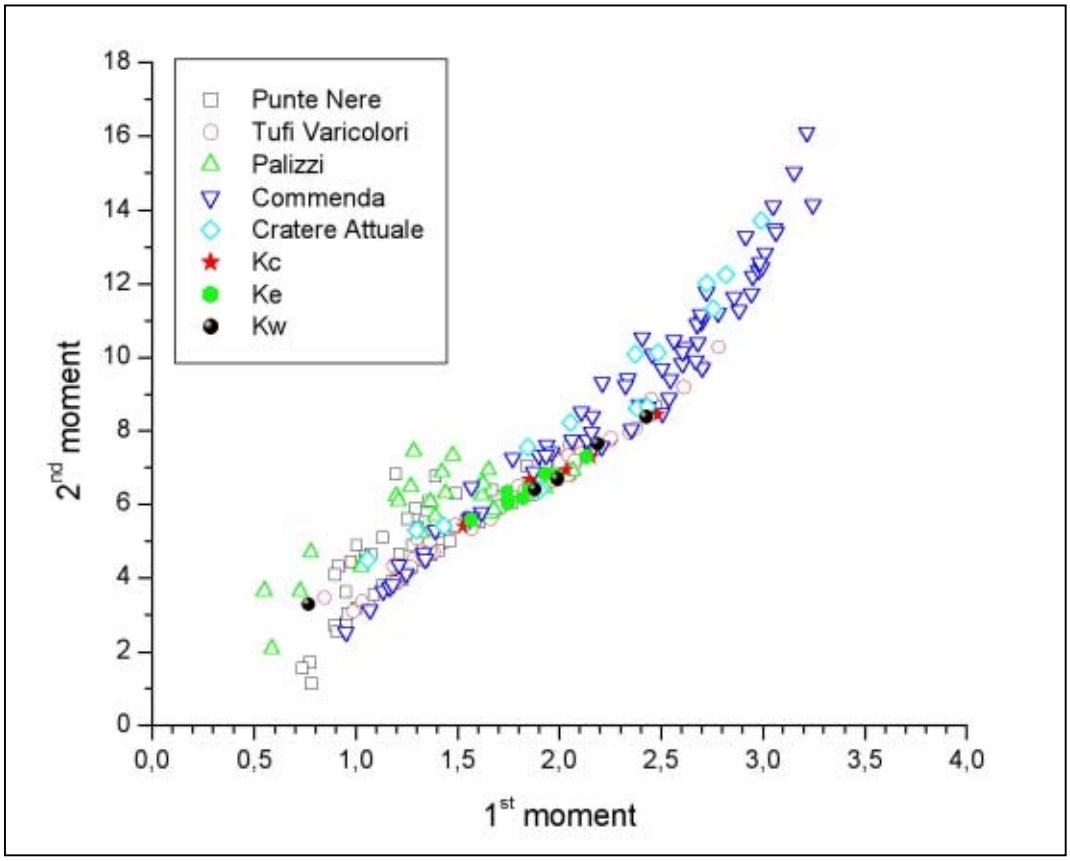

Figure IV.C.3: 1st vs. 2nd moment for outcrop K in comparison with the standard outcrops.

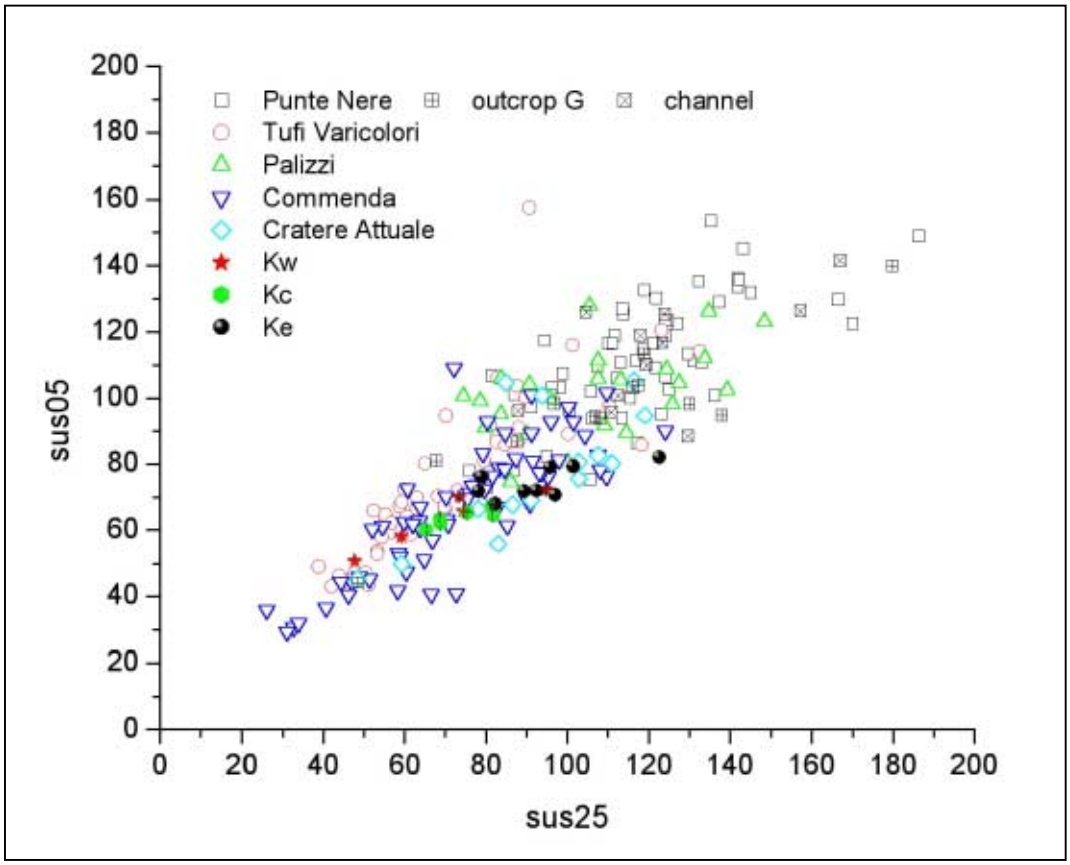

Figure IV.C.4: Scatter plot sus05 vs. sus25 for outcrop K in comparison with the standard outcrops.

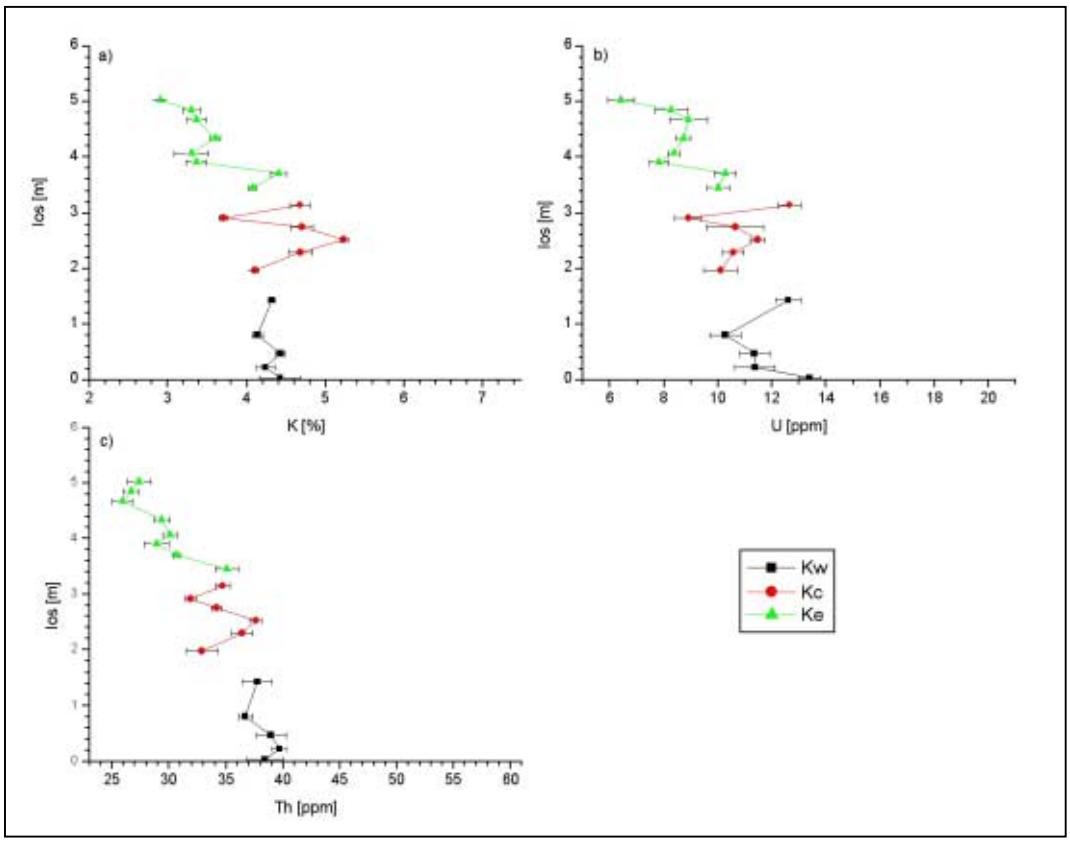

Figure IV.C.5: los. vs. γ-ray values for outcrop K. a) K [%], b) U [ppm], c) Th [ppm].

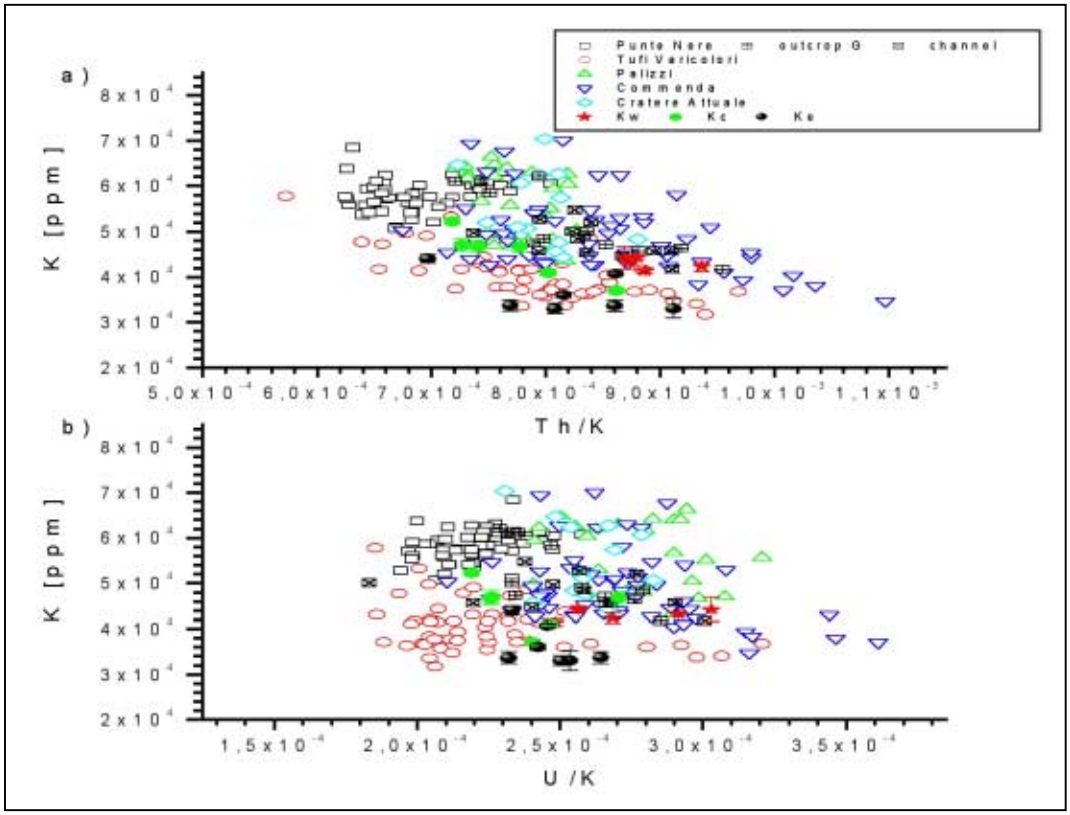

Figure IV.C.6: Scatter plots K vs. Th/K and K vs. U/K for outcrop K in comparison with the standard outcrops. a) K vs. Th/K, b) K vs. U/K.

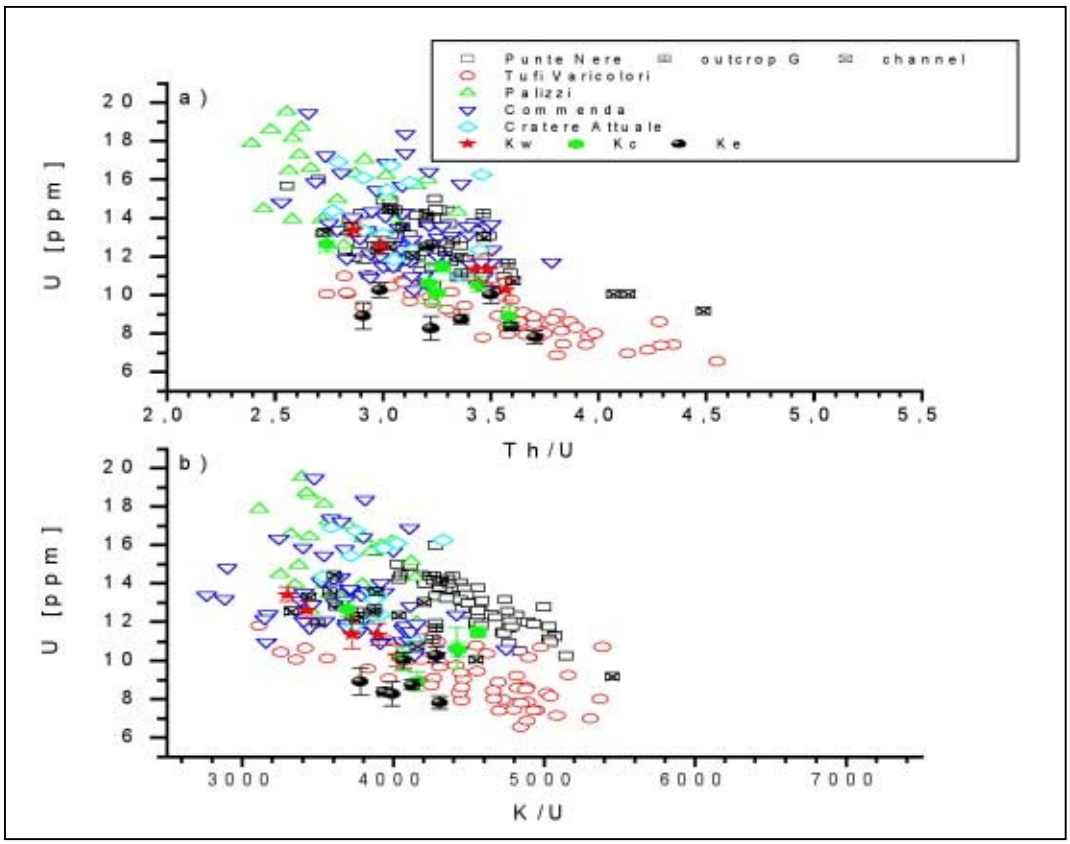

Figure IV.C.7: Scatter plots U vs. Th/U and U vs. K/U for outcrop K in comparison with the standard outcrops. a) U vs. Th/U, b) U vs. K/U.

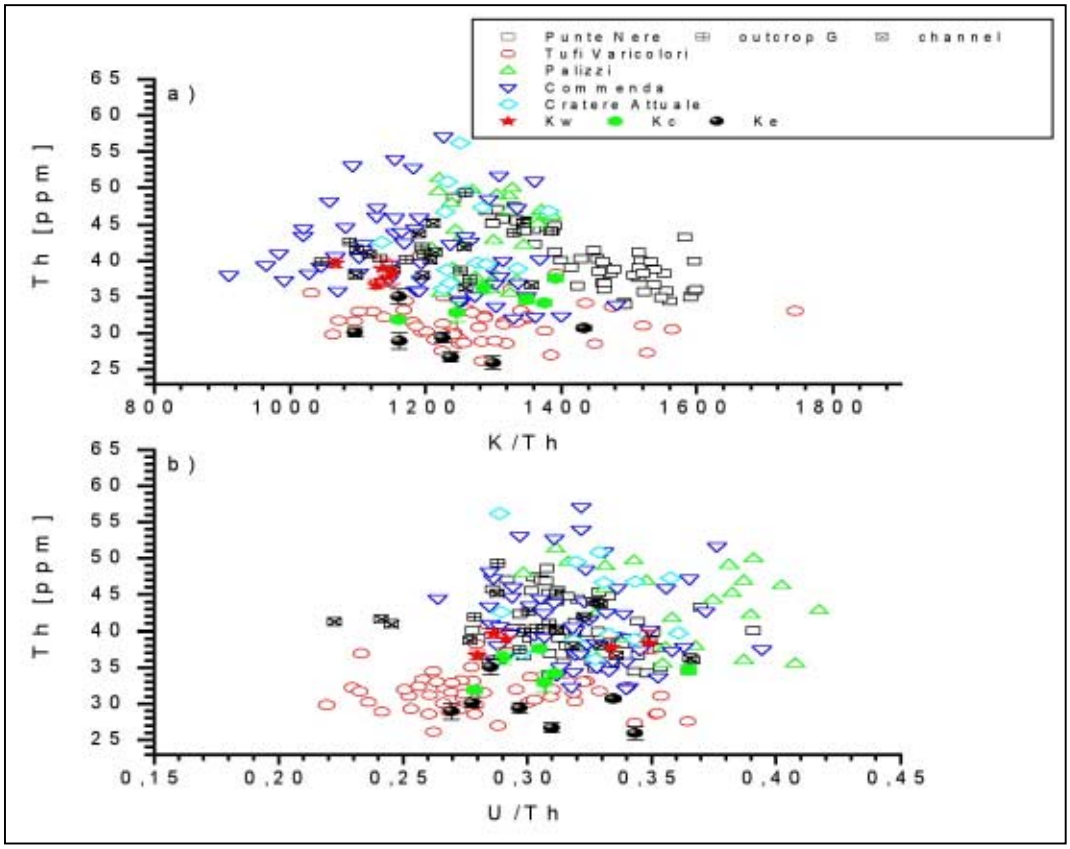

Figure IV.C.8: Scatter plots Th vs. K/Th and Th vs. U/Th for outcrop K in comparison with the standard outcrops. a) Th vs. K/Th, b) Th vs. U/Th.

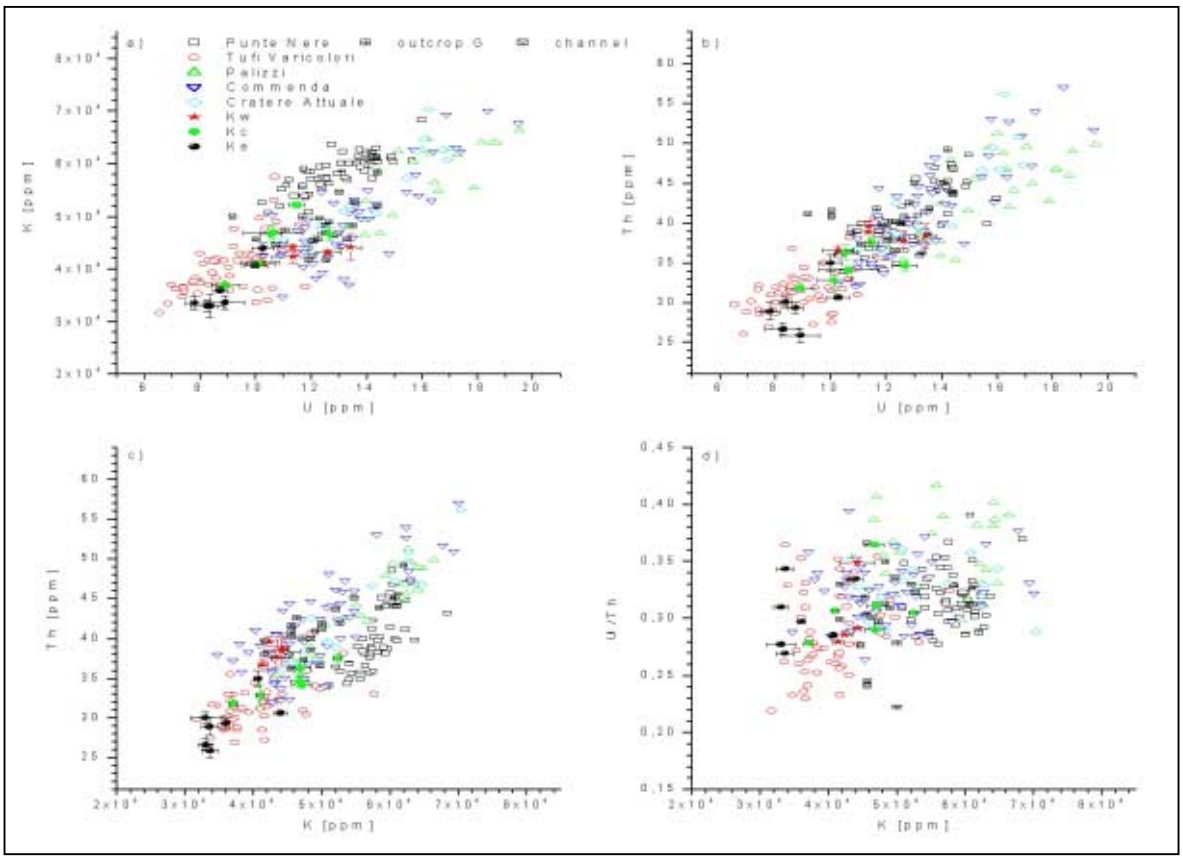

Figure IV.C.9: Scatter plots K vs. U, Th vs. U, Th vs. K, and U/Th vs. K for outcrop K in comparison with the standard outcrops. a) K vs. U, b) Th vs. U), c) Th vs. K, d) U/Th vs. K.

IV. Appendix IVd: Plots for Undefined Outcrops

IV.D. Outcrop L

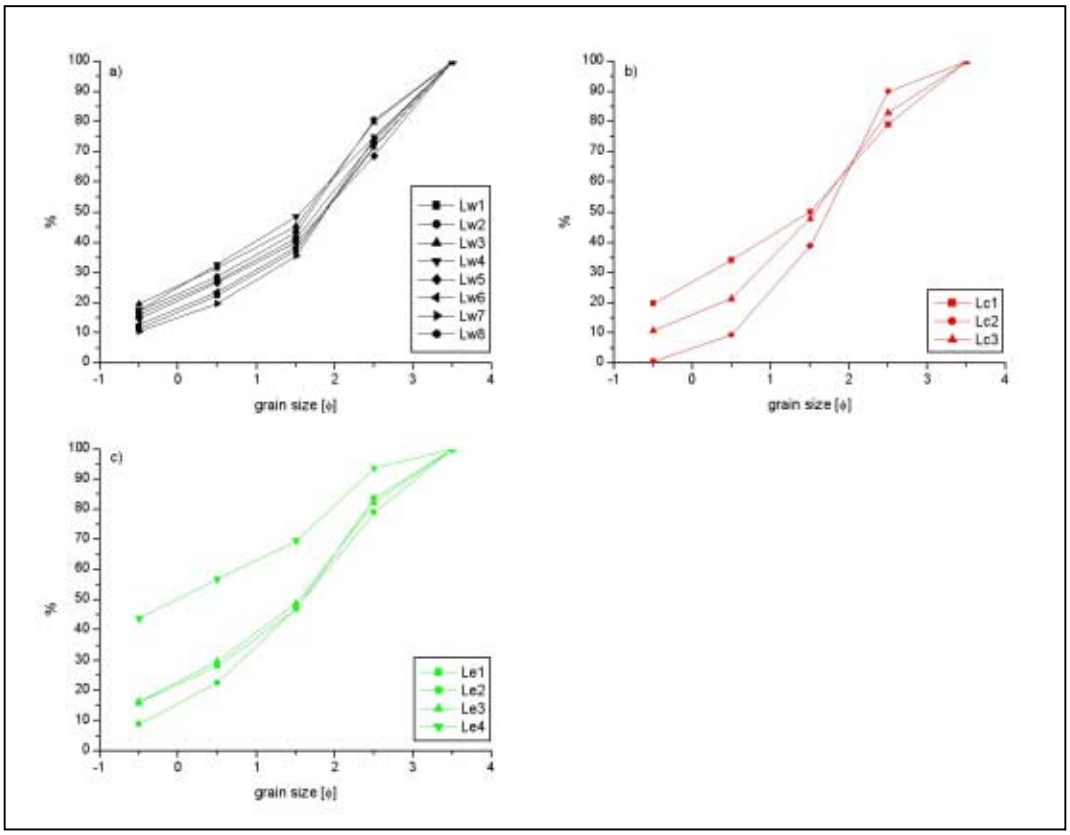

Figure IV.D.1: Cumulative grain size curve for outcrop L. a) unit Lw, b) unit Lc, and d) unit Le.

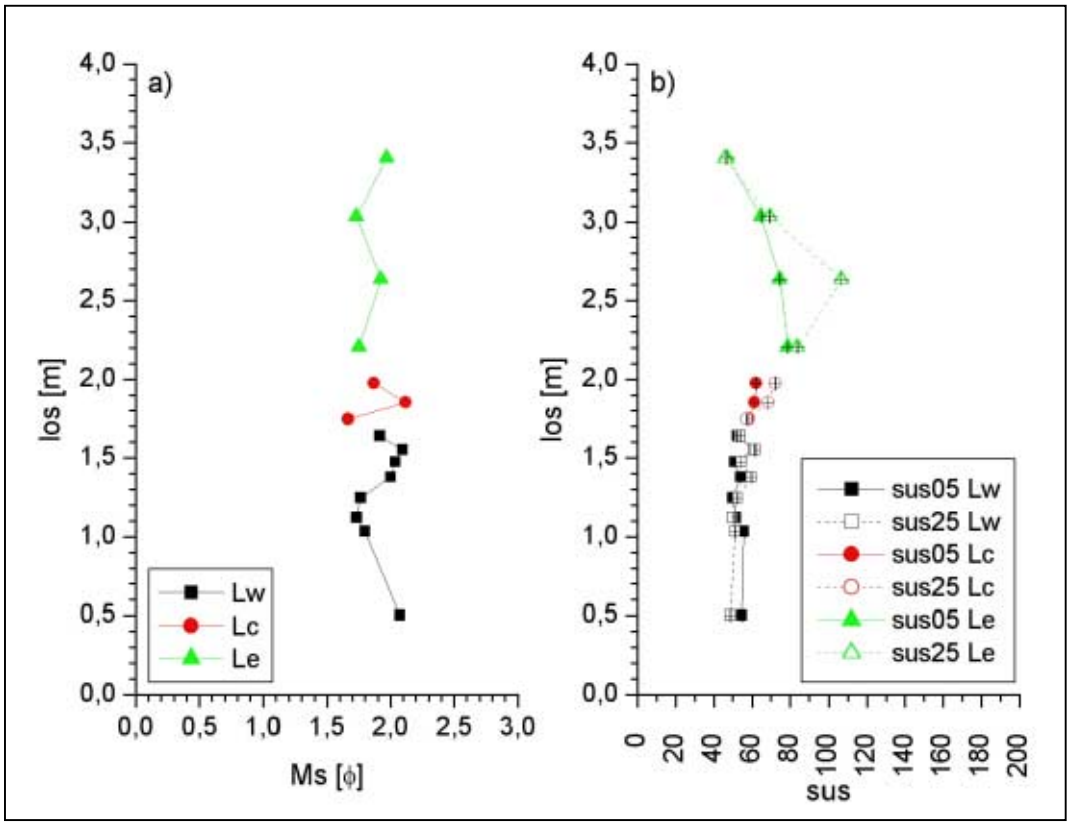

Figure IV.D.2: los vs. Ms [ϕ] and sus for outcrop L. a) los vs. Ms; b) los vs. sus05 and sus25.

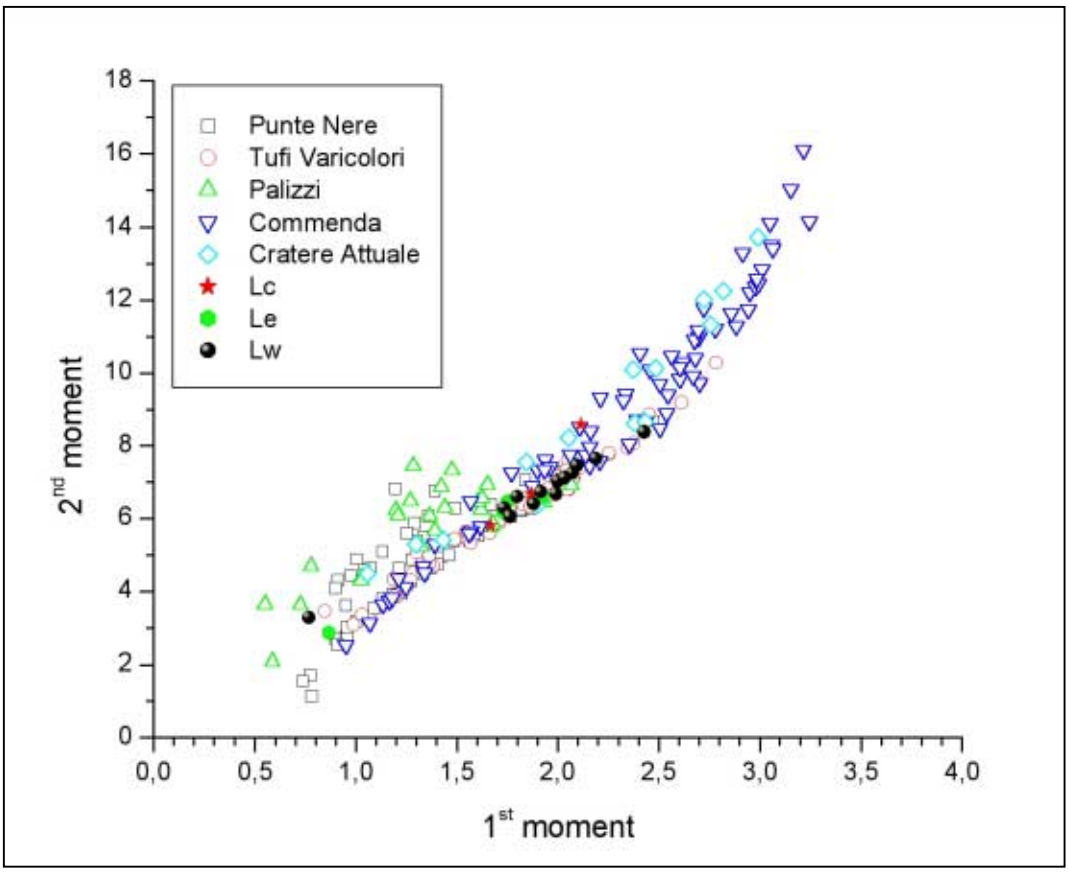

Figure IV.D.3: 1st vs. 2nd moment for outcrop L in comparison with the standard outcrops.

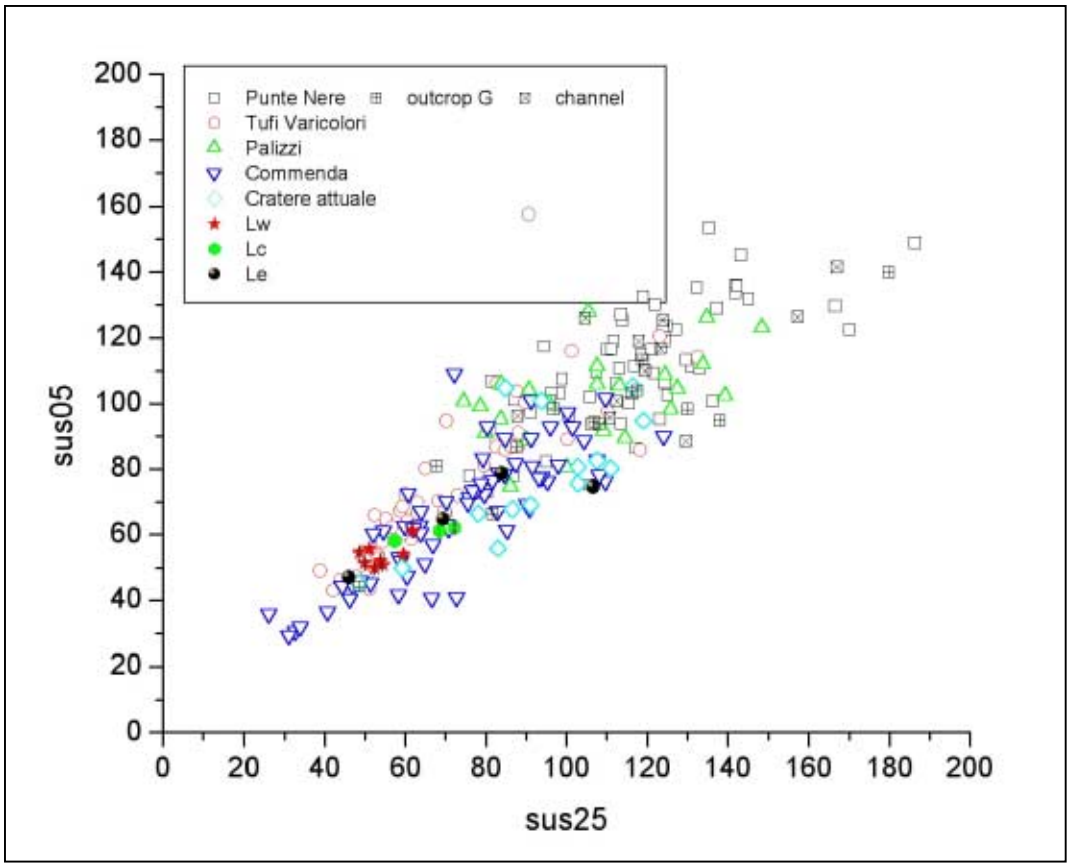

Figure IV.D.4: Scatter plot sus05 vs. sus25 for outcrop L in comparison with the standard outcrops.

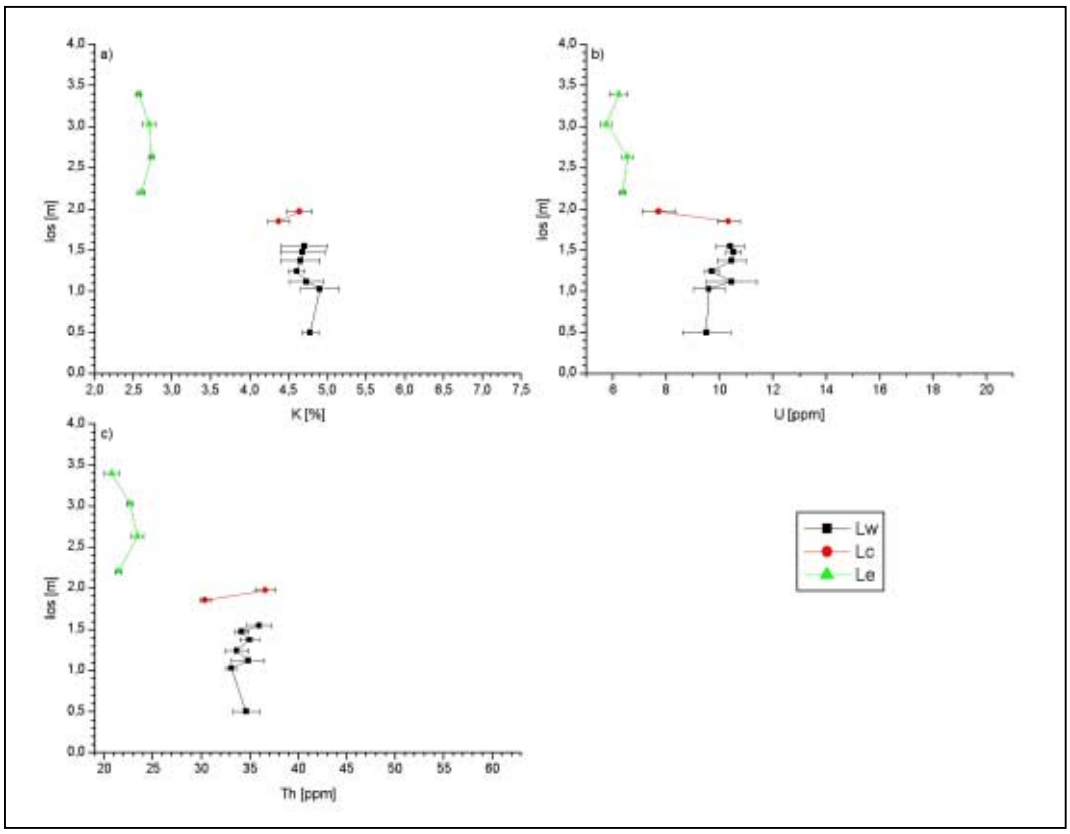

Figure IV.D.5: los. vs. γ-ray values for outcrop L. a) K [%], b) U [ppm], c) Th [ppm].

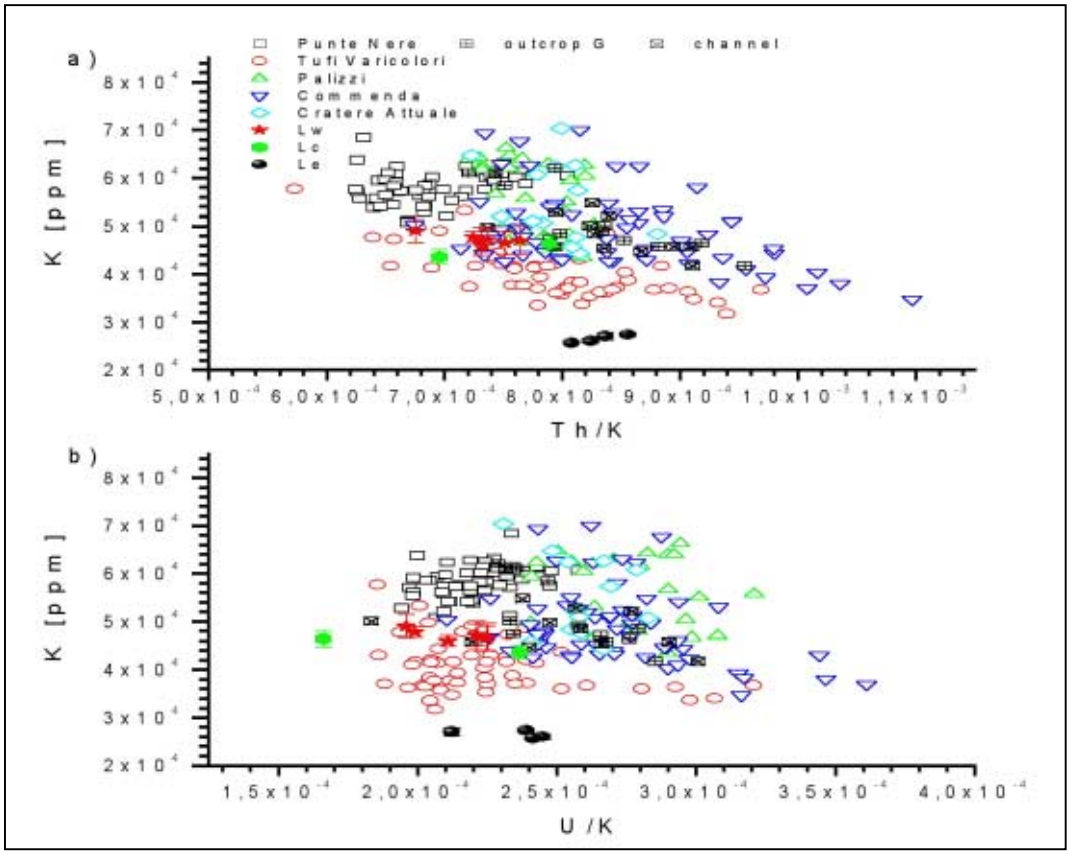

Figure IV.D.6: Scatter plots K vs. Th/K and K vs. U/K for outcrop L in comparison with the standard outcrops. a) K vs. Th/K, b) K vs. U/K.

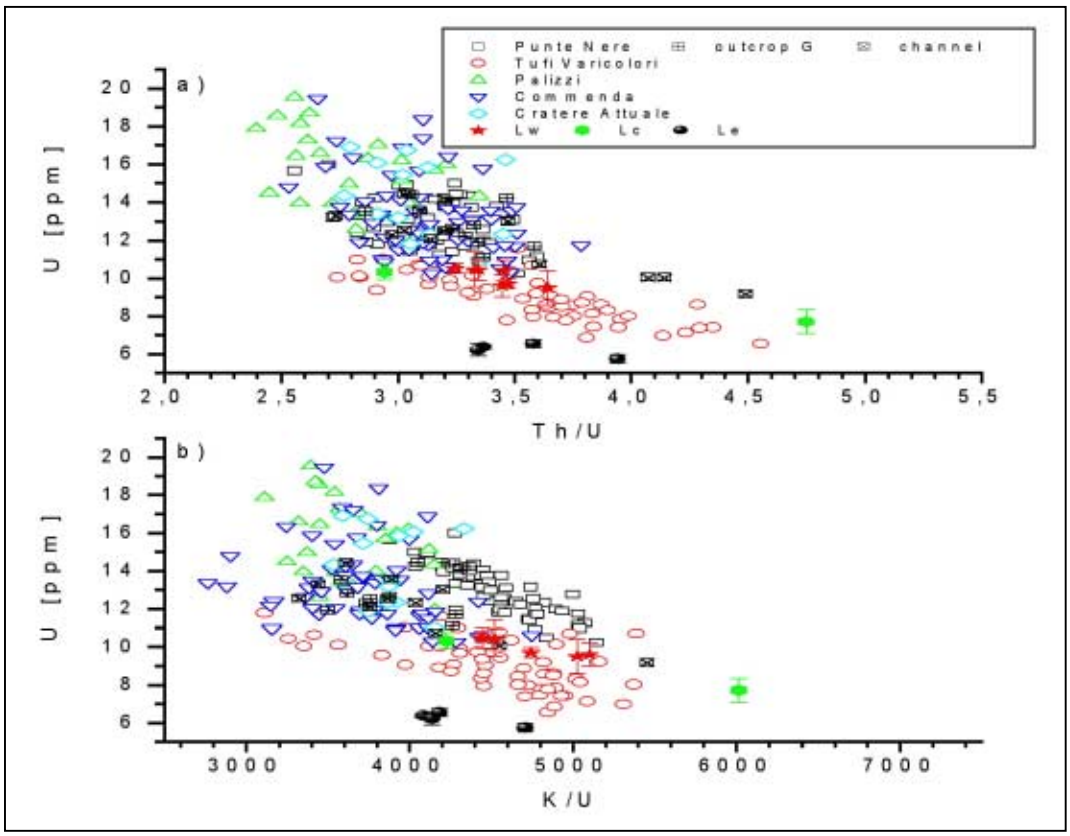

Figure IV.D.7: Scatter plots U vs. Th/U and U vs. K/U for outcrop L in comparison with the standard outcrops. a) U vs. Th/U, b) U vs. K/U.

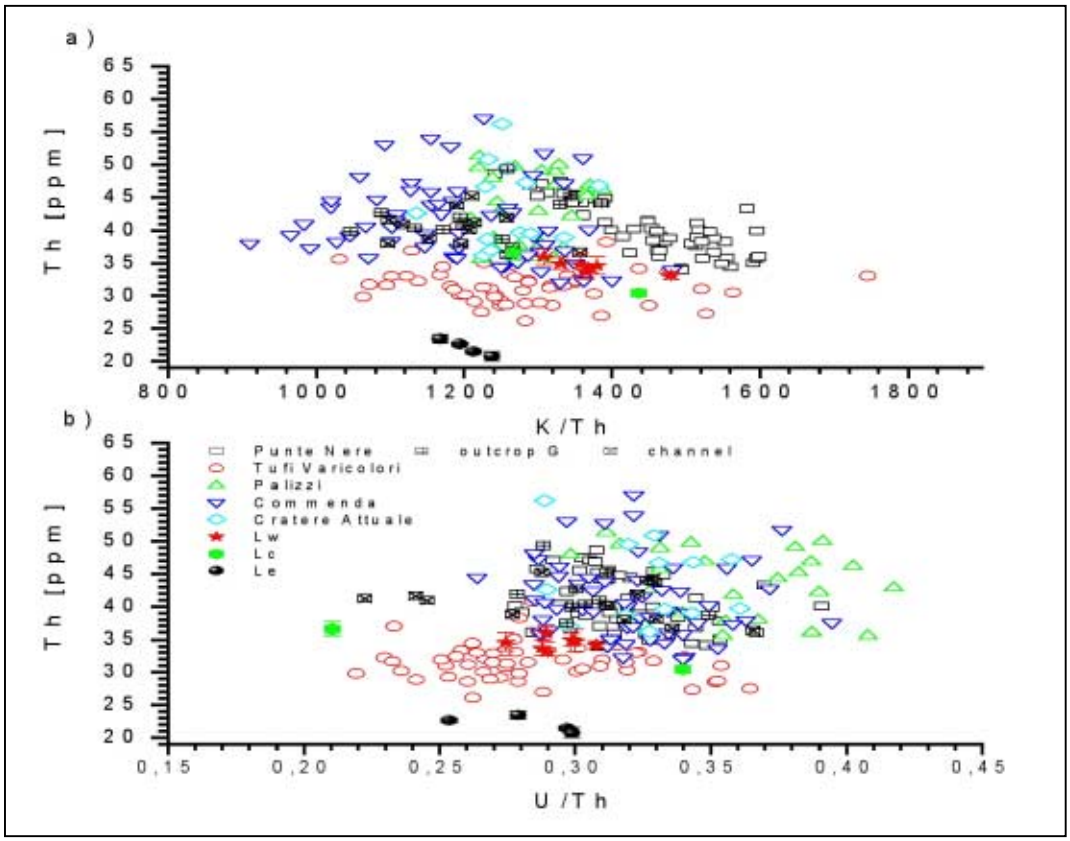

Figure IV.D.8: Scatter plots Th vs. K/Th and Th vs. U/Th for outcrop L in comparison with the standard outcrops. a) Th vs. K/Th, b) Th vs. U/Th.

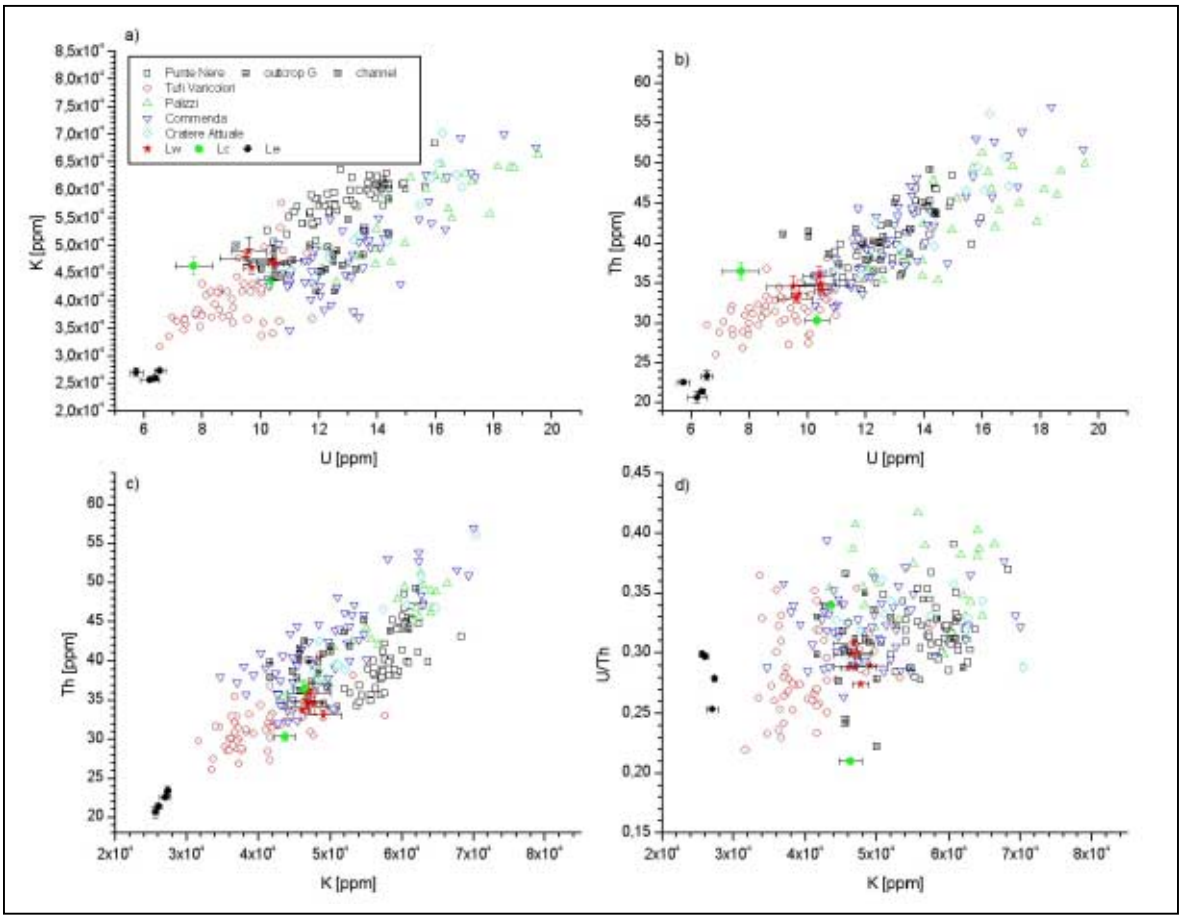

Figure IV.D.9: Scatter plots K vs. U, Th vs. U, Th vs. K, and U/Th vs. K for outcrop L in comparison with the standard outcrops. a) K vs. U, b) Th vs. U), c) Th vs. K, d) U/Th vs. K.

IV. Appendix IVe: Plots for Undefined Outcrops

IV.E. Outcrop M

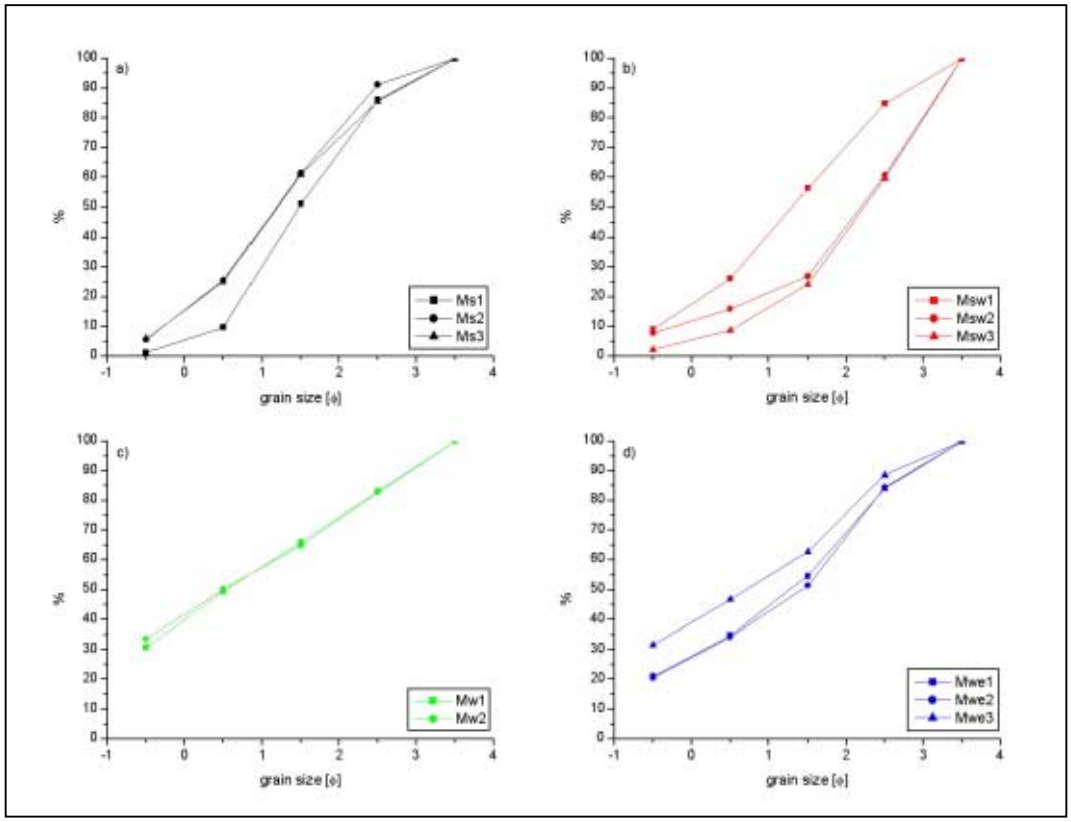

Figure IV.E.1: Cumulative grain size curve for outcrop M. a) unit Ms, b) unit Msw, c) unit Mw, and d) unit Mwe.

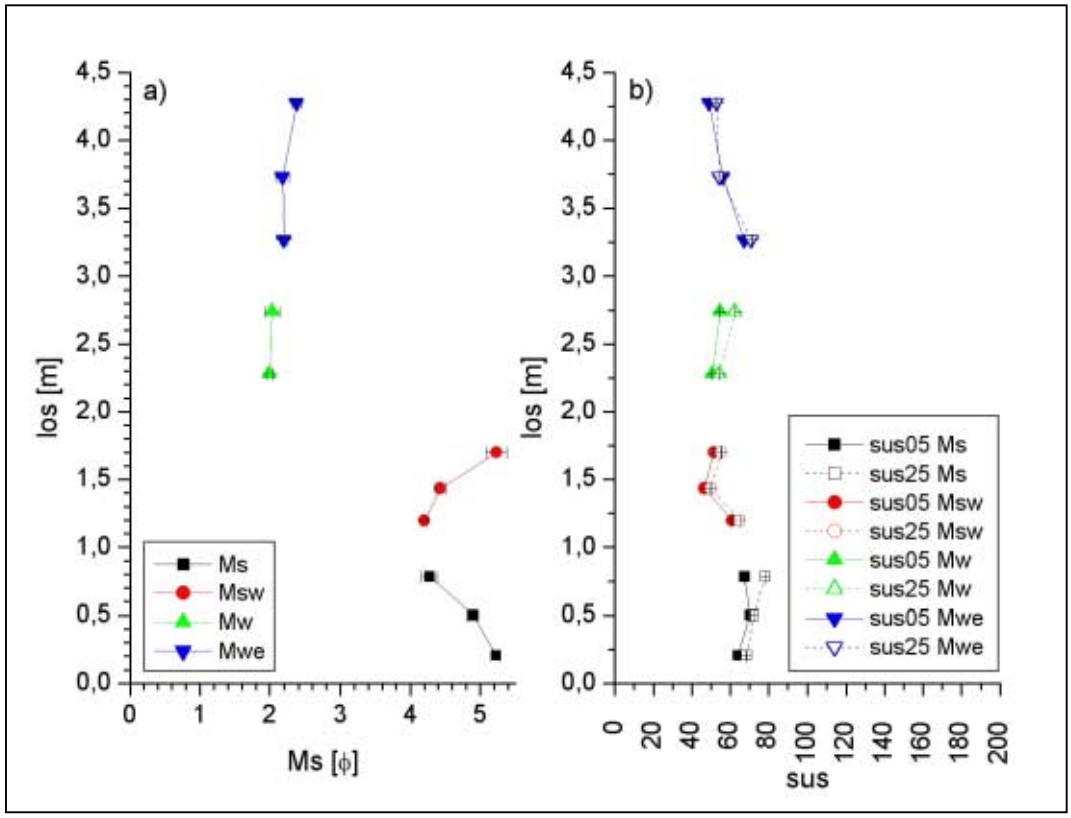

Figure IV.E.2: los vs. Ms [ϕ] and sus for outcrop M. a) los vs. Ms; b) los vs. sus05 and sus25.

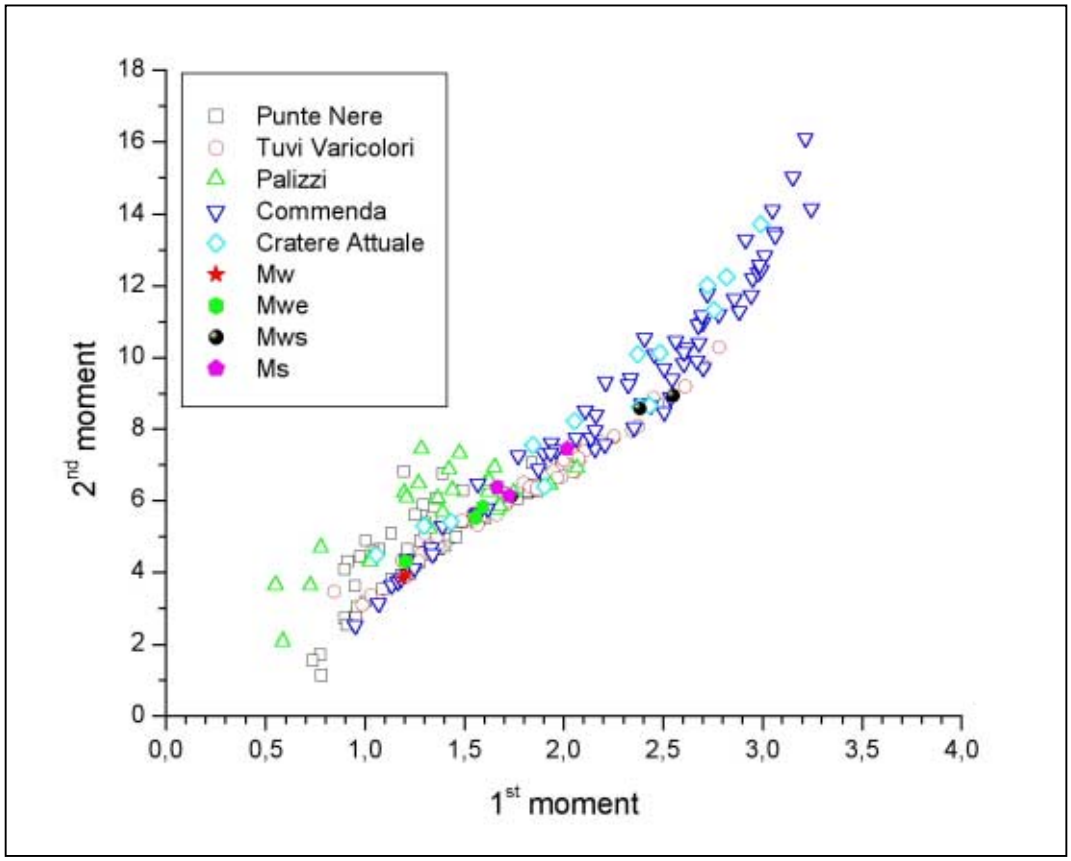

Figure IV.E.3: 1st vs. 2nd moment for outcrop M in comparison with the standard outcrops.

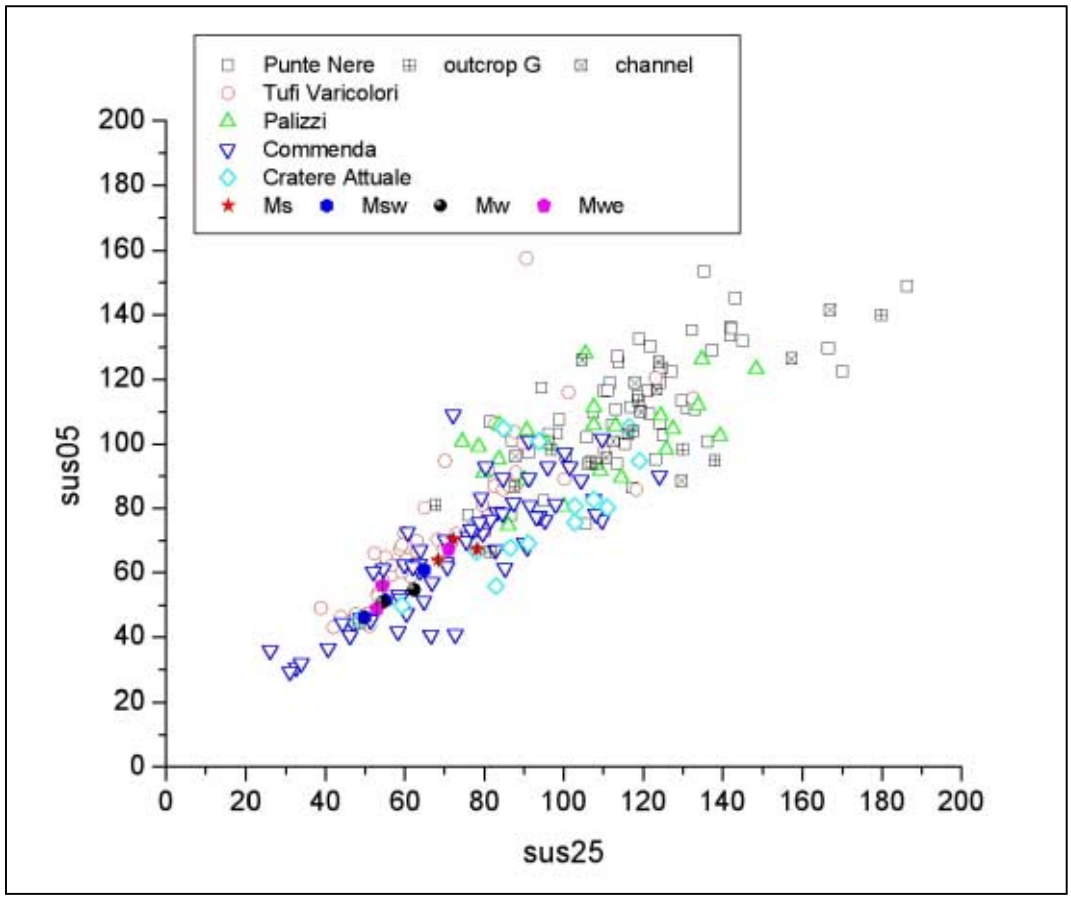

Figure IV.E.4: Scatter plot sus05 vs. sus25 for outcrop M in comparison with the standard outcrops.

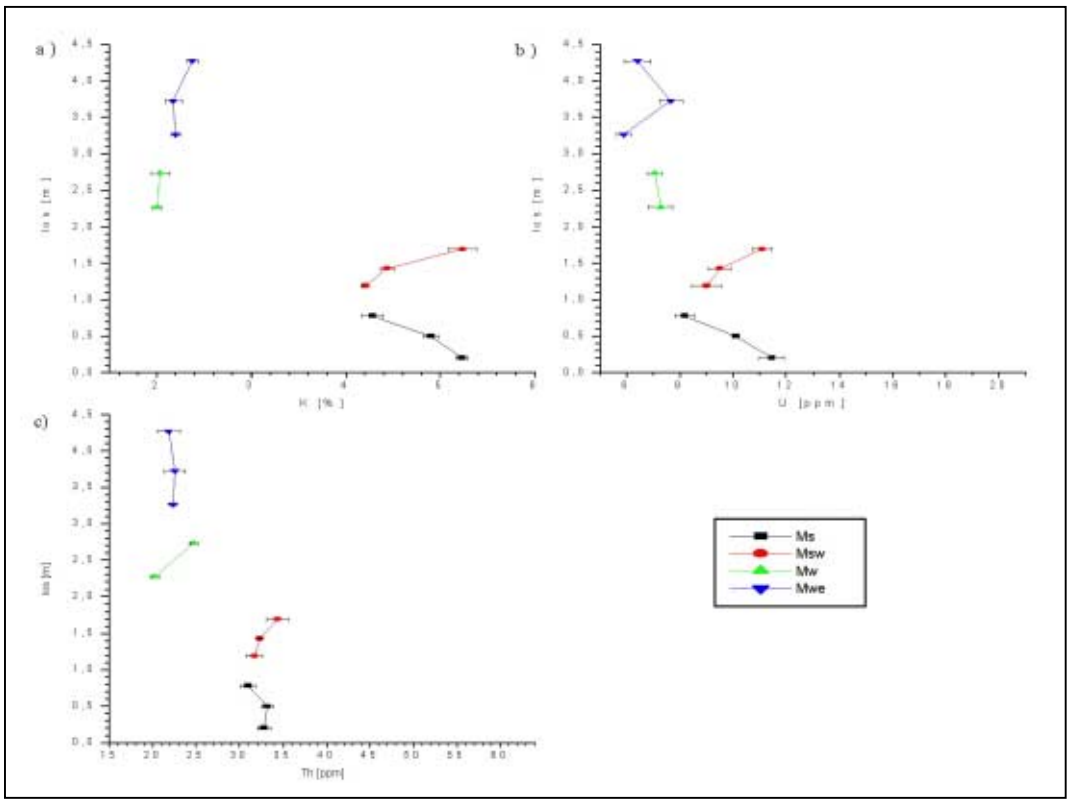

Figure IV.E.5: los. vs. γ-ray values for outcrop M. a) K [%], b) U [ppm], c) Th [ppm].

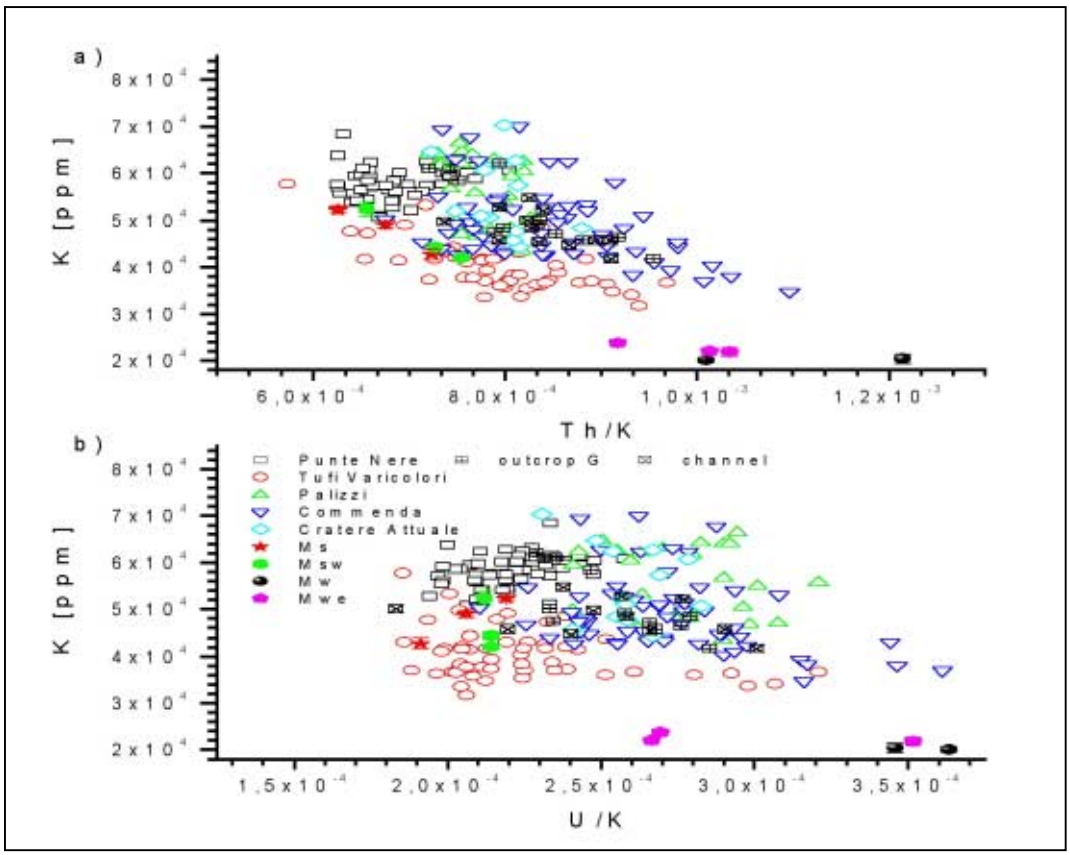

Figure IV.E.6: Scatter plots K vs. Th/K and K vs. U/K for outcrop M in comparison with the standard outcrops. a) K vs. Th/K, b) K vs. U/K.

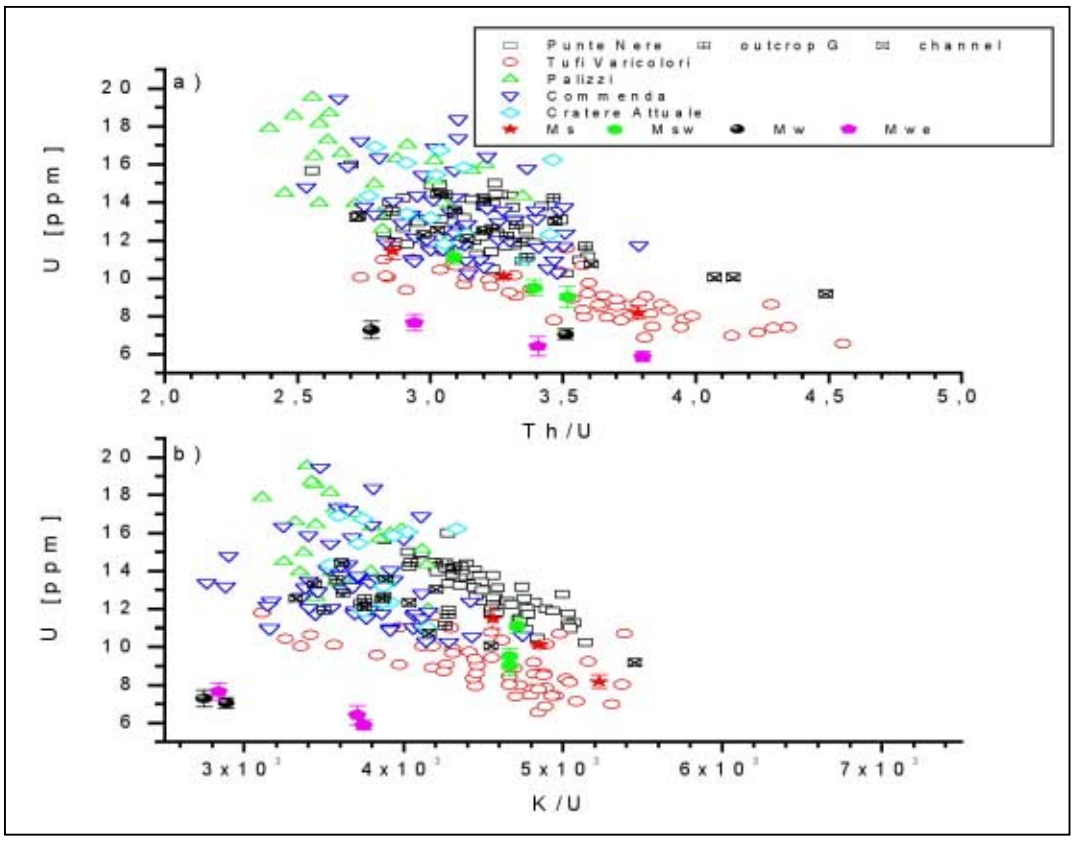

Figure IV.E.7: Scatter plots U vs. Th/U and U vs. K/U for outcrop M in comparison with the standard outcrops. a) U vs. Th/U, b) U vs. K/U.

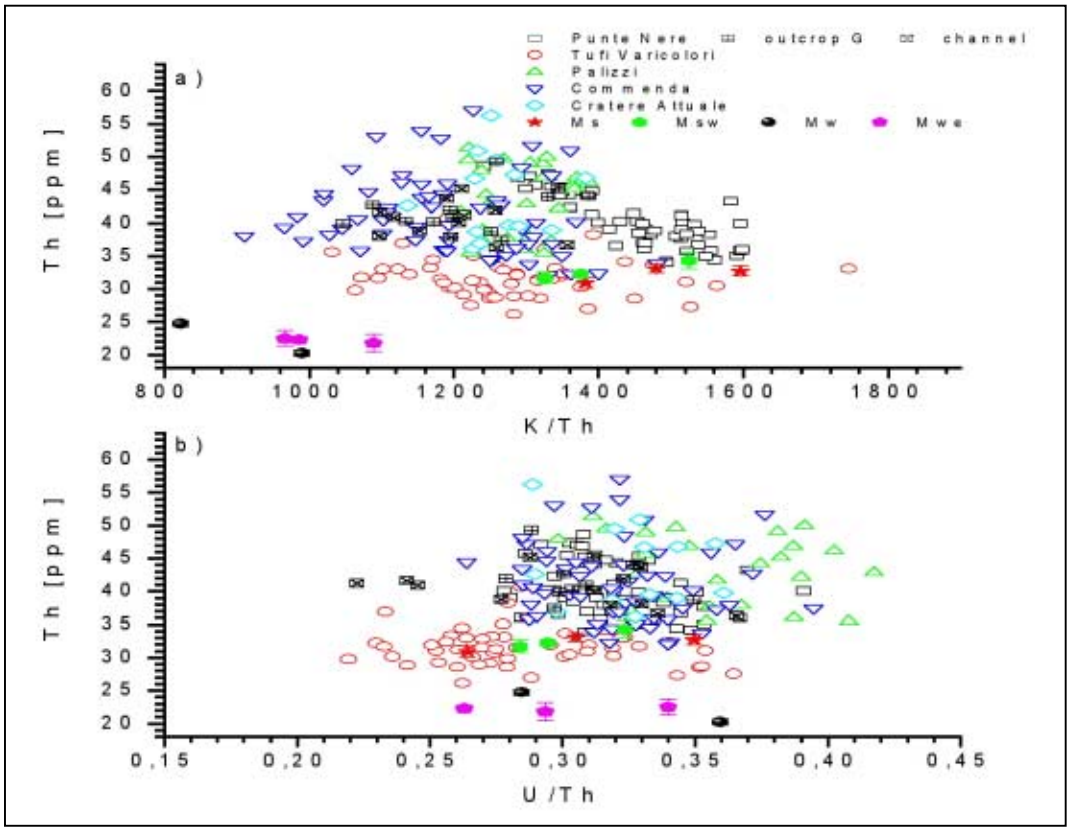

Figure IV.E.8: Scatter plots Th vs. K/Th and Th vs. U/Th for outcrop M in comparison with the standard outcrops. a) Th vs. K/Th, b) Th vs. U/Th.

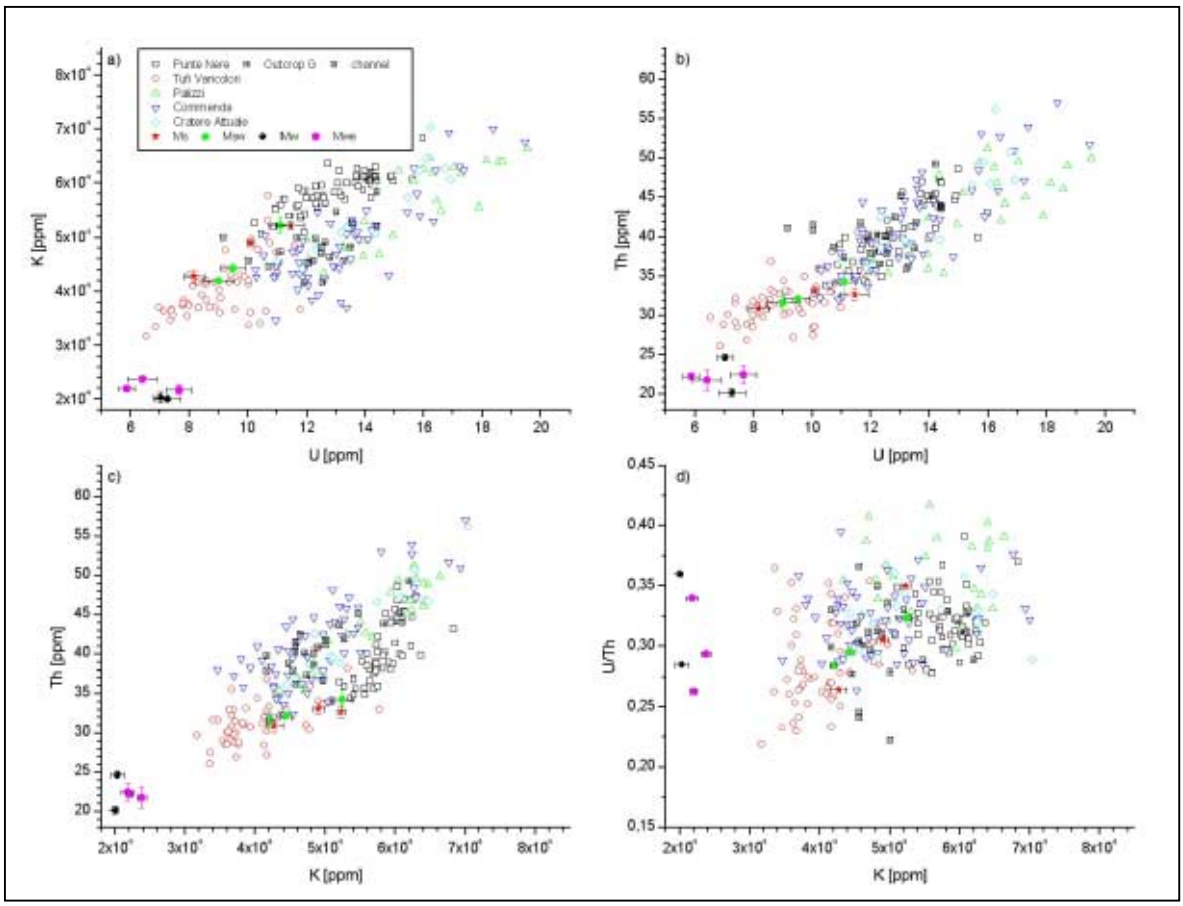

Figure IV.E.9: Scatter plots K vs. U, Th vs. U, Th vs. K, and U/Th vs. K for outcrop M in comparison with the standard outcrops. a) K vs. U, b) Th vs. U), c) Th vs. K, d) U/Th vs. K.

IV. Appendix IVf: Plots for Undefined Outcrops

IV.F. Outcrop N

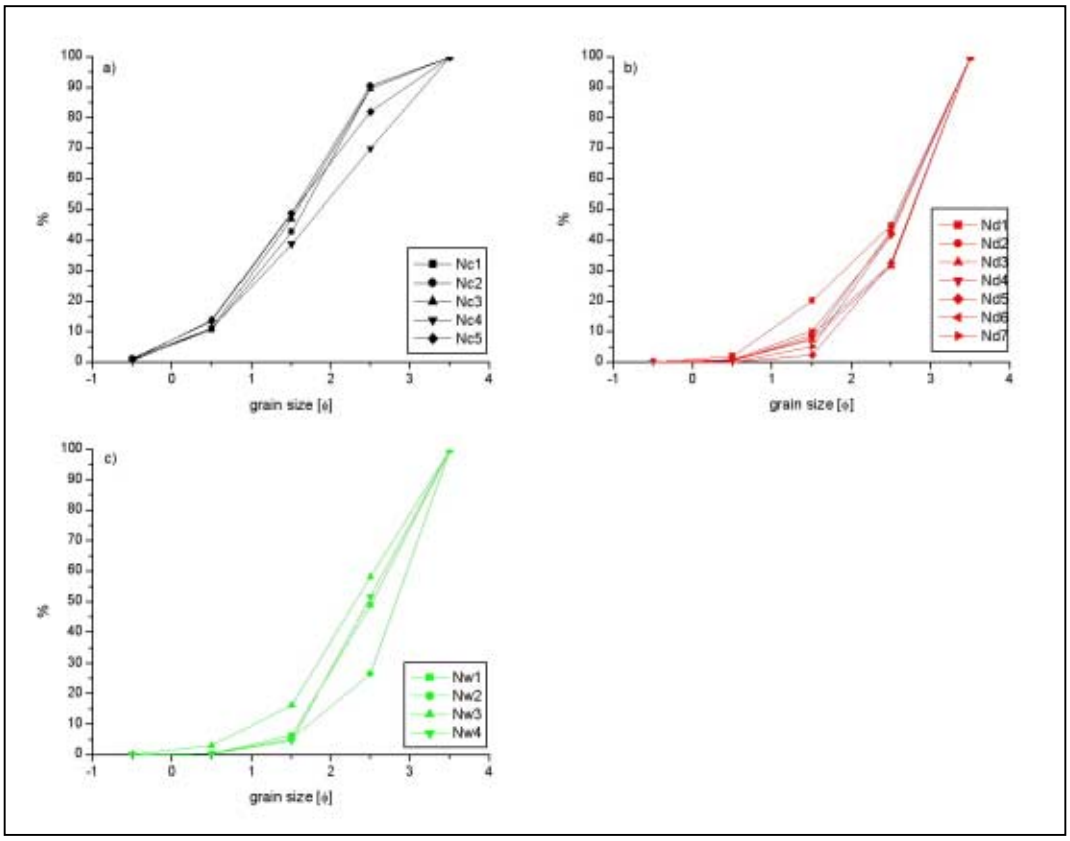

Figure IV.F.1: Cumulative grain size curve for outcrop N. a) unit Nc, b) unit Nd, c) unit Nw

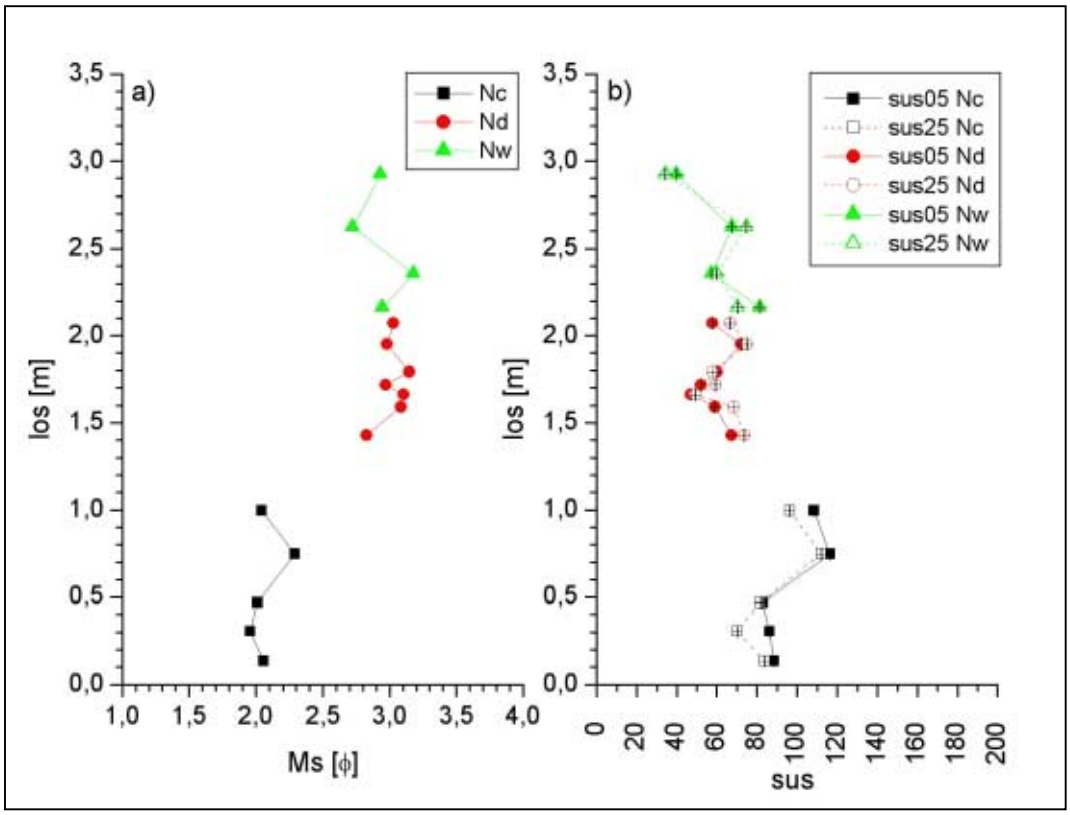

Figure IV.F.2: los vs. Ms [ϕ] and sus for outcrop N. a) los vs. Ms; b) los vs. sus05 and sus25.

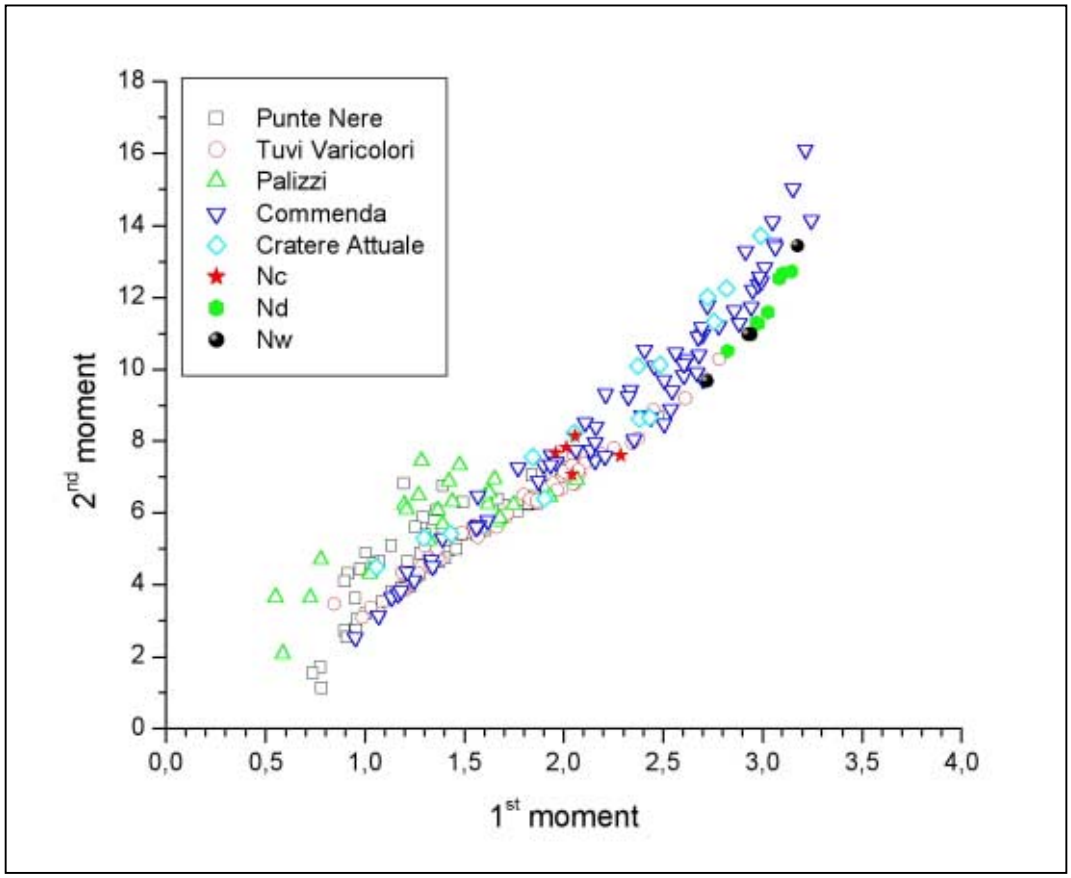

Figure IV.F.3: 1st vs. 2nd moment for outcrop N in comparison with the standard outcrops.

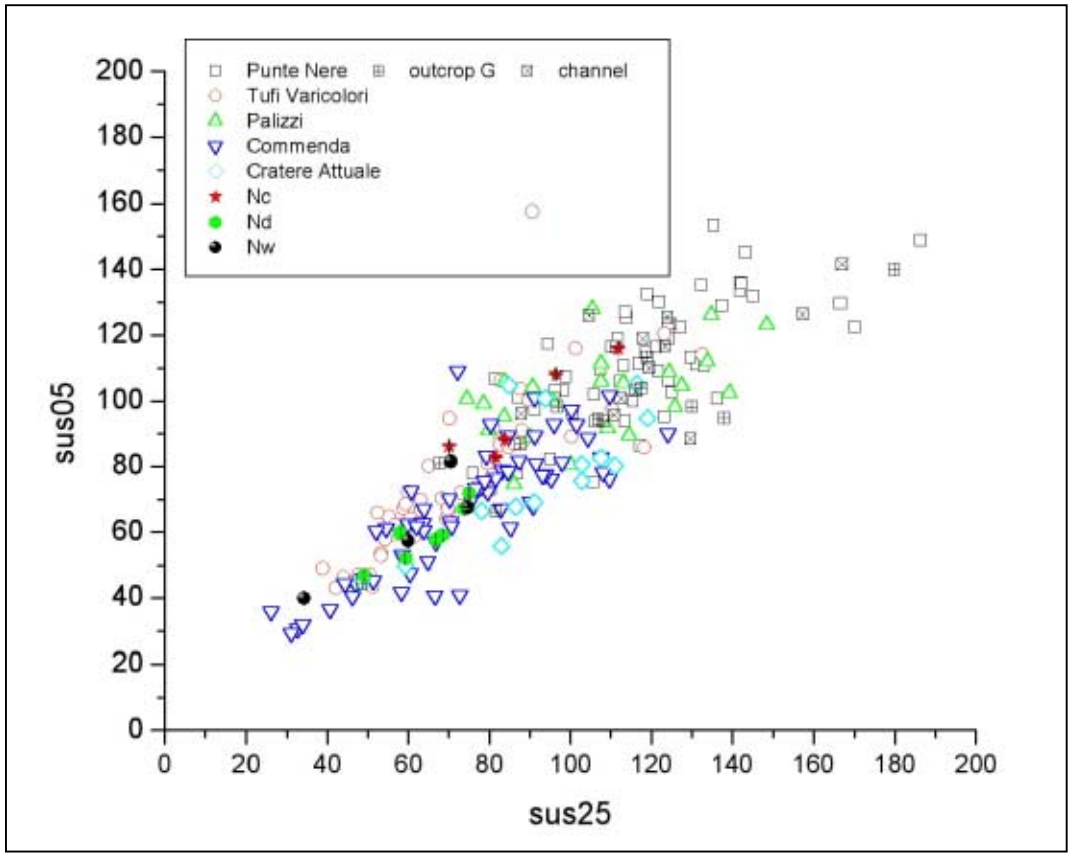

Figure IV.F.4: Scatter plot sus05 vs. sus25 for outcrop N in comparison with the standard outcrops.

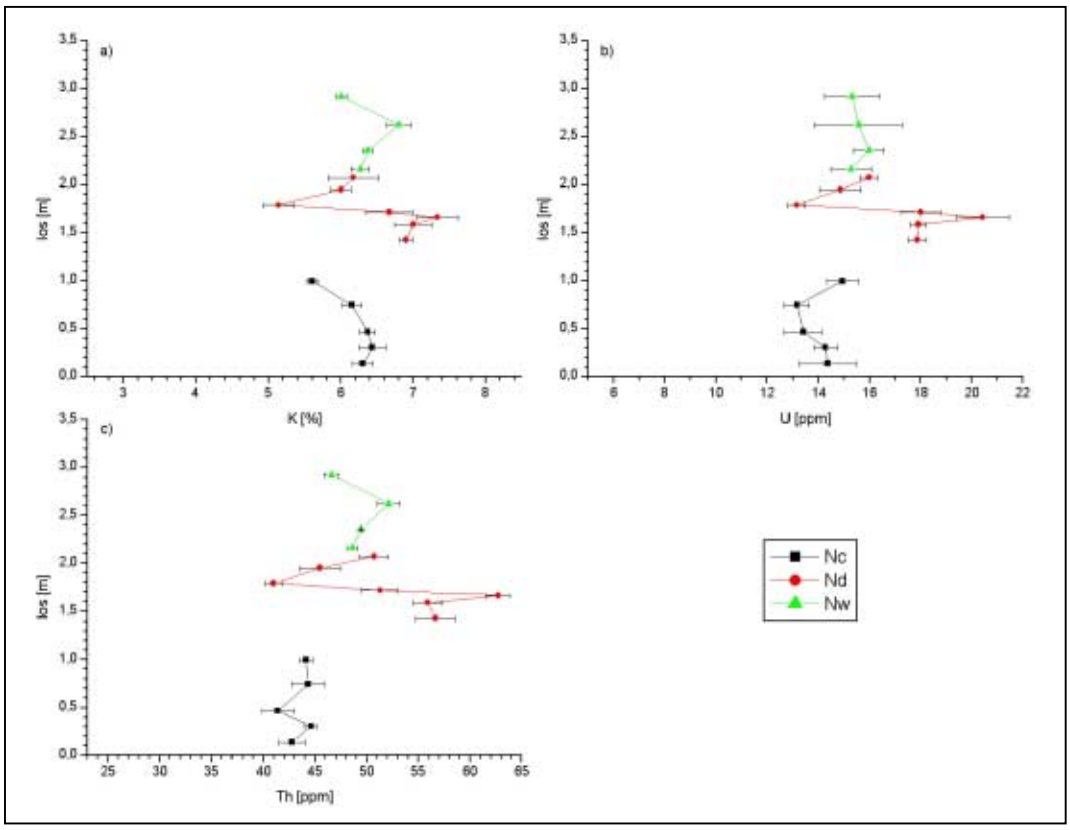

Figure IV.F.5: los. vs. γ-ray values for outcrop N. a) K [%], b) U [ppm], c) Th [ppm].

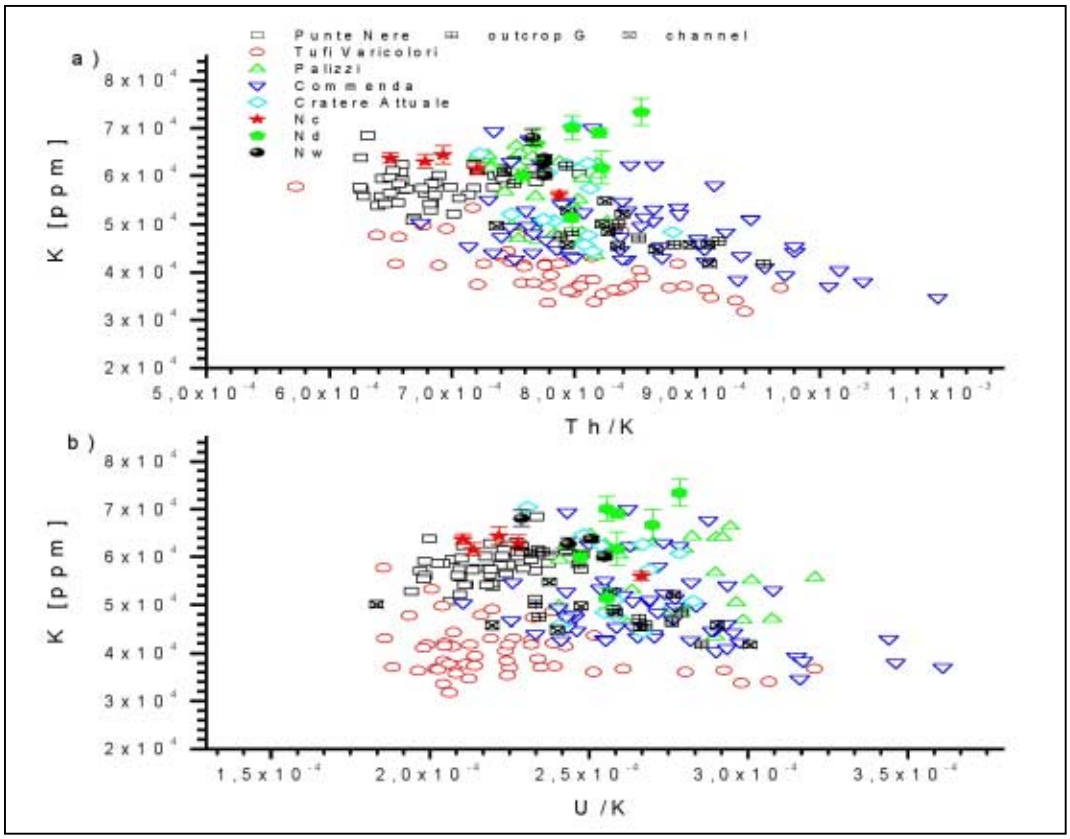

Figure IV.F.6: Scatter plots K vs. Th/K and K vs. U/K for outcrop N in comparison with the standard outcrops. a) K vs. Th/K, b) K vs. U/K.

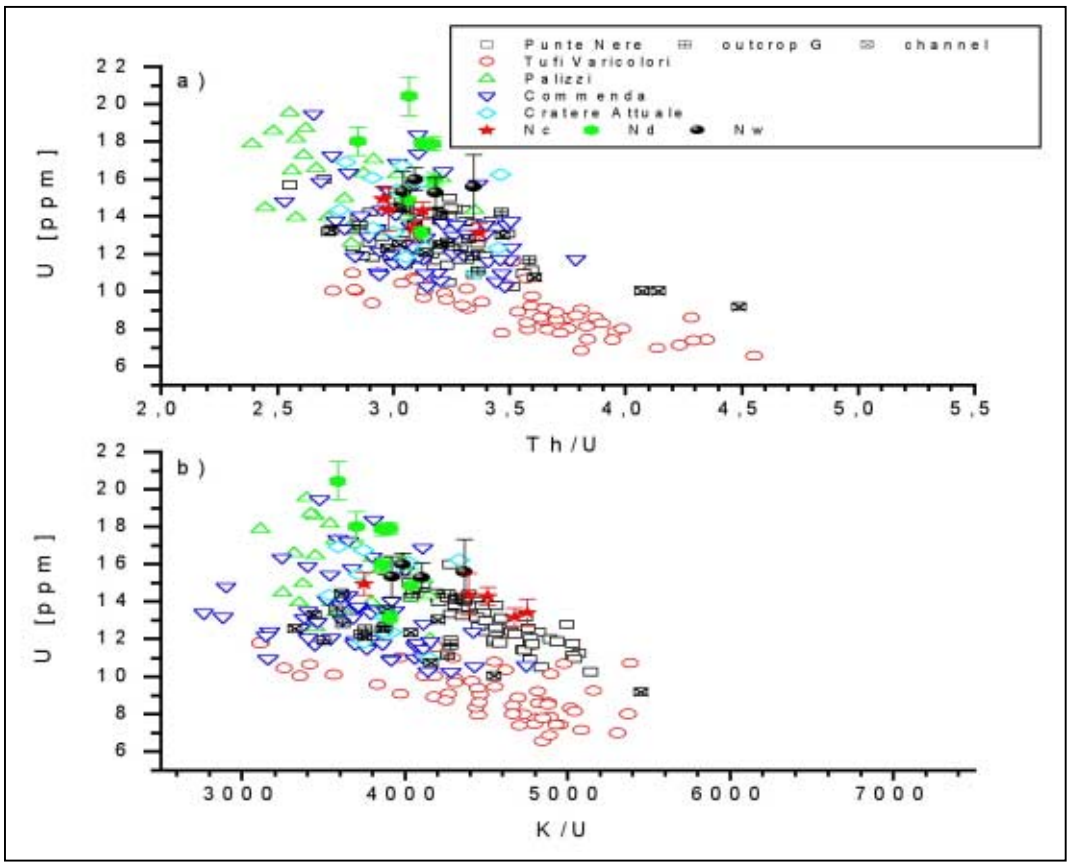

Figure IV.F.7: Scatter plots U vs. Th/U and U vs. K/U for outcrop N in comparison with the standard outcrops. a) U vs. Th/U, b) U vs. K/U.

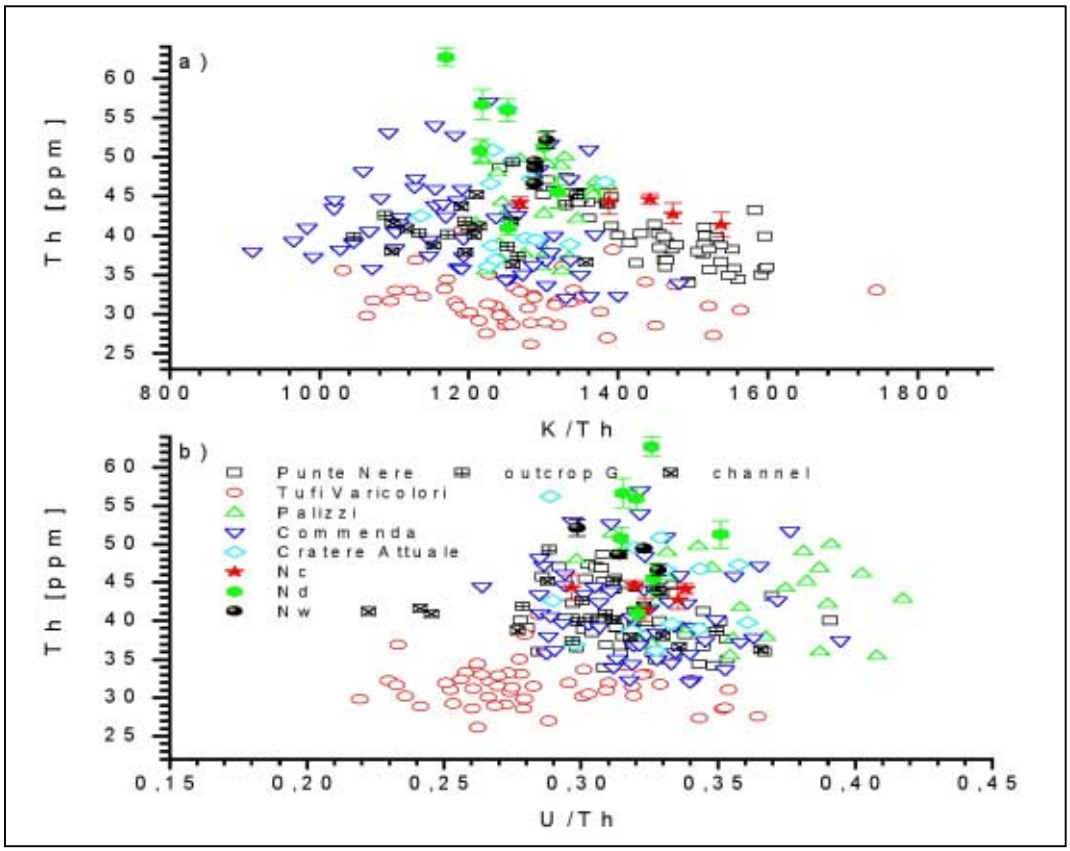

Figure IV.F.8: Scatter plots Th vs. K/Th and Th vs. U/Th for outcrop N in comparison with the standard outcrops. a) Th vs. K/Th, b) Th vs. U/Th.

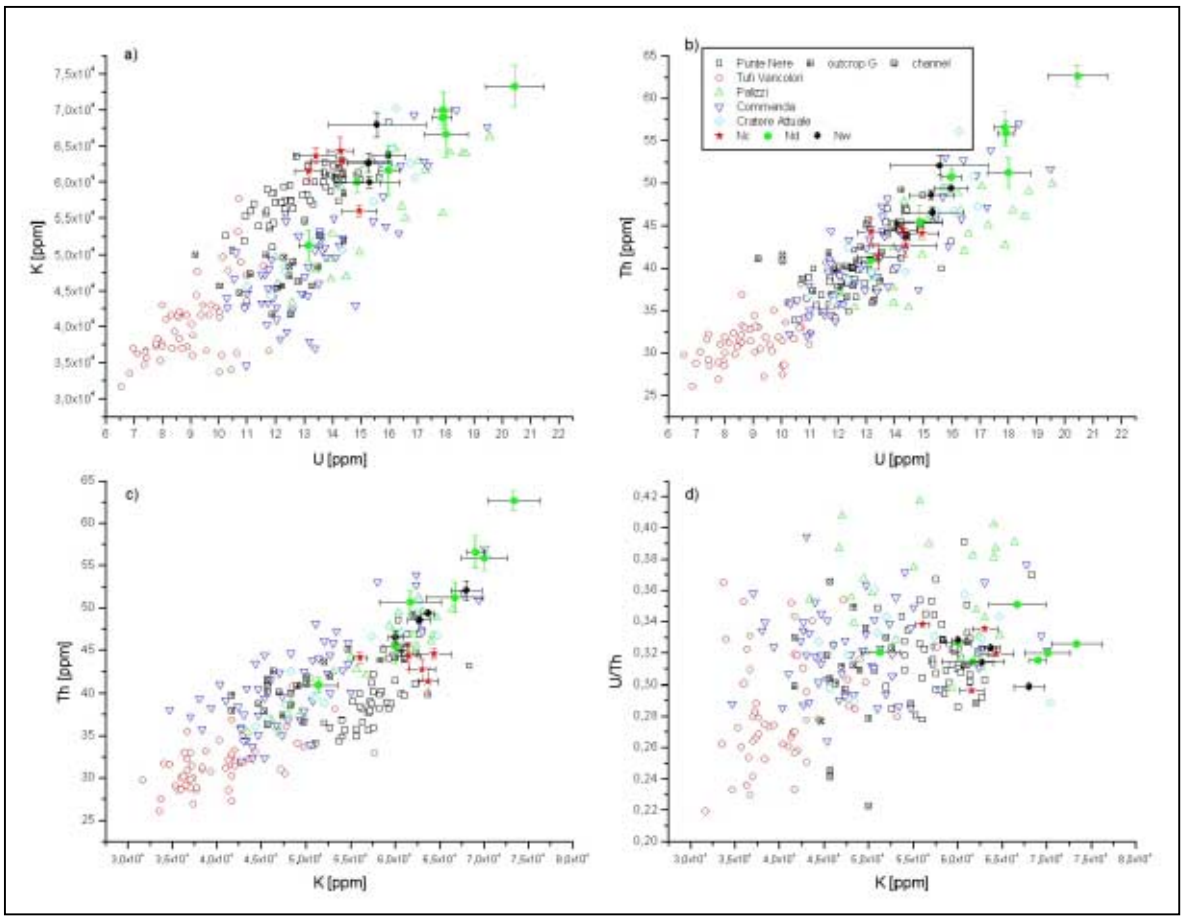

Figure IV.F.9: Scatter plots K vs. U, Th vs. U, Th vs. K, and U/Th vs. K for outcrop N in comparison with the standard outcrops. a) K vs. U, b) Th vs. U), c) Th vs. K, d) U/Th vs. K.

IV. Appendix IVg: Plots for Undefined Outcrops

IV.G. Outcrop P

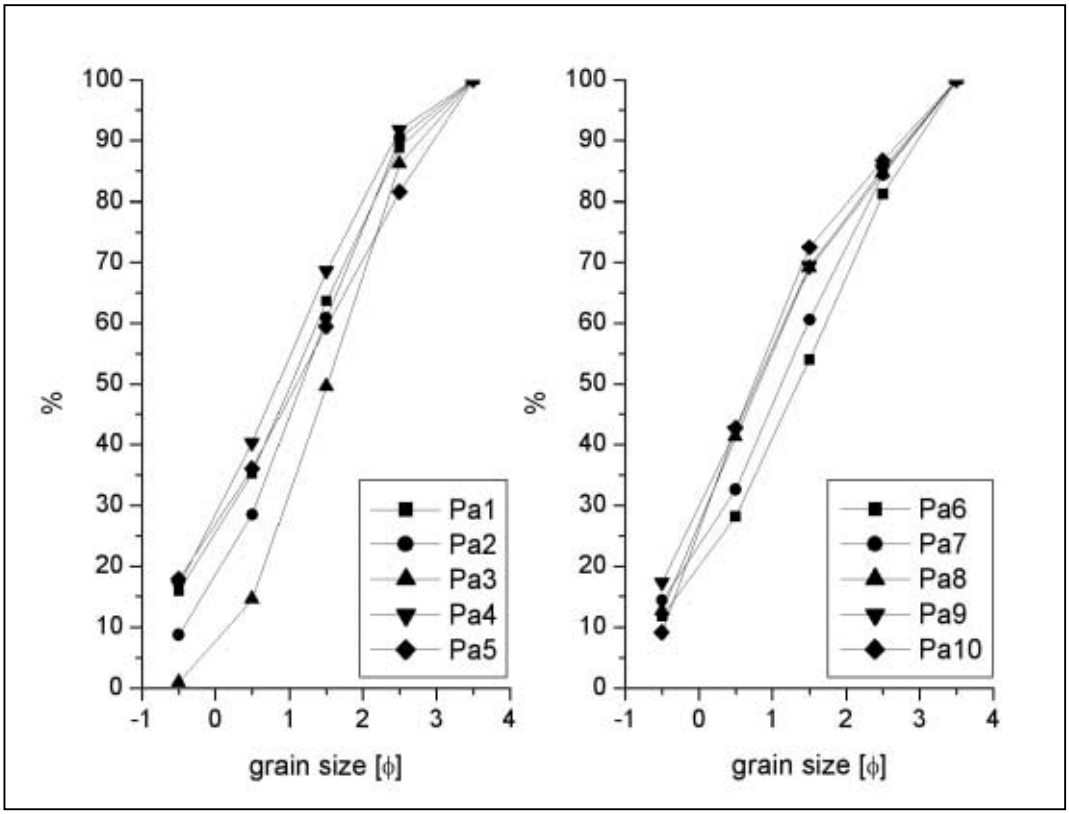

Figure IV.G.1: Cumulative grain size curve for outcrop P.

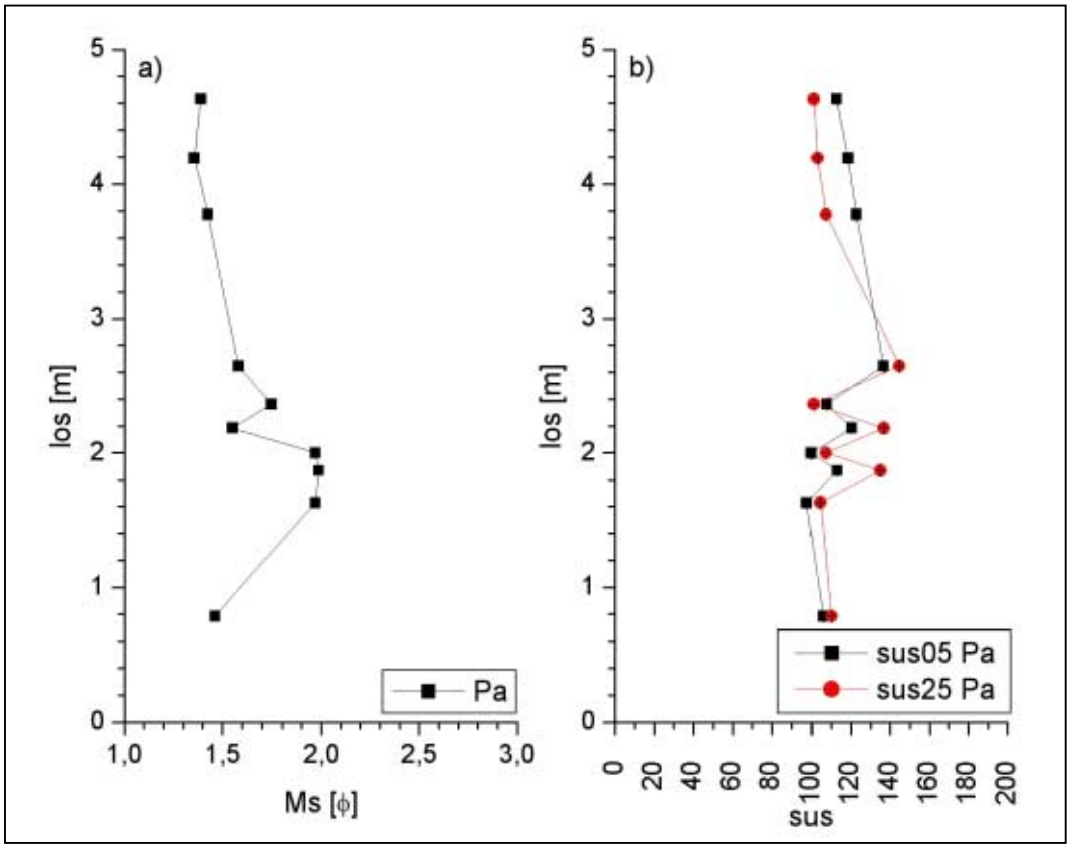

Figure IV.G.2: los vs. Ms [ϕ] and sus for outcrop P. a) los vs. Ms; b) los vs. sus05 and sus25.

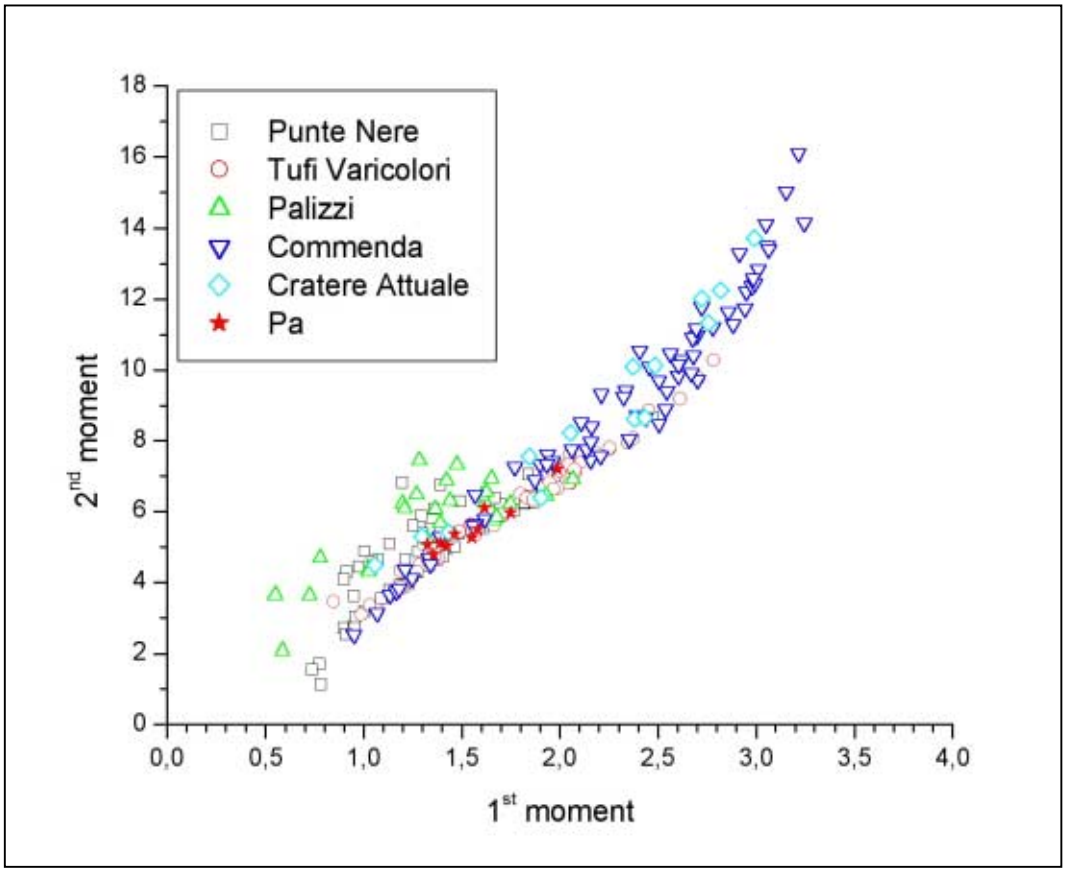

Figure IV.G.3: 1st vs. 2nd moment for outcrop P in comparison with the standard outcrops.

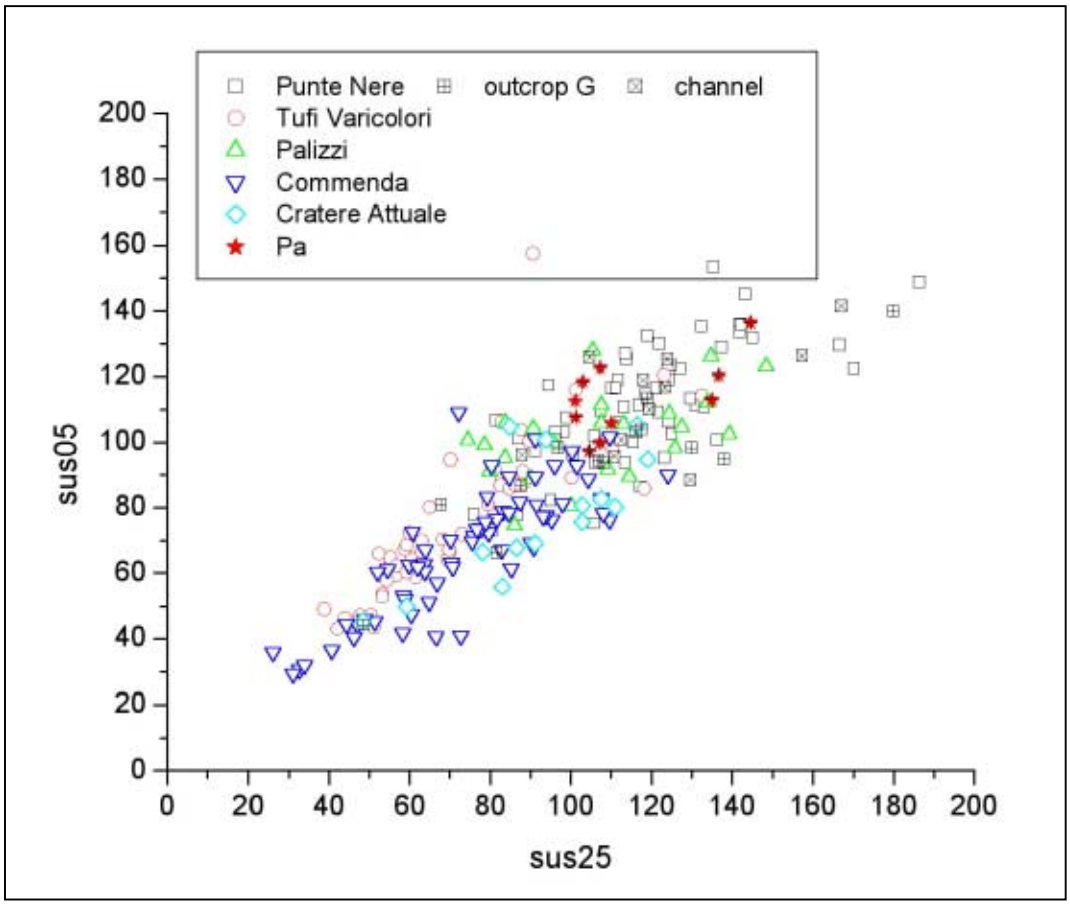

Figure IV.G.4: Scatter plot sus05 vs. sus25 for outcrop P in comparison with the standard outcrops.

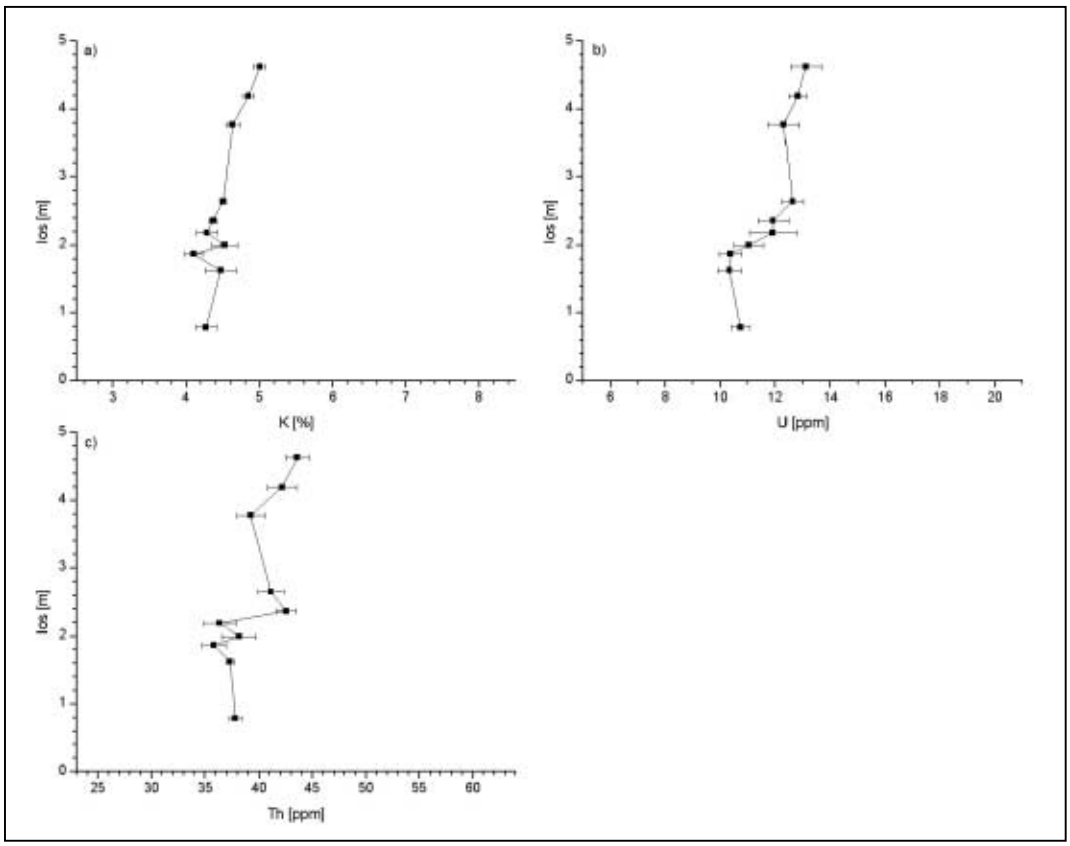

Figure IV.G.5: los. vs. γ-ray values for outcrop P. a) K [%], b) U [ppm], c) Th [ppm].

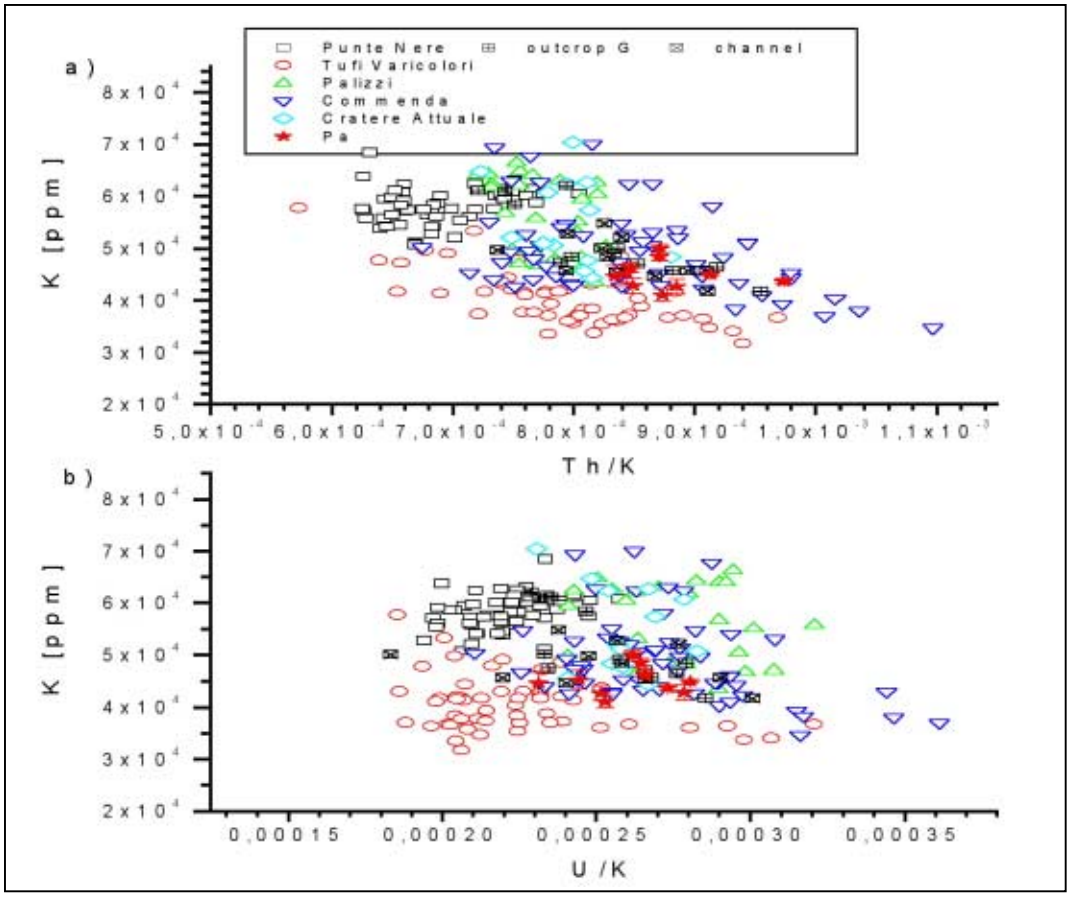

Figure IV.G.6: Scatter plots K vs. Th/K and K vs. U/K for outcrop P in comparison with the standard outcrops. a) K vs. Th/K, b) K vs. U/K.

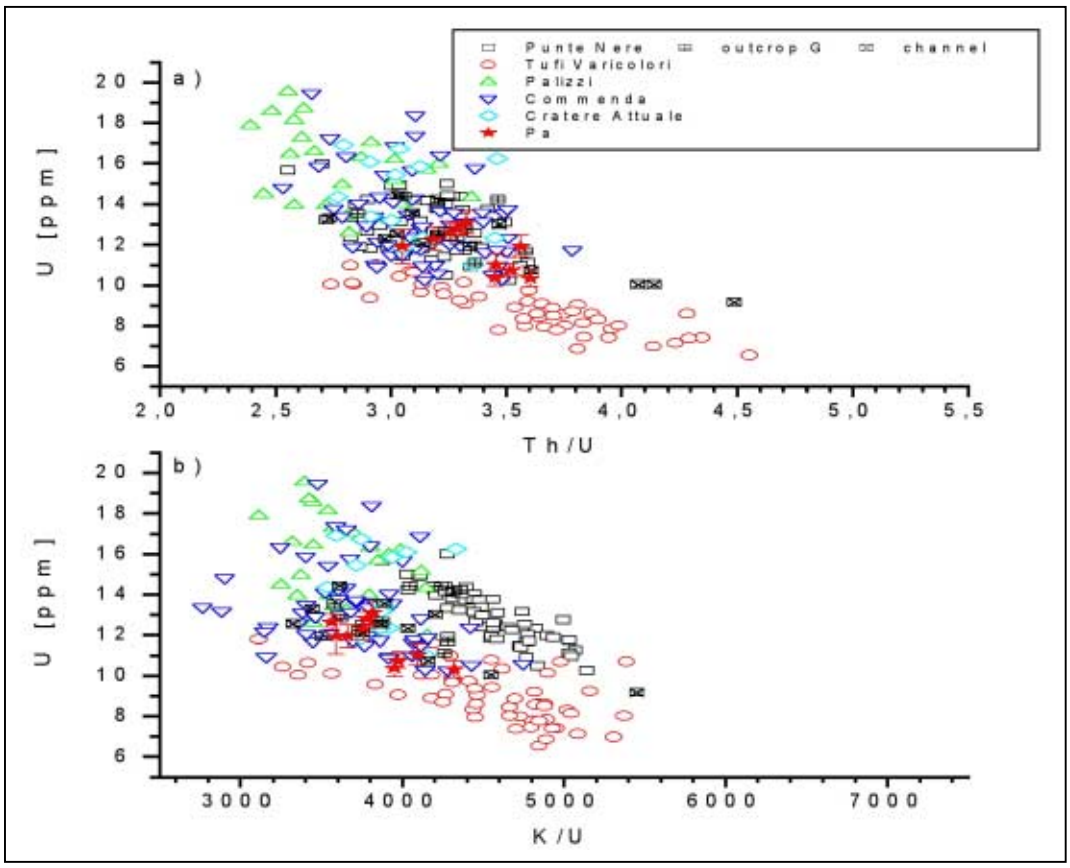

Figure IV.G.7: Scatter plots U vs. Th/U and U vs. K/U for outcrop P in comparison with the standard outcrops. a) U vs. Th/U, b) U vs. K/U.

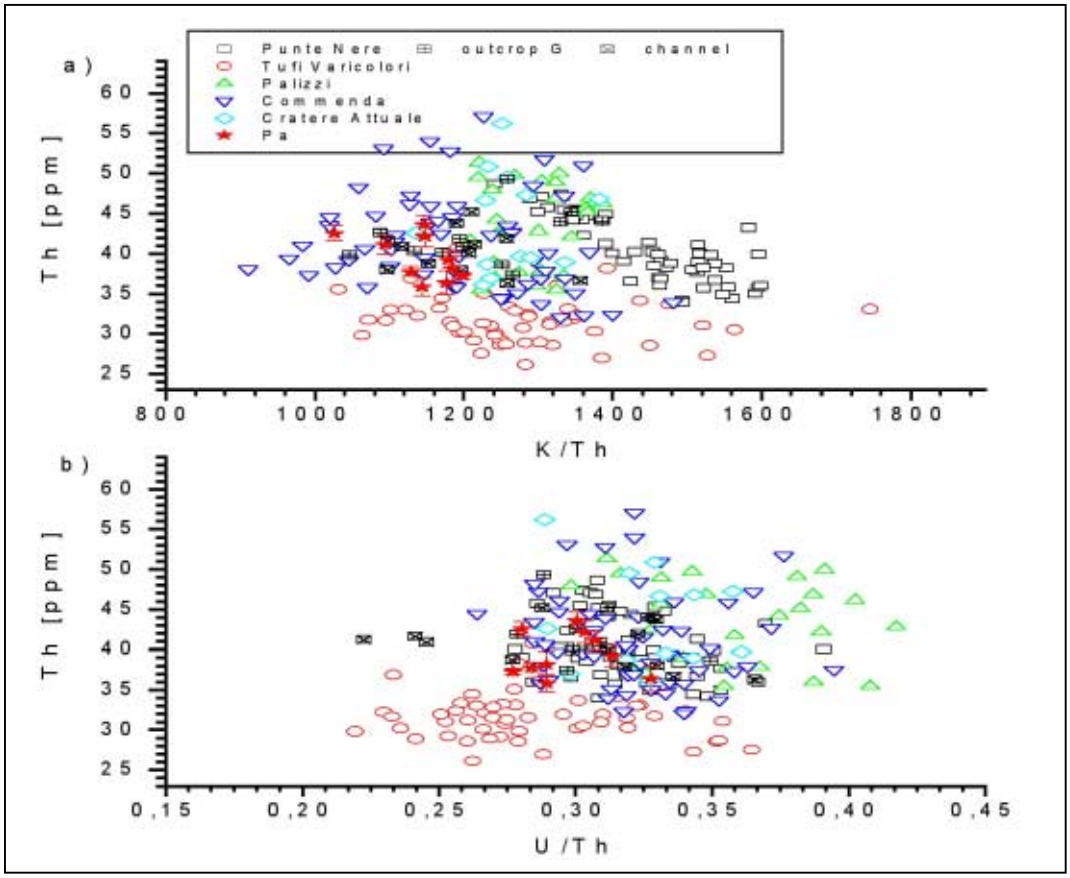

Figure IV.G.8: Scatter plots Th vs. K/Th and Th vs. U/Th for outcrop P in comparison with the standard outcrops. a) Th vs. K/Th, b) Th vs. U/Th.

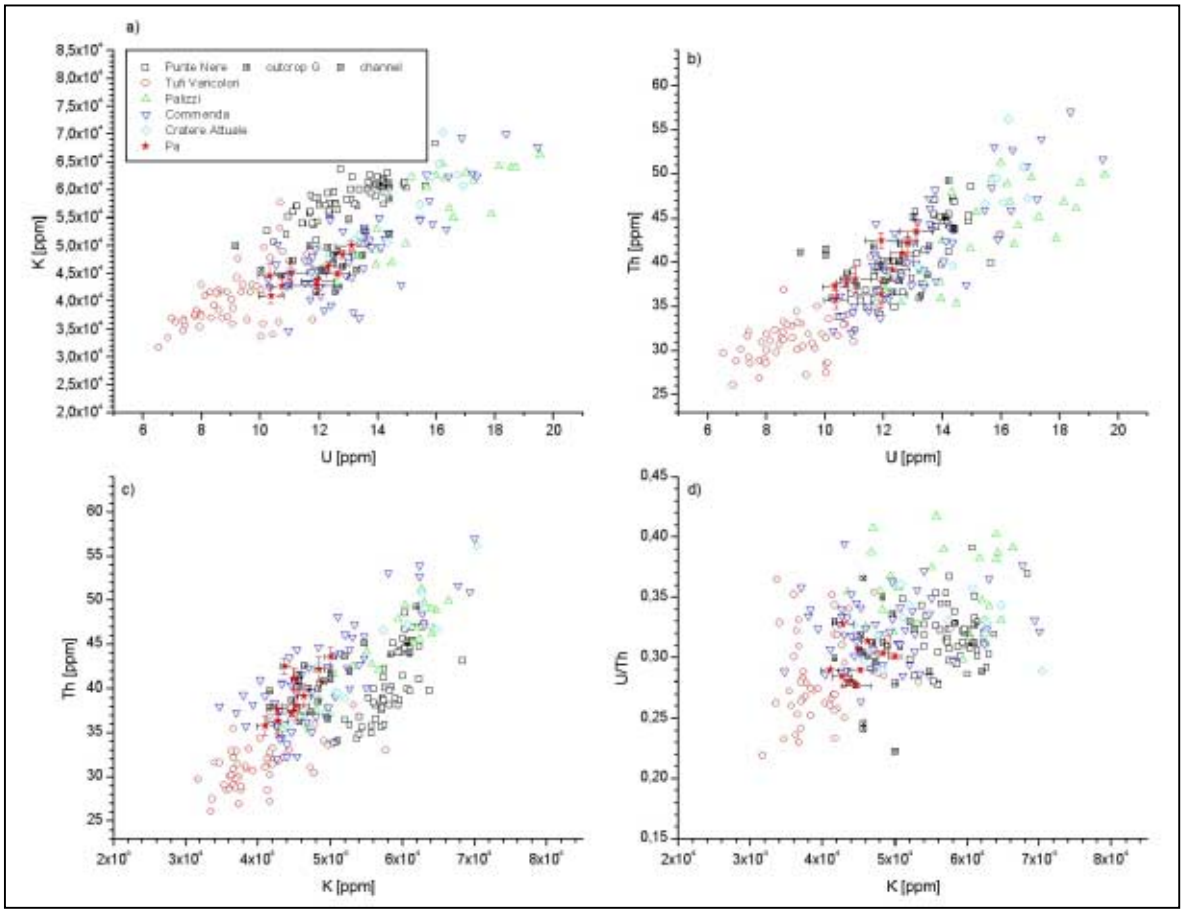

Figure IV.G.9: Scatter plots K vs. U, Th vs. U, Th vs. K, and U/Th vs. K for outcrop P in comparison with the standard outcrops. a) K vs. U, b) Th vs. U), c) Th vs. K, d) U/Th vs. K.

IV. Appendix IVh: Plots for Undefined Outcrops

IV.H. Outcrop Q

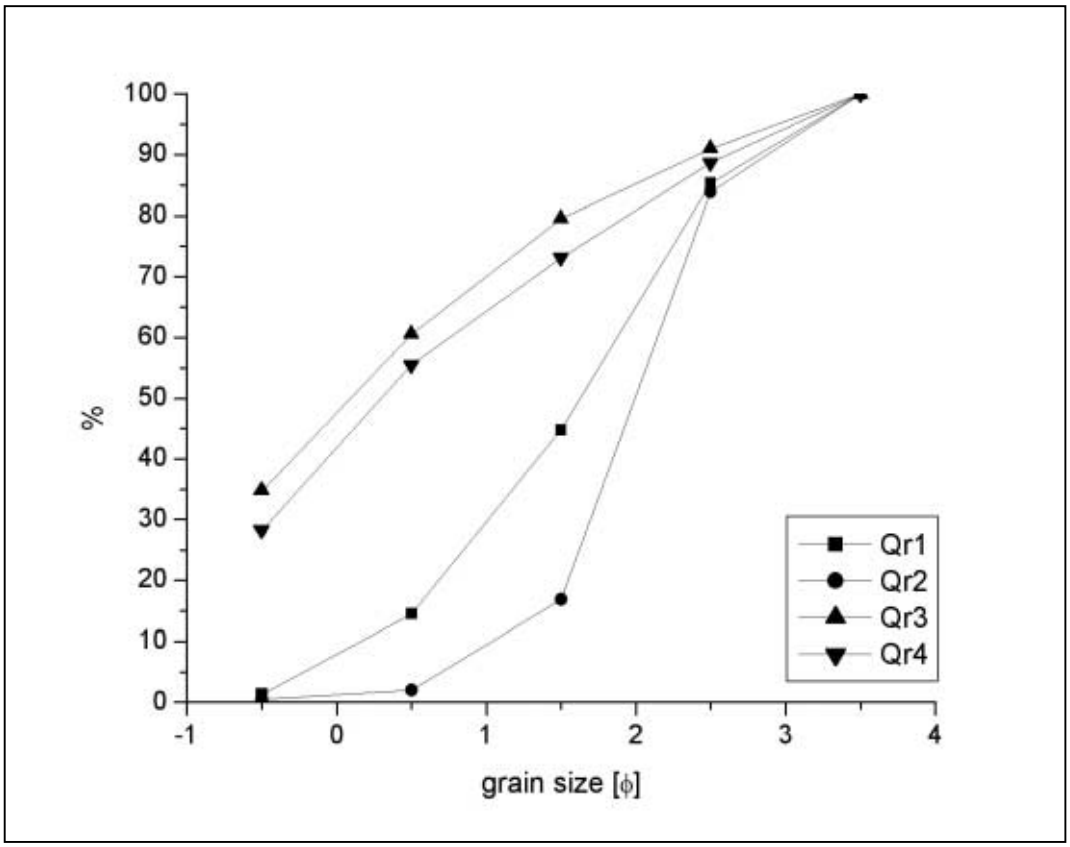

Figure IV.H.1: Cumulative grain size curve for outcrop Q.

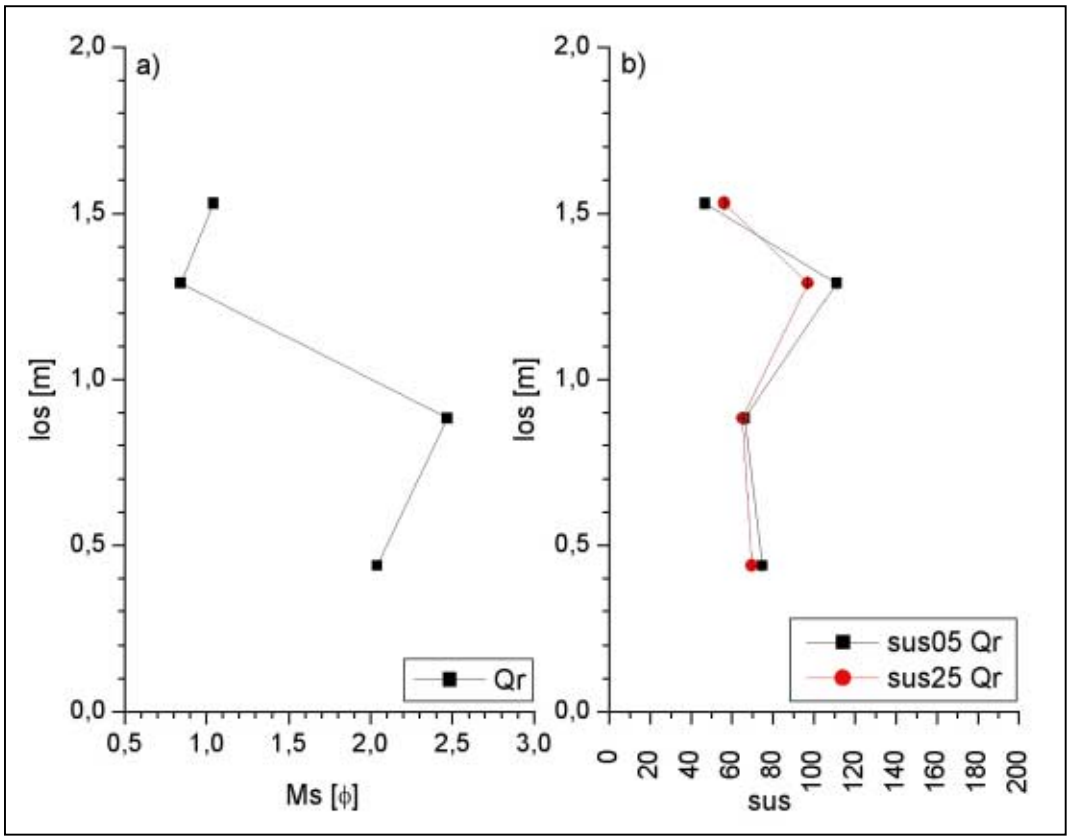

Figure IV.H.2: los vs. Ms [ϕ] and sus for outcrop Q. a) los vs. Ms; b) los vs. sus05 and sus25.

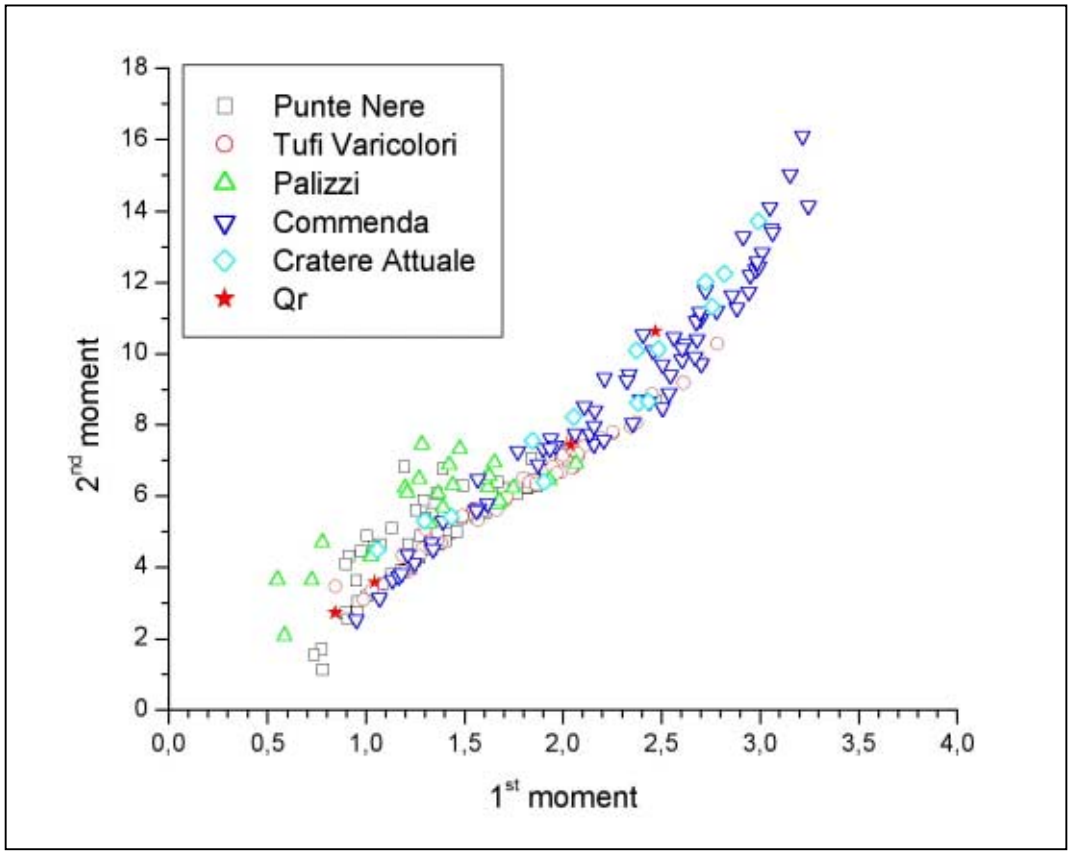

Figure IV.H.3: 1st vs. 2nd moment for outcrop Q in comparison with the standard outcrops.

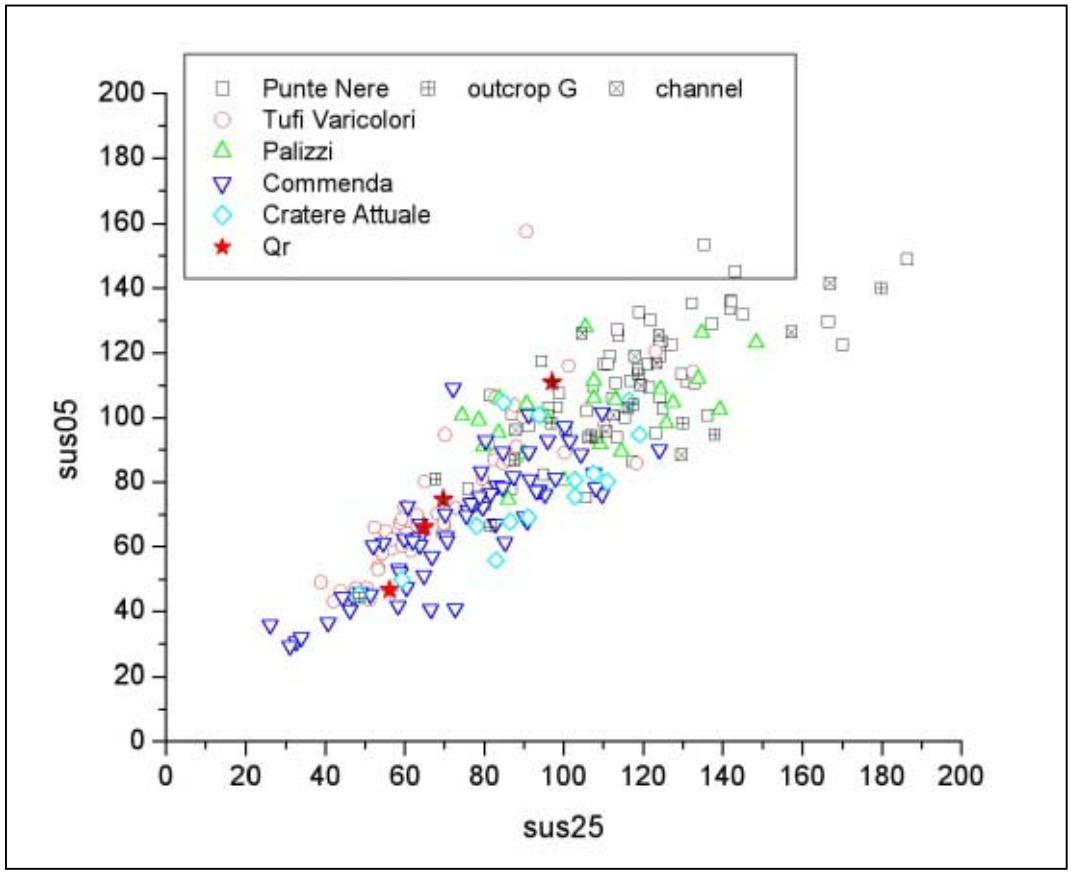

Figure IV.H.4: Scatter plot sus05 vs. sus25 for outcrop Q in comparison with the standard outcrops.

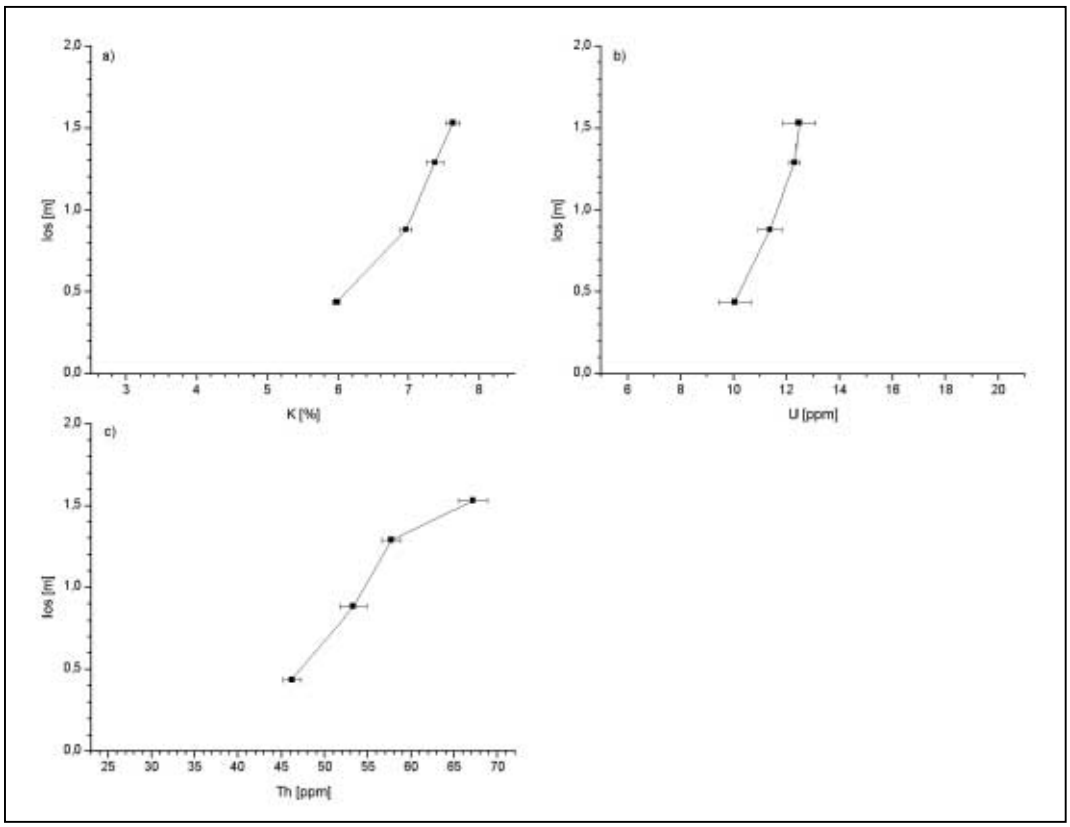

Figure IV.H.5: los. vs. γ-ray values for outcrop Q. a) K [%], b) U [ppm], c) Th [ppm].

IV. Appendix IVi: Plots for Undefined Outcrops

IV.I. Outcrop R

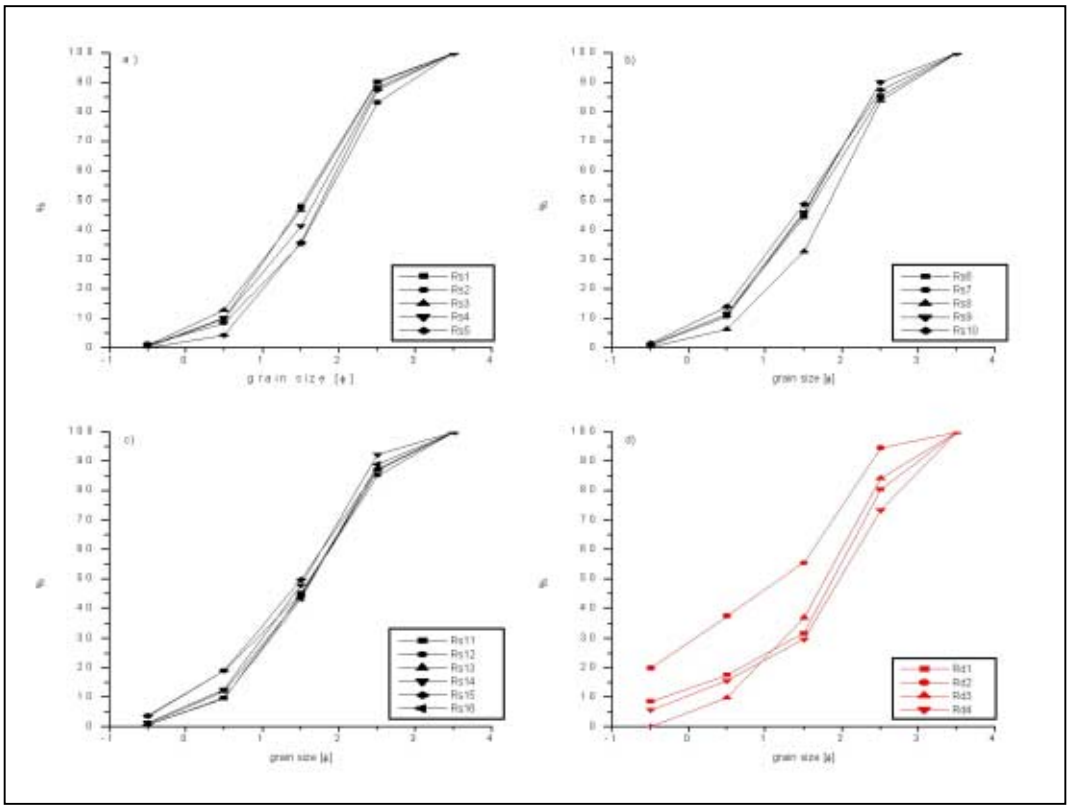

Figure IV.I.1: Cumulative grain size curve for outcrop R. a) to c) unit Rs, d) unit Rd.

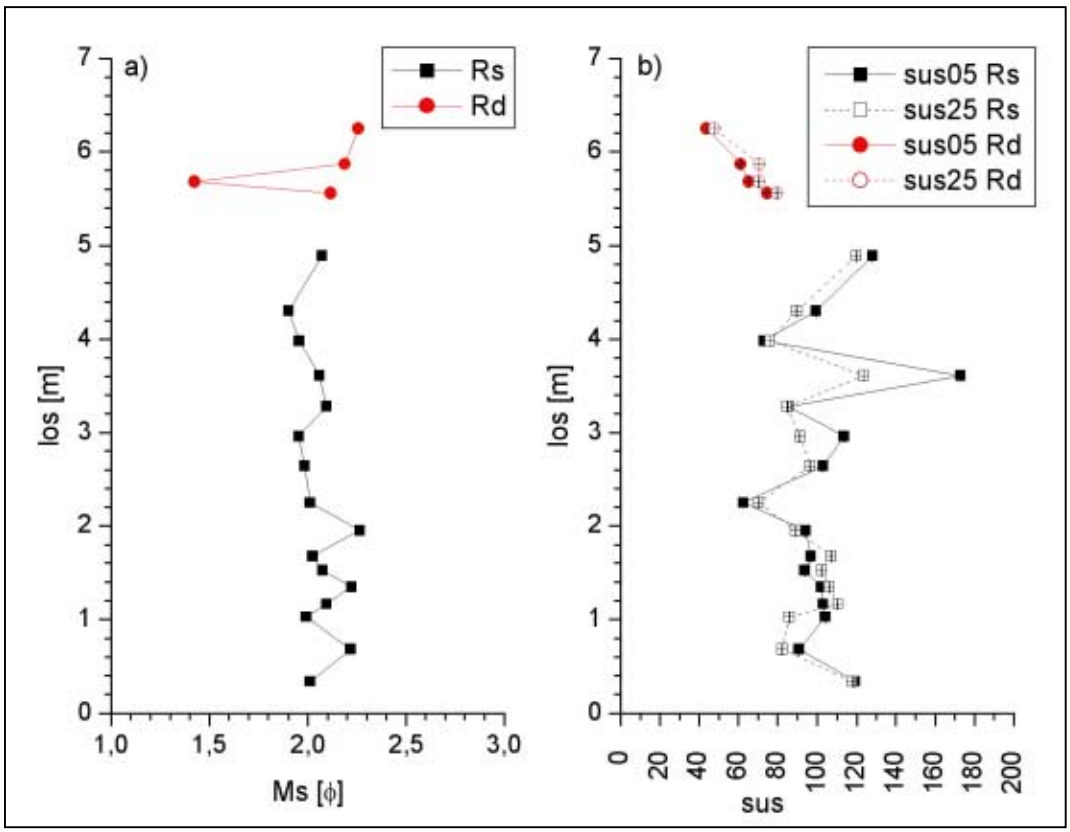

Figure IV.I.2: los vs. Ms [ϕ] and sus for outcrop R. a) los vs. Ms; b) los vs. sus05 and sus25.

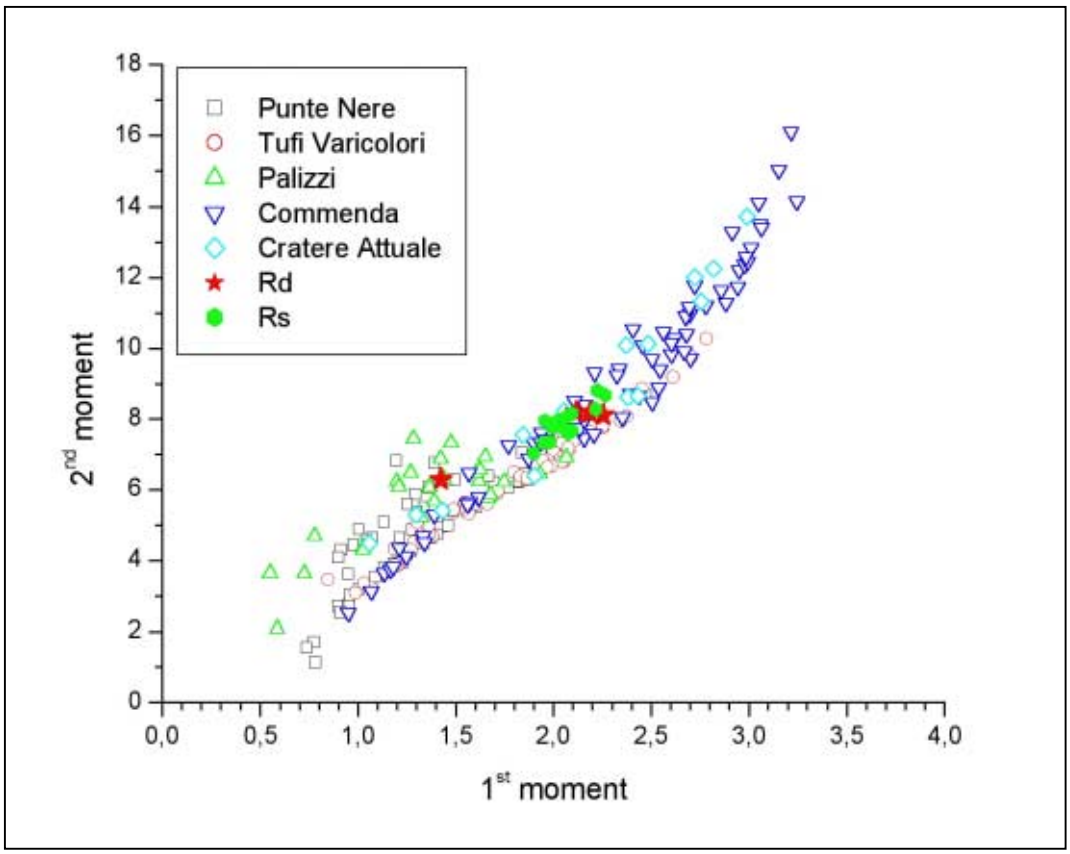

Figure IV.I.3: 1st vs. 2nd moment for outcrop R in comparison with the standard outcrops.

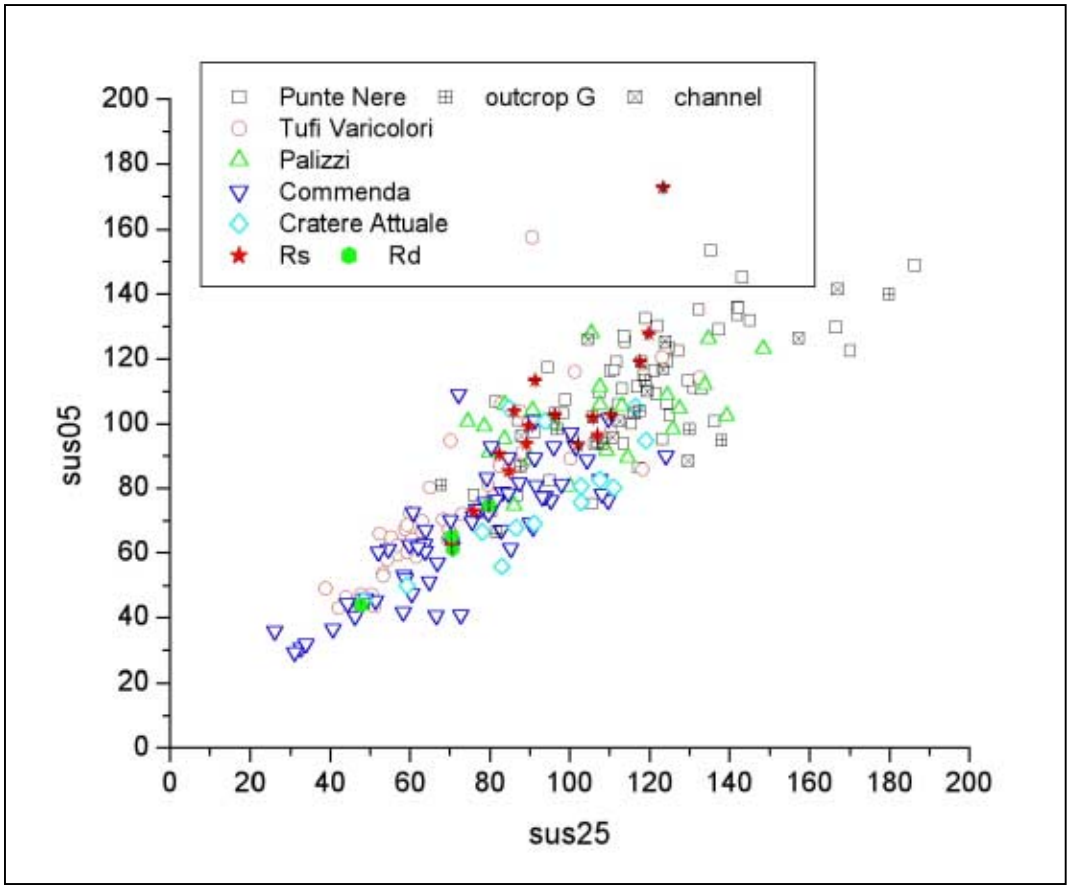

Figure IV.I.4: Scatter plot sus05 vs. sus25 for outcrop R in comparison with the standard outcrops.

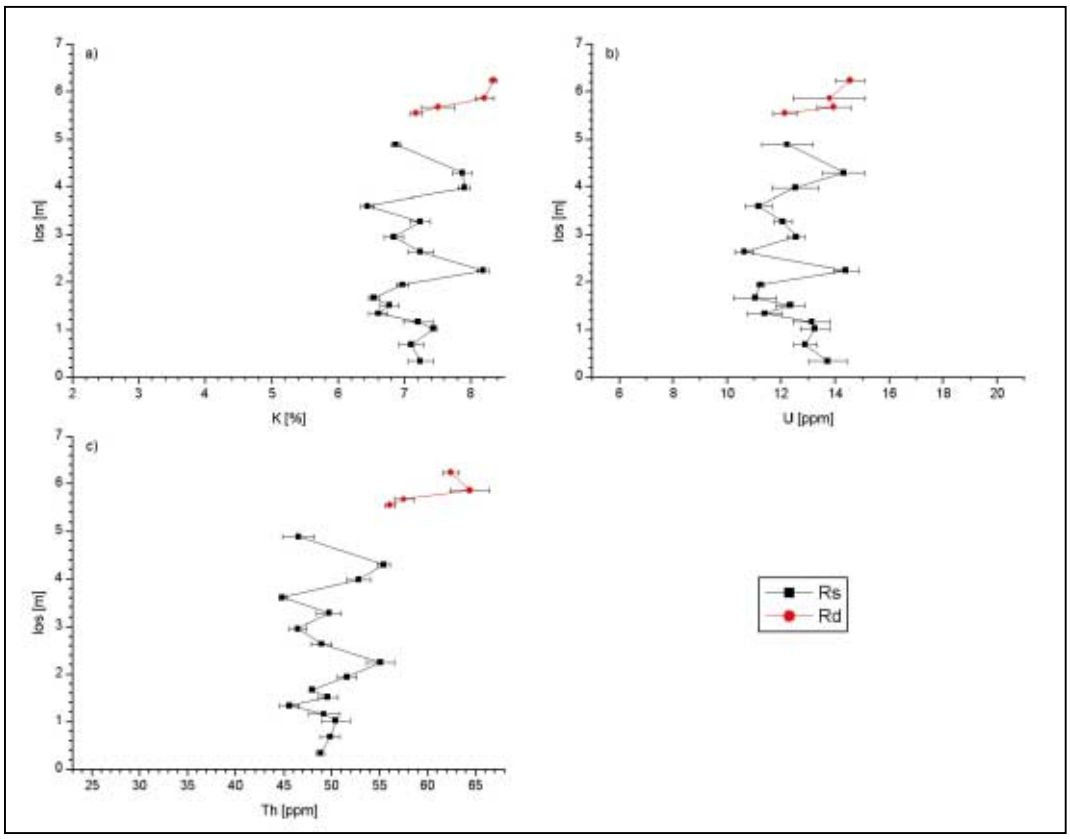

Figure IV.I.5: los. vs. γ-ray values for outcrop R. a) K [%], b) U [ppm], c) Th [ppm].

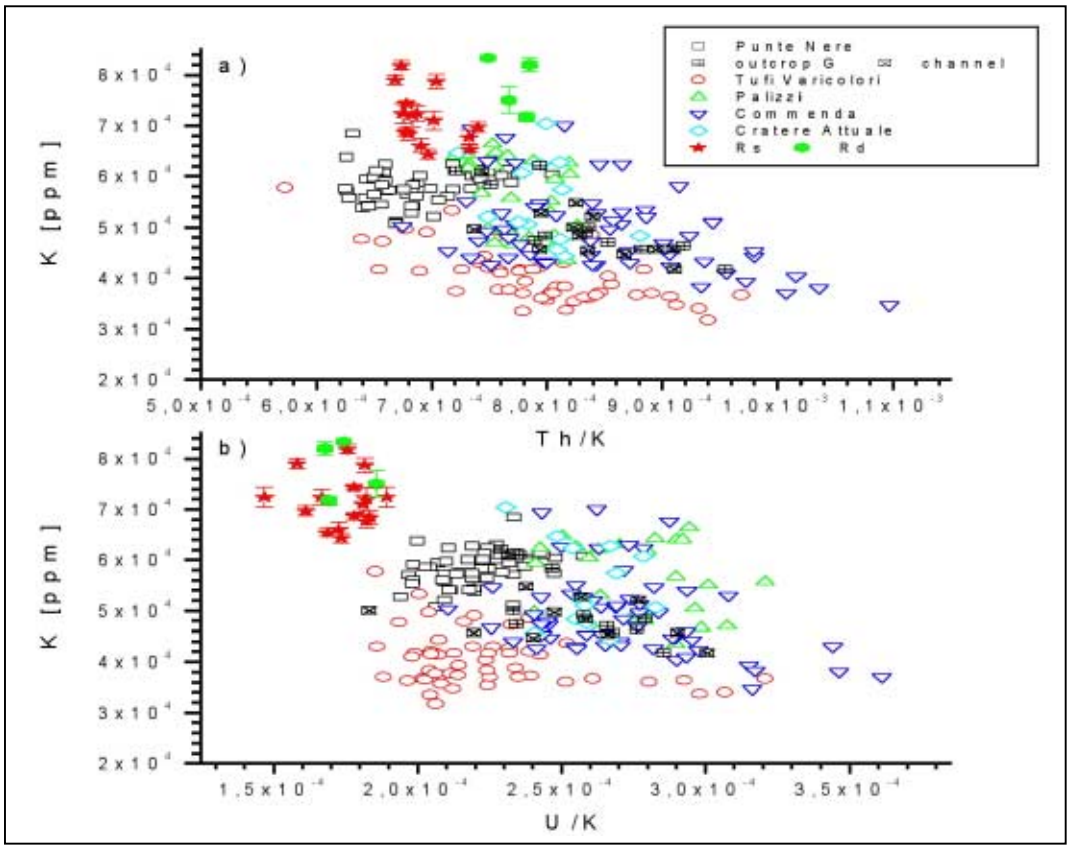

Figure IV.I.6: Scatter plots K vs. Th/K and K vs. U/K for outcrop R in comparison with the standard outcrops. a) K vs. Th/K, b) K vs. U/K.

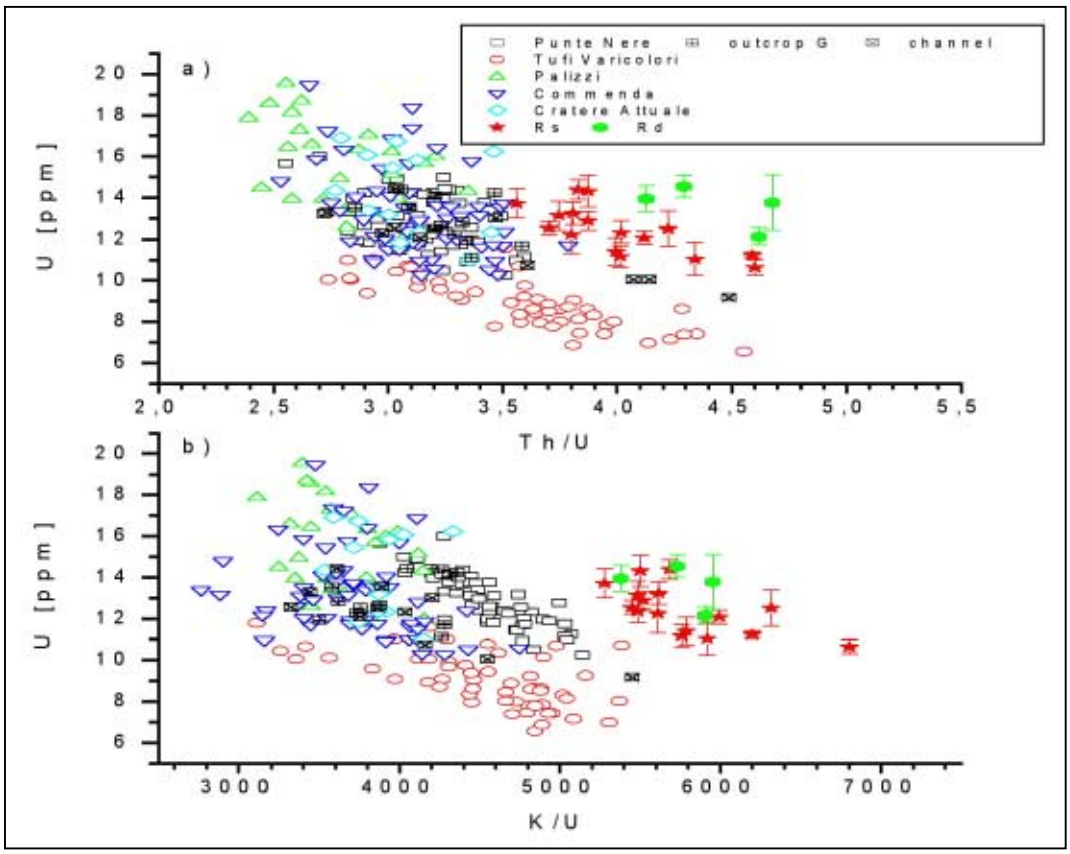

Figure IV.I.7: Scatter plots U vs. Th/U and U vs. K/U for outcrop R in comparison with the standard outcrops. a) U vs. Th/U, b) U vs. K/U.

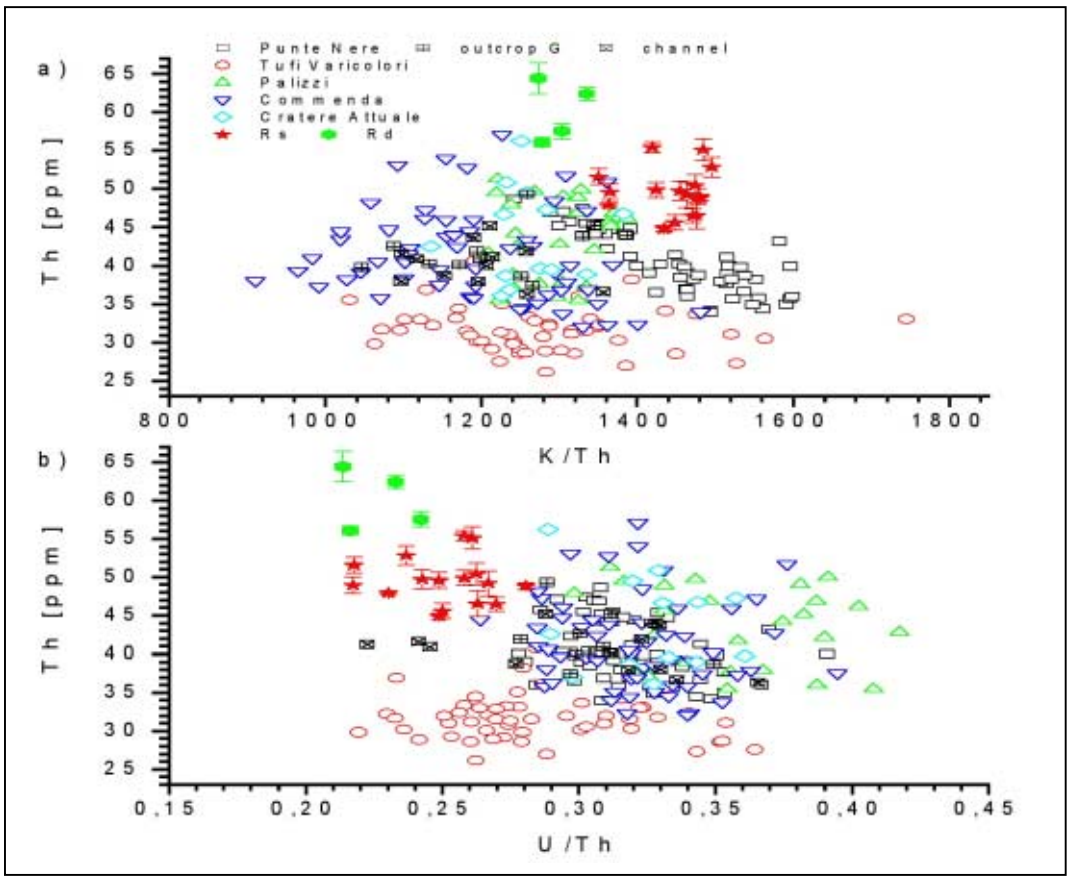

Figure IV.I.8: Scatter plots Th vs. K/Th and Th vs. U/Th for outcrop R in comparison with the standard outcrops. a) Th vs. K/Th, b) Th vs. U/Th.

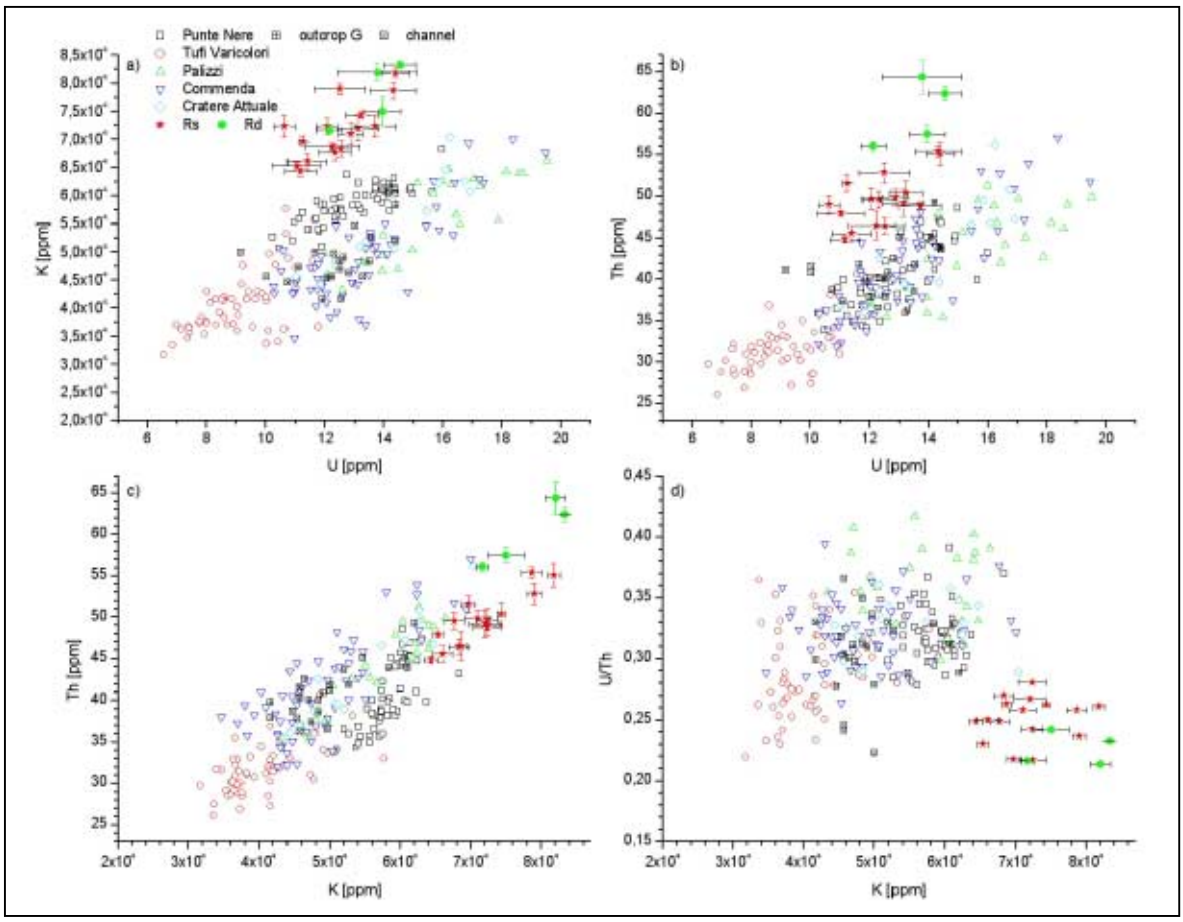

Figure IV.I.9: Scatter plots K vs. U, Th vs. U, Th vs. K, and U/Th vs. K for outcrop R in comparison with the standard outcrops. a) K vs. U, b) Th vs. U), c) Th vs. K, d) U/Th vs. K.

V. Appendix V: Eifel

V.A. Outcrop description

sample	location	description
ULST2	Wingertsberg, Upper Laacher See Tephra ca. 15 m above the top of the marker "Autobahn Mittelstreifen"	• thickness: ca. 30 cm • colour: light grey with lighter spots, thickness changes for the distance • coarse layer with host rocks, lithics, pumice, glass and some scoria. • no grading
ULST1	Wingertsberg, Upper Laacher See Tephra ca. 13 m above the top of the marker "Autobahn Mittelstreifen"	• thickness: ca. 20 cm • colour: light grey • finer grained layer than ULST2 • located in a chute • sometimes signs of a light imbrication, internal bedding in mm to cm scale • some layers are cut
MLST3	Wingertsberg, Middle Laacher See Tephra Marker "Autobahn, obere Fahrspur", located directly above the marker "Autobahn Mittelstreifen"	• thickness: about 60 cm • colour: middle grey • slight internal grading • components angular to subangular, sometimes orientated along their axis • top and base with sharp contact • possibly fall deposits • proper marker for susceptibility an gamma-ray (especially Th and U), possibly leaching
MLST2	Wingertsberg, Middle Laacher See Tephra Marker "Autobahn Mittelstreifen"	• thickness: 5 to 6 cm • colour: grey to ochre • fine grained without visible bedding • the lateral change in the outcrop is not very high/strong
MLST1	Wingertsberg, Middle Laacher See Tephra so called "Tauchschicht", ca. 2 m below the top of the marker "Autobahn Mittelstreifen"	• thickness: on the measuring point 92 cm • fast change of thickness with lateral contribution • colour: creme-grey • macroscopic homogenous, very fine, ash-layer sometimes with lapilli intercalations • near the top intercalations of pumice, without elongated bubbles like LLST deposits • possibly flow deposit
LLST2	Wingertsberg, Lower Laacher See Tephra 6 to 8 m below the top of the marker "Autobahn Mittelstreifen"	• thickness: about 2 m • colour: grey • grain size can change, internal layers with a thickness up to 30 cm possible (not constant in thickness) • sometimes internal grading • intercalations of bombs and impact-structures possible, often concentrated in single layers • sometimes pumice with elongated bubbles
LLST1	Wingertsberg, Lower Laacher See Tephra base of the outcrop 10 to 12 m lower than the top of the marker "Autobahn Mittelstreifen"	• thickness: about 4 m • colour: brownish to grey, depending on the content of weathering • sometimes highly surficial weathering • bedding only sometimes visible

Table V.1: Eifel samples: position and description.

V.B. Gamma-ray

Measuring time 60 seconds, 3 to 6 measurements for each point

sample	K [%]	U [ppm]	Th [ppm]
ULST2	5.87 ± 0.03	2.10 ± 0.08	17.93 ± 0.85
ULST1	5.93 ± 0.07	2.03 ± 0.03	13.70 ± 0.46
MLST3	6.63 ± 0.05	2.93 ± 0.28	19.97 ± 0.41
MLST2	6.88 ± 0.09	3.53 ± 0.25	20.63 ± 1.21
MLST1	5.43 ± 0.07	5.20 ± 0.68	28.13 ± 0.90
LLST2	4.68 ± 0.19	5.74 ± 0.29	32.28 ± 0.61
LLST1	4.78 ± 0.08	7.38 ± 0.52	47.58 ± 0.71

Table V.2: γ-ray values for the measured samples of the Wingertsberg.

V.C. Magnetic Susceptibility

sample	laboratory measurements			
	sus1 [$*10^{-6}$]	**sus05** [$*10^{-6}$]	**sus25** [$*10^{-6}$]	**sus125** [$*10^{-6}$]
ULST2	121.49 ± 1.79	171.48 ± 2.68	111.02 ± 1.28	47.24 ± 0.75
ULST1	107.11 ± 1.05	113.01 ± 0.71	87.61 ± 1.13	60.15 ± 0.73
MLST3	244.74 ± 2.17	253.51 ± 0.88	127.29 ± 0.97	31.77 ± 0.88
MLST2	69.72 ± 0.41	78.10 ± 1.42	44.28 ± 0.73	30.78 ± 0.78
MLST1	32.09 ± 8.68	30.82 ± 0.84	27.87 ± 0.96	24.36 ± 1.08
LLST2	35.58 ± 1.38	32.60 ± 0.96	28.03 ± 0.91	20.37 ± 0.81
LLST1	41.72 ± 1.73	21.81 ± 1.38	16.51 ± 0.82	15.02 ± 0.83
field measurements				
	sus1 [$*10^{-6}$]	**sus05** [$*10^{-6}$]	**sus25** [$*10^{-6}$]	**sus125** [$*10^{-6}$]
ULST2	102.10 ± 7.79	-	-	-
ULST1	-	-	-	-
MLST3	331.48 ± 28.48	-	36.71 ± 7.87	33.39 ± 7.70
MLST2	24.02 ± 7.70	27.42 ± 7.70	25.10 ± 7.86	-
MLST1	-	-	-	-
LLST2	24.95 ± 7.72	16.75 ± 7.70	19.92 ± 7.70	12.75 ± 7.70
LLST1	20.88 ± 7.71	16.43 ± 7.70	-	-

Table V.3: sus-values for the Eifel samples – measured in cgs-mode, standardised to 1g –, values for the laboratory as well as for the field measurements.

V.D. Composition and Grain Size Distribution of the Samples

V.D.1. ULST2

grain size class [mm]	**weight** [%]	**content of lithics** [%]	**juvenile clasts** [%]	**crystal** [%]
16 - 8	30.46	60	40	0
8 - 4	22.54	70	30	0
4 - 2	15.14	80	20	0
2 - 1	11.62	67	40	3
1 - 0.5	9.51	50	40	10
0.5 - 0.25	5.46	50	40	20
0.25 - 0.125	1.94	40	40	20
<0.125	1.94	20	60	20

Table V.4: Grain size distribution and macroscopic composition of sample ULST2.

V.D.2. ULST1

grain size class [mm]	**weight** [%]	**content of lithics** [%]	**juvenile clasts** [%]	**crystal** [%]
16 - 8	1.30	90	10	0
8 - 4	2.99	70	30	0
4 - 2	6.19	39	60	1
2 - 1	9.64	45	50	5
1 - 0.5	18.99	10	70	20
0.5 - 0.25	22.72	10	50	40
0.25 - 0.125	24.18	10	60	30
<0.125	12.08	10	10	80

Table V.5: Grain size distribution and macroscopic composition of sample ULST1.

V.D.3. MLST3

grain size class [mm]	**weight** [%]	**content of lithics** [%]	**juvenile clasts** [%]	**crystal** [%]
16 - 8	19.04	40	60	0
8 - 4	24.02	50	50	0
4 - 2	21.00	60	40	0
2 - 1	13.17	50	50	0
1 - 0.5	4.63	50	40	10
0.5 - 0.25	0.71	0	0	0
0.25 - 0.125	1.25	30	50	20
<0.125	1.07	50	40	10

Table V.6: Grain size distribution and macroscopic composition of sample MLST3.

V.D.4. MLST2

grain size class [mm]	**weight** [%]	**content of lithics** [%]	**juvenile clasts** [%]	**crystal** [%]
16 - 8	0.57	0	100	0
8 - 4	0.57	0	100	0
4 - 2	1.14	0	100	0
2 - 1	2.29	20	80	0
1 - 0.5	82.86	5	90	5
0.5 - 0.25	7.43	5	90	5
0.25 - 0.125	0.29	25	75	5
<0.125	0.29	15	70	15

Table V.7: Grain size distribution and macroscopic composition of sample MLST2.

V.D.5. MLST1

grain size class [mm]	**weight** [%]	**content of lithics** [%]	**juvenile clasts** [%]	**crystal** [%]
16 - 8	0.03	0	100	0
8 - 4	0.07	70	30	0
4 - 2	0.43	30	70	0
2 - 1	1.22	17	80	3
1 - 0.5	6.74	5	90	5
0.5 - 0.25	9.99	10	85	5
0.25 - 0.125	28.09	0	95	5
<0.125	52.45	0	95	5

Table V.8: Grain size distribution and macroscopic composition of sample MLST1.

V.D.6. LLST2

grain size class [mm]	**weight** [%]	**content of lithics** [%]	**juvenile clasts** [%]	**crystal** [%]
16 - 8	16.84	40	60	0
8 - 4	28.32	30	70	0
4 - 2	25.51	20	80	0
2 - 1	20.66	20	80	0
1 - 0.5	15.82	20	80	0
0.5 - 0.25	9.44	20	75	5
0.25 - 0.125	2.04	30	65	5
<0.125	3.83	10	90	0

Table V.9: Grain size distribution and macroscopic composition of sample LLST2.

V.D.7. LLST1

grain size class [mm]	**weight** [%]	**content of lithics** [%]	**juvenile clasts** [%]	**crystal** [%]
16 - 8	11.42	50	50	0
8 - 4	24.11	40	60	0
4 - 2	26.40	30	70	0
2 - 1	18.78	30	70	0
1 - 0.5	11.42	30	70	0
0.5 - 0.25	3.05	20	80	0
0.25 - 0.125	0.25	15	80	5
<0.125	0.25	0	100	0

Table V.10: Grain size distribution and macroscopic composition of sample LLST1.

VI. Appendix VI: Additional Information

VI.A. Calibration Measurements

VI.A.1. Magnetic Susceptibility

VI.A.1.a. Measuring and Sample Mass

	sus05 [*10^{-6}] ❖ sample mass: 10g	**sus05** [*10^{-6}] ❖ sample mass: 7g	**sus25** [*10^{-6}] ❖ sample mass: 10g	**sus25** [*10^{-6}] ❖ sample mass: 7g	**sus125** [*10^{-6}] ❖ sample mass: 10g	**sus125** [*10^{-6}] ❖ sample mass: 7g
	92.70	97.29	109.10	115.29	116.60	122.86
	92.60	97.29	109.00	115.29	116.60	122.86
	92.70	97.29	109.00	115.14	116.50	122.71
	93.90	97.29	109.10	115.43	116.60	122.86
	93.90	97.29	109.00	115.14	116.70	122.86
	93.90	97.29	110.50	115.43	116.60	121.86
	93.90	97.14	110.30	115.43	116.50	121.71
	93.90	97.14	110.40	115.29	116.40	121.86
	93.90	97.29	110.40	115.43	116.50	121.86
	94.00	97.14	110.30	115.43	116.60	121.86
	92.80	97.86	109.70	116.57	117.70	121.71
	92.90	97.86	109.90	116.71	117.70	121.71
	92.90	97.86	109.70	116.71	117.80	121.71
	92.80	97.86	109.80	116.57	117.70	121.71
	92.90	97.71	109.80	116.71	117.90	121.71
	92.80	97.86	108.90	116.86	116.50	121.86
	92.90	97.71	108.90	116.86	116.50	121.71
	92.40	97.71	109.00	116.86	116.60	121.71
	92.40	97.86	109.00	116.86	116.60	121.71
	92.50	97.71	109.00	116.86	116.60	121.86
	92.40	97.43	109.70	116.43	115.20	122.29
	92.50	97.43	109.80	116.57	115.20	122.43
	92.50	97.43	109.70	116.57	115.30	122.57
	92.50	97.57	109.70	116.57	115.20	122.43
	92.40	97.57	109.80	116.43	115.20	122.29
	92.40	97.43	109.10	116.71	116.50	122.43
	92.40	97.43	108.70	116.43	116.50	122.57
	92.60	96.71	109.10	116.43	116.50	122.57
	92.60	96.86	109.00	116.43	116.50	122.57
	92.50	96.71	109.00	116.43	116.50	122.57
	92.70	96.71	109.90	116.14	116.80	122.71
	92.60	96.86	109.90	116.29	116.90	122.86
	92.80	97.29	109.80	116.14	116.80	122.86
	92.70	97.14	109.90	116.29	116.90	122.71
	92.60	97.14	109.90	116.14	116.90	122.71
	92.70	97.29	109.30	115.43	117.70	122.43
	92.60	97.29	109.30	115.43	117.70	122.71
	92.90	97.43	109.40	115.29	117.80	122.57
	92.90	97.43	109.40	115.43	117.90	122.57
	92.90	97.43	109.40	115.43	117.90	122.71
	92.90	97.57	108.80	116.14	117.00	122.57
	92.90	97.43	108.90	116.14	116.90	122.57
	92.70	97.14	108.80	116.14	117.00	122.57

92.60	97.14	109.00	116.29	117.00	122.57
92.60	97.14	109.00	116.29	117.00	122.71
92.50	97.14	110.20	116.00	117.50	122.43
92.60	97.14	110.10	116.00	117.50	122.43
92.40	97.57	110.00	116.00	117.40	122.29
92.30	97.57	110.10	116.00	117.50	122.29
92.30	97.57	110.00	116.00	117.60	122.57
92.40	97.57	109.20	116.00	117.10	122.86
92.30	97.43	109.20	116.00	117.10	122.86
92.50	97.00	109.20	115.86	117.20	123.14
92.40	97.14	109.10	116.00	117.10	123.00
92.40	97.00	109.10	116.00	117.00	123.00
92.40	97.00	109.80	116.00	118.20	122.71
92.50	97.14	109.00	116.14	118.20	122.71
92.40	97.14	109.80	116.14	118.10	122.71
92.40	97.29	109.70	116.00	118.20	122.71
92.50	97.14	109.80	116.00	118.30	122.71
92.50	97.00	109.20	115.86	117.40	122.57
92.50	97.00	109.30	116.00	117.40	122.57
93.80	97.43	109.40	115.86	117.40	122.57
93.80	97.43	109.40	116.00	117.40	122.57
93.80	97.43	109.30	116.00	117.40	122.57
93.80	97.43	110.10	116.71	117.50	122.86
93.80	97.43	110.10	116.43	117.50	122.86
92.40	97.86	110.20	116.57	117.50	122.86
92.40	97.86	110.10	116.71	117.50	123.00
92.40	98.00	110.10	116.71	117.50	122.86
92.30	98.00	109.70	116.29	117.20	123.00
92.40	97.86	109.70	116.29	117.20	123.00
92.80	97.86	109.60	116.14	117.10	122.86
92.80	97.86	109.70	116.29	117.30	122.86
92.70	97.86	109.60	116.14	117.20	122.86
92.70	97.86	109.70	116.43	117.60	123.00
92.80	98.00	109.60	116.57	117.60	122.86
93.00	97.71	109.80	116.43	117.60	123.00
92.80	97.71	109.70	116.57	117.40	123.00
93.00	97.71	109.70	116.57	117.50	122.86
92.90	97.86	109.80	115.86	118.30	122.29
93.00	97.71	109.80	115.86	118.30	122.14
93.20	98.00	109.90	115.57	118.30	122.14
93.30	97.86	109.90	115.71	118.20	122.29
93.40	98.00	109.80	115.57	118.30	122.14
93.20	97.86	109.20	115.71	117.60	122.86
93.40	97.86	109.10	115.71	117.70	122.86
93.50	97.57	109.20	115.71	117.60	122.86
93.50	97.57	109.20	115.71	117.60	122.86
93.40	97.57	109.10	115.86	117.60	122.86
93.50	97.43	108.60	115.71	117.90	123.43
93.50	97.43	108.60	115.71	117.90	123.43
93.40	97.00	108.70	115.86	117.90	123.43
93.50	97.00	108.60	115.71	117.90	123.43
93.50	96.86	108.60	115.71	117.90	123.43
93.40	96.86	109.60	116.00	119.00	122.86
93.50	96.43	109.70	116.00	119.10	122.86
93.10	97.57	109.70	116.00	119.00	122.71
93.00	97.57	109.70	115.86	119.00	122.86
93.10	97.57	109.70	116.00	119.10	122.86
93.00	97.57	109.90	116.00	116.80	122.71
93.10	97.71	109.80	116.00	116.80	122.71

	93.70	96.71	109.80	116.00	116.80	122.57
	93.70	96.86	109.80	116.14	116.80	122.57
	93.70	96.71	109.70	116.14	116.80	122.57
	93.80	96.71	109.60	116.71	118.30	123.00
			109.70	116.71	118.30	122.86
			109.60	116.86	118.20	123.00
			109.60	116.71	118.30	123.00
			109.80	117.00	118.30	123.00
mean	92.93	97.41	109.52	116.11	117.33	122.61
s	0.50	0.36	0.45	0.45	0.80	0.42

Table VI.1: sus values for different sample mass and gsc. ❖: standardised to 1g, measured in cgs-mode

The measurements of different masses do not show significant differences. Due to these values a sample of about 7 g is found to be representative. Repeated measurements for different gsc show a reproducibility of the analysis, whereby 10 measurements for a sample are representative.

VI.A.1.b. Grain Size

The following tables and figures show the differences between the various gsc. sus05 and sus25 are found to be representative.

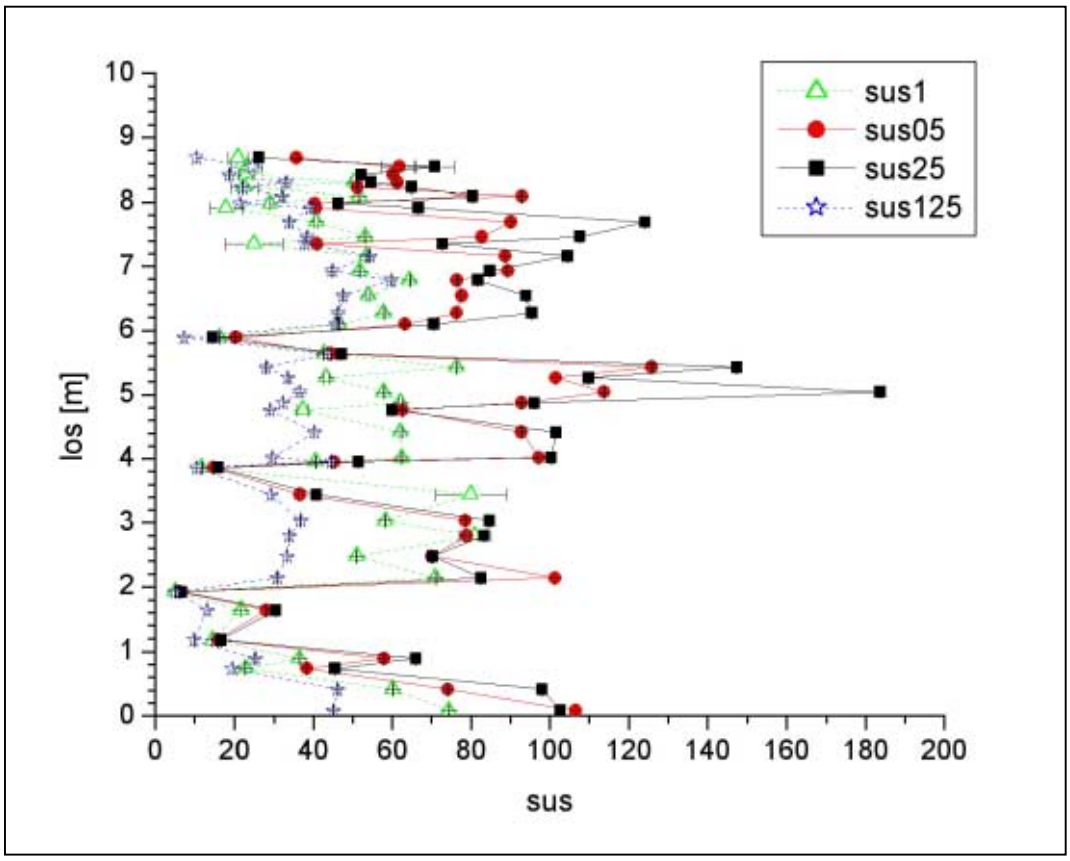

Figure VI.1: los vs. sus of 4 different gsc for outcrop A.

sample	sus1 [*10^{-6}] ❖	sus05 [*10^{-6}] ❖	sus25 [*10^{-6}] ❖	sus125 [*10^{-6}] ❖
Ad1	74.40 ± 0.1	106.53 ± 0.2	102.64 ± 0.1	45.12 ± 0.1
Ad2	60.19 ± 0.1	73.99 ± 0.1	98.00 ± 0.1	46.14 ± 0.1
Ad3	22.75 ± 0.1	38.38 ± 0.1	45.48 ± 0.1	19.50 ± 0.0
Ad4	36.45 ± 0.2	57.91 ± 0.1	65.93 ± 0.1	25.20 ± 0.0
Ad5	14.60 ± 0.0	15.97 ± 0.0	16.78 ± 0.0	9.86 ± 0.0
Ad6	21.69 ± 0.1	27.99 ± 0.1	30.48 ± 0.1	13.18 ± 0.0
Ad7	5.09 ± 0.1	6.06 ± 0.0	6.68 ± 0.0	5.10 ± 0.0
Ad8	71.07 ± 0.2	101.26 ± 0.2	82.48 ± 0.1	30.76 ± 0.1
Ad9	50.99 ± 0.1	70.07 ± 0.1	70.22 ± 0.1	33.31 ± 0.1
Ad10	80.95 ± 3.9	78.90 ± 0.5	83.28 ± 0.1	33.92 ± 0.1
Ad11	58.26 ± 0.1	78.53 ± 0.1	84.72 ± 0.1	36.81 ± 0.1
Ad12	80.00 ± 9.0	36.57 ± 0.4	40.77 ± 0.1	29.20 ± 0.0
Ad13	11.81 ± 0.0	14.94 ± 0.0	15.89 + 0.0	10.48 ± 0.0
Ad14	40.60 ± 0.1	45.30 ± 0.1	51.40 ± 0.1	44.53 ± 0.1
Ad15	62.44 ± 0.2	97.22 ± 0.2	100.37 ± 0.1	29.59 ± 0.0
Ad16	62.17 ± 0.2	92.80 ± 0.2	101.57 ± 0.1	40.20 ± 0.1
Ad17	37.33 ± 1.4	62.53 ± 0.1	59.94 ± 0.1	29.02 ± 0.0
Ad18	62.04 ± 0.3	92.86 ± 0.2	96.14 ± 0.2	32.24 ± 0.1
Ad19	57.86 ± 0.1	113.79 ± 0.2	183.63 ± 0.3	36.44 ± 0.1
Ad20	43.28 ± 0.7	101.53 ± 0.2	109.84 ± 0.2	33.54 ± 0.1
Ad21	76.32 ± 0.2	125.88 ± 0.2	147.47 ± 0.2	28.03 ± 0.0
Ad22	42.65 ± 0.1	44.34 ± 0.1	47.09 ± 0.1	43.60 ± 0.1
Ad23	16.46 ± 0.1	20.42 ± 0.1	14.59 ± 0.0	7.35 ± 0.0
Ad24	46.51 ± 0.1	63.26 ± 0.1	70.51 ± 0.1	45.84 ± 0.1
Ad25	57.86 ± 0.3	76.29 ± 0.1	95.45 ± 0.2	46.20 + 0.1
Ad26	54.01 ± 0.4	77.64 ± 0.2	93.87 ± 0.1	47.56 ± 0.1
Ad27	64.43 ± 0.1	76.49 ± 0.1	81.69 ± 0.1	59.73 ± 0.1
Ad28	51.82 ± 0.2	89.38 ± 0.2	84.79 ± 0.1	44.77 ± 0.1
Ad29	53.61 ± 0.3	88.65 ± 0.1	104.48 ± 0.1	54.24 ± 0.1
Ad30	25.00 ± 7.2	40.80 ± 0.2	72.73 ± 0.1	37.73 ± 0.1
Ad31	53.16 ± 0.2	82.74 ± 0.2	107.64 ± 0.2	38.40 ± 0.1
Ad32	40.75 ± 0.5	90.08 ± 0.2	124.12 ± 0.2	33.91 ± 0.1
Ad33	18.00 ± 4.1	40.68 ± 1.0	66.62 ± 0.1	39.13 ± 0.1
Ad34	29.05 ± 0.1	40.40 ± 0.1	46.24 ± 0.1	21.36 ± 0.0
Ad35	51.54 ± 0.2	92.90 ± 0.2	80.39 ± 0.1	32.08 ± 0.1
Ad36	22.50 ± 3.2	51.19 ± 0.2	64.88 ± 0.1	21.99 ± 0.1
Ad37	50.40 ± 0.7	61.30 ± 0.2	54.64 ± 0.1	33.05 ± 0.0
Ad38	22.86 ± 1.9	60.23 ± 0.3	52.13 ± 0.1	18.78 ± 0.1
Ad39	23.27 ± 3.9	61.80 ± 4.4	70.76 ± 5.1	24.46 ± 1.7
Ad40	20.91 ± 2.3	35.73 ± 0.1	26.11 ± 0.0	10.45 ± 0.0

Table VI.2: sus values for outcrop A. ❖: standardised to 1g, measured in cgs-mode

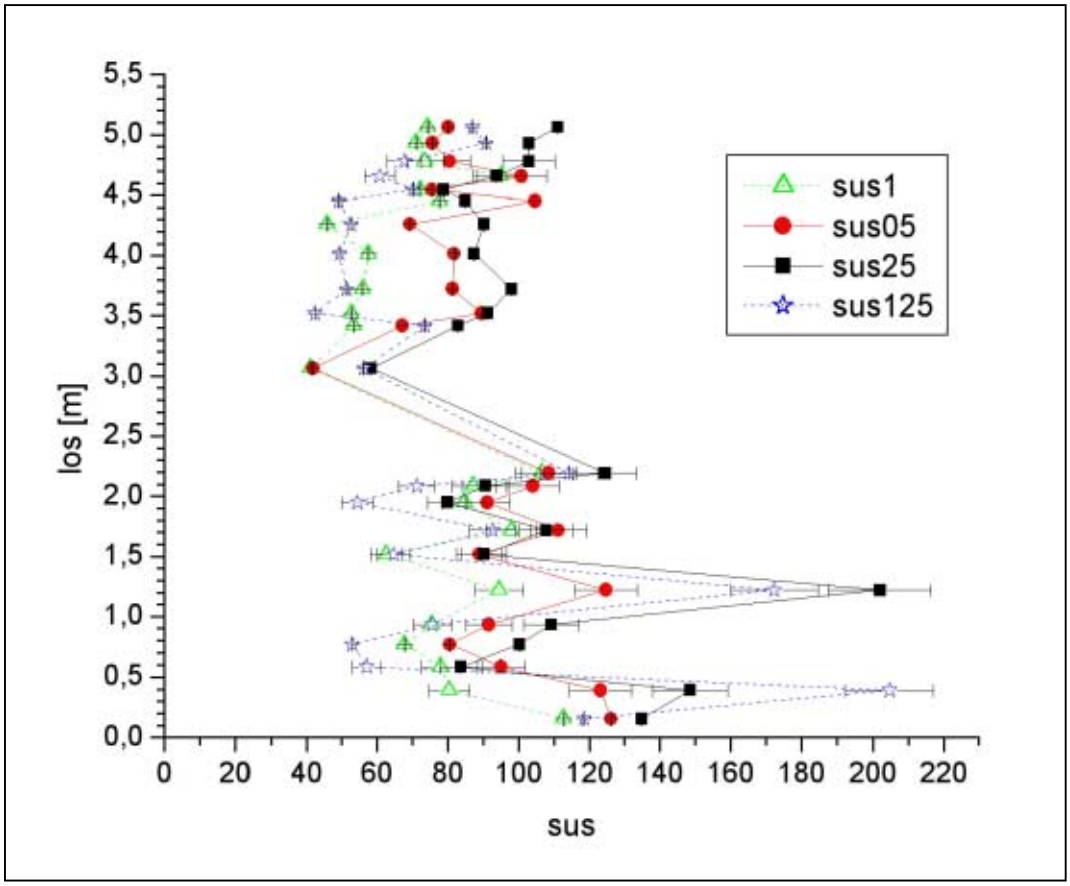

Figure VI.2: los vs. sus of 4 different grain size classes for outcrop E.

sample	**sus1** [*10^{-6}] ❖	**sus05** [*10^{-6}] ❖	**sus25** [*10^{-6}] ❖	**sus125** [*10^{-6}] ❖
Ec1	112.75 ± 0.2	126.15 ± 0.2	134.83 ± 0.2	118.47 ± 0.2
Ec2	80.44 ± 5.7	123.14 ± 8.8	148.53 ± 10.6	204.70 ± 12.4
Ec3	77.97 ± 5.6	95.06 ± 6.8	83.67 ± 6.0	57.0 ± 4.1
Ec4	67.75 ± 0.1	80.45 ± 0.1	100.23 ± 0.2	52.95 ± 0.1
Ec5	75.57 ± 5.4	91.66 ± 6.5	109.23 ± 7.8	75.63 ± 5.4
Ec6	94.49 ± 6.8	124.61 ± 8.9	202.01 ± 14.4	172.31 ± 12.3
Ec7	62.60 ± 4.5	88.77 ± 6.3	90.16 ± 6.4	64.63 ± 4.6
Ec8	97.94 ± 7.0	111.24 ± 7.9	107.71 ± 7.7	92.64 ± 6.6
Ec9	84.69 ± 6.1	91.10 ± 6.5	79.90 ± 5.7	54.40 ± 4.5
Ec10	87.26 ± 6.2	104.07 ± 7.4	90.67 ± 6.5	71.24 ± 5.1
Ec11	106.59 ± 7.6	108.56 ± 7.8	124.46 ± 8.9	114.23 ± 8.2
Ed1	72.20 ± 0.1	75.47 ± 0.1	78.87 ± 0.1	70.08 ± 0.1
Ed2	41.18 ± 0.1	41.77 ± 0.1	58.35 ± 0.1	56.21 ± 0.1
Ed3	53.40 ± 0.1	67.07 ± 0.1	82.83 ± 0.1	73.42 ± 0.1
Ed4	52.71 ± 0.2	89.44 ± 0.1	91.23 ± 0.2	42.36 ± 0.1
Ed5	55.94 ± 0.3	81.30 ± 0.1	98.01 ± 0.2	51.36 ± 0.1
Ed7	57.54 ± 0.1	81.81 ± 0.2	87.41 ± 0.2	49.33 ± 0.1
Ed8	45.81 ± 0.2	69.24 ± 0.1	90.23 ± 0.1	52.60 ± 0.1
Ee1	77.77 ± 0.1	104.59 ± 0.2	84.90 ± 0.1	49.14 ± 0.1
Ee2	95.07 ± 6.8	100.71 ± 7.2	93.81 ± 6.7	60.73 ± 4.3
Ee3	73.47 ± 5.2	80.60 ± 5.8	102.9 ± 7.4	67.73 ± 4.8
Ee4	71.03 ± 0.1	75.62 ± 0.1	102.92 ± 0.2	90.74 ± 0.1
Ee5	74.31 ± 0.1	80.11 ± 0.1	111.02 ± 0.2	86.95 ± 0.2

Table VI.3: sus values for outcrop E. ❖: standardised to 1g, measured in cgs-mode

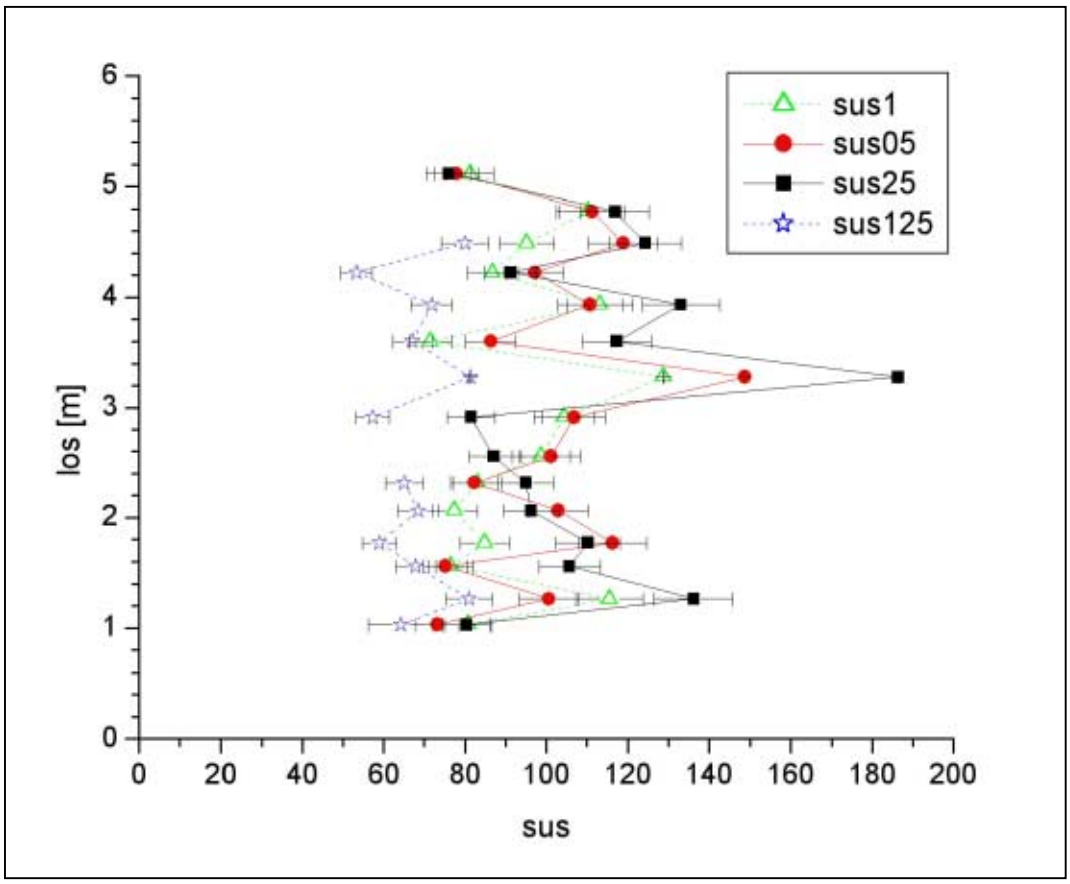

Figure VI.3: los vs. sus of 4 different grain size classes for outcrop I.

sample	**sus1** [*10^{-6}] ❖	**sus05** [*10^{-6}] ❖	**sus25** [*10^{-6}] ❖	**sus125** [*10^{-6}] ❖
Ia1	80.79 ± 5.8	73.16 ± 5.2	80.31 ± 5.7	64.20 ± 8.0
Ia2	115.50 ± 8.3	100.6 ± 7.2	136.23 ± 9.7	80.94 ± 5.8
Ia3	76.56 ± 5.5	75.16 ± 5.4	105.73 ± 7.6	67.87 ± 4.8
Ia4	84.83 ± 6.1	116.29 ± 8.3	110.21 ± 7.9	58.94 ± 4.2
Ia5	77.49 ± 5.5	103.00 ± 7.4	96.27 ± 6.9	68.50 ± 4.9
Ia6	82.99 ± 5.9	82.31 ± 5.9	95.07 ± 6.8	65.01 ± 4.6
Ia7	98.70 ± 7.1	101.16 ± 7.2	87.07 ± 6.2	
Ia8	104.37 ± 7.5	106.81 ± 7.6	81.44 ± 5.8	57.26 ± 4.1
Ia9	128.78 ± 0.2	148.86 ± 0.2	186.31 ± 0.3	81.31 ± 0.1
Ia10	71.56 ± 5.1	86.30 ± 6.2	117.26 ± 8.4	67.00 ± 4.8
Ia11	113.20 ± 8.1	110.64 ± 7.9	133.09 ± 9.5	71.80 ± 5.1
Ia12	86.77 ± 6.2	97.23 ± 6.9	91.20 ± 6.5	53.33 ± 3.8
Ia13	95.17 ± 6.8	118.89 ± 8.5	124.33 ± 8.9	79.96 ± 5.7
Ia14	110.34 ± 7.9	111.30 ± 8.0	116.80 ± 8.3	
Ia15	81.27 ± 5.8	77.94 ± 5.6	75.91 ± 5.4	

Table VI.4: sus values for outcrop I. ❖: standardised to 1g, measured in cgs-mode

VI.B. Error

VI.B.1. Gamma-Ray

VI.B.1.a. Influence of Wetness

moisture [%]	**K** [%]	**U** [ppm]	**Th** [ppm]
sample A			
0	2.38 ± 0.0	4.30 ± 0.2	13.33 ± 0.5
1	2.35 ± 0.1	4.38 ± 0.2	12.95 ± 0.8
2	2.33 ± 0.0	4.15 ± 0.3	12.98 ± 0.6
3	2.20 ± 0.1	4.75 ± 0.2	13.28 ± 0.4
4	2.20 ± 0.0	4.50 ± 0.4	12.43 ± 0.7
7	2.23 ± 0.0	4.30 ± 0.2	13.73 ± 0.5
10	2.20 ± 0.1	5.05 ± 0.3	12.83 ± 1.1
sample B			
0	2.18 ± 0.0	5.40 ± 0.2	12.63 ± 0.5
0.71	2.25 ± 0.0	4.98 ± 0.5	13.30 ± 0.4
1.43	2.23 ± 0.1	5.53 ± 0.3	12.23 ± 0.2
2.14	2.23 ± 0.0	4.48 ± 0.3	12.80 ± 0.4
2.86	2.23 ± 0.1	5.08 ± 0.2	14.15 ± 0.3
5	2.10 ± 0.1	4.33 ± 0.5	16.00 ± 0.9
7.14	2.225 ± 0.0	4.35 ± 0.5	14.40 ± 0.9
sample C			
0	2.23 ± 0.1	4.48 ± 0.3	13.10 ± 0.3
0.63	2.33 ± 0.1	4.48 ± 0.1	14.48 ± 0.8
1.25	2.20 ± 0.1	5.18 ± 0.4	13.15 ± 0.8
1.88	2.15 ± 0.1	4.58 ± 0.2	13.88 ± 0.8
2.5	2.20 ± 0.0	4.58 ± 0.2	14.25 ± 0.6
4.38	2.25 ± 0.0	5.18 ± 0.3	13.05 ± 0.1
6.25	2.10 ± 0.0	4.45 ± 0.4	13.30 ± 0.3

Table VI.5: γ-ray values for different samples of La Fossa cone: influence of wetness. Measured in the laboratory. Measuring time 30 seconds.

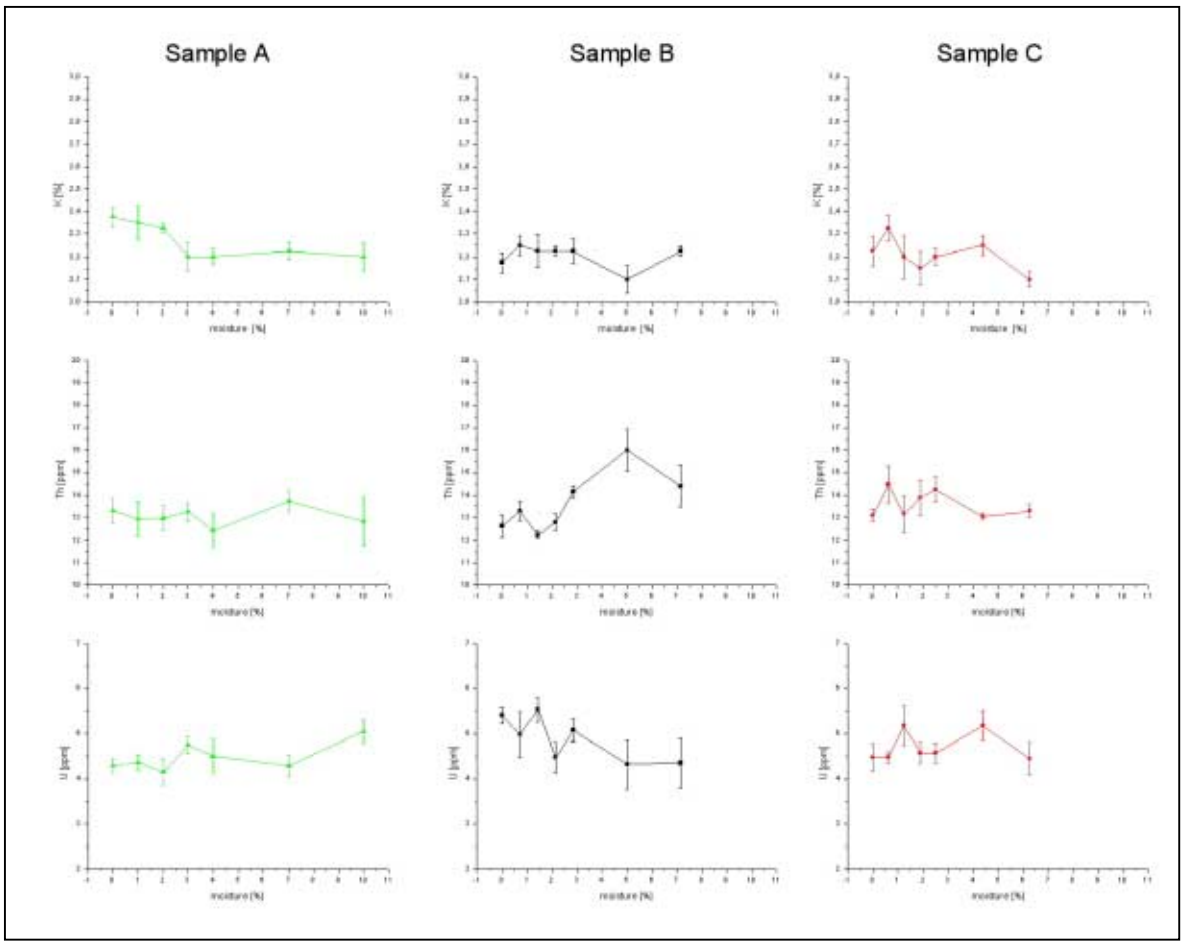

Figure VI.4: Influence of wetness for different samples.

VI.B.1.b. Influence of Thickness

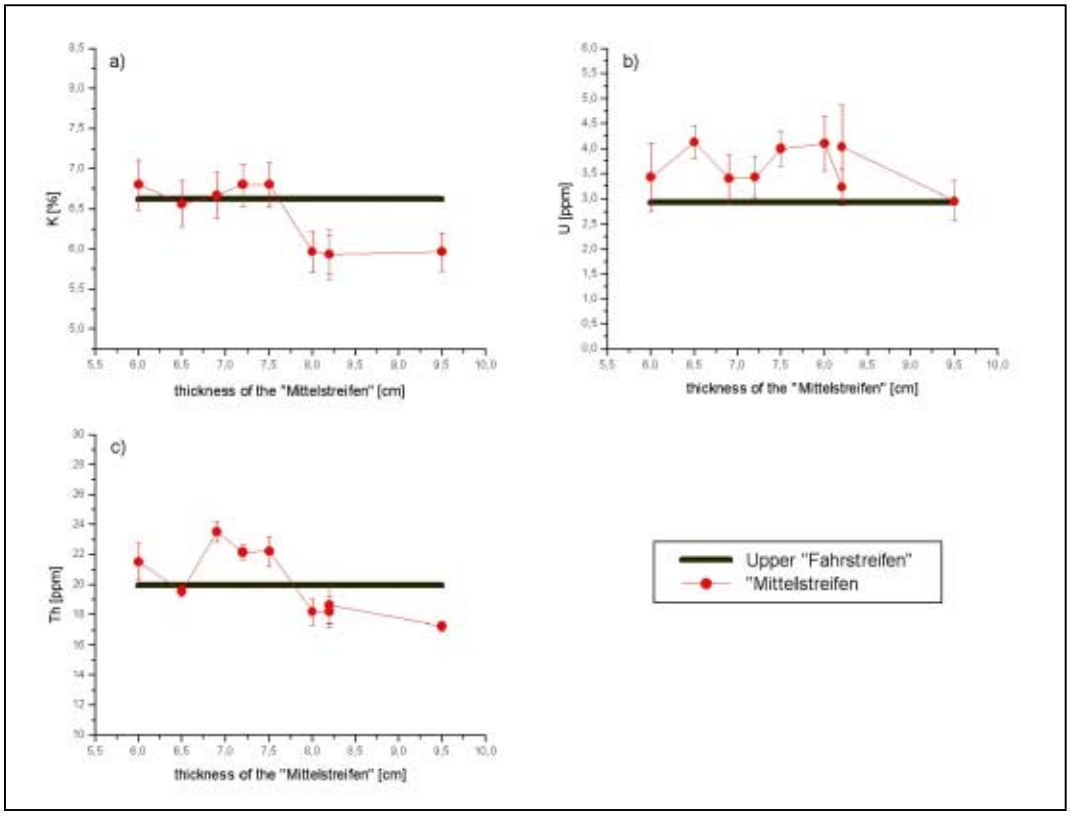

Figure VI.5: : γ-ray measurements of the “Mittelstreifen” (Wingertsberg, Laacher-See, Eifel) in relation to the thickness of the layer for K, U and Th. Values of the overlying Upper “Fahrstreifen” are given for comparison.

VI.C. Distance

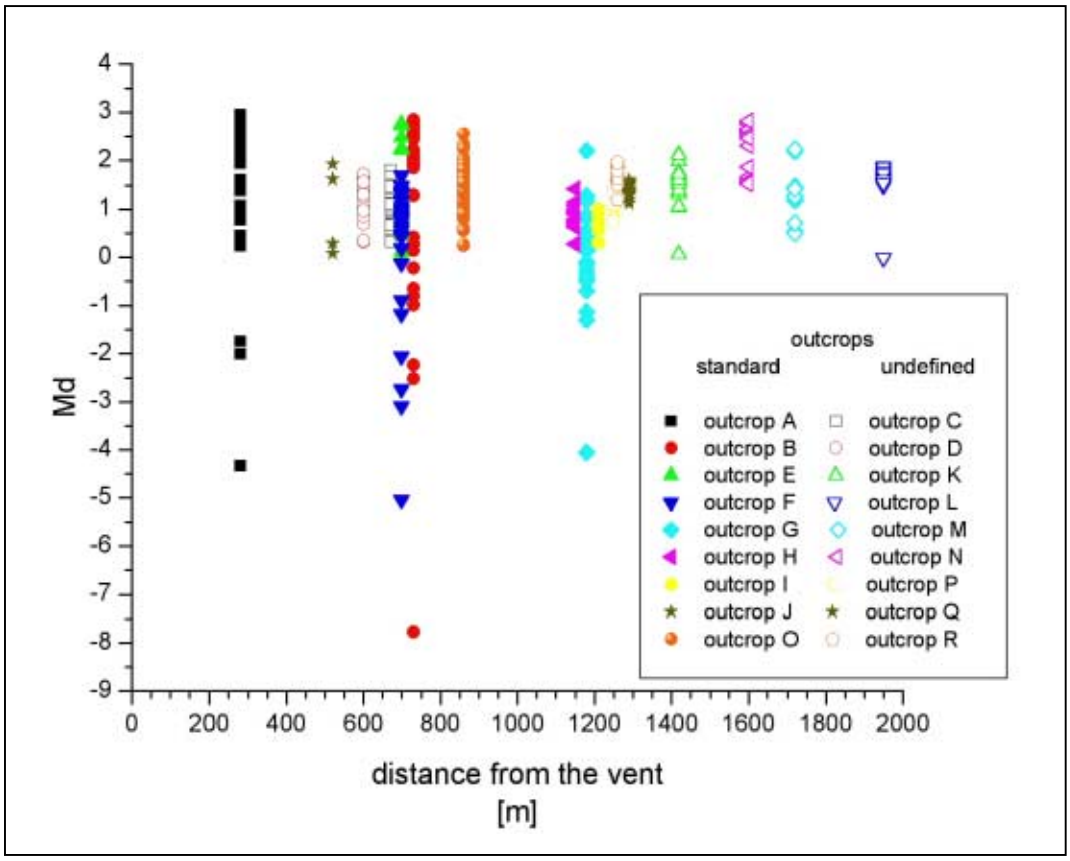

Figure VI.6: Md vs. distance for the different outcrops of La Fossa Cone

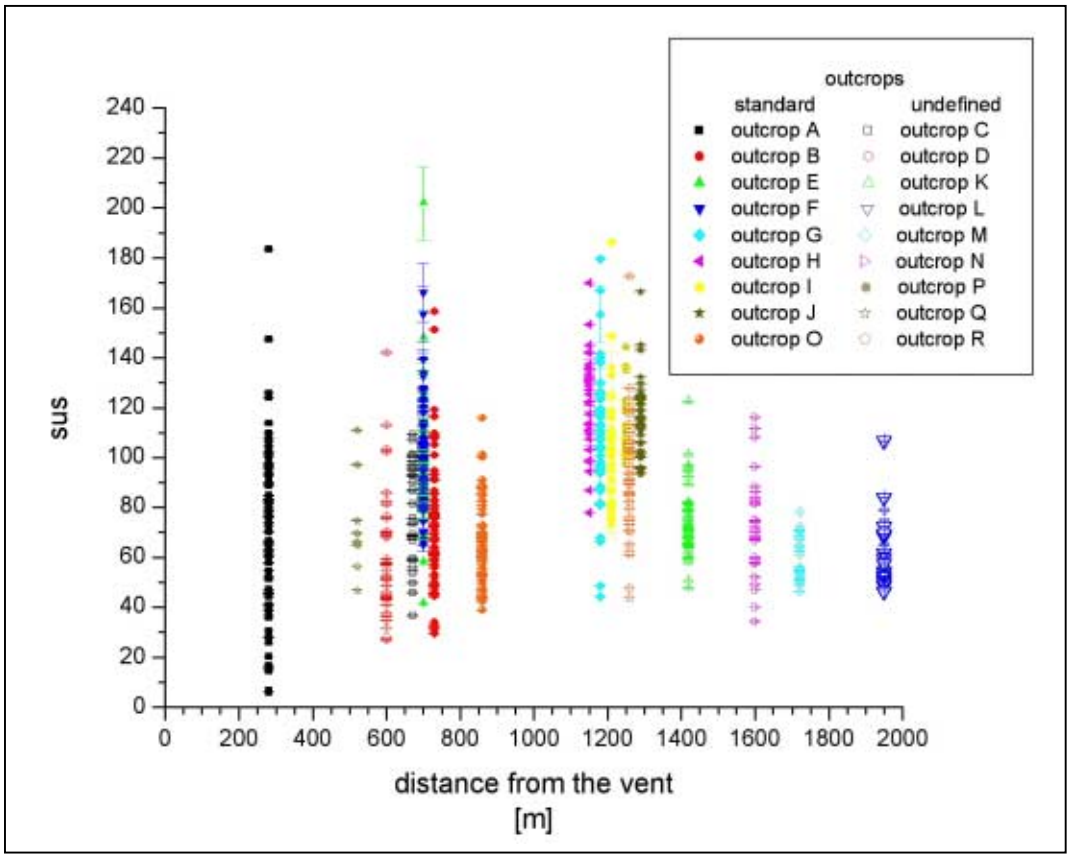

Figure VI.7: sus vs. distance for the different outcrops of La Fossa Cone

VII. Appendix VII: Photo Plates

Figure VII.1: View from Lipari (Quadrocchi) to N-Vulcano.

Figure VII.2: Fumaroles on the Crater of La Fossa di Vulcano, view from the NW-rim.

Figure VII.3: La Fossa Cone, view from outcrop L.

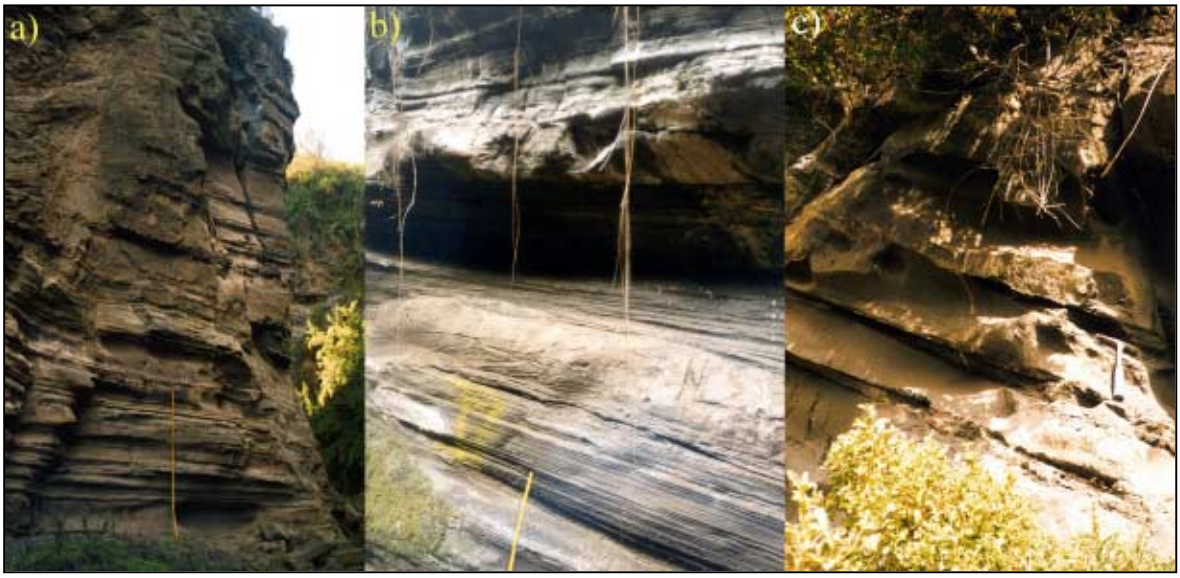

Figure VII.4: Punte Nere a) outcrop G, b) outcrop H dominated by laminated deposits, b) outcrop J dominated by massive deposits.

Figure VII.5: Different wet-surge deposits of Tufi Varicolori. a) outcrop F, b) outcrop O.

Figure VII.6: Outcrop F: Palizzi covered by the 1nd Palizzi pumice.

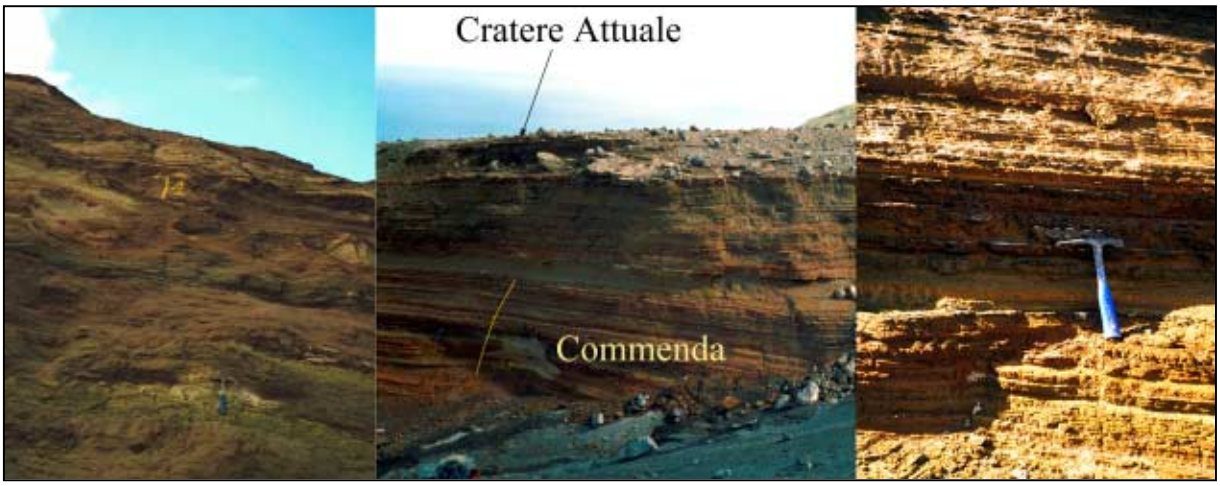

Figure VII.7: Commenda: deposits near the crater rim (left, outcrop A), deposits with increasing distance from the vent (outcrop B). The deposits of Commenda are covered by deposits of Cratere Attuale (middle picture).

Figure VII.8: Cratere Attuale, different dry-surge deposits of outcrop E covered by the Pietre Cotte pumice.